Drug Delivery Approaches

Drug Delivery Approaches

Perspectives from Pharmacokinetics and Pharmacodynamics

Edited by

Bret Berner
Seattle, WA, USA

Toufigh Gordi
South San Francisco, California, USA

Heather A. E. Benson
Curtin University of Technology, School of Pharmacy, Perth, Australia

Michael S. Roberts
University of Queensland, School of Medicine, Brisbane, Australia

WILEY

This edition first published 2021

Registered Office
John Wiley & Sons, Inc., 111 River Street, Hoboken, NJ 07030, USA

Editorial Office
111 River Street, Hoboken, NJ 07030, USA

For details of our global editorial offices, customer services, and more information about Wiley products visit us at www.wiley.com.

Wiley also publishes its books in a variety of electronic formats and by print-on-demand. Some content that appears in standard print versions of this book may not be available in other formats.

Library of Congress Cataloging-in-Publication Data is applied for
Hardback ISBN: 9781119772736

Cover Design: Wiley
Cover Image: © Peshkova/iStock/Getty Images

Set in 9.5/12.5pt STIXTwoText by Straive, Chennai, India

10 9 8 7 6 5 4 3 2 1

Contents

Preface

Drug delivery aims to enable appropriate drug absorption based on the physical and chemical properties, expected dose, and route of administration. For new chemical entities, drug delivery is initially expedient and adapts the dosage form of the active compound to the stage of development based on feedback from the iterative understanding of the pharmacokinetics (PK), pharmacodynamics (PD), and potential sources of variability of the candidate drug. In actual practice, the final formulation is often based at most on the determination of a dose response. Models combining physical and pharmacokinetic properties of a drug candidate with dissolution, in vivo studies, and known transporter and biomarkers have been shown to predict the time course of events successfully in vivo. To improve delivery of older chemical entities, whether controlled release, modified release, temporally or site-controlled delivery, development of a target pharmacokinetic profile to optimize efficacy for duration and/or to reduce adverse events is the starting and ending point for designing a dosage form.

This book discusses the options for drug delivery within the available routes of administration to achieve the target profiles and approaches as defined by these models. It is intended for use by graduate students and novice and skilled practitioners, who are developing either new or re-purposed drugs. In particular, this book should prove useful to pharmaceutical scientists and engineers, including formulators, pharmacokineticists, clinical pharmacologists, and those interested in the interaction of these disciplines.

This book begins with an appreciation of modeling of drug absorption and physiological effects and the use of pharmacokinetic and physiologically based models and follows with an introduction to physiological-based pharmacokinetics (PBPK). For the most common route of delivery, oral administration, there are chapters dealing with both PBPK and the multiplicity of options for oral drug delivery dosage forms. Endpoints that may substitute for measures of delivery or efficacy and rigorous skin permeation testing are discussed as targets for topical drug delivery and may have both development and regulatory applications. In

the case of systemic transdermal delivery, understanding the pharmacokinetics of the formulation and the drug is essential to guide formulation from earliest conception throughout development. Separate chapters discuss the biological and delivery approaches to pulmonary and mucosal delivery. For emergency care settings, the relationship between parenteral infusion profiles and PK/PD is the key topic discussed. The book concludes with some more recent trends with chapters discussing virtual experiments to elucidate mechanisms and approaches to drug delivery and personalized medicine.

We would like to thank all the authors for their contributions to this book. We wish to especially thank our co-editors, Heather Benson and Michael Roberts, for conception, initiation, and review of this book and our editor at Wiley, Jonathan Rose, for his patience and support during the writing of this book.

May 30, 2020

Bret Berner, PhD
Seattle, WA
Toufigh Gordi, PhD
San Carlos, CA

1

Introduction: Utility of Mathematical Models in Drug Development and Delivery

Toufigh Gordi[1] *and Bret Berner*[2]

[1] *Sr. Director of Clinical Pharmacology at Rigel Therapeutics, South San Francisco, CA, USA*
[2] *Formulation and Drug Delivery Consultant, 4011 54 Ave SW, Seattle, WA, USA*

1.1 Introduction

Models, particularly mathematical models, have been widely used to understand different aspects of human lives for a long period of time. Mathematical models not only can help explain observations, but also aid in predicting outcomes of experiments. Models are frequently used in our daily lives. As an example, consider the following equation as a model:

$$\text{Distance} = \text{Speed} \times \text{Time}$$

Knowing the relationship between distance, speed, and time, we use the model to predict the time to reach our destination on a trip. Furthermore, we plan our daily lives by predicting the time it takes for a trip or a simple question of whether we will be on time for a meeting. For this well-established model, instead of performing the experiment of driving from point A to B to know how long it may take, we can have a good estimate of the time by knowing the distance of the destination is from us and how fast we expect to travel. Models can simplify our experiments or even alleviate them. The powerful ability of models to predict outcomes of unknown experiments makes them an essential part of a wide range of modern industries, from aviation to auto to computer and financial entities. New airplane designs are tested less than a handful times in the air before large-scale production starts and they are in regular use. New car crash tests are performed in computer simulations before an actual prototype is crash-tested a few times. Models help advance product development at a faster rate and a fraction of the cost associated with actual experiments. It is not surprising that the use of mathematical models has gained widespread attention within the pharmaceutical industry and

Drug Delivery Approaches: Perspectives from Pharmacokinetics and Pharmacodynamics,
First Edition. Edited by Bret Berner, Toufigh Gordi, Heather A. E. Benson, and Michael S. Roberts.

with regulators. With drug development being a lengthy and enormously expensive process, mathematical models have the potential of optimizing a therapeutic regimen, decreasing costs, and shortening the timelines significantly.

In this chapter, we describe a few mathematical models and their utility in drug development and provide examples of the use of these models in predicting clinical study outcomes or indicating possible causes of the observations, thereby helping researchers focus on areas that have the most impact on the development path of a drug. Within physiologically- based pharmacokinetic (PBPK) in regulatory submissions, only a small fraction, quoted as 6% of PBPK models, focused on drug delivery [1], whether it be food effects or issues in drug absorption. In some exceptional cases, the verification of the PBPK model was sufficient to avoid bioequivalence studies. In this chapter, we focus mostly on models of the drug delivery itself to design or select the target delivery profile or the dosage form itself. Other chapters throughout this book will provide more detailed descriptions of the principles of developing mathematical models in the drug-development process and for the different routes of drug delivery.

1.2 Use of Mathematical Models in Drug Development

The relationship between dose and effect of a remedy must have been known to ancient healers, who often used mixtures of different herbs and other organic material at certain proportions to combat diseases. Despite significant changes to pharmacological intervention aimed at mitigation of symptoms and curing various diseases, drug-development goals today are strikingly similar: find the dose of a compound that provides the maximum desired effect while avoiding unwanted side effects. This central question of what dose (amount, frequency) is a major reason for late-phase, confirmatory clinical development programs [2]. In early stages of the modern pharmaceutical industry, the focus was on establishing a dose–response relationship. With advances in analytical chemistry to allow measurement of drug concentrations in blood, plasma, urine, or other body fluids, the focus has shifted to elucidating a concentration–response, or in broader form, dose–concentration–response relationships. This shift is logical as the larger observed variability in and the complexity of a dose–response relationship is reduced when investigating the concentration–response. Furthermore, concentration measurements offer the possibility to follow the temporal changes of drug concentrations, thereby providing a tool to understand the time course of the pharmacological effect of a compound. Mathematical models that could describe the time course of drug concentrations were first proposed in late 1930s [3, 4]. However, due to the complexity of models required and the lack of computers, only models solved by analytical solutions could be developed. The perceived

complex underlying mathematics resulted in the utility of mathematical models not being appreciated by the medical community. Introduction of physiologically related parameters such as clearance during 1970s made it easier for the medical community to understand and appreciate these models by relating them to the biology of the disease and the pharmacology of the treatment [5]. Furthermore, academic centers contributed to the advancement of general concepts of using mathematical models to describe the time course of drug concentrations in the body (pharmacokinetics, PK) and its effects (pharmacodynamics, PD) [6–8].

Mathematical models have two main functions: describing observations and predicting untested scenarios using simulations. Thus, models are modified when new experimental data becomes available. ~~that are not consistent with the original model~~. The process of model development involves building simple models based on limited available data. This simple model is then used to guide the design of future studies. Once a new study is performed, the generated data are compared to the simulations by the model to test its validity. If the new data agree with the predictions of the model, the experimental data can be added to the data pool and re-estimate the model parameters using a larger data set. On the other hand, if the model was unable to predict the new data, the underlying assumptions or the model may be modified to include new insights gained through the new experiment. This cycle of learning and testing is an essential part of the model development process and is routinely used in drug development [9, 10]. Early development programs of a new drug can be more efficient by developing and enhancing the relevant models, allowing for more accurate and reliable design and prediction of clinical studies.

1.3 Noncompartmental Analysis

Although generally not considered as mathematical modeling, noncompartmental analysis (NCA) of a drug's plasma concentration data over time adds substantial understanding of its PK properties and is therefore briefly described here.

NCA refers to estimating various PK parameters of a compound through simple analysis of its concentration–time profiles at a biological fluid (most commonly plasma), where drug concentrations have been measured. Although the same principles are used when other body fluids, e.g. blood or saliva, are used, in this chapter we will refer to plasma drug levels, the most widely used sample collection medium. Figure 1.1 shows the concentration–time profile of losmapimod, a p38 mitogen-activated protein kinase inhibitor, after intravenous (i.v.) and oral (p.o.) administrations [11]. Since the entire administered dose of the drug is available to the body after an i.v. dose, the bioavailability equals 100% or 1 after an i.v. administration. After a p.o. administration, part of the drug

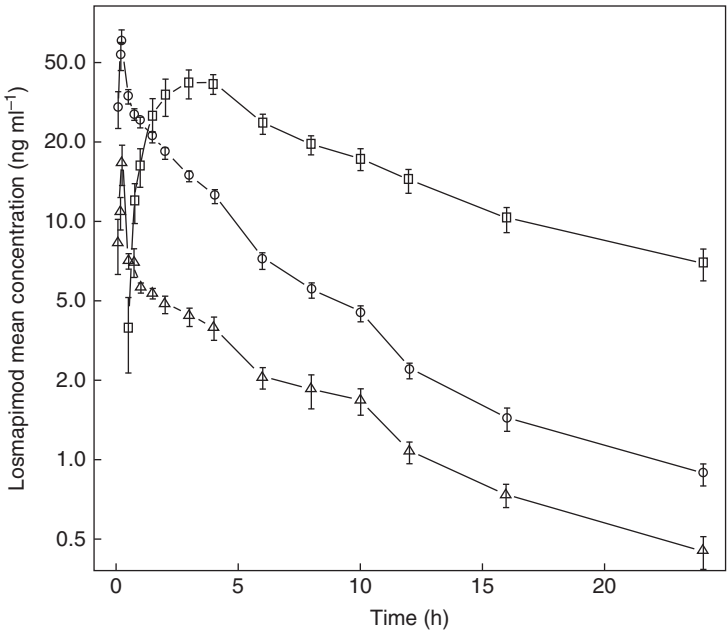

Figure 1.1 Mean losmapimod concentration at each time point with standard error bars: 15 mg orally (squares), 3 mg i.v. (circles), and 1 mg i.v. (triangles). Source: Barbour et al. [11] © 2013, John Wiley & Sons.

may not reach the systemic circulation due to various reasons: it may degrade in the intestinal tract; it may not be fully absorbed; or drug molecules may be metabolized by enzymes in the gut wall or liver before reaching the circulation. Therefore, the bioavailability of the drug may vary from 0 (not at all bioavailable) to 1 (fully bioavailable). Losmapimod in Figure 1.1 has a bioavailability of 0.62.

A simple examination of the concentration–time plots in Figure 1.1 provides several estimates, as listed in Table 1.1. The observations provide the ability to estimate maximum (observed) concentration (C_{max}), exposure to the drug (area under the curve to infinity, AUC), or the time it takes for most of the drug to be eliminated from the body (approximately four to five time its elimination half-life, $t_{1/2}$). Such information may help relate drug concentration and exposure levels to efficacy or toxicity outcomes. However, NCA suffers from certain limitations, including the need for extensive sampling to enable reliable estimation of parameters. Furthermore, by relying on single-point or time-averaged estimates (e.g. AUC, C_{max}, or elimination half-life), information on the time course of the drug concentration changes is lost, despite availability of data.

Table 1.1 NCA parameter estimates (geometric mean except for t_{max} given in median) of losmapimod after single intravenous and oral doses in healthy volunteers.

	i.v. (1 mg)	i.v. (3 mg)	p.o. (15 mg)
$AUC_{0\text{-infinity}}$ (mcg*h/l)	54	171	528
C_{max} (mcg/l)	18	59	46
t_{max} (h)	0.25	0.25	3.5
$t_{1/2}$ (h)	8	6	9

Source: Based on Barbour et al. [11].

1.4 Pharmacokinetic (PK) Models

Pharmacokinetic models are a set of mathematical equations that aim to describe the observed concentration-time data after the administration of a drug. These are often called compartmental models since the models use hypothetical compartments connected to each other allowing for transfer of drug molecules between them. Although these compartments are often given names such as central or peripheral compartments, they do not generally refer to any specific body organ.

Referring to losmapimod in Figure 1.1, the plasma concentrations of drug fall rapidly within a couple of hours after both administration routes. With the passage of time, the decline in concentrations becomes slower toward the end of the sampling period. Although the original authors did not develop a PK model for this set of observations, the two slopes of disappearance can be mathematically described using a two-compartment model (Figure 1.2). The compartments are conveniently named Plasma and Peripheral. In the case of i.v. administration, the dose is given directly into the Plasma compartment, while in the case of p.o. administration the dose is given at the administration site, i.e. the gastro-intestinal tract. The extravascular dose may also be administered elsewhere, e.g. skin (topical or subcutaneous dose) or lungs (inhalation). An extravascular dose is modeled as being transferred to the site of sampling (normally plasma) with a single absorption rate (k_a). During the early period of sampling, losmapimod leaves the Plasma compartment in two ways: transport to the Peripheral compartment and elimination. Transport by passive diffusion to the Peripheral compartment is driven by concentration gradients: as long as the Peripheral compartment has a lower concentration than the Plasma compartment, the net flow will result in disappearance from plasma. Once drug concentrations in the two compartments reach an equilibrium, the net flow becomes zero and hence the disappearance from the Plasma compartment will be driven by the elimination process only.

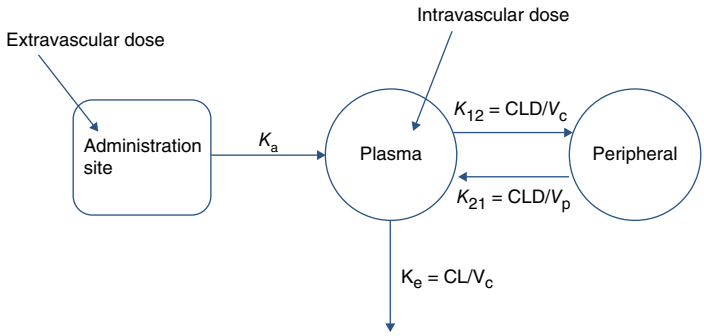

Figure 1.2 Schematic presentation of a two-compartment pharmacokinetic model with extravascular and intravascular administrations. K_a: absorption rate constant, K_{12}, K_{21}: transfer rate from the plasma to the peripheral compartment, and vice versa, respectively, CLD: intercompartmental clearance, V_c and V_p: volume of central (plasma) and peripheral compartments, respectively, K_e: elimination rate constant, CL: drug clearance.

Pharmacokinetic models can be developed to describe drug concentration–time profiles after various routes of administrations (e.g. oral, topical, or i.v.). Furthermore, although plasma is by far the most utilized body fluid used in PK investigations of drugs, other biological media, such as saliva [12] or cerebrospinal fluid [13], may also be used. The choice of the sampling medium is driven by the ease of collection, feasibility, bioanalytical interference, and relevance to the biological activity of interest.

Early development of PK models involved two stages: first, models were fitted to individual drug–concentration–time data and relevant model parameters were estimated for each individual. In a second step, descriptive statistics were performed to estimate various population parameters of the model based on the individual estimates [14, 15]. A major disadvantage of this approach is the need for a large number of samples per individual to build that individual's PK model and estimates one's parameters reliably. Such dependence on the number of samples per individual also means that sparse samples generally collected during late-phase clinical studies cannot be utilized when developing two-stage PK models. These limitations are dealt with in a mixed-effect modeling approach, originally proposed by Sheiner et al. [16–18]. In this approach, all data are pooled and used to develop a universal model. Since individuals exhibit biological differences resulting in different concentration–time data, the modeling approach allows for estimation of structural model parameters (e.g. clearance or absorption rate constant) as well as interindividual variability in model parameters simultaneously. By pooling all data, a major obstacle with two-stage modeling is alleviated: contribution of data from an individual is less critical when estimating the model parameters. Moreover, the mixed-effect modeling

approach allows the use of sparse samples from late-phase clinical studies. In fact, the mixed-effect modeling approach was first developed when dealing with sparse sampling schemes from clinical observations [16, 19]. Furthermore, the mixed-effect modeling approach allows the evaluation of the effect of subject characteristics (e.g. body weight, gender, or age) on various model parameters. The same approach can be applied to other model development practices, e.g. pharmacokinetic/pharmacodynamic (PK/PD) models.

One limitation of PK models is their reliance on observations. Therefore, inadequate sampling may result in developing a simpler model (e.g. a one-compartment model) when a more extensive data set may be best described a more complex model (e.g. three-compartment model). Such misspecification will inevitably result in incorrect model predictions, decreasing the validity or utility to predict future study outcomes. Furthermore, compartments in PK models generally do not have any physiological relevance. In fact, a multicompartmental model may be an exercise in curve fitting when fewer (or more) compartments may better reflect the physiology. Nevertheless, PK models offer the best tools in describing the available data and predict the outcome of untested scenarios using simple simulations compared to performing the actual clinical study.

1.5 Physiologically Based Pharmacokinetic (PBPK) Models

Physiologically based PK (PBPK) models introduce elements of the known physiology when modeling drug concentration–time data. These include adding "compartments" such as liver, lungs, kidneys, or any other organ of interest into the model (Figure 1.3). A considerable amount is known about the blood flow into and out of various tissues and organs and by including other parameters such as drug binding to tissue proteins or distribution of the compound of interest in them, one can estimate drug concentrations within an organ. Such expansion of a model opens new possibilities in using models to predict outcomes of future studies.

An obvious advantage of PBPK models lies in the inclusion of compartments representing distinct organs. This offers several benefits and widens their applications. A major benefit is the use of these models to predict drug pharmacokinetics in certain groups based on data from others. As an example, the pharmacokinetic behavior of a drug in infants can be predicted by applying PBPK models to data from adults [20–23]. Similarly, pharmacokinetic properties of a drug molecule can be predicted in one species based on a model from another species by modifying the model parameters to represent those of the target group [24, 25]. Although not consistently accurate, this approach has been shown to result in better predictions compared to the frequently used allometric scaling, where the clearance

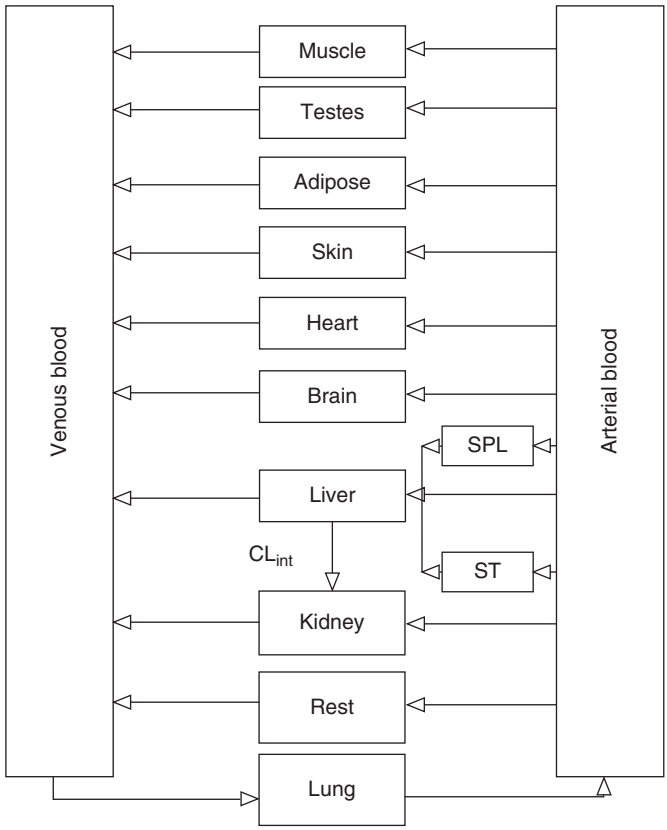

Figure 1.3 An illustration of a physiologically based pharmacokinetics model. Each compartment represents a distinct organ. ST is stomach; SPL are splanchnic organs; and CLint is intrinsic hepatic clearance. Source: Aarons [20] © 2005, John Wiley and Sons.

and volume of distribution terms are scaled up arbitrarily [26, 27]. In addition to intra- or interspecies scaling of pharmacokinetic properties of drugs, PBPK models provide means of estimating drug concentrations at various organs of interest. While plasma monitoring of drugs is easily performed, drug concentrations in certain organs may correlate better with the observed pharmacological and clinical effects of a drug [28, 29]. The increased use of PBPK models in drug development is also evident in the increased number of applications filed with the Food and Drug Administration (FDA), containing such models [30]. Furthermore, the FDA recommends using PBPK models when evaluating drug–drug interactions in a Guidance For Industry document and arranges for regular workshops on the topic [31, 32].

Although implementation of PBPK models is readily made in commonly used modeling software such as NONMEM or Phoenix, highly specialized platforms and software have been developed in recent years. These include, among others, SimCyp®, GastroPlus™, and PK-Sim®. Chapter 3 in this book provides a more in-depth presentation of the most commonly used software packages in the modeling of oral delivery.

1.6 Pharmacokinetic/Pharmacodynamic (PK/PD) Models

Pharmacokinetic and PBPK models provide valuable tools in describing observations and predicting untested scenarios of the expected concentrations after the administration of a certain dose and route of administration. However, such predictions are generally not the focus of interest when developing new medicines. The goal of drug-development programs is to bring effective and safe drugs to the patient population. Therefore, the major focus of such programs is to determine and characterize the efficacy and safety of new drugs. The key question in any drug-development program is "for a given patient what dose of the drug will provide the desired efficacy while avoiding or reducing the undesired effects?" Both PK and PBPK models are important tools to answer this question but only as input into a model that relates drug concentrations at any given time to its pharmacological effect. There is hence another layer of models, generally known as pharmacokinetic/pharmacodynamic (PK/PD) models.

The simplest type of PK/PD model correlates the observed effects directly with drug concentrations [33]. Such effects are observed immediately after the drug concentrations reach a certain minimum level and disappear when drug concentrations decrease below this threshold level. Thus, a major characteristic of such effects is the lack of any significant delay between the observed effect and drug concentration. Such models may include linear or saturable concentration–effect relationships. In reality, these models best characterize data for a steady-state infusion where the time dependence is eliminated.

Although direct concentration–effect relationships are perceived as common, most effects lag behind drug concentrations. In most cases, the maximum drug effect is observed later than the maximum achieved concentration (Figure 1.4) [34–36]. Such delay may result in counterclockwise hysteresis when effect observations are plotted against drug concentrations. This is due to the time delay between the observed effect and measured concentration. Consequently, similar drug concentrations may seem correlated with two different effect magnitudes depending on the time of observation. One of the first PK/PD models developed to capture this delay assumed the lag to result from the movement of minute amounts of drug

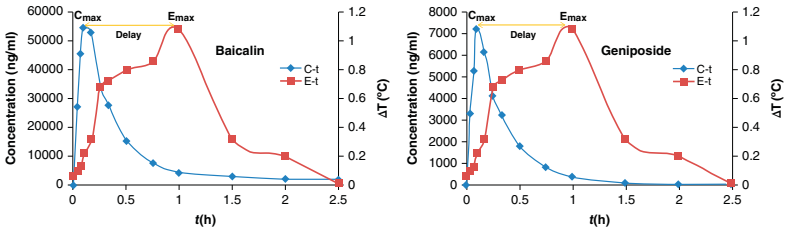

Figure 1.4 The peak effect lags behind the peak concentration of baicalin and geniposide after intraperitoneal administration of quingkailing injection (QKLI). ΔT is the absolute value of the change in rectal temperature. Source: Zhang et al. [34] licensed under CC BY 4.0.

from the site of measurement (mostly plasma) to the site of effect (e.g. brain) [37]. Once drug concentrations reach the threshold levels at the site of action (the effect compartment), there is a direct pharmacological effect. The effect compartment model has successfully been applied to various types of drugs [38–40].

A major shortcoming of the effect compartment model is its prediction of the time of the maximum effect. While the model can predict the increase in the magnitude of the effect with increasing doses of the drug, the time of the maximum effect is predicted to be the same for all doses [41, 42]. This has been shown to be the case for many drugs and their pharmacological effects [43–45]. However, a large number of drugs result in a more complex effect–time relationship, where times to reach the maximum effects increase with dose [42, 46, 47]. This implies a different biological process, where transport time for the drug to reach its site of action may not have any significant impact on the delay of the onset or peak of the effect. Nevertheless, the effect compartment model has its merits when the observed delay is mainly due to the concentration buildup at the site of action. Furthermore, the model can be used when metabolites of the drug are the driving effect, where the delay can be attributed to the formation of the metabolite [48].

Indirect response models assume that the effect of interest is maintained at a baseline level equal to the sum of its production and its disappearance [46]. As an example, body temperature can be seen as a zero-order production of heat and a first-order loss of it. At hemostasis, the net product is kept constant: human body temperature is normally stable around 37 °C. Drugs exert their pharmacological activity by influencing either the production or loss of the effect, which can be an increase or a decrease. A drug that is used against fever, e.g. may decrease the rate of heat production or increase the rate of heat loss, thus resulting in decreased body temperature. Similarly, a drug may increase the production of an endogenous hormone or decrease its elimination, thereby resulting in increased levels of the hormone.

It is noteworthy to realize the difference between these models and the most common form of investigating the exposure–response that is generally limited to evaluating the correlation between a single NCA endpoint, such as AUC or C_{max} and a single-effect measurement (i.e. biomarker levels at the end of treatment). While the noncompartmental parameter estimates may or may not show any correlation with the measured effect, they totally ignore the time course of drug concentrations and their pharmacological effects. In contrast, compartmental PK/PD models describe these time courses and provide means to simulate various scenarios. As an example, knowing the turnover rate of the biological pathway of interest, the effect of formulation changes on the pharmacokinetics of a drug and the subsequent impact on the time course of the effect can be investigated by changing formulation-related model parameters.

1.7 Systems Pharmacology Models

Systems pharmacology (SP) models combine available data with prior knowledge in describing the properties of the underlying biological system that, when perturbed, cause observed pharmacological effects [49]. Although SP models are similar to PK/PD and PBPK models, SP models do not try to describe a set of observations, but to help understand the behavior of the drug and the biological system they exert their pharmacological effect on. By understanding the underlying mechanism of the whole (or parts of a) system, observed changes in measurements can be attributed to specific changes in the biological system affected by a certain intervention, resulting in the observations. Such approach offers significant advantages, albeit at the cost of significantly more effort, compared to PK/PD models. While PK/PD models rely heavily on the existing observations, SP models (and also PBPK models) incorporate the available knowledge from several sources, e.g. experimental data, published literature, or other publicly available information, to build a mathematical description of the interactions between the myriad components of a biological system (Figure 1.5). Furthermore, SP models can be tailored to focus on the specific needs of a project by providing detailed descriptions down to the receptor and gene levels of parts of the system while bundling less relevant parts to a single compartment. Due to the complexity, development of an SP model requires involvement of skilled contributors from several different scientific areas, from engineering to biology, pharmacology, and clinical sciences. Thus, while PK/PD models can be developed by skilled individual modelers, SP model development requires a team effort. However, bringing together teams with different backgrounds in building such models may help breaking down organizational barriers and improve collaboration across different functional areas. Nevertheless, the complexity of SP models has the potential to make use of such models highly unfavorable, either with regard to the expertise needed to use the models or, worse yet, the perception of these models as a "black box," which may result in a less favorable attitude toward its use or incorrect predictions by the end customers.

The utility of SP models stretches into several areas. Once the underlying pathophysiology of a disease is quantitatively described by relating various biological pathways to each other and the disease progress, simulations can be made to find prospective targets for future interventions. By simulating the effects of a hypothetical drug in stimulating or blocking a certain pathway, the relevance and magnitude of the intervention can be modeled. Such practice focuses research in finding new and novel targets for pharmacological interventions. Another potential use is finding relevant biomarkers with high correlation to the disease progression. The levels of each building block of the SP model can be monitored in silico to find biomarkers that can be easily sampled, while informing the progression of the disease, or the lack of it, due to pharmacological intervention. The synergy between

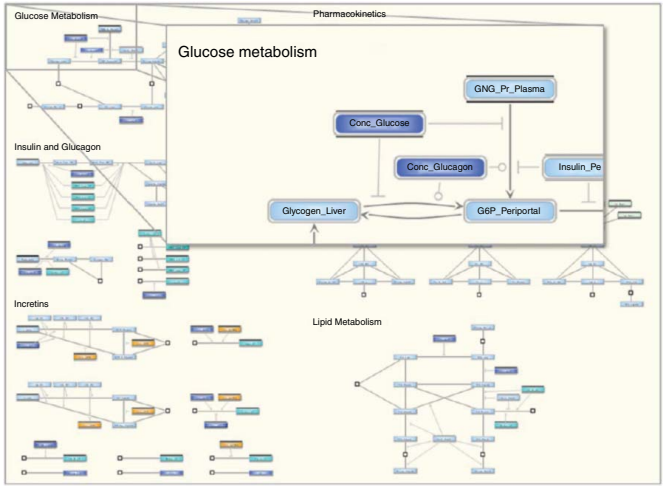

Figure 1.5 A portion of a graphical representation of a type 2 diabetes model. Major biological processes are represented graphically as subsystems or modules (e.g. glucose metabolism, insulin and glucagon, incretins, etc.). They are linked mathematically by the use of an aliasing function that allows display of the same node in multiple places on the diagram. The detailed section represents key regulated processes in glucose metabolism. For example, glycogenolysis (the reaction arrow going from liver glycogen ["Glycogen_Liver"] to glucose 6 phosphate ["G6P_Periportal"]) is regulated by glucose ("Conc_Glucose") and glucagon concentrations ("Conc_Glucagon"). Source: Friedrich [49] © 2016, John Wiley and Sons.

different drugs and finding the best combination may also be evaluated with SP models. Thus, instead of testing several combinations in clinical settings, one or two combinations with the greatest probability of success based on the biology of the disease, the mechanism of action of the drug, and the individual characteristics of the patient can be selected and tested in the clinic. SP models may also be utilized in early discovery studies, when the model can point to areas that need further research to understand the system. Furthermore, SP models can be used to understand the behavior of the observations. An example below highlights the use of one such model to identify the cause of large observed variability in the pharmacokinetics of a drug in neonates.

1.8 Utility of PK/PD Analysis and Models in Drug Development

The following examples describe different instances when evaluating the pharmacokinetics and pharmacodynamics helped address specific questions. Although the first case does not include a modeling approach, it provides an example of how investigating changes in drug concentrations over time can significantly change the conclusions from seemingly straightforward studies. Cases 2 and 3 describe different models and their use in answering different questions of interest.

Example 1.1 ***Toxic or not? It's all about the formulation***
Artemisinin is the parent compound of water- and oil-soluble derivatives used for treatment of malaria [50]. Artemisinin is administered orally, but its water-soluble derivative artesunate is available in oral or i.v. formulation and the oil-soluble derivative artemether is available in oral or intramuscular (i.m.) forms. Artemisinin compounds have been used extensively for treatment of malaria over the past 30 years with minimal adverse effects or signs of toxicity having been reported. However, a series of studies in laboratory animals pointed to potential neurotoxicity, especially with the oil-soluble artemether given i.m. [51]. In general, the preclinical studies were performed by observing physiological changes after single or repeated dosing of the drugs after the administration of high i.m. doses without monitoring drug concentrations. Although such study designs are common in preclinical development and investigations, they may add little to the understanding of the observations or even be misleading. In the case of the toxicity for the artemisinin family of compounds, the observed toxicity in animals was attributed to prolonged exposure to artemether due to a depot effect of the oil-based intramuscular injection [51]. While all artemisinin drugs have a short half-life and are rapidly cleared from the body upon administration, intramuscularly injected oil suspensions result in steady release of the drug

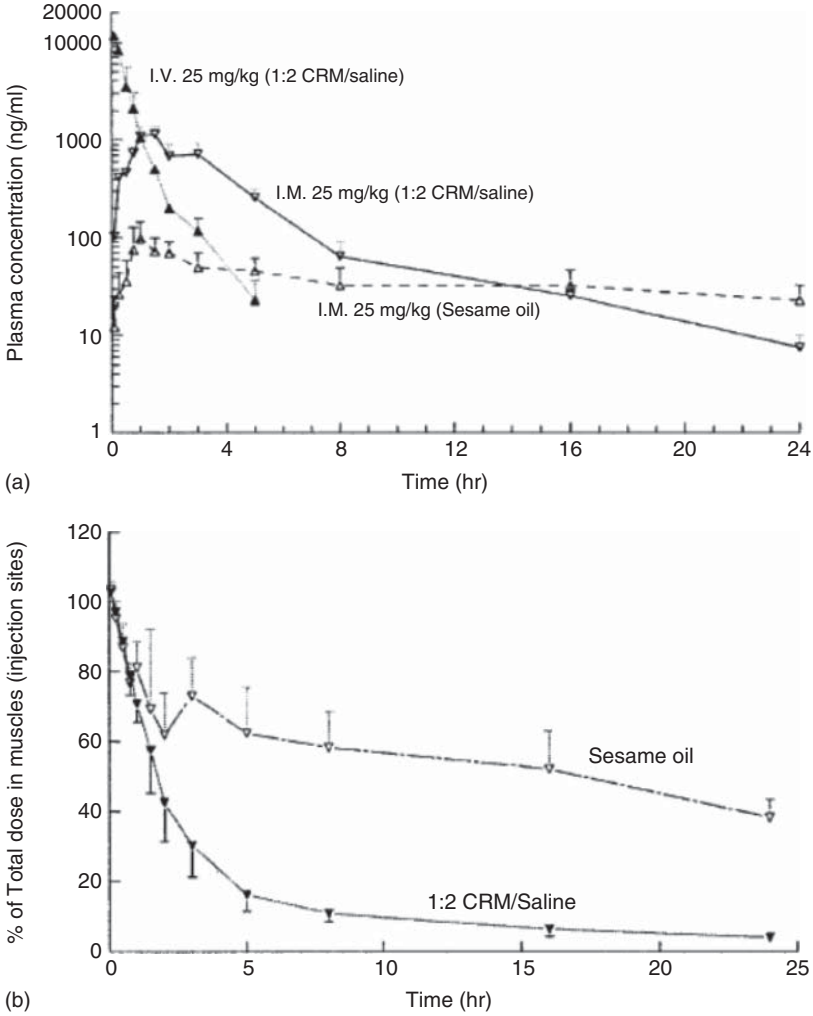

Figure 1.6 Plasma concentration–time profiles of artemether following 25 mg/kg single i.v. and i.m. injections to male rats using sesame oil or the water-based 1 : 2 cremophor/0.9% saline (1 : 2 Cremophor [CRM]/saline) as vehicles (top). The bottom graph shows the muscle concentrations at the site of injections using the two vehicles. Source: Li et al. [52] © 2002, The American Society of Tropical Medicine and Hygiene.

from the site of injection over a long period of time (Figure 1.6) [52]. Such a profound change in the pharmacokinetics of the drug is believed to cause the observed neurotoxic damage. In fact, a single dose of artemether (50 mg/kg), administered using sesame oil as the vehicle, resulted in the death of almost all treated rats. However, none of the rats treated with the same dose of the drug

in a water-soluble vehicle suffered death. It is thus highly recommended that pharmacology studies include a pharmacokinetic investigation, which may help explain findings of the study.

Example 1.2 ***From healthy volunteers to renally impaired subjects***
Regadenoson (Lexiscan®) is a novel, selective A_2A adenosine receptor agonist used as an adjunctive pharmacological stress agent in myocardial perfusion imaging (MPI) procedures [53]. Regadenoson produces coronary vasodilation and increases coronary blood flow by activating the A_2A adenosine receptor. Renal elimination accounts for about 60% of the total clearance of drug. Many subjects undergoing MPI have other comorbidities such as renal insufficiency. Furthermore, a decrease in renal function with age is expected in this generally older patient population. During the clinical development of the compound, renal function was expected to have an impact on drug clearance and potentially result in a longer duration of side effects in patients with decreased renal function. A study in subjects with decreasing levels of renal function was planned to investigate the safety and tolerability of regadenoson in these patients and whether a possible dose adjustment based on renal function was warranted. When designing the study, a major question was the dose to be tested. The perceived clinical dose was 400 μg given as a short i.v. infusion. Considering an expected decrease in the clearance of regadenoson in the new study population, a lower starting dose with a possible escalation to the clinical dose based on clinical safety was contemplated. However, this design implied an exceedingly long and costly study.

During the early clinical development, a randomized, double-blind, crossover, placebo-controlled study was conducted in 36 healthy volunteers to evaluate single intravenous bolus doses of regadenoson that ranged from 0.1 to 30.0 μg/kg [53]. Up to 20 plasma samples were collected from each individual for regadenoson concentration determination within the 24 hours after each dosage. All urine was collected during the 24-hour time period post-dose and an aliquot was used for the determination of the regadenoson concentration. This study provided a rich data set to develop a PK/PD model of regadenoson and its effect on heart rate, the latter being considered as a surrogate marker of efficacy (increased blood flow) as well as safety (tachycardia). Could the results from this study in healthy volunteers be used to design a more realistic study in renally impaired subjects?

Following intravenous bolus dose administration, regadenoson is rapidly distributed throughout the body followed by a relatively fast elimination (terminal elimination half-life of approximately two hours). A nonlinear mixed-effect modeling approach was utilized in describing the plasma and urine concentration-time profiles. Furthermore, the relation between regadenoson plasma concentrations and the increase in heart rate was modeled. During the model-building process, possible influence of several covariates, including body

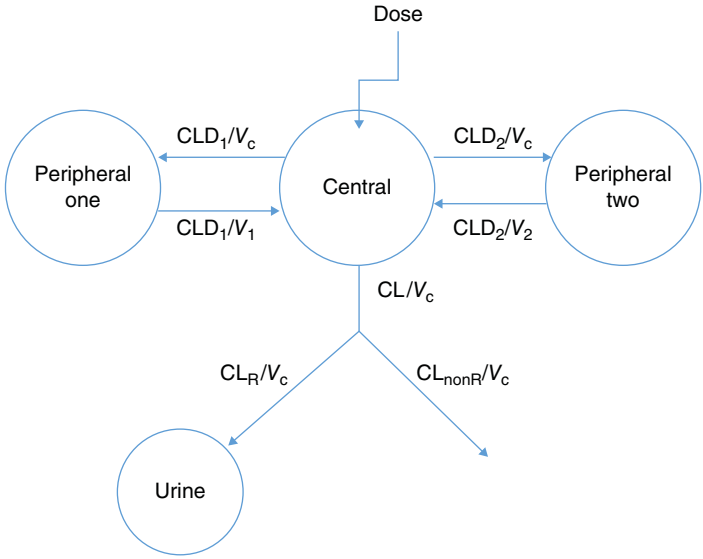

Figure 1.7 Schematic presentation of a three-compartment model describing the pharmacokinetics of regadenoson. A 4th compartment (Urine) accounts for the excreted amounts of regadenoson in urine. CLD (1 or 2): intercompartmental clearances, Vc: volume of the central (plasma) compartment, V1 and V2: volume of the peripheral compartments, CL: clearance, CLR: renal clearance, CLnonR: nonrenal clearance.

weight, body mass index, and age, on pharmacokinetic model parameters was investigated. The pharmacokinetics of regadenoson was successfully described by a three-compartment model with linear clearance (Figure 1.7).

The total clearance of regadenoson was estimated to be 37.8 l/h, with renal excretion accounting for approximately 58% of the total elimination. The renal clearance of the drug was thus estimated to be 21.9 l/h. Regadenoson's volume of distribution of the central compartment and the volume of distribution at steady state were estimated to be 11.5 and 78.7 l, respectively. None of the tested covariates were found to be correlated with any of the pharmacokinetic model parameters.

Individual pharmacokinetic parameter estimates were fixed in the pharmacodynamic model, where changes in heart rate were directly related to plasma drug concentrations using the following equation:

$$\mathrm{HR} = \mathrm{HR}_0 + \frac{\mathrm{HR}_{\max} \times Cp}{\mathrm{EC}_{50} + Cp}$$

where baseline heart rates (HR_0), maximum heart rate increase ($\mathrm{HR}_{\max}$), and plasma regadenoson concentration causing a 50% increase in the maximum heart rate (EC_{50}) were estimated to be 62 beats per minute, 76 beats per minute, and 12.3 ng/ml, respectively.

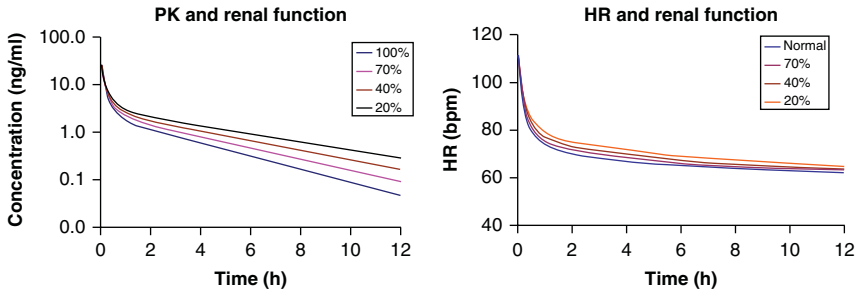

Figure 1.8 Simulated regadenoson plasma concentrations and heart rate in subject with different creatinine clearance values.

The developed model was used to simulate regadenoson plasma concentrations and heart rates over time in subjects with various degrees of decreased renal functions receiving a single dose of 400 μg regadenoson (Figure 1.8). In these simulations, regadenoson renal clearance values were set to lower values to represent subjects with mild, moderate, and severe renal impairment and regadenoson concentrations and heart rates were estimated. The nonrenal clearance was kept unchanged. As seen in Figure 1.8, the model predictions indicated initial regadenoson plasma concentrations remain the same despite decreased renal function. As expected, decreased renal function also leads to a longer elimination half-life and prolonged exposure to regadenoson. However, the greater exposure did not have any clinically significant effect on heart rate. Based on the simulation results, all renally impaired subjects enrolled in the study were administered the 400-μg dose.

The results of the study in renally impaired subjects confirmed the main predictions of the model, including similar maximum concentrations, longer elimination half-lives with decreasing renal function, and similar heart rate changes across the renal function groups [54]. As can be seen in Figure 1.9, the initial regadenoson plasma concentrations were similar in all renal function groups, while the elimination half-lives were prolonged with decreasing renal function. Both of these observations were predicted by the model developed using healthy volunteers data. Furthermore, heart rate changes from baseline confirm the model's predictions of similar heart rate changes across the groups (Figure 1.10).

In conclusion, development of a PK/PD model for regadenoson in healthy volunteers and its utility to simulate untested study design in subjects with renal impairment allowed for better design of a subsequent clinical study aiming to evaluate the impact of decreased renal function on regadenoson's PK and PD properties.

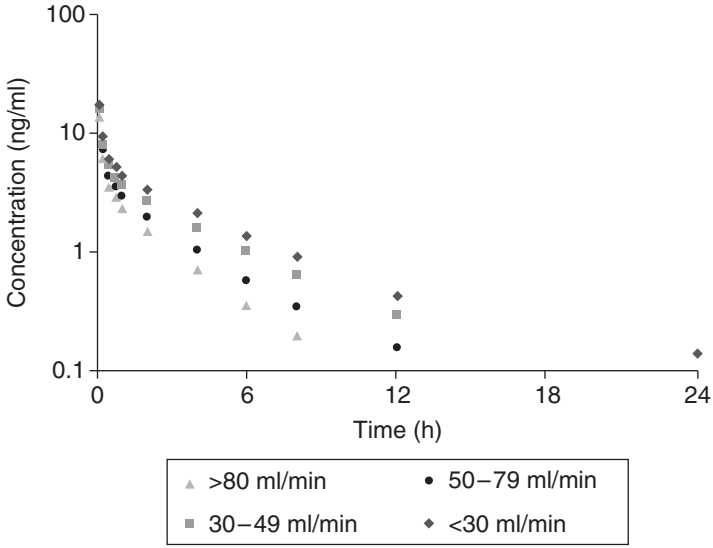

Figure 1.9 Regadenoson plasma concentration in subjects with varying degrees of renal functions, measured as creatinin clearance values. Source: Gordi et al. [54] © 2007, John Wiley and Sons.

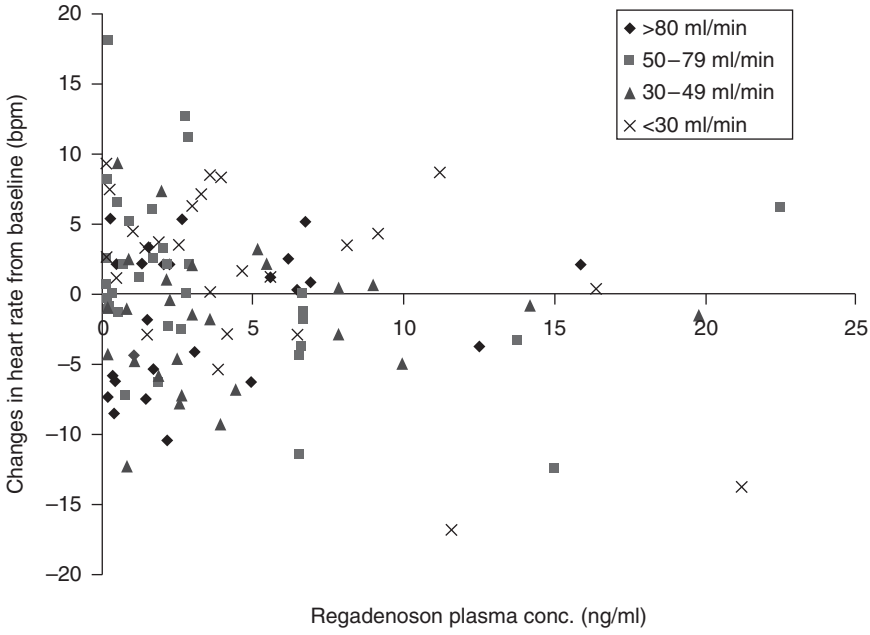

Figure 1.10 Individual heart rate changes from baseline vs. regadenoson plasma concentrations in subjects with varying degrees of renal functions. Source: Gordi et al. [54] © 2007, John Wiley and Sons.

Example 1.3 ***What causes the variability in Ursodiol's pharmacokinetics?***
Ursodiol (Actigall®) is a naturally occurring bile acid approved to treat adult gallstones and primary biliary cirrhosis. It is frequently used off-label to treat neonatal cholestasis, which is a reduction of the normal flow of bile from the liver to the small intestine. Ursodiol pharmacokinetics was studied in neonates using ^{14}C-labeled microdoses of ursodiol alone or in combination with nonlabeled drug [55]. In short, up to five neonates received single ascending doses of ^{14}C-labeled ursodiol (8, 26, 80 ng) 48 hours apart. Another three neonates received a single dose of 80 ng ^{14}C-labeled ursodiol together with a 40-mg/kg non-radiolabeled dose. Blood samples were analyzed using a highly sensitive accelerator mass spectrometry, AMS (Figure 1.11). The use of AMS enables determination of ursodiol concentrations with very small sample volumes needed for the determination of ursodiol concentrations.

A mixed-effect modeling approach was utilized to develop a pharmacokinetic model for ursodiol. A two-compartment model was found to describe the observed plasma concentrations satisfactorily. Ursodiol concentration–time data exhibited a large interindividual variability in the studied neonates, with some subjects showing fast increases followed by rapid decreases of drug concentrations over time, while others had a slower increase and longer half-life upon drug administration. The developed model was able to capture and quantify this variability, as evident by large estimated interindividual variability in parameters for clearance and first-order rate of absorption (Table 1.2).

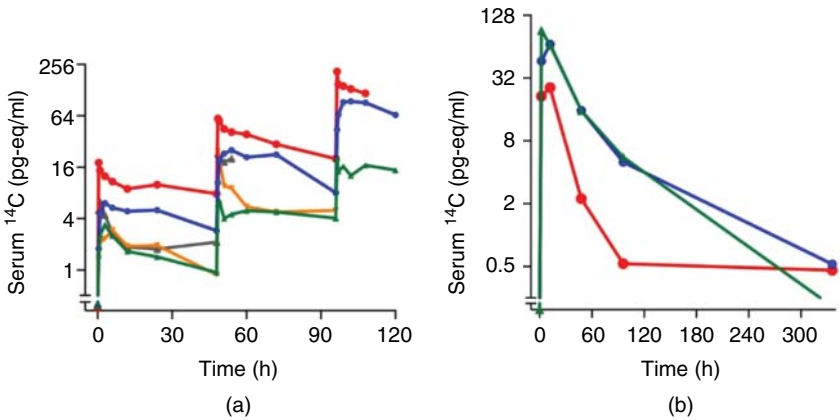

Figure 1.11 Individual ursodiol concentration–time profiles for five infants receiving single ascending doses of ^{14}C-labeled ursodiol (8, 26, 80 ng) 48 hours apart (a) and three infants receiving a single dose of 80 ng ^{14}C-labeled ursodiol together with a 40-mg/kg nonradiolabeled dose (b). Source: Gordi et al. [55] © 2014, John Wiley and Sons.

Table 1.2 Pharmacokinetic model parameter estimates and associated variability terms.

Parameter	Value (RSE)	IIV (RSE)
K_a (h^{-1})	0.04 (0.31)	0.44 (0.35)
CL/F (l/h)	0.034 (0.39)	0.98 (0.62)
CLD/F (l/h)	0.021 (0.55)	—
V2/F (l)	0.012 (1.61)	—
V3/F (l)	1.02 (0.24)	—
Proportional error	0.32 (0.08)	—

Abbreviations: RSE: relative standard error; IIV: interindividual variability; K_a, first-order absorption rate constant; CL, apparent clearance; CLD, apparent intercompartmental clearance; V2, apparent volume of distribution of the central compartment; V3, apparent volume of distribution of the peripheral compartment.
Source: Gordi et al. [55] © 2014, John Wiley and Sons.

A general approach when investigating reasons for interindividual variability is to correlate various subject characteristics with the PK model parameters. By linking subject specific attributes, e.g. age, body weight, body surface area (BSA), gender, or other measured markers to model parameters that are identified as different between subjects, one is often able to attribute differences in drug concentrations between individuals to specific characteristics. These quantitative correlations can explain the cause of the observed variability, and provide a better estimate of the model parameter through the correlation. This practice may have significant implications in patient therapy. As an example, many cancer therapies are dosed based on individual patient's body weight, which directly correlates with the exposure of the drug [56]. Investigating effects of covariates on model parameters can be performed systematically. However, such evaluation normally requires data from a large number of individuals, especially if the effect of the covariate is small. Moreover, finding correlations is an empirical approach: Although the correlation between drug exposure and BSA has been established, this finding does not identify the cause of the observation, just its existence. In the case of ursodiol pharmacokinetics and the observed variability, the small number of neonates in the study ($n = 8$) did not allow for a formal analysis of the effect of subject characteristics on the model parameters.

It was of interest to investigate the physiological basis for the observed variability in the concentration–time profiles of ursodiol in the studied population. Therefore, a quantitative SP model, the Bile Acids PhysioPD™ Platform ("Platform"), was developed and used to identify the cause of the variability. As can be seen in Figure 1.12, the Platform replicates the fate of bile acids in the body: Primary

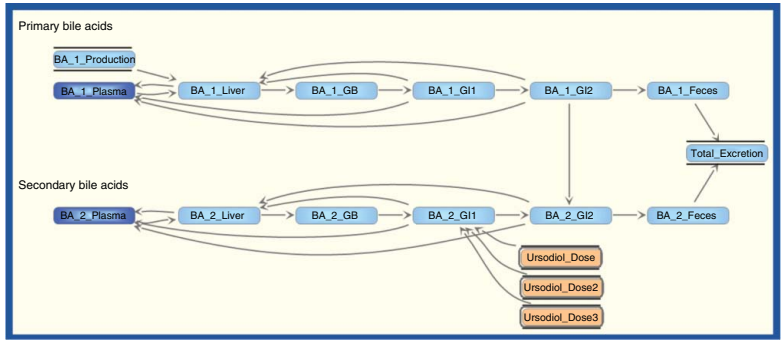

Figure 1.12 The Bile Acid PhysioPD™ Platform.

bile acids (top compartments) are produced (BA_1_Production) and released to the liver (BA_1_Liver), followed by a transfer to either plasma (BA_1_Plasma) or gallbladder (BA_1_GB). While plasma bile acids are recirculated in the liver, the gallbladder releases its content into the gastrointestinal tract (BA_1_GI1). Once in the GI tract, bile acids can be absorbed back to plasma or liver, or moved forward to the lower intestine. In adults, bile acids can then be transformed to secondary bile acids by the bacterial flora (transfer from BA_1_GI2 to BA_2_GI2), while this process is absent in neonates. Similar to the previous stage, the bile acids in the lower GI tract can be either reabsorbed by the liver or into plasma, or move downstream as feces (BA_1_Feces) and excreted (Total_Excretion). Similarly, secondary bile acids undergo the same processes once formed (BA_2_GI2). Ursodiol is a secondary bile acid and in the clinical study was given via a feeding tube, i.e. as an input to the gut (BA_2_GI1).

Data from literature were used to calibrate and qualify the Platform [49]. No detailed data in neonates were available, so the calibration strategy was to use adult data to calibrate the Platform and then emulate the neonate state using appropriate scaling and turning off (setting to zero) the transformation from primary to secondary bile acids. Adult data were available for primary and secondary bile acid concentrations in plasma, primary bile acid synthesis rate, bile acid secretion/recycling rates, the total pool size of bile acids in all compartments, and primary and secondary bile acid excretion rates [57–67]. The Platform was found to be consistent with the available data.

One confirmation that the calibrated dynamics were an appropriate model was obtained from simulating administration of ursodiol in the neonate version of the Platform. The Platform was able to reproduce the observed variable dynamics of ursodiol in plasma. Thus, the Platform reflects the known biology of bile acids and the PK of ursodiol in this study.

The effects of varying parts of the Platform on ursodiol concentration profiles were tested by systematic sensitivity analysis – varying each parameter of the Platform and simulating ursodiol concentrations over time. Figure 1.13 shows three such evaluations: increasing the rate of transfer of ursodiol from gallbladder to gut results in shorter and less pronounced distribution phases (Figure 1.13a) while increasing the rate of transfer from lower GI tract to feces results in prolonged elimination half-lives without any significant change in the distribution phase of ursodiol (Figure 1.13b). When varying the rate of transfer from plasma to liver, the expected ursodiol concentration–time profiles show a resemblance to those observed in the clinical study in neonates (Figure 1.13c) with smaller rates producing monoexponential declines changing to a distinct biexponential pattern with increasing rates. A closer look at the physiology of bile acid transfer from plasma to the liver reveals the involvement of at least two known transporters, Na^+-taurocholate cotransporting polypeptide, NTCP, and organic anion transporting polypeptide, OATP (Figure 1.14) [68, 69]. This explanation is given further

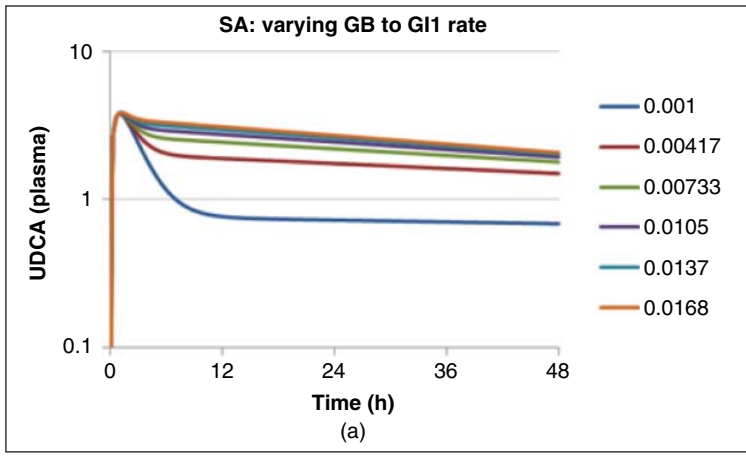

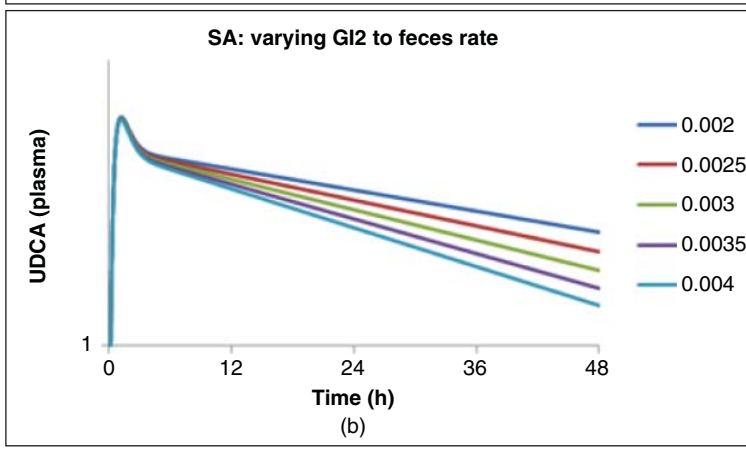

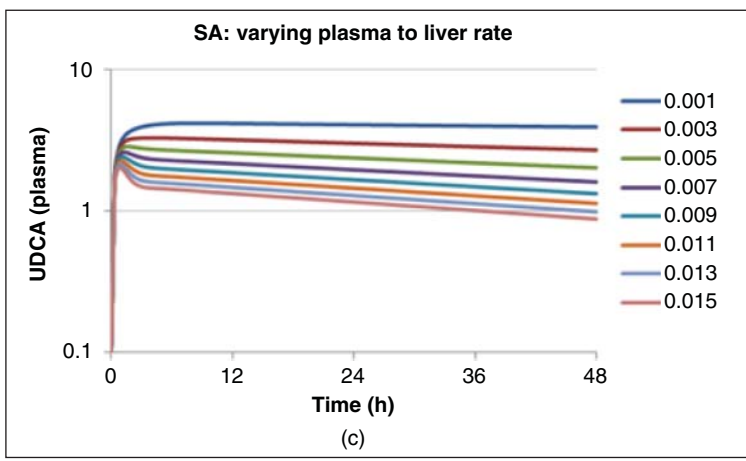

Figure 1.13 (a) Gall bladder secretion rate affects initial distribution and terminal clearance out of plasma, (b) Lower intestine to feces rate affects terminal clearance rate only, (c) Plasma to liver rate affects Cmax, tmax, initial distribution, and terminal clearance.

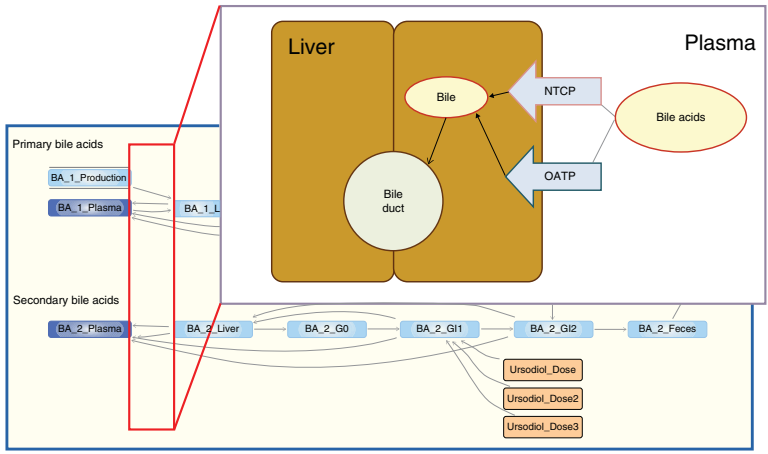

Figure 1.14 Schematic presentation of bile acid transporters and their locations in the liver and the Bile Acid PhysioPD™ Research Platform. Sources: Shitara et al. [68] and Kosters and Karpen [69].

credence by the known pharmacokinetic interaction in adults of ursodiol with certain statins that are affected by the OATP transporters. Simulation results thus indicate a possible role of polymorphisms of these two transporters causing the observed large variability in ursodiol concentration–time profiles in the studied neonates.

1.8.1 Drug Delivery and PK/PD

At the beginning of a drug-development project for a new chemical entity (NCE), little, if anything, is known about the physical properties, absorption, distribution, metabolism, and elimination (ADME) of the drug, its interaction with other excipients, or quantitatively or qualitatively how the drug works therapeutically or adversely. Drug development, at its best, defines through experimental data and models the relationships between the drug for a selected dosage form to provide a drug release profile, the in vivo absorption of the drug, to produce a pharmacokinetic profile if plasma levels are available, and the therapeutic responses in terms of PK/PD models. Generally, this approach is helpful for designing lifecycle extensions of drugs. Typically, however, lifecycle extension is an exercise in sustaining the pharmacokinetic profile for a longer time between administering doses and improving patient compliance. In rational development of an NCE, the pharmacokinetics and PK/PD relationships can be developed often beginning in preclinical studies, in Phase 1 and during Phase 2a Proof-of-Concept studies. A set of target pharmacokinetic profiles can be hypothesized and simulated to achieve potential therapeutic effects. These models and targets are the emphasis of the preceding sections of this chapter.

We now turn to examples of the models and tools to design dosage forms to achieve these target plasma and pharmacodynamic profiles. Some of the variables to design a dosage form are the route of administration (e.g. oral, ocular, parenteral, or transdermal), site of delivery (e.g. stomach, duodenum, or colon), and factors about the dosage form. Examples of important factors for the dosage form are drug loading, physical properties of the drug (i.e. solubility, molecular size, and pK_a), excipients, the geometry of the dosage form, and the mechanism of drug release (e.g. diffusion, an osmotic pump, polymeric dissolution, or degradation). Administration with or without food, the periods of drug administration, and the time between drug administrations are also important. As an example, drugs that are soporific may be best dosed at night or with the evening food. Another example is to model for a water-insoluble drug the effect of drug particle size on dissolution rate and, in turn, its impact on the absorption rate constant with different lipid and protein contents in food versus fasting [70]. If it is acceptable therapeutically to specify administering the drug with food, a dissolution number and solubility in simulated fed intestinal media may be sufficient to estimate the reduced

particle size distribution necessary to achieve efficacious plasma levels, but with a food effect required to achieve this level of bioavailability. If no significant food effect, that is, both fasted and fed administration are recommended, solubility in simulated fasted intestinal media and dissolution number are needed to estimate the particle size distribution to avoid bioavailability being limited by the dissolution rate.

In more complex scenarios, the rate of delivery can be variable and involve control by a device. Prediction of many of these factors from physical properties alone is not that accurate, and iterative experimental data are generally necessary for the development of quantitative models, particularly of in vivo performance of many dosage forms. In the remainder of this chapter, we will discuss a few examples of dosage forms for different routes of administration and their design or use to achieve specific therapeutic or pharmacokinetic targets.

1.8.2 Drug Properties and Mechanism of Release from the Dosage Form

The simplest case for an oral dosage form is an immediate-release capsule of a drug that is both highly water soluble at physiological pH and highly permeable through intestinal mucosa. High water solubility allows for rapid dissolution of the drug, in particular, at least 85% in 15 minutes. The high solubility for all values of physiological pH implies that after leaving the stomach and entering the small intestine, the drug will not precipitate. The high intestinal permeability means the drug in solution will be well absorbed into the bloodstream.

In early drug discovery, permeability may be estimated from the calculated partition coefficient and molecular weight and perhaps polar surface area. In later drug discovery where enough drug substance is available to measure melting point or oil solubility, melting point or solubility in oil and molecular weight may be better predictors of permeability. Even better with sufficient drug substance available, either animal bioavailability or Caco-2 permeability provide direct measurements. A succession of improved estimates as inputs to improve the models is typical of drug development.

Acetaminophen is a good example of a quite old, common drug that is highly water soluble and permeable to the small intestine [71]. The dissolution profile and pharmacokinetic plasma profile for a regular strength 325-mg capsule or tablet is well established. Achieving the specified rapid dissolution and the other good manufacturing practices (GMPs) requirements are sufficient for development. The oral pharmacokinetics for both adults and children can be readily described and predicted with a single PBPK model that accounts for maturation [72].

For the sake of patient convenience, an extended-release acetaminophen tablet 650 mg has been developed to be taken every eight hours. In reality,

these extended-release tablets also often contain an immediate-release portion for rapid pain relief. As in the immediate-release case, the desired therapeutic pharmacokinetic profile is established, and the target in vitro dissolution profile over eight hours and its correlation with the pharmacokinetic profile are already or can easily be established. For simplicity and instructional purposes, this tablet is designed as a hydrophilic polymeric matrix containing acetaminophen and high-molecular-weight hydroxypropyl methylcellulose (HPMC) [73]. After oral administration, water is imbibed by the hydrophilic tablet, and it swells. These high-molecular-weight polymers with many entanglements form a swollen gel through which the highly water-soluble drug, acetaminophen can diffuse into the surrounding fluid. Over much longer time periods, the hydrophilic polymers in the gel dissolve and the tablet erodes. For most of the period of drug release, the cumulative amount of drug released by diffusion of acetaminophen from this swollen hydrophilic matrix is linear with the square root of time. The driving force for this diffusion is the thermodynamic activity gradient or, for an ideal solution, the concentration gradient of acetaminophen across the gel layer. Diffusional release of drug is one of the main mechanisms of drug release from dosage forms. Drug release by diffusion from nonswelling matrices, for example steroids from an ethylene vinyl acetate matrix, generally exhibits linearity with the square root of time [74]. This square root of time input of drug into the gut compartment can be used to simulate the plasma levels of acetaminophen using a pharmacokinetic model based on plasma levels of acetaminophen from the immediate-release dosage form. Alternatively, knowing the plasma levels from both immediate- and extended-release dosage forms, the in vivo input function for the extended-release dosage form can be deconvoluted. This in vivo input function may then be correlated with in vitro dissolution [75]. The effect of polymeric molecular weight and polymeric content on the dissolution profile can be modeled both theoretically and experimentally. Variation in this release profile may be used to vary the extended-release plasma concentration profile based on various absorption or pharmacodynamic hypotheses. For example, a shorter extended-release profile of acetaminophen may be desirable to provide an "off-period" of delivery of acetaminophen to reduce hepatic stress [76]. This same shorter-release profile may result in better absorption by the dosage form releasing a greater percentage of its drug in the upper gastrointestinal (GI) tract [77].

An alternative extended-release dosage form for acetaminophen might be to coat an immediate-release core tablet comprising acetaminophen and fillers, such as microcrystalline cellulose and lactose. This coating would be designed as a rate-controlling membrane and could contain high-molecular-weight HPMC or a methacrylic acid copolymer or other less hydrophilic polymers. For this dosage form after administration, the dissolved acetaminophen in the core would diffuse across the membrane, because there is a concentration gradient of drug across

the membrane. After an initial period, there would be a constant rate of release or zero order from this membrane-controlled dosage form, and the cumulative amount of drug released is linear with time. At later times, the source of drug becomes depleted, the concentration gradient decreases, and the rate of drug release declines with time. For many drugs, this linear concentration profile may have advantages where plasma concentrations are related to known undesired pharmacological effects or to excessive local concentrations of drug in the GI tract that may cause gastrointestinal adverse events [78], such as nausea or diarrhea.

In contrast to acetaminophen, most drugs developed today are insoluble in water. Ibrutinib, a recently approved Bruton's tyrosine kinase (BTK) inhibitor approved for treatment of chronic lymphocytic leukemia, is almost insoluble in water [79]. In addition to filler, superdisintegrant, and lubricant, the approved immediate-release capsule contains micronized drug and sodium lauryl sulfate (SLS), a surfactant. The smaller particle size of drug increases the amount and rate of dissolution into gastric fluid, and the SLS assists the wetting of the hydrophobic drug, thereby increasing the amount dissolved in the micellar solution surrounding the drug particle. For any insoluble drug, the dosage form needs to be designed to increase the amount and rate of dissolution of the drug and to avoid rapid precipitation when the drug empties into the duodenum at a higher pH than the stomach. Micronization is one of the simplest approaches, and many other approaches are discussed in Chapter 4 on oral delivery. The deconvolution of the resulting plasma levels for these rapid dissolution approaches can lead to interesting insights on rates of absorption and sites of absorption within the gastrointestinal tract. As an example, correlation of the AUC or C_{max} with the occupancy for the BTK inhibitors may lead to early predictions of appropriate doses [80].

Extended release of insoluble drugs may require a different mechanism of drug release than for soluble drugs. Carbamazepine is an example of an anticonvulsant used for treatment of epilepsy and pain from trigeminal neuralgia. As a sparingly soluble drug in an immediate-release dosage form without micronization, slow dissolution can result in loss of and variability in bioavailability, and there is often a food effect. With the short half-life, the immediate-release carbamazepine product must be dosed two to three times daily; primarily to improve compliance, and therefore, extended-release dosage forms have been developed. The rate of rise of plasma level, rather than plasma levels, has also shown some correlation with dizziness and other psychomotor impairment [81]. At least two mechanisms of drug release, polymeric erosion and osmotic pumps, have been used in extended-release carbamazepine dosage forms. Carbamazepine has been incorporated in a hydrophilic matrix of somewhat lower-molecular-weight HPMC, and the polymer swells and erodes to release the drug. For less soluble drugs, the contribution of drug release from diffusion is much less, and most of the drug is released by erosion and dissolution of the polymer. Drug release from an

erodible, hydrophilic matrix is often linear with time. The in vitro erosion rate or dissolution rate can be modeled with polymeric content and polymeric molecular weight and can be linearly related to in vivo erosion of the dosage form or in vivo absorption of the drug [82]. For carbamazepine, the HPMC also stabilizes an amorphous form of the drug and aids its dissolution [83]. A second mechanism of release is an osmotic pump, where a membrane, that is semipermeable to water and has at least one hole, surrounds a core containing the carbamazepine and an osmotic agent, typically polyethylene oxide, swell and the osmotic pressure pushes the drug from the hole. The release profile for more soluble compounds is typically linear with time but may be designed to vary. The design of the extended-release product was based on defining a constant input rate that with the extended release the peaks and troughs of steady-state three in a day (TID) administration of the immediate-release carbamazepine bracketed the simulated broader peaks and troughs for the extended-release products. The release profile from the dosage form can be modeled with or without a loading dose portion of an immediate-release coating of drug followed by a constant release for the extended-release portion. The osmogen concentration and the thickness of the membrane are key variables in modeling the release rate and the design of the dosage form [84]. Prototype dosage forms delivering the desired input rate have been compared to the immediate-release product in pilot pharmacokinetic studies. These simple osmotic pumps for less soluble compounds lack the needed osmotic pressure, and push–pull osmotic pumps are more suitable with less variability and more constant release for less soluble drugs, like carbamazepine [85].

1.8.2.1 Temporal Pattern of Delivery

The timing and pattern of timing of drug delivery, for example, as an infusion or a pulse or night as opposed to morning, can have substantive effects on the safety and efficacy of a drug [79, 86]. An example of the importance of the temporal pattern of drug delivery is parenteral delivery of parathyroid hormone (PTH) or its active peptide fragment PTH1-34. Administration of PTH or its fragment as a subcutaneous injection stimulates bone growth. Consequently, it is a treatment for osteoporosis. In contrast, a continuous infusion of PTH can result in severe bone loss [87]. Moreover, infusion of PTH1-34 increases blood pressure in man. A dosage form that achieves the desired intermittent target profile can treat osteoporosis, and an infusion worsens the disease. Transdermal microneedles depending on the materials in the microneedles or containing the drug can resemble a bolus profile or an infusion, and models combined with in vitro skin permeation to define a pulsed profile are critical to designing a product that improves bone growth [88].

Coincident timing of peak drug delivery with the therapeutic need has become established for physiological variation based on circadian rhythms. The greater

incidence of myocardial infarcts in the early morning hours is an example of this circadian rhythm [89]. Increases in blood pressure are most common in the early morning hours [85]. An extended-release dosage form of diltiazem, the calcium-channel blocker, was designed to have its peak delivery approximately 12 hours after dosing with dinner to coincide with early morning hours [89]. Immediate-release drug bead cores containing diltiazem hydrochloride were coated with a membrane comprising a neutral acrylic copolymer, Eudragit NE-30D, HPMC, and polysorbate 80, as a wetting agent and to plasticize and form pores. This membrane became porous in the presence of water and swelled as the core hydrated. The resulting delivery profile of diltiazem had a time lag of approximately four hours followed by diffusion of the drug through the membrane at a constant rate that declined slowly with depletion of the drug from the core [90]. Assuming administration with the evening meal, the time lag followed by the linear cumulative-release profile followed by depletion of diltiazem can be the input function using the pharmacokinetics of immediate-release diltiazem to predict the desired time of onset of the plasma concentrations of drug in this delayed extended-release dosage form [90]. Other hypertensive medications with delayed release have also been developed [91].

Tolerance to a constant infusion of a drug may occur and necessitate clearly defined temporal variation of drug delivery. In some patients, steady-state continuous transdermal delivery of nitroglycerin with a daily patch worn for 24 hours after application leads to tolerance to the therapeutic effects of nitroglycerin [92]. An 8–12-hour rest period without nitroglycerin restores the efficacy of transdermal nitroglycerin [93], and typically the transdermal nitroglycerin patch is removed at night. Patches with delayed onset were developed based on simulated profiles using different time lags and the same steady-state skin permeation of nitroglycerin to give an early morning onset for a transdermal nitroglycerin patch to be applied before bedtime [93]. However, there were potential concerns about patients falling during potential hypotensive episodes in early morning hours and the patients could just remove the patch before bedtime. Consequently, this product was not developed.

Methylphenidate is one of the most widely administered treatments for attention deficit hyperactivity disorder (ADHD), and there has been some interest in the delivery profile and the potential for tolerance. In double-blind trials, flat delivery profiles were compared with a standard twice daily profile and an ascending once daily profile [94]. The constant delivery was less effective in the afternoon than the other two profiles. In a second study, the delivery profile consisted of two boluses either close temporally or separated in time, and there was a reduction in the response to the second bolus for the more closely spaced profile [94]. Both studies were modeled using a tolerance term in a concentration–effect model. The tolerance was generated in this model by the effect generating a hypothesized

antagonist that inhibited the effect [95]. This model is in contrast to models of tolerance that have a given plasma concentration produce an antagonist. While this model successfully explains the efficacy and reduction of the effect with certain timing, the FDA did not accept the model when the dosage form was approved for this indication. Simulation of the desired concentration–response profile leads to a specific drug-delivery profile with an immediate release and separated peaks. To achieve this, an extended-release osmotic pump was designed with an immediate-release drug overcoat over the semipermeable membrane covering two active drug layers and a swelling excipient layer. The contents of the layers and thickness of the membrane are important for controlling the release. A concentration gradient is incorporated into the trilaminate core to produce increasing delivery over the first six to seven hours. Water is imbibed through this membrane and the swelling polyethylene oxide layer pushes the drug through a hole in the semipermeable membrane to give efficacy over 12 hours [95]. With a characterization of the concentration–effect relationship and counterclockwise hysteresis in the effect over time for the plasma concentrations, the drug-delivery profile was optimized and allows for the effect over the waking period.

Temporally controlled drug delivery may require more complex release profiles that are difficult to achieve with standard dosage forms. The advent of 3D printing of dosage forms as well as increasingly miniaturized devices opens opportunities to manufacture dosage forms with more complex and alterable release rates to meet therapeutic needs.

1.9 Discussion

Mathematical models have been utilized in a wide variety of industries for a long period of time. Although the pharmaceutical industry has been late in adopting such models in research and development in large scale, their utility is gaining significant attraction at various organizations, from discovery to preclinical and clinical development. Furthermore, use of such models is encouraged by regulatory agencies such as the U.S. FDA and various other regulatory authorities.

The use of models for formulation and processing of dosage forms can provide target drug dissolution profiles to achieve plasma-level profiles associated with desired pharmacological effects or for avoiding unwanted side effects or with specific timing of efficacy. Simulation of dissolution and pharmacokinetics of dosage forms with a variety of in vitro and in vivo parameters can define the design space needed to optimize dosage forms earlier in development instead of as a lifecycle extension. In dosage form development, this understanding can be related to drug properties, such as particle size, as previously mentioned to mitigate food effects, or for example, to polymer solubility parameters, molecular weights, and polymer

content to predict extended-release delivery profiles and to set specifications on the dosage form. Design of experiments to identify critical variables is typically used both in formulation and in process development and has become embedded in the regulatory and manufacturing frameworks through Quality by Design for predictable batch or continuous manufacturing.

Mathematical models offer several benefits in the lengthy and costly drug development process. A major advantage of having a model is its ability to predict the outcome of untested scenarios through simulations. While a clinical study to investigate certain effects of a drug may cost millions of dollars and take months to years to conduct, computer simulations can normally be made within minutes or hours at a fraction of the cost. Models can also be used to investigate the probability of various study designs to meet the primary endpoint, thereby allowing the researchers to choose the best study design. Thus, while initial development of a model may take time at relatively minor costs, their ability to guide future studies makes them extremely cheap while powerful tools with high impact on the development path of drug candidates.

Another important characteristic of models is their lack of subjectivity and lack of bias to favor a certain hypothesis of the mechanism of action or the ability of a drug or dosage form to perform as thought by individual researchers. A validated model takes into account critical influencing variables and their interactions and counteractions within a system. Such an objective approach is generally difficult to undertake considering the complexity of biological systems.

While models can be developed and used at various stages in drug development, it is imperative to start the modeling process with the end use in mind. In other words, one should start the modeling by asking the simple question of "What question is this model going to answer?" The answer to this question guides the development of the model and sets the degree of complexity the model must have to be relevant. While a more complex model may be highly appealing, a simpler one is often sufficient for the specific question in hand. This is especially the case when developing large systems biology models.

A collaborative approach in developing models may be vital to its use. Developing new medicines requires collaborations across many different disciplines within an organization, with accumulation of knowledge from one group being transferred to another. Since models can be used in various stages of the development of a new drug, it is essential that they are built and refined with input from relevant groups based on expertise or new experimental results to ensure their validity as well as usage. While the actual process of building models, especially the more complex ones, requires skilled and highly specialized personnel, mathematical models should encompass input from the end users, as the models are built to ask specific questions at various stages of the development. Mathematical models developed solely by modelers in silico will have little chance

of appealing to the nonmodeler research teams and will generally not be viewed as an essential tool to answer their questions. Modeling done by those unfamiliar with the assumptions in either developing the models or in the scientific disciplines can be fatal to the models success. The interaction of experts in multiple disciplines and testing and refinement with well-designed experiment are critical components.

In conclusion, mathematical models combined with the tools of well-characterized and modeled drug delivery have enormous potential in improving the drug-development processes, providing a rationally designed dosage form to meet a targeted plasma concentration or therapeutic profile, providing insight and more efficient experimental designs with higher probabilities of success, thereby saving time and funds. Their use can be a critical part of the drug-development process.

References

1 Sager, J.E., Yu, J., Ragueneau-Majlessi, I., and Isoherranen, N. (2015). Physiologically based pharmacokinetic (PBBK) modeling: a systemic review of published models, applications, and model verification. *Drug Metab. Dispos.* 43: 1823–1837.

2 Umscheid, C.A., Margolis, D.J., and Grossman, C.E. (2011). Key concepts of clinical trials: a narrative review. *Postgrad. Med.* 123: 194–204.

3 Teorell, T. (1937). Kinetics of distribution of substances administered to the body, I: The extravascular modes of administration. *Arch. Int. Pharmacodyn. Ther.* 57: 205–225.

4 Teorell, T. (1937). Kinetics of distribution of substances administered to the body, II: The intravascular modes of administration. *Arch. Int. Pharmacodyn. Ther.* 57: 226–240.

5 Rowland, M., Benet, L.Z., and Graham, G.G. (1973). Clearance concepts in pharmacokinetics. *J. Pharmacokinet. Biopharm.* 1: 123–135.

6 Wagner, J.G. and Nelson, E. (1964). Kinetic analysis of blood levels and urinary excretion in the absorptive phase after single doses of drug. *J. Pharm. Sci.* 53: 1392–1403.

7 Levy, G. (1966). Kinetics of pharmacologic effects. *Clin. Pharmacol. Ther.* 7: 362–372.

8 Sheiner, L.B., Rosenberg, B., and Melmon, K.L. (1972). Modelling of individual pharmacokinetics for computer-aided drug dosage. *Comput. Biomed. Res.* 5: 411–459.

9 Sheiner, L.B. (1997). Learning versus confirming in clinical drug development. *Clin. Pharmacol. Ther.* 61: 275–291.

10 Lalonde, R.L., Kowalski, K.G., Hutmacher, M.M. et al. (2007). Model-based drug development. *Clin. Pharmacol. Ther.* 82: 21–32.
11 Barbour, A.M., Sarov-Blat, L., Cai, G. et al. (2013). Safety, tolerability, pharmacokinetics and pharmacodynamics of losmapimod following a single intravenous or oral dose in healthy volunteers. *Br. J. Clin. Pharmacol.* 76: 99–106.
12 Gordi, T., Xie, R., Huong, N.V. et al. (2005). A semiphysiological pharmacokinetic model for artemisinin in healthy subjects incorporating autoinduction of metabolism and saturable first-pass hepatic extraction. *Br. J. Clin. Pharmacol.* 59: 189–198.
13 Kervezee, L., Hartman, R., van den Berg, D.J. et al. (2014). Diurnal variation in P-glycoprotein-mediated transport and cerebrospinal fluid turnover in the brain. *AAPS J.* 16: 1029–1037.
14 Sethi, V.S., Jacksonm, D.V., White, D.R. et al. (1981). Pharmacokinetics of vincristine sulfate in adult cancer patients. *Cancer Res.* 41: 3551–3555.
15 Buerger, C., Plock, N., Dehghanyar, P. et al. (2006). Pharmacokinetics of unbound linezolid in plasma and tissue interstitium of critically ill patients after multiple dosing using microdialysis. *Antimicrob. Agents Chemother.* 50: 2455–2463.
16 Sheiner, L.B., Rosenberg, B., and Marathe, V.V. (1977). Estimation of population characteristics of pharmacokinetic parameters from routine clinical data. *J. Pharmacokinet. Biopharm.* 5: 445–479.
17 Beal, S.L. and Sheiner, L.B. (1982). Estimating population kinetics. *Crit. Rev. Biomed. Eng.* 8: 195–222.
18 Sheiner, L.B. and Ludden, T.M. (1992). Population pharmacokinetics/dynamics. *Annu. Rev. Pharmacol. Toxicol.* 32: 185–209.
19 Martin, E., Tozer, T.N., Sheiner, L.B., and Riegelman, S. (1977). The clinical pharmacokinetics of phenytoin. *J. Pharmacokinet. Biopharm.* 5: 579–596.
20 Aarons, L. (2005). Physiologically based pharmacokinetic modelling: a sound mechanistic basis is needed. *Br. J. Clin. Pharmacol.* 60: 581–583.
21 Diestelhorst, C., Boos, J., McCune, J.S. et al. (2014). Predictive performance of a physiologically based pharmacokinetic model of busulfan in children. *Pediatr. Hematol. Oncol.* 31: 731–742.
22 Strougo, A., Eissing, T., Yassen, A. et al. (2012). First dose in children: physiological insights into pharmacokinetic scaling approaches and their implications in paediatric drug development. *J. Pharmacokinet. Pharmacodyn.* 39: 195–203.
23 Yang, X., Morris, S.M., Gearhart, J.M. et al. (2014). Development of a physiologically based model to describe the pharmacokinetics of methylphenidate in juvenile and adult humans and nonhuman primates. *PLoS One* 9: e106101.
24 Allan, G., Davis, J., Dickins, M. et al. (2008). Pre-clinical pharmacokinetics of UK-453,061, a novel non-nucleoside reverse transcriptase inhibitor (NNRTI),

and use of in silico physiologically based prediction tools to predict the oral pharmacokinetics of UK-453,061 in man. *Xenobiotica* 38: 620–640.

25 Liu, F., Zhuang, X., Yang, C. et al. (2014). Characterization of preclinical in vitro and in vivo ADME properties and prediction of human PK using a physiologically based pharmacokinetic model for YQA-14, a new dopamine D3 receptor antagonist candidate for treatment of drug addiction. *Biopharm. Drug Dispos.* 35: 296–307.

26 Jones, H.M., Parrott, N., Jorga, K., and Lavé, T. (2006). A novel strategy for physiologically based predictions of human pharmacokinetics. *Clin. Pharmacokinet.* 45: 511–542.

27 Espié, P., Tytgat, D., Sargentini-Maier, M.L. et al. (2009). Physiologically based pharmacokinetics (PBPK). *Drug Metab. Rev.* 41: 391–407.

28 Zhu, L., Zhang, Y., Yang, J. et al. (2015). Prediction of the pharmacokinetics and tissue distribution of levofloxacin in humans based on an extrapolated PBPK model. *Eur. J. Drug Metab. Pharmacokinet.* 19: 99–104.

29 Young, J.F., Wosilait, W.D., and Luecke, R.H. (2001). Analysis of methylmercury disposition in humans utilizing a PBPK model and animal pharmacokinetic data. *J. Toxicol. Environ. Health A* 63: 19–52.

30 Wagner, C., Pan, Y., Hsu, V. et al. (2015). Predicting the effect of cytochrome P450 inhibitors on substrate drugs: analysis of physiologically based pharmacokinetic modeling submissions to the US Food and Drug Administration. *Clin. Pharmacokinet.* 54: 117–127.

31 US FDA. (2020). Guidance for Industry: Drug Interaction Studies, Study Design, Data Analysis, Implications for Dosing, and Labeling Recommendations. http://www.fda.gov/downloads/drugs/guidancecomplianceregulatoryinformation/guidances/ucm292362.pdf (accessed 19 December 2020).

32 Wagner, C., Zhao, P., Pan, Y. et al. (2015). Application of physiologically based pharmacokinetic (PBPK) modeling to support dose selection: report of an FDA public workshop on PBPK. *CPT Pharmacometrics Syst. Pharmacol.* 4: 226–230.

33 Meibohm, B. and Derendorf, H. (1997). Basic concepts of pharmacokinetic/pharmacodynamic (PK/PD) modelling. *Int. J. Clin. Pharmacol. Ther.* 35: 401–413.

34 Zhang, Z., Qin, L., Peng, L. et al. (2016). Pharmacokinetic-pharmacodynamic modeling to study the antipyretic effect of qingkailing injection on pyrexia model rats. *Molecules* 21 (3): 317. https://doi.org/10.3390/molecules21030317.

35 Babenco, H.D., Conard, P.F., and Gross, J.B. (2000). The pharmacodynamic effect of a remifentanil bolus on ventilatory control. *Anesthesiology* 92: 393–398.

36 Mager, D.E. and Jusko, W.J. (2001). Pharmacodynamic modeling of time-dependent transduction systems. *Clin. Pharmacol. Ther.* 70: 210–216.

37 Sheiner, L.B., Stanski, D.R., Vozeh, S. et al. (1979). Simultaneous modeling of pharmacokinetics and pharmacodynamics: application to d-tubocurarine. *Clin. Pharmacol. Ther.* 25: 358–371.

38 Francheteau, P., Steimer, J.L., Merdjan, H. et al. (1993). A mathematical model for dynamics of cardiovascular drug action: application to intravenous dihydropyridines in healthy volunteers. *J. Pharmacokinet. Biopharm.* 21: 489–514.

39 Cleton, A., Altorf, B.A., Voskuyl, R.A., and Danhof, M. (2000). Pharmacokinetic-pharmacodynamic modelling of tiagabine CNS effects upon chronic treatment in rats: lack of change in concentration-EEG effect relationship. *Eur. J. Pharm. Sci.* 12: 141–150.

40 Huang, X.H., Qiu, F.R., Xie, H.T., and Li, J. (2005). Pharmacokinetic and pharmacodynamic of irbesartan in renal hypertensive dogs under non-steady-state and steady-state conditions. *Eur. J. Drug Metab. Pharmacokinet.* 30: 121–126.

41 Mager, D.E., Wyska, E., and Jusko, W.J. (2003). Diversity of mechanism-based pharmacodynamic models. *Drug Metab. Dispos.* 31: 510–518.

42 Wright, D.F., Winter, H.R., and Duffull, S.B. (2011). Understanding the time course of pharmacological effect: a PKPD approach. *Br. J. Clin. Pharmacol.* 71: 815–823.

43 Visser, S.A., Smulders, C.J., Reijers, B.P. et al. (2002). Mechanism-based pharmacokinetic-pharmacodynamic modeling of concentration-dependent hysteresis and biphasic electroencephalogram effects of alphaxalone in rats. *J. Pharmacol. Exp. Ther.* 302: 1158–1167.

44 de la Peña, A., Ma, X., Reddy, S. et al. (2014). Application of PK/PD modeling and simulation to dosing regimen optimization of high-dose human regular U-500 insulin. *J. Diabetes Sci. Technol.* 8: 821–829.

45 Simon, N., Viallet, F., Boulamery, A. et al. (2016). A combined pharmacokinetic/pharmacodynamic model of levodopa motor response and dyskinesia in Parkinson's disease patients. *Eur. J. Clin. Pharmacol.* 72: 423–430.

46 Dayneka, N.L., Garg, V., and Jusko, W.J. (1993). Comparison of four basic models of indirect pharmacodynamic responses. *J. Pharmacokinet. Biopharm.* 21: 457–478.

47 Wakelkamp, M., Alván, G., and Paintaud, G. (1998). The time of maximum effect for model selection in pharmacokinetic-pharmacodynamic analysis applied to frusemide. *Br. J. Clin. Pharmacol.* 45: 63–70.

48 Louizos, C., Yáñez, J.A., Forrest, L., and Davies, N.M. (2014). Understanding the hysteresis loop conundrum in pharmacokinetic/pharmacodynamic relationships. *J. Pharm. Pharm. Sci.* 17: 34–91.

49 Friedrich, C.M. (2016). A model qualification method for mechanistic physiological QSP models to support model-informed drug development. *CPT Pharmacometrics Syst. Pharmacol.* 5: 43–53.

50 Chen, C. (2014). Development of antimalarial drugs and their application in China: a historical review. *Infect. Dis. Poverty* 3: 9.

51 Gordi, T. and Lepist, E.I. (2004). Artemisinin derivatives: toxic for laboratory animals, safe for humans? *Toxicol. Lett.* 147: 99–107.

52 Li, Q.G., Mog, S.R., Si, Y.Z. et al. (2002). Neurotoxicity and efficacy of arteether related to its exposure times and exposure levels in rodents. *Am. J. Trop. Med. Hyg.* 66: 516–525.

53 Gordi, T., Frohna, P., Sun, H.L. et al. (2006). A population pharmacokinetic/pharmacodynamic analysis of regadenoson, an adenosine A2A-receptor agonist, in healthy male volunteers. *Clin. Pharmacokinet.* 45: 1201–1212.

54 Gordi, T., Blackburn, B., and Lieu, H. (2007). Regadenoson pharmacokinetics and tolerability in subjects with impaired renal function. *J. Clin. Pharmacol.* 47: 825–833.

55 Gordi, T., Baillie, R., Vuong le, T. et al. (2014). Pharmacokinetic analysis of ^{14}C-ursodiol in newborn infants using accelerator mass spectrometry. *J. Clin. Pharmacol.* 54: 1031–1037.

56 Griggs, J.J., Mangu, P.B., Anderson, H. et al. (2012). Appropriate chemotherapy dosing for obese adult patients with cancer: American society of clinical oncology clinical practice guideline. *J. Clin. Oncol.* 30: 1553–1561.

57 Northfield, T.C. and Hofmann, A.F. (1975). Biliary lipid output during three meals and an overnight fast. I. Relationship to bile acid pool size and cholesterol saturation of bile in gallstone and control subjects. *Gut* 16: 1–11.

58 Roda, E., Aldini, R., Mazzella, G. et al. (1978). Enterohepatic circulation of bile acids after cholecystectomy. *Gut* 19: 640–649.

59 Einarsson, K.A., Gundy, S.M., and Hardison, W.G. (1979). Enterohepatic circulation rates of cholic acid and chenodeoxycholic acid in man. *Gut* 20: 1078–1082.

60 Thistle, J.L., Larusso, N.F., Hofmann, A.F. et al. (1982). Differing effects of ursodeoxycholic or chenodeoxycholic acid on biliary cholesterol saturation and bile acid metabolism in man. A dose-response study. *Dig. Dis. Sci.* 27: 161–168.

61 Fracchia, M., Setchell, K.D., Crosignani, A. et al. (1996). Bile acid conjugation in early stage cholestatic liver disease before and during treatment with ursodeoxycholic acid. *Clin. Chim. Acta* 248: 175–185.

62 Tonelli, D., Gattavecchia, E., Mazzella, G., and Roda, A. (1997). Bile acid kinetics in man studied by radio thin-layer chromatography and densitometry coupling. *J. Chromatogr. B: Biomed. Sci. Appl.* 700: 59–66.

63 Combes, B., Carithers, R.L., Maddrey, W.C. et al. (1999). Biliary bile acids in primary biliary cirrhosis: effect of ursodeoxycholic acid. *Hepatology* 29: 1649–1654.

64 Hofmann, A.F. (1999). The continuing importance of bile acids in liver and intestinal disease. *Arch. Intern. Med.* 159: 2647–2658.

65 Hamilton, J.P., Xie, G., Raufman, J.P. et al. (2007). Human cecal bile acids: concentration and spectrum. *Am. J. Physiol. Gastrointest. Liver Physiol.* 293: G256–G263.

66 Hofmann, A.F. and Hagey, L.R. (2008). Bile acids: chemistry, pathochemistry, biology, pathobiology, and therapeutics. *Cell. Mol. Life Sci.* 65: 2461–2483.

67 Kaddurah-Daouk, R., Baillie, R.A., Zhu, H. et al. (2010). Lipidomic analysis of variation in response to simvastatin in the cholesterol and pharmacogenetics study. *Metabolomics* 6: 191–201.

68 Shitara, Y., Maeda, K., Ikejiri, K. et al. (2013). Clinical significance of organic anion transporting polypeptides (OATPs) in drug disposition: their roles in hepatic clearance and intestinal absorption. *Biopharm. Drug Dispos.* 34: 45–78.

69 Kosters, A. and Karpen, S.J. (2008). Bile acid transporters in health and disease. *Xenobiotica* 38: 1043–1071.

70 Amidon, G.L., Lennernas, H., Shah, V.P., and Crison, J.R. (1995). A theoretical basis for a biopharmaceutic drug classification: the correlation of in vitro drug product dissolution and in vivo bioavailability. *Pharm. Res.* 12: 413–420.

71 International Pharmaceutical Federation (2012). FIP centennial book biowaiver. https://www.fip.org/file/1377 (accessed 19 December 2020).

72 Jiang, X.L., Zhao, P., Barrett, J.S. et al. (2013). Application of physiologically based pharmacokinetic modeling to predict acetaminophen metabolism and pharmacokinetics in children. *CPT Pharmacometrics Syst. Pharmacol.* 2: e80. https://doi.org/10.1038/psp.2013.55.

73 Ghori, M.U. and Conway, B.R. (2015). Hydrophilic matrices for oral controlled delivery. *Am. J. Pharmacol. Sci.* 3: 103–109.

74 Crank, J.C. (1975). *The Mathematics of Diffusion*. London: Oxford University Press.

75 FDA CDER (1997, 1997). *Guidance for Industry: Extended Release Oral Dosage Forms. Development, Evaluation and Application of In Vitro/In Vivo Correlations*. Rockville, MD: Food and Drug Administration, Center for Drug Evaluation and Research (CDER).

76 Larson, A.M., Polson, J., Fontana, R.J. et al., the Acute Liver Failure Study Group (2005). Acetaminophen-induced acute liver failure: results of a United States multicenter, prospective study. *Hepatology* 42: 1364–1372.

77 Birmingham, P.K., Tobin, M.J., Henthorn, T.K. et al. (1997). Twenty-four hour pharmacokinetics of rectal acetaminophen in children. *Anesthesiology* 87: 244–252.

78 Wen, H. and Park, K. (2010). Introduction and overview of oral controlled release formulation design. In: *Oral ControlledRelease Formulation Design and Drug Delivery*, 1–19. Hoboken, NJ: Wiley.

79 FDA (2016). Full prescribing information Imbruvica®. http://www.accessdata.fda.gov/drugsatfda_docs/label/2016/205552s007lbl.pdf (accessed 19 December 2020).

80 Advani, Rh., Buggy, J.J., Sharman, J.P. et al. (2013). Bruton tyrosine kinase inhibitor ibrutinib (PCI-32765) has significant activity in patients with relapsed/refractory B-cell malignancies. *J. Clin. Oncol.* 31: 88–94.

81 Wildin, J.D., Pleuvry, B.J., and Mawer, G.E. (1993). Impairment of psychomotor function at modest plasma concentrations after administration of the liquid suspension to naïve subjects. *Br. J. Clin. Pharmacol.* 35: 14–19.

82 Berner, B. and Cowles, V.E. (2006). Case studies in swelling gastric retentive polymeric tablets. *Expert Opin. Drug Deliv.* 3: 541–548.

83 Qiu, Y. and Zhang, G. (2000). Research and development aspects of oral controlled-release dosage forms. In: *Handbook of Pharmaceutical Technology* (ed. D. Wise), 490. New York: Marcel Dekker, Inc.

84 Wong, P.S.L., Barclay, B., Deters, J.C., and Theuwwes, F. (1988). Osmotic device for administering certain drugs. US Patent 4, 765, 989.

85 Singh, R., Sharma, P.K., and Malviya, R. (2010). Review on chronotherapeutics – a new remedy in the treatment of various diseases. *Eur. J. Biol. Sci.* 2, 67: –76.

86 Smajilovic, S., Shaal-Jensen, R., Jabbari, R. et al. (2010). Effect of intermittent versus continuous parathyroid hormone in the cardiovascular system of rats. *Open Cardiovasc. Med. J.* 4: 110–116.

87 Lee, K., Lee, C.Y., and Jung, H. (2011). Dissolving microneedles for transdermal drug administration prepared by stepwise controlled drawing of maltose. *Biomaterials* 32: 3134–3140.

88 Virag, J.A.I. and Lust, R.M. (2014). Circadian influences on myocardial infarction. *Front. Physiol. Int. Physiol.* 5: 1–10.

89 FDA (2015). Full prescribing Information Cardizem LA®. http://www.accessdata.fda.gov/drugsatfda_docs/label/2015/021392s019lbl.pdf (accessed 19 December 2020).

90 Albert, K.S. and Maes, P.J. (2006). Chronotherapeutic diltiazem formulations and administration thereof. US Patent 7, 108, 866.

91 Patel, H.G., Patel, K., Updhyay, U.M., and Shah, V.H. (2013). Chronomodulated drug delivery system: a review. *Int. J. Pharm. Sci. Rev. Res.* 3: 26–32.

92 Transdermal Nitroglycerin Cooperative Study (1991). Acute and chronic antianginal efficacy of continuous twenty-four hour application of transdermal nitroglycerin. *Am. J. Cardiol.* 68: 1263–1273.

93 Wiegand, A., Bauer, K.H., Bohn, R. et al. (1992). Pharmacodynamic and pharmacokinetic evaluation of a new transdermal delivery system with a time-dependent release of glyceryl trinitrate. *J. Clin. Pharmacol.* 32: 77–84.

94 Swanson, J., Gupta, S., Guinta, D. et al. (1999). Acute tolerance to methylphenidate treatment of attention deficit hyperactivity disorder in children. *Clin. Pharmacol. Ther.* 66: 295–305.

95 Drugs@FDA (2011). Concerta® (methyl phenidate) extended-releasee tablets, Alza Corp. NDA 021121 approval date 8 January 2000 Reference. http://www.accessdata.fda.gov/drugsatfda_docs/nda/2000/21-121_Concerta_biopharmr.pdf (accessed 19 December 2020).

2

Physiologically Based Models: Techniques and Applications to Drug Delivery

Richard N. Upton, Ashley M. Hopkins, Ahmad Y. Abuhelwa, Jim H. Hughes and David J.R. Foster

Australian Centre for Pharmacometrics, Clinical and Health Sciences, University of South Australia, Adelaide, South Australia, Australia

2.1 Introduction

The ultimate goal in drug delivery research is to deliver the optimal amount of drug to the site of drug action, such that a given patient has the optimal balance of therapeutic benefit and unwanted side effects. This entails a quantitative understanding of the sites and mechanisms of drug action and toxicity, and the determinants of the time course of drug concentration in these sites. Given these requirements, it is not surprising that physiologically based pharmacokinetic (PBPK) modeling is often an important component of drug-delivery research. PBPK models potentially allow integrated representations of the time course of drug concentrations in the important organs and sites of drug action, toxicity, absorption, metabolism, and excretion. In this chapter, the applications and techniques of PBPK models are reviewed, with a particular emphasis on the fundamental equations that make up a PBPK model, and how the behavior of these equations can be understood via the simulation of individual components of a larger PBPK model. An example PBPK model (Figure 2.1) is used to illustrate the fundamental equations.

2.2 Types of Pharmacokinetic Models

The classification of pharmacokinetic models is not exact, there being a continuum of model types. In order of increasing structural complexity, models can be classified as Compartmental models, Semi-PBPK models, PBPK models,

Drug Delivery Approaches: Perspectives from Pharmacokinetics and Pharmacodynamics,
First Edition. Edited by Bret Berner, Toufigh Gordi, Heather A. E. Benson, and Michael S. Roberts.

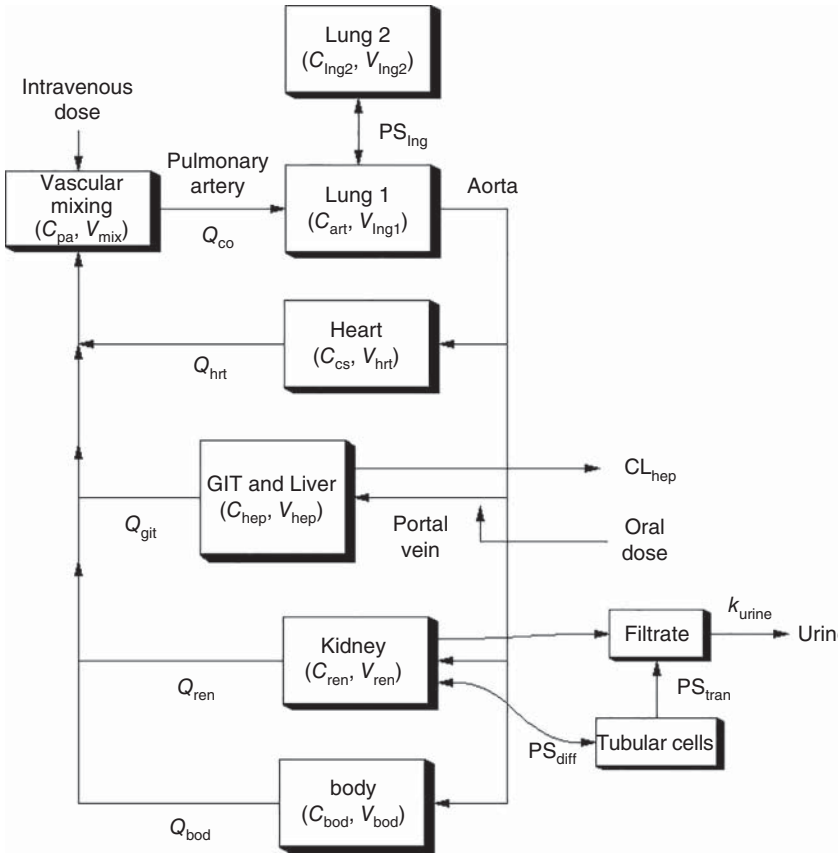

Figure 2.1 An example PBPK model. The code for the model in the R language is given in Table 2.1. The model is used as an example illustrating many of the fundamental features of PBPK models as discussed in the text. Source: Benson and Roberts [1]. Copyright © 2016 Wiley Inc.

and Systems Biology models [2]. At one end of the continuum, Compartmental models have 1–3 compartments with mostly empirical parameters that cannot typically be related to measurable physiological or pharmacological processes (e.g. organ blood flows or volumes, transporter, or enzyme activity or infinity). PBPK models in contrast have multiple compartments representing defined organs or physiological spaces, with parameters that are potentially measurable. PBPK models may be part of a broader Systems Biology approach, which includes models of complex biological systems (e.g. the coagulation network [3]) relating to physiology and pathophysiology. Semi-PBPK models (sometimes called

recirculatory models in anesthesia) are simplifications of PBPK models using lumping of some compartments (e.g. the "rest" of the body).

The lumping of compartments in complex models can be a useful tool for solving specific problems. The lumping process can be formal – for example a Systems Biology model of the coagulation network with 62 compartments could be reduced to a 5-compartment model to describe the brown snake venom–fibrinogen relationship [4]. For intravenous anesthetics, Semi-PBPK models with detailed representations of only the brain and lung were able to capture the important aspects of the induction of anesthesia [5].

There can be distinct differences in how the models at the ends of the continuum are parameterized [6]. Compartmental models are typically parameterized using a "top-down" approach, where the model is fitted to a specific data set to estimate parameter values. PBPK models are typically parameterized using a "bottom-up" approach, where model parameters are derived from literature, in vitro data, or scaled data from another species. Semi-PBPK models can use elements of both approaches.

2.3 Commercial vs. Bespoke PBPK Models

One of the significant developments in the application of PBPK models is the increasing availability and use of commercial software for PBPK modeling. The commercially available whole-body PBPK software includes GastroPlus™, Simcyp®, and PK-Sim®. These evolved from different directions, but all are now sophisticated implementations of complex physiological and pharmacological systems, and are perhaps better described as systems biology. In some research settings, it may be more efficient to use these or similar software rather than "reinvent the wheel."

Nevertheless, it is feasible and common to construct bespoke PBPK for specific projects. Any general-purpose software platform that can solve systems of differential equations can implement a PBPK model. For example, STELLA® or, Berkeley Madonna™ can be used for simulation. R, Python, or MATLAB can be used for simulation and for fitting single-subject data. NONMEM, S-Adapt, or Monolix can be used for simulation and fitting population data. Despite the relative ease of constructing the code for PBPK models, it should be recognized that the more difficult aspect of their implementation is collecting, collating, and justifying the data used to parameterize the model. Furthermore, for complex PBPK models, the task of validating that the model is "fit for purpose" is not trivial [7]. Recent developments in model sharing [8] and the standardization of model terminology [9] will surely make these tasks easier in the future.

2.4 Data Sources

PBPK models can predict the time course of drug concentrations in each organ and site represented in the model. An accurate and useful prediction requires an appropriate model structure for each organ, and reliable values for the parameters of each organ submodel.

Organ blood size and organ blood flows are ubiquitous parameters in PBPK models. For many modeling tasks, parameter values taken from the literature may be sufficient (e.g. where blood flow is not expected to change). For humans, the NHANES database is a useful resource documenting organ size and organ blood flows [10]. Tabulated organ size and organ blood flow data for standard size animals are available for rats, mice, dogs, monkeys, sheep, and pigs [11–13]. Note that organ size and blood flow data can be scaled allometrically to account for subjects of different sizes (See Section 2.6.7). The lung has a special role in the circulation, being connected in series with the other organs of the body and hence receiving the total cardiac output (and thereby being a first-pass organ for most routes of administration [14]).

The other parameters for the models (e.g. relating to binding, enzyme, and transporter kinetics) can come from literature values, in silico predictions, in vitro data, scaled data from another species or direct measurement. An area of particular interest is the "in silico" or near in silico prediction of metabolism, drug–drug interactions [15], and distribution [16] from drug physiochemical properties, enzyme characteristics, and/or binding data. The prediction of in vivo kinetics from these data and PBPK models is clearly of enormous potential in drug screening during drug development. Another area of particular interest is the use of PBPK models for in vitro–in vivo extrapolation (IVIVE) [17]. For example, in vitro data (e.g. microsomes, hepatocytes) have been used to provide parameter estimates for a well-stirred PBPK model of the liver to predict in vivo metabolic clearance [18]. There are a number of IVIVE methods available, which, to varying extents, take account of free fractions in vitro and in vivo [18] and protein abundance [19].

2.5 Applications of PBPK Models

PBPK models are not new, having appeared in the literature in various forms since the 1960s. The term PBPK first appeared in the literature in the 1970s, and the annual publication rate of this term showed an increase in the early 1990s with a plateau until approximately the mid-2000s. Since then there has been a sustained and dramatic acceleration in the number of publications using this term. There are now well over a hundred PBPK papers being published each year, so

any reference to their applications will be selective. Furthermore, it is likely that many PBPK models used to support drug development decisions are unreported in the literature. Indeed, the Food and Drug Administration (FDA) reported that 33 PBPK models were used to support applications in 2012, while this increased to 84 in 2013, with approximately 50% related to drug–drug interactions [20]. Recent reviews are available that provide a broad overview of PBPK models in drug development [21], including candidate selection [22], and in pediatrics specifically [23]. The Accelerating the Development of Therapies for Pediatric Rare Diseases plan released by the FDA in 2014 suggests using PBPK models as a strategy to address difficulties associated with conducting pediatric studies, and they have been used for first-in-pediatric starting dose recommendations (see [24]). In much the same way, PBPK models have been used for first in human dose selection, with examples available after a variety of routes of administration, including subcutaneous [25] or oral routes [26]. Of note, although more limited in the literature, PBPK models have also found utility for this purpose for large molecules in addition to small molecules [27].

Other applications of PBPK models include prediction of drug–drug interactions involving both inhibition and induction, changes in pharmacokinetics due to altered physiology such as hepatic or renal impairment, extrapolation to other patient populations, the implications of variability in transporter activity, the implications of variability in metabolizing enzymes, including genetic polymorphisms, address specific toxicological or pharmacological questions such as predicting exposure of particular target organs and receptor occupancy (see [21, 27, 28]).

In addition to systemic kinetics, PBPK models have been used to better understand drug absorption [29], including food effects [30], formulation effects [31], causes of poor oral bioavailability [32], to describe region specific absorption [33], and to aid formulation development [34]. Furthermore, PBPK models have been shown to be as effective as deconvolution analysis for establishing IVIVC correlations, with the added advantage of having a mechanistic description of the absorption process [35]. There is now a concerted effort to use mechanistic PBPK and other models to understand oral drug absorption [8, 36].

Considering the applications of PBPK models at a more general level, it should be recognized that models should be assessed by their success at being "fit for purpose," and this purpose is likely to differ from application to application. Concepts of validation (using internal or external data) are important for models (of whatever type) used to make predictions, but model validation should be seen as an ongoing and evolving process, particularly for PBPK models. Indeed, in any application, a PBPK model can be considered a mechanistic statement of hypothesis, and hence a platform for further experimentation and a deeper understanding of the drug-delivery problem at hand.

2.6 Techniques of PBPK Modeling

2.6.1 The "Language" of PBPK Models

Regardless of the origin of a PBPK model, users need to be able to understand what the model is representing and how to interpret how the parameters affect the model predictions. PBPK models are by necessity complex. However, this complexity evolves by the joining together smaller, less complex submodels of individual organs that are connected (usually) by the blood circulation as dictated by anatomical considerations. Within each organ, drug absorption, transport, metabolism, or elimination is represented as dictated by the pharmacokinetic role of each organ. The art of PBPK modeling is to find equations and parameter values that represent each of these processes in a way that is fit for purpose. Fortunately, a surprisingly limited number of fundamental equations can be used to build complex PBPK models. Most PBPK models are structured as a system of interconnected compartments and as such can be written as a system of differential equations. A picture of a compartmental system representing a model is easily turned into differential equations. Consider Figure 2.2, which shows a single compartment representing an organ as a single flow-limited compartment with elimination. There are three processes (shown by arrows) contributing to the amount of drug in the compartment – addition of drug via arterial blood, removal of drug via regional venous blood, and removal of drug via clearance. The instantaneous rate of that drug enters the organ is $Q * C_{art}$ (e.g. l/min * mg/l = mg/min). The instantaneous rate that drug leaves the organ is $Q * C_{ven}$ and $C_{art} *$ CL. The amount of drug in the compartment at any time ($A_{(t)}$) is the integral of the net input rate less the net output rate:

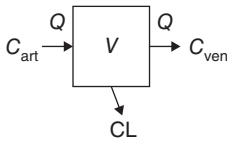

Figure 2.2 A flow-limited compartment model with elimination. This model could be used as a simple representation of a liver or kidney in a PBPK model. The organ is represented as a single compartment of volume *V*, which has blood flow *Q* entering and leaving the organ. The instantaneous rate of that drug enters the organ is the product of arterial drug concentration C_{art} (technically arterial and portal blood for the liver) and blood flow. The instantaneous rate that drug leaves the organ is the product of regional venous drug concentration C_{ven} and blood flow and the product of C_{art} and clearance (CL). Over time, the amount of drug in the compartment is the integral of the net input rate less the net output rate. Source: Benson and Roberts [1]. Copyright © 2016 Wiley, Inc.

$$A_{(t)} = \int_0^t dt\, Q * C_{\text{art}} - \left(Q * C_{\text{ven}} - \text{CL} * C_{\text{art}}\right)$$

Differentiating both sides gives the differential equation for this compartmental system. The differential equation for the system effectively "mass balances" the rate of drug transport entering and leaving the compartment:

$$\frac{dA}{dt} = Q * C_{art} - Q * C_{ven} - CL * C_{art}$$

In practice, it is easier to go directly from a picture to a series of differential equations as each compartment of the system can be stated as the sum of all input rates (positive) and output rates (negative) for the compartment.

$$\frac{dA}{dt} = (\text{All input rates} - \text{All output rates})$$

Using this rule, a complex PBPK model can be constructed as a series of differential equations, with one equation for each compartment in the system.

A system of differential equations needs to be solved to derive the time course of drug concentrations. Note that as the concentration of drug in a compartment is usually more important than the amount in the compartment, amount is converted to concentration by dividing by the compartment volume (V in Figure 2.2). Analytical solutions of large compartment systems are intractable, but they can be solved (approximately but accurately) using differential equation solving routines. In Table 2.1, the code for a simple PBPK model is provided as a series of differential equations. The model without modification could be run in the R language, and with modification in other differential equation solving software. The aim of providing this code is to introduce readers to the common "language" of PBPK models, with examples of how key pharmacokinetic features can be represented as equations. Furthermore, the intention is to show how each submodel within the PBPK model can be examined separately in terms of its input and output. In this way, plots can be used to understand the behavior of the submodel as parameter values are changed. This process of breaking down a PBPK model into its components and understanding the function of each component is important for developing reliable PBPK models.

2.6.2 Oral Absorption Models

As many drugs are taken orally, disintegration, dissolution, absorption, and first-pass metabolism can dominate the kinetics of the drugs through effects on absorption rate and bioavailability. A number of PBPK models have been used to describe the mechanisms underlying these processes. A common approach, as used in the compartmental absorption and transit (CAT) [37] and later in the advanced compartmental absorption and transit (ACAT) [32] models, is to represent the gastrointestinal (GI) tract as a series of compartments representing, for example, stomach, duodenum, jejunum, ileum, cecum, and ascending colon.

Table 2.1 Example model code.

```
#An example PBPK model written in the R language
#www.r-project.org
#Units are mg, L, min

#Load libraries
  library(deSolve) #differential equation solving package

#Define simulation times
   lasttime <- 240
    TIME <- seq(from=0,to=lasttime,by=0.1)

#Subject characteristics
   ID <- 1  #identification number
   WT <- 65  #body weight
   MGKGpo <- 2  #oral dose at time 0 in mg/kg
   MGKGiv <- 1  #iv dose at time 0 in mg/kg

#Oral dose
    Dosemgpo <- MGKGpo*WT  #Calculate total oral dose
    Fpo <- 0.20  #oral bioavailability

    #Dissolution model - enteric coating
    kamax <- 0.1   #maximum absorption rate constant when
pH is not limiting
    theta <- 0.995 #parameter affecting the shape of the
dissolution rate-pH curve
    pH50 <- 4      #parameter affecting the inflection point
in the dissolution rate-pH curve
    Hill <-  10    #parameter affecting the steepness of the
dissolution rate-pH curve
    Tempty <- 30   #time of gastric emptying

    #Define a function that changes pH with time using the
approxfun function of R
    TIMEph <- c(0,Tempty,lasttime) #a sequence of time values
    VALph <- c(1,7,7)              #a sequence of corresponding
pH values
    pHvsT <- approxfun(TIMEph, VALph, method = "const")
#the function.  Takes time as input, returns pH


#IV dose
```

Table 2.1 (Continued)

```
36.    Dosemgiv <- MGKGiv*WT  #calculate total IV dose
37.    Tinfiv <- 15 #duration of infusion
38.    Ratemgminiv <- Dosemgiv/Tinfiv  #calculated infusion rate
39.
40.    #Define a function that changes infusion rate with time
using the approxfun function of R
41.    TIMEinfiv <-c(0,Tinfiv,lasttime) #a sequence of time values
42.    RATEinfiv <-c(Ratemgminiv,0,0)   #a sequence of
corresponding dose rate values
43.    ratevsT <- approxfun(TIMEinfiv, RATEinfiv, method =
"const") #the function.  Takes time as input, returns dose rate
44.
45. #Standard man parameter values
46.     WTstd <- 70   #body weight
47.     AGEstd <- 30   #age in years
48.     PMA <- AGEstd*12*4 + 40 #post menstrual age in weeks
49.
50.     #Tissue pool flows
51.     Qhrtstd <- 1
52.     PSlngstd <- 0.2
53.     Qgitstd <- 1.5
54.     Qrenstd <- 1.5
55.     Qbodstd <- 1.5
56.
57.     #Tissue real volumes
58.     Vmixstd <- 0.25
59.     Vlng1std <- 1
60.     Vlng2std <- 5
61.     Vhrtstd <- 1
62.     Vhepstd <- 1.5
63.     Vrenstd <- 0.5
64.     Vbodstd <- 50
65.
66.     #Renal physiology
67.     GFRstd    <- 0.120 #glomerular filtration rate
68.     PSdiffstd <-  50   #permeability of tubular cells
69.     kurinestd <- 0.8   #rate constant for urine output
70.
71.     #Pharmacodynamic parameters
72.     Ebase <- 2    #baseline drug effect
73.     Emax <- 10    #maximum drug effect
```

(*continued*)

Table 2.1 (Continued)

```
74.     EC50 <- 0.5   #concentration for half-maximum effect
75.
76.     #Drug related parameters
77.     fu <- 0.2     #free fraction in plasma
78.     fuT <- 0.25   #free fraction in tissue (typically differs
by tissue)
79.     Vmax <- 500   #maximum rate of hepatic enzyme activity
80.     km <- 3       #km of hepatic enzyme activity
81.     Ci <- 0       #inhibitor concentration
82.     ki <- 0.5     #inhibitor potency
83.
84.     Vmaxt <- 100  #maximum rate of renal active secretion
85.     kmt <- 50   #km of renal tubular secretion
86.
87.     TM50 <- 47.7  #time for half maturation (weeks)
88.     hillm <- 3.40 #steepness of maturation function
89.
90.
91.     #Allometric scaling of blood flows, clearances and
permeabilities
92.     Qhrt  <- Qhrtstd*(WT/WTstd)^0.75
93.     PSlng <- PSlngstd*(WT/WTstd)^0.75
94.      ETA1  <- rnorm(1, mean=0, sd=0.10)  #sample from a normal
distribution with mean zero and sd=0.1
95.     Qgit  <- Qgitstd*(WT/WTstd)^0.75*exp(ETA1) #adds log-normal
distribution of Qgit via ETA1
96.     Qren  <- Qrenstd*(WT/WTstd)^0.75
97.     GFR   <- GFRstd*(WT/WTstd)^0.75
98.     PSdiff <- PSdiffstd*(WT/WTstd)^0.75
99.     kurine <- kurinestd*(WT/WTstd)^-0.25  #allometric scaling
for rate constant
100.     Qbod  <- Qbodstd*(WT/WTstd)^0.75
101.
102.     Qco <- sum(Qhrt,Qgit,Qren,Qbod)
103.
104.
105.     #Apparent distribution volumes with allometric scaling
106.     Vmix  <- Vmixstd*(WT/WTstd)^1  #vascular compartment,
no apparent distribution volume
107.     Vlng1 <- Vlng1std*(fu/fuT)*(WT/WTstd)^1
108.     Vlng2 <- Vlng2std*(fu/fuT)*(WT/WTstd)^1
109.     Vhrt  <- Vhrtstd *(fu/fuT)*(WT/WTstd)^1
110.     Vhep  <- Vhepstd *(fu/fuT)*(WT/WTstd)^1
```

Table 2.1 (Continued)

```
111.     Vren  <- Vrenstd *(fu/fuT)*(WT/WTstd)^1
112.     Vbod  <- Vbodstd *(fu/fuT)*(WT/WTstd)^1
113.
114.
115. #Function containing differential equations for amounts in
compartments (A) - see help for lsoda
116.    DES <- function(T, A, THETAin)
117.          {
118.
119.             dA <- vector(len=12)
120.
121.             #Infusion specifications
122.             doserateiv <- ratevsT(T)
123.             Ainj <- doserateiv/Qco*Vmix  #amount in mixing
compartment
124.
125.             #Dissolution model
126.             pH <- pHvsT(T)
127.             pHCOV <- theta*pH^Hill/(pH50^Hill + pH^Hill)
128.             ka    <- kamax*pHCOV
129.
130.             #Give names to the state variables for clarity
131.             Apa    <- A[1]
132.             Aart   <- A[2]
133.             Alng2  <- A[3]
134.             Acs    <- A[4]
135.             Agut   <- A[5]
136.             Ahep   <- A[6]
137.             Amet   <- A[7]
138.             Aren   <- A[8]
139.             Atubf  <- A[9]
140.             Atubc  <- A[10]
141.             Aurine <- A[11]
142.             Abod   <- A[12]
143.
144.             #Sum recirculation via venous returns
145.             recirc <- Qhrt*Acs/Vhrt + Qgit*Ahep/Vhep +
Qren*Aren/Vren + Qbod*Abod/Vbod
146.
147.             #Venous mixing compartment - including addition
of recirculation
148.             dA[1] <- (Qco*(Ainj/Vmix-Apa/Vmix) + recirc)
#pulmonary artery
```

(*continued*)

Table 2.1 (Continued)

```
149.
150.              #Lung model
151.              dA[2] <- (Qco*((Apa/Vmix)-(Aart/Vlng1)) +
PSlng*(Alng2-Aart))  #arterial
152.              dA[3] <- (PSlng*(Aart-Alng2))  #peripheral lung
153.
154.              #Heart model
155.              dA[4] <- (Qhrt*((Aart/Vlng1)-(Acs/Vhrt)))  #heart
156.
157.              #Pharmacodynamic model driven by myocardial
concentration (Ccs)
158.              E <- Ebase + (Emax*(Acs/Vhrt))/(EC50+(Acs/Vhrt))
159.
160.              #GIT
161.              dA[5] <- -ka*Agut   #First order oral absorption
162.              Cport <-  ka*Agut/Qgit + Aart/Vlng1
#orally absorbed + recirculated drug
163.              Fmat  <- PMA^hillm/(TM50^hillm + PMA^hillm)
164.              CLint <-  Vmax/(km*(1+(Ci/ki))+Cport)*Fmat
#Competitive inhibition and maturation
165.              CLhep <-  CLint*Qgit/(CLint+Qgit)
#Well-stirred model
166.
167.              dA[6] <- (Qgit*Cport - Qgit*Ahep/Vhep -
CLhep*Cport) #liver
168.              dA[7] <- CLhep*Cport  #cumulative drug amount
metabolised for oral dose
169.
170.
171.              #Kidney
172.              dA[8] <-  Qren*Aart/Vlng1 -Qren*Aren/Vren
-GFR*Aart/Vlng1 -PSdiff*Aren +PSdiff*Atubc   #Kidney plasma
173.              PStran <- Vmaxt/(kmt+(Aren/Vren))
#Saturable excretion driven by renal plasma concentration
174.              dA[9] <-  GFR*Aart/Vlng1 +PStran*Atubc
-Atubf*kurine #Proximal tubule filtrate
175.              dA[10] <- PSdiff*Aren -PSdiff*Atubc
-PStran*Atubc    #Proximal tubule cells
176.              dA[11] <- Atubf*kurine
#Cumulative drug amount in urine
177.
178.              #Pooled Body
179.              dA[12] <- (Qbod*Aart/Vlng1-Qbod*Abod/Vbod)   #Body
```

Table 2.1 (Continued)

```
180.
181.              list(dA,E)
182.   # #end DES
183.
184.      #Set initial conditions
185.      A_0 <- c(A1=0,A2=0,A3=0,A4=0,A5=Dosemgpo*Fpo,
A6=0,A7=0,A8=0,A9=0,A10=0,A11=0,A12=0)
186.
187.      paramlist <- c("ID"=ID,"WT"=WT,"MGKGpo"=MGKGpo,
"MGKGiv"=MGKGiv)
188.
189.      #Run differential equation solver
190.       sim.data <- lsoda(A_0, TIME, DES, paramlist)
191.
192.      #Process the simulated output
193.        sim.data <- data.frame("ID"=ID,"WT"=WT,"MGKGpo"=MGKGpo,
"MGKGiv"=MGKGiv, sim.data)
194.        names(sim.data) <- c("ID","WT","MGKGpo","MGKGiv",
"time","Apa","Aart","Alng2","Acs","Agut","Ahep",
195.                             "Amet","Aren","Atubf","Atubc",
"Aurine","Abod","Effect")
196.
197.      #Convert amounts to concentrations
198.         sim.data$Cpa   <- sim.data$Apa/Vmix
199.         sim.data$Cart  <- sim.data$Aart/Vlng1
200.         sim.data$Clng2 <- sim.data$Alng2/Vlng2
201.         sim.data$Ccs   <- sim.data$Acs/Vhrt
202.         sim.data$Chep  <- sim.data$Ahep/Vhep
203.         sim.data$Cren  <- sim.data$Aren/Vren
204.         sim.data$Cbod  <- sim.data$Abod/Vbod
205.
206.      #Simulated output
207.       head(sim.data)
```

The code for a simple bespoke PBPK model written in the R language (www.r-project.org). The deSolve package of R is used to solve the differential equations. The model can be run copying the code into a text file (removing the line numbering), then sourcing the code from the R console.

Each compartment can have the appropriate representations of drug dissolution, precipitation, efflux or influx transporters, chemical stability, and first-pass metabolism. The Advanced Dissolution, Absorption, and Metabolism (ADAM) model is based on the CAT model with refinements to the dissolution model [38]. An alternative approach is to represent the GI tract as a one-dimensional cylindrical tube with spatially different properties (e.g. pH, length, surface area) rather than a series of transit compartments [39].

A simple dissolution model for an enteric coated formulation is implemented in the example model on lines 22–27 and the behavior of this model is summarized in Figure 2.3. This model assumes dissolution was the rate-limiting step in the oral absorption process (i.e. dissolved drug was rapidly absorbed across the gut wall).

2.6.3 Drug Metabolism and Drug–Drug Interactions

The well-stirred model has been a simple but useful technique for representing the liver in PBPK models. It accounts for the flow limitation of hepatic clearance (CL_{hep}) when intrinsic clearance (CL_{int}, representing the intrinsic capacity of the drug-metabolizing enzymes) is high and not rate limiting, and allows for saturable enzyme kinetics.

$$CL_{int} = \frac{V_{max}}{(k_m + C)}$$

$$CL_{hep} = \frac{CL_{int} * Q_{hep}}{(CL_{int} + Q_{hep})}$$

Here Q_{hep} is liver blood flow, C is the afferent drug concentration, and V_{max} and k_m are the maximum rate and concentration for half maximum rate of drug metabolism, respectively. Note that k_m is most commonly expressed in terms of free drug concentrations, but is shown here without correction for free fraction (f_u) for simplicity.

Metabolism-mediated drug–drug interactions [40] have been an important area of investigation using PBPK models. Drug interactions can be represented as competitive inhibition, which increases k_m but does not affect V_{max}. If I is the inhibitor concentration, and k_i is an indicator of inhibitor potency (a proportionality constant), then:

$$CL_{int} = \frac{V_{max}}{\left(k_m * \left(1 + \frac{I}{k_i}\right) + C\right)}$$

In contrast, noncompetitive inhibition does not affect k_m but decreases V_{max}:

$$CL_{int} = \frac{V_{max} * \left(\frac{k_i}{k_i + I}\right)}{(k_m + C)}$$

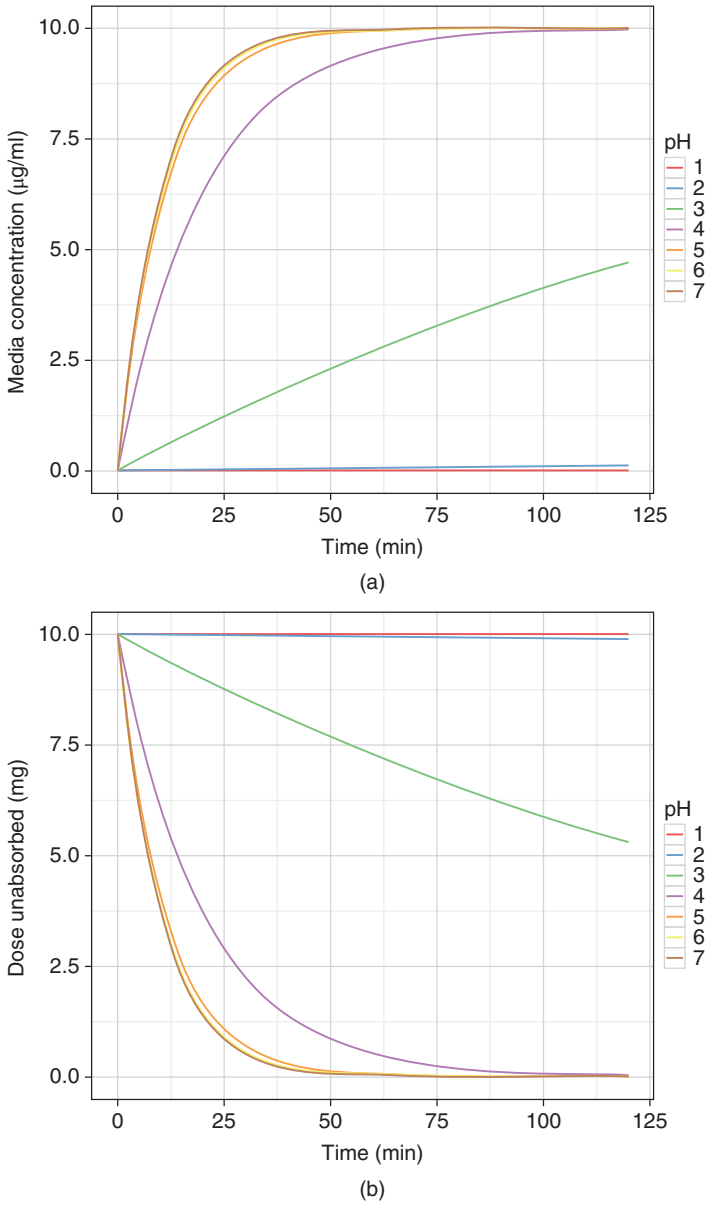

Figure 2.3 Dissolution submodel. A model where the dissolution rate of an oral dose form (10 mg tablet size) is pH dependent. (a) The dissolution characteristics over range of pH values in a dissolution apparatus with a media volume of 1 l. (b) The hypothetical fraction of dose unabsorbed in vivo over range of pH values. In reality, the tablet transitions from an acidic environment in the stomach to the higher pH of the small intestine at a time given by the time of gastric emptying, with a consequent increase in the absorption rate. See lines 22–32 of the example model. Source: Benson and Roberts [1].

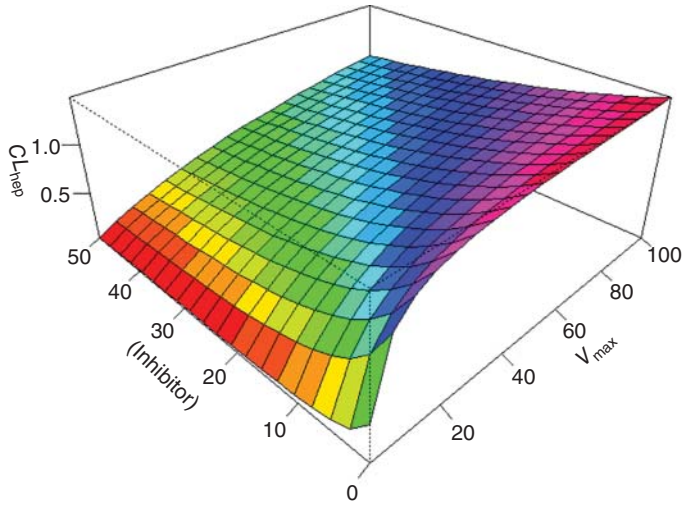

Figure 2.4 Hepatic submodel. A well-stirred hepatic submodel with an implementation of competitive inhibition. The relationship between hepatic clearance (CL_{hep}) and inhibitor concentration [inhibitor] and the maximum rate of metabolism (V_{max}) governing the intrinsic clearance of the drug. When intrinsic clearance is high, the clearance of the drug is less affected by the presence of the inhibitor. See lines 161–168 of the example model. Source: Benson and Roberts [1]. Copyright © 2016 Wiley Inc.

here k_i is the inhibitor concentration associated with 50% inhibition of V_{max}. The cases of mixed and uncompetitive inhibition use derivatives of these equations [40]. Complex, multienzyme systems with many interactions can be built using combinations of these equations.

A well-stirred model is implemented in the example model on line 165. Figure 2.4 presents a model indicating the relationship between organ blood flow, intrinsic clearance, and a competitive inhibitor.

2.6.4 Drug Transporters

To date, PBPK models have generally not featured comprehensive descriptions of transporter kinetics [41]. However, PBPK models are seen as an important tool for developing in vitro–in vivo correlations for transporters, to extrapolate and integrate data from in vitro transporter assays, and for extrapolating preclinical species into humans [42]. The equations describing drug transporter are fundamentally the same as those describing drug metabolism, but the equations represent a transport rate (or clearance) in a given direction rather than the rate (or clearance) of metabolism. For drugs that are transporter substrates yet are sufficiently lipophilic to passively diffuse across membranes, the net transport across the membrane is

theoretically a balance between active transport in one direction and passive diffusion back in the other direction [43]. Active tubular secretion is represented in the example model on lines 173–174.

Drug transporters are often located in a number of tissues other than the kidneys or the blood–brain barrier. Commercially available programs allow for transporters to be present in each tissue with the same transport rate per transporter, but with a different concentration of transport proteins [44]. Relative transporter concentrations can be estimated with sufficient data, but can also be inferred from gene expression data. Care should be taken when using gene expression to guide protein concentration as it typically explains only 40% of the variation in these concentrations [45]. With time, extensive proteomic data may become available in literature removing the need for this surrogate.

2.6.5 Renal Elimination

For renally eliminated drugs or metabolites, the representation of the kidney in a PBPK model requires particular attention. The key processes of renal blood flow, glomerular filtration, passive reabsorption, active tubular secretion, and active tubular reabsorption can be presented with varying degrees of complexity as dictated by need [46]. Glomerular filtration rate (GFR) is generally considered to be synonymous with creatinine clearance. Creatinine clearance can be estimated given age and weight using the equation described by Rhodin et al. [47]. Transporters can be handled using the equations described above. For example, Worley and Fisher were able to describe the transporter-mediated renal elimination of perfluorooctanoic acid in the rat using three compartments: kidney serum, proximal tubule filtrate, and proximal tubule cells [41].

A representation of renal kinetics is implemented in the example model on lines 172–176. Figure 2.5 shows the relationship between GFR and the rate of active tubular transport represented by the model.

2.6.6 Protein Binding

Unbound (free) drug concentrations are increasingly measured due to advances in free fraction methodology and increases in assay sensitivity. Evidence in support of the "free drug hypothesis" continues to accumulate [48], reinforcing the important role of free fraction in plasma (f_u) for drug metabolism, excretion, and distribution as well as IVIVE [18] and pharmacodynamics (PDs) [49]. The simplest description of protein binding is for a single binding site where there is a dynamic equilibrium between drug (D) and protein (P) and the drug–protein complex (DP). The association rate constant is k_{on} and the dissociation rate constant is k_{off}, and

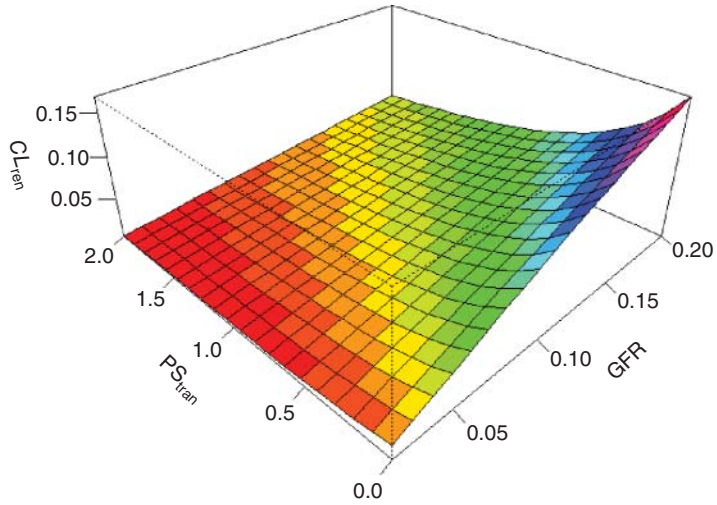

Figure 2.5 Renal submodel. An implementation of a renal submodel, based on Worley and Fisher [41]. The relationship between renal clearance (CL_{ren}) and glomerular filtration rate (GFR) and rate of active tubular uptake (PS_{tran}) is shown. As expected, renal clearance is essentially abolished when GFR is low or tubular uptake is high. See lines 172–176 of the example model. Source: Benson and Roberts [1]. Copyright © 2016 Wiley, Inc.

the equilibrium state (where D is 50% bound to P) is described by the equilibrium dissociation constant K_d:

$$[D] + [P] \leftrightarrow [DP]$$

$$K_d = \frac{k_{on}}{k_{off}}$$

The unbound fraction at equilibrium (f_u) is governed by K_d and the protein concentration.

$$f_u = \frac{1}{\left(1 + \frac{[P]}{K_d}\right)}$$

When [P] is much greater than K_d, f_u tends to 0; conversely when [P] is much less than K_d, f_u tends to 1. Free (C_u) and total (C_{tot}) concentrations can be interconverted if f_u is known:

$$C_u = f_u \cdot C_{tot}$$

$$C_{tot} = \frac{C_u}{f_u}$$

Two general strategies can be employed for representing binding. When protein binding is considered restrictive, k_{off} is relatively slow such that bound drug is not

readily available. It is possible to use free concentrations throughout a model, such that parameters are referenced to the free rather than the total concentration. A binding model can be implemented to describe the relationship between free and total concentrations in plasma, where the binding model predicts total concentrations given free concentration, protein concentration, and the influence of any modifiers of binding [50]. Alternatively, the model can be referenced to total concentrations with f_u used to modify parameters. Using hepatic elimination as an example:

$$\mathrm{CL_{hep}} = \frac{\mathrm{CL_{int}} * f_u * Q_{hep}}{(\mathrm{CL_{int}} * f_u + Q_{hep})}$$

When protein binding is nonrestrictive, k_{off} is relatively rapid such that bound drug is readily available in a "sink" situation. In this case, models incorporating dissociation from protein (with separate compartments for free and bound drug) may be advantageous [51, 52].

The role of protein binding in distribution in PBPK models is often handled by the concept of an organ having a real anatomical volume (V_{real}) and an apparent distribution volume (V_{app}) for a given drug that is a function of the free fraction in plasma (f_u) and the tissue of the organ (f_{uT}):

$$V_{app} = V_{real} * \frac{f_u}{f_{uT}}$$

The free concentration at equilibrium is assumed to be the same in both plasma and tissue (i.e. the case of passive diffusion with no active transport). The extent of distribution at equilibrium may be summarized as a partition coefficient (R), which effectively indicates the ratio of total tissue concentration (C_T) to the total plasma concentration (C_p) at steady state.

$$R = \frac{V_{app}}{V_{real}} = \frac{f_u}{f_{uT}} = \frac{C_T}{C_p}$$

Red blood cell binding and sequestration can be handled in PBPK models using similar approaches to those used for protein binding. Figure 2.6 shows the predictions of a model representing the simple relationship between partition coefficient (R) and the f_u and f_{uT}. A representation of the effect of protein binding on the apparent distribution volumes of a drug is implemented in the example model on lines 107–112.

2.6.7 Accounting for Size

Allometric principles are the foundation of accounting for differences in body size in PBPK models, both within and between species. Biological structures (X) have been found to scale with body weight (WT) by a power equation,

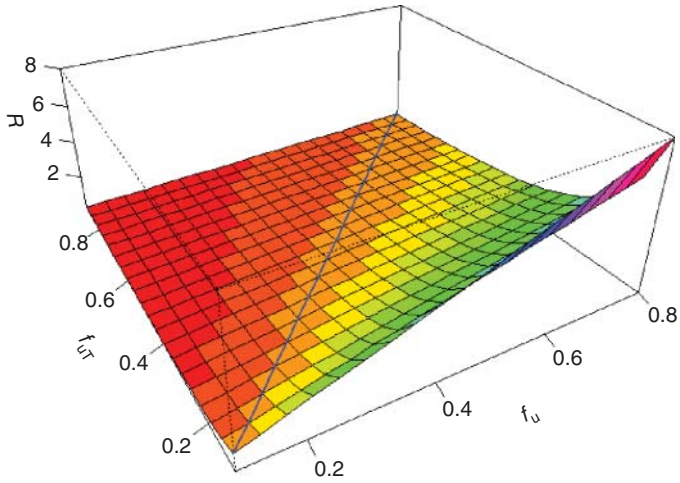

Figure 2.6 The effect of free fraction on partition coefficient. The tissue:plasma partition coefficient (R) as a function of free fraction in plasma (f_u) and free fraction in tissue (f_{uT}). The line where $f_u = f_{uT}$ and partition coefficient is 1 is shown as a diagonal line. High free fraction in plasma (low binding) and low free fraction in tissue (high binding) is associated with the highest partition coefficients. See lines 92–100 of the example model. Source: Benson and Roberts [1]. Copyright © 2016 Wiley Inc.

$X = X_0 \cdot \mathrm{WT}^a$, where a is the allometric coefficient and X_0 is an intercept term. Organ size scales with an allometric coefficient of 1, while metabolic rate and hence organ blood flow scale with an allometric coefficient of ¾ [53]. These values have been observed empirically, and are supported by an underlying theory relating to oxygen delivery in capillary networks [54]. These principles are easily implemented in a PBPK model. Given the flow and weight of a standard reference subject (Q_{std} and $\mathrm{WT}_{\mathrm{std}}$, respectively), the organ blood flow (Q_i) for a subject of weight WT_i is:

$$Q_i = Q_{\mathrm{std}} \left(\frac{\mathrm{WT}_i}{\mathrm{WT}_{\mathrm{std}}} \right)^{0.75}$$

Given the organ volume and weight of a standard reference subject (V_{std} and $\mathrm{WT}_{\mathrm{std}}$, respectively), the organ volume (V_i) for a subject of weight WT_i is:

$$V_i = V_{\mathrm{std}} \left(\frac{\mathrm{WT}_i}{\mathrm{WT}_{\mathrm{std}}} \right)^{1}$$

The standard or reference values for flow and size for man can be taken from literature values [10], where the concept of a "Standard" or "Reference" man, woman or child is sometimes useful [55].

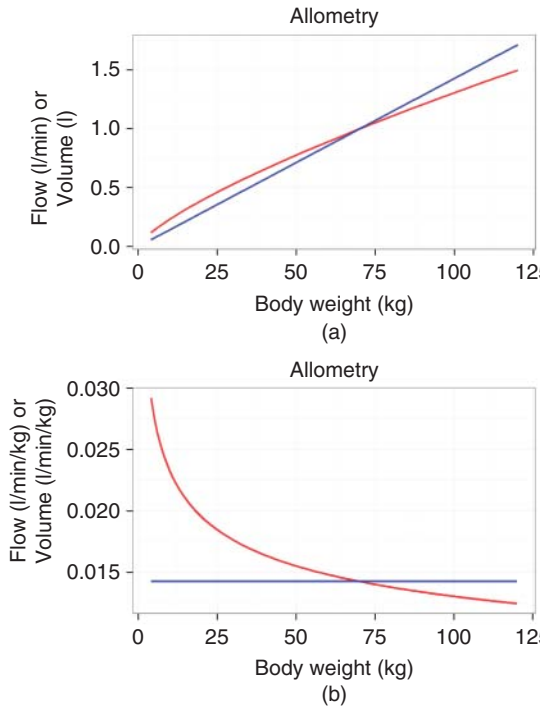

Figure 2.7 Allometric scaling of an organ. Allometric scaling of a single organ with a volume of 1 l and blood flow of 1 l/min at a reference bodyweight of 70 kg. Organ perfusion (light gray) tends to be relatively higher than organ volume (dark gray) at lower body weight, and vice versa (a). This is most obvious when looking at body weight–normalized values (b). Body weight range is 4–120 kg. See lines 92–100 and 106–112 of the example model. Source: Benson and Roberts [1]. Copyright © 2016, Wiley Inc.

Large data sets with a wide range of body weight are needed to reliably estimate allometric coefficients, and hence there are sound arguments for using the theoretical values in many circumstances. Allometric principles do not account for differences in body composition (e.g. obesity), but body composition may be accounted for by considering fat free mass (FFM) and normal fat weight (NFWT) [56] such that fat tissue can be represented as a separate submodel.

Allometric scaling is implemented in the example model on lines 92–100 and 106–112. Figure 2.7 shows the relationship between organ blood flow, organ size, and body weight represented by the model.

2.6.8 Accounting for Age

Accounting for the effect of body size in a PBPK model is fundamental for representing the effect of age, but additional consideration needs to be given to the maturation of biological processes. Maturation for different enzymes occurs at different rates post conception as described by a recent meta-analysis [57], with maturation rates determined from in vivo data appearing more reliable than those determined in vitro. Taking the maturation of hepatic enzymes as an example, this

occurs at different rates for different metabolic pathways but is usually complete by the age of two years [58]. Accounting for maturation effects in PBPK models requires using a time scale that captures the developmental process both before and after birth to properly account for the variable time between conception and birth. Post conception age is ideal, but for practical purposes post menstrual age (PMA) is often used. A number of equations have been used to modify adult clearance. In the following example, both an allometric term and a maturation term [58] modify the standard clearance for a standard weight adult.

$$\mathrm{CL}_i = \mathrm{CL}_{\mathrm{std}} \left(\frac{(\mathrm{PMA}^{\mathrm{hill}})}{(\mathrm{TM50}^{\mathrm{hill}} + \mathrm{PMA}^{\mathrm{hill}})} \right) \left(\frac{\mathrm{WT}_i}{\mathrm{WT}_{\mathrm{std}}} \right)^{0.75}$$

In this equation, as PMA increases the maturation term tends to 1, and is 0.5 at the time of half-maturation (TM50). In a PBPK model describing subjects of a range of ages, underlying data on the relationship between age and weight are crucial. Such data for humans can be found in the published Center for Disease Control (CDC) tables [59] or from the model of Sumpter and Holford [60]. As an example, Figure 2.8 shows the relationship between predicted GFR, weight, and age represented by the two different models [47, 61]. Underlying the predictions is the age–weight relationship of Sumpter and Holford [60]. Maturation effects of GFR are clearly evident below the age of three months. A simple maturation model for intrinsic clearance is implemented in the example model on lines 163–164.

2.6.9 Interspecies Scaling

Scaling of kinetic across species (such as for predicting first in man [FIM] kinetics) is a useful application of PBPK models, and is facilitated by the ability to separate "pharmacology" and "physiology" in PBPK models. Physiology (organ size and blood flows) can be scaled using allometric principles as described above, while pharmacology (protein binding, enzyme, and transporter activity) can be preserved or adapted as inferred from in vitro data or an understanding of mechanisms.

Sources of physiological data for humans and rats, dogs, monkeys, sheep, and pigs have been tabulated [11–13]. However, many of these values are compiled from the literature with measurements made using a variety of methods. There remains a place in the literature for a database of physiological values based on systematic measurement across a range of species, ages, and sex. When scaling across species, it is important to account for differences in body composition as well as size. The percentage of body fat and relative size of the liver for example can vary widely across species [13].

It has been proposed that protein binding is more variable in plasma between species than in tissues [62]; hence, accounting for free fraction differences in plasma is important for scaling between species.

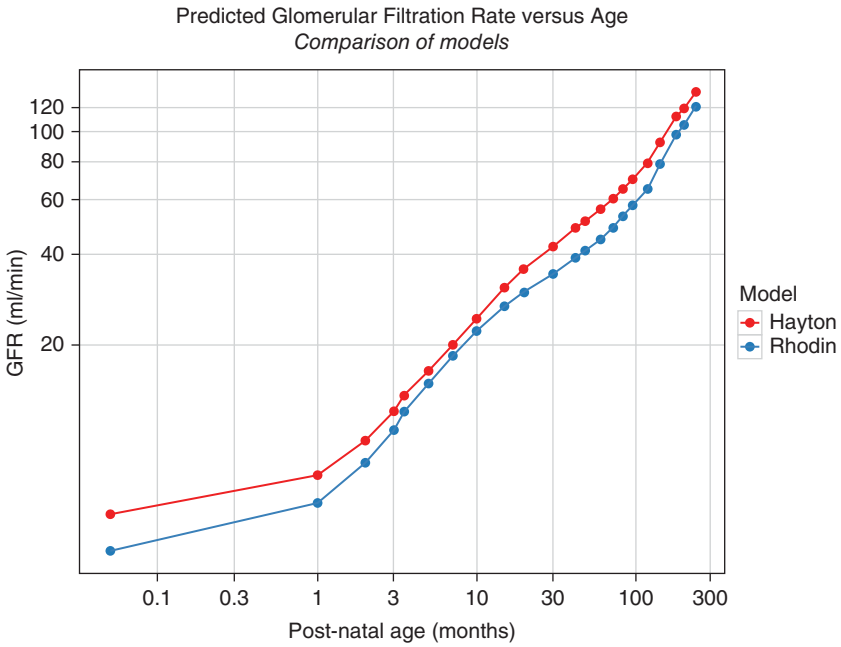

Figure 2.8 Maturation models of glomerular filtration rate (GFR). The relationship between post-natal age and GFR predicted by the submodels of Hayton [61] and Rhodin et al. [47]. Weight for Age was predicted using the Sumpter and Holford model [60] for each. Source: Benson and Roberts [1]. Copyright © 2016 Wiley, Inc.

2.6.10 Between-Subject Variability

PBPK modeling has traditionally been used to represent an "average" or "typical" subject based on parameters that are representative of the average subject in a population. This is often sufficient to examine hypotheses about general mechanisms. However, the utility of "Population"-based analyses [63] with representations of between-subject variability is well established. For example, for drug exposure, it is the subjects at the tails of the distribution of exposure in a population that are of most clinical interest. PBPK models can be used to simulate populations of subjects by assigning distributions (e.g. normal, log-normal, binomial) to the parameters values and randomly sampling parameter values from the distributions [6, 64]. However, a thoughtful covariance structure should ideally be used for the parameter distributions. For example, if separate normal distributions were used for age and weight, without a covariance structure specifying the correlation between them, it is possible to simulate unrealistically young heavy subjects and old light subjects. Using PBPK models to fit multisubject population data is rare in the literature in part due to the long fitting times even with multiprocessor

estimation algorithms, but examples using Semi-PBPK models include models of fentanyl [65] and leflunomide [51]. Between-subject variability is added to the parameter for gastro-intestinal tract (GIT) blood flow in the example model on lines 94–95.

2.6.11 Sensitivity Analysis

PBPK models are characterized by large numbers of parameters, and it is common for some of the parameters to have minimal influence on the predictions of the model in selected scenarios. The importance of parameters in a given scenario can be examined via a simulation-based sensitivity analyses [66]. These methods include local and global sensitivity analyses [66, 67]. In a local sensitivity analysis, model parameters are perturbed one at a time according to predefined fractional changes (e.g. 0.90, 0.95, 1, 1.05, and 1.10 times) from the final parameter values. The resultant changes to model predictions (e.g. exposure through AUC_{inf} and C_{max}) are also summarized as fractional changes from the original model estimations (i.e. when the fractional change in the parameter X was 0.90, the fractional change in AUC_{inf} was Y). The parameter's sensitivity can also be summarized graphically as plots of fractional change in exposure metric vs. fractional change in parameter value for each parameter of the model (Figure 2.9). Sensitivity coefficients can also be calculated and summarized as the average slope of the change in fractional AUC or C_{max} over fractional change in parameter. For sensitivity coefficients, a value of 0 indicates that the exposure metric is not affected by parameter, a value of 1 indicates that the exposure metric doubles for a doubling of parameter value, and a value of −1 indicates that the exposure metric halves for a doubling of parameter value. In a global sensitivity analysis, multiple model parameters are perturbed simultaneously [66, 67]. Using this approach is physiologically more realistic, as typically several model parameters are correlated and would not change independently; albeit it is computationally more difficult, time consuming, and not always necessary to move forward with the model or study design [66, 67].

2.6.12 Pharmacodynamics

Pharmacodynamic (PD) relationships for PBPK models are as important as they are for any other pharmacokinetic model [68]. The principles of linking pharmacodynamic models to PBPK models are generally the same as those for compartmental pharmacokinetic models [69]. However, PBPK models have the advantage that drug concentrations in organs (the target organ) or specific sites in the vasculature (e.g. arterial or venous plasma) or within an organ can be linked to drug effect. This can be advantageous for some classes of drugs where the site of drug action is well understood (e.g. the Central Nervous System [CNS] for anesthetics

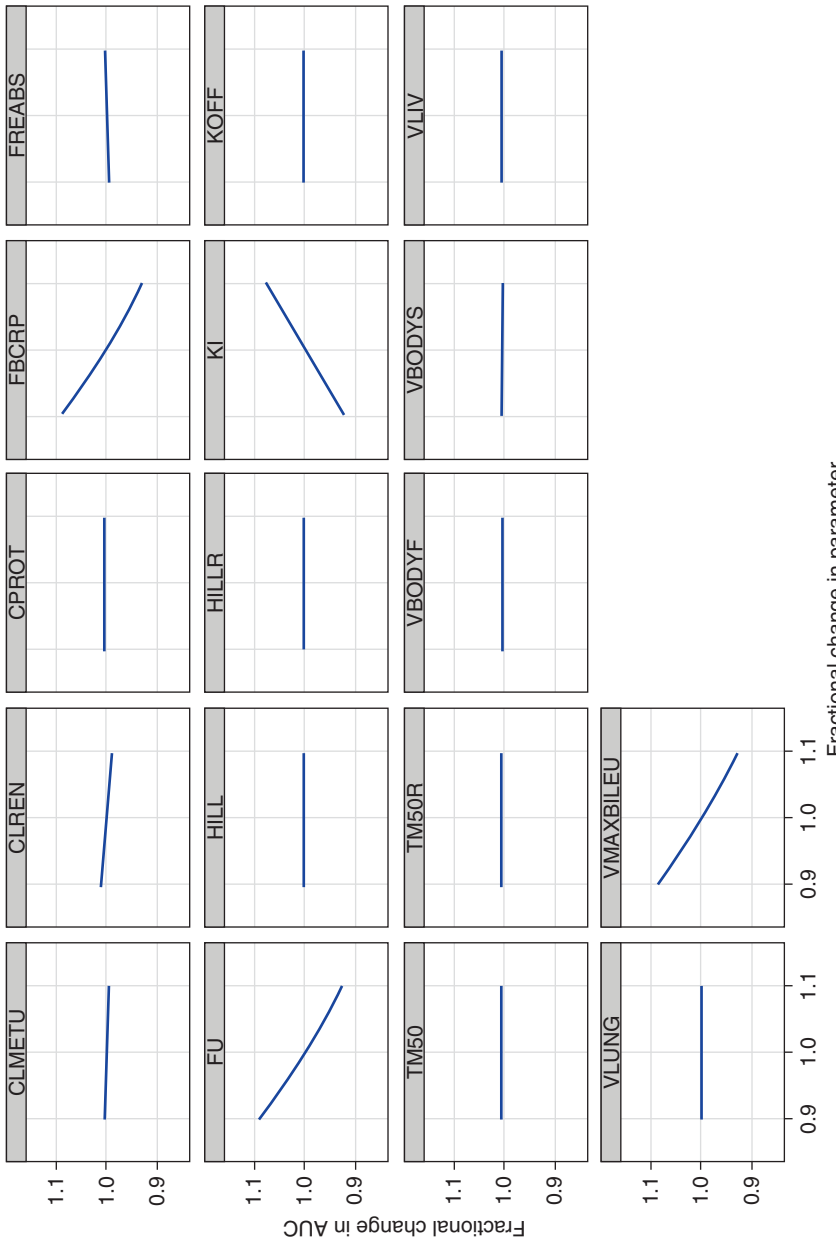

Figure 2.9 Sensitivity analysis of AUC predictions for a semi-PBPK model. Each panel shows sensitivity data for one parameter of the model (the meaning of the parameter is not important here). The fractional change in the exposure metric AUC is shown plotted against the corresponding fractional change in the parameter value. In this model and dosing scenario, AUC is seen to be most sensitive to the parameters FBCRP, FU, KI, and VMAXBILEU.

or the myocardium for cardioactive drugs). Using drug concentrations in the target organ rather than the plasma to drive pharmacodynamic effects may obviate the need for an empirical effect compartment [65]. A simple pharmacodynamic model driven by the myocardial concentrations of a drug is implemented in line 158 of the example model.

2.7 Summary

The current rise in the rate of publication and application of PBPK models is likely to be sustained in the foreseeable future. Contributing factors will likely be the wider use of commercial PBPK models to address drug development and clinical problems, the advent of broader collective efforts to advance and coordinate PBPK [8, 9, 70] and Systems Biology [71] modeling, and the increasing ease with which bespoke PBPK models can be coded and shared [72]. On top of this, there is growing recognition that a literature populated with multiple "top-down" models of the same drug/disease confound rather than contribute to a broader understanding. As efforts move to creating "meta" models from these publications across drugs and diseases, there is likely to be a concurrent move from empirical to mechanistic models that will ultimately improve drug delivery.

References

1 Benson, H.A.E. and Roberts, M. (eds.) (2016). *Encyclopedia of Controlled Drug Delivery*, 2ee. Wiley.
2 Rostami-Hodjegan, A. (2012). Physiologically based pharmacokinetics joined with in vitro-in vivo extrapolation of ADME: a marriage under the arch of systems pharmacology. *Clin. Pharmacol. Ther.* 92 (1): 50–61.
3 Wajima, T., Isbister, G.K., and Duffull, S.B. (2009). A comprehensive model for the humoral coagulation network in humans. *Clin. Pharmacol. Ther.* 86 (3): 290–298.
4 Gulati, A., Isbister, G.K., and Duffull, S.B. (2014). Scale reduction of a systems coagulation model with an application to modeling pharmacokinetic-pharmacodynamic data. *CPT Pharmacometrics Syst. Pharmacol.* 3: e90.
5 Upton, R.N. and Ludbrook, G. (2005). A physiologically based, recirculatory model of the kinetics and dynamics of propofol in man. *Anesthesiology* 103 (2): 344–352.
6 Jamei, M., Dickinson, G.L., and Rostami-Hodjegan, A. (2009). A framework for assessing inter-individual variability in pharmacokinetics using virtual human populations and integrating general knowledge of physical chemistry,

biology, anatomy, physiology and genetics: a tale of 'bottom-up' vs 'top-down' recognition of covariates. *Drug Metab. Pharmacokinet.* 24 (1): 53–75.

7 Rowland, M., Lesko, L.J., and Rostami-Hodjegan, A. (2015). Physiologically based pharmacokinetics is impacting drug development and regulatory decision making. *CPT Pharmacometrics Syst. Pharmacol.* 4 (6): 313–315.

8 Lennernäs, H., Aarons, L., Augustijns, P. et al. (2014). Oral biopharmaceutics tools – time for a new initiative – an introduction to the IMI project OrBiTo. *Eur. J. Pharm. Sci.* 57: 292–299.

9 Swat, M.J., Moodie, S., Wimalaratne, S.M. et al. (2015). Pharmacometrics markup language (PharmML): opening new perspectives for model exchange in drug development. *CPT Pharmacometics Syst. Pharmacol.* 4 (6): 316–319.

10 Price, P.S., Conolly, R.B., Chaisson, C.F. et al. (2003). Modeling interindividual variation in physiological factors used in PBPK models of humans. *Crit. Rev. Toxicol.* 33 (5): 469–503.

11 Brown, R.P., Delp, M.D., Lindstedt, S.L. et al. (1997). Physiological parameter values for physiologically based pharmacokinetic models. *Toxicol. Ind. Health* 13 (4): 407–484.

12 Clewell, R.A. and Clewell, H.J. (2008). Development and specification of physiologically based pharmacokinetic models for use in risk assessment. *Regul. Toxicol. Pharm.* 50 (1): 129–143.

13 Upton, R.N. (2008). Organ weights and blood flows of sheep and pig for physiological pharmacokinetic modelling. *J. Pharmacol. Toxicol. Methods* 58 (3): 198–205.

14 Upton, R.N. and Doolette, D.J. (1999). Kinetic aspects of drug disposition in the lungs. *Clin. Exp. Pharmacol. Physiol.* 26 (5–6): 381–391.

15 Ai, N., Fan, X., and Ekins, S. (2015). In silico methods for predicting drug-drug interactions with cytochrome P-450s, transporters and beyond. *Adv. Drug Delivery Rev.* 86: 46–60.

16 Small, H., Gardner, I., Jones, H.M. et al. (2011). Measurement of binding of basic drugs to acidic phospholipids using surface plasmon resonance and incorporation of the data into mechanistic tissue composition equations to predict steady-state volume of distribution. *Drug Metab. Dispos.* 39 (10): 1789–1793.

17 Yeo, K.R., Jamei, M., and Rostami-Hodjegan, A. (2013). Predicting drug-drug interactions: application of physiologically based pharmacokinetic models under a systems biology approach. *Expert Rev. Clin. Pharmacol.* 6 (2): 143–157.

18 Poulin, P. and Haddad, S. (2013). Toward a new paradigm for the efficient in vitro-in vivo extrapolation of metabolic clearance in humans from hepatocyte data. *J. Pharm. Sci.* 102 (9): 3239–3251.

19 Heikkinen, A.T., Lignet, F., Cutler, P., and Parrott, N. (2015). The role of quantitative ADME proteomics to support construction of physiologically

based pharmacokinetic models for use in small molecule drug development. *Proteomics Clin. Appl.* 9 (7–8): 732–744.

20 Pan, Y., Grillo, J., Hsu, V. et al. (2014). Application of the FDA PBPK knowledgebase in evaluating model predictability for drug-drug interactions. *Clin. Pharmacol. Ther.* 95: S102–S103.

21 Sager, J.E., Yu, J., Ragueneau-Majlessi, I., and Isoherranen, N. (2015). Physiologically based pharmacokinetic (PBPK) modeling and simulation approaches: a systematic review of published models, applications, and model verification. *Drug Metab. Dispos.* 43 (11): 1823–1837.

22 Chen, Y., Jin, J.Y., Mukadam, S. et al. (2012). Application of IVIVE and PBPK modeling in prospective prediction of clinical pharmacokinetics: strategy and approach during the drug discovery phase with four case studies. *Biopharm. Drug Dispos.* 33 (2): 85–98.

23 Maharaj, A.R. and Edginton, A.N. (2014). Physiologically based pharmacokinetic modeling and simulation in pediatric drug development. *CPT Pharmacometics Syst. Pharmacol.* 3: e150.

24 Rioux, N. and Waters, N.J. (2016). Physiologically-based pharmacokinetic modeling in pediatric oncology drug development. *Drug Metab. Dispos.* 44 (7): 934–943.

25 Offman, E. and Edginton, A.N. (2015). A PBPK workflow for first-in-human dose selection of a subcutaneously administered pegylated peptide. *J. Pharmacokinet. Pharmacodyn.* 42 (2): 135–150.

26 Allan, G., Davis, J., Dickins, M. et al. (2008). Pre-clinical pharmacokinetics of UK-453,061, a novel non-nucleoside reverse transcriptase inhibitor (NNRTI), and use of in silico physiologically based prediction tools to predict the oral pharmacokinetics of UK-453,061 in man. *Xenobiotica* 38 (6): 620–640.

27 Jones, H.M., Mayawala, K., and Poulin, P. (2013). Dose selection based on physiologically based pharmacokinetic (PBPK) approaches. *AAPS J.* 15 (2): 377–387.

28 Chetty, M., Rose, R.H., Abduljalil, K. et al. (2014). Applications of linking PBPK and PD models to predict the impact of genotypic variability, formulation differences, differences in target binding capacity and target site drug concentrations on drug responses and variability. *Front. Pharmacol.* 5: 258.

29 Kostewicz, E.S., Aarons, L., Bergstrand, M. et al. (2014). PBPK models for the prediction of in vivo performance of oral dosage forms. *Eur. J. Pharm. Sci.* 57: 300–321.

30 Parrott, N., Lukacova, V., Fraczkiewicz, G., and Bolger, M.B. (2009). Predicting pharmacokinetics of drugs using physiologically based modeling – application to food effects. *AAPS J.* 11 (1): 45–53.

31 Lukacova, V., Woltosz, W.S., and Bolger, M.B. (2009). Prediction of modified release pharmacokinetics and pharmacodynamics from in vitro, immediate release, and intravenous data. *AAPS J.* 11 (2): 323–334.

32 Agoram, B., Woltosz, W.S., and Bolger, M.B. (2001). Predicting the impact of physiological and biochemical processes on oral drug bioavailability. *Adv. Drug Delivery Rev.* 50 (Suppl. 1): S41–S67.

33 Kesisoglou, F., Balakrishnan, A., and Manser, K. (2015). Utility of PBPK absorption modeling to guide modified release formulation development of gaboxadol, a highly soluble compound with region-dependent absorption. *J. Pharm. Sci.* 105 (2): 722–728.

34 Wang, B., Liu, Z., Li, D. et al. (2015). Application of physiologically based pharmacokinetic modeling in the prediction of pharmacokinetics of bicyclol controlled-release formulation in human. *Eur. J. Pharm. Sci.* 77: 265–272.

35 Kesisoglou, F., Xia, B., and Agrawal, N.G.B. (2015). Comparison of deconvolution-based and absorption modeling IVIVC for extended release formulations of a BCS III drug development candidate. *AAPS J.* 17 (6): 1492–1500.

36 Chow, E.C.Y. and Pang, K.S. (2013). Why we need proper PBPK models to examine intestine and liver oral drug absorption. *Curr. Drug Metab.* 14 (1): 57–79.

37 Yu, L.X., Lipka, E., Crison, J.R., and Amidon, G.L. (1996). Transport approaches to the biopharmaceutical design of oral drug delivery systems: prediction of intestinal absorption. *Adv. Drug Delivery Rev.* 19 (3): 359–376.

38 Jamei, M., Marciniak, S., Edwards, D. et al. (2013). The simcyp population based simulator: architecture, implementation, and quality assurance. *In Silico Pharmacol.* 1: 9.

39 Ni, P.F., Ho, N.F.H., Fox, J.L. et al. (1980). Theoretical model studies of intestinal drug absorption V. Non-steady-state fluid flow and absorption. *Int. J. Pharm.* 5 (1): 33–47.

40 Zhang, D., Zhu, M., and Humphreys, W.G. (2007). *Drug Metabolism in Drug Design and Development*. Wiley.

41 Worley, R.R. and Fisher, J. (2015). Application of physiologically-based pharmacokinetic modeling to explore the role of kidney transporters in renal reabsorption of perfluorooctanoic acid in the rat. *Toxicol. Appl. Pharmacol.* 289 (3): 428–441.

42 Feng, B., Varma, M.V., Costales, C. et al. (2014). In vitro and in vivo approaches to characterize transporter-mediated disposition in drug discovery. *Expert Opin. Drug Discovery* 9 (8): 873–890.

43 Upton, R.N. (2002). Theoretical aspects of P-glycoprotein mediated drug efflux on the distribution volume of anaesthetic-related drugs in the brain. *Anaesth. Intensive Care* 30 (2): 183–191.

44 Wang, Q., Zheng, M., and Leil, T. (2017). Investigating transporter-mediated drug-drug interactions using a physiologically based pharmacokinetic model of rosuvastatin. *CPT Pharmacometics Syst. Pharmacol.* 6 (4): 228–238.

45 Vogel, C. and Marcotte, E.M. (2012). Insights into the regulation of protein abundance from proteomic and transcriptomic analyses. *Nat. Rev. Genet.* 13 (4): 227–232.

46 DeWoskin, R.S. and Thompson, C.M. (2008). Renal clearance parameters for PBPK model analysis of early lifestage differences in the disposition of environmental toxicants. *Regul. Toxicol. Pharm.* 51 (1): 66–86.

47 Rhodin, M.M., Anderson, B.J., Peters, A.M. et al. (2009). Human renal function maturation: a quantitative description using weight and postmenstrual age. *Pediatr. Nephrol.* 24 (1): 67–76.

48 Hammarlund-Udenaes, M. (2010). Active-site concentrations of chemicals – are they a better predictor of effect than plasma/organ/tissue concentrations? *Basic Clin. Pharmacol. Toxicol.* 106 (3): 215–220.

49 van Steeg, T.J., Boralli, V.B., Krekels, E.H.J. et al. (2009). Influence of plasma protein binding on pharmacodynamics: estimation of in vivo receptor affinities of beta blockers using a new mechanism-based PK-PD modelling approach. *J. Pharm. Sci.* 98 (10): 3816–3828.

50 Hooker, A.C., Ten Tije, A.J., Carducci, M.A. et al. (2008). Population pharmacokinetic model for docetaxel in patients with varying degrees of liver function: incorporating cytochrome P4503A activity measurements. *Clin. Pharmacol. Ther.* 84 (1): 111–118.

51 Hopkins, A.M., Wiese, M.D., Proudman, S.M. et al. (2015). Semiphysiologically based pharmacokinetic model of leflunomide disposition in rheumatoid arthritis patients. *CPT Pharmacometics Syst. Pharmacol.* 4 (6): 362–371.

52 Baker, M. and Parton, T. (2007). Kinetic determinants of hepatic clearance: plasma protein binding and hepatic uptake. *Xenobiotica* 37 (10–11): 1110–1134.

53 Samant, T.S., Mangal, N., Lukacova, V., and Schmidt, S. (2015). Quantitative clinical pharmacology for size and age scaling in pediatric drug development: a systematic review. *J. Clin. Pharmacol.* 55 (11): 1207–1217.

54 West, G.B. and Brown, J.H. (2005). The origin of allometric scaling laws in biology from genomes to ecosystems: towards a quantitative unifying theory of biological structure and organization. *J. Exp. Biol.* 208 (Pt 9): 1575–1592.

55 (1979). Report of the task group on reference man. *Ann. ICRP* 3 (1–4): iii.

56 Anderson, B.J. and Holford, N.H.G. (2008). Mechanism-based concepts of size and maturity in pharmacokinetics. *Annu. Rev. Pharmacol. Toxicol.* 48: 303–332.

57 Upreti, V.V. and Wahlstrom, J.L. (2016). Meta-analysis of hepatic cytochrome P450 ontogeny to underwrite the prediction of pediatric pharmacokinetics using physiologically based pharmacokinetic modeling. *J. Clin. Pharmacol.* 56 (3): 266–283.

58 Anderson, B.J. and Holford, N.H.G. (2011). Tips and traps analyzing pediatric PK data. *Paediatr. Anaesth.* 21 (3): 222–237.
59 Growth Charts – Percentile Data Files with LMS Values. https://www.cdc.gov/growthcharts/percentile_data_files.htm.
60 Sumpter, A.L. and Holford, N.H.G. (2011). Predicting weight using postmenstrual age–neonates to adults. *Paediatr. Anaesth.* 21 (3): 309–315.
61 Hayton, W.L. (2000). Maturation and growth of renal function: dosing renally cleared drugs in children. *AAPS PharmSci* 2 (1): E3.
62 Rodgers, T., Leahy, D., and Rowland, M. (2005). Physiologically based pharmacokinetic modeling 1: predicting the tissue distribution of moderate-to-strong bases. *J. Pharm. Sci.* 94 (6): 1259–1276.
63 Mould, D.R. and Upton, R.N. (2012). Basic concepts in population modeling, simulation, and model-based drug development. *CPT Pharmacometics Syst. Pharmacol.* 1: e6.
64 Rostami-Hodjegan, A. and Tucker, G. (2004). 'In silico' simulations to assess the 'in vivo' consequences of 'in vitro' metabolic drug–drug interactions. *Drug Discovery Today Technol.* 1 (4): 441–448.
65 Upton, R.N., Foster, D.J.R., Christrup, L.L. et al. (2012). A physiologically-based recirculatory meta-model for nasal fentanyl in man. *J. Pharmacokinet. Pharmacodyn.* 39 (5): 561–576.
66 Felmlee, M.A., Krzyzanski, W., Morse, B.L., and Morris, M.E. (2011). Use of a local sensitivity analysis to inform study design based on a mechanistic toxicokinetic model for γ-hydroxybutyric acid. *AAPS J.* 13 (2): 240–254.
67 Saltelli, A., Tarantola, S., and Chan, K.-S. (1999). A quantitative model-independent method for global sensitivity analysis of model output. *Technometrics* 41 (1): 39–56.
68 Perera, V., Elmeliegy, M.A., Rao, G., and Forrest, A. (2013). The link between pharmacodynamics and physiologically based pharmacokinetic models. *Clin. Pharmacol. Ther.* 93 (2): 151–152.
69 Upton, R.N. and Mould, D.R. (2014). Basic concepts in population modeling, simulation, and model-based drug development: Part 3 – Introduction to pharmacodynamic modeling methods. *CPT Pharmacometics Syst. Pharmacol.* 3: e88.
70 Harnisch, L., Matthews, I., Chard, J., and Karlsson, M.O. (2013). Drug and disease model resources: a consortium to create standards and tools to enhance model-based drug development. *CPT Pharmacometics Syst. Pharmacol.* 2: e34.
71 Dräger, A. and Palsson, B.Ø. (2014). Improving collaboration by standardization efforts in systems biology. *Front. Bioeng. Biotechnol.* 2: 61.
72 Wojciechowski, J., Hopkins, A.M., and Upton, R.N. (2015). Interactive pharmacometric applications using R and the shiny package. *CPT Pharmacometics Syst. Pharmacol.* 4 (3): e00021.

3

Oral Delivery and Pharmacokinetic Models

Wojciech Krzyzanski

University at Buffalo, Department of Pharmaceutical Sciences, Buffalo, NY, USA

3.1 Introduction

Oral drug absorption consists of multiple stages that include delivery to the intestine (disintegration, dissolution, degradation, gastric emptying, intestinal transit), absorption from the lumen (dissolution permeability, intestinal efflux, and transport), first-pass metabolism in the gut, and subsequent first-pass hepatic extraction. The factors controlling the rate and extent of drug absorption are dosage form, physicochemical and biopharmaceutical properties of the drug, and physiology of the gastrointestinal (GI) tract [1]. Additional information about the physiology of the GI tract and about optimizing oral delivery concerning these factors may be found in Chapter 4 of this volume on oral-site-directed delivery. Pharmacokinetic (PK) models of oral drug absorption are meant to quantify in the form of mathematical equations both the processes and factors to describe available data and to predict outcomes of interest under new conditions. The predictive PK absorption models can be used to determine the rate and extent of oral drug absorption, facilitate lead drug candidate selection, establish formulation development strategy, and support the development of regulatory policies [2].

Experimental data used for development of PK models determine the level of adequacy in describing absorption processes. Drug plasma concentration time courses following oral administration are by far most useful sources of information about the absorption rate and extent. To assess the fraction of dose that reaches the systemic circulation, oral data must be accompanied by drug plasma concentration time profiles following an intravenous input. Tablet movement through the GI tract can be studied with magnetic marker monitoring (MMM), an imaging technique for the investigation of the behavior of solid oral

Drug Delivery Approaches: Perspectives from Pharmacokinetics and Pharmacodynamics,
First Edition. Edited by Bret Berner, Toufigh Gordi, Heather A. E. Benson, and Michael S. Roberts.

dosage forms within the GI tract [3]. Plasma concentrations of drug from the superior mesenteric artery and portal vein of the perfused intestinal preparation can be used to assess intestinal metabolism in rats [4]. Total mucosal tissue and microsomes from human and rat small intestines are used to quantify the expression of metabolic enzymes and transporters contributing to the intestinal first-pass metabolism [5]. Monolayers of human colon adenocarcinoma (Caco-2) and Madin-Darby canine kidney (MDCK) cell lines are used to measure passive transport of drug through the intestinal membranes [6, 7].

The purpose of this chapter is to provide a brief overview of current PK modeling approaches for oral absorption. In the following sections, there are introduced the most commonly applied approaches exemplified by a few representative models. Model structures are introduced and the basic properties are briefly explained. Each model is followed by examples of drugs and absorption data the model was applied to.

3.2 Compartmental Models

Mammillary compartmental models are the most commonly applied tools to describe drug disposition. The central compartment is interpreted as the plasma compartment, whereas the peripheral compartments represent tissue, organ, and other possible extravascular distribution sites. The drug absorption process has been also modeled as a single compartment or series of compartments mimicking the stages a drug molecule encounters between its dissolution in the GI tract and reaching the systemic circulation. In the following sections, several compartmental models are discussed as representatives of this modeling approach.

3.2.1 First-Order Absorption

The most commonly used assumption about oral absorption is as a first-order process. The amount of drug in the absorption site A_a is described by one compartment with a first-order absorption rate constant k_a that feeds into the plasma compartment A_p:

$$\frac{dA_a}{dt} = -k_a A_a \tag{3.1}$$

$$\frac{dA_p}{dt} = k_a A_a - k_{el} A_p \tag{3.2}$$

where k_{el} is the elimination rate constant. The initial conditions assume the Dose of the drug was instantaneously administered to the absorption site, but only a

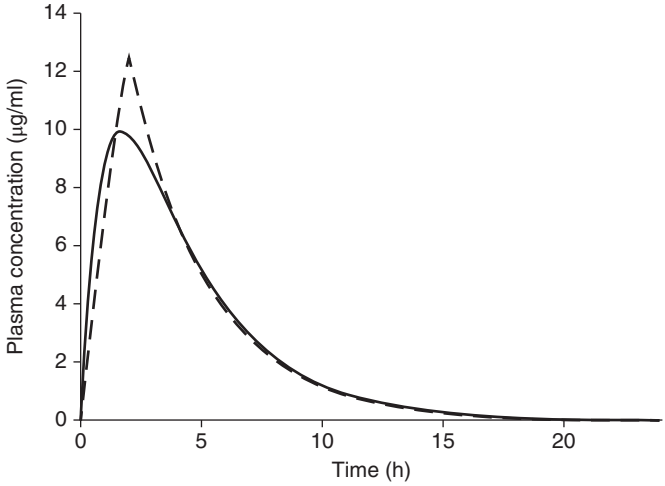

Figure 3.1 Time courses of plasma concentration for the first-order absorption (solid line) and zero-order absorption (dashed line) models. Parameter values used for simulations were Dose = 100 mg, $V_p = 3$ l, $k_{el} = 0.3\,h^{-1}$, $k_a = 1\,h^{-1}$, $F = 0.5$, and $T_{abs} = 2$ h.

fraction $0 < F \leq 1$ reaches the plasma compartment:

$$A_a(0) = F\text{Dose} \quad \text{and} \quad A_p(0) = 0 \tag{3.3}$$

F is referred to as the bioavailability. Bioavailability can be defined as the fraction of administered dose that reaches the systemic circulation. The explicit solution to Eq. (3.2) is known as the Bateman function:

$$A_p = \frac{F\text{Dose}\, k_a}{k_a - k_{el}} \left(e^{-k_{el}t} - e^{-k_a t}\right) \tag{3.4}$$

The time course of the drug concentration in plasma $C_p = A_p/V_p$ described by the Bateman function, where V_p is the volume of the plasma compartment, is shown in Figure 3.1. The peak time t_{max} and the peak concentration C_{pmax} are given by the following equations:

$$t_{max} = \frac{\ln\left(k_a/k_{el}\right)}{k_a - k_{el}} \quad \text{and} \quad C_{pmax} = \frac{F\text{Dose}}{V_p}\left(\frac{k_a}{k_{el}}\right)^{\frac{-k_{el}}{k_a - k_{el}}} \tag{3.5}$$

The one-compartment disposition model Eq. (3.2) can be expanded by a peripheral (extravascular, tissue) compartment or more complex multi compartmental disposition model. An example of a drug successfully described by a first-order absorption model is theophylline administered to healthy subjects as a single oral dose [8].

3.2.2 Zero-Order Absorption

Another assumption about the absorption rate that is often applied is a zero-order process. This is modeled by one compartment (plasma) with an infusion-like input:

$$\frac{\mathrm{d}A_\mathrm{p}}{\mathrm{d}t} = \frac{F\mathrm{Dose}}{T_\mathrm{abs}}\theta\left(T_\mathrm{abs} - t\right) - k_\mathrm{el}A_\mathrm{p} \quad \text{and} \quad A_\mathrm{a}(0) = 0 \tag{3.6}$$

where T_abs is the duration of the absorption process or the constant infusion and $\theta(x)$ is the step function $\theta(x) = 1$ for $0 \le x$ and $\theta(x) = 0$ for $x < 0$. The explicit solution to Eq. (3.6) is identical to the equation for drug amount in the plasma following short infusion:

$$A_\mathrm{p} = \begin{cases} \frac{F\mathrm{Dose}}{T_\mathrm{abs}k_\mathrm{el}}\left(1 - e^{-k_\mathrm{el}t}\right), & \text{if } \ 0 < t < T_\mathrm{abs} \\ \frac{F\mathrm{Dose}}{T_\mathrm{abs}k_\mathrm{el}}\left(1 - e^{-k_\mathrm{el}T_\mathrm{abs}}\right)e^{-k_\mathrm{el}(t-T_\mathrm{abs})}, & \text{if } \ t \ge T_\mathrm{abs} \end{cases} \tag{3.7}$$

A time course of the drug concentration in plasma following the zero-order absorption input is shown in Figure 3.1. The peak time coincides with T_abs and the peak concentration can be obtained from Eq. (3.7) by evaluating C_p at $t = T_\mathrm{abs}$. A typical zero-order absorption can be observed for cyclosporin A administered orally in healthy subjects [9].

3.2.3 Absorption Delay

A standard approach to account for absorption delay is to include a lag time t_lag that passes after dose administration and observation of drug in plasma above the limit of quantification. To introduce a lag time in the absorption model, one needs to delay by t_lag the dosing event and set the initial condition at the time of the lag time to 0. The first-order absorption model Eq. (3.1) with a lag time becomes

$$\frac{\mathrm{d}A_\mathrm{a}}{\mathrm{d}t} = F\mathrm{Dose}\delta\left(t - t_\mathrm{lag}\right) - k_\mathrm{a}A_\mathrm{a} \quad \text{and} \quad A_\mathrm{a}(0) = 0 \tag{3.8}$$

where $\mathrm{Dose}\delta(t - t_\mathrm{lag})$ represents an input of a bolus Dose at time t_lag. Introducing a lag time to the zero-order absorption model requires a start of absorption rate at $t = t_\mathrm{lag}$ and an end at $t = T_\mathrm{abs} + t_\mathrm{lag}$:

$$\frac{\mathrm{d}A_\mathrm{p}}{\mathrm{d}t} = \frac{F\mathrm{Dose}}{T_\mathrm{abs}}\theta\left(T_\mathrm{abs} + t_\mathrm{lag} - t\right)\theta\left(t - t_\mathrm{lag}\right) - \frac{\mathrm{CL}}{V_\mathrm{p}}A_\mathrm{p} \tag{3.9}$$

with the zero initial condition $A_\mathrm{p}(0) = 0$. Time courses of C_p for first-order and zero-order input models with a lag time are shown in Figure 3.2. Addition of a lag time to the model shifts the C_p vs. t curve by t_lag units of time. One-compartment first-order absorption model with a lag time was used to describe plasma concentrations of propoxyphene in healthy volunteers [10].

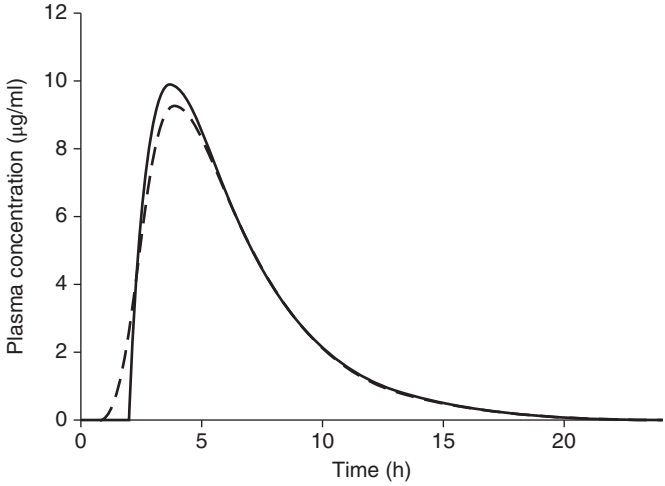

Figure 3.2 Time courses of plasma concentration for the first-order absorption with lag time (solid line) and transit compartment (dashed line) models. Parameter values used for simulations were Dose = 100 mg, $V_p = 3$ l, $k_{el} = 0.3\,h^{-1}$, $k_a = 1\,h^{-1}$, $F = 0.5$, $t_{lag} = 2$ h, and MTT = 2 h, and the number of transit compartments was $n = 10$.

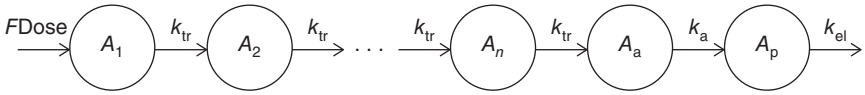

Figure 3.3 Schematic diagram of the transit compartment model of absorption delay.

A major flaw of the lag time-based delay is a discontinuity in the absorption rate. Often a delay manifests itself as a gradual slow increasing onset of the C_p vs. t data indicating a continuous input rate. A transit compartment model has been introduced to alleviate deficiencies of the lag time [11]. In this approach, an absorption delay is described by the mean transit time (MTT) of a drug molecule through a sequence of n compartments connected with each other by the same first-order transfer rate constant k_{tr} (see Figure 3.3):

$$\text{MTT} = \frac{n}{k_{tr}} \tag{3.10}$$

The output from the last nth transit compartment is the input to the absorption compartment:

$$\frac{dA_1}{dt} = -k_{tr}A_1 \quad \text{and} \quad A_1(0) = F\text{Dose} \tag{3.11}$$

$$\frac{dA_i}{dt} = k_{tr}\left(A_{i-1} - A_i\right) \quad \text{and} \quad A_i(0) = 0, \qquad i = 2, \ldots, n \tag{3.12}$$

$$\frac{\mathrm{d}A_\mathrm{a}}{\mathrm{d}t} = k_\mathrm{tr}A_n - k_\mathrm{a}A_\mathrm{a} \quad \text{and} \quad A_\mathrm{a}(0) = 0 \tag{3.13}$$

As for the first-order absorption model, the absorption rate constant k_a determines the input to the plasma compartment Eq. (3.2). An explicit solution for the drug amount in the nth transit compartment,

$$A_n = \frac{F\mathrm{Dose}\left(k_\mathrm{tr}t\right)^{n-1}}{(n-1)!}\mathrm{e}^{-k_\mathrm{tr}t} \tag{3.14}$$

permits substitution of Eq. (3.14) for the input rate in Eq. (3.13) and ignore the transit compartment Eqs. (3.11)–(3.12):

$$\frac{\mathrm{d}A_\mathrm{a}}{\mathrm{d}t} = \frac{F\mathrm{Dose}k_\mathrm{tr}\left(k_\mathrm{tr}x\right)^{n-1}}{\Gamma(n)}\mathrm{e}^{-k_\mathrm{tr}t} - k_\mathrm{a}A_\mathrm{a} \tag{3.15}$$

The gamma function simplifies to $\Gamma(n) = (n-1)!$ for integer n, but it permits any real value of $n > 0$. A time course of C_p for a transit compartment model is shown in Figure 3.2. The transit compartment model was tested on PK data of glibenclamide, furosemide, amiloride, and moxonidine [11].

3.2.4 Parallel Inputs

To account for the double peak phenomenon in the C_p vs. time curve, the concept of parallel inputs has been introduced. In principle, multiple peaks are explained by differences in input rates to the plasma compartment from the absorption site. The parallel input models consist of two processes occurring simultaneously with different rates and different delay times. The two-parallel first-order absorption model consists of two absorption compartments A_a1 and A_a2 with lag times t_lag1 and t_lag2 independently feeding into the plasma compartment A_p:

$$\frac{\mathrm{d}A_\mathrm{a1}}{\mathrm{d}t} = Ff\mathrm{Dose}\delta\left(t - t_\mathrm{lag1}\right) - k_\mathrm{a1}A_\mathrm{a1} \quad \text{and} \quad A_\mathrm{a1}(0) = 0 \tag{3.16}$$

$$\frac{\mathrm{d}A_\mathrm{a2}}{\mathrm{d}t} = F(1-f)\,\mathrm{Dose}\delta\left(t - t_\mathrm{lag2}\right) - k_\mathrm{a2}A_\mathrm{a2} \quad \text{and} A_\mathrm{a2}(0) = 0 \tag{3.17}$$

$$\frac{\mathrm{d}A_\mathrm{p}}{\mathrm{d}t} = k_\mathrm{a1}A_\mathrm{a1} + k_\mathrm{a2}A_\mathrm{a2} - \frac{\mathrm{CL}}{V_\mathrm{p}}A_\mathrm{p} \quad \text{and} \quad A_\mathrm{p}(0) = 0 \tag{3.18}$$

The parameter $0 \le f \le 1$ denotes a fraction of a dose that is absorbed via the first process. A time course of C_p for the two-parallel first-order absorption model is shown in Figure 3.4. The offset part of the curve following the first peak begins during absorption phase of the second slower process resulting in a second peak. Furthermore, the heights of the peaks can be in the opposite order. The first-order

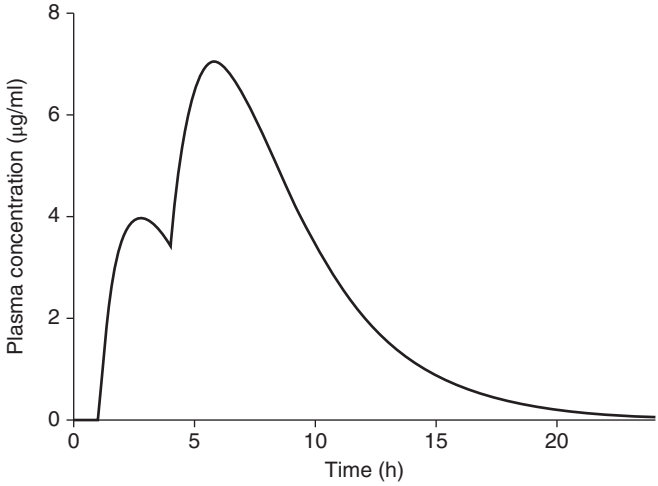

Figure 3.4 Time course of plasma concentration for the parallel input first-order absorption model. Parameter values used for simulations were Dose = 100 mg, $V_p = 3$ l, $k_{el} = 0.3\,h^{-1}$, $k_{a1} = 1\,h^{-1}$, $k_{a2} = 0.6\,h^{-1}$, $F = 0.5$, $f = 0.4$, $t_{lag1} = 1$ h, and $t_{lag2} = 4$ h.

processes can be replaced by the zero-order absorption rates Eq. (3.6). Also, a mixture of the first-order and the zero-order processes can be considered. The absorption delays introduced by the lag times t_{lag1} and t_{lag2} can be modeled using the transit compartments (Eqs. (3.11) and (3.13)) [12].

3.2.5 Discontinuous Absorption

Other concepts than the parallel inputs have been developed to describe the multiple peaks in the C_p vs. time curve. A compartmental model taking into account a discontinuous absorption along the gut has been proposed [13]. In this model, the drug dissolution in the gut is described by a sequence of non-absorbing and absorbing compartments with the last one eliminating drug via the feces. The first-order absorption rate constants from each absorbing compartment into the plasma compartment are allowed to be different from each other. Additionally, each absorption can occur after some time specific for each absorption compartment. This discontinuous absorption model was applied to describe the plasma concentration of ranitidine following a single oral dose administration in healthy subjects [13].

3.2.6 Compartmental Absorption and Transit

The compartmental absorption and transit (CAT) model has been developed to account for gastric emptying and small intestinal transit flow influence on

absorption of drugs in immediate release formulations [14]. The drug transport along the GI tract is described by stomach, seven small intestinal transit, and colonic transit compartments with different transfer rate constants. The absorption to the plasma compartment is possible only from the small intestine and is described as a first-order process. The CAT model was used to simulate oral plasma concentration profiles of atenolol [14]. Atenolol is a β_1-selective β-adrenergic receptor blocking agent.

3.2.7 Gastrointestinal Transit Time

The gastrointestinal transit time (GITT) model extends a drug release, absorption, and disposition model developed by Bergstrand et al. [15] for felodipine extended-release formulation [16]. The drug amount in the tablet is released at zero-order rates to compartments representing regions of the GI tract, fundus, antrum, proximal small intestine, distal small intestine, and colon. The absorption across the GI wall is governed by the first-order rates feeding into the liver compartment that is part of a semi-physiological model that additionally includes a plasma compartment and two peripheral compartments. The discrete movement of tablet along the GI tract is represented by step functions in time, each specific to absorption characteristics of the GI region it is ascribed to [16]. The GITT model was applied to diclofenac data in healthy volunteers receiving enteric-coated tablets. Diclofenac is an anti-inflammatory drug, available in numerous formulations including immediate-, or extended-release tablets.

3.2.8 Other Compartmental Models

The compartmental models presented above do not exhaust a list of mechanistic models describing the oral absorption kinetics which have been developed in the past. For example, a model with different input rates for different time windows has not been discussed [17]. However, provided examples clearly illustrate methodology of modeling the absorption processes using compartmental techniques.

3.3 Empirical Models

Compartmental absorption models often fail to describe plasma concentration–time profiles following oral administration. Less mechanistic empirical models of the absorption rate have been successfully used. They assume that the plasma drug concentration following an oral administration of drug can be decomposed into an independent input process (representing the dissolution and absorption process)

followed by the disposition process. For a simple one compartment disposition model:

$$\frac{\mathrm{d}A_\mathrm{p}}{\mathrm{d}t} = \mathrm{Input}\,(t) - k_\mathrm{el}A \tag{3.19}$$

where k_el is the first-order elimination rate constant from plasma. The amount of drug absorbed up to time t can be calculated by integrating the input rate:

$$A_\mathrm{a}\,(t) = \int_0^t \mathrm{Input}\,(x)\ \mathrm{d}x \tag{3.20}$$

The mean input time can be calculated as:

$$\mathrm{MIT} = \frac{\int_0^\infty t\mathrm{Input}\,(t)\,\mathrm{d}t}{\int_0^\infty \mathrm{Input}\,(t)\,\mathrm{d}t} \tag{3.21}$$

3.3.1 Gamma Model

Various input functions have been proposed. The transit compartment model Eq. (3.15) is a particular case of an empirical model with the input equal to the convolution of $k_\mathrm{tr}A_n$ with $k_\mathrm{a}\exp(-k_\mathrm{a}t)$:

$$\mathrm{Input}\,(t) = \int_0^t \frac{F\mathrm{Dose}\ k_\mathrm{a}k_\mathrm{tr}\left(k_\mathrm{tr}x\right)^{n-1}}{\Gamma\,(n)} \exp\left(-k_\mathrm{tr}x - k_\mathrm{a}\,(t-x)\right)\mathrm{d}x \tag{3.22}$$

where $n > 0$ serves as a shape parameter that for an integer n can be interpreted as the number of transit compartments. The mean input time for the gamma input function is

$$\mathrm{MIT} = \frac{n}{k_\mathrm{tr}} + \frac{1}{k_\mathrm{a}} \tag{3.23}$$

3.3.2 Weibull Model

The flexibility of the Weibull function has been used to reflect the variable drug input rates along the GI tract. It generalizes the first-order absorption model:

$$\mathrm{Input}\,(t) = F\mathrm{Dose}\lambda_\mathrm{a}st^{s-1}\exp\left(-\lambda_\mathrm{a}t^s\right) \tag{3.24}$$

where s is the shape parameter and λ_a can be considered as an analog of the first-order absorption rate constant. If $s = 1$, then the Weibull input reduces to the first-order absorption, as described in Eq. (3.2). The time profile of the Weibull input function and the corresponding of C_p vs. t curve are shown in Figure 3.5. The MIT for the Weibull input is as follows:

$$\mathrm{MIT} = \frac{\Gamma\left(1+\frac{1}{s}\right)}{{\lambda_\mathrm{a}}^{1/s}} \tag{3.25}$$

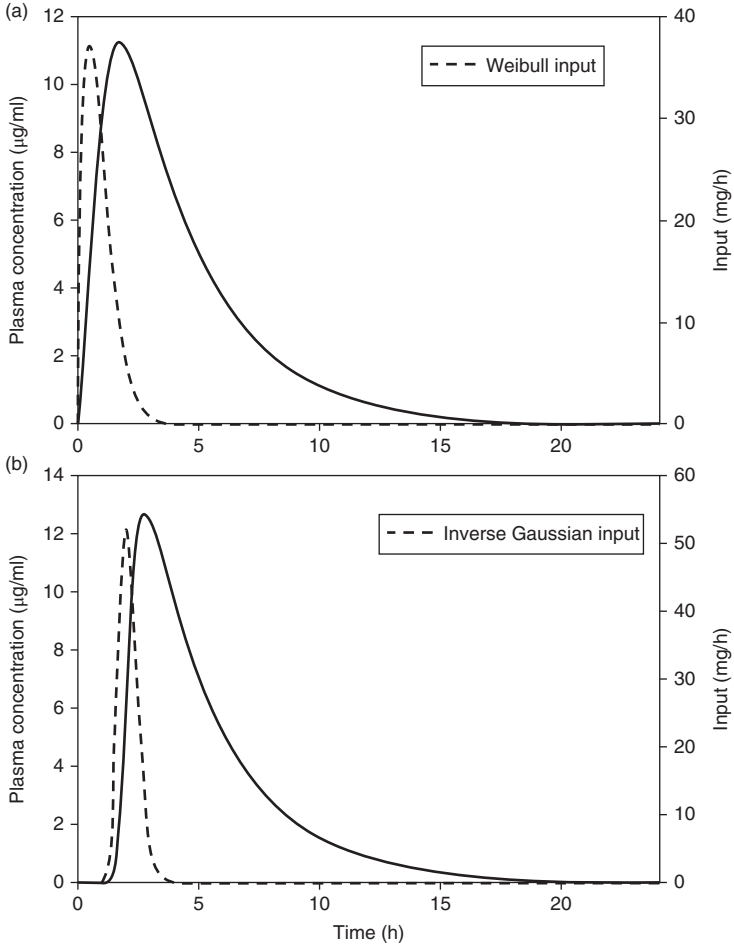

Figure 3.5 Time courses of plasma concentration and input for the Weibull (a) and inverse Gaussian (b) input models. The dashed lines describe the input with reference to the right axis. Parameter values used for simulations were Dose = 100 mg, $V_p = 3$ l, $k_{el} = 0.3\,h^{-1}$, $F = 0.5$, $\lambda_a = 1\,h^{-s}$, $s = 1.5$, MIT = 2 h, and $CV_I = 0.2$.

The amount of absorbed drug is:

$$A_a(t) = F\text{Dose}\left(1 - \exp\left(-\lambda_a t^s\right)\right) \tag{3.26}$$

Piotrovskii [18] first applied the Weibull function to describe the absorption data of theophylline and pantothenic acid. The Weibull input was used to characterize the absorption kinetics of amoxicilline in healthy subjects [19].

3.3.3 Inverse Gaussian Model

The inverse Gaussian (IG) function was introduced by Weiss [20] as a flexible empirical input function to describe drug delivery to the systemic circulation following oral administration. It is of interest to note that the IG is the first passage time distribution of a random walk with drift [21] and the solution of the convection-dispersion equation for pharmacokinetically relevant boundary conditions [22].

$$\text{Input}\,(t) = F\text{Dose}\sqrt{\frac{\text{MIT}}{2\pi \text{CV}_\text{I}^{\,2} t^3}}\exp\left(-\frac{(t-\text{MIT})^2}{2\text{CV}_\text{I}^{\,2}\text{MIT}\,t}\right) \tag{3.27}$$

where MIT represents the mean input time and CV_I is the coefficient of variation of the input times. A plot of C_p vs. t curve for the IG input is shown in Figure 3.5. The IG model was applied to describe the plasma trapidil concentrations in chronic liver disease patients receiving IV and oral dose of 100 mg [23]. Trapidil is a vasodilator used to treat patients with ischemic coronary heart, liver, and kidney disease.

3.4 Physiologically Based Pharmacokinetic Models of Drug Absorption

Physiologically based pharmacokinetic (PBPK) models are compartmental models where compartments represent physiologically realistic body tissues, fluids, and organs. A key difference between a compartmental PK model and a PBPK model is that the structure of a PBPK model is derived from the anatomical and physiological structure of the studied organism, whereas a structure of a compartmental model is based on data of the concentration–time profiles of drug in blood (whole blood, plasma, or serum) and sometimes in other accessible body fluids (e.g. urine, feces) [24]. Consequently, the PBPK model parameters can be obtained from independent experiments, often estimated from in vitro or ex vivo data. In contrast, the compartmental PK model parameters are estimated from the available drug related in vivo data. A major utility of PBPK models is that they can simultaneously describe PKs of drug both in blood and various body tissues and fluids, mechanistically quantifying processes of absorption, distribution, metabolism, and elimination.

PBPK models applied to drug absorption from the GI tract consider the intestine as an organ subdivided into vascular (intestinal blood), cellular (tissue), and luminal subcompartments. Drug permeating the intestinal membrane is subject to intestinal blood flow, metabolism, efflux/influx by transporter proteins, fecal excretion, and protein binding. The blood supply to the small intestine constitutes

about 10% of the cardiac output. Most of the intestinal blood flow is the mucosal flow (Q) that supplies blood to epithelial cells of the villi. Intestinal epithelial cells (enterocytes) express phase I enzymes (CYPs) and phase II enzymes (UDPs, UGTs, SLUTS, and GDTs). The intestinal enzymes involved in the metabolism of the drug contribute to the intrinsic metabolic clearance in the gut (CL_u). The intestinal transporters are expressed in the enterocyte basolateral and lumen membranes. Transporters contribute to the absorption of the substrate across the luminal membrane (k_a) and the intrinsic clearances ($CL_{m,}$ CL_d). Binding to cytoplasmic proteins in enterocytes and plasma proteins in intestinal blood reduces the fraction of free drug (f_u). Passive transport of drug through the intestinal membranes is described by effective permeability (P_{eff}) that is defined as a proportionality coefficient between permeability clearance and surface area of the small intestine. Upon reaching the portal vain drug enters the liver that is yet another part of the physiological model. In the following sections, several examples of PBPK models of drug absorption of varying degree of complexity are discussed.

3.4.1 Traditional and Segregated-Flow Models

In the traditional PBPK model (TM) of absorption only first-order transport and removal processes are considered, and drug is assumed to be unbound [25]. The circulating blood (reservoir) R is connected to the intestine via blood flow Q_I (see Figure 3.6). Removal of drug by other eliminating organs is described by the effective clearance CL_{others}:

$$V_R \frac{dC_R}{dt} = Q_I \left(C_{intb} - C_R\right) - CL_{others} C_R, \quad C_R(0) = \frac{Dose_{iv}}{V_R} \tag{3.28}$$

where C_X denotes concentration of drug in an organ X and V_X is the volume of that organ. The intestine is subdivided into the vascular (intestinal blood) intb, cellular (tissue) int, and luminal lum subcompartments:

$$V_{intb} \frac{dC_{intb}}{dt} = Q_I \left(C_R - C_{intb}\right) - CL_{d1} C_{intb} + CL_{d2} C_{int}, \quad C_{intb}(0) = 0 \tag{3.29}$$

The exchange of substrate between the cellular and vascular compartments is described by the intrinsic transport clearance terms CL_{d1} and CL_{d2}:

$$V_{int} \frac{dC_{int}}{dt} = k_a A_{lum} - \left(CL_{sec} + CL_m\right) C_{int} + CL_{d1} C_{intb} - CL_{d2} C_{int}, \quad C_{int}(0) = 0 \tag{3.30}$$

where CL_{sec} and CL_m denote secretory and metabolic clearances, and $A_X = C_X V_X$ is the amount of drug in organ X. The rate constant for absorption of drug across the luminal membrane is denoted by k_a, whereas luminal removal of the drug, by

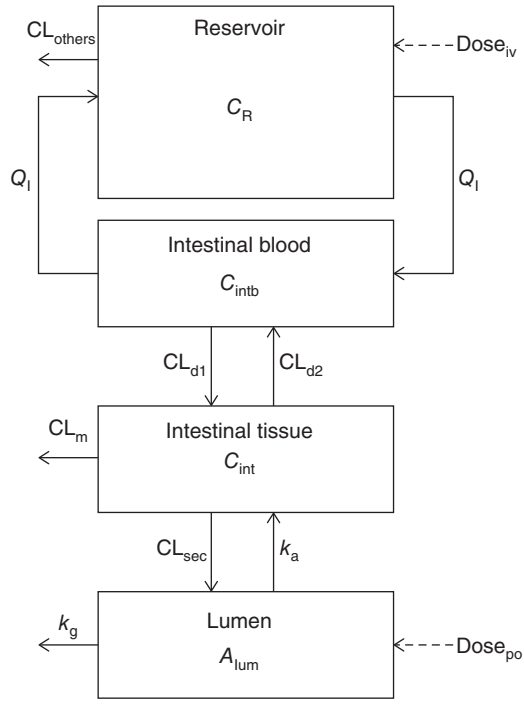

Figure 3.6 Schematic diagram of the traditional PBPK model of absorption.

metabolism, fecal excretion, and GI transit, is represented by rate constant k_g:

$$\frac{dA_{lum}}{dt} = CL_{sec}C_{int} - (k_a + k_g)A_{lum}, \quad A_{lum}(0) = Dose_{po} \tag{3.31}$$

Time courses of fraction of $Dose_{po}$ in the reservoir and intestinal lumen compartments simulated by TM with $CL_{others} = 0$ are shown in Figure 3.7 and the parameter values used for simulations are presented in Table 3.1. The traditional model was applied to describe plasma concentration of morphine (and its metabolite) introduced intraduodenally to the recirculating, vascularly perfused rat small intestine preparation [4, 25].

The TM was extended to the segregated-flow model (SFM). This model adds an additional partition of intestinal tissue into enterocyte and serosal layers. The intestinal blood flow is divided into serosal and enterocyte blood flows. Drug in the serosal and enterocyte blood compartments equilibrates with tissues with the transfer clearances. Remaining lumen and reservoir compartments are identical with ones in the traditional model. The SFM substantially improved the fittings of the morphine data from perfused rat small intestine preparation [25]. Subsequently, a whole body PBPK model was introduced, with the liver and other lumped compartments (highly perfused, poorly perfused) being connected to the

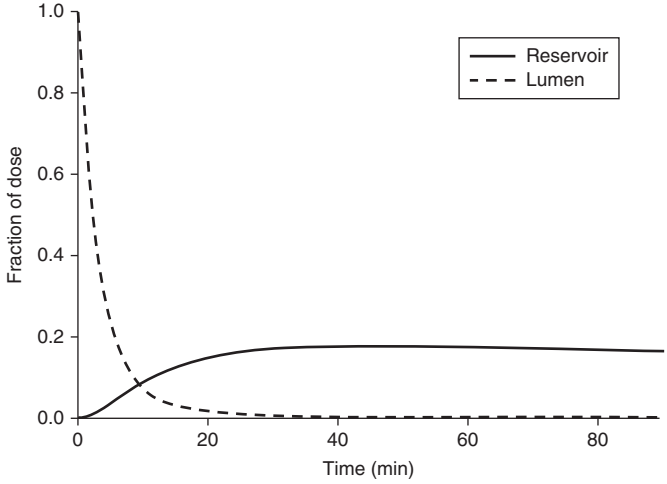

Figure 3.7 Time courses of the fraction of oral dose in the reservoir and intestinal lumen compartments predicted by the traditional PBPK model. Parameter values used for simulations are shown in Table 3.1.

intestine traditional and segregated flow models depicting the intestine and liver as the eliminating organs [26].

3.5 Advanced PBPK Models

Advanced PBPK models involve many compartments and processes which exceeds in number and complexity typical PBPK models. Usually specialized software is needed to implement model equations and perform multiple numerical, statistical, and graphical tasks.

3.5.1 Advanced Compartmental Absorption and Transit Model

The advanced compartmental absorption and transit (ACAT) model is an extension of the CAT model that accounts for dissolution rate, the pH dependence of solubility, controlled release, absorption in the stomach or colon, metabolism in gut or liver, degradation in the lumen, changes in absorption surface area, transporter densities, efflux protein densities, and other regional factors within the intestinal tract [27]. The ACAT model includes linear transfer kinetics and nonlinear metabolism/transport kinetics, six states of drug component (unreleased, undissolved, dissolved, degraded, metabolized, and absorbed), nine compartments (stomach, seven segments of small intestine, and colon), and three

Table 3.1 Parameter values for the traditional PBPK model of intestinal drug absorption in rats.

Parameter	Value
$Dose_{iv}$	0
$Dose_{po}$	100[a)]
V_R (ml)	200
V_{int} (ml)	3
V_{intb} (ml)	1.62
Q_I (ml/min)	8
CL_{d1} (ml/min)	1.73
CL_{d2} (ml/min)	0.207
CL_m (ml/min)	0.0215
CL_{sec} (ml/min)	0.117
CL_{others} (ml/min)	0
k_a (h^{-1})	0.1
k_g (h^{-1})	0.2

a) Unit was not defined.
Source: Based on Cong et al. [25].

states of excreted material (unreleased, undissolved, and dissolved). The ACAT model is implemented in the software package GastroPlus™ (SimulationsPlus Inc., Lancaster, CA). The model predictions of bioavailability, fraction absorbed, and plasma concentrations well agreed with the experimental data for drugs that undergo only liver metabolism (propranolol), gut and liver extraction (midazolam), gut efflux (digoxin), and gut efflux and gut and liver metabolism (saquinavir) [27].

3.5.2 Advanced Dissolution Absorption and Metabolism Model

The advanced dissolution absorption and metabolism (ADAM) model is an extension of CAT and GITT models [28]. It divides the GI tract into nine anatomically defined segments from the stomach through the intestine to the colon. Drug absorption from each segment is described as a function of release from the formulation, dissolution, precipitation, luminal degradation, permeability, metabolism, transport, and transit from one segment to another. The ADAM model assumes that absorption from the stomach is insignificant compared with that from the small intestine, and that the movement of liquid and solid drug through each

segment of the GI tract may be described by first-order kinetics. The ADAM model is implemented in the Simcyp® population-based ADME simulator (Certara Inc., Princeton, NJ) [29]. The ADAM model successfully predicted the plasma concentration profiles for three modified release formulations (fast, moderate, and slow) of metoprolol [30]. Also, the ADAM model predicted percentages of the dose of midazolam absorbed and metabolized in each segment of the small intestine as well as their inter-individual variabilities [28].

3.6 Intestinal First-pass Drug Metabolism

The oral bioavailability F can be determined from in vivo data following sequential intravenous (Dose_{iv}) and oral (Dose_{po}) administration of drug to the same subject:

$$F = \frac{\text{AUC}_{\text{po}}}{\text{AUC}_{\text{iv}}} \frac{\text{Dose}_{\text{iv}}}{\text{Dose}_{\text{po}}} \tag{3.32}$$

assuming linear PKs, where AUC denotes the area under drug plasma concentration vs. time curve. PBPK models of drug absorption allow for calculation of F based on extraction ratios and fraction of drug amount lost during the absorption processes. After oral administration drug passes sequentially from the GI lumen, through the intestinal wall, and through the liver and enters the systemic circulation. Each of these stages potentially involves loss of drug resulting in the oral bioavailability F to be the product of following bioavailabilities:

$$F = F_{\text{a}} F_{\text{G}} F_{\text{H}} \tag{3.33}$$

where F_{a} is the net fraction of dose absorbed from the intestinal tract, F_{G} is the fraction of dose that escapes intestinal first-pass metabolism in the enterocytes, and F_{H} is the fraction of dose that escapes hepatic first-pass metabolism. The intestinal first-pass bioavailability F_{G} can be calculated from PBPK models such as SFM. However, the value of such models in predicting F_{G} is limited by their complexity and the difficulty of obtaining model parameters without actually fitting in vivo data. More operational minimalistic models have been proposed to predict F_{G}.

3.6.1 Well-stirred Gut Model

The well-stirred gut model, similar to the well-stirred model for hepatic clearance [31, 32], assumes that drug is distributed instantly and homogenously throughout the intestinal tissue and that the unbound concentrations in plasma and intestinal tissue are identical. Since $F_{\text{G}} = 1 - E_{\text{G}}$, where E_{G} is the intestinal extraction ratio,

and E_G can be calculated analogously to the hepatic extraction ratio E_H yielding [33, 34]:

$$F_G = \frac{Q_G}{Q_G + f_{uG}CL_{uG}} \tag{3.34}$$

where Q_G is the gut blood flow, f_{uG} is the fraction of drug unbound in the enterocyte, and CL_{uG} is the net intrinsic metabolic clearance in the gut. The gut blood flow Q_G is assumed to be the total intestinal blood flow or mucosal blood flow.

3.6.2 Q_{Gut} Model

The Q_{Gut} model expands the well-stirred gut model by calculating the gut blood flow Q_G as a hybrid of both permeability through the enterocyte membrane and villous blood [35]:

$$Q_G = \frac{Q_{villi}CL_{perm}}{Q_{villi} + CL_{perm}} \tag{3.35}$$

where CL_{perm} is a clearance term defining permeability through the enterocyte and Q_{villi} is villous blood flow. Substituting Eq. (3.35) into (3.34) results in the Q_{Gut} model for F_G:

$$F_G = \frac{Q_{villi}}{Q_{villi} + f_{uG}CL_{uG}\left(1 + Q_{villi}/CL_{perm}\right)} \tag{3.36}$$

The performance of the well-stirred and Q_{Gut} models in predicting F_G was compared based on data for 16 drugs metabolized predominantly by CYP3A [35]. The well-stirred model overpredicted F_G. The Q_{Gut} model substantially improved the predictions only when f_{uG} was assumed to be 1.

3.7 Spatiotemporal Models of Drug Absorption

Compartmental and PBPK models of absorption have a compartmentalized structure of the intestine and drug movement along the GI tract is described as a sequence of first-order processes. The longitudinal location of the drug molecule in the intestine can be considered as an independent variable z that will describe drug concentration in the lumen C_{lum} continuously changing along the GI tract. The spatiotemporal models of drug absorption consider C_{lum} as a function of distance z and time t which require mathematical tools capable of dealing with multi-variable functions such as $C_{lum}(z, t)$. The following examples include models with spatiotemporal changes of drug concentrations.

3.7.1 Dispersion Model

The dispersion model assumes the small intestine can be considered as a uniform tube with constant axial velocity, constant dispersion behavior, and a constant concentration profile across the tube diameter. Then, drug concentration in the lumen of the small intestine can be described by the following convection–dispersion equation [1, 36]:

$$\frac{\partial C_{\text{lum}}}{\partial t} = \alpha \frac{\partial^2 C_{\text{lum}}}{\partial z^2} - \upsilon \frac{\partial C_{\text{lum}}}{\partial z} - k_a C_{\text{lum}} \tag{3.37}$$

where z is the axial distance from an exit of the stomach, k_a is the absorption rate constant, υ is the velocity in the axial direction, and α is the longitudinal lumped diffusion coefficient that accounts for nonconvective transport by both diffusion and physiological effects. For a unique solution Eq. (3.37) requires initial and boundary conditions. Prior to drug administration there is no drug in the intestinal lumen. Thus, the initial condition for the dispersion equation is:

$$C_{\text{lum}}(z, 0) = 0 \quad \text{for } z > 0 \tag{3.38}$$

The boundary condition at $z = 0$ is determined by the drug concentration in the stomach C_{stom}:

$$C_{\text{lum}}(0, t) = C_{\text{stom}}(t) \quad \text{for } t > 0 \tag{3.39}$$

For passively absorbed drugs such as ciprofloxacin, levofloxacin, diclofenac sodium, and oxacillin, the dispersion model predicted the absorption rates and cumulative fraction absorbed very well [37]. However, due to the assumption of negligible first-pass, the dispersion model may overestimate F values for compounds which undergo enzyme-mediated presystemic metabolism such as benazepril and lovastatin [38]. In addition, the dispersion models only taking into account passive intestinal permeability may result in an inaccurate prediction of F values for P-gp substrates such as doxorubicin and ranitidine [39].

3.7.2 Translocation Model

The translocation model (TLM) is based on the concept that a drug is transferred from the lumen to the bloodstream across the enterocytes and lamina propria at an absorption site, which is relocated, expanded, and decreased in size along the length of the GI tract in a time-dependent manner [40]. The locatable absorption site consists of four compartments: solid formulation in the lumen, dissolved drug in the intestinal lumen, concentration in the enterocytes, and concentration in the lamina propria, including the capillaries. The absorption site continuously traverses from the duodenum to the ileum. The stomach and colon are defined as separate compartments. The location and length of the absorption sites in the small

intestine are calculated using $\lambda(t)$, the location function, and $\sigma^2(t)$, the variance function, at time t. The TLM assumes that $C_{\text{lum}}(z, t)$ at the observation time t is constant within the absorption site:

$$\lambda(t) < z < \lambda(t) + 2\sqrt{3}\sigma(t) \tag{3.40}$$

and it is otherwise 0. For drugs which enter the GI tract as a bolus dose, $\lambda(t)$ and $\sigma(t)$ are defined as follows:

$$\lambda(t) = \frac{m_1 t}{m_2 + t} \tag{3.41}$$

and

$$\sigma(t) = s_1 \left(e^{-s_2 t} - e^{-s_3 t}\right) + s_4 \tag{3.42}$$

The parameters m_1, m_2, s_1, s_2, s_3, and s_4 were obtained by fitting of $\lambda(t)$ and $\sigma(t)$ to the observed location and its variance for a nonabsorbable index drug in the intestinal tract [40]. Parameters, such as permeability and clearance, are determined depending on the location of the absorption site. The TLM prediction $F_a F_G$ and plasma concentrations for midazolam agreed well with the observed data. The TLM was validated against F_G and F values reported for 18 and 15 drugs, respectively, which are substrates for CYPA3 enzymes (alfentanil, alprazolam, buspirone, cisapride, felodipine, lovastatin, midazolam, nifedipine, nisoldipine, repaglinide, rifabutin, sildenafil, simvastatin, trazodone, triazolam, zolpidem) and P-gp transporters (cyclosporin, saquinavir, quinidine, verapamil) [40].

3.8 Conclusions

This chapter provides a brief overview of PK models that are representative of current approaches in modeling oral drug absorption. The focus has been on stating the underlying assumptions, explaining model structure and basic properties, and providing examples of applications. Important aspects of modeling drug absorption have not been discussed. While not essential for in vitro data analysis, most in vivo and all clinical PK data exhibit between subject variability. Aspects of population PK modeling approaches need to be considered to address intra- and inter-subject variability. Adequate description of available data is a key feature of a PK model, but to be successful, the model should have a predictive ability beyond the data it has been developed for. This chapter does not provide examples of the utility of PK models for drug development such as prediction of oral bioavailability, in vitro–in vivo correlation, drug–drug interactions, and inter-species scaling. Furthermore, challenges of model software implementation and available programs for modeling absorption data have not been extensively discussed.

There are essentially two approaches to model drug absorption determined by the objectives of interest. For modeling in vivo data and, in particular, clinical data comprising drug plasma concentrations, data driven compartmental and empirical models seem to be most relevant. For modeling in vitro data and in vivo data consisting of drug concentrations in various tissues, mechanistic PBPK models are more appropriate. This classification becomes unclear with increasing complexity of model structure as seen for CAT and ACAT, or GITT and ADAM models. It is difficult to predict directions into which PK modeling of absorption processes will evolve. However, a symptomatic increase in model dimensions (number of compartments) and importance of adequate description of physiological processes imply convergence toward the quantitative systems pharmacology approach that has been proven successful in drug development [41].

References

1 Yu, L.X., Lipka, E., Crison, J.R., and Amidon, G.L. (1996). Transport approaches to the biopharmaceutical design of oral drug delivery systems: prediction of intestinal absorption. *Adv. Drug Delivery Rev.* 19: 359–376.

2 Huang, W., Lee, S.L., and Yu, L.X. (2009). Mechanistic approaches to predicting oral drug absorption. *AAPS J.* 11: 217–224.

3 Weitschies, W., Blume, H., and Monnikes, H. (2010). Magnetic marker monitoring: high resolution real-time tracking of oral solid dosage forms in the gastrointestinal tract. *Eur. J. Pharm. Biopharm.* 74: 93–101.

4 Doherty, M. and Pang, K.S. (2000). Route-dependent metabolism of morphine in the vascularly perfused rat small intestine preparation. *Pharm. Res.* 17: 291–298.

5 Hall, S.D., Thummel, K.E., Watkins, P.B. et al. (1999). Molecular and physical mechanisms of first-pass extraction. *Drug Metab. Dispos.* 27: 161–166.

6 Sun, D., Lennernas, H., Welage, L.S. et al. (2002). Comparison of human duodenum and Caco-2 gene expression profiles for 12,000 Gene sequences tags and correlation with permeability of 26 drugs. *Pharm. Res.* 19: 1400–1416.

7 Irvine, J.D., Takahashi, L., Lockhart, K. et al. (1999). MDCK (Madin-Darby canine kidney) cells: a tool for membrane permeability screening. *J. Pharm. Sci.* 88: 28–33.

8 Boeckmann, A., Sheiner, L., and Beal, S. (1992). *NONMEM Users Guide: Part V*. San Francisco: University of California.

9 Grevel, J., Nüesch, E., Abisch, E., and Kutz, K. (1986). Pharmacokinetics of oral cyclosporin A (Sandimmun) in healthy subjects. *Eur. J. Clin. Pharmacol.* 31: 211–216.

10 Nerella, N.G., Block, L.H., and Noonan, P.K. (1993). The impact of lag time on the estimation of pharmacokinetic parameters. I. One-compartment open model. *Pharm. Res.* 10: 1031–1036.

11 Savic, R.M., Jonker, D.M., Kerbusch, T., and Karlsson, M.O. (2007). Implementation of a transit compartment model for describing drug absorption in pharmacokinetic studies. *J. Pharmacokinet. Pharmacodyn.* 34: 711–726.

12 Godfrey, K.R., Arundel, P.A., Dong, Z., and Bryant, R. (2011). Modelling the double peak phenomenon in pharmacokinetics. *Comput. Methods Programs Biomed.* 104: 62–69.

13 Plusquellec, Y., Efthymiopoulos, C., Duthil, P., and Houin, G. (1999). A pharmacokinetic model for multiple sites discontinuous gastrointestinal absorption. *Med. Eng. Phys.* 21: 525–532.

14 Yu, L.X. and Amidon, G.L. (1999). A compartmental absorption and transit model for estimating oral drug absorption. *Int. J. Pharm.* 186: 119–125.

15 Bergstrand, M., Soderlind, E., Weitschies, W., and Karlsson, M.O. (2009). Mechanistic modeling of a magnetic marker monitoring study linking gastrointestinal tablet transit, in vivo drug release, and pharmacokinetics. *Clin. Pharmacol. Ther.* 86: 77–83.

16 Hénin, E., Bergstrand, M., Standing, J.F., and Karlsson, M.O. (2012). A mechanism-based approach for absorption modeling: the gastro-intestinal transit time (GITT) model. *AAPS J.* 14: 155–163.

17 Lindberg-Freijs, A. and Karlsson, M.O. (1994). Dose dependent absorption and linear disposition of cyclosporin A in rat. *Biopharm. Drug Dispos.* 15: 75–86.

18 Piotrovskii, V.K. (1987). The use of Weibull distribution to describe the in vivo absorption kinetics. *J. Pharmacokinet. Biopharm.* 15: 681–686.

19 Padoin, C., Tod, M., Brion, N. et al. (1995). Pharmacokinetics of amoxicillin coadministered with a salinepolyethylene glycol solution in healthy volunteers. *Biopharm. Drug Dispos.* 16: 169–176.

20 Weiss, M. (1996). A novel extravascular input function for the assessment of drug absorption in bioavailability studies. *Pharm. Res.* 13: 1547–1553.

21 Schrödinger, E. (1915). Zur Theorie der Fall- und Steigversuche an Teilchen mit Brownscher Bewegung. *Phys. Z.* 16: 289–295.

22 Roberts, M.S., Anissimov, Y.G., and Weiss, M. (2000). Commentary: using the convection-dispersion model and transit time density functions in the analysis of organ distribution kinetics. *J. Pharm. Sci.* 89: 1579–1586.

23 Wang, J., Weiss, M., and D'Argenio, D.Z. (2008). A note on population analysis of dissolution-absorption models using the inverse Gaussian function. *J. Clin. Pharmacol.* 48: 719–725.

24 Nestorov, I. (2003). Whole body pharmacokinetic models. *Clin. Pharmacokinet.* 42: 883–908.

25 Cong, D., Doherty, M., and Pang, K.S. (2000). A new physiologically based, segregated-flow model to explain route-dependent intestinal metabolism. *Drug Metab. Dispos.* 28: 224–235.

26 Pang, K.S. and Chow, E.C. (2012). Commentary: theoretical predictions of flow effects on intestinal and systemic availability in physiologically based pharmacokinetic intestine models: the traditional model, segregated flow model, and Q_{Gut} model. *Drug Metab. Dispos.* 40: 1869–1877.

27 Agoram, B., Woltosz, W.S., and Bolger, M.B. (2001). Predicting the impact of physiological and biochemical processes on oral drug bioavailability. *Adv. Drug Delivery Rev.* 50 (Suppl 1): S41–S67.

28 Jamei, M., Turner, D., Yang, J. et al. (2009). Population-based mechanistic prediction of oral drug absorption. *AAPS J.* 11: 225–237.

29 Jamei, M., Marciniak, S., Feng, K. et al. (2009). The Simcyp population-based ADME simulator. *Expert Opin. Drug Metab. Toxicol.* 5: 212–223.

30 Polak, S., Jamei, M., and Turner, D. (2008). Prediction of the in vivo behaviour of modified release formulations of metoprolol from in vitro dissolution profiles using the ADAM model (Simcyp®V8). *Drug Metab. Rev.* 40 (Suppl 1): 45.

31 Gillette, J.R. (1971). Factors affecting drug metabolism. *Ann. N.Y. Acad. Sci.* 179: 43–66.

32 Rowland, M., Benet, L.Z., and Graham, G.G. (1973). Clearance concepts in pharmacokinetics. *J. Pharmacokinet. Biopharm.* 1: 123–136.

33 Gillette, J.R. and Pang, K.S. (1977). Theoretic aspects of pharmacokinetic drug interactions. *Clin. Pharmacol. Ther.* 22: 627–638.

34 Colburn, W.A. and Gibaldi, M. (1978). Pharmacokinetic model of presystemic metabolism. *Drug Metab. Dispos.* 6: 193–196.

35 Yang, J., Jamei, M., Yeo, K.R. et al. (2007). Prediction of intestinal first-pass drug metabolism. *Curr. Drug Metab.* 8: 676–684.

36 Ni, P.F., Ho, N.F.H., Fox, J.F. et al. (1980). Theoretical model studies of intestinal drug absorption V: nonsteady-state fluid flow and absorption. *Int. J. Pharm.* 5: 33–47.

37 Willmann, S., Schmitt, W., Keldenich, J., and Dressman, J.B. (2003). A physiologic model for simulating gastrointestinal flow and drug absorption in rats. *Pharm. Res.* 20: 1766–1771.

38 Willmann, S., Edginton, A.N., and Dressman, J.B. (2007). Development and validation of a physiology-based model for the prediction of oral absorption in monkeys. *Pharm. Res.* 24: 1275–1282.

39 Troutman, M.D. and Thakker, D.R. (2003). Novel experimental parameters to quantify the modulation of absorptive and secretory transport of compounds by P-glycoprotein in cell culture models of intestinal epithelium. *Pharm. Res.* 20: 1210–1224.

40 Ando, H., Hisaka, A., and Suzuki, H. (2015). A new physiologically based pharmacokinetic model for the prediction of gastrointestinal drug absorption: translocation model. *Drug Metab. Dispos.* 43: 590–602.

41 Rostami-Hodjegan, A. (2012). Physiologically based pharmacokinetics joined with in vitro-in vivo extrapolation of ADME: a marriage under the arch of systems pharmacology. *Clin. Pharmacol. Ther.* 92: 50–61.

4

Oral Site-Directed Drug Delivery and Influence on PK

Peter Scholes[1], Vanessa Zann[1], Wu Lin[1], Chris Roe[1] and Bret Berner[2]

[1] *Quotient Sciences, Mere Way, Ruddington Fields Business Park, Ruddington, Nottingham NG11 6JS, UK*
[2] *Drug Delivery Consultant, 4011 54 Ave SW, Seattle, WA 98116, USA*

4.1 Introduction

Oral delivery remains the most common route of administration for existing drug products and new chemical entities, whether to treat local gastrointestinal (GI) disease or to deliver drugs to the systemic circulation to address a broader range of therapeutic indications. Successful performance of an oral dosage form is complex, influenced by many factors and is ultimately dependent upon the interplay between the intrinsic physicochemical properties and biopharmaceutics of the drug substance, the formulation design and technology selection, and the influence of physiological factors in impacting in vivo drug dissolution, solubility and permeability.

In this chapter, we will provide an initial background on GI anatomy and physiology, followed by discussion on the importance of physicochemical properties and biopharmaceutics in drug delivery, the tools that can be used to predict, assess or observe oral transit, metabolism, and absorption, and approaches to formulation to achieve desired delivery goals associated with the therapy. A separate chapter in this volume covers modeling of absorption in the GI tract in more detail, with the results of these models providing valuable insights into dosage form design.

4.2 GI Anatomy and Physiology

Formulation design will be covered elsewhere in this chapter. The pharmaceutical scientist has the ability to modify the solid state characteristics of the drug

Drug Delivery Approaches: Perspectives from Pharmacokinetics and Pharmacodynamics,
First Edition. Edited by Bret Berner, Toufigh Gordi, Heather A. E. Benson, and Michael S. Roberts.

substance (e.g. to influence dissolution or solubility behavior and hence increase absorption and thus bioavailability), or the release rate from the formulation (e.g. to impact control over the plasma concentration – time profile or target different regions of the GI tract). What is more difficult or even impossible to change or control are the multi-variate in vivo environmental conditions into which the drug product is placed post-administration and in the case of non-disintegrating dosage forms, conditions which will change in different anatomical regions of the GI tract through which the dosage form will transit. It is therefore imperative that the formulation scientist has a robust understanding of the GI milieu, transit times and the anatomical, physiological and environmental factors likely to influence dosage form performance in vivo, to ensure the effective design and development of drug product formulations to meet the overall target product profile. Without this integration of scientific thinking, no matter how elegant the formulation design and how positive its assessment in vitro, there will always be significant risks to successful in vivo absorption.

4.2.1 Anatomy

The GI tract is over 7 m in length and can be divided into a number of distinct regions and sub-compartments. The stomach is perhaps the simplest region comprising of four regions (fundus, body, antrum, and pylorus) with collectively a relatively small surface area. It is primarily a secretory rather than an absorptive organ whose main function is to store and grind food, mix it with gastric secretions to initiate the digestive process, and empty the resultant chyme at a controlled rate into the duodenum. While some literature suggests absorption from the stomach can occur [1], at most it represents a very small percentage of the total systemic exposure and consequently, the rate of gastric emptying is often a primary driver of systemic exposure.

The small intestine is approximately 6 m long, and stretches from the pyloric sphincter to the ileocecal junction (ICJ). It can be divided into a proximal region, comprising the duodenum (~30 cm long) and jejunum (~2.4 m long), and a distal region or the ileum (~3.6 m long). The key function of the small intestine is absorption of nutrients as reflected by its large epithelial surface area of over 450 m^2, augmented by intestinal villi and microvilli which increase the absorptive area.

Finally, the large intestine, the colon, is commonly divided into eight regions: caecum, ascending colon, hepatic flexure, transverse colon, splenic flexure, descending colon, sigmoid colon, and rectum. In comparison to the small intestine, the colon has a much reduced length (~1.25 m) and surface area (~1.5 m^2) to reflect its different physiological functionality of absorption of water and storage of fecal matter.

4.2.2 Regional Variations in Physiology Affecting Drug Delivery

The physiology of the GI tract varies from region to region. A wide variety of factors, promoting or impeding drug absorption either into local diseased tissue or the systemic circulation, must be considered for each region, including fluid volumes, composition and pH for drug solubilization, surface area, tissue permeability and transporter expression for drug absorption, and enzyme prevalence for potential intestinal degradation or gut wall metabolism.

4.2.2.1 Fluid Volume and pH

Fluid volumes through the GI tract have been assessed and reviewed by several authors [2–4] and are summarized in Table 4.1. A magnetic resonance imaging (MRI) study [3] reported stomach, small intestine, and large intestine volumes under fasted and fed conditions and confirmed the presence of free water was not uniformly distributed, rather existed in "pockets" presenting another variable to in vivo dissolution and consistency in formulation performance. Reported data consistently show reduced water content in the colon thereby presenting a particular challenge to drug delivery in this region for drug dissolution and hence absorption depending on the dose of drug and its unique physicochemical properties. This is a key consideration for both local delivery and for the development of sustained release dosage forms where colonic absorption is required.

In addition to variable fluid volumes, changes in luminal pH are also significant along the length of the GI tract, ranging from pH 1 to 2 in the fasted stomach, to pH 7–8 in distal regions. Upon gastric emptying, intestinal pH rises slowly through the small intestine from approximately pH 5.5 to above 7 at the ICJ (Figure 4.1). In general, a reduction of at least 1 pH unit is then observed beyond the caecum as a result of local microbial activity [5]. Intersubject variability of pH in healthy

Table 4.1 Mean (sd) fluid volumes (ml) throughout the GI Tract.

	Total fluid (determined post mortem)	Free fluid (determined by MRI)	
	Fasted	Fasted	Fed
Stomach	118 (82)	45 (18)	686 (93)[a)]
Small intestine	212 (110)	105 (72)	54 (41)
Large intestine	187	13 (12)	11 (26)

a) The volume of the stomach after the meal represents the filling volume (not only fluid).

Sources: Adapted from Schiller et al. [3] and McConnell et al.[4].

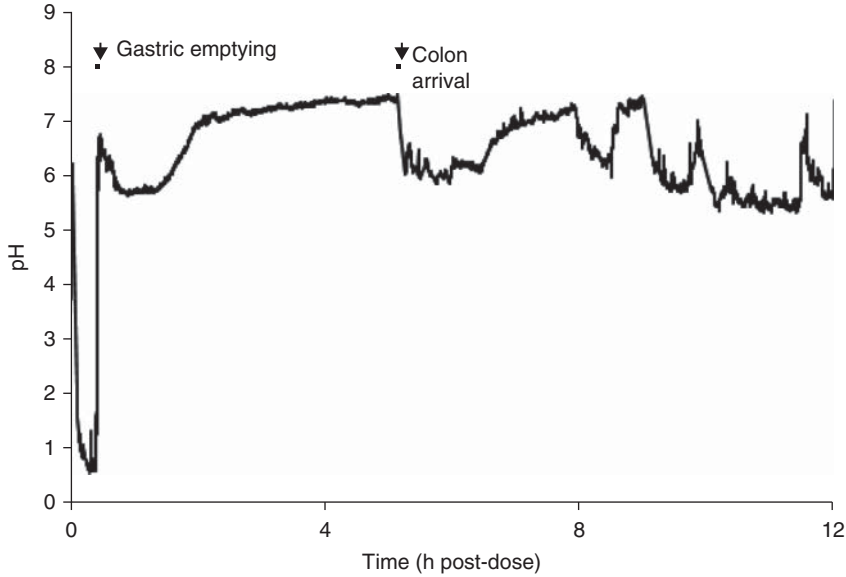

Figure 4.1 Gastrointestinal pH profile from one subject using the SmartPill pH capsule. Source: Unpublished Quotient Sciences data, reproduced with permission from study sponsor.

subjects is typically low, with the variation (CV%) less than 10% in the small intestine [6, 7].

For an ionizable compound, the pH of the local environment will impact solubility and hence the amount of drug available for absorption. Basic molecules have higher solubility in the stomach and lower in the small intestine, which may result in both a burst release effect in the stomach and the potential to precipitate in the small intestine. Conversely, acidic drugs have limited solubility in the stomach and better dissolution in the small intestine. As these molecular types will be subject to variations in pH in vivo, formulation strategies may be required to assure reliable drug delivery as discussed later in this chapter. An additional effect of pH will be discussed later in this chapter in regard to the impact on proton-driven active transporter processes.

4.2.2.2 Enzymes, Gut Wall Metabolism, Tissue Permeability, and Transporters

Evolution has resulted in the presence of many transporters and enzymes within the GI tract, both to aid digestive processes and to protect the body against potential ingestion of harmful toxins. Some transporters and enzymes are ubiquitous throughout and others are expressed preferentially in the certain anatomical

regions. Expression gradients have been documented for a number of enzymes and transporters and their relevance to impacting drug absorption and oral bioavailability is molecule specific.

Enzymes Enzymes in the GI tract arise from three principal GI sources, luminal (e.g. peptidases, esterases), bacterial, and mucosal/gut wall. Combined with hepatic metabolism, these are the key factors in drug biotransformation, absorption, and bioavailability of orally administered drugs. Many enzymes present in the liver are also expressed in intestinal epithelial cells, with the cytochrome P450 (CYP) family being particularly important given its responsibility for the majority of Phase 1 reactions (e.g. oxidation) [8]. CYPs are membrane-associated hemoproteins located within the enterocytes and are expressed and distributed (unequally) as various isoforms throughout the GI tract. The CYP3A subfamily is the most predominant, representing 70–80% of total intestinal CYP content, with CYP3A4 being the main congener [9]. CYP2C is the second most prevalent isoenzyme subfamily at levels of approximately 18% [9]. mRNA analysis from tissue biopsies has confirmed the low-level expression of many other variants in the GI tract, including CYP2D6, CYP2E1, and CYP2J2 [9, 10]; however, their contribution to metabolic activity of drugs is believed to be relatively minimal.

Presystemic metabolism can significantly affect the bioavailability of many orally administered drugs, and is a function of both gut wall and hepatic first-pass processes. The relative contribution of each to the bioavailability of a compound can vary and has been open to conjecture; however, the role of gut wall metabolism should not be underestimated. As an example, studies in a transgenic mouse model [11] have reported how removal of the *CYP3A* genes and selective replacement with the CYP3A4 enzyme in the intestine still ensured significant first-pass metabolism with docetaxel, whereas selective hepatic expression conferred a near-normal systemic clearance of the drug.

Drugs, which are CYP substrates, and hence liable to presystemic metabolism, present several challenges for achieving effective oral drug delivery. They are likely to exhibit supraproportionality in exposure as dose increases due to saturation of CYP-mediated metabolism, as well as potentially demonstrate high intersubject variability as a result of high variability (up to 30-fold) in interindividual CYP3A4 expression [12, 13].

Several strategies have been successfully evaluated to overcome these problems. For antiviral therapies, the coadministration of low-dose ritonavir, a potent albeit nonspecific CYP3A4 inhibitor, was successfully found to increase bioavailability of other protease inhibitors, including saquinavir [14]. A greater than 50-fold enhancement of plasma concentrations was observed in humans following a single codose of ritonavir (600 mg) and saquinavir (200 mg), which was believed to be due to inhibition of both gut wall and hepatic metabolism of saquinavir. This

has led to the design and development of drugs specifically targeting CYP3A4 with reduced off-target effects and with no intrinsic antiviral activity themselves, unlike ritonavir. Cobicistat is a mechanism-based inhibitor of CYP3A enzymes developed and licensed as a pharmacokinetic (PK) enhancer (i.e. booster) of the HIV-1 protease inhibitors (PIs) atazanavir and darunavir in adults, resulting in higher drug levels and slower clearance, comparable to the effects seen with low-dose ritonavir [15].

Other approaches to overcome gut wall metabolism have focused on formulation design, and the use of nonionic and lipid-based excipients such as polysorbate 80, D-α-tocopherol polyethylene glycol (1000) succinate (TPGS), sucrose laurate, Cremophor EL, and Cremophor RH40, which have been shown to reduce the CYP3A4-mediated in vitro metabolism of model drugs, testosterone and diclofenac [16].

An additional drug-delivery strategy for CYP3A4 substrates arises from the observation that enzyme distribution increases in the more proximal regions of the small intestine as evidenced by both CYP3A protein level and the intrinsic clearance of midazolam, a known CYP substrate [12, 17]. As such, the potential to deliver drugs beyond this location, to the more distal regions of the GI tract, offers the potential to increase relative bioavailability. This phenomenon has been reported for simvastatin, which exhibited a threefold increase in bioavailability following delivery to the lower GI tract [18, 19]. Regional delivery offers potential success for the bolus delivery of drugs. However, the presence of saturable processes such as CYP-mediated metabolism (and transporters as described in the next section) needs careful consideration on the design of modified release (MR) formulations. Formulators need to be cognizant of the potential risk of the release rate and hence local concentrations in the GI tract being below saturation thresholds resulting in suboptimal PK.

In common with all CYPs, some drugs or dietary components can also act as inhibitors or inducers of the CYP3A4 enzyme, further complicating the drug-delivery challenge and also raising the potential for drug–drug interactions (DDIs), affecting the safety and efficacy of any comedications, which may be metabolized by CYP3A4. Notable examples reviewed by Thelen and Dressman [8] included ketoconazole and grapefruit juice (both inhibitors) with a concomitant twofold to threefold increase in the bioavailability of coadministered drugs, and rifampicin (an inducer), which has been shown to increase tissue CYP3A4 mRNA levels by a factor of 5–8.

Transporters There are many transporter proteins expressed throughout the body that are responsible for the transport of a wide range of substances. The transporters can be divided into two major classes, the adenosine triphosphate (ATP)-binding cassette family (ABC transporters) and the solute carrier

family (SLC), according to the Human Genome Organisation (HUGO) Gene Nomenclature Committee guideline. Many of these transporters are thought of as cellular gatekeepers as they either limit the entry of substances into cells, or assist thereby increasing the apparent permeability and helping them gain access to cellular targets. Transporters can be divided into active transporters, i.e. requiring energy to affect the movement of the substrate, or facilitated transport, whereby the driving force is diffusion down an electrochemical gradient without using energy [20]. Substances can also pass through membranes by a process referred to as passive diffusion. This is the diffusive movement of a substance through the tight junctional pores, known as paracellular permeability, or through the phospholipid bilayer membrane of the cell referred to as transcellular permeability.

Transporters can be further classified depending on the direction in which they transport substances, either to assist with nutrient and ion absorption (influx transporters) [21] or to expel harmful substances (efflux transporters) such as xenobiotics and prevent absorption into the systemic circulation [22, 23]. The SLC family is typically influx transporters and assists the movement of substances into the intracellular environment through cellular uptake. Movement of substances via influx transporters is powered via a number of mechanisms; diffusion down an electrochemical gradient or transport against a diffusion gradient by a secondary active transporter, whereby the energy is provided via a symport or antiport system transporting ions. However, certain SLC transporters can operate in a bidirectional manner and efflux substances out of the cell as well. The ABC transporters (primary active transporters) are efflux transporters requiring energy from ATP to facilitate the movement of the substance against a concentration gradient. Efflux transporters will prevent absorption into a cell by transporting substances from the intracellular environment to the external environment, and thus limit cellular entry.

Many of the intestinal-based transporters have been shown to influence drug absorption and are also involved in DDIs [24]. Membrane transporters can influence drug absorption by either increasing transport into the intestinal enterocyte via influx transporters or limiting transport into the cell via efflux back into the intestinal lumen.

For compounds requiring permeability enhancement to achieve adequate absorption and therapeutic exposure levels, options for enhancing permeability through formulation are limited, as will be discussed later in this chapter. These types of compounds may lend themselves to structural modification to target intestinal influx transporters to increase absorption [25].

Due to the nature of active transporter processes and their concentration dependence, exposure can be nonlinear due to saturation of the transporter. Once an influx transporter is saturated, the passive permeability process will

become the predominant mechanism as concentration increases, and this can result in a subproportional increase in exposure as the drug dose escalates. For efflux transporters, at low concentrations where the transporter is not saturated, absorption may be limited; however, as the dose and thus local concentration in the GI tract increase, if the efflux transporter becomes saturated, the passive permeability process will become the dominant mechanism. Saturation of an efflux transporter in the intestine can result in a supraproportional increase in exposure as the dose escalates. However, there are a number of other mechanisms that can contribute to nondose proportional PK, e.g. solubility limitations or saturation of clearance processes, and thus, teasing out the underlying causal mechanism is often complicated without extensive investigations both in vitro and in vivo.

Whether a transporter becomes saturated in the GI tract depends on the transporter affinity (substrate-binding affinity [K_m]) and capacity (maximal uptake rate [V_{max}]). Transporters with a high capacity and low affinity only saturate at high concentrations; however, transporters with a low capacity and high affinity saturate at lower concentrations. The impact of the transporter contribution to intestinal absorption depends on the contribution of the active process compared to the passive permeability for the specific drug dose. In vitro cell lines expressing transporters of interest are often used to identify if a drug substance is a substrate for a transporter. If an active transport mechanism is identified using in vitro models, caution should be given to interpreting the in vivo significance of the finding. The clinical relevance of transporter activity and whether it will affect exposure in man is dependent on a number of factors such as solubility, passive permeability, dose, transporter affinity, and capacity.

Table 4.2 and Figure 4.2 provide details of the major intestinal transporters relevant in oral drug absorption. Two recent review articles provide an overview of intestinal transporters and the impact on drug absorption [25, 30]. The main SLC transporters expressed in the intestine are peptide transporter 1 (PepT 1), organic anion polypeptide transporters (OATP1A2 and OATP2B1), monocarboxylate transporter 1 (MCT1), sodium multivitamin transporter (SMVT), organic cation and carnitine transporters (OCTN1 and OCTN2), and the concentrative nucleoside transporters 1 and 2 (CNT1 and CNT2). These SLC intestinal transporters are located at the apical brush-border membrane of the intestinal enterocyte, with the exception of MCT1, which is also expressed at the basolateral membrane. The equilibrative nucleoside transporters 1 and 2 (ENT 1 and 2) are also SLC transporters expressed at the basolateral membrane. Plasma membrane monoamine transporter (PMAT) is an SLC influx transporter located on the apical membrane, which is reported to transport metformin, a drug which displays dose-dependent saturable absorption, with absorption by both passive and facilitated transport [31].

Table 4.2 Human intestinal transporters shown to be involved in the transport of drugs.

Transporter type	Transporter protein	Drug substrates
Apical efflux transporters	P-gp/MDR1	Actinomycin D, cerivastatin, colchicine, cyclosporine A, daunorubicin, digoxin, docetaxel, doxorubicin, erythromycin, etoposide, fexofenadine, imatinib, indinavir, irinotecan, ivermectin, lapatinib, loperamide, losartan, nelfinavir, oseltamivir, paclitaxel, quinidine, ritonavir, saquinavir, sparfloxain, tamoxifen, terfenadine, topotecan, verapamil, vinblastine, vincristine
	BCRP	Abacavir, ciprofloxacin, dantrolene, dipyridamole, enrofloxacin, erlotinib, etoposide, furosemide, gefitinib, genistein, glyburide, grepafloxacin, hydrochlorothiazide, imatinib, irinotecan, lamivudine, lapatinib, methotrexate, mitozantrone, prazosin, rosuvastatin, tamoxifen, triamterene, zidovudine
	MRP2	Indinavir, methotrexate, ritonavir, saquinavir, vinblastine
Basolateral efflux transporters	MRP1	Daunorubicin, doxorubicin, epirubicin, grepafloxacin, methotrexate, vincristine
	MRP3	Etoposide, methotrexate
	ENT1	Cladribine, clofarabine, cytarabine, gemcitabine, ribavirin
	ENT2	Clofarabine, gemcitabine, zidovudine
Efflux transporters	MRP4	Cefizoxine, topotecan
Apical uptake transporters	PepT 1	Ampicillin, bestatin, captopril, cephalexin, enalapril, fosinopril, oseltamivir, valaciclovir
	OATP1A2	Fexofenadine, levofloxacin, methotrexate, ouabain, rosuvastatin, saquinavir
	OATP2B1	Atorvastatin, bosentan, fluvastatin, glyburide, pitavastatin, pravastatin, montelukast, rosuvastatin
	MCT1	Arbaclofen placarbil, carindacillin, gabapentin enacarbil, ketoprofen, naproxen, phenethicillin, propicillin
	SMVT	Gabapentin enacarbil
	OCTN1	Quinidine, verapamil
	OCTN2	Cephaloridine, imatinib, ipratropium, tiotropium, quinidine, verapamil
	CNT1	Cytarabine, gemcitabine, zidovudine
	CNT2	Clofarabine, fluorouridine, ribavirin

Sources: Based on Giacomini et al. [24], Varma et al. [25], Mahar Doan et al. [26], Polli et al. [27], Klaassen and Aleksunes [28], and Murakami and Takano [29].

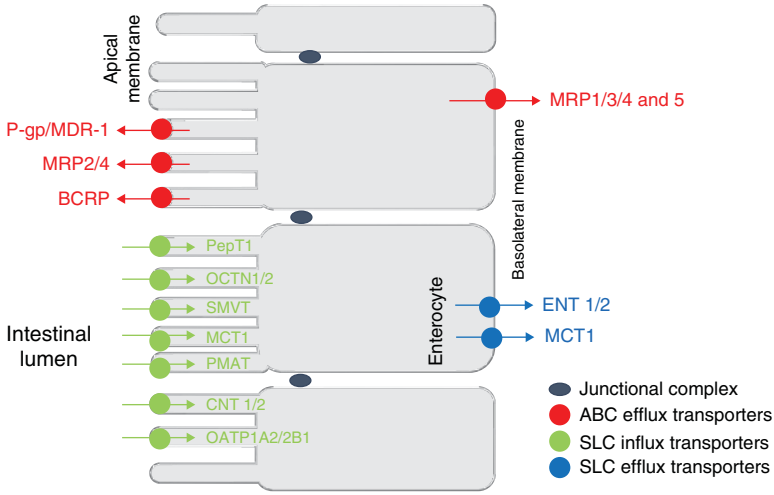

Figure 4.2 Intestinal transporters involved in oral drug absorption.

The main ABC transporters found in the intestine are multidrug resistance 1 (MDR-1) often referred to as P-glycoprotein (P-gp), breast cancer resistance protein (BCRP), and multiresistance proteins 1-5 (MRP1-5). P-gp/MDR-1, MRP2, and BCRP are all located at the apical brush-border membrane, whereas MRP1, 3, and 5 are located at the basolateral membrane, with MRP4 having dual location at both the apical brush border and basolateral intestinal membrane. The apically located ABC transporters (P-gp/MDR-1, MRP2, and BCRP) have been shown to limit absorption of numerous drugs such as the antibiotics, chemotherapy treatments, cardiac drugs, statins and immunosuppressants, and HIV proteases [30].

Intestinal Transporters and Drug Absorption New chemical entities (NCEs) will be evaluated during the drug discovery and development process to assess transporter interactions and thus the implications for absorption and intestinal-based DDIs.

Influx transporters can increase absorption of drug substrates and have been exploited to increase drug exposure. The strategy of creating prodrugs has been used specifically to target increased drug absorption via PepT 1, by introducing peptide-like properties to the parent molecule. The angiotensin-converting-enzyme (ACE) inhibitor Enalapril, an ester prodrug of enalaprilat and a substrate for PepT 1, demonstrates the success of this approach with an increased oral bioavailability of 60–70% compared to 3–12% for enalaprilat [32]. Other examples include the antiviral Valganciclovir, which had a 10-fold increase in plasma exposure compared to ganciclovir, which has been demonstrated in vitro to be attributable to PepT 1 activity [33].

Another example of utilizing intestinal transporters to increase absorption is the prodrug arbaclofen placarbil, which has been designed to target MCT-1. The bioavailability of R-baclofen (active moiety) following dosing with arbaclofen placarbil (pro-drug) was high in monkeys (94%) and dogs (92%), and when compared to dosing oral R-baclofen alone, was approximately two-fold higher [34].

Many drug substances are substrates for efflux transporters and, as such, the implication of the impact of efflux in limiting drug absorption is often assessed during drug discovery. P-gp/MDR-1 is by far the most researched efflux transporter to date. It has a broad substrate range, previously suggested to encompass up to 50% of marketed drugs [35] and can transport small molecules to polypeptides (e.g. 350–4000 Da). The crystal structure of the P-gp protein exhibits partially overlapping binding sites within the internal cavity of the protein, and thus, can explain the broad substrate specificity [36].

Identifying the true role of intestinal P-gp/MDR-1 in drug absorption is often complicated due to a number of factors. CYP3A4 and P-gp/MDR-1 have a large range of overlapping substrate specificities [37]. It has been suggested that they work in conjunction to form a protective barrier, with CYP3A4 metabolizing the drug, while P-gp/MDR1 recycles unmetabolized drug from the enterocyte back into the lumen, thus allowing CYP3A4 prolonged access to the drug for metabolism [38]. Due to the overlap in structure activity with CYP3A4, it is difficult to define if the low absorption of a compound is due to P-gp/MDR-1 efflux back into the intestinal lumen or due to CYP metabolism in the gut [39]. Likewise, when exposure is supraproportional, this could be due to either saturation of efflux or gut metabolism. Location of P-gp/MDR-1 at other sites of the body can also affect systemic exposure and thus present difficulties in assigning a direct link to an intestinal effect.

Digoxin is a well-recognized drug substrate for P-gp/MDR-1 and is often used as a probe substrate to identify P-gp/MDR-1 transporter interactions. It is also a substrate that is not susceptible to CYP metabolism and thus simplifies interpreting the mechanism. Quinidine, a P-gp/MDR-1 inhibitor, has been shown to increase the rate and extent of digoxin absorption in cardiac patients, attributed to inhibiting intestinal P-gp/MDR1 [40]. The clinical impact of P-gp/MDR-1 on digoxin exposure has been demonstrated numerous times in various studies. Fenner et al. [41] compared the area under the curve (AUC) and C_{max} levels of digoxin alone and in the presence of P-gp/MDR-1 inhibitors. In many instances, the impact on AUC and C_{max} of digoxin was less than a two-fold increase in plasma concentrations when coadministered with P-gp/MDR-1 inhibitors; however, given its narrow therapeutic index, a 25% increase in exposure is considered clinically significant due to toxicity resulting from increased plasma levels [42].

The above example highlights that transporter-based DDIs (e.g. inhibition) can occur in vivo, which can affect the PK of the victim drug. The impact of potential

transporter-based DDIs on the overall exposure and safety of that drug would be required to be assessed during development. Both the Food and Drug Administration (FDA) [43] and EMA [44] have recently issued guidances providing details of the preclinical and clinical studies that must be performed to evaluate the transporter-based, drug interaction risks. The EMA guidance recommends that initially the transporter potential be evaluated in vitro using Caco-2 cells and if active transport is observed, then the transporter involved should be identified, if possible. If a clinically relevant transporter DDI is thought to be likely, a clinical study using a strong inhibitor is recommended. If the specific transporter is subject to genetic polymorphisms, in vivo studies with specific genotypes are suggested. The FDA state that all investigational drugs should be evaluated in vitro for being a potential substrate for P-gp/MDR-1 or BCRP. Whether a drug is an inhibitor of P-gp/MDR-1, breast cancer resistance protein (BRCP), and OATP1B1 should also be investigated in vitro based on clinically significant interactions for drugs, which are substrates of these transporters. Decision trees are provided, which give guidance on when a clinical DDI study is required based on the in vitro data generated.

Regional Expression and Polymorphism of Intestinal Transporters and Impact of Drug Variability Variability in the in vivo performance of drug products can be attributed to a number of physiological and formulation causes as described in this chapter. Regional expression and polymorphism of transporters can contribute to these observations, either directly or in conjunction with other causative factors such as drugs and food that alter transit times within the GI tract. In addition, components within food and formulation excipients may alter exposure by inhibiting transporters involved in drug absorption. When grapefruit juice is given with oral talinolol, exposure increases, and the proposed mechanism is inhibition of intestinal P-gp/MDR-1 improving bioavailability by increasing absorption [45]. In vitro studies have also suggested that the breakdown products from a high-fat meal, such as monoglycerides, may increase drug absorption by inhibiting P-gp/MDR-1 [46].

Expression of transporters can vary between regions of the GI tract and between individuals. Polymorphisms of specific transporters may also affect expression levels and functionality, thus having the potential to impact drug absorption.

Transcript levels of several efflux transporters have been measured in human jejunal tissue from 13 healthy volunteers [47], where the levels were found to vary two-fold to threefold only. The BCRP and MRP2 transcript levels were higher than that for P-gp/MDR-1, which was similar to those for MRP1, MRP3, and MRP5, with MRP4 having the lowest transcript level. Expression levels in human duodenal tissue from 14 subjects have shown BCRP expression is greater than P-gp/MDR-1, with MRP2 having the lowest expression level of the

three transporters investigated [48]. However, BCRP expression has previously been shown to be comparable to that of P-gp/MDR-1 in the duodenum, with expression levels decreasing toward the colon [49]. MRP2 expression is highest in the duodenum, then decreases in the terminal ileum and further still in colonic regions [50]. The expression of P-gp/MDR-1 has been shown to vary over the GI tract, with levels increasing from the stomach and duodenum to the colon [51].

PepT 1 is a low-affinity/high capacity transporter known to transport a variety of peptide-like drugs [52]. It has been shown to be expressed at high levels in the small intestine [53]; however, its expression in healthy colonic tissue was not clear, until a recent publication [54] confirmed the presence of PepT 1 in healthy human distal colonic tissue and also showed its functionality in an in vivo mouse model.

Polymorphisms of transporter genes can also lead to variable exposure, if the drug is a substrate for that particular transporter. The variant 1249G>A [V4171] of MRP2 has been associated with higher intestinal activity of the transporter resulting in lower oral bioavailability of talinolol [55].

The variants of the P-gp gene have also been associated with higher serum digoxin concentrations, and could have implications for variable digoxin exposure within a study population, and also safety implications [56]. Whether this effect is at absorption or elimination level is unknown. However, a correlation between a polymorphism in exon 26 (C3435T) of P-gp and duodenal expression levels has been demonstrated. The polymorphism (homozygous) results in significantly lower duodenal P-gp expression and higher digoxin plasma levels [57], which illustrates that polymorphisms of P-gp can affect absorption of P-gp substrates. Another example is the polymorphism of the OATP2B1 gene, which causes a change in amino acid S486F. A clinical study in Japanese subjects has shown that the three genotypes dosed had different exposures (AUC and C_{max}) of fexofenadine, which could not be attributed to changes in clearance, and therefore the effect is a result of altered absorption [58].

Another cause for variability in drug absorption, especially in absorption over time, can be due to downregulation or induction of the transporter protein levels in the intestine, thus affecting the magnitude of the transporter effect [30].

4.2.2.3 Gender and Age Effects

Further implications of variations in GI physiology on oral drug delivery may also need to be considered based upon the sex and age of the target population, which can often require clinical pharmacology studies to be conducted to assess the impact on bioavailability and PK in these specific groups.

A review of the influence of gender was recently reported [59], summarizing how differences in factors with potential to influence bioavailability had been observed, including fasting stomach pH (lower in males), fecal pH (higher in females), gastric emptying and colonic transit time (both longer in females),

enzyme prevalence as well as bile acid secretion and composition. The authors commented how possible gender differences can be influenced by stage of the menstrual cycle as well as the age of the female population. The differences can be substantial, for example a 63% increase in bioavailability of ranitidine, a P-gp substrate, was reported in males but not females when polyethylene glycol (PEG) 400 was included in formulations, which was hypothesized to be due to greater benefits in males from suppressing efflux processes [60].

The impact of age-related differences in physiology is widely acknowledged particularly in regard to pediatric and geriatric populations. For example, in newly born children, the gastric pH is initially elevated at pH 6–7, only dropping over 20–30 months to pH 1–2 [61], presenting significant formulation and delivery implications for oral delivery of ionizable drugs to this age range compared to older children, adolescents, and adults. A further challenge is the observation that intestinal transit times have been reported to be faster in young children, which may reduce the potential for drug absorption, particularly for poorly soluble drugs or sustained-release products [62].

In comparison to younger populations, the increased use of medications to treat chronic diseases has the potential to impact GI physiology in elderly subjects. Furthermore, a recent review article [63] described how the basic GI functions such as motility, secretion, intraluminal digestion, and absorption change with aging. Factors such as delayed gastric emptying, reduced acid secretions, and decreased motility all have potential to affect the in vivo biopharmaceutics performance of the drug substance and dosage form. Such changes can either increase (for example via prolonged intestinal residence) or decrease (for example via elevated gastric pH and hence reduced solubilization of weak bases) the oral absorption of drugs in this population.

4.2.2.4 GI Transit

Since different regions of the GI tract have the potential to affect the systemic exposure of a drug in different ways, it is important to understand typical transit times to aid formulation design, whether for time-based release systems to achieve regional targeting and delivery, or for sustained-release dosage forms to assess what proportion of the drug dose might be delivered to each region. If release over a prolonged period is desired then while release rate will be controlled by the formulation, the length of time that formulation resides in each region and hence the location to which the drug is delivered will be controlled by GI transit time.

In the fasted state, it is widely acknowledged that gastric emptying occurs on average approximately 30 minutes following dosing, with transit through the small intestine having a mean time of around three hours (measured as the time from gastric emptying through to arrival at the ICJ). Subsequent passage through the large intestine generally taking a further 20 hours of which 2 hours, and often

Table 4.3 Mean and range in transit times in anatomical regions of GI tract.

Region	Residence time (h)		
	Mean	Range	Cumulative mean
Stomach	0.5	0–2	0.5
Jejunum	1.25	0.5–2	1.75
Ileum	1.5	0.5–2.5	3.25
ICJ	1.25	0–12	4.5
Colon	20	0–72	24.5

Source: Quotient Sciences, unpublished data.

much longer, is attributed to transit through the ascending colon (Quotient Sciences, unpublished data). There is however significant intra- and intersubject variability in transit times (Table 4.3).

Several factors can substantially impact gastric emptying, not just the contractile stage (Phase III) of the inherent physiological migrating motor complex (MMC) (also known as the migrating myoelectric complex), but also the prandial state (gastroretention of stomach contents occurs post feeding) and the type and size of dosage form itself. Cowles et al. [64] reported how 13 mm × 18 mm tablets had significantly longer gastric residence than those 7 mm × 18 mm in size, while multiparticulate dosage forms have been shown to be less susceptible than monolithic tablets to the effect of food on GI transit [65, 66]. Strategies to deliberately achieve delayed gastric emptying of dosage forms and hence sustained drug delivery to the upper small intestine will be discussed later in this chapter.

Dosage form factors do not influence small intestinal transit to the same extent; however, intra- and intersubject variability does still exist. Transit through the jejunum and ileum can range from 1 to 4.5 hours and residence at the ICJ can be anything from 0 to 12 hours (Table 4.3). Commonly, small intestinal transit is quoted as ranging from one to six hours with two to four being the most commonly cited times [67].

In general terms, however, it can be assumed that, on average, a dosage form administered in the fasted state will arrive in the colon approximately four hours post-dose. Consequently, there is limited time to achieve delivery to and hence absorption from the more favorable environment of the small intestine. In contrast, subsequent transit through the colon is extended, affording the potential to allow prolonged uptake, but only if the drug is sufficiently well absorbed from this region.

The relevance of GI transit time on dosage form design was exemplified by Lobo et al. [68], who described how the performance of a hydroxylpropyl methylcellulose (HPMC) sustained-release matrix formulation developed to release drug over four hours in vitro, was confirmed in vivo with a consistent erosion time ranging from 2.5 to 3.1 hours post dosing (observed via gamma scintigraphy). There was however significant variability in the anatomical location where complete erosion was observed, ranging from the stomach to the colon. Such differences will clearly impact the arising PK from the dosage form in the clinical setting despite its intrinsic performance. The impact of variable colonic transit times has also been exemplified by an investigation on oxprenolol, which correlated plasma concentration time profiles, and extent of absorption with GI transit time and particularly colonic transit [69].

4.2.2.5 Effect of Food

The prandial state can have a variety of effects via multiple mechanisms on GI physiology and hence oral drug delivery, impacting both the rate and extent of absorption. Effects are usually manifested by changes in systemic exposure of the drug and can be either positive or negative. During clinical research food effects on oral bioavailability are assessed by regulatory-defined, adequately powered, clinical pharmacology studies. Increasingly however, exploratory food effect assessments are performed as early as the first-in-human (FIH) study given the potential impact on the development strategy as well as downstream posology and prescribing information. Food effects can arise from modification of gastric pH, delayed gastric emptying, increased drug solubilization, induction of bile release, mechanical formulation stresses, a direct interaction with the drug itself, or a combination of factors. The caloric and fat content of food can impact the magnitude of any effect.

In terms of drug solubility, a key positive effect often observed is with biopharmaceutics classification system (BCS) Class 2 and 4 compounds (low solubility with high and low permeability, respectively) through the presence of lipidic dietary components and bile acids. Alternatively, the typical elevation of gastric pH in the fed state to pH 3–4 or even greater [70], could positively or negatively influence the solubility of acidic or basic drugs, respectively, depending upon individual pK_a values.

The presence of food slows gastric emptying as a result of the physiological response to the ingestion of food; the stomach requires time to grind the food and mix it with gastric secretions to create chyme. The extent of the effect is dependent on the meal provided, with high-fat, high-calorie meals resulting in much slower delivery of the stomach contents to the duodenum. From a PK perspective, this would typically be manifested by a delay in t_{max}. For nondisintegrating solid-dosage forms, emptying from the stomach in the fed state therefore tends to

be delayed and variable. In the majority of cases, the dosage form remains in the stomach for a prolonged period of time, which can present challenges such as an increased burst effect releasing weakly basic drugs, or the premature disintegration and failure of sustained release matrix tablet formulations from contractile forces.

There also exists the potential for direct interactions between food components and drug substances, perhaps the most recognized of which is for divalent cations (e.g. calcium in milk) to complex with tetracycline antibiotics thereby reducing bioavailability. Care is needed from a product formulation perspective where such risks could innocuously exist, for example via the preferred use of sodium stearyl fumarate rather than magnesium stearate as a tablet lubricant.

4.2.2.6 Enterohepatic Circulation

Bile aids the digestive and absorptive process for food nutrients and is discharged into the GI tract in response to gastric emptying and the release of endogenous neurohormones such as secretin and cholecystokinin, resulting in gall bladder contraction. Biliary clearance is also an important route for many drugs especially those undergoing Phase II (conjugated) metabolism, which are lipophilic in nature, of a high molecular weight (350–600 Da), and/or a substrate for active transporter processes [71]. This in turn can have a potentially unique and significant effect on their oral bioavailability through the phenomenon of enterohepatic circulation (EHC) as drug conjugates eliminated in bile can be hydrolyzed by gut bacteria and undergo reabsorption into the systemic circulation from within the GI tract. EHC may therefore prolong the pharmacological effect or cause double peaks in the plasma levels of certain drugs and drug metabolites, as well as be a cause of interindividual differences in drug response observed in healthy subjects and in patients with certain cholestatic liver diseases.

Characterization of biliary clearance in humans is very challenging, because with the exception of special surgical preparations in animal studies, bile is not directly accessible due to the anatomy of the hepatobiliary tract. Collection in humans is limited to postsurgical patients with underlying hepatobiliary disease or, in healthy subjects, the use of feces as a surrogate to quantify the amount of drug excreted via nonurinary pathways (accepting this will be confounded by the presence of nonabsorbed drug and any transitioned back into the GI tract via efflux transporters). The occurrence of EHC is therefore inferred indirectly from evidence of secondary peaks in plasma–time concentration profiles and hence prolonged elimination half-life of the drug following a single oral dose.

A noninvasive method for sampling duodenal fluid has recently been described using the Entero-Test® string [72, 73]. Entero-Test is a gelatin capsule containing a 140-cm-long highly absorbent, weighted nylon string, which is ingested with the other end taped to the subject's mouth. The string passes into and subsequently

resides in the duodenum. The string is withdrawn through the mouth and the recovered bile sample analyzed. The published studies involve the intravenous administration of ^{14}C labeled drugs and describe how baseline samples are obtained by swallowing an Entero-Test capsule on the morning of the day before drug administration (Day-1) and removal of the string before dosing on Day 1. A post-dose bile sample is obtained from a second bile string administered immediately before dosing on Day 1 and removed approximately 24 later in the morning of Day 2.

4.3 Biopharmaceutics Classification System (BCS)

4.3.1 Background and Regulatory Perspectives

The BCS is a tool that was introduced by Gordon Amidon in 1995 [74]. Drug substances are classified into one of the following four categories based on the solubility and permeability properties:

BCS Class 1. High permeability, high solubility
BCS Class 2. High permeability, low solubility
BCS Class 3. Low permeability, high solubility
BCS Class 4. Low permeability, low solubility

The concept and applicability of using BCS to support biowaivers was then published by the FDA in August 2000 [75]. The guidance outlines the framework for the BCS and also its potential uses. Essentially, it has been designed as a mechanism for pharmaceutical companies to apply for biowaivers for certain compound types in place of clinical bioequivalence (BE) studies. It provides recommendations for sponsors of investigational new drug applications (INDs), new drug applications (NDAs), abbreviated new drug applications (ANDAs), and supplements to these applications who wish to request a biowaiver of in vivo bioavailability (BA) and/or BE studies for immediate release (IR) solid oral dosage forms. It outlines a scientific framework for classifying drugs, which accounts for the two factors governing the rate and extent of drug absorption, i.e. aqueous solubility and permeability.

As dissolution of the drug product can have a significant effect on rate of absorption, a rapid or slow dissolution category is also assigned to an IR solid oral dosage form. A BCS Class 1 compound will behave as a solution in vivo, and, if dissolution is fast, then absorption is dependent on gastric emptying, and thus independent of formulation changes.

Since the original guidance was published, there have been a series of literature articles suggesting that the criteria are too strict and biowaivers could be

expanded to other classes [76–79]. A draft guidance was issued in May 2015 to extend biowaivers for BCS Class 3 compounds and also to modify the original permeability and solubility categories [80]. In December 2017 the guidance was finalized [81], with additional information regarding biowaivers for BCS Class 3 compounds, and also dissolution and permeability categories being updated from the draft guidance.

The solubility classification for Class 2 acidic drugs has also been suggested to be too restrictive, considering that the majority of absorption will take place in the small intestine, where the pH is above 5. Therefore, an intermediate solubility class for highly permeable ionizable compounds has been postulated [82]. For Class 2 drugs, in silico absorption modeling has also been highlighted as a potential technique to identify compounds (weak acids and bases in IR dosage forms), which would be suitable as biowaiver candidates, if the dose dissolves completely before reaching the middle jejunum [83].

Currently, biowaivers can be requested for IR solid oral dosage forms, which are defined as BCS Class 1 (highly permeable and highly soluble), rapidly dissolving and meet the following criteria; the drug does not have a narrow therapeutic window, excipients used within the formulation do not affect the rate and extent of drug absorption, and the drug is stable within the GI tract. For highly soluble drugs, whereby dissolution is fast, an IR dosage form will essentially behave as a solution, and gastric emptying will control the rate of absorption. Biowaivers can also now be requested for BCS Class 3 compounds (low permeability and highly soluble), which have very rapid dissolution.

Highly soluble is defined as when the highest dose strength is soluble in <250 ml of aqueous media over a pH range of 1–6.8 (pH 1–7.5 specified in the original FDA 2000 guidance [75]). Highly permeable is defined as when >85% (>90% specified in the original FDA 2000 guidance [75]) of the administered dose is absorbed in humans (as determined by mass balance or absolute bioavailability). Bioavailability data from animals or permeability data for in vitro cells lines, such as Caco-2, may also be used as evidence of high permeability. Rapidly dissolving is defined as when a mean of $\geq$85% of the labeled drug substance dissolves in $\leq$30 minutes using United States Pharmacopeia (USP) Apparatus I or II in a volume of $\leq$500 ml (900 ml specified in the original FDA 2000 guidance [75]), or 900 ml if it can be justified, in each of the following media:

1. 0.1 N HCl or simulated gastric fluid (SGF) USP without enzymes,
2. pH 4.5 buffer,
3. pH 6.8 buffer or simulated intestinal fluid (SIF) USP without enzymes.

Very rapidly dissolving is defined as when a mean of $\geq$85% of the labeled drug substance dissolves within 15 minutes, under all of the above conditions. It is a requirement that validated, stability indicating analytical assays are used to

support the BCS classification for solubility, permeability, dissolution, and GI tract stability.

There are a number of factors that also need careful consideration when requesting a biowaiver; if the formulations contain any excipients that may affect the rate and extent of drug absorption, e.g. new excipients or large quantities of excipients, additional data may be required. As there is a concern that excipients may have a greater impact on the absorption of compounds with poor permeability, for BCS Class 3 drugs it is specified that the test drug product must contain the same excipients as the reference product for a biowaiver to be granted. The test and reference drug product must be qualitatively the same and quantitatively very similar, with the guidance providing specific details on what is acceptable. If the drug in question is a prodrug, consideration to the mechanism and site of conversion is required, and the assessment of permeability, solubility, and dissolution may need to be conducted for both the prodrug and the active moiety. It is also possible to get biowaivers for fixed-dose combinations for BCS Class 1 and BCS Classes 1 and 3 if certain conditions are met.

Biowaivers based on BCS data will not be granted for (i) drugs with a narrow therapeutic index or (ii) products that are absorbed via the oral cavity, i.e. buccal or sublingual dosage forms. However, a BCS-based biowaiver is possible for an orally disintegrating tablet if the sponsor can prove that there is no absorption occurring from the oral cavity.

The FDA formed a CDER (Center for Drug Evaluation and Research) BCS committee in 2004, which consists of members from different offices within the CDER who have the appropriate skills to review the BCS applications. The BCS committee was formed to ensure that there is consistent implementation of the guidance across all therapy areas, and roles include reviewing BCS applications, being a point of contact for BCS questions, etc. and also updating the guidance if required [84].

Although the BCS guideline is a product of the FDA, the principles are accepted by other Regulatory Bodies, and recently BCS-based biowaivers have also been raised as a topic for harmonization by the International Council for Harmonization of Technical Requirements for Pharmaceuticals for Human Use (ICH). The European Medicines Agency (EMA) has issued a document covering the BCS framework and will also accept biowaivers for certain compounds. While the World Health Organization (WHO) is not a regulatory body, its guidances are often given regulatory status by many national regulatory authorities [85]. Guidance on BCS based biowaivers for multisource (generic) products and a WHO model list of essential medicines are covered in Annexes 7 [86] and 8 [87], respectively. The WHO guidelines are often used to direct countries, which do not have a BCS-based guidance or are in the process of developing one [88].

Regions of Asia (Brunei Darussalam, Cambodia, Indonesia, Laos, Malaysia, Myanmar, Philippines, Singapore, Thailand, and Vietnam) follow the Association of Southeast Asian Nations (ASEAN) guideline draft [89], which is adopted from the EMA 2001 guidance on bioavailability and BE, and uses the BCS principles. The Australian regulatory authority (Therapeutic Goods Administration [TGA]) has recently issued an updated guidance [90], which states that the BCS should be used to justify not performing clinical BE studies where relevant, again this being adopted from the recent 2010 EMA guideline. New Zealand also adopts the EMA BCS principles and refers to this within the relevant guideline [91]. Previously, Canada did not consider the use of the BCS appropriate and would not accept biowaivers for BCS Class 1 compounds. However, a new guidance document based on the BCS has recently been released, stating biowaivers can be granted for BCS Class 1 and 3 compounds [92]. All the above guidances are compared in Table 4.4 and state that BCS-based biowaivers are not applicable for drugs with a narrow therapeutic index. Japan does not adopt the BCS principles as the view is that the difference in dissolution and bioavailability between two products is due to difference in formulation variables [93]. Japan has its own specific BE guidelines for approved products, which must be followed for changes in formulation for solid oral dosage forms [88].

4.3.2 Determining a Solubility Class

The FDA guidance also provides details of how to demonstrate that the compound has high solubility. It states that equilibrium solubility should be measured at $37 \pm 1\,^{\circ}\mathrm{C}$, over a pH range from 1 to 6.8, using standard USP buffers, with $n = 3$ replicates. The pH of the solution should be checked after addition of the drug, and adjusted to the target pH if required. The solution pH also needs measuring at the end of the study. Samples should be analyzed by a validated stability indicating assay that can distinguish the drug from its degradation products. The number of buffer conditions tested will depend upon the pK_a of the drug; for example a drug with a pK_a in the range of 3–5 is recommended to be tested at pH 1 and pH 6.8, and $pH = pK_a$, $pH = pK_a + 1$ and $pH = pK_a - 1$. Three replicates are suggested for each buffer condition, and depending on the variability within the data set additional replications may be required. The volume of the buffer required to dissolve the highest dose strength over the pH range should be calculated, and if the volume is $\leq$250 ml, a high solubility classification can be assigned. If the highest dose administered is greater than the highest dose strength tested for solubility, consideration needs to be given to the impact of this on the solubility classification. It is likely additional information such as dose proportionality over a wider dose range will be required.

Table 4.4 Comparison of FDA, EMA, Canada, and WHO guidances covering the BCS principles.

	FDA– BCS guidance 2000 [75]	**FDA– BCS guidance 2017 [81]**	**EMA – BE Guidance 2010 [85]**	**WHO Technical Report Series, No. 937,Annex7[86]**	**Canada–BCS guidance 2014 [92]**
	Highest strength (max dose) dissolvedin pH 1–7.5	Highest strength (max dose) dissolvedin pH 1–**6.8** buffers	Highest single dose administered as an IR is soluble in 250 ml pH 1–6.8 buffer	Highest dose recommended by WHO (if on the WHO model list of essential medicines) or highest dose strength available onthe market(if not onthe WHO list) administered as an IR is soluble in ≤250 ml pH 1.2–6.8 buffer	Highest therapeutic dose is soluble in pH 1.2–6.8
	_90% Mass balance and absolutebioavailability studies inhumans are the preferred approach. Intestinal perfusion methods can be used in human and animals and invitro permeation studies using cell lines or excised tissue. In vitropermeability data acceptable but need to show GI tract stability	**≥85**% Mass balance and absolutebioavailability studies inhumans are the preferred approach. Intestinal perfusion methods can be used in human and animals and invitro permeation studies using cell lines or excised tissue. In vitropermeability data acceptable but need to show GI tract stability	≥85% absorption demonstratedby human studies. In vitrodata considered supportive, as mayBEoral studies using aqueous and solid formulations	≥85% absorption demonstratedbyhuman studies (mass balance or absolutebioavailability). Human intestinal perfusion method isalso acceptable. In vivo or in situ animal perfusion models and in vitrocell-culture model data can be used as supportive	Class 1 ≥ 85% Class 3 ≥ 85% Mass balance and absolute bioavailability studies, data obtained from literature can be used if studies aredesigned appropriately. In vitrodata considered supportive

	FDA – BCS guidance 2000 [75]	FDA – BCS guidance 2017 [81]	EMA – BE Guidance 2010 [85]	WHO Technical Report Series, No. 937, Annex 7 [86]	Canada – BCS guidance 2014 [92]
Dissolution	Dissolution in ≤900 ml 0.1 N HCl or simulated gastric fluid (SGF) USP without enzymes, pH 4.5 buffer and pH 6.8 buffer or simulated intestinal fluid (SIF) USP without enzymes Rapid dissolution, 85% in 30 min	Dissolution in **≤500 ml** 0.1 N HCl or simulated gastric fluid (SGF) USP without enzymes, pH 4.5 buffer and pH 6.8 buffer or simulated intestinal fluid (SIF) USP without enzymes Rapid dissolution mean of ≥85% in ≤30 min **Very rapid dissolution mean of ≥85% in ≤15 min**	Dissolution in ≤900 ml pH 1–1.2 (usually 0.1 N HCl or SGF without enzymes), 4.5, and 6.8 (or SIF without enzymes) Rapid dissolution ≥85% in ≤30 min Very rapid dissolution ≥85% in ≤15 min	Dissolution in ≤900 ml of pH 1.2 HCl solution, pH 4.5 and pH 6.8 buffer Rapid dissolution ≥85% in ≤30 min Very rapid dissolution ≥85% in ≤15 min	Dissolution in ≤900 ml pH 1–1.2, 4.5, and 6.8 Rapid dissolution >85% in ≤30 min Very rapid dissolution >85% in ≤15 min SGF and SIF without buffers may also be used
Excipients	Yes for currently approved IR products, new excipients or very large quantities used will require additional supporting data	Class 1 – product does not contain any excipients that will affect the rate and extent of absorption of the drug **Class 3 – test product formulation is qualitatively the same and quantitatively very similar**	Class 3 – excipients are qualitatively the same and quantitatively very similar Excipients that might affect bioavailability should be qualitatively and quantitatively the same	Evidence is required, that excipients present in the product are well established and do not affect GI motility, or absorption. Excipient is present in the comparator, or in a number of other products, which contain the same active pharmaceutical ingredient (API). The excipient is present in a similar amount to the comparator, or in an amount typically used for that type of dosage form.	Class 1 – excipients affecting bioavailability should be the same as in the reference Class 3 – excipients should be qualitatively the same and quantitatively very similar to the reference

(*continued*)

Table 4.4 (Continued)

	FDA– BCS guidance 2000 [75]	FDA– BCS guidance 2017 [81]	EMA – BE Guidance 2010 [85]	WHO Technical Report Series, No. 937, Annex7 [86]	Canada–BCS guidance 2014 [92]
Biowaivers	Class I	Class 1–rapid dissolution **Class 3–very rapid dissolution**	Class 1–very rapidor similarly rapid dissolution, applicable for different salt forms if both salts areClass 1 Class 3–very rapid dissolution, biowaiver decision will be more critically reviewed.	Class 1–rapidly dissolving and meets the criteria of dissolution profile similarity $f_2 \geq 50$ Class 1–very rapidly dissolving, f^2 comparison is not required Class 3– eligible for biowaivers if the following are considered; similarity of the test and reference dissolution profiles, excipients used in the formulation and risk of incorrect decision. Class 2– high solubility at pH 6.8 (but not at pH 1.2 and pH 4.5), high permeability, rapid dissolution (85% in ≤30 min) in pH 6.8, and test displays similar dissolution (determined by f_2)tothe comparator at three pH values (pH 1.2, 4.5, and 6.8). Excipients and risk of incorrect decision also need consideration	Class 1–very rapidand rapid dissolution, for rapid dissolution, f_2 test is required. Class 3–Very rapid dissolution

Bold text highlight differences between FDA 2000 [75] and 2017 [81] guidances.

4.3.3 Determining a Permeability Class

The preferred methods for determining the permeability classification are human studies, either mass balance, absolute bioavailability, or intestinal perfusion studies (Loc-I-Gut procedure). For the mass balance and absolute bioavailability studies, an adequate number of subjects are required to determine a reliable estimate of absorption. Other methods, which can be used to determine a permeability classification, include in situ intestinal perfusion in suitable animals (e.g. rats), in vitro permeability assessments using excised intestinal tissue, or epithelial cell monolayers (e.g. Caco-2 cells). If the data are conclusive, a single method is often sufficient for defining a permeability classification. Examples of this would include when bioavailability is 85% or greater, 85% or more of the drug is excreted unchanged in the urine, or when 85% or greater is recovered in the urine as parent and metabolites. For the last method mentioned, data must also be provided to illustrate that the drug is stable within the GI tract. Significant potential for poor stability is suggested when greater than 5% degradation of the drug occurs in gastric fluid for one hour or intestinal fluid for three hours.

The guidance advises that, when a single method fails to conclusively demonstrate a permeability class, providing data using two methods may be advantageous. Human data are viewed as the gold standard, and these data will supersede those from other models.

The intestinal permeability methods (e.g. Loc-I-Gut, animal in situ perfusion models, intestinal tissue methods, and cell-culture models) are considered suitable for passively transported drugs (e.g. no involvement from active influx or efflux transporter systems). A requirement for using the above methods is that the systems are appropriately validated. The regulators have insisted on characterization of the systems to ensure that misclassification of the permeability class is avoided. There is a concern that, if active transport systems (e.g. P-gp, BCRP, and MRP2 efflux systems) are not expressed in the in vitro models or the expression is low compared to that seen in humans, the permeability classification from these models may be overestimated. For permeability investigations using in vivo or in situ animal models and in vitro permeability investigations, the guidance requires permeability to be investigated at three concentrations (e.g. 0.01, 0.1, and 1 times the highest dose strength dissolved in 250 ml).

A passive transport mechanism can be defined when one of the following are met: (i) a proportional relationship between dose (over the relevant clinical range) and bioavailability in humans or linear PK in humans, (ii) a lack of dependence of the permeability on the initial drug concentration when using the in vivo or in situ animal models, or (iii) a lack of dependence on the initial drug concentration or on transport direction (e.g. the rate of transport across the cell monolayer is the same in both directions) for in vitro cell-culture models expressing efflux

transporters such as P-gp, BCRP, and MRP2. However, the guidance also states that if the in vitro method demonstrates active transport but the human PK is linear, there are fewer concerns suggesting that this combined information would support a permeability classification.

Validation of the permeability model to illustrate that the system is suitable for defining a permeability classification is required. This is assessed by establishing a rank-order relationship between measured permeability values of model drugs in the various models and the extent of absorption of these drugs in humans. The guidance provides a list of suggested model drugs and the relationship established must allow differentiation between high and low permeability with the model drugs chosen representing zero, low (<50% F_{abs}), moderate (50–84% F_{abs}), and high ($\geq$85% F_{abs}) absorption. For the human intestinal perfusion method (Loc-I-Gut model) 6 model drugs are recommended, while the other models require a larger validation set using 20 drugs. Once the relationship is established and the model validated, a high and low permeability model drug should be used as internal standards (included in the donor fluid with the test drug) in future studies, and therefore it is not necessary to rerun the validation model drug set with each study. The data subsequently generated using the internal standards should not differ significantly between tests or from the validation test.

The guidance advises that there must be acceptance criteria set for the high, low, and zero permeability standards and that membrane retention (for tissue or cell monolayers) needs to be calculated. The new guidance provides more clarification around this and states that tissue/cell/membrane analysis is only required at the end of the study to assist in mass balance calculations, if recovery from the apical and basolateral chambers are <80%. When selecting a high permeability internal standard, the proximity of the permeability of the internal standard to the high and low boundaries is important. The lower the permeability is for the high permeability internal standard, the greater the chance of demonstrating high permeability for the compound in question. To demonstrate that a compound has high permeability, its permeability value must be greater than or equal to that of the high permeability internal standard. A rationale for the concentrations of drugs (which is assumed to be both markers and test drug) used in the permeability studies is also required to be included in the regulatory application.

When permeability methods are used to support a high permeability classification, evidence of the stability of the drug within the GI tract is required. This is also required for mass balance studies.

The guidance provides limited details on how to perform the in vitro permeability assessment; a minimum of three replicates per condition are suggested in the updated guidance [81]; however, additional suggestions on using $n = 6$ monolayers for each condition and demonstrating the compounds stability in the cell-culture media/conditions have been made [93]. No guidance is given on the

pH conditions for permeability assessments for in vitro cell-culture models, and this can impact the permeability data generated. Consideration needs to be given to the pH at which these studies are conducted. The suggested pH conditions to mimic in vivo situation are apical pH 6.5 and basolateral pH 7.4. However, for acidic and basic compounds, this will affect the permeability data generated due to a change in the percentage of neutral species (pH partition theory) at these different pH values and can give rise to false-positive results for active transport systems. For a basic compound such as propranolol, if studied at pH 6.5 and 7.4, the permeability data generated will suggest efflux [94], and for an acidic compound such as indomethacin, active influx will be observed [95]. Reliable transporter effects when using a bidirectional permeability assay can only be assessed using an iso pH gradient. A recent article has provided pH-dependent permeability and solubility criteria that can be used to assign a provisional BCS classification early in discovery [96].

The Caco-2 cell line is often used to support permeability classifications for BCS. However, Madin-Darby canine kidney type II cell line heterogeneously expressing the human P-gp transporter (MDCKII-MDRI) has recently been validated for BCS permeability classification [97]. Interestingly, the validated method is performed using GF120918 (a specific P-gp inhibitor) in the media, and therefore theoretically the nontransfected cell line (MDCKII) should generate the same results and thus raises questions about the necessity for this transfected cell line for this purpose. This method uses a unidirectional assay (apical to basolateral) and dual pH conditions; pH 5.5 and pH 7.4 apical conditions and pH 7.4 basolateral conditions [97].

A single method to support a permeability classification may not always be appropriate and may lead to misclassification. For example, Sotalol has been shown to have high F_{abs} (90%), and yet the Caco-2 permeability was low [98]. However, investigations using the rat intestinal perfusion model have shown that sotalol has high permeability in the distal ileum and, thus, is suggested to be responsible for the high F_{abs} observed in man [99].

4.3.4 Determining Dissolution of the Drug Product

Biowaivers can be granted for BCS Class 1 compounds if the test formulation dissolves rapidly and does not contain excipients that will affect drug absorption. Certain BCS Class 3 compounds are also applicable for biowaivers. In this instance, the test and reference drug product must dissolve very rapidly, with the caveat that the test formulations are qualitatively the same and quantitatively very similar. Dissolution apparatus should meet the USP requirements and the FDA's guidance on Mechanical Calibration of Dissolution Apparatus I and II [100]. Dissolution should be performed using USP Apparatus I (100 rpm) or USP Apparatus II

(50 rpm), with a 500-ml volume (900 ml maybe used with appropriate justification) of the following media:

- 0.1 N HCl or SGF USP without enzymes
- pH 4.5 buffer
- pH 6.8 buffer or SIF USP without enzymes

These conditions can be modified under certain circumstances, for example the rpm can be changed to 75 rpm if justification can be provided and for formulations containing a gelatin component, enzymes can be added to the media. Dissolution should be performed using at least 12 dosage units of both test and reference for each dose strength, with samples collected at appropriates times to characterize the full dissolution profile. Similarity between the test and reference product should be established using the similarity factor (f_2), with an f_2 value of $\geq$50 illustrating similarity. The f_2 test is not required if both the reference and test drug product dissolve $\geq$85% within 15 minutes in all three media.

4.3.5 GI Stability

When using mass balance studies by total radioactivity in the urine to demonstrate absorption, this analysis does not take into consideration any instability in the GI tract. If the radioactive compound is broken down in the gut lumen and the breakdown products are absorbed, this could lead to an overestimation of absorption. Therefore, when using this method, it is necessary to demonstrate stability in the gut lumen. This can be performed using simulated gastric and intestinal fluids. The experimental design is such that the compound is incubated with the appropriate fluids for a time representative of the in vivo contact time (one hour in gastric and three hours in intestinal fluid) at 37 °C. If there is greater than 5% degradation, this could suggest potential instability.

4.3.6 Applications and Limitations of BCS Classification

Although the BCS guideline has been generated to facilitate biowaivers using in vitro data, the BCS structure has been embraced during drug development to help assist not only at the discovery stage in selecting compounds with good biopharmaceutic properties to ensure successful formulation development, but also to highlight where enabling formulation strategies will be required and to assess the risk of formulation switches and data required to support them, e.g. in vitro or BE studies. During the development of Pregabalin, in vitro dissolution data (pH range 1.2–6.8) was used to show that three different series of formulations and the commercial formulation were all rapidly dissolving and had similar dissolution profiles. The data were subsequently used to support biowaivers [99]. Using

the BCS in this instance was estimated to have saved more than US$ 1 000 000 in research and development costs.

A number of articles have been published whereby lists of oral drugs have been provisionally classified according to BCS based on available literature data, including the Model list of Essential Medicines of the WHO, which were assigned a BCS classification based on data available in the public domain [101]. Thirty-two out of the 89 listed were given a BCS Class 1 classification (either certain or provisional) and the publication states that these could be considered for biowaiver status based on in vitro dissolution data as opposed to BE studies in man. It has also been estimated that 30% of the oral IR drug products on the US top 200 oral drug products can be classified as BCS Class 1 [102]; thus, there is potential to save the industry over US$ 35 000 000 per year by applying the BCS [99]. Furthermore, 55% of these drugs have been given a provisional high solubility definition (BCS Classes 1 and 3) [102] thus the actual potential saving may be greater. The literature clearly highlights the potential additional use of the BCS-based biowaiver systems, especially now the draft guidance has been updated to include certain BCS Class 3 compounds. However, it must be noted that the classification of compounds within the literature is often based on using available aqueous solubility data (often performed using a limited pH range) and correlations with $C \log P$ and $\log P$ for permeability, and thus may represent a best case scenario. In reality, a number of high-solubility compounds may potentially change class when the full BCS recommended package is generated, as stated in the current guideline.

A review comparing global regulations regarding biowaivers for IR solid oral dosage forms concluded that biowaivers for BCS Class 1 compounds have not been used to their full potential, with the following reasons being given [103]:

- Limited number of BCS Class 1 compounds are being developed in the US and EU
- Risk that rejected biowaiver applications may result in the regulatory agency requesting a BE study
- Biowaivers are not acceptable in all countries (e.g. Japan) and therefore a BE study may be required anyway

It was also suggested in this article that a relaxation on the criteria is required to overcome these barriers, as well as possible global harmonization of the guidelines [103]. However, it will take time before the impact of the refined BCS biowaiver criteria in the recent updated FDA guidance can be assessed.

However, a recent publication by Mehta et al. reviewed the impact of the BCS on drug development and also the number of BCS applications to the FDA from 2004 to 2017 (first three months) [84]. There was no clear trend in the rate of uptake of the BCS over the 12-year period assessed; however out of 73 applications, 70% were

approved (58% as new drugs and 92% as generic drugs). The approval rate indicates that the industry is using the BCS process successfully with a high acceptance rate.

The BCS is also used in developing the formulation strategy, in assessing the risk associated with formulation switches, process parameter changes, setting dissolution specifications, managing drug substance form change, and deciding whether a clinical BE study is required or if in vitro supporting data are adequate. When managing risk during development for formulation switches, the BCS provides guidance on whether dissolution assessments are adequate to assess the impact on in vivo performance or if a clinical BE study is required. For BCS Class 1 and rapidly dissolving Class 3 compounds, dissolution is appropriate. However, for BCS Class 3 slow dissolving and Class 4 compounds, a clinical bioavailability or BE study will be required. For Class 2 compounds, a clinical BE study or an in vitro in vivo correlation (IVIVC) study may be used. As there is no regulatory requirement to perform clinical BE studies prior to pivotal safety and efficacy studies, the BCS provides pharmaceutical companies a tool to guide development [99].

For generic-based companies submitting ANDA, the BCS biowaiver system offers a significant advantage compared to performing a clinical BE study.

A recent case example questioned the use of the f_2 dissolution test similarity criteria for BCS Class 1 drugs that release <85% in 15 minutes [99]. The compound in question failed to meet the $f_2 > 50$ criteria for three formulations due to large differences in the initial dissolution rate, and the biowaiver route was not progressed. However, BE was shown for the two formulations, which showed the largest difference in the early dissolution time points. For rapidly dissolving BCS Class 1 compounds, it was concluded that dissolution profiles at the early time points may not be predictive of the in vivo performance [99].

Another potential limitation seen by pharmaceutical companies with applying for BCS-based biowaivers is time. If the process for receiving formal approval from the agency is not sufficiently fast, the risk of not getting a positive response may be too great and delay the development program [99]. A recent article analyzing the application of BCS biowaivers for generic oncology drug products highlighted that the time for FDA BCS biowaiver applications containing in vitro studies is often as long as those containing in vivo BE studies, due to inadequate information in the submissions [104]. Examples of the missing information included:

- *Permeability studies*. Permeability data for the model drugs were missing, such as too few replicates preventing statistical assessment of the variability of the study data, validation reports for analytical methods, and relevant method standard operating procedures (SOPs) were not submitted
- *Solubility studies*. pH measurement after addition of the drug substance was missing, data were not collected under equilibrium conditions, a stability

indicating assay was not used and copies of validation reports for analytical methods and relevant method SOPs were not submitted

- *Dissolution studies*. Description of the dissolution method was missing, validation reports for analytical methods and the relevant method SOPs were not submitted [104].

The recent review of BCS applications to the FDA also highlighted deficiencies in the submitted BCS work packages, and examples given of missing information were dissolution data not provided for all dose strengths, solubility data generated with inappropriate methods and also lack of multi-pH profiles, no efflux data for the cell line model used, lack of bidirectional transport of the validation marker compounds in the in vitro models and missing SOPs for the analytical methods [84].

It is hoped highlighting these deficiencies will help future applicants to generate acceptable work packages.

In 2005 the Biopharmaceutics Drug Disposition Classification System (BDDCS) was introduced [105], which originated from the BCS. The BDDCS substitutes extensive and poor metabolism in place of high and low permeability, while using the same solubility classification as the original BCS guidance. It was suggested that regulatory authorities adapt the BCS guidance to incorporate drug metabolism as an alternative method to classify Class 1-marketed drugs suitable for BE biowaivers [106]. In particular, if a drug is $\geq$90% metabolized, it should be considered $\geq$90% absorbed. If an orally administered drug has $\geq$90% metabolism by Phase 1 oxidative and Phase 2 conjugative processes, the drug must have $\geq$90% absorption. The theory underpinning the relationship between permeability category and level of metabolism is thought to be due to the fact that a high-permeability compound will be able to enter metabolic cells and thus be metabolized. The application of the BDDCS was proposed to facilitate a number of marketed drugs being appropriately assigned as BCS Class 1. A more recent publication proposed the BDDCS as a method to predict drug disposition, a tool that may prove useful during the early stages of drug discovery [107]. It estimated that the difference between classification using the BCS and BDDCS is approximately 10%. However, the difference is estimated to be higher (40%) for Class 1 drugs, where the FDA has granted biowaivers [107].

4.3.7 "Developability Classification System"

The BCS classification system is often used by pharmaceutical companies to assist in candidate drug selection in a transition from discovery to development, to ensure that the selected candidates have suitable biopharmaceutics properties for successful oral formulation development. If a BCS classification is assigned

early in the drug discovery process, it is common that during development the classification may change.

This may be due to changes in the dose range or the solid-state form/salt or also a more thorough permeability classification study being conducted as opposed to the high-throughput screen used earlier in discovery. The BCS is a regulatory framework to allow in vitro assessments to be used in place of clinical BE studies for low-risk compounds (Classes 1 and 3). It is a regulatory tool and therefore somewhat conservative, to ensure that changes in drug products do not result in changes in exposure and therefore pose no risk to patient safety. A BCS Class 4 compound can actually have 80% absorption, with high solubility in intestinal fluid. Thus, is the traditional BCS really the best assessment on which to base the formulation or development strategy? The BCS was adapted in 2010 to the developability classification system (DCS) with the focus being on the developability of the compound and the factors that are critical to in vivo performance [108]. The DCS has been designed to better assess the factors that limit drug absorption and, as such, is deemed more appropriate to support product development and quality-by-design (QbD) concepts. The BCS categorizes solubility over the GI pH range (pH 1.2–6.8) in simple buffer systems. However, this is likely to be an underestimation of the true in vivo solubility at the site of absorption, as many drugs have pH-dependent solubility and the intestinal fluid have components such as bile acids and phospholipids, which can increase solubilization. In the fed state, lipids or proteins contained within the food can also increase drug solubility. The use of more biorelevant gastric- and intestinal-simulated media has therefore been used to improve the assessment of GI dissolution and solubility. These media have been developed to reflect both fasted and fed states and hence four core biorelevant media have been proposed [109]. The DCS has been adapted from the BCS to incorporate a more biorelevant solubility assessment by using Fasted State Simulated Intestinal Fluid media (FaSSiF) to estimate the extent of human absorption, dissolution rate based on particle size instead of dose-to-solubility ratio, and a solubility-limited absorbable dose (SLAD) for Class 2 compounds [108]. The main difference of the DCS to the BCS is that Class 2 compounds are subdivided into 2a (dissolution rate-limited) and 2b (solubility-limited), and thus this information can be used to define strategies for formulation optimization. The DCS utilizes for understanding BCS Class 2 compounds their positive food effects. The solubility in FaSSiF is used as a worst case for the dose-to-solubility ratio and clearly delineates where a food effect on bioavailability will occur independent of particle size without additional enhancement in solubility. Conversely, it also indicates the particle size distribution needed to mitigate the food effect or reduced bioavailability. For those therapeutic indications where prescribing administration with food is therapeutically acceptable, FeSSiF may be used to determine whether particle size reduction is sufficient to increase bioavailability for BCS Class 2 compounds without too much variability.

4.4 Applications and Limitations of Characterization and Predictive Tools

Oral administration is the most widely used route for delivery of drugs into the systemic circulation, primarily due to its convenience, which provides the highest levels of patient compliance [110, 111]. As discussed above, understanding the factors influencing oral absorption is the key to ensure successful oral formulation development. The following section illustrates the wide variety of techniques available for the study/prediction of intestinal permeability and, in particular, highlights the differing levels of complexity, reliability, and physiological relevance between the various techniques. Figure 4.3 highlights examples of such techniques organized by aspects such as biological relevance or throughput.

4.4.1 In Silico Tools: Predictive Models, Molecular Descriptors, and ADMET

Although the models themselves may be complicated to build, computational, or in silico, predictive models are by far the simplest in terms of generating a permeability number and are consequently used during the early stages of drug discovery and development. These computational tools are based on calculations and predictions from molecular structures and can be used to support the development of molecules with suitable absorption, distribution, metabolism, elimination, and toxicity (ADMET) properties [112, 113].

The main advantages in using computational models, which are able to predict or assess key ADMET and permeability-related physicochemical properties, are that they can be rapidly applied and performed. Parameters such as molecular weight, partition coefficients at specific pHs, solubility, lipophilicity, and polar surface area (PSA) can be studied. This allows for virtual screening of large numbers of potential candidates. Screening with in silico tools can support the selection of a limited number of potential drug molecules with appropriate physicochemical properties for later development. This can reduce the risk of poor candidates being taken forward into downstream labor-intensive and costly investigations. These include the use of in vivo models or animal tissue, which, from an ethical perspective, should be minimized wherever possible. One of the simplest examples of this type of tool is Lipinski's "rule of 5," which, based on an assessment of around 2200 drug candidates, predicts that poor permeation is more likely when there are more than 5 hydrogen bond donors, 10 hydrogen bond acceptors, the molecular weight is above 500 or log *P* is greater than 5 for a given drug compound. Relatively simple models such as this, focused on a few easily interpreted parameters, can be more readily understood and can be used to build structure–property relationships, but are limited in the accuracy of the predictions generated [114].

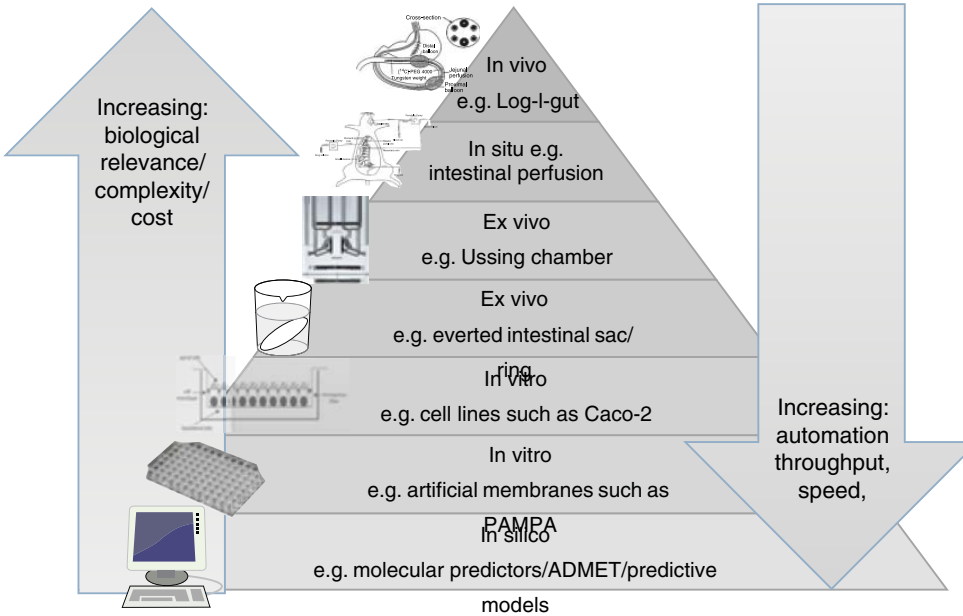

Figure 4.3 Examples of predictivetools used to estimateintestinal permeability.

More complex multivariate data analysis models, based on a number of molecular properties or "descriptors" combined, can improve the applicability of the predictions and enable the creation of quantitative structure–property relationships (QSPRs) [115]. Combining models in a "consensus-modeling" approach can improve predictions even further by reducing the impact of outlier results from any individual model. A disadvantage of the more complex models is the requirement for expert user interpretation such as that from a computational chemist.

Predictive software tools are commercially available such as ADMET predictor™ from SimulationsPlus, VolSurf+ from Molecular Discovery, and QikProp from Schrödinger, which can take molecular structures, in 2D or 3D and predict ADMET parameters such as solubility, $\log P/\log D$, Caco-2 permeability and human permeability in the intestine, blood–brain barrier permeability, volume of distribution among other things at capacities up to hundreds of thousands of compounds per hour. A significant limitation for both simple and this type of complex predictive model is that the chemical space covered by the datasets used to build and train them may limit applicability to new chemical entities within the same or a similar space [113]. Another factor, which may need to be considered, is the potential for molecular descriptors to be impacted by conformational changes, such as PSA, particularly for large molecules with high intramolecular flexibility.

4.4.2 In Vitro Tools

4.4.2.1 PAMPA

Generally speaking, in vitro tools to investigate permeability should ideally mimic the epithelial wall of the intestinal tract. Early stage screening tools, however, have been developed to study transcellular passive permeability – the most common mechanism drug molecules use to cross cell membranes. These early stage permeability models measure the permeability of the drug molecule through artificial membranes, e.g. a semipermeable plastic or cellulose filter coated with lipids to mimic the lipid bilayer found in the human epithelial wall. These artificial membrane systems offer the advantage of being reproducible, rapid, and simple as well as being both high-throughput and cost effective to run. One such in vitro tool is the parallel artificial membrane permeability assay (PAMPA), which has been studied widely [116]. The PAMPA system involves a membrane formed from a lipid (such as phospholipids or lecithin), contained within an inert organic solvent. The lipid/solvent solution is stored within a porous hydrophobic filter plate. The filter plate is then filled with the donor solution – containing the test drug, and is suspended over the receptor plate, which contains the acceptor buffer solution. The plates are incubated for a period of time, sometimes with stirring, shaking, or rotationally introduced convection to account for the potential impact of an aqueous unstirred boundary layer for rapidly permeating molecules [117]. At specific

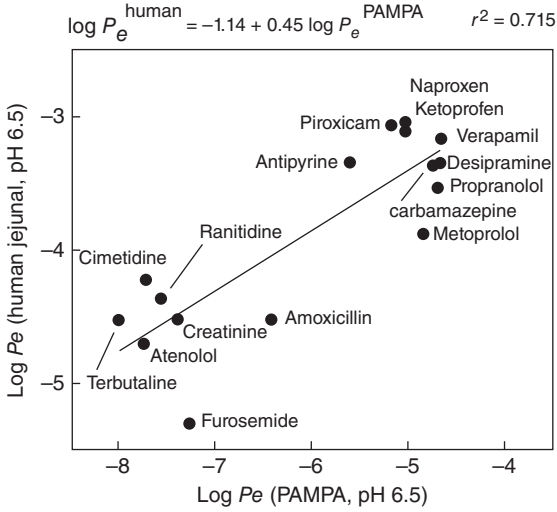

Figure 4.4 Correlation between human jejunal and PAMPA permeabilities. Source: Van de Waterbeemd et al. [119]. © 2003, John Wiley & Sons.

time points, the amount of drug is measured in all compartments. The amount of drug present in the lipid membrane can then be calculated through mass balance. PAMPA is generally used to screen drugs into approximate rankings or categories such as high, intermediate, and low permeability and has been demonstrated to correlate with GI permeation [118]. Figure 4.4 shows a correlation plot based on a pH 6.5 PAMPA model utilizing a 20% soy lecithin-dodecane membrane with 35-mM sodium lauryl sulfate in the acceptor compartment [119].

The main limitations of PAMPA are that it can only approximate the measurement of transcellular passive diffusion-based permeability since the system has no active transport, paracellular pathway (permeation of material through tight junctions between epithelial cells), or metabolizing enzyme capability. Another limitation is that studies must be performed at room temperature since the membrane becomes unstable at the more physiologically relevant 37 °C. A further disadvantage of the PAMPA system, along with other artificial membranes, is that the pores of the filter plate where lipid multilamellar bilayers form are much longer than an epithelial cell membrane lipid bilayer, thereby slowing the apparent permeation rate compared to the equivalent in vivo situation. Calculations and pH shift studies have been employed to address the impact of this issue [120].

Other artificial systems, which measure lipophilicity characteristics, include immobilized artificial membranes (IAMs) and the related immobilized liposome chromatography (ILC), micellar electrokinetic chromatography (MECK), and biopartitioning micellar chromatography (BMC). All of these techniques result in lipophilicity indices, which may better relate to membrane interactions and

passive permeability than simple octanol/water partitioning evaluations [119]. Nevertheless, the correlation of these results with solubility in selected oils is also apparent.

4.4.2.2 Cell Lines

The most routinely used in vitro methods for assessing intestinal drug permeability are cell-culture-based monolayer models. Among these, one of the most commonly used is the Caco-2 human colon carcinoma–based cell line. When this cell line is grown on a microporous filter (see Figure 4.5) under standard culture conditions for around 16–21 days, monolayers are formed that have morphological and functional characteristics similar to that of human intestinal epithelial cells [121].

The Caco-2 cell line is the only one to have been found to undergo enterocytic differentiation and become polarized during culturing to resemble the human epithelial cell wall. This results in a morphology with tight cellular junction formation and microvilli at the apical surface, alongside functional expression of many transporter and enzymes found in the small intestine. Transporters expressed include efflux transporters, such as P-gp/MDR1, which actively transport a wide range of chemical molecules back out of the small intestine in vivo, therefore potentially limiting their absorption [122]. It should be noted that the transporters expressed can be different depending upon the culture conditions used. FDA guidance recommends cell lines such as Caco-2 as the preferred method for in vitro mechanistic investigation of DDIs [123]. Caco-2 cell line investigations can be performed with different pH and/or osmolality in the apical and basolateral chambers to mimic different regions of the GI tract in vivo. The impact of different formulation components on pH and permeability can also be studied. In a similar manner to PAMPA studies, Caco-2 cell permeability investigations are performed with the monolayer held between an apical and a basolateral chamber into which test compound or blank receiver buffer media can be added. Following incubation with orbital shaking, the apical and basolateral chamber solutions are sampled at selected time points and the amount of test compound in the compartments is measured. Absorption is indicated by the appearance of more drug in the basolateral chamber following apical application of test compound compared to that found in the apical chamber following basolateral application of the same amount of drug. Apical secretion, or efflux, is

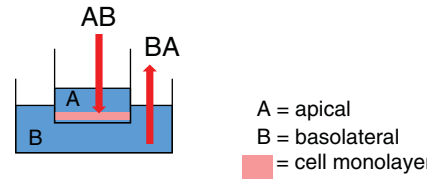

Figure 4.5 Schematic of drug transport assay in cell monolayers cultured on a culture insert containing a permeable membrane.

indicated by a greater amount of drug appearing in the apical chamber following basolateral application of test compound compared to that found in the basolateral chamber following apical application of the same amount of drug. The apparent permeability (P_{app}) of a test compound is calculated by dividing the quantity of compound reaching the receiver chamber (normalized to the filter surface area per unit time) by the initial drug concentration in the donor chamber. P_{app} can be used to rank compounds in terms of oral absorption potential [124, 125]. An advantage of the Caco-2 cell line over artificial membranes is the ability to assess paracellular tight-junction permeability, thought to be important in the absorption of low-molecular-weight, hydrophilic drugs. Tight junctions can be assessed using hydrophilic-marker paracellular compounds such as mannitol and/or through monitoring the transepithelial electrical resistance (TEER) of the monolayers. Caco-2 cells mainly display tight junctions, which match the smaller of the two pore populations found in the human small intestine. This cell line is therefore limited in its ability to identify molecules with significant levels of paracellular permeability in vivo in comparison to alternative cell lines, such as the conditionally immortalized rat fetal intestinal cell line 2/4/A1 [126]. However, it should be noted that the 2/4/A1 cell line is more difficult to culture, is poorly differentiated morphologically, and does not express many of the enzymes and transporters found in the Caco-2 cell line. The 2/4/A1 cell line should therefore be used to study passive transport only.

Standard culture Caco-2 cell lines show low and unstable expression levels of the major metabolizing enzymes of the CYP [127]. Clones of Caco-2 cells such as TC-7 express greater levels of enzymes such as cytochrome P4501A1 and UDP-glucuronosyltransferase (UGT) and can be used as an alternative intestinal model [128].

A disadvantage the majority of cell lines used for modeling intestinal permeability (including Caco-2) is the lack of a mucus layer, produced in vivo by goblet cells. The human intestinal epithelial colon carcinoma cell line, HT29, can be grown to become a polarized monolayer of mucus secreting cells. This can be used to investigate the impact of mucus found in vivo, which can be a barrier to intestinal permeability [129]. Attempts made to coculture Caco-2 cells with HT29-H and HT29-MTX (HT29 clones), to more closely mimic the in vivo cell population diversity, were not successful due to insufficient mixing between cell lines [130, 131].

Another popular cell line used to investigate intestinal drug permeability is the Madin-Darby canine kidney cell line (MDCK). Monolayers produced from this cell line have the advantage of being fully differentiated after only around three to seven days of culturing. Despite being derived from a dog kidney epithelium with resulting potential differences in transporter expression, correlation to Caco-2 in terms of passive transport has been reported [132]. It should be noted that there are two subclones of MDCK with high or low resistance in terms of TEER values,

and that this cell line is not suitable for prediction of active transport or efflux due to the potentially different transporters expressed in dog. Transporters, however, are expressed at low levels and so transfected MDCK cells have been used to investigate specific transport mechanisms such as P-gp/MDR1 impact on permeability through MDR1-MDCK cells. An alternative cell line suitable for transfection is the Lewis lung carcinoma-porcine kidney cell (LLC-PK1). Both MDCK and LLC–PK1 cells have shown improved stability and enzymatic activity when transfected with CYP 3A4 compared to Caco-2 transfected cells. A summary of the characteristics of the different in vitro cell lines used for intestinal permeability investigations is provided in Table 4.5.

4.4.3 Ex Vivo Tools

Although the in vitro tools described previously can address specific mechanistic questions and inform decisions regarding intestinal permeability, models utilizing living and functioning tissue isolated from an animal or human, also known as ex vivo models, reflect the in vivo situation in a more comprehensive way. Ex vivo small intestinal tissue models have beneficial features, which differentiate them from the cell based in vitro models, such as a mucus layer, representative paracellular permeability, expression of transport proteins, and gut-metabolizing enzymes. They can be readily used to evaluate permeability in different regions of the GI tract and compare intestinal permeability between species [111, 133, 134].

The two main ex vivo models used to investigate intestinal permeability are diffusion chamber-based models such as the Ussing chamber [135, 136] and the everted intestinal sac [137].

4.4.3.1 Ussing Chambers

Ussing chambers are the most commonly used diffusion chamber model for intestinal permeability studies. Ussing chambers are available in different sizes but are all based on the same principle of using an excised section of intact mucosal intestinal tissue. The tissue is cut into small segments of appropriate size and opened to form a flat epithelial sheet. This sheet is mounted, usually vertically, between two chambers containing physiological buffer oxygenated with carbogen (95% O_2, 5% CO_2) and maintained at 37 °C (see Figure 4.6).

The continuous oxygenation with carbogen supports functionality of the tissue while also providing circulation of fluid within the chambers, which reduce unstirred water layer effects that could impact permeability assessment of poorly soluble compounds [139]. The study commences when test drug is added to the donor chamber and test samples are removed at defined time intervals from the receiver chamber for analysis and quantification. The removed sample volume is then immediately replaced with fresh, prewarmed physiological buffer. P_{app} or flux

Table 4.5 Cell-culture models used for drug permeability assessment.

Cell line	Species of origin	Special characteristics
Caco-2	Human colon adenocarcinoma	Most well-established cell model
		Differentiates and expresses some relevant efflux transporters
		Expression of uptake transporters is variable
MDCK	Mardin-Darby canine kidney cells	Polarized cells with low intrinsic expression of ABC transporters
		Ideal for transfections. (e.g. MDR1-MDCK)
LLC-PK1	Pig kidney epithelial cells	Polarized cells with low intrinsic transporter expression
	Lewis lung carcinoma-porcine kidney	Ideal for transfections
2/4/A1	Rat fetal intestinal epithelial cells	Temperature-sensitive
		Ideal for paracellularly absorbed compounds because of leakier pores with 9.0 ± 0.2 Å, similar to human small intestine pores. TEER of $50\,\Omega\,cm^2$
		Contains brush-border enzymes as well as transporter proteins
TC-7	Caco-2 subclone	Similar to Caco-2
T84	Human carcinoma	Have receptors for many peptide hormones and neurotransmitters; maintains vectorial electrolyte transport
HT-29	Human colon	Contains mucus-production goblet cells
IEC-18	Rat small intestinal cell line	Provides a size-selective barrier for paracellularly transported compounds
HEK	Human embryonic kidney	Used for transfections
HeLa	Cervical cancer cells	Wide use in research

Source: Estudante et al. [30] © 2013, Elsevier.

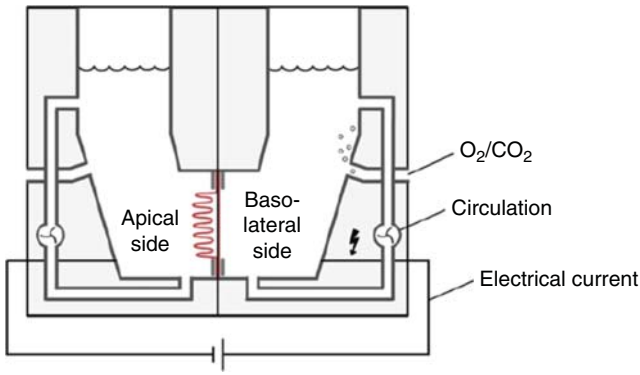

Figure 4.6 Schematic of a small piece of intestinal epithelial tissue mounted in the Ussing chamber. Source: Verhoeckx [138]. © 2015, Springer Nature.

is calculated as the rate of drug accumulation in the receiver chamber normalized for tissue surface area. Bidirectional transport studies can be conducted with the drug being exposed initially to either the mucosal or the serosal (basolateral) surface of the tissue. Continuous monitoring of the integrity and activity of the excised tissue membrane can be performed through the use of electrodes positioned in each chamber of the apparatus, measuring the TEER, potential difference, and short-circuit current (SCC) [140]. The provision of electrodes and functionality of the tissue membrane used within Ussing chambers additionally allows measurement of changes in ion transport across the membrane in the presence of drug compounds [141].

Ussing chamber models also allow the study of intestinal permeability and DDIs in combination with intestinal metabolism [142]. The opportunity to utilize human tissue from a target patient population, which will confer mechanistic features of the disease state, is a distinct advantage models such as the Ussing chamber can offer. As with in vitro cell lines, permeability can be studied under different physiological conditions (e.g. pH and osmolality) using Ussing chambers. Since the intestinal tissue segments used in the Ussing chamber model retain the morphological architecture and physiological features of the intestine, the complex interplay of the multicellular environment is also retained [142]. Human tissue studies using the Ussing chamber can be used to troubleshoot unanticipated clinical findings, e.g. where preclinical species did not show the same PK observations as found in human clinical studies.

Many of the limitations and disadvantages of Ussing chamber studies are associated with the practical aspects of excision and preparation of the tissue itself, which can be very difficult to source [134]. One major challenge is the coordination and logistics of sourcing fresh, viable tissue, especially human tissue from

both healthy and specific patient groups. Interindividual variability between tissue segments and membranes can also be an issue, particularly as these models are low throughput and take prolonged periods of time to set up and run. Muscle layers present an extraneous barrier to permeability; hence, they are often removed from the serosal side of the tissue (stripping) to provide a membrane, which better represents the physiological permeation of drugs. The muscle layer can also cause potential bias in electrical properties due to sporadic contractions, or limit viability through decreased efficiency of oxygenation of the epithelial cells [143]. Complete removal of the muscle layers is normally not feasible, and there is also a risk of damage to the mucosal membrane during the intricate process of excision, dissection, stripping, and mounting of the membrane in the chamber. This can cause changes to morphology and the functionality of transporter proteins and enzymes [144]. Another limitation of the use of ex vivo intestinal segments is the limited viability of the tissue to around 2–2.5 hours during experiments.

The Ussing chamber model has been found to appear unsuitable for evaluation of ester prodrugs, such as adefovir and dipivoxil, because it failed to provide evidence of significant transport enhancement for this type of drug, as was demonstrated with Caco-2 and rat in situ intestinal perfusion [145]. The model is also unsuitable for use with rabbit duodenal and jejunal intestinal tissue sections as they are too thick to mount within the apparatus [146]. Comparison of rat and human small intestinal active and passive permeability using Ussing chambers seems to show good correlation however [147].

Attempts to address the disadvantage that the classical Ussing chamber model does not allow simultaneous preparation and analyses of a large number of epithelial tissue segments have been made more recently. Systems, which use multiple horizontally orientated membranes, have been developed, such as Netherlands Organization for Applied Scientific Research (TNO's) porcine intestinal tissue–based InTESTine™ medium-throughput multiwell system. This system uses pig tissue, which demonstrates high similarity in anatomy and physiology to human intestinal tissue, and allows potential studies such as parallel regional intestinal permeability assessments to be performed [148].

4.4.3.2 Everted Intestinal Sac/Ring

Many of the advantageous attributes of the Ussing chamber model run with animal tissue can also be applied to the everted intestinal sac (or everted gut sac) model. In this model, either a 2–6 cm section or the whole of the intestine is rapidly removed from an anesthetized animal (typically a rat), and flushed with physiological buffer before being everted (turned inside-out) over a glass rod or tube. The everted intestinal tissue is then either tied at both ends to create a sac or cannulated with tubing in an apparatus designed to make subsequent sampling easier, as illustrated in Figure 4.7 [149].

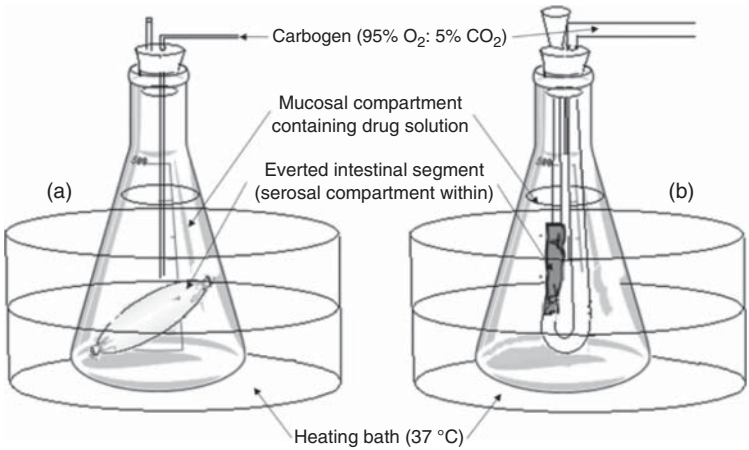

Figure 4.7 Schematic of ex vivo everted intestinal sac experiment. (a) Intestinal sac tied at both ends. (b) Modified apparatus with cannulation. Source: Based on Ungell [149].

In this model, the mucosal surface becomes the outside layer while the serosal surface becomes the inside surface. Physiological buffer is filled both inside the sac (or cannulated everted tissue "tube") and outside in the outer container of either sac or cannulation apparatus. The system is oxygenated continuously with carbogen as described for the Ussing model to maintain viability of the tissue, which may only have integrity for around an hour or two after preparation.

The everted intestinal sac model is rapid, relatively inexpensive, reproducible, and can be particularly useful for analysis of low permeability compounds as the volume of fluid within the serosal compartment, i.e. inside the sac or tube, is low [150]. This model provides a relatively large surface area for permeability, has a mucus layer present, and is most commonly used to assess the impact of enzyme activity and transporters. The data generated are affected by the donor animal's age, sex, species, disease state, diet, and treatments. The major limitations and disadvantages of the technique are maintaining tissue viability, potential morphological damage caused during harvesting and eversion, plus the retention of an intestinal muscle layer (muscularis mucosa), which can affect both the permeation observed and the oxygenation efficiency of the model [151]. Studies are generally run at 37 °C and gentle shaking can be applied to minimize tissue damage. Drug molecules under test can be analyzed in both the fluid inside the everted intestinal sac and in the surrounding chamber as well as in the tissue itself. The everted sac viability and integrity can be monitored through glucose concentration measurements from the solutions outside and inside of the sac [152]. In addition to following drug permeability through timed sampling and analysis of the media from the outer container and internal compartment of the everted intestinal sac,

the model can be used to screen the impact of particular pharmaceutical excipients or entire formulations on permeability, such as mucoadhesive properties of bioadhesive formulations. In vitro and in vivo findings are often in agreement between the rat everted intestinal sac model and human data and, as such, the everted intestinal sac model is a useful screening tool for permeability investigations.

An adaptation from the everted intestinal sac is the everted intestinal ring system in which slices of intestine around 2–5 mm in width are prepared and placed in well-oxygenated buffer containing test drug. This model offers the advantages of having many intestinal samples from one animal, allowing different intestinal regions, drug concentrations, drug molecules or formulations to be tested. Everted intestinal rings are relatively simple and quick to prepare and require limited maintenance. The model is used for measuring uptake into intestinal cells and metabolism. One of the limitations of this technique is the potential analytical challenge of low drug concentrations within the ring slices. However, this is often addressed by using radiolabeled drug [153]. Other specific limitations include the inability to define which surface (serosal or mucosal) the uptake is occurring at, as both surfaces are exposed to the buffer containing drug. Also the increased number of cuts made during preparation of multiple rings increases the risk of damage to edge cells, which can lead to false uptake levels being recorded [154].

4.4.4 In Situ Tools

There are a number of intestinal perfusion methods available, which offer the advantages of providing an intact intestinal mucosa, nerve system, lymphatic system, and blood flow, alongside expression of enzymes and transporters. This allows for the assessment of permeability in viable tissue under conditions mimicking the in vivo environment closely. In these studies, animals are typically anesthetized and heated to maintain 37 °C using pads and lamps. An additional advantage of intestinal perfusion models is that regional differences in permeability and metabolism can be investigated without interference from gastric emptying and/or small intestinal transit times, which can impact in vivo permeability and absorption studies. In addition, these models can be used to investigate drugs, which require complex dosing vehicles to overcome poor solubility, which can result in sensitivity issues when presented to other less complex models such as cell-culture systems. In situ perfusion models, for instance, can be used to perform kinetic studies. Rat in situ perfusion models have been shown to correlate, at least in terms of rank ordering of compounds, with in vivo human data for both passive and carrier mediated drug transport [155–157]. Tissue viability and integrity, a potential limitation as with other ex vivo models, can be monitored through the use of markers such as phenol red, inulin, or ^{14}C-PEG-4000. It should be noted though that these marker compounds may alter

membrane function themselves [158]. Oxygen and glucose consumption, pH of perfusate, and morphological examination can also be monitored within these systems. One of the limitations of running such a model is that specialist surgical manipulation is required to expose the abdominal cavity and withdraw the region of the intestine to be cannulated at both ends for perfusion.

4.4.4.1 Closed Loop Intestinal Perfusion

In the closed loop intestinal perfusion model, a selected region of intestine is cannulated and washed with perfusion solution before being filled with perfusion solution containing a drug or formulation. The intestinal lumen content is then sampled at predetermined time intervals and the concentration of drug is analyzed [159]. Within 10–30 seconds of sampling, the perfusion solution is returned to the isolated intestine lumen. The method can be run with syringes fitted with stopcocks to enable solution transfer and sampling. Alternatively, an adaptation using an inline peristaltic pump to allow recirculation of the luminal media can be applied. The inline pump set up has the advantages of providing constant and gradual mixing and reducing the risk of mechanical trauma during liquid transfer when compared to the syringe method. A potential limitation of the closed-loop perfusion model is that the drug is exposed to the entire mucosal surface of the intestinal segment throughout the study. This may not reflect the in vivo situation, where a drug product will transit through the small intestine. However, it may allow more precise control of drug concentration and benefit the assessment of low permeability/high-efflux compounds through higher disappearance rates [160].

4.4.4.2 Single-Pass Intestinal Perfusion

The single pass (or open loop) intestinal perfusion model is similar in set up to the closed loop model except that an infusion pump is used to perfuse the liquid containing drug, at around 0.1–0.3 ml/min continuously down a fixed-length intestinal segment [161]. Although permeability estimates generated from both closed and single-pass perfusion methods are similar when normalized for perfused volume and intestinal length, the single-pass method has been shown to be more robust and reproducible [162]. Samples collected from the ileal-end cannulation are assayed for drug and the permeability estimated through calculation of the concentration difference between ingoing and outgoing perfusate, once outgoing concentration has stabilized and steady state has been achieved. Perfusion studies can be run in situ with the closure of the bile duct to prevent entero-hepatic recirculation of drug as part of building a mechanistic understanding of the process of absorption.

4.4.4.3 Intestinal Perfusion with Venous Sampling

An adaptation of the closed-loop and single-pass intestinal perfusion models incorporates plasma sampling through cannulation and drainage of a vein, such as the

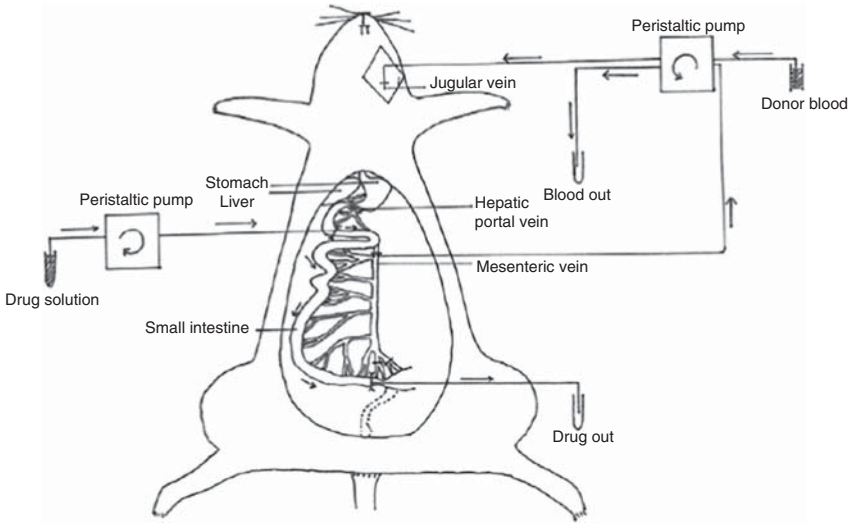

Figure 4.8 Schematic drawing of in situ intestinal perfusion with venous sampling. Source: Luo et al. [133]. © 2013, Elsevier.

mesenteric vein of an intestinal segment, with donor blood replacement from, e.g. the jugular vein (Figure 4.8). This provides a means to quantify drug flux through the intestinal wall rather than only quantifying uptake by the wall and is sometimes referred to as the "auto-perfused" method [163]. In this technique, intestinal permeability can be estimated from the rate of drug appearing in the blood and it can be performed with either closed- or open-loop methodologies.

4.4.4.4 Vascularly Perfused Intestinal Models

A further level of model complexity has been investigated through isolation and cannulation of an intestinal segment, alongside cannulation of a supply artery such as the mesenteric artery plus a drainage vein. Perfusate monitoring, after drug input from the lumen of the intestinal segment and from the artery, can be compared to quantify intestinal-mediated extraction of drug [164].

4.4.4.5 Other Animal Models

The vascularly perfused intestine-liver model can be used to study first-pass metabolic effects without limitations associated with portal vein cannulation such as liver blood loss and engorgement of intestinal veins [165].

The Thiry–Vella fistula is a perfusion loop in rat or dog in which the intestinal permeability can be estimated in an unanesthetized animal with the advantage of the intestine being kept at close to physiological conditions [166].

4.4.5 In Vivo Tools

A number of open and closed in vivo perfusion techniques have been reported for estimating intestinal permeability, drug dissolution, secretion, and metabolism in humans. The most commonly used of these techniques is the Loc-I-Gut method, which consists of a six-channel polyvinyl disposable tube [158]. Two of these channels are linked to balloons used to occlude a 10-cm segment of the intestine, one channel is for drug perfusate infusion, another is for luminal content sampling and the final two channels are for viability marker administration of compounds such as phenol red as mentioned earlier [167]. The balloons, when inflated through the multichannel tube, create a closed section of intestine, which has the advantage of minimal contamination from luminal fluid from the rest of the intestine, plus improved control of hydrodynamics within the occluded segment, as shown in Figure 4.9.

Another advantage of this technique is that transit time and regional pH differences do not influence studies. Potential factors to account for when running this method include correcting for any binding of the drug to the tubing, chemical and/or enzymatic degradation of drug in the luminal contents, and possible accumulation of drug in the intestinal wall, which could affect sink conditions across the epithelium. Drug permeability is estimated from the rate of disappearance of drug from the perfused intestinal segment. The technique also allows the measurement of absolute bioavailability through the use of IV dosing and peripheral blood sampling and analysis for drug in the systemic circulation. Major limitations with the in vivo human techniques such as the Loc-I-Gut are the high cost and ethical issues associated with running such a model. As a result, the Loc-I-Gut is not used routinely, e.g. for early permeability screening but is applied in later development phases, for example to generate permeability values for in vitro–in vivo correlations. It is also used to investigate enzyme and transporter expression

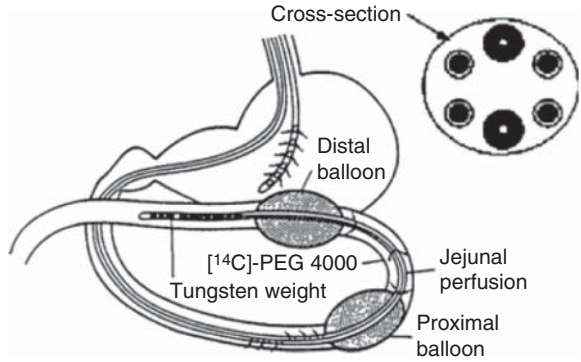

Figure 4.9 Schematic drawing of the Loc-I-Gut instrument. Source: Ehrhardt and Kim [158] © 2008, Springer Nature.

levels and functionality measurements or to evaluate food–drug interactions, drug dissolution, and intestinal drug secretion [168].

The Loc-I-Gut was used to develop an in vivo human permeability database as a basis of BCS for oral IR dosage forms [74, 75]. This exemplifies that this technique is viewed as a gold standard for intestinal permeability and absorption models. Table 4.6 summarizes the strengths and limitations of ex vivo and in situ intestinal permeability models.

4.4.6 In Silico Tools for Prediction of PK and PK/PD

The use of in silico tools to model, simulate, and predict the anticipated clinical performance of dosage forms following oral delivery continues to attract increasing industry attention. Rudimentary noncompartmental simulations based upon single-dose human PK data are routinely utilized to predict, for example, the impact of different multiple dosing regimens during a FIH study, or how a particular MR input function could achieve a desired plasma concentration – time profile. Crucially, however, noncompartmental approaches do not take into consideration the biopharmaceutics aspects of oral drug delivery and how the dose and intrinsic properties of drug, coupled with formulation design and anatomical variability in the GI environment, can affect the dissolution, solubility, absorption, and hence bioavailability.

Over the last decade, physiological-based pharmacokinetic (PBPK) modeling and simulation has emerged as a recognized tool to guide oral drug product design and development [169–172]. In-house or commercially available software tools, such as GastroPlus™ (Simulations Plus, Lancaster, CA, USA) and SimCyp® (Certara, Princeton, NJ, USA), are utilized, where through the input of in vitro, preclinical, and clinical datasets modeling and simulation activities in regard to potential in vivo performance can be performed, in the context of the physiological GI environments. Within GastroPlus, this functionality is further enhanced by the multicompartmental ACAT™ (Advanced Compartmental Absorption and Transit) model, which describes changes in conditions as a function of GI transit.

Many different factors can be assessed to aid an understanding of how variations in physicochemical properties and dosage form design can influence PK outcomes (Table 4.7).

A common application given the dominating feature of BCS Class 2 compounds in the industry pipeline is to probe the interplay between particle size, pH, and oral bioavailability. Mathias and Crison [170] described how for a weak base with pH-dependent solubility, PBPK modeling was used to describe the impact of both food and coadministered proton pump inhibitors (PPIs) (i.e. elevated gastric pH) on the plasma concentration – time profile, to define a preferred formulation development strategy. The model accurately described comparable effects from the two

Table 4.6 Strengths and limitations of ex vivo and in situ intestinal permeability models.

	Strengths	Limitations
Ex vivo intestinal perfusion	The model has a viable mucosa, and it is a quick, simple technique for estimating of intestinal drug transport	Tissue viability and integrity of the intestinal respiratory system havea marked effect on the results. And the barrier imposed by the intestinal wall and serosa may result in slower absorption rates than those obtained in intact animals
Ex vivo everted gut sac experiments	The model is simple, and it is very useful for predicting the extent of transfer and intestinal metabolism of drugs	The everted intestinal sacs gradually lose structural integrity
Ex vivo Ussing chamber	The method is well validated and it can be used to study the permeability of drugs that are poorly absorbed, the absorption mechanisms of different compounds, the drug–drug interactions, and drug transport processes	The Ussing chamber method appears to be unsuitable for evaluating ester prodrugs. And it is also not suitable for use with rabbit tissues as the duodenal and jejunal sections aretoo thick for the diffusion chambers and leaks are observed
In situ closed-loop method	It enables intestinal absorption to occur at body temperature for an appointed time. The model also allows absorption to be measured separately at different regions of rat intestine, jejunum, ileum, and colon. And it avoids the uncertainty of gastric emptying time	The procedure does not allow estimation of absorption at steady state. It is also necessary toundertakea large number of experiments before statistically significant results can be obtained. And the operative procedure is complex
In situ Thiry-Vella	It enables intestinal absorption to be studied in conscious animals with an intestine maintained at near-normal physiological conditions	It requires sophisticated surgical procedures and instrumentations

(*continued*)

Table 4.6 (Continued)

	Strengths	Limitations
In situ intestinal single-pass perfusion	It significantly reduces the number of animals utilized and animals act as their own controls for analyzing segmental-dependent membrane permeability	It requires sophisticated surgical procedures and instrumentations
In situ intestinal recirculating perfusion	It can magnify the concentration changes, which is suitable for studying drugs, which are absorbed slowly	It requires sophisticated surgical procedures and instrumentations
In situ intestinal perfusion with venous sampling	It is a useful method for obtaining realistic drug absorption rates, and it allows the determination of intestinal metabolism without interference by the confounding effects of hepatic first-pass metabolism	It requires sophisticated surgical procedures and instrumentations
In situ vascularly perfused intestine-liver	It allows the investigation of the hemodynamics and metabolism for each organ, as well as the inter-relationships between the small intestine and liver	It requires sophisticated surgical procedures and instrumentations
In situ Loc-I-Gut	It is an accurate method that provides direct estimates of local drug absorption in human subjects. And it is not influenced by other gastrointestinal factors such as transit time and regional pH differences	It requires sophisticated surgical procedures and instrumentations

Source: Luo et al. [133]. © 2013, Elsevier.

Table 4.7 Applications of PBPK modeling and simulation for oral drug delivery.

Parameter	Attribute	Outputs
Drug substance	Pharmaceutical form	Maximum absorbable dose
	Particle size	
Drug product	Formulation design	Fraction absorbed
	Solubilization strategy	
	Modified release modality	PK profiles
	In vitro–in vivo correlations	
Physiological	Gastric pH	Bioavailability
	Gastric emptying time	
	In vivo precipitation time	In vitro–in vivo correlations
	Saturable GI processes (metabolism, efflux)	
	Food effect	Biowaivers
	Pediatric and geriatric populations	

conditions allowing the authors to conclude that reduced solubility with elevated pH was a rate-limiting feature and not delayed gastric emptying in the fed state. Further simulations then evaluated the impact of particle size on the PK to conclude that the adverse pH and food effects could be mitigated by ensuring a smaller particle size specification (<100 μm) for the drug.

PBPK modeling is also widely applied in the design and development of MR dosage forms, whether the formulation strategy is to ameliorate C_{max}-related adverse events or to overcome short-half lives and achieve once or twice daily dosing. In one example, an assessment of a BCS Class 1 compound was performed utilizing the PK data from the FIH study coupled with laboratory-derived physiochemical and biopharmaceutics data [171]. Simulations were then used to predict PK profiles from three different input rates for drug release over 8–16 hours at different unit dose levels to achieve a target $C_{24,}$ plasma concentration at 24 hours. The risks were highlighted with the slower release rates due to the potential for variation in GI transit times and hence prolonged residency in the colon, which, as previously described in this chapter, presents unique challenges for regional absorption. A 12-hour release profile was subsequently proven to give an optimal PK profile.

In silico tools have the potential to assess potentially complex problems in regard to oral drug product design. As an example, Brown et al. [173] describe

the prediction of the oral bioavailability of BMS-626529, a molecule with solubility-limited absorption, following delivery of the nonabsorbed phosphonooxymethyl ester prodrug, BMS-663068, which requires enzymatic conversion to the active moiety immediately before absorption. Compartmental absorption modeling was used to predict the potential feasibility of an MR dosage form given the short half-life of BMS-626529. Regional bioavailability data from a site of absorption study were incorporated in the model to improve the colonic compartmental assumptions. The authors described that while the model predicted the rank order of three extended-release (ER) formulations tested in humans, only one system achieved the target C_{max}:C_{12} ratio.

4.4.7 Preclinical PK Models

Independent of mandatory pharmacological, toxicological, and safety studies in preclinical species, an industry norm where possible is to assess the performance of pharmaceutical dosage forms in animals, to generate in vivo PK data, prior to clinical testing. The main driver for this paradigm is the perceived cost effectiveness of screening and selecting formulations in rats, dogs, or primates to identify a limited number of drug products to take forward into human studies. As already discussed in this chapter, however, the environment of the human GI tract is complex, variable, and significantly affects dosage form performance and hence bioavailability. Several authors have reported interspecies differences in physiology, which must be accounted for when considering the utility of preclinical PK data in regard to predicting drug dissolution, solubility, absorption, and bioavailability outcomes in humans (Table 4.8).

Given these differences coupled with unique transporter expressions and variations in tight junction permeability, it is perhaps not surprising that the

Table 4.8 Comparison of animal and human gastrointestinal systems.

	Rat	Dog	Nonhuman primate	Human
Gastric pH	3.3–5.0	3.4–5.5	2.8–4.8	1.5–3.5
Small intestine pH	6.5–7.1	6.2–7.5	5.6–6.0	5.0–7.0
Small intestine length (cm)	102–148	414		525–625
Small intestine transit(h)	>3	2.8	2.9 (range: 2.2–4.2)	3 (range: 1–6)
Large intestine pH	6.6–7.6	6.4–6.5	5.0–5.1	5.5–7.0
Large intestine length (cm)	9–11	60		125–150
Large intestine transit (h)				20 (range: 1–60)

Sources: Kararli [174], Ikegami et al. [175], Lennernas and Regardh [176], and Quotient Sciences, unpublished data.

correlation between observed animal and human bioavailability data can be erratic. Although a 0.97 correlation coefficient for 64 compounds when comparing rat-to-human absorption data has been reported [177], there is an accepted position that for bioavailability predictions it is high risk to rely on data from preclinical species. Two separate meta-analyses of extensive published literature reported a decade apart concluded the lack of correlation between animal and human data (Figure 4.10) [178, 179]. While some data points lie on a linear regression line in the graphs, for an NCE this can only be proven following clinical testing. As such, product performance observed in preclinical testing may not be reflective of that in human studies and caution should be exercised in an over-reliance on preclinical PK data in determining clinical formulation development.

These challenges were illustrated by Reddy et al. [180], who reported data on danoprevir, an NS3/4A PI, which suffered from a short-half life, poor solubility and permeability. To investigate the potential to develop a once-daily controlled-release drug product an in silico model (GastroPlus) was first developed, which predicted human colonic bioavailability between 4% and 28%. The potential for once-daily dosing was confirmed in preclinical experiments in monkeys with a bioavailability (relative to oral administration) of 30% from the colon reported. To validate the model, a human regional drug absorption study was performed, which demonstrated the actual drug absorption from the colon was just 0.6% and 6.5% for particulate and solution formulations, respectively. As such, human colonic absorption was overestimated by both the preclinical and in silico model of human absorption indicating that an important mechanism impacting human colonic absorption was not fully understood, thereby both limiting the usefulness of such models for determining the potential development of a once-daily dosage form, and indicating the continued need for improved predictive tools.

Differences in intestinal and hepatic metabolism among species may also contribute greatly to prediction of human bioavailability. Even between cynomolgus monkeys and humans, important differences in intestinal absorption and first-pass metabolism have been observed. [181, 182].

4.5 Tools to Probe Regional Bioavailability in Humans: Case Studies

4.5.1 Site-Specific Delivery Devices

The assessment of regional bioavailability is an important scientific capability to inform oral formulation strategies. Studies can be performed proactively to understand the preferred site for drug delivery or to explore potential development

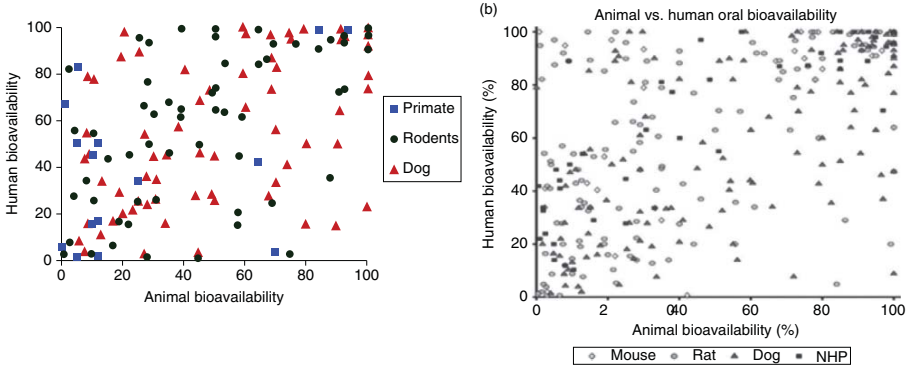

Figure 4.10 Comparisons of human and animal bioavailability. Source: (a) Grass and Sinko [178] © 2002, Elsevier and (b) Musther et al.[179] Licensed under CC BY 3.0.

of an MR formulation to deliver a target PK profile (and hence the design features required). Alternatively, the approach can be applied retrospectively to diagnose the reasons why an engineered formulation did not perform as expected. A simplistic approach is the use of intubation to introduce solution formulations directly to regions of the GI tract via oro- or naso-gastric tubes [183]; however, the technique is invasive for subjects and requires intervention by a gastroenterologist. Moreover, for colonic studies, the removal of the tube can be quite painful. More commonly, the method of choice has been the use of a remote-controlled capsule technology where the drug can be delivered to a specific anatomical region of interest prior to PK sampling and analysis [184–187]. A range of electromechanical capsules have been evaluated clinically, as summarized in Table 4.9. The most commonly used and reported remote-controlled device is the Enterion™ capsule [184], which has been used in over 120 clinical investigations, involving the administration of over 4000 capsules [188]. For completeness, Table 4.9 also contains a summary of other related devices used to monitor physiological conditions in the GI tract and/or disease diagnosis and assessment.

Typically, a regional absorption clinical study will be based upon a four- or five-way crossover design. Following administration of a reference oral drug product, test formulations are delivered to different regions of the GI tract (e.g. upper small intestine, lower small intestine, and colon) to profile a regional absorption map for the drug molecule. Bioavailability data are expressed relative to that for the reference oral dose. The driver for performing this type of investigation has typically been as a prelude to the informed design of an MR formulation to achieve a specific target PK profile. Alternatively, studies can be performed in response to suboptimal PK profiles obtained from clinical testing of a prototype formulation with the aim of diagnosing whether the (unexpected) poor performance was a result of regional differences in absorption [188].

Studies can be augmented by the repeat delivery of different formulations to the same target site to evaluate the impact of various formulation parameters on bioavailability. Published examples have included (i) solution and particulate formulations (to tease apart solubility vs. permeability drivers) [180], (ii) different solubilization technologies (to determine optimum formulation strategies for BCS Class 2 compounds), (iii) different P-gp inhibitors and concentrations to assess potential to overcome efflux, and (iv) different enhancers to improve absorption of BCS Classes 3 or 4 compounds.

As described both earlier and later in this chapter, the colonic environment presents significant challenges to drug delivery with a general trend of reduced rate and extent of absorption when delivered to the colon. Regional bioavailability studies have therefore been used extensively to study this potential risk with demonstrated examples, including Ticagrelor (oral P2Y12 receptor antagonist), which had 32% relative bioavailability from the colon [189] and bevirimat (an HIV

Table 4.9 Summary of electromechanical capsules and devices utilized to assess GI drug delivery, physiology, and disease.

	Purpose	Keyfeatures
IntelliCap® (Medimetrics,	GI drug-delivery system for human drug absorption studies and therapeutic treatments	• 0.3–0.5 ml formulation chamber • Temperature and pH sensors • Formulations released by motorized piston • Programmable delivery profiles • Location tracked via real-time pH measurements • Battery powered and has a wireless link to the outside for reporting and adjustment of medication delivery • Potential for GI fluid sampling
Enterion™ (Quotient Sciences, UK)	Drug-delivery tool for human drug absorption studies	• 1-ml formulation chamber • Tracked via sealed radiolabel tracer • Activation via RF signal torelease piston and bolus drug • Feedback signal confirms device activation • Capable of delivering all solution and solid formulation types
IntelliSite® (Innovative Devices, US)	Drug-delivery tool for human drug absorption studies	• 0.8- and 1-ml formulation chambers • Tracked via radiolabeling of formulations • Activation via Radiofrequency (RF) signal • Original version passive delivery of solution formulations only • "Companion" capsule has active drug-delivery feature for viscous solutions, suspensions, and powders
HF capsule (Battelle-Institute,	Drug-delivery tool for human drug absorption studies	• Tracking using fluoroscopy • Activation via RF signal producing heat to melt athread, release a needle, and pierce alatex balloon • Suitability for solutions, not particulates as passive delivery

Capsule	Purpose	Keyfeatures
Telemetric capsule (Inserm, France)	Drug-delivery tool for hydrogen-donating ability (HDA) study	• 20×39 mm in dimension and 3.5 g in weight • Contains a location detector,aradiotransmitter,a lithium battery, and an interchangeable tip. • Battery powered, limited to eight-hours duration • Primarily for solution delivery • Magnet-triggered release • Location estimated by rotation of on-board cogwheel as an indicator of transit distance
PillCam® (Given Imaging Ltd., Israel)	Endoscopy capsule	• Capsule variants for visualization of esophagus (PillCam ESO), small intestine (PillCam SB) and colon (PillCam Colon 2) • Battery powered • Images transmitted real time • >140° field of view • Noremote control (activated prior toingestion) • FDAapproved
EndoCapsule 10 (Olympus, Japan)	Endoscopy capsule	• Aimed at visualization of small intestine • Battery powered (minimum 12h life) • 160° field of view • Twoimages taken per second, which can be monitored real time • Belt-type antenna worn by patients • FDAapproved
Sayaka capsule (RF SystemLab, Japan)	Endoscopy capsule	• Replaced previous Norika3 technology • Focus and view field can be controlled by an external system • No battery required • Sayaka: Camera positioned in the capsule barrel rather than at the end and can rotate through 360° • Captured images transmitted toreceiver for data processing
MiroCam® (IntroMedic, South Korea)	Endoscopy capsule	• 10.8 × 24.5 mm in size aids ease of swallowing • Three images taken per second over 11h • 170° view field • Uses an oxide silicone chip for imaging • Uses twoexternal capsule electrodes to transmit and a single skin electrode toreceive the data

(*continued*)

Table 4.9 (Continued)

Capsule	Purpose	Keyfeatures
OMOM (Jinshan Science and Technology,China)	Endoscopy capsule	• Made up of three parts: a disposable CE, an image recorder, and an image workstation. • 13× 27.9 mm in size, weighs <6 g • 140° field of view and aresolution of 0.1 mm • Battery life of approximately 6~8 h • Pictures aretaken continuously at arate of twoper second and transmitted real time to the image recorder
CapsoCam Plus ™ (CapsoVision, US)	Endoscopy capsule	• Four laterally oriented cameras provide a full 360° panoramic image of the mucosa • 11×31 mm capturing color high-resolution images at 4 frames per second • Large-capacity onboard storage system completely eliminates the need for external receiver equipment
Bravo™ (Given Imaging, US)	pH monitoring system	• Used for monitoring pH in the esophagus and GI tract and diagnosis of gastroesophageal reflux disease (GERD). • Capsule consists of a battery,radio transmitter, pH electrode • 25 ×6× 5.5 mm in size • Noremote control (activated prior toingestion) • pH measured every 6s and data transmitted every 12s for 48hto an external receiver unit worn by the patient
SmartPill® (Given Imaging, US)	A multifunctional GI monitoring system	• Measures pressure, pH, and temperature throughout GI tract • Battery powered • Cylindrical in shape (26.8 mm long, 11.7 mm in diameter) • Noremote control (activated prior toingestion) • Data extracted and analyzed post recovery • FDAapproved

maturation inhibitor) with 28% relative bioavailability [190]. Conversely, however, there are many reports of drugs being well absorbed from the colon, despite suboptimal characteristics. When fasudil, a kinase inhibitor for the treatment of stable angina, was delivered to the colon comparable exposure to the oral dose was observed with 114% relative bioavailability [191]. Similarly with ATHX-105 phosphate, a 5-HT_{2c} receptor agonist for the treatment of obesity, relative bioavailability of 121% compared to the oral dose was observed from the colon [192]. In theory, it should also be possible to demonstrate dramatically increased relative bioavailability from the colon, for example, for a CYP substrate by bypassing the small intestine.

Regional drug absorption studies have also been used to study the benefits of administering prodrugs vs. active metabolites. Zhu et al. [193] reported on the delivery of fenofibrate, an approved treatment for dyslipidemia, and fenofibric acid, the active metabolite of fenofibrate, as nanocrystal suspensions. Fenofibric acid had improved bioavailability throughout the entire GI tract when given direct in comparison to conversion from the parent compound – approximately 1.5 times higher in the proximal and distal small bowel and 5 times higher following colon delivery. The authors concluded that an oral MR fenofibric acid formulation would therefore be less affected by physiological variability in the GI tract, for example as a result of differences in transit and residence times.

More recently, the Intellicap® capsule has been used for clinical trials with the differentiating feature of being able to simulate an MR input function through the controlled administration of drug over a period of time, in contrast to previous devices only capable of bolus release. Becker et al. [187] reported the use of Intellicap to deliver diltiazem with a first-order release profile over 24 hours, matching the in vitro dissolution profile of a commercial once daily formulation, which in vivo gave highly comparable PK profiles.

4.5.2 Gamma Scintigraphic Imaging

The ability to visualize drug product performance in vivo provides unequivocal evidence as to whether the desired functionality designed and observed under laboratory conditions is actually elicited in the physiological environment. With oral dosage forms, in particular, this also enables a contemporaneous comparison with PK profiles, thereby allowing relationships between formulation parameters controlling drug release (such as disintegration and erosion), anatomical location, and systemic bioavailability to be assessed. Such techniques also provide key insights into intra- and intersubject variability as to whether causes may pertain to the drug product or inherent physiological factors such as differences in GI transit. For MR formulations seeking to deliver drug throughout or to targeted regions of the GI tract, regional bioavailability therefore can be assessed.

The established "gold standard" technique is arguably that of gamma scintigraphy first used to investigate the in vivo release properties of drug formulations in 1976 [194]. The technique has since been used extensively in the development and evaluation of pharmaceutical drug-delivery systems, including enteric-coated tablets and complex MR formulations [195–198]. A variety of techniques have been utilized for labeling oral drug products with short half-life radioisotopes such as ^{99m}Tc or ^{111}In, with the preferred approach determined by dosage form type and study objectives [199].

An example of the use of the gamma scintigraphy to aid targeted delivery was described by Hilton [200], in studies to optimize targeted drug delivery of a novel multiparticulate formulation of prednisolone to the colon. Particles were coated with an amylose/ethylcellulose solution with the aim of triggering drug release in the colon as a result of amylose degradation by bacterial enzymes. Scintigraphy was used to correlate anatomical location of the formulations with PK (prednisolone absorption is reduced in the colon compared to small intestine), and hence inform the adjustment of the coating composition to achieve the desired delivery performance.

Gamma scintigraphy has also been applied extensively to the study of monolithic dosage forms to study a variety of release modalities and durations. In a study performed by Nicholson et al. [201], hydrophilic matrix MR tablet formulations of 6-hydroxybuspirone were prepared and tested in healthy volunteers. Both scintigraphic and PK data confirmed that release of drug was predominantly via a diffusion-controlled mechanism, given plasma concentrations were detected prior to the observed physical release of the radiolabeled marker, and that the release rate was relatively independent of environmental pH. The formulation-controlled drug release and the PK profile were successfully modified in comparison to a solution reference formulation, reducing the maximum plasma concentration to 64–70% (to ameliorate adverse event potential) while maintaining exposure and presumably efficacy. Deconvolution of the PK data confirmed that drug absorption continued through 14 hours with no impact on relative bioavailability, indicating good colonic bioavailability.

The use of scintigraphy to optimize performance of a hydroxypropyl methylcellulose (HPMC) erosion-controlled matrix tablet containing LY545694 Tosylate, a prodrug for compound 645838, was reported by Lobo et al. [68]. Deconvolution techniques had shown that the preferred site of absorption for LY545694 was in the small intestine and hence targeted release through the jejunum and ileum was required. The clinical assessment of an initial 35-mg prototype MR formulation was deemed unsuccessful given delivery of a significant proportion of the drug to the nonabsorptive colonic region. Gamma scintigraphy was therefore utilized to aid development of a revised formulation composition capable of achieving the same exposure and plasma concentration-time profile but with a lower dose

(25 mg) by optimizing drug delivery to the small intestine where absorption was greater. A different grade of HMPC was selected to ensure a faster in vivo release profile, and tablets were radiolabeled with ≤1 MBq ^{111}In resin. A six-arm, flexible study in 16 healthy volunteer subjects was conducted with an adaptive protocol, which, together with an ability to manufacture drug products in reaction to the clinical results, enabled formulation compositions (within an HPMC range of 20–50% w/w) to be adjusted based on observed scintigraphic and PK data. Study data confirmed that formulations demonstrated slower erosion in vivo than those observed in vitro. With the combined use of scintigraphic imaging and an ability to modify tablet composition and performance, an optimal composition that achieved the target PK was identified.

4.5.3 Magnetic Resonance Imaging (MRI)

The use of magnetic imaging for continuously observing the in vivo performance of pharmaceutical dosage forms in motion in the GI tract has also been extensively studied over the last 20 years [202–204]. Initial research utilized the incorporation of a magnetic material (e.g. ferromagnetic iron oxides) into the capsule or tablet, analogous to radioisotopes labeling in gamma scintigraphy, followed by detection with biomagnetic measurement instrumentation to track anatomical location and formulation behavior.

The use of MRI originated as a noninvasive clinical diagnostic tool to identify and characterize diseased tissues and is widely established in medical practice today. There is also increasing research interest to utilize MRI to track pharmacodynamic endpoints to monitor disease progression and the success of therapeutic treatments. Its use to visualize "unadulterated" dosage forms, however, has been cited as problematic due to both prolonged imaging times (and hence impact of transient GI motility and motions on quality of image acquisition) and poor signal-to-noise ratios (which can impact the ability to discern drug products from GI artifacts such as food or air pockets) [203]. This in turn has driven researchers to include paramagnetic or ferromagnetic materials in the dosage form.

Schiller et al. [3] using model nondisintegrating capsules illustrated how MRI could be used to concurrently track anatomical location and to assess free volume of fluids throughout the GI tract. The study also demonstrated that it is erroneous to assume that dosage forms will always be in contact with free water in the GI milieu, as this was observed for only ~50% of capsules in the small intestine and <10% of capsules in the colon in the fasted state. MRI showed fluid was present as discrete pockets, which in the small intestine increased in number and reduced in volume post ingestion of food, while in the colon there was an increase in number, but not volume. Further research has been conducted to characterize volumes and distribution of water in the GI tract and to provide further insights into potential

performance of oral dosage forms with regard to disintegration, dissolution, and absorption as a function of anatomical location and GI transit [205, 206]. These observations further confirm the challenge and complexity for successful design and development of delivery systems to achieve consistent in vivo performance with low intra- and intersubject variability in bioavailability.

4.6 Rational Formulation Design and Effective Clinical Evaluation: Case Studies Describing How to Achieve Desired Release Modality and Target PK

4.6.1 Formulation Strategies to Address BCS Classification Challenges

4.6.1.1 Solubilization

As indicated earlier in this chapter, low solubility and slow dissolution are the characteristics of BCS Classes 2 and 4 drugs. As such, these drugs have potential for low absorption after oral administration and can be associated with low bioavailability, high intra- and intersubject variability, potential food effects, and a lack of dose proportionality [207]. Although the absorption of BCS Class 4 drugs can be also affected by limitations in their permeability, increasing the solubility or dissolution rate of both BCS Class 2 and 4 drugs can often improve their in vivo absorption.

Different technologies have been developed for improving the solubility and/or dissolution rate. These technologies fall into two categories – chemical modification (e.g. salt forms, cocrystals, or prodrugs) and or the use of formulation strategies. The first of these is outside the scope of this review. For the formulation strategies the technologies are mainly particle size reduction, cosolvent, pH adjustment, micelle system, amorphous forms or less stable but more soluble crystalline forms, inclusion complexes, and lipid formulations. Selection of a technology will be based on the physicochemical and biopharmaceutics properties of the drug such as pK_a, stability, crystal form, permeability, and dosage form requirements.

Particle Size Reduction Particle size reduction is one of the simplest approaches to deal with poorly soluble drugs. The strategy is mainly to accelerate the drug dissolution rate. The impact of particle size reduction on the drug's dissolution rate can be explained by the Noyes–Whitney equation below [208], whereby decreasing the particle size, the specific surface area (total surface area per fixed amount of a drug) increases, hence accelerating dissolution of the drug. The effective thickness of the unstirred or Nernst layer may also decrease with particle size to increase the

dissolution rate.

$$\frac{dW}{dt} = \frac{DA(C_s - C)}{L}$$

where:

dW/dt	=	rate of dissolution
D	=	diffusion coefficient
A	=	surface area (of the solid)
C_s	=	saturated solubility concentration in the diffusion layer
C	=	bulk solution concentration
L	=	diffusion layer thickness

Drug solubility can also potentially be improved via particle size reduction. The Freundlich–Ostwald equation describes the relationship between drug solubility and particle size [209]. The inference of particle size on the solubility is also observed as Ostwald ripening phenomenon [210]. However, this effect may not be notable for larger or micronized particles, but can be prominent if in the nanosized range [209].

One of the most common technologies for particle size reduction is micronization via air jet milling due to its high efficiency, scalability, and the fact that the milled drug intermediate can be further developed into a wide range of dosage forms [211]. It is a dry milling process based on interparticle and particle–wall impactions/collisions in the milling chamber under high velocity air fluid. The efficiency of particle size reduction via jet milling depends on the design of the mill, the drug properties, and milling conditions such as feeding rate, injector, and grinding pressures [211]. Increasing air flow pressure or multiple cycles can also lead to smaller particle sizes. In addition, it is relatively easier to achieve smaller particle sizes from brittle drug forms. For softer drug substance materials, it can be helpful to find a more compact crystalline form or to seek specialized mills or use chilling. The particle size generated using this technology is normally less than 10 μm with a lower limit of just below 3 μm. However, as jet milling is a dry process, the resulting micronized drug particles can be electrostatic and difficult to wet for dissolution [212]. Comilling with additional excipients has been reported to improve the drug dispersion and dissolution [212, 213]. Incorporation of a wetting agent is also commonly used during suspension or solid dosage form development.

Further reduction of particle size can be achieved using ball or bead milling, by compaction of drug particles between the milling beads or grinding media and between the beads and the wall of the milling chamber [213]. Wet bead milling is a more effective method for generating nanometer-sized drug particles as small as ≤200 nm [206, 214]. The classic wet bead milling is a slow process during which the drug powders are suspended in a vehicle and filled into a cylinder-shaped jar

loaded with milling beads. The jar is then horizontally rotated on a roller. The more advanced method such as NanoCrystal® Technology utilizes a static milling container with a milling shaft to agitate the milling beads for grinding the drug particles [215, 216]. Process parameters, which affect the milling efficiency, include the formulation composition and concentration, bead density and size, bead-filling ratio, speed, and flow rate [215, 216], Wet-milling processes are very effective and scalable; however, physical stability of the nanoparticle suspension requires addition of polymeric stabilizers or surfactants.

An alternative formulation strategy approach for particle size reduction is high-pressure homogenization (HPH) – a process initially developed for the manufacturing of colloidal dispersions, especially emulsion formulations for parenteral administration [217]. It can also be used for particle size reduction by utilizing the high mechanical energy to force the drug suspensions through a very small gap, creating a high stream velocity fluid, which causes particle size reduction via collision, impaction, shear force, and cavitation [209, 217–219]. To avoid the blockage of the small gap, the drug substance needs to be premicronized before suspending in a medium for HPH processing. The size reduction efficiency depends on the drug loading, flow rate, operating pressure, and physical properties of the drug. Similar to other "top-down" technologies, brittle drug particles are relatively easy to size-reduce compared with elastic drugs. To achieve small particles with narrow particle size distributions, multiple cycles are normally required. The advantages of HPH are good reproducibility and continuous production for a wide scale range and narrow particle size distribution.

Controlled precipitation is a low-energy "bottom-up" process for the preparation of drug nanocrystals or drug-loaded nanoparticles [219, 220]. The drug solution is first dissolved in a suitable solvent, usually a water-miscible organic solvent. The solution is then mixed with a second aqueous medium, possibly chilled, in which the solvent is miscible but the drug is poorly soluble and acts as an antisolvent. Once the solvent disperses, the poorly soluble drug will precipitate to form a suspension. By controlling the drug concentration in the solvent and the mixing of the two media, and by introducing stabilizers in the media, the balance between the drug precipitation (seed forming) and increasing crystal size (crystal growth) can be managed and hence drug particles with a size as low as the nanometer range can be generated [220]. The solvent in the final nanosuspension needs to be removed before further use, typically by drying. The controlled precipitation process can also be combined with a top-down process. The NANOEDGE™ technology is such an example where controlled precipitation is followed with HPH [221]. With this combination, the precipitated nanoparticles can be further stabilized with improved particle size distribution during high-energy processing. The heat generated during the HPH process can also help to remove residual solvent.

Cosolvent and pH Adjustment For pediatric patients or those with difficulty swallowing a solid dosage form, a liquid formulation may be a preferred approach. In early-phase development, where possible, liquid formulations are also commonly used to assess drug safety and PK profiles, due to simplicity of preparation and flexibility for dose escalation. To achieve the maximum possible exposure from liquid formulations of poorly soluble drugs, a solubilized solution that does not precipitate upon dilution or change of pH will always be the preferred choice, although other approaches such as micro- or nanosuspensions and lipid formulations can also be used. The use of cosolvent or pH adjustment are simple and cost effective methods. Cosolvents are water miscible and should be selected to exhibit no pharmacological effect at the used concentrations. Common solubilization vehicles used are propylene glycol, low-molecular-weight PEGs, e.g. PEG300 or PEG400, and glycerol [222].

For ionizable acidic or basic drugs, adjusting the pH of the vehicle can effectively solubilize the drug in the solution. The ionized form of the drug is normally more hydrophilic and hence has higher solubility in aqueous media. The solubility of acidic drugs increases at pH values above the pK_a, whereas the solubility of basic drugs increases at pH values below its pK_a [222]. The solubility profile of zwitterionic drugs, i.e. those that exhibit both acidic and basic properties, is complicated, but in general, the drug solubility increases when the pH is sufficiently above or below its isoelectric point (the pH value at which the drug molecule carries no net electrical charge) [223]. The pH range used in oral liquid formulations is normally between 3 and 9, but can go as low as pH 2 [222]. For some poorly soluble drugs, the pH adjustment is commonly combined with the cosolvent approach to improve the solubilization efficiency [222, 223].

Surfactants Surfactants with a relatively high hydrophilic–lipophilic balance (HLB) value are water soluble and can solubilize poorly soluble drugs via either a cosolvent effect or incorporation into the micelles formed above the critical micelle concentration [222]. Apart from direct solubilization, surfactants are also widely used as wetting agents in suspensions and solid dosage forms to help disperse and dissolve drug particles. In lipid formulations, surfactants can also be mixed with oil lipid and/or cosolvent to improve the drug solubility and dispersion of the formulation. Polysorbate (Tween 20 or 80), PEGylated castor oil (Cremophor EL or RH40), D-α-tocopherol polyethylene glycol 1000 succinate (Vitamin E TPGS), and polyoxylglycerides (Labrasol or Softigen) are commonly used low-toxic nonionic surfactants for solubilization of poorly soluble drugs [222]. These surfactants or also anionic surfactants, such as sodium lauryl sulfate or sodium docusate, or the cationic surfactant, such as cetyl triethyl ammonium bromide, may also be used to improve wetting and solubility as discussed in the previous section on particle size reduction.

Inclusion Complexes Cyclodextrin (CD) is a cyclic oligosaccharide consisting of a hydrophilic outer exterior and a hydrophobic inner cavity. Common CDs include those formed by six-, seven-, or eight-saccharide monomers, classified as α, β, or γ CD, respectively [224, 225]. They can also be further modified by introducing additional functional groups to improve the solubility or enhance the interaction with the guest drug. Examples of these modified CDs are hydroxypropyl-β-cyclodextrin (HPβCD) and sulfobutylether β-cyclodextrin (SBEβCD). Due to specific structure CDs can accommodate whole or partial molecules of drugs in their cyclic cavities to form dynamic inclusion complexes leading to an increase in the apparent solubility of the drug. The host/guest molar ratio of such inclusion complexes are most frequently at 1 : 1, but more complicated complexes can also exist depending on the molecular size, structure, and process [225, 226]. β form CDs such as HPβCD are the most used excipients to form inclusion complexes for poorly soluble drug solubilization for oral administration. 1 : 1 CD complexes often do not precipitate upon dilution. Solubilized drugs in CD solutions can also be further formulated into tablet or capsule solid dosage forms [227]. Addition of water-soluble polymers can provide synergistic effects on solubilization, hence significantly reducing the usage of CD and eliminating the incidence of diarrhea [228]. The additional polymer can also reduce the drug precipitation after dilution with biological fluids post dosing. The use of CDs are currently limited to nonchronic therapeutic indications. Examples of marketed formulations that use CD complexation for oral administration are Sporanox® Oral Solution (Itraconazole) and Surgamyl®(Tiaprofenic acid). For use in the earliest clinical trials or short-term therapeutic applications only, CD solutions, where the solubility of the drug is maintained in the linear range with CD concentration, is one of the simpler and most rapid formulations to develop and present the drug as a nonprecipitating solution. At higher drug concentrations, taste masking or flavoring may be required.

Solid Dispersions Solid dispersion refers to the dispersion of one or more active ingredients in an inert water-soluble carrier matrix in the solid state [228]. The drug can be dispersed in the carrier either at a molecular level, as amorphous particles or as a very fine crystalline material, and the carrier can be either crystal or amorphous in form [229, 230]. The dissolution rate of a poorly water soluble drug in a solid dispersion is increased either by converting the drug crystal to the amorphous form or increasing the surface area of the drug as a result of a reduction in drug particle size in the dispersion. Solid dispersions that contain drug in the amorphous form usually show much faster dissolution rates than those containing crystalline drug, as no lattice structure has to be disrupted for dissolution to take place [231]. As such the amorphous solid dispersion is always the first choice for this technology to achieve faster drug dissolution and hence better

drug absorption. The water-soluble carrier can also improve the drug wettability, prevent drug from aggregation, and even inhibit precipitation to maintain the drug as a supersaturated solution post dissolution [230, 231]. It has been observed that dissolution under nonsink conditions, where a supersaturated solution forms, can be stable beyond the dissolution experiment. The increased rate of dissolution and the "improved solubility" should be directly determined by measuring the kinetic solubility over several hours at different conditions to understand the rate of precipitation. Selection an enteric polymeric excipient, such as hydroxypropyl methylcellulose acetate succinate (HPMCAS) or an anionic acrylate, to stabilize the amorphous dispersion can delay dissolution until the small intestine and aid in avoiding precipitation of the dissolved drug in its supersaturated state.

The amorphous dispersions are metastable and the less soluble, higher melting point form is the stable form. The ratio of the glass transition of the amorphous form to the melting point of the stable form is a measure of the energy released by converting to the more stable form. It is critical in developing these amorphous dispersions to assess differential scanning calorimetry and X-ray powder diffraction data on stability samples to ensure that the metastable form still exists [232]. It has been observed that dissolution under nonsink conditions, where a supersaturated solution forms, can be stable beyond the dissolution stage. Accelerated conditions with direct exposure to temperature and humidity aid in screening for stable formulations.

The first solid dispersion was manufactured using a eutectic mixture method by Sekigushi and Obi [233]. Since then various technologies have been developed, including solvent evaporation, supercritical fluid, hot-melt extrusion, spray-drying, spray coating, and freeze-drying technologies [234–239]. Among these, hot-melt extrusion and spray drying are advanced methods for manufacture of amorphous-based solid dispersion. Other advantages of these technologies are a robust and continuous manufacturing process, suitable for commercial scale production. Two additional approaches to stabilizing amorphous dispersions that are very effective at increasing absorption of drugs are antisolvent precipitation of basic drugs with methacrylic acid copolymers, referred to as microprecipitated bulk powder (MBP) [240] and entrapment of a weakly acidic drug with an anion exchange resin, Amberlite [241]. MBP relies on dissolution of the basic drugs in a cold acidic aqueous solution followed by precipitating the drug rapidly as an amorphous dispersion. Both methods use the strongest intermolecular interaction, i.e. the ionic interaction between the drug and the polymer to stabilize the amorphous dispersion.

Lipid-Based Formulations Most poorly water-soluble drugs are hydrophobic with relatively high log P and hence have higher solubility in organic solvents and lipidic excipients. Lipid-based formulations have been widely used for solubilizing

hydrophobic drugs or food supplements for oral administration. As the absorption of these drugs is typically positively impacted in the presence of food due to solubilization in lipids and adsorption on proteins in the meal, lipid-based formulations provide similar effects and can potentially avoid restrictive labeling for product administration, where large food effects are observed.

A wide range of lipidic and other excipients can be used for formulations in which a drug is solubilized in a lipid vehicle. The Lipid Formulation Classification System (LFCS) introduced by Pouton [242, 243] defines the type of lipid formulations based on the formulation compositions and their associated behavior on dispersion and digestion (Table 4.10).

Type I formulations are simple drug-in-oil solutions in which the drug is dissolved in a digestible oil such as triglyceride, diglyceride, monoglyceride, or their mixtures. While all lipid-based formulations are somewhat limited to more potent drugs, the solubility capacity of Type I formulations is not high, but can be sufficient for some potent, highly hydrophobic drugs. As the oil vehicle is not water miscible, this formulation has poor dispersibility and needs to be digested by enzymes before releasing the loaded drug for absorption [243, 244]. However, there are a number of advantages of this formulation, including protection for the loaded drugs susceptible to enzymes or the acidic environment in the stomach [245].

Type II formulations contain 20–60% water-soluble hydrophobic surfactants in the lipid vehicle and therefore will self-emulsify on contact with aqueous media. The oil droplet size of such emulsion is around 200 nm to 1 mm. This type of lipid formulation is normally referred to as SEDDS (self-emulsifying drug-delivery system) and the ability of emulsification and the resulting droplet size are affected by the type and concentration of the surfactants used. As the droplet size after dispersion is relatively large, digestion is still likely to be required for complete release of the loaded drug.

Type III formulations incorporate cosolvents and more hydrophilic surfactants such as Cremophor EL, Cremophor RH40, or Tween 80. These formulations can rapidly emulsify as microemulsions, a true equilibrium state, and generate finer oil droplets (50–250 nm) upon dispersion and hence are commonly described as SMEDDS (self-microemulsifying drug-delivery system). Based on the level of oil and cosolvent, this type can be further divided into two subgroups as Type IIIA and IIIB, with the latter containing less oil and more cosolvent enabling production of relatively smaller oil droplets. Due to quick self-emulsification into fine oil droplets, fast drug release from these formulations can be achieved without involving enzyme digestion. However, this can also cause precipitation of the released drug after dilution in vivo. Therefore, incorporation of a drug precipitation inhibitor may need to be considered to maintain the released drug in the solution [246]. Careful characterization of the multicomponent phase diagram is required for successful Type III formulations.

Table 4.10 Characterizations of the lipid formulation classification system.

	Type I	Type II	Type III		Type IV
			IIIA	IIIB	
Composition					
	100%	40–80%	40–80%	40–80%	—
Surfactant	—	20–60% (HLB <12)	20–60% (HLB >12)	20–60% (HLB >12)	30–100% (HLB >12)
Cosolvent	—	—	0–40%	20–50%	0–50%
Impact of dispersion	Limited dispersion	Emulsion with droplet size 250 nm to >1μm	Fine emulsion with droplet size 100–250 nm	Fine emulsion with droplet size <100 nm	Micelle solution
Impact of digestion	Digestion required	Likely torequire digestion	Mayrequire digestion	May not require digestion	Digestion not required
Solubility capacity	Low ⇨				High
Precipitation up on dispersion	Low risk ⇨				High risk

Type IV systems are not true lipid formulations as they contains no oil component but only water-miscible surfactants and cosolvents. They can potentially provide higher solubilization capacities than other lipid formulation types. Upon dilution with aqueous media, the formulation can be rapidly dispersed to form surfactant micelles from which the loaded drugs tend to be quickly released and precipitated as the solubility capacity in the resulting micelles is much lower than the undiluted formulation [243].

Other lipid formulations not included in the LFCS are solid lipid nanosuspension [247, 248] and ionic liquid salt-based lipid formulations [249]. Most lipid formulations on the market are in liquid form or liquid filled into gelatin capsules (Agenerases, Neorals, Kaletra). However, the use of solid lipids can provide some advantages, such as mitigating the potential risks of capsule leakage and achieving relatively longer shelf lives. The liquid lipid formulations can also be incorporated into mesoporous absorbent to generate free flow powder for capsule filling or tablet manufacture [250, 251].

4.6.1.2 Permeability Enhancement

The poor permeability of BCS Classes 3 and 4 drugs limits their oral absorption. For these drugs, one of the strategies to improve the permeability is to use permeability enhancers in the formulation. Permeability enhancers are functional excipients, which can improve the drug permeability through the mucosal membrane resulting in enhanced drug absorption [252].

Open Tight Junctions The poor membrane permeability of some drugs can be due to their large-molecular weights or insufficient lipophilicity to partition into biological membranes. For such drugs, paracellular permeation through the tight junctions in the intestinal enterocytes can play an important role in absorption [253–256]. Medium-chain fatty acids and their derivatives have long been recognized as having the ability to regulate the tight junction and hence facilitate the paracellular absorption of drugs [253]. However, a number of these enhancers may disrupt the membrane at higher concentrations, thereby inducing biochemical changes. Consequently, their enhancement and safety must be balanced. The sodium salt of capric acid (C10) is the most common example and has been used as an absorption enhancer in the suppository product Doktacillin®, marketed in Japan, Denmark, and Sweden. It has also been shown to enhance the oral absorption of different drugs in humans [254]. Examples of other permeability enhancers under investigation for modulating tight junctions and enhancing paracellular absorption are chitosan [255], salcaprozate sodium (SNAC) [256], and 8-(*N*-2-hydroxy-5-chloro-benzoyl)-amino-caprylic acid (5-CNAC) [257, 258]. Positive results from clinical trials have been reported for the use of SNAC and 5-CNAC in improving the oral absorption of a number of peptides [252, 259]. In

addition, Peptelligence™ technology (Enteris Biopharma) combines a proteinase inhibitor (citric acid) with an absorption enhancer (Lauroyl-L-carnitine) in an enteric coated form for the oral delivery of peptides. Citric acid itself can also modulate the tight junctions via calcium chelating although not as effectively as other tight junction modulators [260], although positive Phase III data using this approach have been reported for the oral delivery of Tarsa's calcitonin formulation TBRIATM™ for treatment of postmenopausal osteoporosis [261].

Ion-pair Approach The ion-pair concept is based on the fact that some molecules are in an ionized form in the intestine and absorption subsequently relies on the formation of electrically neutral and more lipophilic species between a drug and an endogenous counter ion [262]. The potential of ion-pair formation to improve the oral absorption has been explored in vitro and animal models [262–264]. The use of more polarizable counterions to form salts may have the same effect. The effect of ion-pair formation on intestinal absorption and oral bioavailability of amifostine, a cytoprotective adjuvant with low lipophilicity and ionized at physiological pH range, was conducted and the results demonstrated a 20–30-fold increase in bioavailability with succinic acid and a 10-fold increase with phthalic acid as ion pair [263]. Formation of an ion-pair between sodium caprate (C10) and a cationic drug has also been observed (Quotient Sciences, unpublished data). Both sodium caprate and the drug were water soluble, but the result of a stoichiometric titration indicated that at 1 : 1 molar ratio a hydrophobic sodium caprate-drug pair was formed and precipitated from the aqueous medium. The solubilization of the formed poorly soluble ion-pair was achieved by further addition of the sodium caprate to 1 : 2 ratio and such formulation has improved the drug absorption in rats from 2.3% to 19.5%.

P-gp Inhibitor As noted previously, P-gp located in the apical membrane of the epithelial cells in the intestine can pump drugs back into the gut lumen and hence reduce oral bioavailability [265, 266]. Inhibition of the efflux via P-gp is one strategy used to improve the oral absorption of drugs, which are P-gp substrates. Certain drugs, such as verapamil and cyclosporine, and synthesized small molecules such as KR30031, XR9576, and LY335979, can inhibit P-gp efflux resulting in increased drug absorption [267, 268]. However, such inhibitors will also exert their own intended pharmacological activities or may cause toxic side effects. A formulation approach, using pharmacologically inactive excipients, can provide a safer and more economical way to inhibit P-gp efflux if this is thought to limit absorption [267, 269, 270].

The majority of the excipients inhibiting P-gp are polyethylene glycol (PEG) or PEG containing surfactants such as Cremophors, Tweens, Vitamin E-TPGS, Labrasol, and poloxamers [271, 272]. Li et al. investigated the effects of PEG400,

Tween-80, Cremophor EL, and Poloxamer 188 on the intestinal absorption of ganciclovir, a P-gp substrate, by assessing its in vitro transfer from mucosa to serosa and in situ transepithelial permeation [272]. Drug permeability was significantly increased by all excipients. Cornaire et al. used an improved everted gut sac technique to screen 11 excipients for their ability to enhance the absorption of the P-gp substrates, digoxin and celiprolol, and found that Labrasol had the most effective P-gp inhibition effect [265]. Lo investigated the effects of a series of pharmaceutical excipients, including Span 80, Brij 30, Tween 20, Tween 80, Myrj 52, and sodium lauryl sulfate on the intracellular accumulation, transport kinetics, and intestinal absorption of a P-gp substrate, epirubicin [273]. These results indicated that the optimal effect on epirubicin uptake was characteristic of PEGylated excipients with intermediate HLB values ranging from 10 to 17.

In addition to PEG-containing surfactants, lipid excipients such as medium-chain triglyceride (Miglyol) [265] and water-soluble polymers such as chitosan have also been reported to have an inhibitory effect on P-gp efflux [274]. It was indicated that thiolated chitosan could significantly increase the oral bioavailability of P-gp substrate Rho-123 in rats [274]. The use of novel formulation technologies such as nanoencapsulation can also reduce P-gp efflux and increase the relative oral bioavailability of the P-gp substrate tacrolimus in rats and pigs, 4.9 and 2.45-fold, respectively, when compared to the commercial product [275].

4.6.1.3 Concluding Remarks on Strategies for BCS Challenges

Different formulation strategies have been developed in an attempt to address BCS classification challenges. Selection of a suitable strategy should be based on the physicochemical and biopharmaceutical properties of the molecule of interest and its dosage form requirements. It is common that poor drug absorption can be associated with a number of causes with, for example, a BCS Class 4 drug exhibiting both poor solubility and low permeability. Many formulation strategies and functional excipients can be deployed to address these drug-delivery challenges, in some cases providing benefits not only to increase solubility but also improve permeability. As such, selection of the correct formulation strategy can be critical for achieving the target drug pharmacotherapeutic profiles.

4.6.2 Formulation Strategies for Chronotherapeutic and Regional GI Delivery for Local or Systemic Delivery

4.6.2.1 Gastric Retention

Swellable Formulations For over 40 years, several approaches to gastric-retained drug-delivery systems have been studied to extend the duration of drug absorption in the upper GI tract, to the stomach and upper small intestine, the regions with the greatest absorptive surface area [276–282]. Such gastric retentive systems avoid

delivery to the colon, where many classes of drugs show reduced absorption [283, 284]. In particular, drugs that could benefit from gastric retention are (i) ionized over the relevant physiological pH range, in particular zwitterions or multipolar ions [284, 285], (ii) insoluble drugs i.e. BCS Classes 2 and 4, and (iii) drugs for treating local disorders of the stomach, e.g. Helicobacter pylori infections [286, 287]. In addition, drugs with side effects from delivery to the colon, such as certain antimicrobials or other agents causing diarrhea, may benefit from gastric retention.

Many designs of gastric retentive systems are intended to remain in the stomach for unrealistically prolonged times, including in the fasted stomach through the MMC or housekeeping wave. However, this approach is fighting the existing physiology of the housekeeping wave and has had quite limited success due to variable gastric emptying. Moreover, retention of very large dosage forms in the fasted state has only been evaluated in small populations. The retention of the dosage form in a fasted stomach is promoted after swallowing by a rapid increase in size of the formulation to greater than 2–3 cm by swelling, mechanical means, or gas production, and then significant reduction in size after delivery of the drug to allow the system to exit the digestive tract [281, 282, 288–292].

In contrast to this aforementioned approach to gastric retention in the fasted state, other delivery systems are designed to utilize the natural physiology of digestion in the fed state that delays emptying from the stomach for four to six hours followed by relatively reproducible small intestinal transit of two to four hours [276–278]. In the fed mode, three approaches have been used to achieve gastric retention: size large enough to be retained in the stomach to avoid passage through the contracted fed pylorus, floating in the stomach to avoid the pyloric opening, and adhesion to mucosa.

Optimization of the tablet size, combined with administration of a large daily meal, has led to effective drug delivery to the upper GI tract for up to 10 hours [293]. The sieving mechanism for emptying large particles from the stomach resembles sedimentation, with a strong dependence on particle size relative to the pyloric opening and a weaker dependence on density [294]. For single-unit, nondisintegrating tablets, typical delivery to the upper GI tract is about six hours, which is the sum of gastric emptying times of 2.7 ± 1.5 hours and small intestinal transit time of 3.1 ± 0.4 hours [295]. Multiparticulates, with their more limited size, tend to empty faster than larger single unit tablets, but may have somewhat less variation [296] and have a smaller food effect. Pellets are retained in the stomach for only 1.2 ± 1.3 hours [296]. Addition of flotation to multiparticulate systems has resulted in retention times similar to larger single unit, floating, or nonfloating systems [275, 297, 298].

Among the multiple sources of variation in gastric residence that impact delivery in the fed mode, the fat content of the meal is the dominant correlate with longer retention. Other factors are caloric content, the relative sizes of the pyloric opening

and the tablet or pellet, the erosion of the tablet by disintegration or grinding in the stomach, and inter- and intraindividual variation in the duration of the fed mode. Timmermans and Moes have reported that during the fed mode the pylorus remained mostly contracted, and the mean pyloric diameter was 12 ± 7 mm [299]. Only a gradual cutoff for gastric emptying of 13 mm was observed with mean emptying times of approximately six hours and no clear trend for particles between 12 and 18 mm. While half of the osmotic pumps administered with a light breakfast emptied the stomach within three hours, a heavy breakfast resulted in all of the osmotic pumps remaining in the stomach over eight hours [300]. After dosing with a light breakfast, a 12.5-mm-diameter hypromellose tablet comprising 34% lactose and phenylpropanolamine exited the stomach within one hour [301]. With enteric-coated 12 mm tablets, gastric emptying times were reported as 5.1 ± 0.8 and 7.7 ± 0.7 hours after administration with light and heavy breakfasts, respectively [302].

In a pharmacoscintigraphic study, a nondisintegrating capsule that was 3.5 cm long and 1.2 cm wide was used to measure the onset of the MMC. This huge capsule was compared with a swelling metformin ER tablet, comprising high-molecular-weight polyethylene oxide and hypromellose [278, 303]. These tablets were 12 mm in the minor dimension when dry and swelled to a maximum of approximately 18 mm, gradually eroding over a period of 14–15 hours with most of the drug release being complete within approximately 8 hours [278, 304]. When the healthy volunteers ate three high-fat meals (1000 calories, at least 50% fat) during the day, the large, nondisintegrating capsule resided in the stomach for 20.9 ± 1.8 hours indicating that the MMC was essentially absent throughout the day. By comparison, these metformin ER tablets were last observed in the stomach at 12.6 ± 6.1 hours. With the exception of one tablet that was first seen in the colon at 20 hours, all other metformin tablets disintegrated in the upper GI tract, and consequently with high-fat meals, most of the drug was delivered to the upper GI tract. When the same metformin dosage forms and large nondisintegrating capsules were investigated after administration of low-fat meals (less than 30% fat content), the swelling metformin tablets were last seen in the stomach at 8.5 ± 7 hours and emptied in two populations from 3 to 6 hours and greater than 19 hours. These tablets were last observed in the upper GI tract at 11 ± 3 hours and even under low-fat conditions exceeded the 8 hour drug-delivery period for most of the population. In contrast, large nondisintegrating capsules were last seen in the stomach at 12.8 ± 8.9 hours and also showed the same two populations of short and long emptying times. With the lower-fat content meal, the coefficient of variation for gastric emptying time was 70% in contrast to 9% for the high-fat meal [304]. The much larger capsule does not provide a reproducible longer retention time beyond the swelling tablets. After low-fat meals, the MMC may return and empty both sizes of dosage forms. Moreover, when given with food, the relative

bioavailability of this metformin ER dosage form, given as a single 500-mg tablet once daily, was approximately 115% that of a single 500-mg metformin IR tablet. In the fasted state, however, the relative bioavailability of metformin ER was only approximately 2/3 that of metformin IR tablets [305]. This emphasizes the difficulties in gastric retention through the fasted state with any dosage form and the necessity of administration with food.

For swelling, hydrophilic matrix, gastric retentive dosage forms administered with food, there are two limiting cases for the mechanism of drug release: (i) diffusional release of water-soluble drugs from high-molecular-weight, entangled hydrophilic polymers that form a gel [296, 306–308], and (ii) erosional release of poorly soluble drugs usually from erosional lower-molecular-weight polymers [309].

The diffusional mechanism is confirmed by the cumulative amount of drug released being linearly proportional to the square root of time, which is typical of diffusional release from a dispersed monolith. With the higher-molecular-weight polymer, the tablet forms a strong gel that disintegrates or erodes slowly compared to the time period for drug delivery, and consequently, these diffusional swelling dosage forms given with food can support delivery to the upper GI tract for 8–10 hours. Two drugs released by diffusion from gastric retentive, swelling hydrophilic matrix dosage forms are metformin HCl [296, 306–308], a biguanide antihyperglycemic agent for treatment of Type 2 diabetes, and gabapentin [293], a GABA analog used for treatment of epilepsy and for neuropathic pain from post-herpetic neuralgia (PHN). Both drugs show at least partially saturable absorption from the small intestine with reduced absorption in the lower GI tract [310, 311]. This nonlinear, saturable absorption combined with slower release and absorption from the ER dosage form linearizes the dose-plasma concentration relationships for both ER products [293, 312]. As compared to IR tablets, metformin ER tablets resulted in lower incidences of nausea and diarrhea, presumably due to the lower concentration of drug in the GI tract and administration with food that in itself leads to better tolerability [312]. It is hypothesized that the combination of more linear absorption with better tolerability allows for more rapid and more successful dose titration of therapy.

The efficacy of IR metformin was noted to last longer than the plasma levels [313], and the development of metformin ER was based on the hypothesis that once-daily administration of metformin over about eight hours could lead to good glycemic control. This was demonstrated in clinical trials comparing an IR dosage form and the once-daily ER regimen [312, 313].

A 1000-mg metformin HCl ER tablet [40] was also developed that was bioequivalent to two hydrophilic swelling matrix tablets each with 500 mg. This 1000-mg tablet consisted of a nondisintegrating tablet with a somewhat elastic, plasticized polymethacrylate-based membrane coating that allowed some swelling. The

size of this 1000 mg nondisintegrating dosage form is sufficiently large to show reproducible delivery to the upper GI tract, and it is an approach that has also been used for gastric retention with food of large osmotic pumps [314, 315]. Since FDA guidelines for BE allow and suggest testing of only the highest dose, it is not clear whether the 500-mg tablets designed with identical dosage form mechanisms also can reproducibly deliver the same fraction of drug to the upper GI tract.

ER dosage forms of gabapentin [293] also showed comparable bioavailability when 1800 mg (600 mg tablets) given once a day (QD) (three tablets with the evening meal) or asymmetrically twice a day (BID) (two tablets with evening meal and one tablet at breakfast) as compared to IR gabapentin three times a day (TID) (one tablet with each meal). In contrast to the conventional ER regimen, administration of ER gabapentin as either once-daily dosing or asymmetric dosing with a larger nocturnal dose was found to reduce the adverse effect of somnolence by its timing of C_{max}, while providing optimal pain relief at night from PHN. Using conventional approaches to ER and therapeutic windows, the regimen for administration would have been 900 mg BID, and the peaks and troughs of the ER dosage form would then be bracketed by the higher peaks and lower troughs for the IR gabapentin TID regimen with a shorter duration of efficacy and more side effects. This novel asymmetric approach allowed for a more convenient dosage regimen that was at least as well tolerated and provided pain relief [316].

Less soluble or slower-diffusing drugs may be incorporated into swelling hydrophilic, gastric retentive dosage forms given with food. Lower- or medium-molecular-weight hydrophilic polymers, such as alkyl celluloses or polyethylene oxides, swell in aqueous media and erode to release the drug. The size of the swollen tablet remains close to its swollen peak until much of the drug is released. For this erosional release, the cumulative amount of drug released in dissolution testing is linear with time. However, in the upper GI tract in the fed state, the hydrodynamics and grinding from peristaltic contractions may cause the rate of drug release from erosional dosage forms to be much faster than seen in standard dissolution testing. The cumulative drug release or size of the tablet measured instead in a disintegration tester correlated with in vivo determination of erosion of the tablet in dogs by fluoroscopy and in humans by scintigraphy [309, 317]. Two examples of sparingly soluble drugs that were studied in swelling hydrophilic dosage forms are furosemide, a loop diuretic for treating edema in congestive heart failure patients, nephritic syndrome, and cirrhosis, and ciprofloxacin HCl, a fluoroquinolone antimicrobial agent.

Furosemide has a short duration of action of approximately four hours, during which frequent urination may prevent normal activities. Based on infusion studies [317], continuous delivery of furosemide was hypothesized to be more convenient by spreading out the diuresis over several hours and reducing the

antidiuretic period to allow for potentially superior efficacy [318]. Furosemide, an insoluble drug, is well absorbed in the duodenum and jejunum, but not in the ileum or colon. Therefore, a gastric retentive ER formulation was designed [318] to release the drug over six hours from an erosional, lower-molecular-weight, polymeric swelling matrix. To improve the gastroretention of the tablet remaining in the stomach and drug release to the upper GI tract throughout the six hour drug-delivery period, bilayer tablets were fabricated with a second higher-molecular-weight, hydrophilic matrix to swell and maintain its size in the fed stomach.

Pharmacokinetics, pharmacodynamics, and transit and in vivo erosion of furosemide bilayer tablets when dosed with a meal were studied in 14 healthy volunteers [318]. The tablets were last visualized in the stomach 10.6 hours after administration (range: 3.9–16.5 hours) with the active furosemide layer eroding in 5.7 ± 2 hours (range: 2.6–9.1 hours). This threefold range of erosion rates is typical of in vivo erosion and can provide sufficiently reproducible drug delivery for many therapies. With the exception of one subject, for whom erosion and drug delivery was completed in the upper small intestine, complete erosion of the active layer was observed in the stomach. The six-hour target of erosional drug release from disintegration testing agreed well with the in vivo erosion time of 5.7 hours.

With the short ER bilayer tablet, t_{max} was delayed compared to an IR formulation by a couple of hours, while C_{max} was decreased to about 2/3. While the total urinary outputs were similar for both formulations, the diuresis and natriuresis were more gradual for the ER tablets.

The most common reason for discontinuation of ciprofloxacin antimicrobial therapy is GI adverse events, in particular, nausea and diarrhea [319, 320]. To treat uncomplicated urinary tract infections with a once-daily administration, an erodible, gastric retentive, hydrophilic swelling matrix tablet was developed that delivered over six hours ciprofloxacin HCl to the upper GI tract, where ciprofloxacin is best absorbed [321].

A flat plasma profile is not desirable for an ER ciprofloxacin, because the two important pharmacodynamic parameters for antimicrobial efficacy of a fluoroquinolone anti-infective are AUC/minimum inhibitory concentration (MIC) and C_{max}/MIC [322, 323], with the latter parameter being important for avoiding microbial resistance. The six-hour delivery profile for the ER formulation was designed, when dosed QD with food, to provide comparable AUC and C_{max} to the IR dosage form given BID while substantially reducing the concentration of ciprofloxacin in the GI tract. Two different ER formulations were tested in single-dose PK studies in man: a single layer, erodible, swelling matrix and a bilayer with a high-molecular-weight swelling layer for retention and an erodible, swelling active layer [318, 324]. For ciprofloxacin HCl, the key PK parameters

were comparable in both magnitude and variability. In contrast to furosemide, ciprofloxacin is absorbed throughout the small intestine and is somewhat soluble. While a bilayer formulation resulted in more reproducible gastric retention times and PK profiles for furosemide, a single layer was sufficient for ciprofloxacin.

The efficacy of ER ciprofloxacin HCl given QD with the evening meal was noninferior to IR ciprofloxacin administered BID in a study with 1037 women with uncomplicated urinary tract infections [324]. Both treatments were well tolerated, but the frequencies of nausea and diarrhea were statistically lower in the ER treated group.

Floating Gastric Retentive Dosage Forms The effect of the density of dosage forms on gastric emptying times has been investigated both for densities greater than gastric fluid (submerged or sunken) and for less than gastric fluid (floating). Devereux [325] observed that multiparticulate systems with a density of 2.8 g/cm^3 exhibited delayed emptying in the fasted and fed state. Clarke et al. [326] investigated multiparticulates between 1.18 and 1.40 mm in diameter and with densities of 1.5, 2.0, and 2.4 g/cm^3 and observed no differences in gastric emptying. If there is a critical density greater than gastric fluid for gastric retention, it appears to be between 2.4 and 2.8 g/cm^3.

Many recent gastric retentive dosage forms have focused on floating dosage forms. While the review by Moes [276] remains the most comprehensive on floating dosage forms, there are a number of recent reviews [298, 327].

Floating dosage forms administered in an erect position may delay emptying from the stomach by maintaining a larger distance from the pyloric opening. Nevertheless, floating dosage forms also rely on food in the stomach both to be retained and to float away from the pylorus. The ability of a dosage form to float can be measured both in vitro and in vivo and depends on the resultant weight, which is the difference between the buoyancy force submerged and the gravitational force or weight [297]. When the resultant weight is positive, the dosage form floats; with a negative resultant weight the dosage form is submerged. Through gamma scintigraphy, in vivo flotation can be quantitated as the relative intragastric height, which is defined as the ratio of the distance from the craniocaudal height of the dosage form from the lowest gastric region to the entire gastric height. The relative intragastric height should be interpreted relative to the gastric fluid level. Body posture may have a profound effect on emptying of floating gastric dosage forms. In particular, the influence of supine posture with lying on the left or right side should be studied for gastric emptying and drug delivery. The in vivo performance should also be characterized in terms of the time of onset or lag time to begin floating, the duration of floating, and the effect of frequency of food and fluid intake on floating.

In eight healthy volunteers using gamma scintigraphy, Davis et al. [300] examined nonfloating vs. floating tablets and floating capsules given in the fasted state and after a light breakfast. All dosage forms emptied from 0.8 to 1.7 hours in the fasted state. With food both tablets showed variable gastric emptying after four hours, and the floating capsule emptied after seven hours.

Light and heavy capsules (both were 6 mm × 6 mm × 20 mm) each labeled with two different gamma emitters were studied by scintigraphy in healthy volunteers after dosing either in the fasted state or after a light meal [328]. Food intake was the main determinant of gastric emptying time, while density had only a minor effect. Floating capsules were retained longer in two of eight subjects in both fed and fasted conditions.

The gastric emptying times of floating (initial densities of 0.5–0.7 g/cm^3) and nonfloating (initial densities of 1.1–1.2 g/cm^3) capsules were observed after administration with breakfast to volunteers in the upright and supine positions [297]. Three capsule sizes were investigated: 8–9 mm, 11–12 mm, and 14–15 mm. The size of the nonfloating capsules was correlated with the emptying time and the results were variable. The residence time for floating capsules increased from the smallest- to medium-sized capsules, and was similar for the medium and larger capsules. Floating capsules trended to longer mean gastric emptying times than the nonfloating capsules for all capsule sizes, i.e. 3 vs. 1.5 for the smallest, 4 vs. 2 for the medium, and 4 vs. 3.5 for the largest. Note that these differences between floating and nonfloating dosage forms were smallest or nonexistent at the largest size. While nonfloating capsules had similar emptying times when subjects were in the erect and supine positions, floating capsules emptied earlier in the supine position than nonfloating capsules, and nonfloating capsules emptied earlier than floating capsules in the upright position.

Floating dosage forms have been designed as a bilayer with a drug release layer and a floating layer, the latter consisting of hydrocolloid gelling polymer, such as hypromellose or gums. This has been developed into a marketed product that delivers misoprostol [329]

Matrix non-gas-generating floating tablets are usually composed of gelling hydrophilic polymers, typically hypromellose, that form a lower-density gel on the outside of the tablet core. Sheth and Tossounian [330] developed a hydrodynamically balanced system, which has been used for two marketed products, Valrelease® (diazepam) and Madopar (levodopa and benserazide). Flotation times and gastric emptying times of up to six hours were observed.

Gas-generating floating systems may produce carbon dioxide that is trapped inside the dosage form. Bicarbonate or calcium carbonate, either with or without an acid, such as citric, fumaric, or tartaric acids are most often used to generate the gas. Different capsule sizes (#5, 0, 000) with Methocel K4M and sodium

bicarbonate (2% w/w) as a gas-generating agent were studied [297]. Flotation times as long as eight hours were observed in vitro, and in vivo in fed (650-kcal continental breakfast) upright subjects. Constant relative gastric heights were achieved for up to 200 minutes.

A number of monolithic gas generating tablets have been developed and marketed. A gas-generating tablet containing superdisintegrant as swelling polymer, a gelling polymer, sodium bicarbonate, and ciprofloxacin [331] has been marketed in India (Cifran OD) [298]. The sparingly soluble ciprofloxacin allows for a slower release rate with a small amount of polymer. The plasma concentration–time profiles for ciprofloxacin reflect a relatively short ER similar to that for the previously described non-gas-generating swelling tablet. This gas-generating tablet also shows a longer in vitro dissolution profile and could benefit from disintegration testing of the drug-release profile to obtain better correlation with in vivo performance.

A gas-generating swelling hydrophilic matrix system was developed to deliver metformin while being bioequivalent to the marketed ER tablet [332]. While both the innovator and the ANDA dosage forms contained swelling hydrophilic polymers, metformin HCl, and an esthetic, rapidly dissolving coating, sodium bicarbonate was also added as a gas-generating agent.

Multiparticulate dosage forms are frequently cited as advantageous over single-unit dosage forms, because all-or-nothing emptying is avoided. Aggregation of multiple units may occur in gastric fluid as a raft or mass floating on top of the fluid. While this raft has been an intentional design for gastric retentive floating dosage forms, it also loses this particular advantage of multiparticulate systems. With alginate beads, these gels may float for even three hours after dosing, and only dissolve with ingestion of hot liquid or food [333, 334].

Using lyophilized calcium alginate beads with a mean diameter of 2.15 mm and 0.33 g/cm^3 density, Whitehead et al. [335] reported gastric emptying times in excess of 5.5 hours after a high-fat breakfast for the floating beads as opposed to approximately one hour for nonfloating beads. In vitro a positive resultant weight was observed and floating was maintained for 12 hours. Alginate beads with dissolved amoxicillin exhibited superior flotation to those loaded with suspended amoxicillin [335].

While the advantages of the larger floating tablets are less apparent, for equivalent small pellets, beads, or minitabs, these multiple unit dosage forms provide more reproducible emptying as a probability distribution of particles. Moreover, there are longer retention times for these smaller particles when in an upright position. Such floating multiparticulates have the potential of being used in a specialized dosage form for patients with difficulty swallowing, a potential issue with the large expanding tablets. Using liquid floating alginate beads (Topalkan, Pierre-Fabre, France) and effervescent floating alginate solution

(Liquid Gaviscon, GSK, India), retentive aluminum–magnesium antacid products have been developed. The latter forms a raft by forming a floating, colloidal gel in the stomach.

Bioadhesion or Mucoadhesive Systems Mucoadhesion or sticking to mucin, the glycoprotein on the GI tissue surface, has been reviewed with the purpose of gastric retention [295, 336], and this is a small subset of the field of bioadhesion. The mechanisms of bioadhesion include gastric bonding mediated (mechanical and chemical bonding; nonspecific), hydration mediated, and receptor mediated (specific) [295, 337]. Bioadhesive polymers may be classified as anionic, cationic, and neutral, and the ionic classes are the most relevant to this discussion.

Reproducible gastric retention resulting from mucoadhesion has been elusive, as a result of rapid gastric mucosal turnover, limited penetration into the mucus layer, and the limited surface area of the stomach. In the stomach, the mucus layer is thicker and turnover more rapid than the intestine with greater motility and proteolytic activity. With its greatly limited surface area, there are fewer binding sites in the stomach compared to the intestine. With either a specific binding mechanism, such as antibody targeting to mucin, or nonspecific polymeric carriers, only about 2% of microparticles or nanoparticles exhibited prolonged adhesion to the upper GI tract (unpublished data by the authors).

Acrylic acid/acrylamide copolymers showed bioadhesion below pH 4.7. Adhesion increased directly with the density of carboxyl groups and inversely with the crosslink density [338]. Chain flexibility may be critical to form entanglements for proper hydrogen bonding between polymer chains and the glycoprotein [337]. In an in vitro study, where porcine gastric mucosa was continuously washed with SGF, 3% dispersions of polyacrylic acid showed good adhesion [339]. Carbopol (carbomer) 934P, in which ion exchange resin particles were microencapsulated, had no significant effect on gastric residence in rats [340].

Chitosans, the cationic polysaccharides derived by partial deacetylation of chitin, interact with mucin, according to atomic force microscopy studies, mainly by electrostatic interactions through the NH^{4+} moieties on chitosan with the COO^{-} and SO^{3-} groups on mucins [341]. Chitosan granules loaded with furosemide were studied in healthy volunteers [342]. While the in vitro studies showed adhesion, there was no change in t_{max}, and with slower delivery there was decreased bioavailability, indicating a lack of significant prolongation of gastric emptying. Only 10% of tetracycline-loaded chitosan microspheres remained after two hours in the fasted stomach of gerbils [286].

A short-term treatment for duodenal ulcers, sucralfate, an aluminum salt of an anionic sulfated polysaccharide, adheres to the surface of gastric and duodenal ulcers [343]. Matrix tablets of sucralfate and Methocel E4M loaded with theophylline exhibited good adhesion and release in vitro [344]. A lyophilized solid

dispersion of sucralfate and tetracycline was compared in fasted rats with a physical blend of the two [345]. The dispersion exhibited the greatest tetracycline on the mucosal surface and was consistent with prolonged residence.

Approaches for the Fasted State Gastric retention through Phase 3 of the MMC or housekeeper wave has been the "holy grail" of oral controlled-release technology [282, 288, 290] and reproducible and safe residence through the fasted state sufficient for a commercialized pharmaceutical product has not been demonstrated. This part of the discussion will concentrate on three of the more interesting approaches in the last three decades: a gas-generating expanding membrane device [346], superporous hydrogels [347], and the "accordion pill" [348].

The dosage form developed by Sinnreich [346] consisted of a polyvinyl alcohol membrane bag that contained the drug, usually baclofen, a gas-generating agent, sodium bicarbonate, and optionally an acid, such as citric acid, to avoid variation in gastric pH from PPIs, food, or achlorhydria or to shorten the time lag for inflation.

When collapsed, the bag could be rolled and fit into a capsule. In gastric fluid, the dosage form expands to about 2–2.5 cm in diameter and then deflates when the gas source is depleted. To visualize the baclofen-containing dosage form and the gas in the dosage form in beagle dogs, radiopaque strings were incorporated into the bag [349]. In both fasted and fed states, all dosage forms inflated within 0.5 hours followed by deflation within 1–4 hours when fasted and 3–6 hours when fed. In the fed beagles, the dosage form remained in the stomach for at least 10 hours in five of six dogs and emptied between 6 and 7 hours in the remaining dog. The plasma profile of baclofen was consistent with a gastric retentive, ER dosage form with a comparable bioavailability, reduced C_{max}, and longer t_{max} compared to the IR formulation [349].

Samarium oxide was added to the baclofen dosage form [346] followed by neutron activation [350] to observe its transit using gamma scintigraphy [351] in a crossover study involving healthy volunteers in the fasted state or with a low- or high-fat meal. Relative bioavailability in these same volunteers after a low-fat meal and a high-fat meal was 80% and 90%, respectively, compared to the bioavailability of the IR baclofen. After a high-fat meal, all 13 dosage forms remained in the stomach at 16 hours and 7 were still in the stomach at 24 hours. In the fasted state, the dosage forms emptied in 2 hours in three volunteers while four still were observed in the stomach at 16 hours. Following the low-fat, low-calorie meal, four systems were last observed in the stomach at 6 hours, 60% of the dosage forms resided in the stomach at 16 hours, and one remained at 24 hours. This remains one of the most successful cases of retention with a low-fat meal. A limitation of this dosage form is that relatively potent drugs are required.

To develop very large expanding gastric retentive systems, Park and Park [347] investigated superporous hydrogels, dried open channel hydrogel foams with large

pores greater than 100 μm in diameter. Superporous hydrogels and their biological applications are reviewed by Mastropietro et al. [352]. These are lightly crosslinked with an interconnecting series of pores and swell greatly with the use of appropriate monomers, particularly polyacrylic acid, polyacrylamide, polyhydroxyethylmethyl methacrylate, or hydroxypropylmethylmethacrylate. Residual monomers for these hydrogels need to be substantially removed and controlled below tight control limits. Control of the washing and pore size can be challenging. To create a foam of these hydrogels, a protein, poloxamer, gas, or a chemical foaming agent may be used.

After rapid swelling to a large size, these hydrogels have poor mechanical strength and fall apart. The superdisintegrant, sodium croscarmellose, improves its mechanical strength [353, 354]. While these hydrogels emptied the stomach in 2–3 hours in fasted beagles, in fed dogs they remained in the stomach for 24 hours. In second-generation superporous hydrogels, additional mechanical strength was gained with less swelling [352]. Carbohydrate superporous hydrogels have been developed and degraded by amylase [355]. By incorporating the drug in a separate region, dosage forms have been designed [356].

The "accordion pill," an unfolding multilayer, expanding compressed dosage form that resides in the stomach, was developed in the laboratories of Hoffman and Friedman [348, 357–360], and a BID carbidopa–levodopa treatment for treatment of Parkinson's disease is entering Phase III trials (Intec Press Release 14 December 2015).

In their early studies, the basic unit of the accordion dosage form was a trilayer with an inner polymeric drug layer shielded by two outer glutaraldehyde crosslinked gelatin layers that were coated with microcrystalline cellulose on the outside to prevent adhesion. A rigid biodegradable frame of polylactic acid and ethyl cellulose (9 : 1) surrounded the inner layer [359]. This unfolded 2.5×5 cm system was folded and placed in a large capsule. Like the previous two systems, the accordion pill also required specialized manufacturing considerations. The handling of the multilaminate, slitting, die cutting, and folding made this stage of the manufacturing more analogous to the converting operations in transdermal systems and in packaging than typical oral solid dosage forms.

A prototype system with riboflavin, which is absorbed only in the duodenal cap and exhibits saturated absorption [361, 362], remained in the stomach of fasted dogs for 13 hours [357, 359]. Moreover, the riboflavin bioavailability was four times greater than from an IR dosage form.

Klausner et al. [348] pretreated fasted beagles with carbidopa and administered three prototype accordion dosage forms containing L-dopa. In these fasted dogs, the prototype with the longest dissolution time of 4.2 hours produced plasma levels greater than 500 ng/ml for over 9 hours, which was significantly longer than standard controlled-release dosage forms.

Gastric retention was studied by MRI in 11 subjects fed a moderate-calorie, high-fat breakfast (552 kcal, 48% fat), followed by a low-fat lunch (862 kcal, 26.5% fat) at 4 hours after administration, and then a nonstandardized dinner at 10 hours [363]. In 80% of the subjects, the dosage form remained in the stomach for 8 hours, and almost 20% remained at 24 hours. In a Phase 2 study in Parkinson's patients ($n = 8$), comparable plasma level data were shown for a gastric retentive carbidopa-L-dopa dosage forms administered every eight hours and IR dosage forms given every four hours. In Phase II trials, when compared to conventional therapy, this unfolding dosage forms showed statistically different (shorter) off periods, the period where medication does not work as indicated by increased difficulty in movement. With the entry of this gastric retentive carbidopa-L-dopa dosage form into Phase 3 trials, there is a promise both for improving therapy and for pursuing longer durations of drug delivery to the upper GI tract than were previously feasible. A similar duration with twice daily delivery of carbidopa L-dopa has been studied and achieved with swelling hydrophilic matrices with food [364].

4.6.2.2 Enteric-Coated Dosage Forms and Delayed Release to the Small Intestine

Enteric-coated dosage forms or multiparticulates are the most common approach to delayed drug release for either chronotherapy or delivery to lower regions of the GI tract and/or to avoidance of delivery to the stomach. The reader is referred to reviews of coating [365] or enteric coating [366, 367] for details of the materials, excipients, and processes. The typical reasons for avoiding drug delivery to the stomach are (i) instability of the drug, such as for pepsin-sensitive enzymes or for acid instability, for example, omeprazole, (ii) for preventing gastric irritation such as with nonsteroidal inflammatory agents, like ibuprofen or diclofenac, (iii) to avert nausea, for example with iron or magnesium salts, or (iv) to avoid GI side effects as with valproic acid. In cases of acid unstable active agents, such as omeprazole, the drug may need to be protected not just from the gastric acid, but also from the acidic polymers in enteric coats. In particular, a rapidly dissolving hypromellose subcoat can separate and protect the acid unstable drug. Certain drugs may also be better absorbed if delivered as a bolus directly to the upper small intestine. For example, some actives requiring enhancers to increase their permeability or alternatively, acid-soluble drugs may benefit from inclusion of an acidic excipient, such as fumaric or citric acids, to increase the solubility of the drugs, Other water-insoluble agents may have improved bioavailability by bolus delivery to the small intestine as amorphous dispersions or nanoparticles to maintain a metastable supersaturated state. Formulations, including acids, may also cause interference with the rate of dissolution of the enteric coating and, thus, a subcoat may be useful. For peptides, some clinically successful oral delivery has been

shown by coating first with an HPMC subcoat and then enteric coating a tablet containing a peptide or protein, such as parathyroid hormone (1–31) or salmon calcitonin, 500 mg citric acid, and lauroyl-L-carnitine, as an enhancer [368]. Other reasons for enteric coating are (i) to provide a delay or part of a timed delay for applications to chronotherapy, (ii) to define a time separation in absorption of a combination drug, where one drug is IR and the other is enteric coated, for example to avoid a metabolic drug interaction, or (iii) to deliver drugs to other regions of the GI tract, i.e. jejunum, ileum, or colon. The latter will be discussed in Sections 4.6.2.3 and 4.6.2.4 of this chapter.

Enteric coatings are generally usually based on charged polymers that are largely impermeable at acidic pH, such as SGF, and become permeable and dissolve at values of pH close to neutral or basic, as exists in the duodenum and jejunum. There is considerable variability in pH of fasted (often 1–2) and fed states (4–5 and then decreasing with added gastric acid secretion). Some causes of variation in GI pH are: (i) different meals and drinks, for example, from acidic sodas to pH in excess of 5 for most meals, (ii) various medications, in particular, proton-pump inhibitors that reduce gastric acid secretion, (iii) in the elderly or pernicious anemia patients that frequently have achlorhydria, or low gastric acid production, and (iv) different regions of the GI tract.

Enteric coating materials offer a range of pH to select as a target pH above which is the onset of drug release, and may be applied with either aqueous or organic coating (Table 4.11). The cellulosic enteric-coating materials are subject to hydrolysis at elevated temperatures and relative humidity with HPMCAS and polyvinyl acetate phthalate (PVAP) being less susceptible. Hydrolysis may substantially alter the enteric coating properties. Shellac may suffer from variability. MA-EA copolymers, HPMCAS-HF, and shellac release at relatively high pH for delivery to the duodenum or jejunum, but may have uses for other sites in the GI tract. In contrast, PVAP and HPMCP 50 may have unplanned release in the stomach with certain meals and in certain patient populations.

In vitro dissolution testing of enteric-coated dosage forms are intended to demonstrate avoidance of release in the stomach (i.e. less than 2%) by testing at pH 1 or 2 for one to two hours, and to characterize the simulated rate of drug release in the small intestine by dissolution at pH 6 or greater, showing greater than 80% drug release in a relevant defined time, such as 20 minutes or over an extended period. The rate of dissolution of the enteric coating at near-neutral pH may be influenced by many factors including the following: (i) the properties of the drug or excipient, in particular plasticizers, (ii) the pH and the polymer or mixture of polymers in the coating, (iii) the coat weight or thickness, (iv) dissolution media, including pH, buffer, and ionic strength, and (v) holes or fissures in the barrier, which may be generated by porosogens.

Table 4.11 Enteric-coating polymers.

EC polymer	pH for onset of release	Coating solutions
Hydroxypropyl methylcellulose phthalate (HPMCP)	4.5–5.5 HPMPCP 50 5.0 HPMPCP 55 5.5	Organic Aqueous
Polyvinyl acetate phthalate (PVAP)	5.0	Organic Aqueous mixture
Cellulose acetate trimellitate (CAT)	5.2	Organic Ammoniacal aqueous
Poly methacrylic acid ethyl methacrylate or MA-EA	Eudragit L30-D/L-100-55 5.5	Aqueous Organic
Poly methacrylic acid methyl methacrylate or MA-MMA	Eudragit L 6.0 Eudragit S 7.0 Eudragit FS 30D 7.0	Aqueous Organic Aqueous
Cellulose Acetate Phthalate (CAP)	6.2	Aqueous Organic
Hydroxypropyl methylcellulose acetate succinate (HPMCAS)	HPMCAS LF 5.0 HPMCAS MF 5.5 HPMCAS HF 7.0	Aqueous
Shellac	7.0	Organic Aqueous

The use of enteric-coated granules, pellets, or beads instead of enteric-coated tablets or capsules can make for a more reproducible product with respect to drug-delivery onset time or t_{max} when given with food. While food effects refer to changes in AUC and C_{max}, for enteric-coated tablets or capsules, variable t_{max} is a more likely effect of nondisintegrating tablets administered with food. For example, EC-Naprosyn® (FDA approved label) is a 500-mg enteric-coated tablet and exhibited t_{max} at 4–6 hours (range: 2–12 hours) in the fasted state and at 12 hours (range: 4–24 hours) in the fed mode. That is, drug delivery may essentially be delayed one day in some patients due to delayed gastric emptying. In contrast, for granules, pellets, and beads, there is a distribution of much shorter gastric emptying times and much less of a difference between fasted and fed administration in t_{max} and less variability of t_{max} with food. Note that the size of enteric-coated enhancer tablets or tablets where acid is included to shift local intestinal pH briefly may be a balancing act between the tablet size needed for a sufficient local effect to enhance absorption and longer and erratic gastric emptying times in the presence of food.

4.6.2.3 Delivery to the Jejunum and Ileum

Delivery to the stomach can be achieved with IR dosage forms, and bypassing the stomach usually involves enteric coating as a delay with a difference in pH between the stomach and the small intestine as a trigger for release. Initiation of drug delivery further down the intestine may involve either a single longer delay mechanism or both a delay mechanism and a different trigger-second delay mechanism to start delivery to the desired area of the small intestine or colon. While delivery to the jejunum or ileum may be used to improve bioavailability for drugs susceptible to enzymes or transporters that reside in the duodenum or upper jejunum, colonic delivery is more typically used for local treatment of the colon, for example, inflammatory bowel disease (IBD), Crohn's disease, or colorectal cancer. Colonic delivery has also been studied for delivery of macromolecules, particularly proteins and peptides, to avoid digestion [369]. However, most studies still report bioavailability of at most a few percentages for these proteins [369].

Delivery to the jejunum and ileum can be achieved with enteric coating with release at pH 5.5–6.0 and then a delay for about 40 minutes to 1 hour, which is generally greater than transit through the duodenum. This additional delay can be accomplished with the use of a single, slower-dissolving enteric coating or a separate delay mechanism. Dissolution of the enteric coating can be slowed by a thicker coating, addition of insoluble excipient to the coating, a mixture of two enteric coating materials, one with less solubility or releasing at a higher pH, or other means. This enteric coating with a delay approach removes the variability of gastric emptying and relies on the relative consistency of intestinal transit time.

Delayed release beyond the dissolving of the enteric coating may be achieved by a subcoat that dissolves or erodes over a defined period of time. The erosion times for these subcoatings are better predicted in a disintegration tester than in the standard dissolution apparatus. There can be a threefold to fourfold range in the erosion times in vivo and, therefore, targeted erosion times should be selected as shorter than the desired mean. Another approach is to have a semipermeable membrane subcoating, such as plasticized cellulose acetate, surrounding an osmotic agent that induces increased pressure from the influx of water and eventually causes the membrane to rupture after a determined time to initiate drug release.

To initiate delivery in the ileum, particularly the distal ileum where a pH value slightly greater than 7 is common, enteric coatings that dissolve near pH 7 have been used [4]. There are two potential issues with this pH approach. The pH along the intestine may vary considerably, and the pH may peak near the ICJ and then decrease in the colon [6]. Moreover, transit through the small intestine slows distally. Considerable time can be spent at the ICJ, and this time can vary. The variation in pH and ileal transit will be discussed in Section 4.6.2.4 in terms of its impact on colonic delivery.

4.6.2.4 Colonic Delivery

Colonic delivery is generally used for local treatment of the colon to reduce the amount of drug needed by localizing it in the colon to optimize efficacy while reducing side effects. Either prodrugs activated in the colon, colonic drug-delivery systems, or carriers digested in the colon may be used. Delivery to the colon relies on three potential triggers: (i) the pH of the colon decreasing to 6.4 ± 0.6 upon entering and rising to 7.0 ± 0.7 in the descending colon, (ii) relatively reproducible small intestinal transit of two to four hours after gastric emptying, and (iii) digestion by colonic microflora. The decrease in pH upon entering the colon results from bacterial fermentation, e.g. producing lactic acid and short-chain fatty acids. Bacterial growth in the colon is typically 10^{11}–10^{12} colony forming units (CFUs) and is 3–5 orders of magnitude greater than in the small intestine.

pH as a Trigger for Colonic Delivery A simple mechanism of targeting drug delivery to the colon is enteric coating the formulation to release the drug near pH 7. Since the ICJ is near pH 7 with a slightly more acidic pH in the initial portion of the colon and then returning to pH 7 in the descending colon, the site of drug release is often in the ileum [370]. Use of an enteric coating that dissolves at a more acidic pH would result in even more drug release earlier in the small intestine. A gamma scintigraphic study was conducted in eight fasted healthy volunteers of three dosage forms enteric coated with an aqueous dispersion of Eudragit S, an ethanolic solution of Eudragit S, and an aqueous dispersion of Eudragit FS-30D, all of which release drug above about pH 7.0 [371]. When coated with the aqueous Eudragit S dispersions, the tablets were observed in all subjects to disintegrate in the mid-to-proximal small intestine. In contrast, the tablets coated with the ethanolic solution of Eudragit S did not disintegrate in three of the eight participants and in the other three subjects disintegrated in the ICJ. The tablets coated with Eudragit FS disintegrated in 14 of 16 administrations either in the ileocecal region or the ascending colon.

While some of the drug may be absorbed in the ileum, most of the drug may still be delivered to the colon. It is useful to consider marketed enteric-coated dosage forms of mesalazine or 5-aminosalicylic acid (5-ASA) to treat IBD or ulcerative colitis. Asacol® is a marketed dosage form of 5-ASA 400 mg coated with Eudragit S in an 80-μm-thick layer that releases drug above pH 7. Using barium-loaded tablets, the tablets were visualized disintegrating in the distal ileum and the right colon [370]. Almost 90% of the 5-ASA was delivered to the colon in an ileostomy study [372]. Although Robinson and coworkers [373] indicate that pH alone is too variable to deliver drug only to the colon, much of the drug still can be delivered to the colon using pH as a trigger.

Another marketed 250-mg 5-ASA product, Claversal®, is coated with a thick coating of Eudragit L that releases drug above pH 6. Since the lower pH would

initiate drug release in the upper small intestine, this thicker enteric coat delays the drug release until the distal ileum and right colon.

To treat distal idiopathic colitis, capsules were enteric coated with cellulose acetate phthalate to release drug above pH 6 to the distal small intestine and ileum [374].

Dissolution testing of pH triggered colonic delivery dosage forms is analogous to enteric-coated tablets with at most a few percentages of the drug released in two hours at pH 1–2 and greater than 80% of the drug released in a specified time for a pH slightly greater than 6 or 7 depending on the coating polymer. If a slow-dissolving enteric coat is used, multiple time points should be used to specify the lag.

Time Delay or pH and Time Delay Triggers for Colonic Delivery A lag time before drug release is initiated has been used as a trigger mechanism for colonic delivery. In the fasted state, gastric emptying is generally less than two hours, and the small intestinal transit time is typically two to four hours. Consequently, entrance into the colon generally occurs 2.5–6 hours after fasted administration. The Pulsincap® dosage form uses an impermeable capsule with a hydrogel plug that swells and is expelled from the capsule after an approximate delay period. The dosage form subsequently releases the drug after this delay.

While this time-delayed approach may work in the fasted state, there is too much variability in the gastric emptying times with food, particularly of large single-unit, nondisintegrating dosage forms. Multiparticulate dosage forms may incorporate an osmotic agent and a semipermeable membrane that bursts and releases drug after a fixed time or alternatively be coated with an erodible coating after which drug is released. While these approaches are somewhat less affected by administration with food, there is still considerable variation in the emptying time distribution of the particulates. Moreover, this timed approach does not account for other sources of individual variation.

A combination of two trigger mechanisms of pH for entering the small intestine followed by timed delay to release drug in the colon after small intestinal transit provides a solution to the variability of transit with food. For example, if a Pulsincap dosage form or a coated microparticulate with either erodible coatings or osmotic burstable coatings were over coated with an enteric coating that dissolves above pH 5.5 or 6, the gastric-emptying variability is accounted for by the enteric coating and a three to four-hour delay would allow delivery to the colon. The arrival time to the colon and for drug release would still show the same variability with food, but the delivery to the colon would be less variable.

Rather than two delay mechanisms, Wong and Theeuwes [375, 376] coated osmotic pumps with cellulose acetate phthalate to release drug in the distal small interesting above pH 6 and then deliver the drug at a constant zero order

rate based on the osmotic pressure. For more restricted delivery to the colon, such as for ulcerative colitis, this enteric-coated osmotic pump has an additional three to four-hour delay after the pump membrane becomes permeable through dissolution of the enteric coating and prior to initiating the zero-order drug delivery [377]. In an osmotic pump designed for colonic delivery of proteins, a core of an active and an osmotic agent was enveloped by a delay coating with an external semipermeable membrane over coated with an enteric polymer to delay dissolution until arrival in the small intestine [378]. These combined trigger mechanisms provide a method of overcoming the variability in delivery to the colon due to transit with administration with food, but the timing of the onset of drug release in the colon still shows the variability of large, nondisintegrating tablets.

To understand how sustained-release dosage forms deliver drug to the colon without the enteric coat or any delay, it is useful to consider a conventional sustained-release dosage form of 5-ASA. This conventional sustained release 5-ASA product, Pentasa®, consists of microgranules coated with ethyl cellulose, provides sustained release of 5-ASA throughout the entire GI tract, and does not target delivery to the colon, the region needing treatment [379]. This is in contrast to the other mechanisms discussed for targeting to the colon. Since the transit time through the colon is longer than the rest of the GI tract, most of the drug is still delivered to the colon. IBD can accelerate transit times and it has been shown that even in patients with IBD nearly 90% of the drug is delivered. Nevertheless, the drug delivered to the stomach is unstable and absorbed systemically from the small intestine [380].

Dissolution testing of dosage forms with delays triggered by a change in pH requires demonstrating minimal drug release over two hours at pH 1.2 and determining at least 80% release in a specified time at a pH where the enteric coating dissolves. When an ER profile is also involved, dissolution should use multiple time points to characterize the delay and the full drug-release profile through at least 80% release. If pH trigger and ER are combined, the multiple time points should be characterized at a high enough pH to ensure dissolution of the enteric coating.

Digestion by Microflora to Trigger Drug Release in the Colon Both prodrugs and dosage forms for targeted delivery to the colon have been based on drug liberation through either azo reductases or hydrolysis by glycosidases both located almost exclusively in colonic microflora.

The classic prodrug of 5-ASA targeted to the colon is sulfasalazine, which is 5-ASA conjugated to sulfapyridine (SP) through an azo bond and digested mostly in the colon by bacterial azoreductases to yield free 5-ASA and SP. Many of the adverse events from this drug are associated with the SP, and attempts to provide

an improved prodrug focused on increasing the mole ratio of 5-ASA:SP in the prodrug. Olsalazine [381] through cleavage of azo bonds in the colon releases 2 mol of 5-ASA for every mole of SP. Both drugs show little absorption intact, and most of the free 5-ASA and its acetylated metabolite are found in the feces. This approach was extended to an azo-linked pendant azo linkage of 5-ASA to polysulfonamidoethylene polymer [382, 383].

Drug glycosides and particularly glucuronides are metabolized by both bacterial enzymes and are suitable for targeting the colon. These compounds are polar and poorly absorbed in the small intestine and are metabolized in the colon. With certain plant glycosides, this leads to toxicity, but also demonstrates the potential for colonic prodrugs. β-Glucosides of prednisolone and dexamethasone and β-glucuronides of budesonide and dexamethasone have been demonstrated in vitro and in vivo as colonic prodrugs [369]. Naloxone and nalmefene were conjugated with a glucuronide linkage and tested in a rat model with the goal of blocking morphine-induced constipation [384].

CDs have been used as carriers of drugs and as linkages of prodrugs for colonic delivery. CDs, which are polar and molecular weights in an excess of 1000, are poorly absorbed or metabolized by glycosidases in the small intestine and not digested until the colon by microbial flora to maltose and glucose. CD complexes of insoluble drugs generally lead to rapid absorption of the drug in the small intestine and an early peak plasma concentration. For CD complexes to be effective for colonic delivery, the dissociation kinetics of the complex must be quite slow.

CDs are, however, applicable as prodrugs for colonic delivery. Conjugates of prednisolone were made with α, β, and γ- CDs, and the α-conjugate was tested in a rat IBD model. The side effects were reduced compared to free prednisolone [385–387].

The second basic approach that relies on colonic bacteria as a trigger mechanism involves degradation of the dosage form or its coating by the microbial flora. Early work on delivery of proteins or peptides to the colon to avoid digestion in the small intestine utilized degradation by azo-reductases of either hydrogels or coatings. Kopecek and coworkers prepared hydrogels of acrylic acid and acrylamide derivatives crosslinked with 4,4-(dimethylacetoamino)azobenzene [388] with entrapped proteins. The acrylic acid content provided little swelling in the acidic stomach and swelled at intestinal pH. In the colon, the azo crosslinks in the swollen hydrogel were slowly degraded by the colonic bacterial azo-reductases, which are macromolecular enzymes and as a result of their high-molecular weight had slow diffusional access to the crosslinks.

Saffran et al. [389, 390] prepared hydrogel coatings of hydroxyethylmethacrylate (HEMA) crosslinked with divinylazobenzene and coated pellets of insulin and capsules and pellets of vasopressin. While the drug release in rats was considerably delayed, the pharmacological response was very variable.

Polysaccharide matrices and coatings provide more readily acceptable pharmaceutical excipients that may provide trigger mechanisms for colonic delivery. In particular, guar gum, pectin, and alginic acid remain intact through the human upper GI tract and can be digested by colonic flora [391]. An amylose and ethyl cellulose coating was applied to a dosage form of prednisolone metasulfobenzoate and relied on colonic bacteria for drug release. Positive Phase II trial results were observed in IBD [392].

The ability of pectin- and guar gum-based matrices to disintegrate in the colon was studied by gamma scintigraphy [393]. A calcium pectinate blend with pectin was designed to disintegrate quickly in the ascending colon, and a calcium pectinate blend with guar gum was intended to disintegrate more slowly throughout the transverse colon. Studies with rat fecal fluid in vitro were used to screen these formulations for degradation in the presence of colonic bacteria. The scintigraphic study confirmed that the calcium pectinate blend with pectin disintegrated faster in the colon and more reproducibly than the calcium pectinate blend with guar gum.

A dual trigger mechanism of a colonic capsule coated with a single-layer coating, including both Eudragit S and polysaccharide, was studied in eight healthy volunteers by gamma scintigraphy in a three-way crossover design when given fasting, with breakfast or 30 minutes before breakfast. Independent of the food condition, the radiolabeled capsules were observed to disintegrate consistently in the ileocecal region or in the colon [394]. A rat fecal slurry was used to examine dissolution in vitro. When this dual mechanism dosage form was administered in the fasted state, six capsules disintegrated in the ascending colon, and one at the left splenic flexure at the distal end of the transverse colon. In comparison in the fasted state with a dosage form coated only with Eudragit S using only a pH-dependent mechanism, four capsules disintegrated in the ascending colon and four capsules exited the colon.

Finally, in a recent gamma scintigraphy study in six healthy volunteers [395], theophylline tablets compression coated with guar gum were investigated as a treatment for nocturnal asthma by delayed release to the colon. Dissolution was studied at pH 1.2 and at pH 6.8 with and without galactomannanase to digest the guar gum. Up to 3% of the drug was released in the acidic dissolution media. While 27–54% of the theophylline was released over 10 additional hours at pH 6.8 without enzyme, the rate of dissolution increased substantially 82–104% over 12 hours with the added galactomannase. The tablets were observed to reach the colon at five, six, and eight hours in three of the six subjects. With variation in gastric emptying with food, the variability of drug release and onset of therapy for these microbial release nondisintegrating tablets is quite problematic. Delayed-release dosage forms are certainly applicable to chronotherapy, but multiparticulates and timed delays are more reproducible.

4.7 Conclusions

There are many potential barriers to a successful development of oral dosage forms, whether the goal is to achieve adequate absorption and systemic bioavailability or to target a specific anatomical location for the treatment of local GI disease. Physiological variability in pH, water content, surface area, and enzyme and transporter expression throughout the intestines presents unique challenges for any NCE with its own unique physicochemical and biopharmaceutics properties, affecting the fundamental in vivo drug-delivery parameters of dissolution, solubility, absorption, metabolism, and hence bioavailability.

To assess challenges and strategies for successful oral delivery, a range of tools exist to characterize the properties of candidate drugs. Development teams also have access to a wide range of in silico, in vitro, and in vivo models to aid prediction of clinical performance based on these input data. Nevertheless, evidence suggests that caution should be observed in regard to assuming extrapolation to man, which is perhaps not surprising given the aforementioned complexity of biological systems.

Over recent decades, scientific approaches have been developed to aid understanding of drug and formulation performance in humans, which can provide valuable insights in regard to either anticipating or explaining the clinical successes and failures of dosage forms.

Based on a combined knowledge of GI anatomy and physiology and drug substance properties coupled with an appreciation of likely performance in humans, the pharmaceutical scientist has access to a wide range of formulation technologies to design and develop a drug product capable of achieving the desired performance in vivo. Due to trends in molecular chemistry and emerging pharmacological targets, it is increasingly unlikely that a simple IR dosage form will be sufficient for development. More typically, to identify clinically and commercially successful drug products, strategies will be required either to overcome solubility and permeability challenges to absorption and presystemic metabolism, and/or deliver drugs to specific anatomical regions of the GI tract.

References

1 Castelli, M.C., Connor, A.L., Wilding, I.R., and Riley, M.G. (2011). A gamma scintigraphic clinical study of the absorption of insulin co-formulated with Eligen® absorption enhancer 4-CNAB. *FASEB J.* 25 (S1): 7.1-lb646. Experimental Biology 2011 Meeting Abstracts.

2 Dressman, J.B. (1986). Comparison of canine and human gastrointestinal physiology. *Pharm. Res.* 3: 123–130.

3 Schiller, C., Frohlich, C.-P., Giessmann, T. et al. (2005). Intestinal fluid volumes and transit of dosage forms as assessed by magnetic resonance imaging. *Aliment. Pharmacol. Ther.* 22: 971–979.

4 McConnell, E.L., Fadda, H.M., and Basit, A.W. (2008). Gut instincts: explorations in intestinal physiology and drug delivery. *Int. J. Pharm.* 364: 213–226.

5 Zarate, N., Mohammed, S., O'Shaughnessy, E. et al. (2009). Accurate localisation of a fall in pH within the ileo-caecal region. *Neurogastroenterol. Motil.* 21 (s1): 21–43. Abstracts of the 3rd International Meeting of Neurogastroenterology and Motility, 27–30 August 2009, Chicago, USA, 1–104.

6 Evans, D.E., Pye, G., Bramley, R. et al. (1988). Measurement of gastrointestinal pH profiles in normal ambulant human subjects. *Gut* 29: 1035–1041.

7 Connor, A.L., Evans, P., Church, A. et al. (2013). A phase I study to investigate the impact of gastrointestinal site of delivery, gastrointestinal pH and formulation composition, on the bioavailability of AK106–001616 in healthy subjects. *American Association of Pharmaceutical Scientists Annual Meeting and Exposition*, San Antonio, US. Poster presentation R6043.

8 Thelen, K. and Dressman, J.B. (2009). Cytochrome P450-mediated metabolism in the human gut wall. *J. Pharm. Pharmacol.* 61: 541–558.

9 Paine, M.F., Hart, H.L., Ludington, S.S. et al. (2006). The human intestinal cytochrome P450 'pie'. *Drug Metab. Dispos.* 34: 880–886.

10 Thorn, M., Finnstrom, N., Lundgren, S. et al. (2005). Cytochromes P450 and MDR1 mRNA expressions along the human gastrointestinal tract. *Br. J. Clin. Pharmacol.* 60: 54–60.

11 van Herwaaden, A.E., Wagenaar, E., van der Kruijssen, C.M.M. et al. (2007). Knockout of cytochrome P450 3A yields new mouse models for understanding xenobiotic metabolism. *J. Clin. Invest.* 117: 3583–3592.

12 Paine, M.F., Khalighi, M., Fisher, J.M. et al. (1997). Characterization of interintestinal and intraintestinal variations in human CYP3A4-dependent metabolism. *J. Pharmacol. Exp. Ther.* 283: 1552–1562.

13 Von Richter, O., Burk, O., Fromm, M.F. et al. (2004). Cytochrome P450 and P-glycoprotein expression in human small intestinal enterocytes and hepatocytes: a comparative analysis in paired tissue specimens. *Clin. Pharmacol. Ther.* 75: 172–183.

14 Kempf, D.J., Marsh, K.C., Kumar, G. et al. (1997). Pharmacokinetic inhibitors of the human immunodeficiency virus protease by co-administration with ritonavir. *Antimicrob. Agents Chemother.* 41: 654–660.

15 Deeks, E.D. (2014). Cobicistat: a review of its use as a pharmacokinetic enhancer of atazanavir and darunavir in patients with HIV-1 infection. *Drugs* 74: 195–206.

16 Christiansen, A., Backensfeld, T., Denner, K., and Weitschies, W. (2011). Effects of non-ionic surfactants on cytochrome P450-mediated metabolism in vitro. *Eur. J. Pharm. Biopharm.* 78: 166–172.

17 Beaumont, K. (2003). The importance of gut wall metabolism in determining drug bioavailability. In: *Drug Bioavailability*, 1e (eds. H. van de Waterbeemd, H. Lennernäs and P. Artursson), 311–328. Weinheim: Wiley-VCH.

18 Jones, K., Connor, A., and Paterson, M. (2007). Development of oral formulations to overcome gut wall metabolism. *10th Annual AAPS North East regional Discussion Group (NERDG) Conference,* Conneticut, US. Poster presentation.

19 Tubic-Grozdanis, M., Hilfinger, J.M., Amidon, G.L. et al. (2008). Pharmacokinetics of the CYP 3A substrate simvastatin following administration of delayed versus immediate release oral dosage forms. *Pharm. Res.* 25: 1591–1600.

20 Hediger, M., Clemencon, B., Burrier, R., and Bruford, E. (2013). The ABCs of membrane transporters in health and disease (SLC series): introduction. *Mol. Asp. Med.* 34: 95–107.

21 Russell, F. (2010). Transporters: importance in drug absorption, distribution, and removal. In: *Enzyme- and Transporter- Based Drug-Drug Interactions*, Chapter 2,, 1e (eds. S. Pang, D. Rodrigues and R. Peter), 27–49. New York: Springer-Verlag.

22 Huls, M., Russell, F., and Masereeuw, R. (2009). The role of ATP binding cassetts transporters in tissue defense and organ regeneration. *J. Pharmacol. Exp. Ther.* 328: 3–9.

23 Leslie, E., Deeley, R., and Cole, S. (2005). Multidrug resistance proteins: role of P-glycoprotein, MRP1, MRP2, and BCRP (ABCG2) in tissue defense. *Toxicol. Appl. Pharmacol.* 204: 216–237.

24 Giacomini, K., Huang, S., Tweedie, D. et al. (2010). Membrane transporters in drug development. *Nat. Rev. Drug Discovery* 9: 215–236.

25 Varma, M., Ambler, C., Ullah, M. et al. (2010). Targeting intestinal transporters for optimizing oral drug absorption. *Curr. Drug Metab.* 11: 730–742.

26 Mahar Doan, K., Humphreys, J., Webster, L. et al. (2002). Passive permeability and P-glycoprotein-mediated efflux differentiate central nervous system (CNS) and non-CNS marketed drugs. *J. Pharmacol. Exp. Ther.* 303: 1029–1037.

27 Polli, J., Wring, S., Humphreys, J. et al. (2001). Rational use of in vitro P-glycoprotein assays in drug discovery. *J. Pharmacol. Exp. Ther.* 299: 620–628.

28 Klaassen, C. and Aleksunes, L. (2010). Xenobiotic, bile acid, and cholesterol transporters: function and regulation. *Pharmacol. Rev.* 62: 1–96.

29 Murakami, T. and Takano, M. (2008). Intestinal efflux transporters and drug absorption. *Expert Opin. Drug Metab. Toxicol.* 4: 923–939.

30 Estudante, M., Morais, J., Soveral, G., and Benet, L. (2013). Intestinal drug transporters: an overview. *Adv. Drug Delivery Rev.* 65: 1340–1356.
31 Zhou, M., Xia, L., and Wang, J. (2007). Metformin transport by a newly cloned proton-stimulated organic cation transporter (plasma membrane monoamine transporter) expressed in human intestine. *Drug Metab. Dispos.* 35: 1956–1962.
32 Zhang, E., Phelps, M., Chen, C. et al. (2002). Modeling of active transport systems. *Adv. Drug Delivery Rev.* 54: 329–354.
33 Sugawara, M., Huang, W., Fei, Y.-J. et al. (2000). Transport of valganciclovir, a ganciclovir prodrug, via peptide transporters PEPT1 and PEPT2. *J. Pharm. Sci.* 89: 781–789.
34 Lal, R., Sukbuntherng, J., Tai, E. et al. (2009). Arbaclofen placarbil, a novel *R*-bacolfen prodrug: improved absorption, distribution, metabolism, and elimination properties compared with *R*-baclofen. *J. Pharmacol. Exp. Ther.* 330: 911–921.
35 Akamine, Y., Yasui-Furukori, N., Leiri, I., and Uno, T. (2012). Psychotropic drug-drug interactions involving P-glycoprotein. *CNS Drugs* 11: 959–973.
36 Aller, S., Yu, J., Ward, A. et al. (2009). Structure of P-glycoprotein reveals a molecular basis for poly-specific drug binding. *Science* 323: 1–10.
37 Zhou, S. (2008). Drugs behave as substrates, inhibitors and inducers of human cytochrome P450 3A4. *Curr. Drug Metab.* 9: 310–322.
38 Cummins, C., Jacobsen, W., and Benet, L. (2002). Unmasking the dynamic interplay between intestinal P-glycoprotein and CYP3A4. *J. Pharmacol. Exp. Ther.* 300: 1036–1044.
39 Kivisto, K., Niemi, M., and Fromm, M. (2004). Functional interaction of intestinal CYP3A4 and P-glycoprotein. *Fundam. Clin. Pharmacol.* 18: 621–626.
40 Pedersen, K., Christiansen, B., Klitgaard, N., and Nielsen-Kudsk, F. (1983). Effect of quinidine on digoxin bioavailability. *Eur. J. Pharmacol.* 24: 41–47.
41 Fenner, K.S., Troutman, M.D., Cook, J.A. et al. (2009). Drug-drug interactions mediated through P-glycoprotein: clinical relevance and in vitro-in vivo correlation using digoxin as a probe drug. *Clin. Pharmacol. Ther.* 85: 173–181.
42 Tunock, Y., Hazan, E., Oto, O. et al. (1997). Relationship between high serum digoxin levels and toxicity. *Int. J. Clin. Pharmacol. Ther.* 35: 366–368.
43 CDER/FDA (2012). Guidance for industry drug interaction studies-study design, data analysis, implications for dosing, and labeling recommendations.
44 European Medicines Agency (EMA) (2012). Guideline on the Investigation of drug interactions. CPMP/EWP/560/95/Rev. 1 Corr. 2**, Committee for Human Medicinal Products (CHMP).
45 Spahn-Langguth, H. and Langguth, P. (2001). Grapefruit juice enhances intestinal absorption of the P-glycoprotein substrate talinolol. *Eur. J. Pharm. Sci.* 12: 361–367.

46 Custodio, J., Wu, C.-Y., and Benet, L. (2008). Predicting drug disposition, absorption/elimination/transporter interplay and the role of food on drug absorption. *Adv. Drug Delivery Rev.* 60: 717–733.

47 Taipalensuu, J., Tőrnblom, H., Lindberg, G. et al. (2001). Correlation of gene expression of ten drug efflux proteins of the ATP-binding cassette transporter family in normal human jejunum and in human intestinal epithelial Caco-2 cell monolayers. *J. Pharmacol. Exp. Therapeutics* 299: 164–170.

48 Tucker, T., Milne, A., Fournel-Gigleux, S. et al. (2012). Absolute immunoquantification of the expression of ABC transporters P-glycoprotein, breast cancer resistance protein and multidrug resistance-associated protein 2 in human liver and duodenum. *Pharmacology* 83: 279–285.

49 Gutmann, H., Hruz, P., Zimmermann, C. et al. (2005). Distribution of breast cancer resistance protein (BCRP/ABCG2) mRNA expression along the human GI tract. *Biochem. Pharmacol.* 70: 695–699.

50 Zimmermann, C., Gutmann, H., Hruz, P. et al. (2005). Mapping of multidrug resistance gene 1 and multidrug resistance-associated protein isoform 1 to 5 mRNA expression along the human intestinal tract. *Drug Metab. Dispos.* 33: 219–223.

51 Thörn, M., Finnström, N., Lundgren, S. et al. (2005). Cytochromes P450 and MDR1 mRNA expression along the human gastrointestinal tract. *Br. J. Clin. Pharmacol.* 60: 54–60.

52 Daniel, H. and Kottra, G. (2004). The proton oligopeptide cotransporter family SLC15 in physiology and pharmacology. *Eur. J. Physiol.* 447: 610–618.

53 Meier, Y., Eloranta, J.J., Darimont, J. et al. (2007). Regional distribution of solute carrier mRNA expression along the human intestinal tract. *Drug Metab. Dispos.* 35: 590–594.

54 Wuensch, T., Schulz, S., Ullrich, S. et al. (2013). The peptide transporter PETP1 is expressed in distal colon in rodents and humans and contributes to water absorption. *Am. J. Physiol., Gastrointest. Liver Physiol.* 305: G66–G73.

55 Haenisch, S., May, K., Wegner, D. et al. (2008). Influence of genetic polymorphisms on intestinal expression and rifampicin-type induction of ABCC2 and on bioavailability of talinolol. *Pharmacogenet. Genomics* 18: 357–365.

56 Aarnoudse, A.-J., Dieleman, J., Visser, L. et al. (2008). Common ATP-binding cassette B1 variants are associated with increased digoxin serum concentrations. *Pharmacogenet. Genomics* 18: 299–305.

57 Hoffmeyer, S., Burk, O., von Richter, O. et al. (2000). Functional polymorphisms of the human multidrug-resistance gene: multiple sequence variation and correlation of one allele with P-glycoprotein expression and activity in vivo. *Proc. Natl. Acad. Sci. U.S.A.* 97: 3473–3478.

58 Nakanishi, T. and Ikumi, T. (2012). Genetic polymorphisms of OATP transporters and their impact on intestinal absorption and hepatic disposition of drugs. *Drug Metab. Pharmacokinet.* 27: 106–121.

59 Freire, A.C., Basit, A.W., Choudhary, R. et al. (2011). Does sex matter? The influence of gender on gastrointestinal physiology and drug delivery. *Int. J. Pharm.* 415: 15–28.

60 Ashiru, D.A., Patel, R., and Basit, A.W. (2008). Polyethylene glycol 400 enhances the oral bioavailability of a BCS class III drug (ranitidine) in male subjects but not females. *Pharm. Res.* 25: 2327–2333.

61 Kaye, J.L. (2011). Review of pediatric gastrointestinal physiology data relevant to oral drug delivery. *Int. J. Clin. Pharm.* 33: 20–24.

62 Pedersen, S. and Steffensen, G. (1987). Absorption characteristics of once-a-day slow-release theophylline preparation in children with asthma. *J. Pediatr.* 110: 953–959.

63 Grassi, M., Petraccia, L., Mennuni, G. et al. (2011). Changes, functional disorders, and diseases in the gastrointestinal tract of elderly. *Nutr. Hosp.* 26: 659–668.

64 Cowles, V.E., Gusler, G., Chen, T.-F. et al. (2004). Gastric emptying and intestinal transit of gastroretentive tablets in the fed state: effect of meal content and tablet size. *Gasteroenterology* 126 (Suppl. 2): A489–A490.

65 Coupe, A.J., Davis, S.S., and Wilding, I.R. (1991). Variation in gastrointestinal transit of pharmaceutical dosage forms in healthy volunteers. *Pharm. Res.* 8: 360–364.

66 Hardy, J.G., Harvey, W.J., Sparrow, R.A. et al. (1993). Localization of drug release sites from an oral sustained-release formulation of 5-ASA (Pentasa) in the gastrointestinal tract using gamma scintigraphy. *J. Clin. Pharmacol.* 33: 712–718.

67 Davis, S.S., Hardy, J.G., and Fara, J.W. (1986). Transit of pharmaceutical dosage forms through the small intestine. *Gut* 27: 886–892.

68 Lobo, E.D., Argentine, M.D., Sperry, D.C. et al. (2012). Optimization of LY545694 tosylate controlled release tablets through pharmacoscintigraphy. *Pharm. Res.* 29: 2912–2925.

69 Davis, S.S., Washington, N., Parr, G.D. et al. (1988). Relationship between the rate of appearance of oxprenolol in the systemic circulation and the location of an oxprenolol Oros 16/260 drug delivery system within the gastrointestinal tract as determined by scintigraphy. *Br. J. Clin. Pharmacol.* 26: 435–443.

70 Dressman, J.B., Berardi, R.R., Dermentzoglou, L.C. et al. (1990). Upper gastrointestinal (GI) pH in young, healthy men and women. *Pharm. Res.* 7: 756–761.

71 Ghibellini, G., Leslie, E.M., and Brouwer, K.L.R. (2006). Methods to evaluate biliary excretion of drugs in humans: an updated review. *Mol. Pharm.* 3: 198–211.

72 Guiney, W.J., Beaumont, C., Thomas, S.R. et al. (2011). Use of entero-test, a simple approach for non-invasive clinical evaluation of the biliary disposition of drugs. *Br. J. Clin. Pharmacol.* 72: 133–142.

73 Stevens, L., Collier, J., Cozens, S. et al. (2012). Application of the Entero-Test® String for Assessing Biliary Secretion of Camicinal (GSK962040) and its Metabolites in Healthy Subjects. AAPS 2012 poster T2307.

74 Amidon, G., Lennern's, H., Shah, V., and Crison, J. (1995). A theoretical basis for a biopharmaceutical drug classification: the correlation of in vitro drug product dissolution and in vivo bioavailability. *Pharm. Res.* 12: 413–420.

75 FDA (2000). Waiver on in vivo bioavailability and bioequivalence studies for immediate-release solid oral dosage forms based on the Biopharmaceutics Classification System, Guidance for Industry. U.S. Department of Health and Human Services, FDA, Centre for Drug Evaluation and Research (CDER).

76 Blume, H. and Schug, B. (1999). The biopharmaceutics classification system (BCS): class III drugs- better candidates for BA/BE waiver? *Eur. J. Pharm. Sci.* 9: 117–121.

77 Yu, L., Amidon, G., Polli, J. et al. (2002). Biopharmaceutics classification system: the scientific basis for biowaiver extensions. *Pharm. Res.* 19: 921–925.

78 Jantratid, E., Prakongpan, S., Amidon, G., and Dressman, J. (2006). Feasibility of biowaiver extension to biopharmaceutics classification system class III drug products: cimetidine. *Clin. Pharmacokinet.* 45: 385–399.

79 Polli, J., Abrahamsson, B., Xu, L. et al. (2008). Summary workshop report: bioequivalence, biopharmaceutics classification systems and beyond. *AAPS J.* 10: 373–379.

80 FDA (2015). Waiver on in vivo bioavailability and bioequivalence studies for immediate-release solid oral dosage forms based on the Biopharmaceutics Classification System, Guidance for Industry, Draft Guidance. U.S. Department of Health and Human Services, FDA, CDER.

81 FDA (2017). Waiver on in vivo bioavailability and bioequivalence studies for immediate-release solid oral dosage forms based on the Biopharmaceutics Classification System, Guidance for Industry. U.S. Department of Health and Human Services, FDA, CDER.

82 Yazdanian, M., Briggs, K., Jankovsky, C., and Hawi, A. (2004). The "high solubility" definition of the current FDA guidance on biopharmaceutical classification system may be too strict for acidic drugs. *Pharm. Res.* 21: 293–299.

83 Tubic-Grozdanis, M., Bolger, M., and Langguth, P. (2008). Application of gastrointestinal simulation for extensions for biowaivers of highly permeable compounds. *AAPS J.* 10: 213–225.

84 Mehta, M.U., Uppoor, R.S., Conner, D.P. et al. (2017). Impact of the US FDA "biopharmaceutics classification system" guidance on global drug development. *Mol. Pharm.* 14: 4334–4338.

85 EMA (2010). Guideline on the Investigation of Bioequivalence. CPMP/EWP/QWP/1401/98 rev.1/Corr**.

86 WHO Technical Report Series, No.937. (2006). Multisource (generic) pharmaceutical products: guidelines on registration requirements to establish interchangeability Annex 7.

87 WHO Technical Report Series, No.938. (2006) Proposal to waive in vivo bioequivalence requirements for *WHO Model List of Essential Medicines* immediate-release, solid oral dosage forms. Annex 8.

88 Davit, B., Braddy, A., Conner, D., and Yu, L. (2013). International guidelines for bioequivalence of systemically available orally administered generic drug products: a survey of similarities and differences. *AAPS J.* 15: 974–990.

89 Asean Guideline Draft (2004). The Conduct of Bioavailability and Bioequivalence studies.

90 TGA (2015). *Guidance 15: Biopharmaceutics Studies*. Australian Government, Department of Health.

91 Med Safe (2015). Guideline on the Regulation of Therapeutic products in New Zealand, Part 6: Bioequivalence of medicines, Ed. 2.

92 Health Canada (2014). Guidance Document, Biopharmaceutics Classification System based Biowaiver.

93 Volpe, D., Xu, L., and Mőller, H. (2002). *Cell Culture Models of Biological Barriers: In vitro Test Systems for Drug Absorption and Delivery* (ed. C.-M. Lehr), 130–139. London, Chapter 9: CRC Press - Taylor and Francis Group.

94 Zheng, Y., Benet, L., Okochi, H., and Chen, X. (2015). pH dependent but not P-gp dependent bidirectional transport study of S-propranolol: the importance of passive diffusion. *Pharm. Res.* 32: 2516–2526.

95 Neuhoff, S., Ungell, A.-L., Zamora, I., and Artursson, P. (2005). pH-dependent passive and active transport of acidic drugs across Caco-2 cell monolayers. *Eur. J. Pharm. Sci.* 25: 211–220.

96 Varma, M., Gardner, I., Steyn, S. et al. (2012). pH-Dependent solubility and permeability criteria for provisional biopharmaceutics classification (BCS and BDDCS) in early drug discovery. *Mol. Pharm.* 9: 1199–1212.

97 Thiel-Demby, V., Humphreys, J., Williams, L. et al. (2009). Biopharmaceutics classification system: validation and learnings of an in vitro permeability assay. *Mol. Pharm.* 6: 11–18.

98 Dahan, A., Miller, J., Hilfinger, J. et al. (2010). High-permeability criterion for BCS classification: segmental/pH dependent permeability considerations. *Mol. Pharmaceutics* 7: 1827–1834.

99 Cook, J., Addicks, W., and Wu, Y. (2008). Application of the biopharmaceutical classification system in clinical drug development – an industrial view. *AAPS J.* 10: 306–310.

100 FDA (2010). The Use of Mechanical Calibration of Dissolution Apparatus 1 and 2 – Current Good Manufacturing Practice (CGMP). Guidance for Industry. U.S. Department of Health and Human Services, FDA, CDER.

101 Lindberg, M., Kopp, S., and Dressman, J. (2004). Classification of orally administered drugs on the world health organisation model list of essential medicines according to the biopharmaceutics classification system. *Eur. J. Pharm. Biopharm.* 58: 265–278.

102 Takagi, T., Ramachandran, C., Bermejo, M. et al. (2006). A provisional biopharmaceutical classification of the top 200 oral drug products in the United States, Great Britain, Spain and Japan. *Mol. Pharm.* 3: 631–643.

103 Gupta, E., Barends, D., Yamashita, E. et al. (2006). Review of global regulations concerning biowaivers for immediate release solid oral dosage forms. *Eur. J. Pharm. Sci.* 29: 315–324.

104 Tampal, N., Mandula, H., Zhang, H. et al. (2015). Biopharmaceutics classification system-based biowaivers for generic oncology drug products: case studies. *AAPS PharmSciTech* 16: 5–9.

105 Wu, C. and Benet, L. (2005). Predicting drug disposition via application of the BCS:transporter/absorption/elimination interplay and development of a biopharmaceutics drug disposition classification system. *Pharm. Res.* 22: 11–23.

106 Benet, L., Amidon, G., Barends, D. et al. (2008). The use of the BDDCS in classifying the permeability of marketed drugs. *Pharm. Res.* 25: 483–488.

107 Benet, L., Broccatelli, F., and Oprea, T. (2011). BDDCS applied to over 900 drugs. *AAPS J.* 13: 519–547.

108 Butler, J. and Dressman, J. (2010). The Developability classification system: application of biopharmaceutics concepts to formulation development. *J. Pharm. Sci.* 99: 4940–4954.

109 Jantratid, E. and Dressman, J. (2009). Biorelevant dissolution media simulating the proximal human gastrointestinal tract: an update. *Dissolut. Technol.* 16 (3): 21–25. Special Edition on Biorelevant Dissolution: Methodology and Applications.

110 Rosen, H. and Abribat, T. (2005). Timeline: the rise and rise of drug delivery. *Nat. Rev. Drug Discovery* 4: 381–385.

111 Li, J., Wang, Q., and Hidalgo, I.J. (2016). *New Horizons in Predictive Drug Metabolism and Pharmacokinetics*, Chapter 2, RSC Drug Discovery Series number 49 (ed. A. Wilson), 27–52. London: RSC.

112 Lipinski, C., Lombardo, F., Dominy, B., and Feeney, P. (2001). Experimental and computational approaches to estimate solubility and permeability in drug discovery and development settings. *Adv. Drug Delivery Rev.* 46: 3–26.

113 Bergström, C., Charman, W., and Porter, C. (2016). Computational prediction of formulation strategies for beyond-rule-of-5 compounds. *Adv. Drug Delivery Rev.* 101: 6–21.

114 Wessel, M., Jurs, P., Tolan, J., and Muskal, S. (1998). Prediction of human intestinal absorption of drug compounds from molecular structure. *J. Chem. Inf. Comput. Sci.* 38: 726–735.

115 Egan, W., Merz, K., and Baldwin, J. (2000). Prediction of drug absorption using multivariate statistics. *J. Med. Chem.* 43: 3867–3877.

116 Kansy, M., Senner, F., and Gubernator, K. (1998). Physicochemical high throughput screening: parallel artificial membrane permeation assay in the description of passive absorption processes. *J. Med. Chem.* 41: 1007–1010.

117 Molloy, B., Tam, K., Matthew Wood, J., and Dryfe, R. (2008). A hydrodynamic approach to the measurement of the permeability of small molecules across artificial membranes. *Analyst* 133: 655.

118 Avdeef, A., Artursson, P., Neuhoff, S. et al. (2005). Caco-2 permeability of weakly basic drugs predicted with the double-sink PAMPA method. *Eur. J. Pharm. Sci.* 24: 333–349.

119 Van de Waterbeemd, H., Lennernäs, H., and Artursson, P. (eds.) (2003). *Drug Bioavailability: Estimation of Solubility, Permeability, Absorption and Bioavailability*, Methods and Principles in Medicinal Chemistry, vol. 18, 12–69. Weinheim: Wiley-VHC.

120 Avdeef, A., Bendels, S., Di, L. et al. (2007). PAMPA—critical factors for better predictions of absorption. *J. Pharm. Sci.* 96: 2893–2909.

121 Hidalgo, I., Raub, T., and Borchardt, R. (1989). Characterization of the human colon carcinoma cell line (Caco-2) as a model system for intestinal epithelial permeability. *Gastroenterology* 96: 736–749.

122 Hunter, J. and Hirst, B. (1997). Intestinal secretion of drugs. The role of P-glycoprotein and related drug efflux systems in limiting oral drug absorption. *Adv. Drug Delivery Rev.* 25: 129–157.

123 Food and Drug Administration, Center for Drug Evaluation and Research (CDER) (2017). In Vitro Metabolism-and Transporter-Mediated Drug-Drug Interaction Studies, Guidance for Industry, Draft Guidance.

124 Artursson, P. and Karlsson, J. (1991). Correlation between oral drug absorption in humans and apparent drug permeability coefficients in human intestinal epithelial (Caco-2) cells. *Biochem. Biophys. Res. Commun.* 175: 880–885.

125 Lennernäs, H., Palm, K., Fagerholm, U., and Artursson, P. (1996). Comparison between active and passive drug transport in human intestinal

epithelial (Caco-2) cells in vitro and human jejunum in vivo. *Int. J. Pharm.* 127: 103–107.

126 Linnankoski, J., Mäkelä, J., Palmgren, J. et al. (2010). Paracellular porosity and pore size of the human intestinal epithelium in tissue and cell culture models. *J. Pharm. Sci.* 99: 2166–2175.

127 Brimer, C., Dalton, J., Zhu, Z. et al. (2000). Journal search results - cite this for me. *Pharm. Res.* 17: 803–810.

128 Caro, I., Boulenc, X., Rousset, M. et al. (1995). Characterisation of a newly isolated Caco-2 clone (TC-7), as a model of transport processes and biotransformation of drugs. *Int. J. Pharm.* 116: 147–158.

129 Wikman, A., Karlsson, J., Carlstedt, I., and Artursson, P. (1993). A drug absorption model based on the mucus layer producing human intestinal goblet cell line HT29-H. *Pharm. Res.* 10: 843–852.

130 Wikman-Larhed, A. and Artursson, P. (1995). Co-cultures of human intestinal goblet (HT29-H) and absorptive (Caco-2) cells for studies of drug and peptide absorption. *Eur. J. Pharm. Sci.* 3: 171–183.

131 Hilgendorf, C., Spahn-Langguth, H., Regårdh, C. et al. (2000). Caco-2 versus Caco-2/HT29-MTX co-cultured cell lines: permeabilities via diffusion, inside- and outside-directed carrier-mediated transport. *J. Pharm. Sci.* 89: 63–75.

132 Irvine, J., Takahashi, L., Lockhart, K. et al. (1999). MDCK (Madin-Darby canine kidney) cells: a tool for membrane permeability screening. *J. Pharm. Sci.* 88: 28–33.

133 Luo, Z., Liu, Y., Zhao, B. et al. (2013). Ex vivo and in situ approaches used to study intestinal absorption. *J. Pharmacol. Toxicol. Methods* 68: 208–216.

134 Nunes, R., Silva, C., and Chaves, L. (2016). *Concepts and Models for Drug Permeability Studies*, Woodhead Publishing Series in Biomedicine number 79, Chapter 4.2 (ed. B. Sarmento), 203–236. Elsevier.

135 Ussing, H. and Zerahn, K. (1951). Active transport of sodium as the source of electric current in the short-circuited isolated frog skin. *Acta Physiol. Scand.* 23: 110–127.

136 Grass, G. and Sweetana, S. (1988). In vitro measurement of gastrointestinal tissue permeability using a new diffusion cell. *Pharm. Res.* 5: 372–376.

137 Wilson, T. and Wiseman, G. (1954). The use of sacs of everted small intestine for the study of the transference of substances from the mucosal to the serosal surface. *J. Physiol.* 123: 116–125.

138 Verhoeckx, K. (ed.) (2015). *The Impact of Food Bio-Actives on Gut Health*, 264. Cham, Switzerland: Springer International.

139 Buckley, S., Fischer, S., Fricker, G., and Brandl, M. (2012). In vitro models to evaluate the permeability of poorly soluble drug entities: challenges and perspectives. *Eur. J. Pharm. Sci.* 45: 235–250.

140 Barthe, L., Woodley, J., and Houin, G. (1999). Gastrointestinal absorption of drugs: methods and studies. *Fundam. Clin. Pharmacol.* 13: 154–168.

141 Bunton, D.C. (2015). *Human Based Systems for Translational Research*, RSC Drug Discovery Series number 41, Chapter 2 (ed. R. Coleman), 17–37. London: RSC.

142 Rozehnal, V., Nakai, D., Hoepner, U. et al. (2012). Human small intestinal and colonic tissue mounted in the Ussing chamber as a tool for characterizing the intestinal absorption of drugs. *Eur. J. Pharm. Sci.* 46: 367–373.

143 Nejdfors, P., Ekelund, M., Jeppsson, B., and Westrom, B.R. (2000). Mucosal in vitro permeability in the intestinal tract of the pig, the rat and man: species- and region-related differences. *Scand. J. Gastroenterol.* 35: 501–507.

144 Haslam, I., O'Reilly, D., Sherlock, D. et al. (2011). Pancreatoduodenectomy as a source of human small intestine for Ussing chamber investigations and comparative studies with rat tissue. *Biopharm. Drug Dispos.* 32: 210–221.

145 Annaert, P., Tukker, J., van Gelder, J. et al. (2000). In vitro, ex vivo, and in situ intestinal absorption characteristics of the antiviral Ester prodrug adefovir dipivoxil. *J. Pharm. Sci.* 89: 1054–1062.

146 Abaut, A., Chevanne, F., and Le Corre, P. (2007). Oral bioavailability and intestinal secretion of amitriptyline: role of P-glycoprotein? *Int. J. Pharm.* 330: 121–128.

147 Lennernäs, H. (2014). Human in vivo regional intestinal permeability: importance for pharmaceutical drug development. *Mol. Pharm.* 11: 12–23.

148 Westerhout, J., Steeg, E., Grossouw, D. et al. (2014). A new approach to predict human intestinal absorption using porcine intestinal tissue and biorelevant matrices. *Eur. J. Pharm. Sci.* 63: 167–177.

149 Ungell, A. (1997). In vitro absorption studies and their relevance to absorption from the GI tract. *Drug Dev. Ind. Pharm.* 23: 879–892.

150 Bohets, H., Annaert, P., Mannens, G. et al. (2001). Strategies for absorption screening in drug discovery and development. *Curr. Top. Med. Chem.* 1: 367–383.

151 Alam, M., Al-Jenoobi, F., and Al-mohizea, A. (2011). Everted gut sac model as a tool in pharmaceutical research: limitations and applications. *J. Pharm. Pharmacol.* 64: 326–336.

152 Yang, Y. and Yu, L.X. (2009). *Developing Solid Oral Dosage Forms: Pharmaceutical Theory and Practice. Oral Drug Absorption, Evaluation, and Prediction*, Chapter 12 (eds. Y. Qiu, Y. Chen, G.G.Z. Zhang, et al.), 289–308. San Diego, CA: Academic Press.

153 Hillgren, K., Kato, A., and Borchardt, R. (1995). In vitro systems for studying intestinal drug absorption. *Med. Res. Rev.* 15: 83–109.

154 Leppert, P. and Fix, J. (1994). Use of everted intestinal rings for in vitro examination of oral absorption potential. *J. Pharm. Sci.* 83: 76–981.

155 Fagerholm, U., Johansson, M., and Lennernäs, H. (1996). Comparison between permeability coefficients in rat and human jejunum. *Pharm. Res.* 13: 1336–1342.

156 Salphati, L., Childers, K., Pan, L. et al. (2001). Evaluation of a single-pass intestinal-perfusion method in rat for the prediction of absorption in man. *J. Pharm. Pharmacol.* 53: 1007–1013.

157 Cao, X., Gibbs, S., Fang, L. et al. (2006). Why is it challenging to predict intestinal drug absorption and oral bioavailability in human using rat model. *Pharm. Res.* 23: 1675–1686.

158 Ehrhardt, C. and Kim, K.-J. (2008). *Drug Absorption Studies: In Situ, In Vitro and In Silico Models*, Chapter 2, vol. 7, 59. New York: Springer.

159 Doluisio, J., Billups, N., Dittert, L. et al. (1969). Drug absorption I: an in situ rat gut technique yielding realistic absorption rates. *J. Pharm. Sci.* 58: 1196–1200.

160 Ruiz-Balaguer, N., Nacher, A., Casabo, V.G., and Sanjuan, M. (2002). Intestinal transport of cefuroxime axetil in rats: absorption and hydrolysis processes. *Int. J. Pharm.* 234: 101–111.

161 Ho, N. and Higuchi, W. (1974). Theoretical model studies of intestinal drug absorption IV: bile acid transport at premicellar concentrations across diffusion layer-membrane barrier. *J. Pharm. Sci.* 63: 686–690.

162 Schurgers, N., Bijdendijk, J., Tukker, J., and Crommelin, D. (1986). Comparison of four experimental techniques for studying drug absorption kinetics in the anesthetized rat in situ. *J. Pharm. Sci.* 75: 117–119.

163 Windmueller, H.G. and Spaeth, A.E. (1981). Vascular autoperfusion of rat small intestine in situ. *Methods Enzymol.* 77: 120–129.

164 Miyazaki, K., Sunada, K., Iseki, K., and Arita, T. (1986). Simultaneous vascular and luminal perfusion of rat small intestine. *Chem. Pharm. Bull.* 34: 3830–3835.

165 Pang, K.S., Cherry, W.F., and Ulm, E.H. (1985). Disposition of enalapril in the perfused rat intestine-liver preparation: absorption, metabolism and first-pass effect. *J. Pharmacol. Exp. Ther.* 233: 788–795.

166 Clarke, E.W. and Smyth, D.H. (1950). Technique for perfusion of the Thiry-Vella loop in dogs. *J. Physiol. (London)* 112: 45P–46P.

167 Lennernäs, H., Ahrenstedt, Ö., Hällgren, R. et al. (1992). Regional Jejunal perfusion, a new in vivo approach to study oral drug absorption in man. *Pharm. Res.* 9: 1243–1251.

168 Lennernäs, H. (1998). Human intestinal permeability. *J. Pharm. Sci.* 87: 403–410.

169 Agoram, B., Woltosz, W., and Bolger, M. (2001). Predicting the impact of physiological and biochemical processes on oral drug absorption. *Adv. Drug Delivery Rev.* 50: S41–S67.

170 Mathias, N.R. and Crison, J.C. (2012). The use of modelling tools to drive efficient oral product design. *AAPS J.* 14: 591–600.

171 Kesisoglou, F. and Mitra, A. (2015). Application of absorption modelling in rational design of drug product under quality-by-design paradigm. *AAPS J.* 17: 1224–1236.

172 Kesisoglou, F., Chung, J., van Asperen, J., and Heimbach, T. (2016). Physiological based absorption modelling to impact biopharmaceutics and formulation strategies in drug development – industry case studies. *J. Pharm. Sci.* 105 (9): P2723–P2734.

173 Brown, J., Chien, C., Timmins, P. et al. (2013). Compartmental absorption modeling and site of absorption studies to determine feasibility of an extended-release formulation of an HIV-1 attachment inhibitor phosphate ester prodrug. *J. Pharm. Sci.* 102 (6): 1742–1751.

174 Kararli, T.T. (1995). Comparison of the gastrointestinal anatomy, physiology and biochemistry of humans and commonly used laboratory animals. *Biopharm. Drug Dispos.* 16: 351–380.

175 Ikegami, K., Tagawa, K., Narisawa, S., and Osawa, T. (2003). Suitability of the cynomolgus monkey as an animal model for drug absorption studies of oral dosage forms from the viewpoint of gastrointestinal physiology. *Biol. Pharm. Bull.* 26: 1442–1447.

176 Lennernas, H. and Regardh, C.-G. (1993). Regional gastrointestinal absorption of the beta-blocker pafenolol in the rat and intestinal transit rate determined by movement of ^{14}C-polyethylene glycol (PEG) 4000. *Pharm. Res.* 10: 130–135.

177 Chiou, W.L. and Barve, A. (1998). Linear correlation of the fraction of oral dose absorbed of 64 drugs between humans and rats. *Pharm. Res.* 15: 1792–1795.

178 Grass, G.M. and Sinko, P.J. (2002). Physiologically-based pharmacokinetic simulation modelling. *Adv. Drug Delivery Rev.* 54: 433–451.

179 Musther, H., Olivares-Morales, A., Hatley, O.J.D. et al. (2014). Animal versus human oral drug bioavailability: do they correlate? *Eur. J. Pharm. Sci.* 57: 280–291.

180 Reddy, M., Connor, A., Brennan, B.J. et al. (2011). Physiological modelling and assessment of regional drug bioavailability of danoprevir to determine whether a controlled released formulation is feasible. *Biopharm. Drug Depos.* 32: 261–275.

181 Takahashi, M., Washio, T., Suzuki, N. et al. (2009). The species differences of intestinal drug absorption and first-pass metabolism between cynomolgus monkeys and humans. *J. Pharm. Sci.* 98: 4343–4353.

182 Takahashi, M., Washio, T., Suzuki, N. et al. (2010). Investigation of the intestinal permeability and first-pass metabolism of drugs in cynomolgus monkeys using single-pass intestinal perfusion. *Biol. Pharm. Bull.* 33: 111–116.

183 Sutton, S.C. (2009). The use of gastrointestinal intubation studies for controlled release development. *Br. J. Clin. Pharmacol.* 68: 342–354.

184 Wilding, I., Hirst, P., and Connor, A. (2000). Development of an engineering based capsule for human drug absorption studies. *Pharm. Sci. Technol. Today* 3: 385–392.

185 Wilding, I. and Prior, D.V. (2003). Remote controlled release capsules in human drug absorption (HDA) studies. *Crit. Rev. Ther. Drug Carrier Syst.* 20: 405–431.

186 McGirr, M.E.A., McAllister, S.M., Peters, E.E. et al. (2009). The use of the InteliSite® companion device to deliver mucoadhesive polymers to the dog colon. *Eur. J. Pharm. Sci.* 36: 386–391.

187 Becker, D., Zhang, J., Heimbach, T. et al. (2014). Novel orally swallowable IntelliCap® device to quantify regional drug absorption in human GI tract using diltiazem as model drug. *AAPS PharmSciTech* 15: 1490–1497.

188 Connor, A.L. (2012). Location, location, location: gastrointestinal delivery site and its impact on absorption. *Ther. Delivery* 3: 575–578.

189 Teng, R. and Maya, J. (2014). Absolute bioavailability and regional absorption of ticagrelor in healthy volunteers. *J. Drug Assess.* 3: 43–50.

190 Connor, A.L., Evans, P., Doto, J. et al. (2009). An oral human drug absorption study to assess the impact of site of delivery on the bioavailability of bervirimat. *J. Clin. Pharmacol.* 49: 606–612.

191 Hinderling, P.H., Karara, A.H., Tao, B. et al. (2007). Systemic availability of the active metabolite hydroxyl-fasudil after administration of fasudil to different sites of the human gastrointestinal tract. *J. Clin. Pharmacol.* 47: 19–25.

192 Limb, M.C., Starling, R.D., Connor, A.L. et al. (2009). Absorption of ATHX-105 phosphate from the human gastrointestinal tract. *AAPS Annual Meeting and Exposition*, Los Angeles, CA, USA. Poster Presentation.

193 Zhu, T., Ansquer, J.-C., Kelly, M.T. et al. (2010). Comparison of the gastrointestinal absorption and bioavailability of fenofibrate and fenofibric acid in humans. *J. Clin. Pharmacol.* 50: 914–921.

194 Casey, D.L., Beihn, R.M., Digenis, O.A., and Shambhu, M.B. (1976). Method for monitoring hard gelatin capsule disintegration times in humans using external scintigraphy. *J. Pharm. Sci.* 65: 1412–1413.

195 Connor, A.L., Wray, H., Cottrell, J., and Wilding, I.R. (2001). A scintigraphic study to investigate the potential for altered gut distribution of loperamide from a loperamide-simethicone formulation in man. *Eur. J. Pharm. Sci.* 13: 369–374.

196 Cole, E., Scott, R., Connor, A.L. et al. (2002). Enteric coated HPMC capsules designed to achieve intestinal targeting. *Int. J. Pharm.* 231: 83–95.

197 Katsuma, M., Watanabe, S., Takemura, S. et al. (2004). Scintigraphic evaluation of novel colon-targeted delivery system (CODES™) in healthy volunteers. *J. Pharm. Sci.* 93: 1287–1299.

198 Hodges, L.A., Connolly, S.M., Band, J. et al. (2009). Scintigraphic evaluation of colon targeting pectin-HPMC tablets in healthy volunteers. *Int. J. Pharm.* 370: 144–150.

199 McDermott, J., Scholes, P.D., and Connor, A.L. (2008). Radiolabelling technologies for evaluation of oral pharmaceutical dosage forms. *AAPS Annual Meeting and Exposition*, Atlanta, GE. Poster Presentation.

200 Hilton, J. (2008). Delivering drugs to the colon using COLAL®: a modified release delivery system. *Eur. J. Pharm. Sci.* 13: 43–49.

201 Nicholson, S.J., Timmins, P., Dockens, R.C. et al. (2012). Development of oral extended release formulations of 6-hydroxybuspirone. *Biopharm. Drug Dispos.* 33: 522–535.

202 Weitschies, W., Wedemeyer, J., Stehr, R., and Trahms, L. (1994). Magnetic markers as a noninvasive tool to monitor gastrointestinal transit. *IEEE Trans. Biomed. Eng.* 41: 192–195.

203 Weitschies, W. and Wilson, C.G. (2011). In vivo imaging of drug delivery systems in the gastrointestinal tract. *Int. J. Pharm.* 417: 216–226.

204 Hoad, C.L., Marciani, L., Foley, S. et al. (2007). Non-invasive quantification of small bowel water content by MRI: a validation study. *Phys. Med. Biol.* 52: 6909–6922.

205 Mudie, D.M., Murray, K., Hoad, C.L. et al. (2014). Quantification of gastrointestinal liquid volumes and distribution following a 240 mL dose of water in the fasted state. *Mol. Pharm.* 11: 3039–3047.

206 Junghanns, J.A.H. and Muller, R.H. (2008). Nanocrystal technology, drug delivery and clinical applications. *Int. J. Nanomed.* 3: 295–310.

207 Tang, J., Sun, J., and He, Z.G. (2007). Self-emulsifying drug delivery systems: strategy for improving oral delivery of poorly soluble drugs. *Curr. Drug Ther.* 2: 85–93.

208 Noyes, A.A. and Whitney, W.R. (1897). The rate of solution of solid substances in their own solutions. *J. Am. Chem. Soc.* 19: 930–934.

209 Muller, R.H. and Peters, K. (1998). Nanosuspensions for the formulation of poorly soluble drugs I. Preparation by a size-reduction technique. *Int. J. Pharm.* 160: 229–237.

210 Tadros, T. (2013). Ostwarld ripening. In: *Encyclopedia of Colloid and Interface Sciences* (ed. T. Tadros), 820. Berlin, Heidelberg: Springer-Verlag. ISBN: 978-3-642-20664.

211 Midoux, N., Hosek, P., Pailleres, L., and Authelin, J.R. (1999). Micronization of pharmaceutical substances in a spiral jet mill. *Powder Technol.* 104: 113–120.

212 Jain, R.A., Brito, L., Straub, J.A. et al. (2008). Effect of powder processing on performance of fenofibrate formulations. *Eur. J. Pharm. Biopharm.* 69: 727–734.

213 Vogt, M., Kunath, K., and Dressman, J.B. (2008). Dissolution improvement of four poorly water soluble drugs by cogrinding with commonly used excipients. *Eur. J. Pharm. Biopharm.* 68: 330–337.

214 Merisko-Liversidge, E., Liversidge, G.G., and Cooper, E.R. (2003). Nanosizing: a formulation approach for poorly-water-soluble compounds. *Eur. J. Pharm. Sci.* 18: 113–120.

215 Merisko-Liversidge, E. and Liversidge, G.G. (2011). Nanosizing for oral and parenteral drug delivery: a perspective on formulating poorly-water soluble compounds using wet media milling technology. *Adv. Drug Delivery Rev.* 63: 427–440.

216 Peltonen, L. and Hirvonen, J. (2010). Pharmaceutical nanocrystals by nanomilling: critical process parameters, particle fracturing and stabilization methods. *J. Pharm. Pharmacol.* 62: 1569–1579.

217 Jahnke, S. (1998). The theory of high-pressure homogenization. In: *Emulsions and Nanosuspensions for the Formulation of Poorly Soluble Drugs* (eds. R.H. Muller, S. Benita and B. Bohm), 177–200. Stuttgart: Medpharm Scientific.

218 Gao, L., Zhang, D., and Chen, M. (2008). Drug nanocrystals for the formulation of poorly soluble drugs and its application as a potential drug delivery system. *J. Nanopart. Res.* 10: 854–862.

219 Sinha, B., Muller, R.H., and Moschwitzer, J.P. (2013). Bottom-up approaches for preparing drug nanocrystals: formulations and factors affecting particle size. *Int. J. Pharm.* 453: 126–141.

220 List, M. and Sucker, H. (1988). Pharmaceutical colloidal hydrosols for injection. GB Patent 2200048.

221 Moschwitzer, J. and Müller, R.H. (2006). New method for the effective production of ultrafine drug nanocrystals. *J. Nanosci. Nanotechnol.* 6: 3145–3153.

222 Strickley, R.G. (2004). Solubilizing excipients in oral and injectable formulations. *Pharm. Res.* 21: 201–230.

223 Li, P., Tabibi, S.E., and Yalkowsky, S.H. (1999). Solubilization of flavopiridol by pH control combined with cosolvents, surfactants, or complexants. *J. Pharm. Sci.* 88: 945–947.

224 Loftsson, T., Brewster, M.E., and Masson, M. (2004). Role of cyclodextrins in improving oral drug delivery. *Am. J. Drug Delivery* 2: 1–15.

225 Loftsson, T. and Duchene, D. (2007). Cyclodextrins and their pharmaceutical applications. *Int. J. Pharm.* 329: 1–11.

226 Salústio, P.J., Pontes, P., Conduto, C. et al. (2011). Advanced technologies for oral controlled release: cyclodextrins for oral controlled release. *AAPS PharmSciTech* 12: 1276–1292.

227 Challa, R., Ahuja, A., Ali, J., and Khar, R.K. (2005). Cyclodextrins in drug delivery: an updated review. *AAPS PharmSciTech* 6: E329–E357.

228 Loftsson, T. and Fridriksdóttir, H. (1998). The effect of water soluble polymers on the aqueous solubility and complexing abilities of β-cyclodextrin. *Int. J. Pharm.* 163: 115–121.

229 Chiou, W.L. and Reigelman, S. (1971). Pharmaceutical applications of solid dispersion systems. *J. Pharm. Sci.* 60: 1281–1302.

230 Newman, A., Knipp, G., and Zografi, G. (2012). Assessing the performance of amorphous solid dispersions. *J. Pharm. Sci.* 101: 1355–1377.

231 Vasconcelos, T., Sarmento, B., and Costa, P. (2007). Solid dispersions as strategy to improve oral bioavailability of poor water soluble drugs. *Drug Discovery Today* 12: 1068–1075.

232 Hancock, B.C. and Zografi, G. (1997). Characteristics and significance of the amorphous state in pharmaceutical systems. *J. Pharm. Sci.* 86: 1–12.

233 Sekigushi, K. and Obi, N. (1961). Studies on absorption of eutectic mixtures. I. A comparison of the behavior of eutectic mixture of sulfathiazole and that of ordinary sulfathiazole in man. *Chem. Pharm. Bull.* 9: 866–872.

234 Broman, E., Khoo, C., and Taylor, L.S. (2001). A comparison of alternative polymer excipients and processing methods for making solid dispersions of a poorly water soluble drug. *Int. J. Pharm.* 222: 139–151.

235 Repka, M.A., Majumdar, S., Battu, S.K. et al. (2008). Applications of hot-melt extrusion for drug delivery. *Expert Opin. Drug Delivery* 5: 1357–1376.

236 Yasujia, T., Takeuchib, H., and Kawashimac, Y. (2008). Particle design of poorly water-soluble drug substances using supercritical fluid technologies. *Adv. Drug Delivery Rev.* 60: 388–398.

237 Betageri, G.V. and Makarla, K.R. (1995). Enhancement of dissolution of glyburide by solid dispersion and lyophilization techniques. *Int. J. Pharm.* 126: 155–160.

238 Friesen, D.T., Shanker, R., Crew, M. et al. (2008). Hydroxypropyl methylcellulose acetate succinate-based spray-dried dispersions: an overview. *Mol. Pharm.* 5: 1003–1019.

239 Paudel, A., Worku, Z.A., Meeus, J. et al. (2013). Manufacturing of solid dispersions of poorly water soluble drugs by spray drying: formulation and process considerations. *Int. J. Pharm.* 453: 253–284.

240 Shah, N., Sandh, H., Puapradit, W. et al. (2012). Development of novel microprecipitated bulk powder (MBP) technology for manufacturing stable amorphous formulations of poorly soluble drugs. *Int. J. Pharm.* 438: 53–60.

241 Kulthe, V.V. and Chaudhari, P.D. (2013). Drug resinates as an attractive approach of solubility enhancement of atorvastatin calcium. *Indian J. Pharm. Sci.* 75: 523–532.

242 Pouton, C.W. (2000). Lipid formulations for oral administration of drugs: non-emulsifying, self-emulsifying and 'self microemulsifying' drug delivery systems. *Eur. J. Pharm. Sci.* 11 (Suppl. 2): S93–S98.

243 Pouton, C.W. (2006). Formulation of poorly water-soluble drugs for oral administration: physicochemical and physiological issues and the lipid formulation classification system. *Eur. J. Pharm. Sci.* 29: 278–287.

244 Porter, C.J.H., Wasan, K.M., and Constantinides, P. (2008). Lipid-based systems for the enhanced delivery of poorly water soluble drugs. *Adv. Drug Delivery Rev.* 60: 615–616.

245 Aldwell, F.E., Keen, D.L., Parlane, N.A. et al. (2003). Oral vaccination with Mycobacterium bovis BCG in a lipid formulation induces resistance to pulmonary tuberculosis in brushtail possums. *Vaccine* 22: 70–76.

246 Warren, D.B., Benameur, H., Porter, C.J.H., and Pouton, C.W. (2010). Using polymeric precipitation inhibitors to improve the absorption of poorly water-soluble drugs: a mechanistic basis for utility. *J. Drug Targeting* 18: 704–731.

247 Bunjes, H. (2010). Lipid nanoparticles for the delivery of poorly water-soluble drugs. *J. Pharm. Pharmacol.* 62: 1637–1645.

248 Das, S. and Chaudhury, A. (2011). Recent advances in lipid nanoparticle formulations with solid matrix for oral drug delivery. *AAPS PharmSciTech* 12: 62–76.

249 Sahbaz, Y., Williams, H.D., Nguyen, T.-H. et al. (2015). Transformation of poorly water-soluble drugs into lipophilic ionic liquids enhances oral drug exposure from lipid based formulations. *Mol. Pharm.* 12: 1980–1991.

250 Gumaste, S.G., Pawlak, S.A., Dalrymple, D.M. et al. (2013). Development of solid SEDDS, IV: effect of adsorbed lipid and surfactant on tableting properties and surface structures of different silicates. *Pharm. Res.* 30: 3170–3185.

251 Jain, A.K., Thanki, K., and Jain, S. (2014). Solidified self-nanoemulsifying formulation for oral delivery of combinatorial therapeutic regimen: Part I. Formulation development, statistical optimization, and in vitro characterization. *Pharm. Res.* 31: 923–945.

252 Aungst, B.J. (2012). Absorption enhancers: applications and advances. *AAPS J.* 14: 10–18.

253 Lindmark, T., Kimura, Y., and Artursson, P. (1998). Absorption enhancement through intracellular regulation of tight junction permeability by medium chain fatty acids in Caco-2 cells. *J. Pharmacol. Exp. Ther.* 284: 262–369.

254 Leonard, T.W., Lynchb, J., McKennac, M.J., and Brayden, D.J. (2006). Promoting absorption of drugs in humans using medium-chain fatty acid-based solid dosage forms: GIPET™. *Expert Opin. Drug Delivery* 3: 685–692.

255 Ranaldi, G., Marigliano, I., Vespignani, I. et al. (2002). The effect of chitosan and other polycations on tight junction permeability in the human intestinal Caco-2 cell line. *J. Nutr. Biochem.* 13: 157–167.

256 Deli, M.A. (2009). Potential use of tight junction modulators to reversibly open membranous barriers and improve drug delivery. *Biochim. Biophys. Acta* 1788: 892–910.

257 Alani, A.W.G. and Robinson, J.R. (2008). Mechanistic understanding of oral drug absorption enhancement of cromolyn sodium by an amino acid derivative. *Pharm. Res.* 25: 48–54.

258 Karsdal, M.A., Byrjalsen, I., Henriksen, K. et al. (2008). The effect of oral salmon calcitonin delivered with 5-CNAC on bone and cartilage degradation in osteoarthritic patients: a 14 day randomized study. *Osteoarthr. Cartil.* 18: 150–159.

259 Castelli, M.C., Wong, D.F., Friedman, K., and Riley, G.M.I. (2011). Pharmacokinetics of oral cyanocobalamin formulated with sodium N-[8-(2-hydroxybenzoyl)amino] caprylate (SNAC): an open-label, randomized, single-dose, parallel-group study in healthy male subjects. *Clin. Ther.* 33: 934–945.

260 Welling, S.H., Hubálek, F., Jacobsen, J. et al. (2014). The role of citric acid in oral peptide and protein formulations: relationship between calcium chelation and proteolysis inhibition. *Eur. J. Pharm. Biopharm.* 86: 544–551.

261 Binkley, N., Bolognese, M., Sidorowicz-Bialynicka, A. et al. (2012). A phase 3 trial of the efficacy and safety of oral recombinant calcitonin: the oral calcitonin in postmenopausal osteoporosis (ORACAL) trial. *J. Bone Miner. Res.* 27: 1821–1829.

262 Song, I.S., Choi, M.K., Shim, W.S., and Shim, C.K. (2013). Transport of organic cationic drugs: effect of ion-pair formation with bile salts on the biliary excretion and pharmacokinetics. *Pharmacol. Ther.* 138: 142–154.

263 Samiei, N., Mangas-Sanjuan, V., González-Álvarez, I. et al. (2013). Ion-pair strategy for enabling amifostine oral absorption: rat in situ and in vivo experiments. *Eur. J. Pharm. Sci.* 49: 499–504.

264 Miller, J.M., Dahan, A., Gupta, D. et al. (2010). Enabling the intestinal absorption of highly polar anti-viral agents: ion-pair facilitated membrane permeation of zanamivir heptyl ester and guanidino oseltamivir. *Mol. Pharm.* 7: 1223–1234.

265 Cornaire, G., Woodley, J., Hermann, P. et al. (2004). Impact of excipients on the absorption of P-glycoprotein substrates in vitro and in vivo. *Int. J. Pharm.* 278: 119–131.

266 Varma, M.V.S., Perumal, O.P., and Panchagnula, R. (2006). Functional role of P-glycoprotein in limiting peroral drug absorption: optimizing drug delivery. *Curr. Opin. Chem. Biol.* 10: 367–373.

267 Varma, M.V.S., Ashokraj, Y., Dey, C.S., and Panchagnula, R. (2003). P-glycoprotein inhibitors and their screening: a perspective from bioavailability enhancement. *Pharmacol. Res.* 48: 347–359.

268 Woo, J.S., Lee, C.H., Shim, C.K., and Hwang, S.J. (2003). Enhanced oral bioavailability of paclitaxel by coadministration of the P-glycoprotein inhibitor KR30031. *Pharmacol. Res.* 20: 24–30.

269 Constantinides, P.P. and Wasan, K.M. (2007). Lipid formulation strategies for enhancing intestinal transport and absorption of P-glycoprotein (P-gp) substrate drugs: in vitro/in vivo case studies. *J. Pharm. Sci.* 96: 235–248.

270 Werle, M. (2008). Natural and synthetic polymers as inhibiotrs of drug efflux pumps. *Pharm. Res.* 25: 500–511.

271 Johnson, B.M., Charman, W.N., and Porter, C.J.H. (2002). An in vitro examination of the impact of polyethylene glycol 400, pluronic P85, and vitamin E D-α-tocopheryl polyethylene glycol 1000 succinate on P-glycoprotein efflux and enterocyte-based metabolism in excised rat intestine. *AAPS Pharm. Sci.* 4: 193–205.

272 Li, M., Si, L., Pan, H. et al. (2011). Excipients enhance intestinal absorption of ganciclovir by P-gp inhibition: assessed in vitro by everted gut sac and in situ by improved intestinal perfusion. *Int. J. Pharm.* 403: 37–45.

273 Lo, Y.L. (2003). Relationships between the hydrophilic-lipophilic balance values of pharmaceutical excipients and their multidrug resistance modulating effect in Caco-2 cells and rat intestines. *J. Controlled Release* 90: 37–48.

274 Foger, F., Hoyer, H., Kafedjiiski, K. et al. (2006). In vivo comparison of various polymeric and low molecular mass inhibitors of intestinal P-glycoprotein. *Biomaterials* 27: 5855–5860.

275 Nassara, T., Roma, A., Nyskab, A., and Benita, S. (2009). Novel double coated nanocapsules for intestinal delivery and enhanced oral bioavailability of tacrolimus, a P-gp substrate drug. *J. Controlled Release* 133: 77–84.

276 Moes, A. (1993). Gastroretentive dosage form. *Crit. Rev. Ther. Drug Carrier Syst.* 10: 143–195.

277 Hwang, S.J., Park, H., and Park, K. (1998). Gastric retentive drug delivery systems. *Crit. Rev. Ther. Drug Carrier Syst.* 15: 243–284.

278 Hou, S.Y., Cowles, V.E., and Berner, B. (2003). Gastric retentive dosage forms: a review. *Crit. Rev. Ther. Drug Carrier Syst.* 20: 461–498.

279 Sheth, P.J. and Tossounian, J.L. (1978). Sustained release pharmaceutical capsules. US Patent 4,126,672.

280 Sheth, P.J. and Tossounian, J.L. (1979) Sustained release tablet formulations. US Patent 4,140,755.

281 Michaels, A.S., Bashaw, J.D., and Zaffaroni, A.. (1975). Gastro-inflatable drug delivery device. US Patent 3,901,232.

282 Banker, G.S. (1975). Sustained release film-coated preparations. US Patent 3,896,792.

283 Rouge, N., Buri, P., and Doelker, E. (1996). Drug absorption sites in the gastrointestinal tract and dosage forms for site-specific delivery. *Int. J. Pharm.* 136: 115–122.

284 Kim, J.S., Oberle, R.L., Krummel, D.A. et al. (1994). Absorption of ACE inhibitors from small intestine and colon. *J. Pharm. Sci.* 83: 1350–1356.

285 Dressman, J.B., Amidon, G.I., and Fleischer, D. (1985). Absorption potential: estimating the fraction absorbed for orally administered compounds. *J. Pharam. Sci.* 74: 588–589.

286 Hejazi, R. and Amiji, M. (2003). Stomach-specific anti-*H. pylori* therapy II: gastric residence studies of tetracycline-loaded chitosan microspheres in gerbils. *Pharm. Dev. Technol.* 8: 253–262.

287 Baumgartner, S., Tivadar, A., Vrecer, V., and Kristl, J. (2001). Development of floating tablets as a new approach to the treatment of *Heliobacter pylori* infections. *Acta Pharm.* 51: 21–33.

288 Curatolo, W.J. and Lo, J. (1991). Gastric retention system for controlled drug release. US Patent 5,002,772.

289 Curatolo, W.J. and Lo, J. (1995). Gastric retention system for controlled drug release. US Patent 5,443,843.

290 Caldwell, L.J., Gardner, C.R., and Cargill, R.C. (1988). Drug delivery device which can be retained in the stomach for a controlled period of time. US Patent 4,767,627.

291 Cargill, R.C., Caldwell, R.J., Engle, K. et al. (1989). Controlled gastric emptying 1: effects of physical properties on the residence times of non-disintegrating geometric shapes in beagle dogs. *Pharm. Res.* 5: 533–536.

292 Cargill, R.C., Engle, K., Gardner, C.R. et al. (1989). Controlled gastric emptying 2: in viro erosion and gastric residence time erodible device in beagle dogs. *Pharm. Res.* 6: 506–509.

293 Gordi, T., Hou, E., Kasichayanula, S., and Berner, B. (2008). Pharmacokinetics of gabapentin after a single day and at steady state following the administration of gastric retentive-extended-release and immediate-release tablets; a randomized, open label, multiple dose, three-way crossover exploratory study in healthy subjects. *Clin. Ther.* 30: 909–916.

294 Meyer, J.H., Dressman, J., Fink, A., and Amidon, G. (1985). Effect of size and density on canine gastric emptying of non-digestible solids. *Gastroenterology* 89: 805–813.

295 Chawla, G., Gupta, P., Koradia, V., and Bansal, A.K. (2003). Gastroretention; a means to address regional variability in intestinal drug absorption. *Pharm. Technol.* 27: 50–68.

296 Shell, J.W., Louie-Helm, J., and Markey, M. (2002). Extending the duration of drug release within the stomach during the fed mode. US Patent 6,340,475.

297 Timmermans, J. and Moes, A.J. (1994). Factors controlling the buoyancy and gastric retention capabilities of floating capsules: new data for reconsidering the controversy. *J. Pharm. Sci.* 83: 18–24.

298 Shashank, C., Prabha, K., Sunil, S., and Kumar, A.V. (2013). Approaches to increase the gastric residence time: floating drug delivery systems – a review. *Asian J. Pharm. Clin. Res.* 6: 1–9.

299 Timmermans, J. and Moes, A.J. (1993). Cutoff size for gastric emptying of dosage forms. *J. Pharm. Sci.* 82: 854.

300 Davis, S.S., Hardy, J.G., Taylor, M.J. et al. (1984). The in vivo evaluation fo an osmotic device (Osmet) using gamma scintigraphy. *J. Pharm. Pharmacol.* 36: 740–742.

301 Feeley, L.C. and Davis, S.S. (1989). Correlation of phenylpropanolamine bioavailability with gastrointestinal transit by scintigraphic monitoring of ^{111}In-labeled hydroxypropylmethylcellulose matrices. *Pharm. Res.* 6: 274–278.

302 Davis, S.S., Norring-Chrestensen, F., Khosla, R., and Feeley, L.C. (1988). Gastric emptying of large single unit dosage forms. *J. Pharm. Pharmacol.* 40 (3): 205–207.

303 Gusler, G., Berner, B., Chau, M., and Padua, A. (2004). Optimal polymer mixtures for gastric retentive tablets. US Patent 6,723,340.

304 Gusler, G., Hou, S.Y.E., Connor, A.L. et al. (2003). Pharmacoscintigraphic evaluation of metformin ER in healthy volunteers. *Pharm. Sci.* 5: S1.

305 Gusler, G., Gorsline, J., Levy, G. et al. (2001). Pharmacokinetics of metformin gastric retentive tablets in healthy volunteers. *J. Clin. Pharmacol.* 41: 655–661.

306 Timmins, P., Dennis, A.B., and Vyas, K.A. (2002). Biphasic controlled delivery systems for high solubility pharmaceuticals and method. US Patent 6,475,521.

307 Timmins, P., Dennis, A.B., and Vyas, K.A. (2003). Method of use for a biphasic controlled delivery system for high solubility pharmaceuticals. US Patent 6,660,300.

308 Shell, J.W., Louie-Helm, J., and Markey, M. (2003). Extending the duration of drug release within the stomach during the fed mode. US Patent 6,635,280.

309 Berner, B., Louie-Helm, J., and Shell, J.W. (2011). Gastric retentive oral dosage form with restricted drug release to the lower gastrointestinal tract. US Patent 7,976,870.

310 Stewart, B.H., Kugler, A.R., Thompson, P.R., and Bockbrader, H.N. (1993). A saturable transport mechanism in the intestinal absorption of gabapentin is the underlying cause of the lack of proportionality between increasing dose and drug levels in plasma. *Pharm. Res.* 10: 276–281.

311 Scheen, A.J. (1996). Clinical pharmacokinetics of metformin. *Clin. Pharm.* 30: 359–371.

312 Schwartz, S., Wu, J., and Berner, B. (2006). Extended-release metformin for the treatment of diabetes mellitus. *Expert Opin. Pharmacother.* 7: 803–809.
313 Dunn, C.J. and Peters, D.H. (1995). Metformin. A review of its pharmacological properties and therapeutic uses in non-insulin dependent diabetes mellitus. *Drugs* 49: 721–749.
314 Frisbee, S. (2012). Controlled release dosage forms. US Patent 8,323,692.
315 Cheng, X.X., Steve, J., Chou, J., and Chen, C.M. (2013) Controlled release metformin formulations. US Patent 8,475,841.
316 Chen, C., Han, C.H., Sweeney, M., and Cowles, V.E. (2013). Pharmacokinetics, efficacy, and tolerability of a once-daily gastroretentive dosage form of gabapentin for the treatment of postherpetic neuralgia. *J. Pharm. Sci.* 102: 155–1164.
317 Berner, B. and Cowles, V.E. (2006). Case studies in swelling gastric retentive polymeric tablets. *Expert Opin. Drug Delivery* 3: 541–548.
318 Brater, D.C. (1991). Clinical pharmacology of loop diuretics. *Drugs* 41: 14–22.
319 Blondeau, J.M. (2004). Current management in the treatment of urinary tract infections: extended-release ciprofloxacin as a novel treatment option. *Drugs* 64: 611–628.
320 Davis, R., Markham, A., and Balfour, J.A. (1996). Ciprofloxacin: an updated review of its pharmacology, therapeutic efficacy, and tolerability. *Drugs* 51: 1019–1074.
321 Harder, S., Fuhr, U., Beerman, D., and Staib, A.H. (1990). Ciprofloxacin absorption in different regions of the human gastrointestinal tract. Investigations with the hf-capsule. *Br. J. Clin. Pharmacol.* 30: 35–39.
322 Aminimanizani, A., Beringer, P., and Jelliffe, R. (2001). Comparative pharmacokinetics and pharmacodynamics of the newer fluoroquinolone antibacterials. *Clin. Pharm.* 40: 169–187.
323 Turnidge, J. (1999). Pharmacokinetics and pharmacodynamics of fluoroquinolones. *Drugs* 58: 29–36.
324 Fourcroy, J.L., Berner, B., Chiang, Y.K. et al. (2005). Efficacy and safety of a novel once daily extended-release ciprofloxacin tablet formulation for treatment of uncomplicated urinary tract infections in women. *Antimicrob. Agents Chemother.* 49: 4137–4143.
325 Devereux, J.E., Newton, J.M., and Short, M.B. (1990). The influence of density on the gastrointestinal transit of pellets. *J. Pharm. Pharmacol.* 42: 500–501.
326 Clarke, G.M., Newton, J.M., and Short, M.B. (1995). Comparative gastrointestinal transit of pellet systems of varying density. *Int. J. Pharm.* 114: 1–11.
327 Bhusnure, O., Marde, A.G., and Chandrakant, A.S. (2015). Floating drug delivery system a novel approach for gastro retentive delivery. *World J. Pharm. Pharm. Sci.* 4: 1114–1143.

328 Muller-Lissner, S.A. and Blum, A.L. (1981). The effect of specific gravity and eating on gastric emptying of slow-release capsules. *N. Engl. J. Med.* 304: 1365–1366.

329 Franz, M.R. and Oth, M.P. (1993). Sustained release, bilayer buoyant dosage form. US Patent 5,232,704.

330 Sheth, P.R. and Tossounian, J. (1984). The hydrodynamically balanced system (HBSTM): a novel drug delivery system for oral use. *Drug Dev. Ind. Pharm.* 10: 319–339.

331 Talwar, N., Sen, H., and Staniforth, J.N. (2001). Orally administered controlled drug delivery system providing temporal and spatial control. US Patent 6,262,601.

332 Dudhara, K.M., Dharmadhikari, N.B., and Dhavse, V.V. (2010). Gastric retention controlled drug delivery system. US Patent 7,776,345.

333 Whitehead, L., Fell, J.T., Collett, J.H. et al. (1998). Floating dosage forms: in vivo study demonstrating prolonged gastric retention. *J. Controlled Release* 55: 3–12.

334 Fell, J.T., Whitehead, L., and Collett, J.H. (2000). Prolonged gastric retention: using floating dosage forms. *Pharm. Technol.* 24: 82–89.

335 Whitehead, L., Collett, J.H., and Fell, J.T. (2000). Amoxycillin release from a floating dosage form based on alginates. *Int. J. Pharm.* 210: 45–49.

336 Jimenez-Castellanos, M.R., Hussein, Z., and Rhodes, C.T. (1993). Mucoadhesive delivery systems. *Drug Dev. Ind. Pharm.* 19: 143–194.

337 Park, H. and Robinson, J.R. (1987). Mechanisms of mucoadhesion to poly(acrylic acid) hydrogels. *Pharm. Res.* 4: 457–464.

338 Park, H. (1986). On the mechanism of bioadhesion. PhD dissertation. The University of Wisconsin-Madison.

339 Riley, R.G., Smart, J.D., Tsibouklis, J. et al. (2002). An in vitro model for investigating the gastric mucosal retention of ^{14}C-poly(acrylic acid) dispersions. *Int. J. Pharm.* 236: 87–96.

340 Cuna, M., Alonso, M.J., and Torres, D. (2001). Preparation and in vivo evaluation of mucoadhesive microparticles containing amoxicillin-resin complexes for drug delivery to the gastric mucosa. *Eur. J. Pharm. Biopharm.* 51: 199–205.

341 Deacon, M.P., McGurk, S., Roberts, C.J. et al. (2000). Atomic force microscopy of gastric mucin and chitosan mucoadhesive systems. *Biochem. J* 348: 557–563.

342 Sakkinen, M., Jurjenson, H., Marvola, M. et al. (2003). Evaluation of microcrystalline chitosans for gastro-retentive drug delivery. *Eur. J. Pharm. Sci.* 19: 345–353.

343 American Society of Health-System Pharmacist (2003). *AHFS Drug Information*, 2834–2836. Bethesda, MD: American Society of Health-System Pharmacist.

344 Li, S.P., Pendharkar, C.M., Mehta, G.N. et al. (1993). Sucralfate as a bioadhesive gastric intestinal retention system: preliminary evaluation. *Drug Dev. Ind. Pharm.* 19: 2519–2537.

345 Higo, S., Kawashima, Y., Takeuchi, H. et al. (1997). Gastric mucoadhesive properties of the solid dispersed complex of sucralfate and tetracycline for *Heliobacter pylori* eradication. *Pharm. Res.* 14: S537–S538.

346 Sinnreich, J. (1991). Covered retard forms. US Patent 4,996,058.

347 Park, K. and Park, H. (1998). Super absorbent hydrogel foams. US Patent 5,750,585.

348 Klausner, E.A., Eyal, S., Friedman, M., and Hoffman, A. (2003). A novel levodopa gastroretentive dosage form in vivo evaluation in dogs. *J. Controlled Release* 88: 117–126.

349 Wilson, A.M., McKenna, B., Gudipati, M. et al. (2001). Evaluation of endogastric therapeutic system (EGTS) containing a GABA receptor agonist in dogs. *AAPS Pharm. Sci.* 3: 3.

350 Wilding, I.R., Davis, S.S., Sparrow, R.A. et al. (1995). Pharmacoscintigraphic evaluation of a modified release (Geomatrix) diltizem dosage. *J. Controlled Release* 33: 89–97.

351 Cumming, K.I., Wilson, A.M., McKenna, B. et al. (2001). The pharmacokinetic and pharmacoscintigraphic evaluation of endogastric therapeutic systems in the fasted and fed state in healthy volunteers. *AAPS Pharm. Sci.*: 3.

352 Mastropietro, D.J., Omidian, H., and Park, K. (2012). Drug delivery applications for superporous hydrogels. *Expert Opin. Drug Delivery* 9: 71–89.

353 Chen, J., Blevins, W.E., Park, H., and Park, K. (2000). Gastric retention properties of superporous hydrogel composites. *J. Controlled Release* 64: 39–51.

354 Chavda, H.V. and Patel, C.N. (2010). Preparation and characterization of swellable polymer-based superporous hydrogel composite of poly(acrylamide-co-acrylic acid). *Trends Biomater. Artif. Organs* 24: 83–89.

355 Kuang, J., Yuk, K.Y., and Huh, K.M. (2011). Polysaccharide-based superporous hydrogels with fast swelling and superabsorbent properties. *Carbohydr. Polym.* 83: 284–290.

356 Gutierrez-Rocca, J., Dunne, L., and Lally, M. (2003). Release pharmaceutical construct for gastric retention. US Patent Application 2003/0008007 A1.

357 Lavy, E., Klausner, E., Hoffman, A., and Friedman, M. (2001). Evaluation of a novel sustained – release gastroretentive dosage form of riboflavin in dogs. *J. Vet. Intern. Med.* 15: 304.

358 Klausner, E.A., Lavy, E., Stepensky, D. et al. (2003). Furosemide pharmacokinetics and pharmacodynamics following gastroretentive dosage form administration to healthy volunteers. *J. Clin. Pharmacol.* 43: 711–720.

359 Klausner, E.A., Lavy, E., Stepensky, D. et al. (2002). Novel gastroretentive dosage forms evaluation of gastroretentivity and its effect on riboflavin absorption in dogs. *Pharm. Res.* 19: 1516–1523.

360 Klausner, E.A., Lavy, E., Friedman, M., and Hoffman, A. (2003). Expandable gastroretentive dosage forms. *J. Controlled Release* 90: 143–162.

361 Jusko, W.J. and Levy, G. (1970). Pharmacokinetic evidence for saturable renal tubular reabsorption of riboflavin. *J. Pharm. Sci.* 59: 765–772.

362 Jusko, W.J., Rennick, B.R., and Levy, G. (1970). Renal excretion of riboflavin in the dog. *Am. J. Physiol.* 4: 1046–1053.

363 Dagan, L. (2014). *Intec Pharma the Accordion Pill™*. Berlin, Germany: World Drug Delivery & Formulation.

364 Verhagen Metman, L., Stover, N., Chen, C. et al. (2015). Gastroretentive carbidopa/levodopa, DM-1992, for the treatment of advanced Parkinson's disease. *Mov. Disord.* 30: 1222–1228.

365 Porter, S.C. and Bruno, C.H. (1990). Coating of pharmaceutical solid-dosage forms. In: *Pharmaceutical Dosage Form: Tablets*, vol. 3 (eds. H.A. Lieberman, L. Lachman and J.B. Schwartz), 77–160. New York: Marcel Dekker, Inc.

366 Signorino, C.A., Levine, S., Barkley, A., and Forcellini, L. (2004). The use of acrylic resins for improved aqueous enteric coating. *Pharm. Technol.* 6: 32–39.

367 Singh, D.H., Roychowdhury, S., Verma, P., and Bhandari, V. (2012). A review on recent advances in enteric coating. *IOSR J. Pharm.* 2: 5–11.

368 Stern, W. and Consalvo, A.P. (2014). Peptide pharmaceutical for oral delivery. US Patent 8,664,178.

369 Friend, D.R. (1991). Colon-specific drug delivery. *Adv. Drug Delivery Rev.* 7: 149–199.

370 Dew, M.J., Ryder, R.E.J., Evans, N. et al. (1982). Colonic release of 5-aminosalicylic acid from an oral preparation in active ulcerative colitis. *Br. J. Clin. Pharmacol.* 16: 185–187.

371 Ibekwe, V.C., Fadda, H., Khela, M.K. et al. (2006). An investigation into the in vivo performance variability of pH responsive polymers for ileo-colonic drug delivery using gamma scintigraphy in humans. *J. Pharm. Sci.* 95: 2760–2766.

372 Riley, S., Tavares, I.A., Bennet, A., and Mani, V. (1988). Delayed-release mesalazine (5-aminosalicylic acid), coat dissolution and excretion in ileostomy subjects. *Br. J. Clin. Pharmacol.* 26: 173–177.

373 Gruber, P., Longer, M.A., and Robinson, J.R. (1987). Some biological issues in oral, controlled drug delivery. *Adv. Drug Delivery Rev.* 1: 1–18.

374 Thomas, P., Richards, D., Richards, A. et al. (1985). Absorption of delayed-release prednisolone in ulcerative colitis and Crohn's disease. *J. Pharm. Pharmacol.* 37: 757–758.

375 Wong, P.S.I. and Theeuwes, F. (1986). Colonic therapeutic delivery system. US Patent 4,627,851.

376 Wong, P.S.I. and Theeuwes, F. (1987). Colon delivery system. US Patent 4,693,895.

377 Swanson, D., Barclay, B., Wong, P., and Theeuwes, F. (1987). Nifedipine gastrointestinal therapeutic system. *Am. J. Med.* 8: 3–9.

378 Savastano, L., Carr, J., Quadros, E. et al. (1997). Controlled release drug delivery. US Patent 5,681,584.

379 Rasmussen, S.N., Bondesen, S., Hvidberg, E.F. et al. (1982). 5-Aminosalicylic acid in a slow-release preparation: bioavailability, plasma level, and excretion in humans. *Gastroenterology* 83: 1062–1070.

380 Haagen Nielsen, O.H. and Bondesen, S. (1983). Kinetics of 5-aminosalicylic acid after jejunal instillation in man. *Br. J. Clin. Pharmacol.* 16: 738–740.

381 Willoughby, C.P., Aronson, J.K., Agback, H. et al. (1982). Distribution and metabolism in healthy volunteers of disodium azodisalicylate, a potential therapeutic agent for ulcerative colitis. *Gut* 23: 1081–1087.

382 Brown, J.P., McGarraugh, G.V., Parkinson, T.M. et al. (1983). A polymeric drug for treatment of inflammatory bowel disease. *J. Med. Chem.* 26: 1300–1307.

383 Klotz, U. (1985). Clinical pharmacokinetics of sulphasalazine, its metabolites and other prodrugs of 5-aminosalicylic acid. *Clin. Pharmacokinet.* 10: 285–302.

384 Simpkins, J.W., Smulkowski, M., Dixon, R., and Tuttle, R. (1988). Evidence for delivery of narcotic antagonists to the colon as their glucuronide conjugates. *J. Pharmacol. Exp. Ther.* 244: 195–205.

385 Yano, H., Hiroyama, F., Arima, H., and Uekama, K. (2001). Preparation of prednisolone-appended α-, β- and γ-cyclodextrins: substitution at secondary hydroxyl groups and in vitro hydrolysis behavior. *J. Pharm. Sci.* 90: 493–503.

386 Yano, H., Hiroyama, F., Arima, H., and Uekama, K. (2001). Prednisolone appended α-, β-, and γ-cyclodextrins: alleviation of systemic side effect of prednisolone after intracolonic administration in 2,4,6-trinitrobenzenesulfonic acid-induced colitis rats. *J. Pharm. Sci.* 90: 2103–2112.

387 Yano, H., Hiroyama, F., Kamada, M. et al. (2002). Colonic delivery of prednisolone appended α-cyclodextrin conjugates: alleviation of systemic side effect after oral administration. *J. Controlled Release* 79: 103–112.

388 Brondsted, H. and Kopecek, J. (1991). Hydrogels for site-specific oral drug delivery: synthesis and characterization. *Biomaterials* 12: 584–592.

389 Saffran, M., Kumar, G.S., Savariar, C. et al. (1986). A new approach to the oral delivery of insulin and other peptide drugs. *Science* 223: 1081–1084.

390 Saffran, M. and Neckers, D.C. (1987). Method of use polymers containing cross-linked azo bonds for releasing therapeutic agents in the lower gastrointestinal tract. US Patent 4.663,308.

391 Rubinstein, A. (1990). Microbially controlled drug delivery to the colon. *Biopharm. Drug Dispos.* 11: 465–475.

392 Hanauer, S.B. and Sparrow, M. (2004). COLAL-PRED Alizyme. *Curr. Opin. Invest. Drugs* 5: 1192–1197.

393 Adkin, D.A., Kenyon, C.J., Lerner, E.I. et al. (1997). The use of scintigraphy to provide "proof of concept" for novel polysaccharide preparations designed for colonic delivery. *Pharm. Res.* 14: 103–107.

394 Ibekwe, V.C., Kheka, M.K., Evans, D.F., and Basit, A.W. (2008). A new concept in colonic drug targeting: a combined pH responsive and bacterially triggered drug delivery technology. *Aliment. Pharmacol. Ther.* 28: 911–916.

395 Akkas, B.E., Guner, L., Gokcora, N., and Acarturk, F. (2015). The use of scintigraphy for in vivo evaluation of guar gum-based compressed coated tablets for colonic delivery of theophylline. *J. Nucl. Med.* 56: 1670.

5

The Vasoconstrictor Assay (VCA): Then and Now

Isadore Kanfer[1,2] and Howard Maibach[3]

[1] *Faculty of Pharmacy, Rhodes University, Grahamstown, South Africa*
[2] *Leslie Dan Faculty of Pharmacy, University of Toronto, Toronto, Canada*
[3] *Department of Dermatology, School of Medicine, University of California San Francisco, San Francisco, CA 94143, USA*

5.1 Introduction

In June 1995, the US FDA introduced a Guidance which described a surrogate method for the assessment of the bioequivalence (BE) of topical dermatological corticosteroids [1]. This guidance made provision for a "non-clinical" end point study for use to obtain market approval of generic topical corticosteroid products intended for local action. The method is based on a pharmacodynamic (PD) response following application of topical corticosteroids to the skin of human subjects where a skin-whitening effect or "blanching" may occur. This method, commonly known as the vasoconstrictor assay (VCA) is also sometimes referred to as the human skin blanching assay (HSBA).

The production of blanching in human skin is a side effect of the topical corticosteroid application and was first observed by Hollander et al. [2]. They noticed that intra-articular administration of topical corticosteroids produced blanching of the engorged synovial membrane and subsequently, Ashton and Cook [3] also observed that skin-whitening occurred in rabbits following topical treatment with cortisone which was presumed to be an apparent vasoconstriction response on the blood vessels in rabbit ear chambers. Some 10 years later, McKenzie and Stoughton [4] realized after observation that topical corticosteroids produced blanching of psoriasis lesions and the surrounding skin and that this skin whitening effect may be used as a measure of subcutaneous penetration of corticosteroids from topical formulations. Hence, they proposed that this unique

Drug Delivery Approaches: Perspectives from Pharmacokinetics and Pharmacodynamics,
First Edition. Edited by Bret Berner, Toufigh Gordi, Heather A. E. Benson, and Michael S. Roberts.

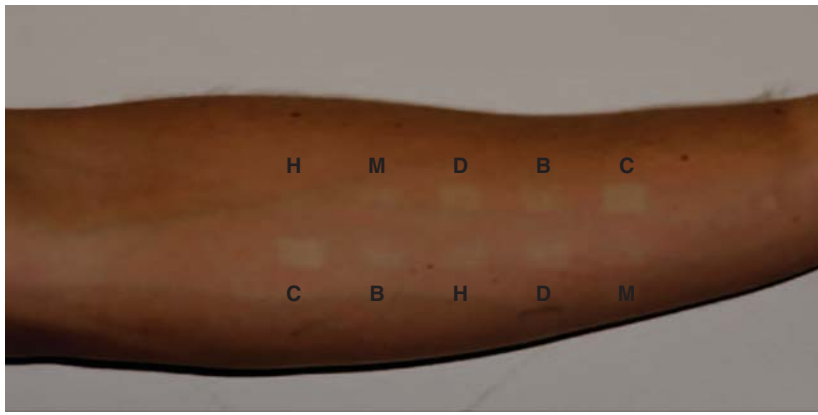

Figure 5.1 Typical blanching responses following application of topical corticosteroids to the volar aspect of the forearm of a human subject. H = hydrocortisone 17-butyrate cream (0.1%). C = clobetasol propionate cream (0.05%). B = betamethasone valerate cream (0.1%). D = desoximetasone ointment (0.25%). M = mometasone furoate cream (0.1%). Source: Kanfer [5].

ability of topical corticosteroids to produce skin blanching (Figure 5.1) may be applicable for use as an assay since it relates to the amount of corticosteroid that has penetrated into the skin [6]. Subsequently, the vasoconstriction assay was correlated with clinical activity in psoriasis [7].

5.1.1 Applications and Procedures

Initially, visual observations and measurements of skin blanching were made and investigated using a simple Yes/No assessment to establish whether a blanching response was present or absent after application [8–10]. However, this type of assessment does not provide useful information on the degree of bioavailability of the product and it is thus not suitable for the assessment of bioequivalence by comparing bioavailability between different topical corticosteroids and/or their formulations.

To be eligible for a PD endpoint-based BE study, the drug product must meet the following criteria [11]:

- A dose–response relationship is demonstrated;
- The PD effect of the selected dose should be at the rising phase of the dose–response curve, as shown in Figure 5.2;

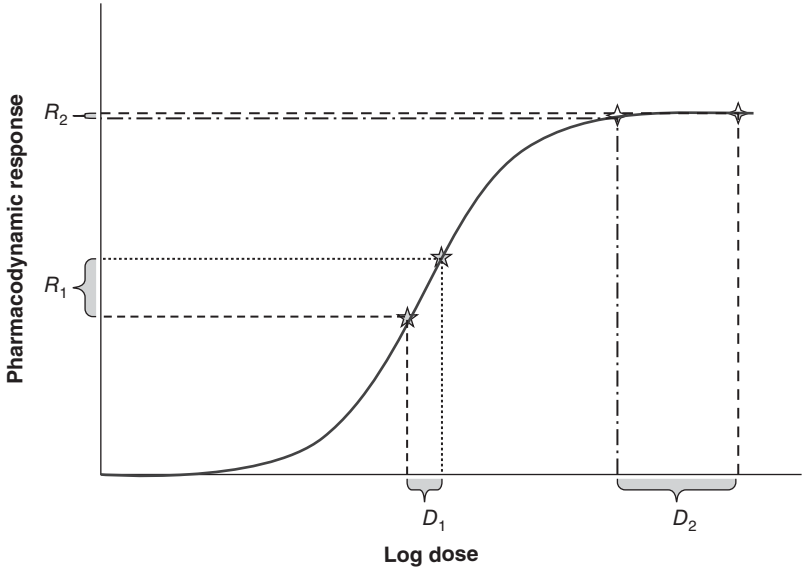

Figure 5.2 Sigmoidal dose-response curve. R_1 and R_2 represent the pharmacodynamic responses (skin blanching) following administration of dose 1 (D_1) and dose 2 (D_2) respectively.

- Sufficient measurements should be taken to assure an appropriate PD response profile; and
- All PD measurement assays should be validated for specificity, accuracy, sensitivity, and precision.

Following the introduction of the FDA Guidance document [1], the use of an instrumental method was recommended. However, the visual assessment method has also been retained as an option [1] of measuring the vasoconstrictor response, viz. Section 2, B, states:

> The Division of Bioequivalence currently considers the use of a chromameter to be applicable to bioequivalence studies based on the vasoconstrictor assay, and therefore recommends that pharmaceutical sponsors incorporate the use of a chromameter into their study designs. However, with acceptable validation, which includes establishing the correlation between chromameter measurements and visual estimation data, sponsors may rely on visual estimation of the degree of vasoconstriction.

This is somewhat intriguing since this option is probably redundant, and it is highly unlikely that a sponsor would resort to submitting visual data to support market approval.

In this guidance, the VCA was optimized to facilitate comparisons by evaluating time-response profiles, potencies, and formulations of topical corticosteroids. The optimizations included the application of appropriate statistics, establishment of requisite duration of application of the drug or drug product (dose duration) and intervals of time following application at which the response should be assessed and also a scoring system to facilitate visual assessment [12–14].

The FDA Guidance recommends a pilot study with the reference listed drug (RLD) to investigate the dose–response relationship and to determine the number of subjects to be used in the BE study and a pivotal study be conducted to assess bioequivalence. The pilot study provides information on an appropriate dose duration required for bioequivalence testing in a subsequent pivotal study. The pilot study provides information regarding the amount of topical corticosteroid being delivered within the period of time that the formulation/product is left in contact with the skin. This study is usually conducted only using the reference product. Dose durations required for the pivotal study as per FDA guidance [1] are ED_{50}, D_1 (i.e. ½ED_{50}) and D_2 (i.e. $2ED_{50}$), where ED_{50} is the dose duration at which 50% of the maximum blanching response is achieved. The ED_{50} is chosen since it represents the portion of a dose–response relationship plot where the optimum discrimination of relevant differences can be detected. The development and validation of a dose–response curve is therefore essential to determine ED_{50}, D_1, and D_2. These values are determined from an E_{max} model, in accordance with the FDA guidance [1]. The pivotal study is subsequently conducted where a comparison between the responses of a test and reference product is investigated for bioequivalence using the ED_{50}. In addition, the Guidance further stipulates that a subject must be a "detector" in order for inclusion of their data for statistical analyses supporting in vivo bioequivalence assessment. Hence, subjects' responses are expected to meet the specified minimum D_2/D_1 ratio of area under the effect curve (AUEC) values in the pivotal study as shown in the equation below.

$$\frac{\text{AUEC at } D_2}{\text{AUEC at } D_1} \geq 1.25$$

5.1.2 Visual Assessment

As previously mentioned, the initial method to determine bioequivalence of topical corticosteroid products involved the visual assessment of the degree of skin blanching following application of a topical corticosteroid to human skin in vivo. Although, the human eye may be sufficiently sensitive to discriminate small color changes in skin blanching, this approach is considered to be observer dependent

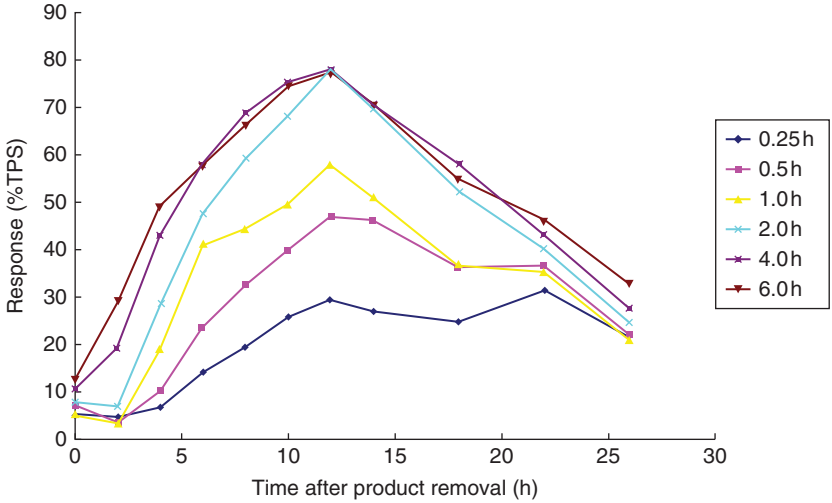

Figure 5.3 Visual response profiles of different dose durations.

and thus too subjective and perceived as an apparent weakness when using the human eye to evaluate skin whitening. A further criticism relates to the inability to validate the eye as one is able to do when using an instrument.

However, if the observers undergo sufficient training and acquire experience in visual evaluation of skin blanching, reproducibility and reliability of visual assessment can be established [15–17].

A scoring system for visual assessment was developed and involved a graded response based upon the following criteria: absent, faint, faint–moderate, moderate–strong, and strong–intense blanching using the scores of 0, 1, 2, 3, and 4, respectively. The data are plotted in terms of the percentage of the total possible score (TPS) vs. time (Figure 5.3) and calculated as follows [14]:

The maximum score per site = 4
The number of independent observers = n
The number of sites per preparation per arm = S
The number of volunteers = V
Total possible score (TPS) = $4 \times n \times S \times V$
Percent total possible score (%TPS) = (Actual score/TPS) × 100

5.1.3 Chromameter Assessment

The Minolta® chromameter, which is a portable instrument that uses tristimulus colorimetry involving reflectance spectroscopy, was adapted to measure skin

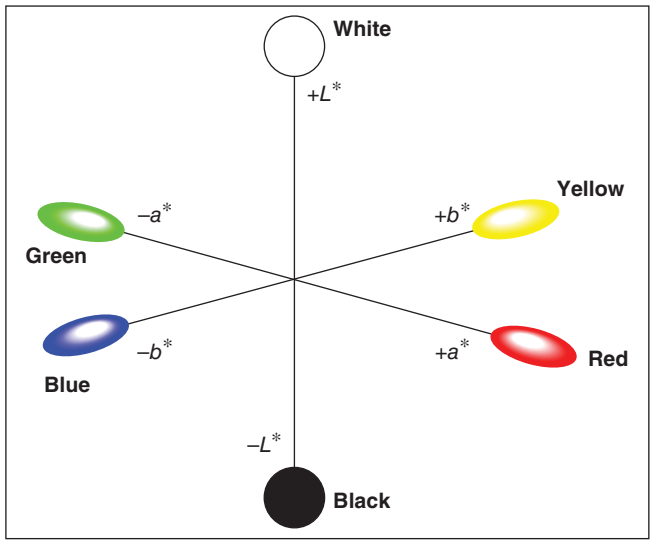

The L*a*b* color space (adapted from Waring [21])

Figure 5.4 Tristimulus colorimetry where the reflected light is recorded in a three-dimensional color system using a Chromameter. Source: Waring et al. [20]. © 1993, Elsevier.

blanching [18, 19]. The chromameter functions by emitting a white light (using a pulsed xenon arc lamp) onto the chosen area of assessment and measuring the intensity of reflected light through three particular wavelength filters (analyzed at wavelengths of 450, 560, and 600 nm) or using a photodiode array in more recent instruments. The detected signal is converted into three coordinates: L^* (luminosity), a^* (the amount of green or red), and b^* (the amount of yellow or blue). These three coordinates record color in a three-dimensional color system (Figure 5.4) recommended by CIE (Commission International de l'Eclairage) [20–23]. As skin blanching develops, the skin becomes lighter and its redness fades and as the skin becomes more pale, the L^* scale increases, a^* scale decreases, and b^* scale increases very slightly. It has been shown that the L^* and a^* coordinates are more discriminative than the b^* coordinate in determining skin blanching responses, thus the latter coordinate is omitted from data analysis. Furthermore, following release of the FDA guidance, only the a-scale data has been recommended for use in the statistical analysis [1].

5.1.3.1 Comparison Between Visual and Chromameter Assessment

Although visual assessment is not recommended and has been replaced with assessment by chromameter, published data have confirmed the utility of visual

assessment. In a dose duration study by Au et al. [24] using a 0.05% clobetasol propionate cream, visual assessment was performed by three trained observers and a chromameter was also used to assess the degree of skin blanching at various time intervals over a period of 26 hours. The E_{max} model fitting using AUEC data from the visual and chromameter assessments showed that in both instances, the AUEC of the blanching/vasoconstriction response approached a maximum at ~1 hour dose duration. Using the resulting ED_{50} of 0.6 hour and D_1 and D_2 values of 0.3 and 1.2 hours, respectively, a subsequent pivotal study was conducted in 34 healthy human subjects. The same clobetasol propionate cream used in the dose duration study was used as both reference and test product for the determination of bioequivalence. Skin blanching was evaluated over a period of 30 hours after the removal of the applied products. The results revealed that 23 subjects were found to be "detectors" in the pivotal study, but the data for all 34 subjects were included for comparison purposes. The skin blanching profiles were found to be very similar when comparing the data between the two different assessment methods or between "detectors" and "non-detectors" and clearly indicated that the visual and chromameter assessment methods are comparable to each other and both are equally applicable for use to assess bioequivalence. Interestingly, the inclusion of "non-detectors" data did not seem to have a significant effect on the skin blanching profiles nor on the outcomes of the comparisons for the assessment of bioequivalence.

Whereas the acceptance criteria for the declaration of bioequivalence generally specify that the 90% confidence intervals (CIs) for the ratios of the log-transformed C_{max} and area under the curve (AUC) for orally administered test and reference products must fall within the range of 80–125% [25], the FDA guidance [1] recommends that only the ratios of the untransformed AUECs should be used as assessment criteria. The data in Table 5.1, indicate that both assessment methods complied with the bioequivalence criteria except for the data for "detectors" using the chromameter where the 90% CI as 86.5–129.3.

This usually suggests that the power of the study was too low and more subjects should therefore be included in order to increase the power of the study when

Table 5.1 Ninety percent confidence intervals (CIs) using Locke's method for visual and chromameter data.

	Visual		Chromameter	
	Mean ratio % (T/R)	**90% CI**	**Mean ratio % (T/R)**	**90% CI**
Detectors ($n = 23$)	104.6	99.3–111.6	104.6	86.5–129.3
All subjects ($n = 34$)	102.9	97.9–109.2	104.3	90.2–120.7

Source: Au et al. [24]. © 2008, Canadian Society for Pharmaceutical Sciences.

using the chromameter as the assessment tool. On the other hand, the visual assessment data clearly indicated that the study population of 23 subjects was sufficient to confirm bioequivalence. Hence, it implies that although the use of the chromameter is generally recommended as the "preferred" assessment method in favor of visual assessment due to the subjectivity; the above data has shown that visual assessment is a reliable and appropriate assessment technique to assess the bioequivalence of a topical corticosteroid formulation. Previous studies using visual assessment [26, 27] also confirmed the high degree of reproducibility and excellent correlations where two different creams containing betamethasone valerate (0.12%) were compared in three separate trials using three trained independent observers. The results obtained by each of the observers for each trial were similar where the rank order between the two different creams were found to be consistent throughout each trial and for each observer. A further study investigating possible correlations between the visual and chromameter assessments indicated excellent correlations using a mometasone cream product (1%) and the data collected by two independent observers [15].

The foregoing data provide compelling evidence that the visual method of assessment which has largely been discarded by regulatory authorities can provide the same or similar blanching data compared with the chromameter. However, validation of the visual assessment method remains in contention, whereas the use of a chromameter lends itself to a more feasible and practical approach to ensure appropriate validation of an instrumental method and procedures.

5.2 Issues and Controversies

5.2.1 Fitting of PD Response Data

To characterize the response vs. dose–duration relationship and to determine the population ED_{50} and E_{max} estimates, the guidance [1] recommends that the PD response data should be fitted using either naïve pooled data or a parametric nonlinear mixed effect (NLME) modeling method [28]. A study case example is included in the guidance where the NLME algorithm, as implemented in P-PHARM®, was used. The value of the ED_{50} has important implications for the design of the pivotal skin blanching study in the bioequivalence evaluation of topical corticosteroids products. Although several different population modeling methods, algorithms, and software are available, the guidance does not provide information whether different types of NLME methods can provide differing results, and if so, which one is preferred. Results from different population modeling methods can vary due to their different estimation approaches in data analysis [28–31]. Some studies obtained different population mean estimates

when using different population modeling methods [28, 29, 32–34], some others found comparable results [35–37].

Furthermore, the recommended NLME method requires setting distribution assumptions, which are absent in the guidance since it is not specified whether normal or ln-normal distribution of the ED_{50} should be assumed in the process of population modeling. Interestingly, in a letter published by FDA in 1998 [37] in response to Demana et al. [38], the absence of any consideration for the nature of the distribution (normal or ln-normal) of population parameters was mentioned among the reasons to discourage the use of naïve pooled data method since naïve pooled data does not consider inter-individual variability when estimating population parameters. As a result, population estimates based on the naïve pooled data method may poorly correlate with the observed data and thus may not accurately represent the study population [39, 40], and should thus not be the method of choice. Hence, an NLME should therefore be the preferred option to be used for the determination of the population parameters of interest such as the ED_{50} and the E_{max}.

As population ED_{50} estimates play a critical role in the BE assessment of topical corticosteroid products, any difference in estimated PD parameters could influence the outcome of BE evaluation for these products. Due to the availability of several methods for performing population modeling and their parametric approach in data analysis, updating the US FDA 1995 Guidance [1] with more specific instructions related to the population approach and normality assumptions, would favor a more consistent approach to be followed by pharmaceutical manufacturers, and would increase the confidence in BE assessment results of these products.

5.2.2 Circadian Activity

The influence of treatment duration and time of day of application of a topical corticosteroid was investigated by Pershing et al. [41]. Since circadian activity of topical corticosteroids may compete with endogenous circulating cortisol for activity in the skin, the possible influence of circadian activity of topically applied corticosteroids may have implications for the degree of skin blanching and thus, bioequivalence assessment using the VCA. Pershing et al. [41] found that the maximal betamethasone dipropionate activity in skin was around midnight which coincides with minimal circulating blood concentrations of endogenous cortisol that occur between 20.00 and 04.00 hours [42]. These data indicate the importance of considering circadian activity and time of maximal skin response to a particular topical corticosteroid when designing a BE study and which could be particularly useful for those topical corticosteroids which exhibit very low blanching response such as hydrocortisone and clocortolone pivalate, among others.

5.2.3 BE Studies Performed Under Occlusion

Various approaches have been used to enhance the percutaneous penetration of drugs. In particular, following the application of a topical corticosteroid, the application site can be occluded using an occlusive dressing such as a plastic covering. The enhanced pharmacological effect of occlusion has been demonstrated by McKenzie [6]. When considering the use of the VCA for BE of topical corticosteroid products, although the usual experimental design involves assessing blanching following application in the non-occluded mode, the FDA [1] permits the use of occlusion provided occlusion is allowed in the labeling of the specific reference listed drug. Furthermore, caution is emphasized in the guideline since it has been shown that the ED_{50} decreases with increasing topical corticosteroid product potency [43]. Hence, since very short dose durations are generally impractical to perform, occlusion is recommended only for lower potency products.

There are several practical implications which need to be considered when using occlusion such as a requirement to also occlude untreated sites. Whereas all the treated sites will be affected, occlusion would certainly only be a factor on untreated site skin tone no longer than the time of the first post-dose reading. It is unlikely that it is even a factor 10–15 minutes after removal of the occlusive covering, as the effect would almost certainly have to be related to heat and moisture retention. Once the occlusive covering is removed, the untreated site skin tone would acclimate to what it would have been had it not have been occluded. However, this raises the issue regarding whether there would likely be differences in the readings at the treated sites comparted to the non-occluded untreated sites. Any difference could have an impact on inclusion of the required "detectors" based on D_2/D_1 response ratio and also on the Test-to-Reference ratio, as well as on the variances used in the 90% CI calculation. However, any occlusive effects on the skin tone of an untreated site would likely have dissipated by the time of the first post-dose blanching readings.

5.2.4 Erythema Response at Application Sites

At times a paradoxical redness may occur at the site of application of a topical corticosteroid product in some subjects during a VCA study which is generally mild and short-lived. This phenomenon may cause concern when one or more chromameter readings are taken when this response is still evident thereby resulting in a decision to exclude such a subject from the study. However, it would be prudent to retain such data unless the response was considered severe enough by the investigator to be listed as moderate-to-severe which would be then be a reasonable justification to exclude the subject and consequently require a follow-up investigation regarding the safety of the particular product.

5.2.5 Use of VCA for Market Approval in the European Union

In February 1987, the European Medicines Agency (EMA) issued a Guideline entitled "Clinical Investigation of Corticosteroids Intended for Use on the Skin (Legislative basis Directive 75/318/EEC)," which was enforced in August 1987 [44].That note for guidance was intended to assist applicants for a marketing authorization with respect to the clinical testing of topical corticosteroids which are intended to be used on the skin. Perusal of that guideline indicates that it is primarily intended for new topical corticosteroid products since there is no clear directive for use to obtain marketing authorization of generic topical corticosteroid products using the VCA. It is also interesting to note that document has not been revised since its issuance. Subsequently in 2006, the European Medicines Evaluation Agency (EMEA) issued a Questions and Answers on Guideline Title: Clinical Investigation of Corticosteroids Intended for Use on the Skin, CHMP/EWP/21441/2006, on 16 November 2006 [45]. Whereas inferences are made to generic topical corticosteroid products in the Q&A document, certain requirements are quite intriguing and seemingly misconstrued. For example, Question 2 presents the following:

How to use vasoconstriction assays for comparisons?

The answer includes a reference to the FDA's Guidance [1] and also provides a summary of the general testing principles which relate to a pretest (dose duration) and subsequent pivotal study requirements. However, it also stipulates an intriguing requirement that the reference products should include different potency classes (suggested equally potent, more potent, and less potent) and have received a Marketing Authorization based on a full dossier. Seemingly, this statement has been inappropriately extracted from the 1987 Guideline which applies to clinical testing of new topical corticosteroid products. Since the primary objective in BE testing is to determine equivalence between a test and reference product, inclusion of different potency classes in a BE study makes no sense. Furthermore, when including an equally potent, more potent, and less potent product, it would be meaningless to attempt any evaluation apart from the Test and Reference products since the ED_{50} and hence the appropriate dose durations for those other products may be entirely different from those data established for the reference product used in the initial dose duration study. Furthermore, no information has been provided for interpreting the results or acceptance criteria.

A further intriguing statement is also included under the heading:

Assessment of the vasoconstriction response: In this section of the answer to Question 2, mention is made of the use of a chromameter to measure the vasoconstriction response but adds the following statement: "However, although this

technique may be very useful in the future, comparison with human eye assessment shows that it still requires refinement and optimization. Until these refinements have been researched and implemented, evaluators should continue to use the visual and chromameter-based methods of comparison of topical corticosteroids."

The above implies that both visual and chromameter-based methods are required for inclusion in the application dossiers.

These above-mentioned anomalies can likely result in difficulties in attempts to use the VCA to establish BE and obtain marketing approval for generic topical corticosteroid products in the EU.

5.2.6 Potency Ranking of Topical Corticosteroid Products

The human skin blanching method has been used for the potency ranking of corticosteroid products [4]. However, it was also found that the method has limitations and does not necessarily rank the corticosteroid products in the same order when compared to other assessment methods [8, 46]. This is unsurprising since the method used was relatively imprecise as it relied solely on the appearance of a vasoconstriction response on the skin following application of the topical corticosteroid for several hours (generally 15 or 16 hours) and a single blanching observation an hour or two later. Furthermore, in practice, topical corticosteroid products are usually applied to diseased skin thus penetration of the drug will differ due to less resistance by the *stratum corneum* barrier. As a result, information on topical bioavailability [47] obtained from studies on healthy skin may not reflect the penetration of the drug into diseased skin.

It is of interest to note that several lists ranking various topical corticosteroid formulations in order of potency have been published where these rankings are largely based on clinical data. There are many topical corticosteroid products available on the market and the current potency rankings have been developed to differentiate between different corticosteroid products according to their relative clinical anti-inflammatory activities without taking into account differences in the concentrations of the active ingredients, ignoring molecular weight differences between compounds and also differences between specific formulations.

According to Hepburn et al. [48] in the United States topical corticosteroids are ranked into seven classes based entirely on the vasoconstrictor assay giving no weight to clinical outcome, safety, or cost, whereas a four category system is used in northern Europe, UK, Germany, Netherlands, and New Zealand to classify potency of topical corticosteroids [49–51]. In New Zealand, class I is the strongest while in continental Europe class I is mildly potent and class IV is very

highly potent [50, 51]. However, the system may not be sufficient to indicate significant biological differences among various corticosteroid preparations available because it only has four different classes compared to US ranking with seven different classes [52]. Ference and Last [53] stated that the preferred way to determine potency of topical corticosteroids is the vasoconstrictor assay. The latter supported Hepburn et al. [48] that the method is imperfect for predicting clinical effectiveness of steroids and also highlighted the need for development of a ranking system that compares clinical outcomes to safety ratio which will be of greater benefit.

The published literature has, however, shown discrepancies in the classification of topical corticosteroid potency. A study conducted by Brown [54] showed no significant differences in potency between Eumovate® (clobetasone butyrate 0.05%) ointment classified as moderately potent and Betnovate® (betamethasone valerate 0.1%) and Propaderm® (Beclomethasone dipropionate 0.025%) ointments classified as potent preparations. Allenby and Sparkes [55] also supported the findings by demonstrating that Eumovate is clinically equal or even superior to Locid® (hydrocortisone butyrate 0.1%) which is classified as a potent preparation. At times different dosage forms of the same formulation will have different potencies; e.g. Halcinonide cream 0.1% (class 2) is more potent than Halcinonide ointment 0.1% (class 3).

Current published literature relating to potency often does not indicate how some of the potency classifications were done but lists are available depicting the different potency classes and ranking of corticosteroid products. Furthermore, ranking of the inherent potency of active pharmaceutical ingredients (APIs) is conspicuous by its absence.

There is clearly a need to develop standard procedures and protocols to properly classify topical corticosteroids in terms of their inherent potencies and considering the dose response for each based on relevant ED_{50} data. Furthermore, it is also important to consider the effects of formulation factors which may enhance or reduce potency.

The HSBA has, nevertheless, been found to be very effective for screening and for the determination of the effect of formulation on the activity and efficacy of topical corticosteroid products as well as to examine the comparative bioavailabilities of such topical preparations as indicators of the efficacy of those products [46]. Whereas one of the initial objectives was to utilize the HSBA for potency ranking with a view to predict clinical outcome, and while the vasoconstriction rankings predict percutaneous absorption, correlation of the vasoconstrictor assay with clinical outcomes is considered an approximation – vasoconstriction rankings do not reliably predict clinical outcomes [48].

5.2.7 Sensitive Region of the Dose–Response Curve

Critical to the use of the VCA in BE testing, is that the dose duration at which the test and reference products are compared fall within the sensitive and discriminating region of the dose–response curve.

The E_{max} model considered operative in the dose–response relationship for topical corticosteroids is given by the equation:

$$E = (E_{max} \times \text{Dose duration})/(ED_{50} + \text{Dose duration})$$

where

E = Pharmacodynamic effect metric (area under the effect curve. AUEC)
Dose duration = duration of exposure (minutes) to the topical corticosteroid
E_{max} = Maximum possible value for "E"
ED_{50} = Dose duration needed to achieve 50% of the E_{max} response

According to the FDA guidance [1], the determination of D_1 and D_2 corresponds to approximately one-half ED_{50} and two times ED_{50}, respectively, for use in the pivotal study. These values bracket ED_{50} and correspond to approximately 33% and 67%, respectively of the maximal response, and represent the sensitive portion of the dose duration-response curve [56]. It is thus permitted to round up the observed ED_{50} value by up to 15 minutes to obtain the ED_{50} value used in the pivotal study. In practice, a demonstration of dose duration-response based on D_1, within 0.25–0.5 times the observed ED_{50} and D_2 within 2–4 times the observed ED_{50} is acceptable. For potent corticosteroids with short ED_{50} values, these recommendations may require adjustment.

The following examples illustrate the effects of using the ED_{50} and a dose duration lower than the ED_{50}.

Presume that the ED_{50} was determined to be 400 minutes and that the ED_{50} dose duration was used for the testing duration for bioequivalence. The reference product response would be 50% of E_{max}. Table 5.2 provides the expected Test and Reference responses for a generic product which, when applied for the same duration as the reference product, only delivers an effective dose equal to 80% that of the Reference product and for a second generic product that delivers an effective dose equal to 125% of that of the Reference dose.

If a 200-minute testing duration had been used instead of the 400-minute ED_{50}, the reference product response would be 33.33% of the E_{max}. Table 5.3 provides the expected Test and Reference responses for a generic product which delivers an effective dose equal to 80% (i.e. 160-minute dose) of that of the Reference product and for a product which delivers an effective dose that is 125% (i.e. 250-minute dose) of that of the Reference product.

Table 5.2 Dose duration used for testing = 400 min and ED_{50} = 400 minutes.

Effective test dose duration (min)	Reference dose duration (min)	Test response (%E_{max})	Reference response (%E_{max})	Test/reference response ratio (%)
320	400	44.44	50.00	88.9
500	400	55.56	50.00	111.1

Table 5.3 Dose duration used for testing = 200 minutes when ED_{50} = 400 minutes.

Effective test dose duration (min)	Reference dose duration (min)	Test response (%E_{max})	Reference response (%E_{max})	Test/reference response ratio (%)
160	200	28.57	33.33	85.7
250	200	38.46	33.33	115.4

It is thus evident from the test-to-reference response ratios in Tables 5.2 and 5.3 that the use of a lower dose duration for testing instead of the ED_{50} dose did not decrease, but actually increased the sensitivity to detect differences between a test product that is equivalent to the Reference product in its delivered dose. In both the 80% and 125% cases, the Test/Reference response ratio was farther removed from 100% at the lower testing dose duration, 200 minutes, than when the ED_{50} dose duration of 400 minutes was used for testing [57].

Based on the above premise, it is acceptable to adjust dose durations to a value lower than the ED_{50} in the VCA instead of using the actual fitted ED_{50} value.

5.2.8 Correlation of ED_{50} with Potency Classification of a Product?

Singh et al. reported that ED_{50} values were inversely related to drug potency based on nonlinear mixed effects modeling (NONMEM) analysis. They asserted that values for population ED_{50} decreased with increase in dermatologic corticosteroid product potency [43]. This was based on the premise that the ED_{50} value relates to the dose duration corresponding to half-maximal response, and as such, to the speed of absorption of a medication. However, the absorption velocity of a medication is strongly influenced by a number of factors including, release capability of the formulation, degree of penetration into the skin, stability of the drug, and potency among others. Hence, the ED_{50} value does not only reflect the potency of the product but is clearly influenced by additional factors [58]. In the study

reported by Keida et al. [58], 0.05% betamethasone butyrate propionate (BBP) cream, a purported potency class II corticosteroid equivalent to betamethasone dipropionate and 0.01% hydrocortisone butyrate (HCB), a purported potency class III corticosteroid equivalent to betamethasone valerate, were studied to determine their respective ED_{50}s. Their results revealed that the ED_{50} of the corticosteroid which represented a stronger potency class was almost 50% higher than that of the weaker potency class whereas the respective E_{max} values were somewhat similar, E_{max} BBP = 89.2 and for HCB = 72. These findings suggest that E_{max} is the more appropriate parameter which correlates with potency and not the ED_{50}.

5.3 Conclusions

The official regulatory acceptance of the VCA has been a major contribution in the realm of BE assessment of topical corticosteroid products. Unlike other generic topical dermatological products where clinical trials in patients are required resulting in a dearth of such products, use of the VCA has facilitated the availability of generic topical corticosteroid products in numerous countries making such products cost-effective and more accessible to the wider communities around the world. Whereas the VCA has undoubtedly served relevant beneficiaries well over the years since its introduction, there remain several issues which need to be re-visited to optimize this unique technique and facilitate the revision of an improved and more informative guidance.

References

1 FDA (1995). *Guidance for Industry – Topical Dermatological Corticosteroids: In Vivo Bioequivalence*. Centre for Drug Evaluation and Research. Food and Drug Administration.
2 Hollander, J.L. and Brown Jr EM, S.E.K. (1950). The use of intra-articular temperature measurement in the evaluation of anti-arthritic agents. *J Clin Invest.* 29 (6): 822–823.
3 Ashton, N. and Cook, C. (1952). In vivo observation of the effects of cortisone upon the blood vessels in rabbit ear chambers. *Br. J. Exp. Pathol.* 33: 445–450.
4 McKenzie, A. and Stoughton, R. (1962). Method of comparing percutaneous absorption of steroids. *Arch. Dermatol.* 86: 608–610.
5 Kanfer, I. (2015). Methods for the assessment of bioequivalence of topical dosage forms: correlations, optimization strategies and innovative approaches. In: *Topical Drug Bioavailability, Bioequivalence and Penetration*, 2e (eds. J. Jenner, V.P. Shah and H.I. Maibach), 113–151. New York: Springer Science.

6 McKenzie, A. (1962). Percutaneous absorption of steroids. *Arch. Dermatol.* 86: 91–94.

7 Cornell, R. and Stoughton, R. (1985). Correlation of the vasoconstriction assay and clinical activity in psoriasis. *Arch. Dermatol.* 121: 63–67.

8 McKenzie, A. (1966). Comparison of steroid induced vasoconstriction. *Br. J. Dermatol.* 78: 182–183.

9 Poulsen, B.J., Young, E., Coquilla, V., and Katz, M. (1968). Effect of topical vehicle composition on the in vitro release of fluocinolone acetonide and its acetate ester. *J. Pharm. Sci.* 57 (6): 928–933.

10 Heseltine, W., McGilchrist, J., and Gartside, R. (1964). Comparative vasoconstrictor activities of corticosteroids applied topically. *Br. J. Dermatol.* 76: 71–73.

11 Zou, P. and Yu, L. (2014). Pharmacodynamic endpoint bioequivalence studies. In: *FDA Bioequivalence Standards* (eds. L. Yu and B. Li), 217–241. New York: Springer.

12 Clanachan, I., Devitt, H., Foreman, M., and Kelly, I. (1980). The human vasoconstrictor assay for topical steroids. *J. Pharmacol. Methods* 4: 209–220.

13 Pepler, A., Woodford, R., and Morrison, J. (1971). The influence of vehicle composition on the vasoconstrictor activity of betamethasone-17-valerate. *Br. J. Dermatol.* 85: 171–176.

14 Haigh, J. and Kanfer, I. (1984). Assessment of topical corticosteroids preparations: the human skin blanching assay. *Int. J. Pharm.* 19: 254–262.

15 Schwarb, F., Smith, E., Haigh, J., and Surber, C. (1999). Analysis of chromameter results obtained from corticosteroid-induced skin blanching assay: comparison of visual chromameter data. *Eur. J. Pharmacol.* 47: 261–267.

16 Haigh, J. and Smith, E. (1991). Topical corticosteroid-induced skin blanching measurement: eye or instrument? Letter to the editor. *Arch. Dermatol.* 127: 1065.

17 Skelly, J., Shah, V., and Peck, C. (1991). Topical corticosteroid-induced skin blanching measurement: eye or instrument? Response to the editor. *Arch. Dermatol.* 127: 1065.

18 Kanfer, I., Tettey-Amlalo, R., and Au, W. (2010). Assessment of topical dosage forms intended for local or regional activity. In: *Generic Drug Product Development: Specialty Dosage Forms* (eds. L. Shargel and I. Kanfer), 54–103. New York: Informa Healthcare.

19 Kanfer, I. (2015). Methods for the assessment of bioequivalence of topical dosage forms: correlations, optimization strategies and innovative approaches. In: *Topical Drug Bioavailability, Bioequivalence and Penetration*, 2e (eds. J. Jenner, V.P. Shah and H.I. Maibach), 4–7. New York: Springer Science.

20 Waring, M., Monger, L., Hollingsbee, D. et al. (1993). Assessment of corticosteroid-induced skin blanching: evaluation of the Minolta chromameter CR200. *Int. J. Pharm.* 94: 211–222.

21 Piérard, G. (1998). EEMCO guidance for the assessment of skin colour. *J. Environ. Eng. Div. ASCE* 10: 1–11.

22 Taylor, S., Westerhof, W., Im, S., and Lim, J. (2006). Noninvasive techniques for the evaluation of skin color. *J. Am. Acad. Dermatol.* 54: S282–S290.

23 Chan, S. and Po, A. (1992). Quantitative skin blanching assay of corticosteroid creams using tristimulus colour analysis. *J. Pharm. Pharmacol.* 44: 371–378.

24 Au, W., Skinner, M., and Kanfer, I. (2008). Bioequivalence assessment of topical clobetasol propionate products using visual and chromametric assessment of skin blanching. *J. Pharm. Pharm. Sci.* 11: 147–153.

25 (2002). *FDA Guidance Industry: Bioavailability and Bioequivalence Studies for Orally Administered Drug Products—General Considerations*. 5600 Fishers Lane Rockville, MD 20857: U.S. Department of Health and Human Services Food and Drug Administration Center for Drug Evaluation and Research (CDER).

26 Haigh, J., Meyer, E., Smith, E., and Kanfer, I. (1997). The Human skin blanching assay for in vivo topical corticosteroid assessment. I. Reproducibility of the assay. *Int. J. Pharm.* 152: 179–183.

27 Haigh, J., Meyer, E., Smith, E., and Kanfer, I. (1997). The human skin blanching assay for in vivo topical corticosteroid assessment. II. Subject- and observer-dependent variation in blanching responses. *Int. J. Pharm.* 152: 185–192.

28 Ozdin, D., Sharma, N., Lujan-Zilbermann, J. et al. (2018). Revisiting FDA's 1995 guidance on bioequivalence establishment of topical dermatologic corticosteroids: new research based recommendations. *J. Pharm. Pharm. Sci.* 21: 413–428 (www.cspscanada.org).

29 Plan, E., Maloney, A., Mentre, F. et al. (2012). Performance comparison of various maximum likelihood nonlinear mixed-effects estimation methods for dose response models. *AAPS J.* 14 (3): 420–432.

30 Roe, D. (1997). Comparison of population pharmacokinetic modeling methods using simulated data: results from the population modeling workgroup. *Stat. Med.* 16 (11): 1241–1257; discussion 57-62.

31 Bauer, R., Guzy, S., and Ng, C. (2007). A survey of population analysis methods and software for complex pharmacokinetic and pharmacodynamic models with examples. *AAPS J.* 9 (1): E60–E83.

32 Staatz, C. and Tett, S. (2002). Comparison of two population pharmacokinetic programs, NONMEM and P-PHARM, for Tacrolimus. *Eur. J. Clin. Pharmacol.* 58 (9): 597–605.

33 Bennett, J. and Wakefield, J. (1996). A comparison of a Bayesian population method with two methods as implemented in commercially available software. *J. Pharmacokinet. Biopharm.* 24 (4): 403–432.

34 Girard P., Mentré F. A comparison of estimation methods in nonlinear mixed effects models using a blind analysis. PAGE 14 (2005) Abstr 834 (www.page-meeting.org/?abstract=834).

35 Mentré, F. and Gomeni, R. (1995). A two-step iterative algorithm for estimation in nonlinear mixed-effect models with an evaluation in population pharmacokinetics. *J. Biopharm. Stat.* 5 (2): 141–158.

36 McLachlan, A. and Tett, S. (1996). Pharmacokinetics of fluconazole in people with HIV infection: a population analysis. *Br. J. Clin. Pharmacol.* 41 (4): 291–298.

37 Singh, G., Fleischer, N., Lesko, L., and Williams, R. (1998). Evaluation of the proposed FDA pilot dose–response methodology for topical corticosteroid bioequivalence testing. *Pharm. Res.* 15 (1): 4–7.

38 Demana, P., Smith, E., Walker, R. et al. (1997). Evaluation of the proposed FDA pilot dose–response methodology for topical corticosteroid bioequivalence testing. *Pharm. Res.* 14 (3): 303–308.

39 Bonate, P. (2005). Recommended Reading in population pharmacokinetic pharmacodynamics. *AAPS J.* 7 (2): E363–E373.

40 Sheiner, L. and Beal, S. (1983). Evaluation of methods for estimating population pharmacokinetic parameters. III. Monoexponential model: routine clinical pharmacokinetic data. *J. Pharmacokinet. Biopharm.* 11 (3): 303–319.

41 Pershing, L., Corlett, J., Lambert, L., and Poncelet, C. (1994). Circadian activity of topical 0.05% betamethasone dipropionate in human skin in vivo. *J. Invest. Dermatol.* 102: 734–739.

42 Krieger, D., Allen, W., Rizzo, F., and Krieger, H. (1971). Characterization of the normal temporal pattern of plasma corticosteroid levels. *J. Clin. Endocrinol. Metab.* 32: 266–284.

43 Singh, G., Adams, W., Lesko, L. et al. (1999). Bioequivalence methodology for dermatologic corticosteroids based on pharmacodynamic modelling. *Clin. Pharmacol. Ther.* 66: 346–357.

44 EMEA. (1987) Guideline: "Clinical Investigation of Corticosteroids Intended for Use on the Skin (Legislative basis Directive 75/318/EEC EMEA Note for Guidance on the Clinical Investigation of Corticosteroids Intended for Use on the Skin.

45 EMEA. (2006) Questions and Answers on Guideline Title: Clinical Investigation of Corticosteroids Intended for Use on the Skin, CHMP/EWP/21441/2006.

46 Coldman, M., Lockerbie, L., and Laws, E. (1971). The evaluation of several topical corticosteroid preparations in the blanching tesT. *Br. J. Dermatol.* 85: 381–387.

47 Baker, H. and Sattar, H. (1968). The assessment of four new fluocortolone analogues by a modified vasoconstriction assay. *Br. J. Dermatol.* 80: 46–53.
48 Hepburn, D., Aeling, J., and Weston, W. (1996). A reappraisal of topical steroid potency. *Pediatr. Dermatol.* 13 (3): 239–245.
49 Ashworth, J. (1988). Potency classification of topical corticosteroids: modern perspectives. *Acta dermato-venereologica* 151 (Supplementum): 20–25.
50 Oakley, A. (2012). Topical steroids (corticosteroid creams) [Internet] (cited 2012 October 12). http://dermnetnz.org/treatments/topical-steroids.html (accessed 18 December 2020).
51 Green, C., Colquitt, J., Kirby, J. et al. (2004). Clinical and cost-effectiveness of once-daily versus more frequent use of same potency topical corticosteroids for atopic eczema: a systematic review and economic evaluation. *Heal. Technol. Assess. Winch. Engl.* 8 (47): iii, iv, 1–120.
52 Cope, C.L. (ed.) (1972). *Adrenal Steroids and Disease*, 2e, xi–883; illustrated. £l0-00. London: Pitman Medical Publishing.
53 Ference, J. and Last, A. (2009). Choosing topical corticosteroids. *Am. Fam. Physician* 79 (2): 135–140.
54 Brown, G. (ed.) (1981). *British National Formulary*, 277. London: British Medical Association and the Pharmaceutical press.
55 Allenby, C. and Sparkes, C. (1981). Halogenation and topical corticosteroids: a comparison between the 17-butyrate esters of hydrocortisone and clobetasone in ointment bases. *Br. J. Dermatol.* 104 (2): 179–183.
56 Holford, N. and Sheiner, L. (1981). Understanding the dose–effect relationship: clinical application of pharmacokinetic-pharmacodynamic models. *Clin. Pharmacokinet.* 6: 429–453.
57 Bon, C. (2016). *Personal Communication*. Wilmington, NC: Biostudy Solutions LLC.
58 Keida, T., Hayashi, N., and Kawashima, M. (2006). Application of the food and drug administration (FDA) bioequivalent guidance of topical dermatological corticosteroid in yellow-skinned Japanese population: validation study using a chromameter. *J. Dermatol.* 33: 684–691.

6

Topical Delivery: Toward an IVIVC

Sam G. Raney[1] *and Thomas J. Franz*[2]

[1] *Office of Research and Standards, Office of Generic Drugs, U.S. Food and Drug Administration, Silver Spring, MD 20993, USA*
[2] *10716 SE Forest View Lane, Happy Valley, OR 97086, USA*

6.1 Introduction

Our progress in understanding the fundamentals of topical and transdermal drug delivery has benefited immensely from the availability of a simple model system involving ex vivo human skin mounted in diffusion chambers. The demonstration more than 70 years ago that the water barrier of skin "lives on" in the ex vivo state was the foundation on which the initial use of this model was based [1–3]. Those studies helped to not only establish the location of the skin's rate-limiting barrier, the stratum corneum, but also found that (i) the barrier generally remains structurally and functionally intact for many days under in vitro conditions; and (ii) it is generally not damaged by freezing for long periods of time and subsequent thawing. The latter properties contribute to the simplicity and utility of the model and underscore why an in vitro permeation test (IVPT) with excised human skin has become the method of choice for evaluating percutaneous absorption.

6.2 In Vitro–In Vivo Correlation: Validating the Model of Topical Delivery

From its initial use forward, it has generally been accepted that data arising from studies conducted using an IVPT should correlate with those obtained in vivo. However, this assumption was based on early work that was largely of a qualitative, rather than quantitative nature. Enhanced drug absorption through ex vivo skin specimens produced by increased temperature, increased hydration,

Drug Delivery Approaches: Perspectives from Pharmacokinetics and Pharmacodynamics,
First Edition. Edited by Bret Berner, Toufigh Gordi, Heather A. E. Benson, and Michael S. Roberts.

or the application of dimethylsulfoxide was shown to correlate with either an improved clinical response or an increased pharmacodynamic (vasoconstrictor [VC]) response [4, 5]. The sole quantitative evidence that supported the validity of the model was based on the demonstration that the magnitude of outward movement of water through the skin (transepidermal water loss, TEWL) was the same in vitro as in vivo [1].

The earliest systematic attempt to validate the IVPT was that of Franz [6] in which the absorption of 12 organic compounds was measured in vitro and the data compared to those obtained in living humans by Feldmann and Maibach [7]. Both studies were conducted using radioactive compounds and the metric for comparison was total absorption, measured in vitro as the total radioactivity recovered in the receptor solution bathing the underside of the skin over 48 hours, and in vivo as the total radioactivity recovered in the urine over five days, after correcting for incomplete urinary excretion as determined following an intravenous dose of the same compound.

A comparison of the in vitro and in vivo data found a clear, direct relationship between the two. However, the quantitative relationship was not 1 : 1, and with 4 of the 12 compounds (caffeine, hippuric acid, nicotinic acid, and thiourea), there were 4- to 10-fold differences in total absorption between the two data sets. A follow-up study explored reasons for the lack of in vitro–in vivo correlation (IVIVC) in which new in vitro studies as well as new in vivo studies were conducted with the four questionable compounds, and changes were made to both in vitro and in vivo protocols in order to better align and bring them into harmony [8]. Both sets of experiments (in vitro and in vivo) were conducted on abdominal skin using radiolabeled compounds dissolved in acetone and applied at an identical dose (of the compound). The application sites were protected nonocclusively to prevent rub-off (in vivo only), and the skin surface was washed at 24 hours. Moreover, urine collection was extended until the detectable radioactivity approached background levels and was not limited to five days (as had been the case in the first in vivo study). This modification to the in vivo study design was necessary because several compounds in the original study showed significant levels of radioactivity in the fifth day's samples, suggesting an ongoing elimination and an incomplete collection/recovery of the total amount of test compounds absorbed. Thus, although the in vitro study duration was only two days, it was recognized that longer periods of time might be required in vivo to assess the total amount that was absorbed through the skin for some compounds due to slow systemic clearance and elimination.

An excellent IVIVC was found in the new study, and some of the reasons for the discrepancies in the original comparison were identified (Table 6.1). Longer urinary collection times were demonstrated to have been necessary for two compounds in particular, thiourea, and nicotinic acid, for which it took 21 days for the radioactivity in the samples to reach background levels. It was also noted that an incorrect urinary correction factor had been used for nicotinic acid in the original

Table 6.1 Total absorption from an IVIVC study conducted with a harmonized protocol.

Compound	In vitro[a] (% dose)	In vivo[a] (% dose)	# of days (urine collection)
Hippuric acid	1.25 ± 0.5 (4)	1.0 ± 0.4 (6)	3
Nicotinic acid	2.3 ± 0.9 (4)	2.1 ± 0.7 (3)	21
Thiourea	4.6 ± 2.3 (5)	3.7 ± 1.3 (4)	21
Caffeine	24.1 ± 7.8 (4)	22.1 ± 15.8 (4)	7

a) Mean ± SD (# of subjects or donors).

study. It had been assumed that nicotinic acid followed the same excretory pattern as nicotinamide, for which 90% of the radioactivity was excreted in the urine. In fact, it was found that only 15% of ^{14}C-nicotinic acid was excreted in the urine following intravenous administration in the rhesus monkey [6]. Regional variation (forearm vs. abdomen) undoubtedly also contributed to some of the differences noted in the first study.

Similar problems (i.e. differences between in vitro and in vivo protocols) were noted by Lehman et al. [9] when surveying the literature to collect absorption data on all compounds for which both in vitro and in vivo data were available. Out of a total of 92 data sets representing 30 separate compounds, only 11 sets could be found where the protocols were reasonably the same. The major differences included (i) anatomical site, (ii) composition of vehicle, (iii) test compound dose, (iv) vehicle dose, and (v) length of exposure/wash time. Using total absorption as the metric for comparison, expressed as percent of applied dose, they found a clear tendency for the data to follow the line of perfect 1 : 1 correlation when all data sets were included (Figure 6.1). However, IVIVC was distinctly better with the harmonized data set (Figure 6.2). When all data were included (including those from unharmonized in vitro and in vivo studies) the average in vitro–in vivo (IVIV) ratio was only 1.6, but the difference in the amount of any individual compound that was absorbed in vitro vs. in vivo could be as high as 20-fold (the range of IVIV ratios was 0.18–19.7). Not only was the average IVIV ratio of 0.96 almost perfect with the harmonized data set, but strikingly, the mean in vitro and mean in vivo amount absorbed of any compound was now be less than twofold different (the range of IVIV ratios was 0.58–1.28). This was a remarkably good IVIVC for the 11 harmonized data sets, particularly considering the fact that bioequivalence (BE) limits for a study of sufficient size to have adequate statistical power is 0.80–1.25.

The analysis made it very clear that in vitro data obtained from IVPT studies would closely replicate in vivo data in humans when the in vitro and in vivo study protocols are well matched. Although the magnitude of the error introduced by small deviations between protocols in past studies is impossible to assess, the two most common discrepancies in the in vitro vs. in vivo protocol conditions, which led us to exclude 81 of the 92 data sets from the harmonized set of studies was (i)

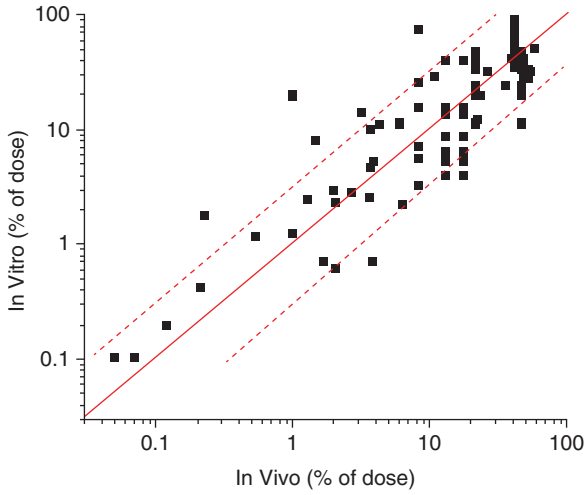

Figure 6.1 IVIV ratios of total absorption for all 92 data sets plotted on log–log scale. Solid line represents the ideal one-to-one correlation and dashed lines represent ±3-fold difference from ideal. The IVIV ratios ranged from 0.18 to 19.7 with an overall mean of 1.6.

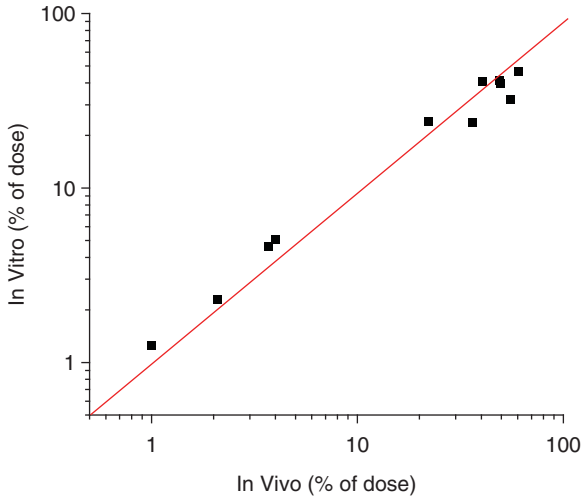

Figure 6.2 IVIV ratios of total absorption for 11 fully harmonized data sets plotted on log–log scale. Line represents the ideal one-to-one correlation. The IVIV ratios ranged from 0.58 to 1.28 with an overall mean of 0.96.

the use of skin from different body sites and (ii) formulation differences; either a compositional difference or a difference in the dose applied. Both are factors that have been well documented as having a great impact on the absorption process.

6.3 In Vitro–In Vivo Correlation: Transdermal Delivery

Additional evidence supporting the validity of the excised skin model comes from the field of transdermal drug delivery, in which measuring the absorption of various prototype formulations of the active pharmaceutical ingredient (API)

is an essential part of the product development process. Since the development of transdermal dosage forms for any given drug generally follows after the development of other dosage forms, the steady-state therapeutic blood concentration (C_{ss}) and systemic clearance (Cl_s) are already known and it is only necessary to find a formulation with a sufficient steady-state flux (analogous to a constant intravenous infusion rate) to achieve the necessary C_{ss}.

$$J_{ss} \times A = C_{ss} \times Cl_s \tag{6.1}$$

where

J_{ss} = steady state flux through skin;
C_{ss} = steady state blood concentration;
Cl_s = systemic clearance;
A = skin application area.

As the screening of multiple prototype formulations can be relatively easily accomplished using the in vitro model, the lengthy process of formulation development is greatly simplified, obviating the need to conduct trial-and-error clinical studies. The utility of this strategy was initially demonstrated by the Alza Corporation during the development of the first transdermal product (Transderm-Scop®) and led them to the conclusion that the in vitro data accurately predicted the in vivo results [10]. Additional studies of transdermal products have also found excellent correlation between in vitro data and that obtained in vivo for several drugs including nitroglycerin [11], ketorolac acid [12], selegiline [13], and estradiol [14].

One striking example of the excellent IVIVC found during the development of two transdermal products, testosterone (Androderm®) and estradiol (Alora®), is that reported by Srinivasan [15] (erroneously ascribed to Venkateschwaran in prior citations [16, 17]). When expressed as average cumulative absorption, the in vitro rate of absorption profiles closely matched those obtained in vivo by measuring the rate of drug loss from the transdermal delivery system (TDS)/patch (Figure 6.3). The difference between in vitro and in vivo results noted for estradiol after 48 hours occurred because the TDS/patch was larger than the chamber used in the in vitro study. Only 67% of the total patch area was in contact with the skin, and this resulted in a slower rate of drug depletion from the patch in vitro than that which would occur in vivo. Consequently, the steady-state rate of absorption in vitro was maintained for a longer period of time.

6.4 In Vitro–In Vivo Correlation: Bioavailability and Bioequivalence

The long history of using excised human skin as a widely accepted in vitro model for the study of percutaneous absorption has logically led to its consideration as

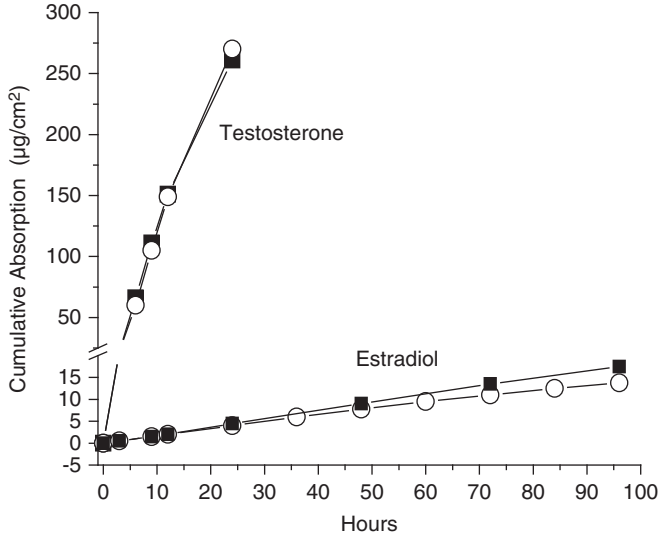

Figure 6.3 Comparison of the rate of absorption of estradiol and testosterone from separate transdermal systems as measured in vitro (filled square, excised skin) and in vivo (open circle, human subjects). The in vivo rate was determined by measuring drug loss from the patch. Source: Redrawn from Srinivasan [15].

a surrogate for comparative clinical endpoint studies or human pharmacokinetic studies in determining the bioavailability (BA) and BE of topical drug products. The rationale for this use is quite obvious since it provides an exceptionally efficient means by which to measure the rate and extent of absorption of the API at or near the site of action in the skin under well-controlled laboratory conditions. Whereas the prior sections focused on IVIVC from the perspective of percutaneous absorption, this section examines data correlating conclusions about the relative BA/BE of test and reference products based upon IVPT results with the corresponding conclusions about the relative BA/BE of those same products based upon clinical results.

A prime attribute of the IVPT model with excised human skin that strongly supports its use as a surrogate for comparative clinical endpoint BE studies is its sensitivity to changes in the composition of the vehicle. An example of this is illustrated by the process used in the development of a generic ketoconazole cream [16]. In that instance, reverse engineering was not able to accurately determine the concentration of two cosolvents in the reference product. So a series of prototype formulations were prepared by the generic manufacturer in which the concentration of the cosolvents were varied, and ketoconazole absorption from each was compared head-to-head with the reference product. The first series of prototype

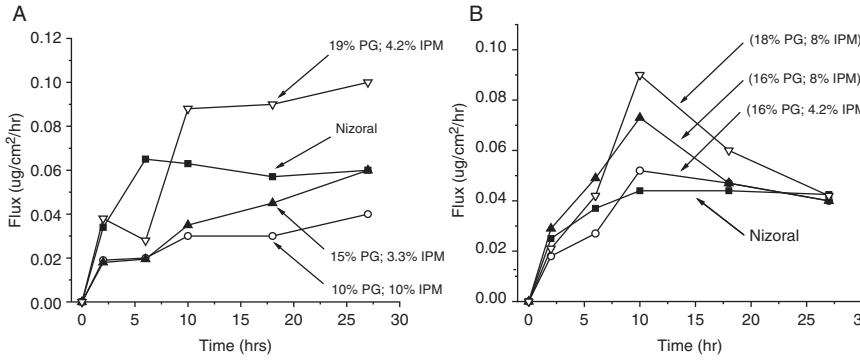

Figure 6.4 Comparison of in vitro rate of absorption profiles of prototype formulations of ketoconazole, with varying levels of propylene glycol (PG) and isopropyl myristate (IPM), to determine which best matches the reference product (Nizoral). (a) None of the first three prototype formulations tested match the reference product. (b) One formulation from the second group of three prototype formulations closely approximated the reference product.

formulations were unsuccessful in matching the BA of the reference product, but the data obtained suggested that BA was largely controlled by the propylene glycol (PG) concentration, and this led to the preparation of additional prototype formulations in which the PG concentration was varied between 16% and 18%. This time the absorption profile of one prototype formulation did match that of the reference product (Figure 6.4). A test product with this prototype formulation was subsequently shown by a comparative clinical endpoint study to be bioequivalent to the reference product and approved by the US Food and Drug Administration (FDA) as therapeutically equivalent to the reference product.

In a similar manner, the IVPT model with excised human skin has been used to assure in vivo BE (based upon the results of an IVPT study) for a test product compared to its reference product by evaluating a number of prototype formulations, prior to conducting the pivotal comparative clinical endpoint BE study. Franz et al. [17] evaluated the absorption of the API from seven prospective generic drug products during their preclinical development (two tretinoin gels and five glucocorticoid formulations) and compared it to that of the reference products in side-by-side IVPT studies. The test products were later evaluated either by a comparative clinical endpoint BE study (tretinoin) or by a VC assay in humans (glucocorticoids), and all the prospective generic products were confirmed to be bioequivalent to their respective reference products and subsequently approved by the FDA.

The in vitro tretinoin product comparisons were designed as a simulated BE study with a sufficient number of replicate skin specimens evaluated to calculate confidence intervals as recommended by the FDA. Both test products (0.01% gel,

Table 6.2 Comparison of primary endpoints for test and reference tretinoin gels.

	Test	Reference	Test/Reference	90% CI
	0.01% tretinoin gel			
Total absorbed	2.9961	2.9742	1.022 66	97.07, 107.46
J_{max}	0.5492	0.5716	1.037 89	92.53, 115.05
T_{max}	3.5957	3.5726	1.043 00	92.23, 116.37
	0.025% tretinoin gel			
Total absorbed	3.4921	3.4709	1.027 98	95.14, 110.45
J_{max}	0.9058	0.8840	1.114 81	95.08, 127.88
T_{max}	3.6642	3.7248	0.983 89	97.26, 99.52

Statistical analysis was based on natural log transformed data. The estimated error standard deviation was used to compute the 90% confidence intervals for the ratios of the means (test/reference) of the listed parameters.

0.025% gel) were estimated to be bioequivalent to the corresponding strength of the reference product, Retin-A® based upon IVPT studies (Table 6.2). The 90% confidence interval was within the required interval (80–125%) for all three primary endpoints with 0.01% tretinoin gel and for two of three primary endpoints with 0.025% tretinoin gel; the third endpoint (maximum flux) just slightly exceeded the BE limits in vitro (95.1–127.9%).

The in vitro glucocorticoid data were also in agreement with the clinical study data recommended to support FDA approval (i.e. a VC assay in humans) and found the test products to be equivalent to the reference products in four of five cases, with test:reference ratios ranging from 0.96 to 1.14 (Table 6.3). The sole exception, mometasone furoate ointment, was found to have a test:reference ratio of only 0.63 in vitro. Yet, by a VC assay in humans, the generic formulation was found to be bioequivalent to the reference product. This single discrepancy was not necessarily due to a failure of the in vitro method to correlate with or be predictive of in vivo BA/BE, but rather, likely a result of the greater sensitivity of the IVPT method to detect differences in BA/BE between products. Evidence supporting the greater sensitivity of the IVPT method relative to in vivo methods can be seen in the alclometasone data in Table 6.3. Alclometasone dipropionate absorption is approximately 15 times greater from the ointment product than the cream product. However, there is no difference in their potency as assessed by a VC assay in humans. Equivalence of the cream and ointment products in this VC assay has also been noted by Stoughton [18].

The observation that an IVPT study appears to be more sensitive than the VC assay in humans at discriminating differences in the relative BA/BE of test and

Table 6.3 In vitro–in vivo comparison of five generic glucocorticoid test products vs. the corresponding reference (Ref) products.

	In vitro absorption[a] ($ng/cm^2/48\,h$)			In vivo VC assay[a] ($-AUEC_{0-24\,h}$)		
	Test	Ref	Test/Ref	Test	Ref	Test/Ref
Alclometasone cream	4.52	4.39	1.03	18.5	16.8	1.10
Alclometasone ointment	66.95	70.0	0.96	16.0	17.4	0.92
Halcinonide cream	110.4	96.9[b]	1.14	33.1	30.7	1.08
Halcinonide ointment	246.7	256.4	0.96	28.6	28.5	1.00
Mometasone ointment	213.4	338.7	0.63	13.7	12.3	1.11

a) Listed numbers are mean values.
b) Average of three reference product lots, none of which were used in the VC study. In all other comparisons identical lots of test and reference products were used in both the in vitro and in vivo studies.

reference products is highly significant, and other examples exist to support this conclusion. For example, as part of a program to develop a more efficacious topical formulation of betamethasone valerate, a new and innovative thermolabile foam formulation of the drug was developed and compared to a traditional lotion formulation in the treatment of scalp psoriasis. An IVPT study found a threefold greater rate of absorption of the drug from the foam formulation than the marketed lotion product, and this produced a highly significant 50% increase in therapeutic efficacy at the end of a 28-day treatment period [19]. However, when the two products were compared by a VC assay in humans, no difference in potency was found [20].

Another study comparing the sensitivity of an IVPT study to the VC assay in humans obtained similar results. The relative BA of five topical clobetasol propionate products was assessed using both, in vitro and in vivo methods [21]. The IVPT study found total clobetasol absorption to vary 10-fold between the two products with the highest and lowest BA, whereas the VC assay in humans found the difference between the same two products to be less than twofold. The coefficient of variation ranged from 78% to 126% in the VC assay, but ranged from only 30% to 43% for the IVPT study. Statistically, the IVPT study could separate the five products into three groups: (i) ointment; (ii) cream and gel; and (iii) emollient cream and solution. However, due to its greater variability as well as saturation of the pharmacodynamic response at higher flux levels, the VC assay found all products except the solution to be equipotent.

6.5 Summary

A substantial body of data now exists demonstrating that the in vitro measurement of percutaneous absorption using an IVPT with excised human skin is a valid method by which to predict in vivo absorption in humans. Studies specifically designed to quantify the relationship between in vitro and in vivo data have shown an excellent IVIVC when the critical protocol parameters (study conditions) under which in vitro studies are performed are appropriately controlled so that they adequately duplicate in vivo conditions. Two protocol parameters that are critical for a good IVIVC are the use of skin from the same body sites in vitro and in vivo, and the use of the same prototype formulations or products in vitro and in vivo.

A comparison of IVPT data with that obtained from clinical endpoint studies as well as a VC assay in humans also support the validity of the excised skin model by demonstrating the typical accuracy of predictions obtained in vitro with those obtained by clinical evaluation. The results of several prospective studies, in which a number of test and reference products were shown to have equivalent BA in an IVPT study, have all been validated when subsequent clinical testing found the test and reference products to be bioequivalent in vivo. Taken collectively, the conclusion of a large number of studies is that data obtained in the IVPT model with excised human skin consistently and accurately correlated with and was predictive of relative BA/BE in vivo in humans, whether the comparator endpoint is a rigorous quantifiable metric such as total absorption or a clinical outcome (endpoint) such as the VC score, discussed in Chapter 5, or therapeutic efficacy.

Disclaimer

The views expressed in this chapter do not reflect the official policies of the Department of Health and Human Services; nor does any mention of trade names, commercial practices, or organization imply endorsement by the US government.

References

1 Winsor, T. and Burch, G.E. (1944). Differential roles of layers of human epigastric skin on diffusion rate of water. *Arch. Intern. Med.* 74: 428–436.
2 Burch, G.E. and Winsor, T. (1944). Rate of insensible perspiration (diffusion of water) locally through living and through dead skin. *Arch. Intern. Med.* 74: 437–444.
3 Burch, G.E. and Winsor, T. (1946). Diffusion of water through dead plantar, palmar and torsal human skin and through toe nails. *Arch. Derm. Syphilol.* 53: 39–41.

4 Fritsch, W.C. and Stoughton, R.B. (1963). The effect of temperature and humidity on the penetration of C^{14} acetylsalicylic acid in excised human skin. *J. Invest. Dermatol.* 41: 307–311.

5 Stoughton, R.B. and Fritsch, W. (1964). Influence of dimethylsulfoxide (DMSO) on human percutaneous absorption. *Arch. Dermatol.* 90: 512–517.

6 Franz, T.J. (1975). Percutaneous absorption on the relevance of in vitro data. *J. Invest. Dermatol.* 64 (3): 190–195.

7 Feldmann, R.J. and Maibach, H.I. (1970). Absorption of some organic compounds through the skin in man. *J. Invest. Dermatol.* 54: 399–404.

8 Franz, T.J. (1978). The finite dose technique as a valid in vitro model for the study of percutaneous absorption in man. *Curr. Probl. Dermatol.* 7: 58–68.

9 Lehman, P.A., Raney, S.G., and Franz, T.J. (2011). Percutaneous absorption in man: in vitro–in vivo correlation. *Skin Pharmacol. Physiol.* 24: 224–230.

10 Shaw, J.E., Chandrasekaran, S.K., Michaels, A.S., and Taskovich, I. (1975). Controlled transdermal derlivery, in vitro and in vivo. In: *Animal Models in Dermatology* (ed. H.I. Maibach), 138–146. New York: Churchill-Livingstone.

11 Hadgraft, J., Beutner, D., and Wolff, H.M. (1993). In vivo–in vitro comparison in the transdermal delivery of nitroglycerin. *Int. J. Pharm.* 89: R1–R4.

12 Roy, S.D., Manoukian, E., and Combs, D. (1995). Absorption of transdermally delivered ketorolac acid in humans. *J. Pharm. Sci.* 84: 49–52.

13 Rohatagi, S., Barrett, J.S., McDonald, L.J. et al. (1997). Selegiline percutaneous absorption in various species and metabolism by human skin. *Pharm. Res.* 14: 50–55.

14 Rohr, U.D., Altenburger, R., and Kissel, T. (1998). Pharmacokinetics of the transdermal reservoir membrane system delivering beta-estradiol: in vitro/in vivo-correlation. *Pharm. Res.* 15: 877–882.

15 Srinivasan, V. (1997). In vitro–in vivo correlation for transdermal delivery. In: *IBC International Conference on Transdermal Drug Delivery*, 15–16. Coronado, CA, 12–13 December.

16 Franz, T.J., Lehman, P.A., and Raney, S.G. (2008). The cadaver skin absorption model and the drug development process. *Pharmacopeial Forum.* 34: 1349–1356.

17 Franz, T.J., Lehman, P.A., and Raney, S.G. (2009). Use of excised human skin to assess the bioequivalence of topical products. *Skin Pharmacol. Physiol.* 22: 276–286.

18 Stoughton, R.B. (1992). Vasoconstricto assay – specific applications. In: *Topical Corticosteroids* (eds. H.I. Maibach and C. Surber), 42–53. Basel: S. Karger.

19 Franz, T.J., Parsell, D.A., Halualani, R.M. et al. (1999). Betamethasone valerate foam 0.12%: a novel vehicle with enhanced delivery and efficacy. *Int. J. Dermatol.* 38: 628–632.

20 FDA, CDER (1999). Summary Basis of Approval, NDA 20-934, Luxiq (Betamethasone Valerate) Foam, Clinical Pharmacology and Biopharmaceutics Review. Rockville, MD. http://www.accessdata.fda.gov/drugsatfda_docs/nda/99/20934.cfm (accessed 18 December 2020).

21 Lehman, P.A. and Franz, T.J. (2014). Assessing topical bioavailability and bioequivalence: a comparison of the in vitro permeation test and the vasoconstrictor assay. *Pharm. Res.* 3: 3529–3537.

7

Integrated Transdermal Drug Delivery and Pharmacokinetics in Development

Bret Berner[1] *and Gregory M. Kochak*[2]

[1] *Consultant, 4011 54 Ave SW, Seattle, WA, USA*
[2] *Kochak Consulting, 647 Woody Drive, Auburn, AL, USA*

7.1 Introduction

Transdermal delivery has enabled a steady trickle of novel controlled-release drug products over more than three decades. Patches have significant advantages over the more traditional oral delivery route in terms of avoiding first-pass metabolism, circumventing potentially saturable transporters, providing the capability of maintaining nearly constant delivery for up to one week, and easy termination of dosing by removal of a patch. Successful development of a transdermal product is encumbered by selection of a suitable drug that is both highly potent and sufficiently permeable through skin as a result of relatively low molecular weight and good oil solubility of the drug. Moreover, the drug must have an acceptable level of skin irritation and sensitization. Design of a transdermal system involves achieving the desired skin permeation to achieve a target plasma concentration associated with either a known therapeutic dose or a pharmacodynamic effect.

This chapter reviews the fundamentals of skin structure, skin permeation, pharmacokinetics of delivery through skin, and practical aspects of patch development, and emphasizes deconvolution as a method to determine and compare in vitro and in vivo absorption. Over the past two decades, a number of active technologies that can achieve greater permeation and temporally varying delivery have been developed. These active technologies rely on the combination of devices with transdermal delivery to improve permeation. The cost of the various devices must justify the added therapeutic benefit provided by this active patch. These new technologies and some resulting products are briefly reviewed.

Drug Delivery Approaches: Perspectives from Pharmacokinetics and Pharmacodynamics,
First Edition. Edited by Bret Berner, Toufigh Gordi, Heather A. E. Benson, and Michael S. Roberts.

7.2 Fundamentals of Transdermal Delivery

7.2.1 Architecture of Skin

The large accessible surface area and the chemical protective barrier properties of the multilayer organ, skin, provide the unique advantages and limitations of transdermal delivery. Skin architecture has been extensively reviewed [1, 2]. The three layers of skin from internal to external are the dermis, the viable epidermis, and the stratum corneum.

The dermis, which ranges from 1 mm in thickness on the scalp to 4 mm on the back, constitutes the bulk of the skin and is comprised mostly of the fibrous protein, collagen, that provides the dermis with its tensile strength. Elastin, a second fibrous protein, is located as networks between the bundles of collagen and returns skin to its normal structure after deformation. The elastin and collagen are located in a mixture of anionic polysaccharides, chondroitin 4-sulfate, dermatin sulfate, and heparin, and this carbohydrate mixture contains the fibroblasts that synthesize and lay down these fibrous proteins and carbohydrates.

Arteries are located just below the dermis and increasingly smaller blood vessels penetrate throughout the dermis up to the most external convoluted portion of the dermis and the dermal–epidermal junction, a basement membrane that attaches and supports the epidermal membrane and filters the flow of macromolecules across the junction. Drugs permeating through skin for systemic delivery must diffuse through the epidermis to the blood vessels in the upper dermis.

In addition to the small blood vessels residing within the dermis, hair, sweat glands, and sebaceous glands form shunt pathways from the dermis to the surface of the skin. These shunt pathways may be important for polar transport, such as with iontophoresis, and in general, may be important for early transient transport through skin in topical or transdermal delivery [3, 4].

The epidermis, which is composed of keratinocytes, keratin-containing cells, is a thin sheet approximately 70–150 μm thick covering the body except as a much thicker layer on the palms and soles. Epidermal keratinocytes initiate from the basal cells, ovoid cells that are attached to the basal laminate and produce the daughter cells, some of which rapidly differentiate and mature as they migrate through the epidermis to the surface of the stratum corneum, where about one layer of keratinocytes is shed each day. As the epidermal cells migrate from the basal cells through the spinous layer, they lose the ability to divide and begin to flatten. Fibrils are aggregates formed from the keratin filaments, and these intracellular fibrils connect to desmosomes on the cell surface. In the granular layer, keratinocytes lose the organelles, and membrane-coating granules are secreted into the intercellular space. In the cell membrane, the protein, involucrin, is synthesized and eventually becomes the stratum corneum cell envelope.

While the phospholipid content of the cell membrane substantially decreases, the ceramide, sterol, and fatty acid content increases greatly.

There are other types of cells in the epidermis that can be important in understanding local adverse skin reactions. The dendrites of the Langerhans cells extend through the epidermis and are critical in skin immunology including skin contact allergy. When skin is damaged, neutrophils, macrophages, and lymphocytes, that are associated with destruction and removal of debris with inflammation or skin irritation, are present in the epidermis.

In the stratum corneum, there is a sharp transition to flat hexagonal elongated cells, about 1 μm thick. The stratum corneum is a multi-laminate consisting of 15–20 flattened keratinocyte cell layers. This cell shape seems almost ideally designed for barrier and mechanical properties with the cells forming layers with the protein fibrils of keratin and filaggrin attached to desmosomes acting as bridges between cells. Although present in the deeper stratum corneum, filaggrin is absent in the upper stratum corneum. The cell envelope forms an excellent barrier with the structure determined by the cross-linked protein. About 30% by volume of the stratum corneum is constituted by lipids in the cell envelopes and the intercellular space [5]. Phospholipids are essentially absent in the stratum corneum, and the lipids consist mainly of sterols, ceramides, and fatty acids [6].

There is a water gradient across stratum corneum [3] with the viable epidermis being essentially fully hydrated at close to unit thermodynamic activity. The outer surface is maintained at ambient relative humidity and a temperature of approximately 32 °C. The flux of water across skin, transepidermal water loss, is readily measured in vitro or in vivo, and is one method of determining the integrity of skin in permeation studies [7, 8]. Water serves as a plasticizer for keratins and skin, and at low relative humidity, the stratum corneum can dry and crack. Hydration is also important to increase the rate of skin permeation [3].

At the outer surface of stratum corneum, the cells are desquamated generally in clusters with a stratum corneum turnover time of two to three weeks. Cell cohesion weakens near the outer surface, and the partly detached stratum corneum cells are referred to as the stratum disjunctum. For topical delivery, this region is important both for establishing the skin reservoir of precipitated drug and also for loss of drug with shed skin in accounting for mass balance.

There are three regions by which drugs can penetrate stratum corneum: through the intercellular lipids; through skin appendages; and through the keratin bundles in the stratum corneum (SC) [9].

7.2.2 Skin Permeation and Transdermal Delivery

In an in vitro skin permeation experiment, isolated skin, preferably either isolated human epidermis or stratum corneum, is mounted in a diffusion cell

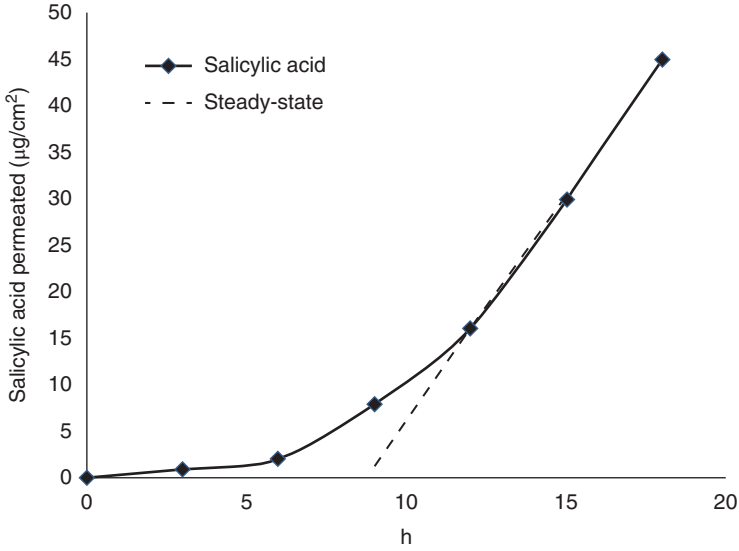

Figure 7.1 Amount of salicylic acid (1%) w/v transported across isolated human epidermis from propylene glycol with oleic acid.

between the donor solution with the drug or a portion of a transdermal patch and the aqueous receiver solution in which the drug is appropriately soluble. The amount of drug permeating through the skin, Q, is then measured over time [10]. Assuming there is no significant depletion of the permeating drug and that the skin is not damaged by the drug or a solvent, at long times J, the flux or amount transported/cm^2-h, becomes a constant known as the steady-state-flux, $J_{s,}$ and Q is linear with time (Figure 7.1). Q, represented by the terminal asymptotic region, is the steady-state region as shown for 1% salicylic acid penetrating human epidermis from the enhancing cosolvents of propylene glycol and oleic acid [11]. Q obeys the asymptotic equation:

$$Q = A \cdot J_s \left(t - t_L\right) \tag{7.1}$$

where A is the area, t is time, and t_L is the time lag or the extrapolated time intercept of the steady-state line. J_s is the most important parameter determined in skin permeation and is often directly related to delivery in vivo. t_L is short for salicylic acid, but for permeants of higher molecular weight may be closer to 12–24 hours. Analysis of Q, the cumulative amount, reduces the variability over time of in vitro skin permeation data and allows trends to be most easily observed. Analysis of the flux vs. time presents skin permeation data in its most variable form, but allows careful study of variation with time, approach to steady state, and depletion of drug.

A fundamental thermodynamic relationship between the chemical potential, μ, and the chemical activity, a, is

$$\mu = \mu^{\circ} + RT \cdot \ln(a) \tag{7.2}$$

where μ° is chosen to be the reference chemical potential of the pure solid or a saturated solution, R is the gas constant, and T is absolute temperature. The gradient in chemical potential or activity across the skin membrane is the driving force for transport [12]. Activity is the product of the activity coefficient and concentration, and for skin permeation, the most useful approach is to select the pure solid as the reference chemical potential, and therefore, to a first approximation, the activity coefficient is the reciprocal of the solubility. Then the activity is the fraction of solubility, and the flux may be written as a function of activity as follows:

$$J = -\left(\frac{D \cdot C}{a}\right) \cdot \frac{\partial a}{\partial x} \tag{7.3}$$

where D is the diffusion coefficient, C is the concentration, and x is the distance across the stratum corneum. The activity gradient and not just the concentration gradient is the driving force for transport. Since the solubility is inversely related to the activity, this is critical in comparing permeation from a series of solvents or for a homologous series of permeants. For example, the amounts of salicylic acid transported across stratum corneum from saturated aqueous solution (0.2% w/v) as compared to saturated propylene glycol (20% w/v) were not statistically different. For transdermal delivery, the effectiveness of a penetration enhancer is judged by comparing the flux from different compositions at constant activity and usually from saturated solutions. In addition, minimizing the amount of residual drug in used patches has been requested by regulatory officials. Therefore, knowledge of solubility and activity in the patch is needed.

The simplest case is an ideal membrane that is homogeneous, not influenced by the drug or vehicle, and where the solubility and diffusion constant are constant [10]. In this ideal case,

$$J_{\mathrm{s}} = \frac{D \cdot K \cdot C_{\mathrm{v}}}{l} \tag{7.4}$$

where l is the stratum corneum thickness, C_{v} is the concentration in the vehicle, and K is the partition coefficient between the stratum corneum and the vehicle defined as

$$K = \frac{C_{\mathrm{s}}}{C_{\mathrm{v}}} \tag{7.5}$$

C_{s} is the concentration in the stratum corneum. The steady-state flux is then a predictor of the rate of drug delivery across skin to the systemic circulation in vivo, and the product, KC_{v}, is proportional to the amount in the stratum corneum in vitro (divided by 2 at steady-state for an ideal membrane) and a predictor of the

residual drug reservoir left in skin in vivo after removal of a patch. For this ideal membrane, the time lag is inversely related to the diffusion constant as follows:

$$t_L = \frac{l^2}{6D} \tag{7.6}$$

The time lag is a measure of the time to achieve steady-state delivery.

The steady-state flux, J_s, is the primary derived quantity for in vitro skin permeation, and for determining the feasibility of transdermal delivery. Since adequate flux across stratum corneum is critical to transdermal feasibility, it is useful to consider the key physical properties of any permeant to enable skin penetration. Since the greatest flux from any vehicle or patch is from a saturated solution or patch, and saturation is the appropriate thermodynamic reference state, Eq. (8.4) for the maximum flux of drug from a given vehicle or patch across stratum corneum may be stated as follows:

$$J_s = \frac{D \cdot S}{l} \tag{7.7}$$

where S is the solubility of drug in stratum corneum.

Most biological permeation studies are performed at constant concentration, and when skin permeation is conducted in this manner, it can lead to fallacious interpretation. At constant concentration, the permeability, P, by this biological definition equals the flux, J, divided by the concentration gradient, which for nearly zero concentration on the receptor side approximately equals the donor concentration. While flux is directly the measurement of interest, permeability is a convoluted variable that is a mixture of a kinetic variable (diffusion coefficient), a physiological parameter (membrane thickness), and an equilibrium variable (partition coefficient defined in Eq. (7.5)). This partition coefficient is a measure not only of the membrane property of the solubility of the drug in the membrane but also confounds interpretation by including how much the drug likes the vehicle. When skin permeation from two vehicles is compared at constant concentration, it may falsely be concluded that the vehicle showing the greater permeability is an enhancer. The drug may just be less soluble in that vehicle. As stated earlier, an enhancer may be judged by comparing skin permeation from saturated solutions.

Species differences in transdermal permeation or site of application differences within a species may be due mainly to variations in skin thickness, the composition of intercellular stratum corneum lipids, and in the number of skin shafts. The amount of free fatty acids and triglycerides and the density of hair follicles are important factors causing differences between skin barriers among species [5, 13]. Artificial lipid impregnated membranes have been designed to chemically mimic biological membranes but lack their regional organization. However, they have been reported to strongly correlate with human cadaver skin for a number of drug molecules (Strat-M™ product literature, EMD Millipore Corp., Billerica, MA). Human skin is the only proven relevant biological membrane. Porcine skin is widely available and often encountered in transdermal drug development. In

particular, pig ear skin is relatively free of coarse hair follicles and easy to prepare. Porcine skin has been shown to resemble the histology, thickness of stratum corneum, and biochemistry of human skin [14, 15].

In a comparative study of human, domestic pig, minipig, rat, and two tissue-culture based human skin equivalents (Graftskin LSE™ (Apligraf), Organogenesis, Inc., Canton, MA and RHE (reconstituted human epidermis), SkinEthic, Nice, France), the percutaneous flux of four drugs with diverse polarities was determined in a Franz-type diffusion cell at 48 hours [16]. All were applied superficially as a 1% solution in propylene glycol or propylene glycol/water. In another study [17], the apparent permeability coefficient was determined for theophylline, sodium diclofenac, and benzoic acid in a similar diffusion cell at 37 °C. Note that actual skin temperature is 32 °C and may only approach 37 °C under complete occlusion. Permeation rates are given in Table 7.1.

Table 7.1 Different skin permeation rates in static Franz-type diffusion cells.

From Ref. [16]	Flux (μg/cm²/h)			
	Terbinafine	Clotrimazole	Hydrocortisone	Salicylic acid
Human	<0.01	0.02 ± 0.01	0.023 ± 0.007	21.9 ± 1.8
Domestic pig	0.010 ± 0.004	0.02 ± 0.01	0.011 ± 0.009	12.7 ± 0.5
Minipig	0.011 ± 0.005	0.02 ± 0.01	0.010 ± 0.03	9.6 ± 2.1
Rat	0.55 ± 0.21	0.055 ± 0.027	1.16 ± 0.73	24.2 ± 9.0
Graftskin™ LSE	0.28 ± 0.21	20.4 ± 3.1	4.86 ± 0.07	45.5 ± 15.7
RHE SkinEthic	0.37 ± 0.02	18.8 ± 2.7	5.29 ± 0.09	152.8 ± 15.7

From Ref. [17]	Permeability coefficient (mm/h)		
	Theophylline	Sodium diclofenac	Benzoic acid
Nude mice skin	0.041 ± 0.021	0.043 ± 0.011	0.978 ± 0.209
Sprague–Dawley rat skin	0.017 ± 0.002	0.063 ± 0.001	0.935 ± 0.140
Porcine skin	0.018 ± 0.006	0.138 ± 0.031	0.299 ± 0.076
Human prepuce skin	0.016 ± 0.010	0.056 ± 0.008	0.843 ± 0.144
Human thigh skin	0.016 ± 0.009	0.009 ± 0.008	0.666 ± 0.156

Similar permeation rates were observed between human and porcine skin for the hydrophobic drugs terbinafine, clotrimazole, and hydrocortisone, while the hydrophilic molecule salicylic acid showed better correspondence between human and rat skin. The permeability coefficients of sodium diclofenac and benzoic acid also showed better correspondence between rat and human skin. Other studies have also demonstrated the similarities between human and porcine skin for hydrophobic molecules, and between human and rat skin regarding hydrophilic molecules [9]. The veracity of this conclusion needs further testing. The obvious differences in skin thickness, lipids, and density and structure of hair follicles predict these differences. Only for iontophoretic delivery where the use of constant current through pores ensures comparability of rat and human skin is this model relevant. Microneedles may also use a rat model, but it is not usually appropriate for passive skin permeation.

To predict the steady-state flux through human stratum corneum as shown in Eq. (7.8), it is instructive to examine the dependence of solubility and diffusion coefficient on the physicochemical properties of the permeants. Since many drugs are lipophilic and permeate skin by dissolving in a portion of the lipid matrix, ideal solution theory should be a reasonable approximation. X_s, the mole fraction solubility of the drug in stratum corneum, is given by [18, 19]

$$X_s = e^{\left[\Delta H_f (T - T_m)/R \cdot T \cdot T_m\right]} \tag{7.8}$$

where ΔH_f is the heat of fusion, R is the gas constant, T is the absolute temperature, and T_m is the melting point. Using approximations developed by Yalkowsky for solubility in water [18], expressions can be developed for rigid aromatics and for flexible chains that depend only on T_m as a measure of the crystalline lattice energy of the drug. In particular, for rigid aromatics [18],

$$X_s = e^{\left[6.79\left(1 - \frac{T_m}{T}\right)\right]} \tag{7.9}$$

For rigid molecules, diffusion according to free volume theory [20] depends on the size of the hole established in the fluid for a diffusional jump, and to a first approximation, this energy is related to the product of the surface tension and the molecular surface area. Using this approach, the diffusion constant may be expressed as

$$D = D_0 e^{-a \cdot M} \tag{7.10}$$

where D_0 and a are constants and M is the molecular weight of the drug.

Based on Eq. (7.7), the predicted flux is the product of D and X_s and large fluxes across stratum corneum should be correlated with small M and low T_m. Quantitative structure-permeation relationships have been explored for these two variables and others [21–23]. The Potts and Guy equation [21] relates the skin permeability, P expressed in cm/s, to the molecular weight, M, and octanol–water partition

coefficient, K_{oct}, through Eq. (7.11),

$$Log\,P = 6.3 + 0.71 \cdot \log\left(K_{oct}\right) - 0.0061 \cdot M \tag{7.11}$$

To calculate the predicted steady-state flux from Eq. (7.11), P must be multiplied by the solubility in water. During early drug discovery where the melting point may be unknown, Eq. (7.11) can be particularly helpful.

Skin permeation enhancers [24, 25] are used in transdermal formulations to increase the flux and enable the delivery of adequate therapeutic amounts from a patch of smaller, practical surface area. As can be seen from Eq. (7.8) for the steady-state flux, an enhancer must alter the diffusion constant or solubility of the drug in the stratum corneum. The test for an enhancer is to demonstrate an increase in flux from a saturated transdermal patch by the addition of the enhancer. For any patch, it is important to establish the solubility of the drug in the reservoir or in the adhesive matrix. For polymeric pressure-sensitive adhesives that are solvent cast, it is easy to obtain a supersaturated system that is often in a metastable state. This occurred with both scopolamine and rotigotine in commercial products and resulted in transdermal systems with a decrease in driving force and in dissolution. Methods of measuring solubility in adhesives can be performed either by comparing the flux from systems to systems seeded with crystals or alternatively from a patch with crystalline material [26–29]. In estradiol adhesive matrix patches, crystallization and reduced flux were often observed during product development, because the more stable and less soluble hemihydrate crystal form was formed during storage from the anhydrous form [30]. Exposure to high relative humidity outside of the pouch can be used to accelerate and study such crystallization. Transdermal rotigotine exhibited crystallization with reduced bioavailability and resulted from a stable and a metastable polymorph in the adhesive [31].

One class of permeation enhancers is solvents, which are typically incorporated into liquid reservoir systems that then permeate through a membrane or porous membrane and an adhesive layer. The original estradiol transdermal system, Estraderm®, and the original fentanyl transdermal system, Duragesic®, used ethanol as an enhancer [32–35], and the flux of the drug across stratum corneum was linear with the ethanol flux. This linear relationship allowed control of the skin permeation of the enhancing ethanol, which would promote the skin transport of the drug. The classical solvent enhancer is dimethyl sulfoxide [36].

Another class of enhancers is surfactants, which were demonstrated to interact with polar transport through proteins in the stratum corneum [37]. The optimal chain length for many physical properties of surfactants is 12 carbons [38, 39], and the ability of surfactants to enhance permeation correlates with the hydrophilicity of the polar head group [11, 40]. Fatty acids and esters have both been used as penetration enhancers in adhesive matrix systems. Binary, tertiary, and quaternary

mixtures of semipolar solvents, such as propylene glycol, butanediols, dimethyl sulfoxide, or *N*-methyl pyrrolidone, may be combined with surfactants to obtain very effective enhancement of drug permeation [25]. For adhesive matrix systems, the amount of these volatile solvents including overages must be carefully controlled in the coating process.

Enhancers may also affect adhesion of patches and may produce skin irritation. In the aforementioned patches, ethanol resulted in mild erythema in 10–20% of the patient population. The irritation of skin and other membranes has long been established for surfactants [41]. Development of a patch with an enhancer can be a balance between increasing the flux and minimizing skin irritation. Skin irritation of the drug and its flux may also be important. The pK_a of the drug at constant flux is predictive of primary skin irritation [42, 43]. Delivery of nicotine at lower fluxes allowed for acceptable levels of skin irritation from transdermal nicotine [44].

7.2.3 Basic Pharmacokinetics of Transdermal Delivery

A typical single-dose, pharmacokinetic study of a transdermal patch involves application of an adhesive patch to a selected skin site and fixed surface area for a fixed application time ranging from 12 hours to 7 days, and then removing the patch. To avoid contamination or locally high concentrations, plasma samples are taken from the contralateral side at predetermined times throughout the application period and after removal to determine terminal half-lives. Skin permeation data are most variable when presented as flux and yet best to study changes with time carefully. Trends are most easily understood with less variability from analysis of the cumulative amount over time. In the same way, pharmacokinetic data are best studied as concentration profiles over time to study temporal variation, and less variable and easier to see trends when the area under the curve (AUC) is examined over time instead of as the usual at a single time or at infinite time after administration.

To understand the important features of transdermal pharmacokinetics, it is best to start with this AUC analysis in the simplest case, a linear one-compartment model. If C_p is the plasma (or body compartment) concentration of drug, V_c is the volume of the body compartment, and k_e is the elimination rate constant of the drug from the body compartment, then by mass balance with the only input as a transdermal flux, J, from a patch of area, A, the change in amount in the plasma compartment with time is [45, 46]:

$$V_c \cdot \frac{dC_p}{dt} = -k_e \cdot V_c \cdot C_p + AJ \tag{7.12}$$

When a transdermal patch is administered sufficiently long that steady-state transport is achieved, the pharmacokinetics may be interpreted with a meaning similar to transport experiments. Note that steady-state refers to constant transport and not to the typical pharmacokinetic meaning of steady-state profiles for

multiple dosage applications. At steady-state for a single pharmacokinetic compartment, the steady-state plasma concentration, C_{ss}, is IR, the drug input rate, divided by the intravenous drug clearance, CL. IR at steady-state equals $A{\cdot}J_s$, and CL equals $k_e{\cdot}V_c$. Consequently, as shown in Eq. (7.13):

$$C_{ss} = \frac{A \cdot J_s}{k_e \cdot V_c} = \frac{\mathrm{IR}}{\mathrm{CL}} \tag{7.13}$$

This result is completely analogous to a steady-state drug infusion, and the utility of this equation is that based on a target plasma concentration, the required transdermal input rate can be calculated, and based on estimated patch sizes, the necessary flux across skin can be determined. Note this assumes that there is no cutaneous metabolism to decrease the transdermal bioavailability. In particular, transdermal nitroglycerin has been shown to have somewhat reduced bioavailability due to cutaneous metabolism [47]. Ethanol has been shown to inhibit the cutaneous metabolism of estradiol during in vitro skin permeation through hairless mouse skin [48]. While the extent of cutaneous metabolism is less than hepatic, it can influence systemic bioavailability by the transdermal route [49, 50]. Moreover, Eq. (7.13) can be scaled to the bioavailable flux, $F{\cdot}J_s$, where F can always be determined with corresponding intravenous drug administration.

In a similar manner, the AUC is obtained by integration of the plasma concentration over time. In contrast to normal pharmacokinetic use, AUC is examined as a function of time as opposed to a single fixed time or infinite time after administration. At long times, the steady-state plasma concentration C_s yields a linear steady-state asymptote, AUC_{ss},

$$\mathrm{AUC}_{ss} = C_{ss}\left(t - t_L^k\right) = \frac{A \cdot J_s}{k_e \cdot V_c}\left(t - t_L^k\right) \tag{7.14}$$

where t_L^k is the pharmacokinetic time lag and for a single compartment model is equal to

$$t_L^k = \frac{1}{k_e} + t_L \tag{7.15}$$

That is the pharmacokinetic time lag (defined here as time to steady state not the time to first observed plasma level) is the sum of the reciprocal drug elimination constant and the diffusional time lag. For drugs with short half-lives, the diffusional time lag across skin will determine the onset of drug delivery. Note that the slope of the long-time asymptote of the AUC is the steady-state plasma level and related to the ratio of input rate and clearance, and the time intercept is the pharmacokinetic time lag. In Figure 7.2, a plot of AUC in units of pg-h/ml and C_p in pg/ml × 100 vs. time after patch application is shown for a 10 cm^2 buprenorphine transdermal system [51]. The region for fitting the linear asymptote is selected from the profile for C_s and include neither the rising concentration profile prior to steady-state nor the decline on the seventh day that results from depletion of drug and/or of the enhancer, levulinic acid. The steady-state plasma concentration or

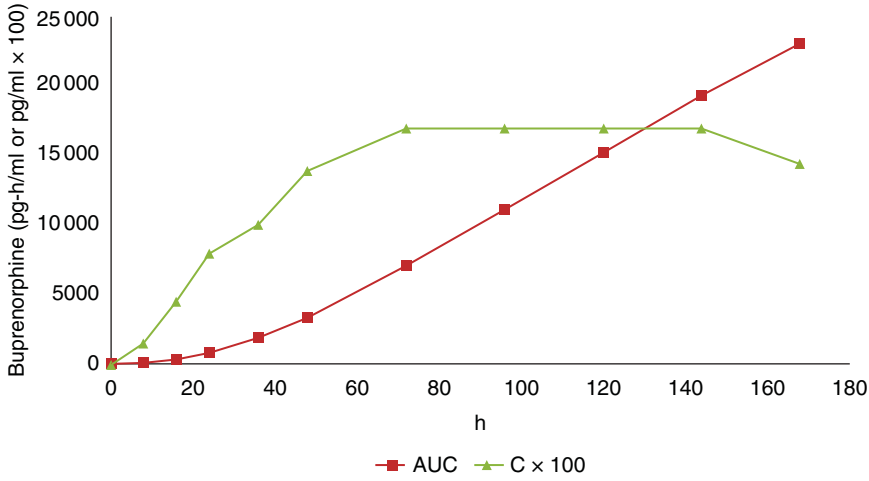

Figure 7.2 AUC and C_p profiles vs. time for a 10 cm^2 transdermal buprenorphine patch. Source: Adapted from Drugs@FDA [51].

slope is 170 pg/ml, and the pharmacokinetic time lag is approximately 30 hours. For a patch application time of one week, a time to steady-state of more than one day is not necessarily an issue.

Transdermal patches contain a well-defined, finite amount of drug, and typically, the amount delivered toward the end of the wearing period declines relative to the maximum delivery. This depletion may be due to either depletion of drug from the reservoir or depletion of enhancer from the reservoir. The Food and Drug Administration (FDA) issued a guidance to reduce the amount of residual drug in used patches [52] for both safety and environmental reasons, for example, the drug content in some used patches may still be lethal or abused. This depletion of a finite dose has been modeled [46, 53] and may be used to define a useful wearing period for a patch, t_u, if one can define a criterion, Y, that is the ratio of the lowest acceptable flux at the end of the wearing period to the maximum flux. Then t_u can be estimated by and related to t_L by the following [46]:

$$t_u = t_L\left(1 - \frac{\ln Y}{\alpha_l^2}\right) \tag{7.16}$$

And, α_1 may be found in tables [54] and is the first solution to Eq. (7.17),

$$\alpha_l \tan \alpha_l = B \tag{7.17}$$

B is the ratio of the solubility of drug (or enhancer) in the patch to that in the stratum corneum, and for all existing patches, $B \ll 1$, which implies that the

permeation behaves like an infinite dose at short times and a finite dose at long times [46].

Removal of a patch can similarly be understood by depletion of the residual steady-state profile of drug in stratum corneum after the wearing period. The observed half-life after removal of a patch can be controlled by either the pharmacokinetic half-life, $-\ln(2)/k_e$, or by diffusion from the skin reservoir, $t_{L,}$ and it is useful to define a ratio, r, as follows:

$$r = k_e \cdot t_L \tag{7.18}$$

If $r \ll 0.4$, pharmacokinetic elimination from the plasma is the rate-limiting process and plasma levels decline as $e^{-k_e t}$. Transdermal donepezil with a half-life of approximately 70 hours [55] is an excellent example of this case. If $r \gg 0.4$, diffusion from the stratum corneum is rate-limiting, and plasma levels decline as $e^{(-2.4t/t_L)}$. The characteristic time to empty the stratum corneum is 2.4 times longer than the time to reach steady state. Scopolamine, for example, has an elimination constant of $0.62\,h^{-1}$ and for skin permeation $t_L = 2$ hours [56]. Consequently, $R = 1.2$ and therefore, the observed patch half-life upon removal should reflect 2.4 times the time lag for permeation and be approximately five hours. Since the skin site after patch removal is no longer occluded or hydrated, the time to empty the stratum corneum may be even longer. Toon et al. compared the transdermal absorption from a $2.5\,cm^2$ clonidine patch over seven days with a two hours intravenous infusion of 150 μg of clonidine in a two-way crossover study in 12 healthy volunteers [57]. Using the intravenous clearance of 10.6 ± 2.2 l/h, the steady-state rate of delivery from the patch was 4.3 ± 1.7 μg/h. After removal of the clonidine patch, the elimination half-life was 14–26 hours [58] and is consistent with a residual depot in nonoccluded skin.

In actual multiple dosing of patches, a second patch is applied to a new skin site after the old patch is removed from the old skin site. By superposition of the declining delivery from the skin site for the old patch with rising delivery from the new patch, diffusion of drug from the old skin site theoretically can be shown to more than compensate for the delayed onset of drug delivery from the new patch in the new site. That is, for ideal membranes, the steady-state plasma level should always be overshot by a factor of 1–1.4 and then return to steady state [59]. Importantly, this implies that the time lag period is not of therapeutic significance during multiple dosing. While the first dose of transdermal nicotine (21 mg per day) exhibited an 8–19 hours period before steady-state plasma levels were achieved, the fifth dose applied was initially close to the steady-state level, rose to 1.3 times the steady-state level and then in 8–10 hours obtained a multiple dose steady-state level not different than the single dose steady-state concentrations [60]. During multiple dosing, some transdermal patches may exhibit a short dip after application of a new patch, and then a rapid return to steady state. This dip instead

of an overshoot may be due to slower permeation from lack of hydration of the unoccluded, old skin patch site.

7.3 In Vivo Assessment of Drug Input and Pharmacokinetic Disposition

7.3.1 Deconvolution

Understanding the in vivo delivery from a transdermal patch is critical to designing and confirming the onset of delivery, the appropriate rate of delivery, and the total drug loading. This critical information for patch development is obtained quantitatively by comparing the pharmacokinetic concentration profiles from a candidate patch with an immediate release product, preferably by the parenteral route, and then deconvolution is used to calculate the in vivo input rate over time. Under the right circumstances, this information can also be used to develop in vitro–in vivo correlations (IVIVCs) and obtain biowaivers.

Deconvolution is an important process used to interrogate extravascular drug input into the systemic circulation. It is intrinsically a heuristic technique and is best implemented with knowledge of the disposition of a drug in the systemic circulation, although it is not required. Deconvolution methods generally fall into two broad categories: model-dependent and model-independent. In pharmacokinetics, model-dependent methods are based on mass balance and require complete inter-compartmental distribution and elimination parameter values obtained from regression analysis of an independent disposition function, i.e. intravenous drug administration. Prominent models are the Wagner–Nelson and Loo–Riegleman methods [61]. The main drawback to model-independent methods is that Wagner–Nelson method is limited to drugs with one compartment model kinetics, and the Loo–Riegleman method requires drug concentrations be measured following extravascular and intravascular administration at the same times, although this limitation can be circumvented by computing comparable concentration values after curve fitting the intravascular concentration-time data. Model-independent methods usually are considered more robust, because they require fewer assumptions concerning drug input and output kinetics. They do not require advance knowledge with regards to the number of distribution compartments, although curve fitting of the intravascular drug concentrations and using least-squares estimates of concentration values in the deconvolution process enhances robustness. Compartmental models offer simplicity and often insight into the kinetic processes and the differences between the different routes of administration or dosage forms being compared.

Most of this discussion will investigate basic principles regarding two types of model-independent deconvolution, direct matrix inversion (numerical

deconvolution), and the use of trial generalized parametric input functions. However, in order to develop a deconvolution process, one must first understand what convolution is and how it pertains to an output response function.

7.3.2 Convolution

Pharmacokinetic models are solutions to systems of linear differential equations where time (t) is the independent variable. A very useful method to solve systems of linear differential equations is by converting t in rate expressions to the complex domain of the Laplace operator s. This reduces differential equations into ordinary simultaneous linear expressions which can be solved by algebra.

Solutions corresponding with $\mathcal{L}\{C_{ev}(t)\}$, where $\mathcal{L}$ refers to the Laplace transform, can be recognized as the product of an input rate function and disposition function. $\mathcal{L}\{C_{ev}(t)\}$ is referred to as the response function and may be exemplified as the Laplace transform of the amount or concentration of drug in the plasma after oral or transdermal drug administration. Then,

$$\mathcal{L}\left\{C_{ev}(t)\right\} = \mathcal{L}\{I(t)\} \cdot \mathcal{L}\{\mathrm{d}(t)\} = \mathcal{L}\{I(t)\} \cdot \mathcal{L}\left\{C_{v}(t)\right\}, s > a \geq 0 \tag{7.19}$$

where, a is a parametric constant of a function of exponential order (i.e. rate constant), $I(t)$ is an input rate function, $\mathrm{d}(t)$ is the disposition function, and $C_{ev}(t)$ is a response function. For example, in transdermal delivery, the input function is the area times the flux as a function of time, the disposition function is the pharmacokinetic plasma concentration to unit impulse or specifically, a unit dose intravenous bolus, and the response function is the plasma concentrations for the transdermal patch. A property of the product solution is that when the anti-Laplace or inverse Laplace of $\mathcal{L}\{I(t)\}$ and $\mathcal{L}\{\mathrm{d}(t)\}$ have identifiable independent inversions, a solution for the response function can always be constructed. Here, $\mathrm{d}(t)$ corresponds to instantaneous intravascular drug administration expressed as normalized plasma concentration such that $C_{v,N} = C_v(t)/C_v(0)$. $I(t)$ corresponds to the input rate, for example, first-order drug absorption for an oral tablet corrected for oral bioavailability or surface area multiplied by transdermal flux for a patch. $C_{ev}(t)$ corresponds to the drug concentration in the plasma resulting from extravascular drug administration, for example, from the patch.

Furthermore, $C_{ev}(t) \neq I(t) \cdot C_{v,N}(t)$, but $C_{ev}(t)$, $I(t)$, and $C_{v,N}(t)$ are related by the convolution integral such that,

$$C_{ev}(t) = \int_0^t I(u) \cdot C_{v,N}(t-u)\,\mathrm{d}u = \int_0^t I(t-u) \cdot C_{v,N}(t)\,\mathrm{d}u \tag{7.20}$$

This is the convolution theorem where $C_{ev}(t)$ is known as the convolution of I and $C_{v,N}$, written as $C_{ev}(t) = (I^{*}C_{v,N})(t)$. Thus provided that $\mathcal{L}\{C_{ev}(t)\} = \mathcal{L}\{I(t)\} \cdot \mathcal{L}\{\mathrm{d}(t)\}$, and the anti-Laplace of $\mathcal{L}\{I(t)\}$ and $\mathcal{L}\{\mathrm{d}(t)\}$ are determined or

can be determined by formal inversion [62], then the concentration in the plasma arising from extravascular administration can be determined.

Deconvolution is the reverse process and is the main approach to calculating the in vivo drug delivery rate from a dosage form when the plasma concentrations resulting from both that dosage form and from a unit dose intravenous bolus are already determined. If $C_{ev}(t)$ and $C_{v,N}(t)$ are known, then how can $I(t)$ be determined? Usually, $C_{v,N}(t)$ is represented by the response to an independent intravenous bolus injection normalized by the initial drug concentration. A typical pharmacokinetic model is a sum of exponentials given by, $C_v = \sum_1^n A_i \cdot e^{-\lambda_i t}$. $C_{v,N}(t)$ is then represented as the response to a unit impulse function by dividing C_v by $C_v(t=0) = \sum_1^n A_i$. The response function to the dosage form is defined by C_{ev} which is equal to X_{ev}/V_c, where X_{ev} is the amount of drug in the vascular compartment resulting from extravascular input into the vascular compartment, and V_c is the volume of the vascular compartment. Then Eq. (7.20) is approximated as a discrete sum such that

$$C_{ev}(t_n) = \sum_{k=1}^{n} I(t_k) \cdot C_{v,N}(t_n - t_k) \cdot (t_k - t_{k-1}) \tag{7.21}$$

where t is the value of the ordered set $t_n \in \{t_1, t_2, t_3, \ldots, t_n\}$ and $C_{v,N}$ is the response to the unit impulse function. Equation (7.21) can be expanded into a set of n linear equations corresponding with the number of concentration-time data points,

$$\begin{aligned}
C_{ev}(t_1) &= I(t_1) \cdot C_{v,N}(0) \cdot (t_1 - t_0) \\
C_{ev}(t_2) &= I(t_1) \cdot C_{v,N}(t_2 - t_1) \cdot (t_1 - t_0) + I(t_2) \cdot C_{v,N}(0) \cdot (t_2 - t_1) \\
C_{ev}(t_3) &= I(t_1) \cdot C_{v,N}(t_3 - t_1) \cdot (t_1 - t_0) + I(t_2) \cdot C_{v,N}(t_3 - t_2) \cdot (t_2 - t_1) \\
&\quad + I(t_3) \cdot C_{v,N}(0) \cdot (t_3 - t_2) \\
&\cdots \\
&\cdots \\
&\cdots \\
C_{ev}(t_n) &= I(t_1) \cdot C_{v,N}(t_n - t_1) \cdot (t_1 - t_0) + I(t_2) \cdot C_{v,N}(t_n - t_2) \cdot (t_2 - t_1) \\
&\quad + I(t_3) \cdot C_{v,N}(t_n - t_3) \cdot (t_3 - t_2) + \cdots \\
&\quad + I(t_n) \cdot C_{v,N}(0) \cdot (t_n - t_{n-1})
\end{aligned} \tag{7.22}$$

or, in matrix form,

$$\boldsymbol{C}_{\mathbf{ev}}(t_k) = \left[\boldsymbol{C}_{\mathbf{v.N}}(t_n - t_k) \cdot (t_k - t_{k-1})\right] \cdot [\mathbf{I}(t_k)] \tag{7.23}$$

This equation is solved for $[I(t_k)]$ by matrix inversion such that,

$$\left[\boldsymbol{I}(t_k)\right] = \left[\boldsymbol{C}_{\mathbf{ev}}(t_k)\right] \cdot \left[\boldsymbol{C}_{\mathbf{v.N}}(t_n - t_k) \cdot (t_k - t_{k-1})\right]^{-1} \tag{7.24}$$

where $[\boldsymbol{I}(t_k)]$ is a vector array containing the in vivo input rates from extravascular administration of the dosage form corresponding to each time point. As mentioned above, a reduction in error excursions which are multiplicative in the right side of Eq. (7.24) can be realized by using regression estimates for $C_v(t)$ [63]. In addition, since the same sampling times are required for both extravascular and intravascular concentration profiles, flexibility is gained by using calculated values for the intravascular concentrations at the time points that match the sampling times for the plasma concentrations measured for administration of the dosage form.

From Eqs. (7.21) and (7.24), the $[\boldsymbol{I}(t_k)]$ array of input rates, i.e. absorption, is represented in terms of concentration in the central compartment. This array is converted to the mass delivery rate by multiplying by V_c which is determined from the bolus injection.

$\boldsymbol{C}_{\mathbf{v,N}}(t_n - t_k)$ is dimensionless. When integrated, the cumulative amount of drug delivered to the systemic circulation is obtained. Integration can be either numerical or analytical with appropriate curve fitting. Preferably, input rates can be modeled analytically using least-squares regression techniques. The cumulative amount of drug delivered is then explicitly calculated.

7.3.3 Instability in Deconvolution

Deconvolution is inherently ill-conditioned, which can lead to spurious excursions at discrete time nodes as the result of approximating a continuous function, and the contamination of experimental data by random error. Numerous methods have been developed for spectral deconvolution including filters and constraining routines [64]. Iterative algorithms based on Van Cittert's method are progressive with each observation node or time point estimated based on all previous estimates or near neighbor estimates. Nomenclature is not common between disciplines and can be confusing. For instance, response, input rate, and disposition functions as used in this chapter and the pharmacokinetic literature correspond with image, transfer, and response functions in the spectral literature. Kiwada et al. proposed constraints applicable to linear pharmacokinetic models [65]. As mentioned, the deconvolution process is heuristic. Intervening least-square regression minimizes random error and can provide optimal estimates for the input rate and disposition functions. The input rates can be modeled and reconvolved with the disposition function to produce the response function. In this way, the input rate function can be interrogated comparing various models.

Another consideration, unlike spectral deconvolution, is that pharmacokinetic response models are generally rather simple functions, that is, monotonic input and disposition functions. Deconvolution is far less demanding than in the spectral case where the function analogous to the disposition function is multimodal and polyphasic. Li and Cutler demonstrated that stable and robust estimates of the

cumulative amount of drug absorbed were obtained when the disposition function was the response to an intravenous unit dose bolus injection [63]. When the disposition function was polyphasic corresponding to the response to an immediate release, oral drug input, estimates were only acceptable with an optimal sampling scheme. When the sampling scheme was not optimal, erratic estimates were obtained. Nevertheless, a least-squares derivable model appeared to still be possible and is routinely used for in vitro/in vivo correlations for oral controlled release dosage forms.

A search of the literature did not find any pharmacokinetic deconvolution commercial software employing advanced filtering and smoothing of raw direct inversion estimates of the input rate function. If one considers the regression estimates of the disposition function as error-free, then two sources of error remain inherent to deconvolution [63]. First is the error associated with the numerical integration of the discrete convolution approximation which leads to estimate bias. This source of error can be minimized by dense sampling of response data. The second source of error is random experimental error associated with the response function data which can be minimized by local smoothing.

In order to investigate the effect of local smoothing on deconvolution estimation, a nearest-neighbor smoothing (NNS) technique as proposed by Altman [66] was employed. In particular, a two-compartment pharmacokinetic model with first-order input was tested. $\boldsymbol{C}_{\mathbf{ev}}(t_k)$ and $\boldsymbol{C}_{\mathbf{v,N}}(t_n - t_k)$ were directly calculated and $(t_k - t_{k-1})$ was uniformly one hour. The theoretical first-order mass input rate is

$$\text{Input rate} = \frac{\mathrm{d}X}{\mathrm{d}t} = X(0) \cdot k_a \cdot e^{-k_a \cdot t} \tag{7.25}$$

where $X(0)$ is the bioavailable dose. $\boldsymbol{C}_{\mathbf{v,N}}(t_n - t_k)$ was used as calculated (error-free) and entered into Eq. (7.22). Normally distributed random error was superimposed on $\boldsymbol{C}_{\mathbf{ev}}(t_k)$ with $\mu = 0$ and $\sigma^2 = 0.0011$ and 0.0025 corresponding with error excursions of −10% to 10%, and −15% to 15% to produce corrupt $\boldsymbol{C}_{\mathbf{ev}}(t_k)$ values. Errors were generated using the random number generator software contained in Microsoft Excel 2007. These values were then entered into Eq. (7.22) and matrix Eq. (7.24) was solved for $\boldsymbol{I}(t_k)$ using the matrix inversion function in Excel. The directly inverted $\boldsymbol{I}(t_k)$ values were considered unprocessed raw deconvolution values. Subsequent processing used three-point NNS such that,

$$\left\langle I\left(t_k\right)\right\rangle = {}^1\!/_3 \cdot \sum_{j=-1}^{j=1} I\left(t_{k+j}\right) \tag{7.26}$$

where $\langle I\ (t_k)\rangle$ is the local input rate average about t_k. The bioavailable dose (F · Dose) was regarded as equal to the dose.

The results are shown in Figures 7.3 and 7.4. In Figure 7.3, the effect of random error averaging was evaluated. The imposition of NNS data processing shows

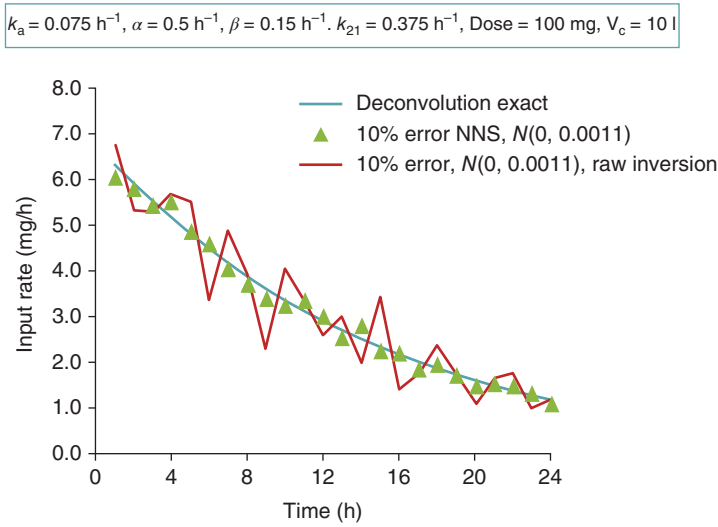

Figure 7.3 Deconvolution of an input rate-limited pharmacokinetic model: effect of error averaging using local nearest-neighbor smoothing.

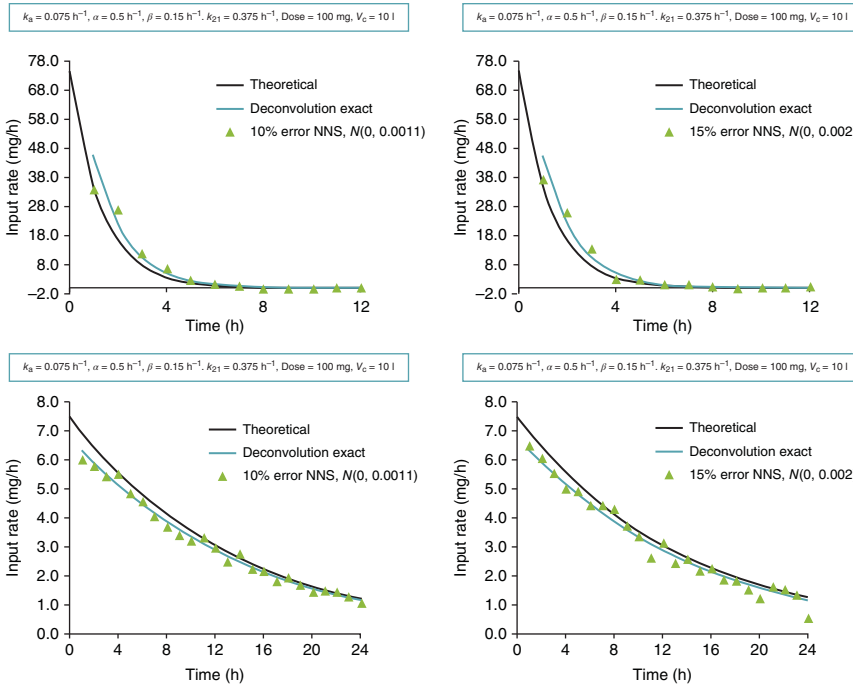

Figure 7.4 Effect of error on estimation bias resulting from discrete convolution approximation for rapid and rate-limited input pharmacokinetic models.

significant benefit resulting in a sharpened regular input rate without compromising accuracy relative to error-free deconvolution. NNS reduces random error by local averaging of error which is distributed $N(0, \sigma^2)$. The resulting processed data facilitates model elucidation for subsequent curve-fitting by nonlinear regression analysis and further error minimization.

In Figure 7.4, estimation bias from the discrete sum approximation of the convolution integral was evaluated.

Estimation bias arising from discrete approximation convolving the input function with the unit impulse disposition function appears to be more problematic, although not necessarily limiting with regards to IVIVCs, where a scaling factor can be utilized. Deconvolution of error-free data resulted in a 6.7% bias relative to theoretical values. The addition of error increases bias for rapid input to 22% and rate-limited input to 9% for estimates of k_a by nonlinear regression. In the case of rapid input, sampling was limited in the first four hours and most likely contributed to the extent of error illustrating the need for well-designed clinical studies with appropriate sampling scale which may not be obvious from plasma concentration–time profiles alone. Within the limitations of deconvolution and variability associated with clinical trials, however, deconvolution with NNS produces reasonable profiles and estimates which may be suitable for input rate function interrogation and modeling.

Direct inversion deconvolution is attractive since it facilitates model interrogation. Furthermore, the theoretical basis of convolution and deconvolution remains the standard for establishing an input function. Results using NNS are intriguing and suggest the potential for error filtering and smoothing using advanced algorithms. Reports of pharmacokinetic applications of deconvolution processing appear to be absent. Many of these methods are frequently used in the physical sciences.

7.3.4 Generalized Input and Convolution

Most reports of deconvolution applied to pharmacokinetics employ a method known as analytical deconvolution. Analytical deconvolution is actually not "deconvolution" in a strict sense, but trial-and-error convolution. It has been reported to be the preferred method to evaluate the input rate function [67]. In this approach, a known disposition function is convolved with a generalized empirical input rate function to produce an analytical expression for the response function. Real data is then curve-fit to the response function using least-squares regression. Parameters associated with the input rate function are estimated iteratively using statistical techniques to minimize error. It is important that the chosen trial input rate function is flexible and robust. Various input rate functions have been used including polynomials [68–70], B-spline function [71, 72], and

the gamma function [73, 74]. Once parameter estimates are obtained, the input rate function is easily retrieved, since it is known, and integrated to give the cumulative input to the central vascular compartment.

Analytical deconvolution has its limitations as well. Nonlinear regression analysis of polyphasic functions is often difficult with iterative convergence to local minima. The congruency of the generalized input function with known physical and pharmacokinetic functions may be complex to interpret. Analytical deconvolution requires the prescription of an input function which defeats the purpose of using deconvolution as an investigative tool to elucidate a proper input function usually based on mechanistic considerations. The exception is where a physiological or physical based model is used as the analytical model and allows direct mechanistic interpretation. Currently available pharmacokinetic software (i.e. WinNonlin7, GastroPlus™), however, appear to use analytical deconvolution.

7.4 In Vitro Testing: Drug Release from Transdermal Systems

The purpose of in vitro release testing is for quality control to assess measures of the rate and extent of the delivery of the drug from the transdermal patch. It is important in formulation development, maintaining quality specifications, to identify critical manufacturing variables, to assess in vivo performance when predictive, and to track product performance during development including postapproval changes. Sink conditions are critical to the ability of the test to discriminate and for the only test of transdermal system performance that is independent of the skin and hydrodynamics.

Current compendial methods for testing transdermal delivery systems are the paddle over disk, or disk assembly using US pharmacopaeia (USP) apparatus 5, or the rotating cylinder using USP apparatus 6 [75]. While the pH of the receiver medium is best when it reflects physiological skin conditions, pH 5–6, it is more important to use a dissolution media that allow sink conditions for the labeled theoretical drug content. Extended range testing in at least three media, pH 1.2, 4.5, and 6.8, has been recommended for buprenorphine [76]. Recommended temperature of the media is typically 32 °C. The agitation speed and testing time are experimentally determined and should reflect the amount of drug to be delivered. The conditions and time points for generic transdermal patches may be found on the FDA website. The final time point studied at least for the pivotal batches generally reflects delivery of at least 80–85% of the contents of the transdermal patch and may exceed the duration of the normal quality control method. If aqueous solvents alone are inappropriate, aqueous and organic solvent mixtures or surfactants or other solubilizers, such as cyclodextrins, can be used with justification.

The cumulative amount of drug released into the receiver is measured. The USP paddle over disk method has been adapted, for example for use with transdermal rotigotine into 900 ml of pH 4.5 phosphate buffer. The bath is stirred at 50 rpm with sampling times of 0.25, 1, and 2 hours [76]. In contrast, the rotating cylinder method is used for transdermal methylphenidate into 900 ml of 0.1 N hydrochloric acid solution stirred at 50 rpm and sampled at 0.5, 1.5, and 3 hours [77]. The rotating cylinder method is also applied to transdermal rivastigmine base into 0.9% sodium chloride solution.

In general, in vitro dissolution testing of transdermal systems has no relationship to in vivo delivery and should be viewed as a method for quality control and understanding of the transdermal patch. One difference is the insensitivity of the dissolution test to changes in thermodynamic activity or solubility in the patch. Permeation across skin or a membrane depends on the thermodynamic activity of the drug. Moreover, especially for matrix transdermal patches, the dissolution rate is much faster than the in vitro or in vivo skin permeation rate, and consequently, changes in the dissolution rate may not be relevant to in vivo delivery.

Rivastigmine was delivered orally for treatment of Alzheimer's disease and especially during titration, produces a high incidence of nausea and vomiting that may be due to either local concentrations in the stomach or systemically mediated effects with its high C_{max} [78]. A transdermal patch was developed to reduce the incidence of these adverse events by flattening the peak plasma levels and local gastrointestinal drug concentration. During the development of transdermal rivastigmine [79], the rate of dissolution from the rivastigmine patch was found to decrease up to 20% on stability at 36 months at 25 °C/60% RH (relative humidity). The sponsor successfully argued that the observed changes in dissolution were not indicative of any changes in vivo based on clinical efficacy. The in vitro skin permeation across the same donor skin from freshly made transdermal patches and from this 36-month old batch with much slower dissolution rates were not statistically different.

While at most about half of the rivastigmine is delivered in vivo during the one day wearing period, substantially more rivastigmine is released after seven hours of dissolution testing. Since the rate of dissolution greatly exceeds the rate of skin permeation, the skin permeation is rate-limiting for these matrix systems, and there was in this example, no relationship to in vivo drug delivery. In addition to providing skin permeation data for the fresh and old transdermal patches from the same lots, the permeation across 9% ethylene vinyl acetate (EVA) membranes demonstrated that approximately 35% of the drug permeated in one day from fresh and old patches. This lack of in vivo correlation with dissolution testing is generally true for almost all transdermal patches and reinforces its use as a quality control method, but not for in vivo prediction.

Validated in vitro testing for iontophoretic sumatriptan succinate depended on the use of a membrane of sufficient resistance that limits passive diffusion and

permits the iontophoretic systems to operate within its design specifications [80]. The flux was determined for each stage of operation of the device and for the total amount of drug released over the test period.

7.5 In Vitro/In Vivo Correlation

Dosage form design to achieve the desired pattern of drug delivery based on pharmacokinetic objectives requires a significant amount of time as well as financial investment. Formulation optimization may require various compositions, manufacturing processes, and equipment. Traditionally, changes in any of these factors of an approved product required an in vivo bioequivalence (BE) study. The guidance on IVIVC was promulgated by the FDA in order to reduce the impact of product changes on product development [81]. The main objective of an IVIVC is to enable the dissolution or release test to serve as a surrogate for clinical bioavailability trials. In Chapter 6 in this volume, in vitro skin permeation is discussed in terms of its predictive ability for in vivo delivery from topical dosage forms.

The FDA defines an IVIVC as a predictive mathematical model describing the relationship between an in vitro property of a dosage form and an in vivo response. The in vitro physicochemical property is the in vitro dissolution or release profile into biologically relevant media, or cumulative release. The in vivo response is the plasma concentration-time profile. In order to relate the in vivo plasma concentration-time profile to the in vitro cumulative release profile, the in vivo drug input rate needs to be determined and the cumulative extent of absorption profile established.

The FDA defines three levels or correlation, Levels A, B, and C, between in vitro drug release and in vivo rate and extent of absorption into the systemic circulation. A Level A correlation is usually estimated by deconvolution of plasma concentration-time profile followed by comparison of the fraction of drug absorbed to the fraction of drug dissolved. The deconvolution may be either model-dependent or model-independent. A correlation of this type is generally linear, but does not have to be, and represents a point-to-point mapping between in vitro dissolution and the in vivo input function. In a linear correlation, the in vitro dissolution and in vivo input curves may be directly superimposable or may be made to be superimposable by the use of a scaling factor. Nonlinear correlations, while not as common, may also be appropriate.

Alternative approaches to developing a Level A IVIVC are possible. One alternative is based on a convolution procedure that models the relationship between in vitro dissolution and plasma concentration in a single step. Plasma concentrations predicted from the model and those observed are compared directly.

Whatever the method used to establish a Level A IVIVC, the model should predict the entire in vivo time course from the in vitro data. In this context, the model

refers to the relationship between in vitro dissolution of an extended release dosage form and an in vivo response such as plasma drug concentration or amount of drug absorbed. A Level A correlation is the only level acceptable for a biowaiver of clinical bioavailability trials. The model for the Level A correlation must be adequate to include accurate prediction of actual in vivo performance of transdermal patches that release drug in dissolution testing both slower and faster than the approximate specifications for dissolution.

Levels B and C are primarily developed for optimizing formulation development, selecting appropriate excipients, optimizing manufacturing processes, quality control, and characterizing the release patterns of newly formulated immediate release and modified release products relative to the reference listed drug. They may also be supportive of expected in vivo performance.

IVIVC's have been determined for a number of drug formulations and products, although in general, they are not common [82–87]. Level A IVIVC for prolonged release dosage forms is expected for highly permeable drugs which are application site independent. An IVIVC is expected for immediate release drug products that have low aqueous solubility but have high permeability and highly soluble drug products that are dissolution rate limited with high permeability. Low or highly soluble drug products with low permeability have little or no IVIVC.

The lack of IVIVC for matrix transdermal systems is particularly easy to understand. Cumulative release into a dissolution bath from a transdermal matrix whether a drug solution (for the first 60% of drug release) or dispersion (greater than 60% or 70% of drug release) in a polymer is generally proportional to the square root of time. Most of the drug is released in a period much faster than delivery in vivo. The in vivo delivery is controlled by transport across the stratum corneum and is linear with time. Consequently, in vitro skin permeation may be predictive of in vivo delivery, but cumulative release from a matrix transdermal system is generally not predictive.

In contrast, cumulative release from a membrane-controlled transdermal system may or may not exhibit good correlation with in vivo performance. Membrane systems usually have a membrane-adhesive laminate that the drug must diffuse across from the drug reservoir before reaching the skin. The series resistance approximation, which is the diffusional analog of electrical resistance and is the reciprocal permeability, may be used to understand these membrane systems. The total resistance through the skin-membrane-adhesive multilayer system is the sum of the resistances through each layer or written in terms of fluxes as follows:

$$\frac{1}{J_T} = \frac{1}{J_M} + \frac{1}{J_A} + \frac{1}{J_S} \tag{7.27}$$

where J_i indicates the fluxes through the ith layer, T, M, A, S are the total multilayer, the membrane, the adhesive, and the skin, respectively. Most commercial membrane transdermal systems have fluxes through the membrane that are

greater than or equal to the flux through skin alone, and consequently, the skin becomes the dominating barrier in determining the flux across the total multilayer as much or more than the membrane system. Nevertheless, cumulative release will be linear with time, but faster than in vivo delivery, and some correlation may be obtained. However, the membrane-adhesive laminate is equilibrated in the package, and the drug partitions into the entire membrane adhesive laminate. This drug loading contributes a burst or shortens the diffusional time lag. Initial cumulative release is dominated by this nonlinear burst from the membrane system and further hinders correlation with a membrane transdermal system. One approach is to use a silicone adhesive where the solubility of drug is very low and diffusion fast to minimize this burst.

There are two examples of true membrane-controlled patches that should produce good IVIVCs. A user-activated nicotine patch [88] was studied, where the transdermal system had a truly rate-controlling membrane, that is, the permeability of the drug through the membrane was much less than through the skin alone, and prior to activation, there was no drug in the membrane or adhesive layers. Since the amount of drug delivered in cumulative release testing and in vivo was determined essentially by the membrane, a Level A correlation should have been possible. The nicotine user-activated systems consisted of a compartment with nicotine hydrochloride salt and another compartment with sodium hydroxide solution system separated by a rupturable seal. Just prior to use, this seal was broken, and the hydrochloride salt was converted to the free base. Consequently, there was no "burst of drug" from the adhesive typically observed in cumulative release for a transdermal patch. Then the nicotine base diffused through the 2% EVA membrane-adhesive laminate with a steady-state flux of $81 \pm 6\ \mu g/cm^2/h$. For comparison, when this laminate was placed on skin in vitro, the steady-state flux of nicotine was $78 \pm 5\ \mu g/cm^2/h$ and not statistically different [44]. The nicotine transdermal system was applied to eight healthy smokers, who abstained from smoking for 12 hours prior and during the single-dose pharmacokinetic study [88]. The in vivo absorption was calculated by the Wagner–Nelson method [61] and the excellent correlation with the in vitro dissolution is visually obvious in Figure 7.5. To create this figure, the in vivo cumulative release is assumed without fitting to lag behind the in vitro cumulative release by two hours. The longer time lag for in vivo absorption of nicotine is as per equation 16 accounted for the time lag for diffusion through skin and the elimination half-life of four hours.

Pharmacokinetic concentration profiles from two prototype membrane-controlled, ethanol-enhanced nitroglycerin transdermal patches were compared with a commercial transdermal nitroglycerin patch in six healthy subjects in a three-way crossover study [89]. The two ethanolic prototypes differed by the fill volume of ethanolic solution. An intravenous stable isotope ^{15}N-infusion was administered concurrently with each transdermal administration. The ratio

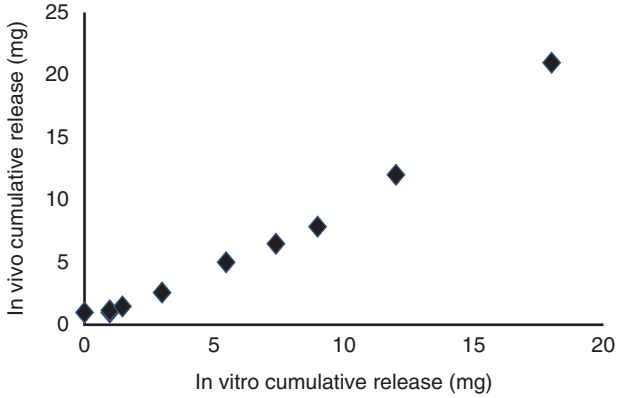

Figure 7.5 In vitro vs. in vivo nicotine cumulative release from a nicotine transdermal system. Source: Based on Chan et al. [88].

of the plasma concentrations of the two isotopic forms and the infusion rate provided the stationary transdermal delivery rate from each transdermal system. This approach of simultaneous stable isotope infusions can greatly decrease the size of the population needed for a bioequivalence study. From an analysis of variance (ANOVA), the intersubject coefficient of variation was reduced in both ethanol-enhanced systems. For one of the prototypes, the intersubject variation was half that for the commercial transdermal system, while that prototype maintained a delivery of twice the flux from the commercial system. The flux of the enhancer, ethanol, through the selected EVA membrane was approximately equal to that through skin. Nitroglycerin flux through the multilayer correlated linearly with the ethanol flux, and thus, control of the ethanol flux controls the flux of nitroglycerin. A silicone adhesive was used to minimize the burst of ethanol and drug. These systems may also be capable of developing a Level A correlation. Since these EVA membranes have permeability approximately the same as that of skin, slow transdermal systems with a thicker membrane delivering 25% less drug and fast systems with thinner membranes delivering 25% more drug could be developed and tested. Based on the series resistance membrane model in Eq. (7.21), it would be expected that the measured flux across the slow system and skin in vivo would be 86% of the normal system through skin as compared to cumulative release from the slower system being 75% that from the normal system. Similarly, the expected flux from the faster system and skin in vivo would be 111% of that from the normal system and skin in vivo as compared to cumulative release from the faster system being 125% that from the normal system. While the in vivo data would be less discriminating, it is likely that a

good correlation could be developed. Finally, the ethanolic prototype that was optimized with a lower fill volume only had 55% residual drug after use, while the commercial patch without enhancer had 84% residual drug after use. This is a good example of optimally loading an enhancer in order to substantially reduce the amount of residual drug after application.

An example of a Level C correlation [90], which describes the relationship between the amount of drug released at one time point and one pharmacokinetic parameter, is the iontophoretic fentanyl system (E-TRANS®).This E-TRANS system is designed to function for as long as 24 hours or 80 doses, whichever comes first. Steady-state absorption of fentanyl is observed in about 24 hours in vivo. For development of an IVIVC, the in vivo plasma AUC (23–24 hours), which is the area under the curve from the 23 to 24 hours after application and corresponded to the 47th dose activation, was correlated with the amount of fentanyl released from the 45th dose activation in vitro. The amount absorbed in vivo is related to the AUC at steady state by the following pharmacokinetic relationship.

$$\text{Amount absorbed } \left(\text{E-TRANS}^{®}\right) = \text{AUC}_{\text{E-TRANS}}\ (23 - 24\,\text{hours}) \times \text{CL} \tag{7.28}$$

where CL is the systemic clearance after intravenous fentanyl administration.

This IVIVC was demonstrated in the new drug application [90] and is shown in Figure 7.6.

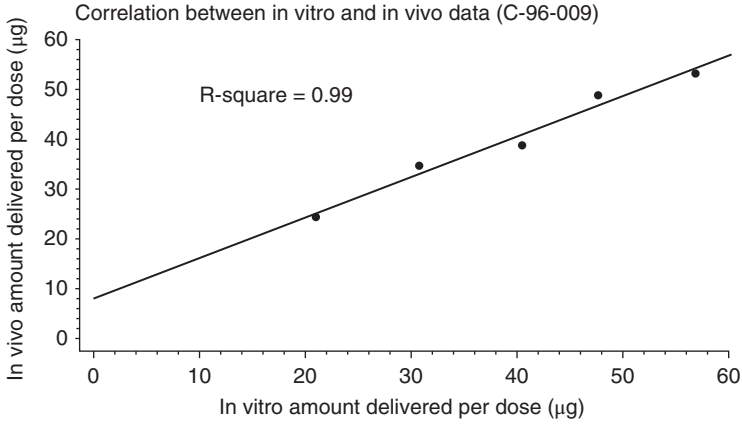

Figure 7.6 In vivo–in vitro correlation of between the amount of fentanyl hydrochloride delivered in vivo and in vitro by iontophoresis. Source: From Drugs@FDA [90].

7.6 Clinical Safety and Efficacy Studies for Dermal Drug Development

Bioequivalence testing of transdermal dosage forms is a mainstay and concern of product development due to the complexity of transdermal devices and dermal formulations. Even minor manufacturing differences can lead to failure of bioequivalence. Current regulations demand a complete characterization of the formulation in terms of physicochemical properties, pharmacokinetics disposition, residual content, and skin irritation and sensitization. Efficacy studies are required when drug plasma concentration-time curves are significantly different from established products such as the conversion from an immediate release product to a prolonged release product with minimal steady-state oscillations. For example, approval of the estradiol matrix system with relatively flat plasma levels included a requirement to establish safety and efficacy even though the ethanolic transdermal estradiol reservoir system with multiple delivery peaks was already marketed [60]. A change of route of administration usually also necessitates at least one pivotal safety and efficacy study. There have been exceptions where there was an established pharmacokinetic/pharmacodynamic (PK/PD) relationship and daily AUC and the bounds of the plasma levels from the patch were within the limits for those from the oral dosage form.

Table 7.2 lists required clinical studies for dermal drug development. Adhesion, skin irritation, skin sensitization, and residual content may be incorporated into the bioavailability or bioequivalence studies or into safety and efficacy studies.

Table 7.2 Required or supportive clinical studies in support of transdermal drug development.

Bioavailability or bioequivalence
Adhesion
Skin irritation and sensitization
Dosage form and dose proportionality
Residual content analysis in transdermal patches and content minimization for certain drug classes
At least one pivotal clinical study validating efficacy and demonstrating safety
Supporting in vitro studies defining mechanism of skin permeation
Bioequivalence studies demonstrating the comparative bioavailability, adhesion, and skin irritation for different skin sites
Safety studies related to environmental conditions such as heat, sauna, and abuse potential

7.6.1 Bioavailability and Bioequivalence

Bioavailability (BA) studies are required to support systemic drug availability and are preferably done relative to an intravenous injection (absolute bioavailability) or to a reference product by a different route of administration (relative bioavailability). When comparing a product to a reference listed drug product, a comparative bioavailability study is appropriate for a 505(b)(2). A bioequivalence study is required, if an abbreviated new drug application (ANDA) is the goal. Bioequivalence is established when the criteria of 80–125% of log transformed variables AUC and C_{max} are met for the test product vs. the reference product based on the 90% confidence interval. When multiple strengths are available, usually a single strength of product needs to be tested clinically. Other strengths are supported by in vitro dissolution or release testing when bioequivalence is established provided that proportional similarity exists across all formulation strengths. The European Medicines Evaluation Agency (EMEA) requires single-dose and multiple-dose bioequivalence.

Adhesion and skin irritation studies of the transdermal patch are often conducted in conjunction with the BA or BE study. For these studies, the patch should be identical with the commercial product. Formal adhesion performance of the intact transdermal test product must be evaluated for the full duration of the intended application. Adhesion of a larger system or higher strength may be more problematic and should be evaluated. No patch reinforcement is allowed when the study is being used to characterize acceptable adhesion performance to support product approval. Since there is a learning curve evident in adhesion studies when patients apply a patch, the patch should be applied by trained clinical personnel. Adhesion scoring is performed daily. A scoring system is recommended by the FDA with scores ranging from 0 corresponding with ≥90% adhesion, essentially no lift off the skin, to a score of 4 for a detached patch. The use of grids can aid this evaluation. Adhesive residue on the skin site due to cold flow should also be evaluated. While good adhesion is essential for bioavailability, for certain therapies, in particular, contraception, adhesion is critical to efficacy by the transdermal route.

The skin sites of application need to be investigated in terms of comparative bioavailability, skin irritation, and adhesion. Transdermal rivastigmine (10 cm^2) was applied to the chest, upper back, upper arm, abdomen, and thigh [91]. The bioavailability was greatest for the upper back, chest, and upper arm while the rank of skin sites for adhesion was thigh, abdomen, upper arm, chest, and upper back. Erythema was lower for the upper back, chest, and upper arm. The patient instructions for transdermal estradiol for hormone replacement therapy stated that delivery to the abdomen, buttocks, and back were bioequivalent, but recommended

application to the buttocks to decrease skin irritation for those patients experiencing skin irritation on the abdomen [60].

7.6.2 Skin Irritation and Sensitization Study

While certain FDA guidance recommend that irritation and sensitization be evaluated in a single study, this may confound adequate definition of the separate phenomena. Irritancy studies follow either concurrently worn (randomized by left or right side or by site) or cross-over designs comparing the active transdermal test product to a comparable placebo batch with active drug. For generics, the reference listed drug would also be compared. High (0.1% sodium lauryl sulfate) or low (0.9% saline) irritancy active controls may also be included as positive controls. The duration of exposure is generally 21 days for an ANDA. Scoring of dermal reactions should include erythema, edema, and other features indicative of irritation. Observations of dermal reactions are made daily. Grading should be done at one hour after removal and followed daily until sufficient resolution of the reaction occurs. While mechanical irritation peaks immediately after removal of a patch, chemical irritancy arises one hour after removal and may persist for days. Irritation studies for an ANDA only require 30 subjects. However, for weak irritants including the enhancers, in innovator patches, skin irritation or sensitization studies may require a total of 100–200 subjects. Combinations of BA studies and evaluation of irritation in clinical studies may be used to define a more realistic incidence.

Skin sensitization is usually conducted under conditions of maximal stress and may be used during the assessment of transdermal drug products for generics. Sensitization studies follow the same clinical cross-over design as irritation studies. In the studies recommended in the guidance on skin irritation and skin irritation for generic transdermal products [92], the duration of the study is six weeks which is divided into three phases, the induction phase, the rest phase, and the challenge phase. During the induction phase, application of test materials are made to the same skin sites three times weekly for three weeks for a total of nine applications. The test products are to remain in place for 48 hours on weekdays and 72 hours on weekends. Scoring of skin reactions are to be made using an appropriate scale. The induction phase is followed by the rest phase for two weeks, during which no applications are made. The challenge phase follows where test materials are applied to new skin sites for 48 hours. Evaluation of immunogenic-elicited skin reactions is made at 1 hour and 24, 48, and 72 hours. Skin reactions are graded and tabulated as a percentage of subjects. The comparison with placebo challenges, the type of skin reaction, and the onset, severity, and persistence of the reaction help separate irritation from sensitization. The sensitization study requires 200 subjects. For characterization of weak sensitizers, a longer induction phase of four weeks may be necessary. A rechallenge phase may also be added to confirm sensitization.

7.7 Dosage Form Proportionality Scaling and Dose Proportionality

Dose scaling or dosage form proportionality is assessed during pharmacokinetic studies in a similar manner as for any extravascular administered drug. Dose proportionality is usually only required for new molecular entities, although it may be required for special dosage forms. For drugs with greater skin permeation, the residual drug content is usually easy to measure reliably, and the residual drug content can be a good confirmation of dose proportionality.

7.7.1 Residual Content of the Dosage Form

The amount of active pharmaceutical ingredient (API) remaining in a patch after the recommended time of application is used as one of the methods to assess BA/BE. The apparent transdermal dose delivered needs to be calculated by subtracting the residual content of these used transdermal systems from the residual content of matched unused patches, preferably also returned from the same lot in the clinic. There is often a strong linear correlation between the amount delivered calculated from the residual content and the AUC. Residual content of the API has an impact on the product's safety, including environmental safety, potential child safety, and abuse potential. There is a clear guidance [52] to reduce the residual content of the transdermal patch as an element of patch design.

7.7.2 Comparative Toxicity and Efficacy

At least one clinical trial is required to support changes in the route of delivery or substantial differences in transdermal delivery characteristics when the C_{max} to C_{min} ratio at steady state is altered. Conversion from conventional immediate-release dosage forms may also impact C_{max} requiring an efficacy trial if average exposure has not been established as the determinant of efficacy. For innovative transdermal products, a nonclinical study in a suitable nonrodent species, usually minipig or a primate, is recommended for multiple months [93]. For a 505(b)(2), the study should be designed to bridge the toxicity to the reference product. A toxicokinetic bridge is also appropriate.

For chronic transdermal therapy with an innovator product, a carcinogenicity study by the dermal route may be required.

7.8 Supporting In Vitro Studies

Supporting in vitro dissolution studies are required for all transdermal dosage forms and for quality control in manufacturing. Assay, content uniformity, and

related substances are required as for any dosage form. An enhancer is considered a critical component, and the enhancer content should be determined. The in vitro studies and specifications developed from these studies is part of the Chemistry, Manufacturing, and Control (CMC) section of an ANDA or new drug application (NDA) submission. Extensive screening and characterization of the transdermal dosage form is expected to form the basis of the development of the product as well as establishing the appropriate residual content. The methods employed have been discussed above.

In addition, extensive characterization of the adhesive, a critical component of any transdermal matrix patch is required. This generally includes adhesion, tack, and peel testing and potentially shear and cold flow.

7.9 Safety Studies Related to Environmental Conditions Such as Heat and Storage Conditions

These studies fall under the category of stability studies which are required in the CMC section. Other tests include leak test, water vapor permeability test, heat effect on rheological properties and skin permeation, and crystallization of the drug. Pharmacokinetic safety studies to define the effect of heat or other factors may also be required.

7.10 Active Transdermal Systems That Enhance Barrier Penetration

7.10.1 Microneedles

The stratum corneum is a formidable barrier especially for proteins and macromolecules. Microneedle arrays provide a mechanical solution to dermal delivery of drugs by puncturing the stratum corneum with minimal elicitation of pain. Considerable interest in microneedle delivery of vaccines has been elicited in the past two decades due to prevalence of antigen-presenting cells in the epidermis and advances in micro- and nanofabrication technology [94–100].

Microneedles are an array of thin projectiles of micron length that are used to pierce the stratum corneum. They do not penetrate into the dermis and with the small diameter are painless and bloodless. These devices can be designed for either immediate or sustained drug delivery. Since microneedles are self-administered, there are no ancillary health care providers, who may be necessary for drug administration by a hypodermic syringe. Special applicators are

often used for reproducible insertion into the skin. There are currently four types of microneedles: (i) Solid projectiles made of silicon, metal, glass, or ceramics are used to pretreat an area of skin by pressing an array of projectiles against the skin to create an array of pores [99]. The projectile array is removed, and the drug is applied topically in a patch. To reduce the area of drug to the region with pores, printed patches may be used that align the printed area with drug over the pores. Ceramic microneedles are retained in place once applied for a specified period of time. Drug is loaded into the porous ceramic material by osmosis, and after application, the drug is released in a similar manner. (ii) Hollow projectiles for infusion of larger quantities of drug into the skin. Drug delivery through hollow microneedles is essentially intradermal injection and is similar to conventional parenteral delivery except the needles are 0.5–1 mm in length and deliver volumes of <200 µl. These devices require positive pressure for liquid delivery. (iii) Coated or arrowhead tipped solid projectiles are applied similarly to solid microneedles. They are retained on the skin like ceramic microneedles for a specified period of time. Once the coating dissolves, the array is removed. For arrowhead tipped microneedles, once the device is applied, it is removed, dislodging the arrowhead tip, which is retained in the skin. Arrowheads or tips are usually polymeric. (iv) Dissolving projectiles in which the microneedles are made of a water-soluble material. Drug is impregnated in the material and released upon dissolution. Novel designs include biocompatible polymeric material microneedle arrays laminated on water soluble rapid dissolving flexible backings [98]. The polymeric material is slow dissolving providing for sustained release. There is no need to remove these biodegradable devices. For dissolving microneedles, establishing rapid and complete dissolution reduces the total drug content of the patch. Furthermore, they reduce biohazard residual washed from device disposal. Biodegradable microneedles of polylactic acid (PLA) and polylactic glycolic acid (PLGA) copolymers were produced in polydimethylsiloxane micromolds. The forces to fracture the microneedles greatly exceeded the force of insertion into the skin. The in vitro skin permeation through human skin of calcein (623 Da) and bovine serum albumin was increased over 1000-fold compared to passive skin permeation [100]. With dissolving and biodegradable microneedles, the amount of drug may be especially restricted to highly potent drugs or vaccines, particularly when the drug is coated on the surface of these small needles.

The main limitations for microneedle development are problems associated with large-scale microfabrication, the range of molecules suitable for this mode of delivery, and the amount of drug needed to be delivered. Moreover, any small pore can tend to clog, close, or tear and maintaining its patency for the desired time can be a challenge. Reductions in the size of pore diameter have been observed within 15 minutes [101], but pores have been shown to remain open for two to three days under occlusion [102]. Another restriction is the need for potent drugs since

the quantity that can be delivered is still limited, but generally much greater than passive diffusion of drugs through skin. Dissolving microneedles with drug in the baseplate are less limited by drug potency. In recent clinical studies, neither skin infection nor skin irritation was problematic with the use of microneedles [103].

Solid microneedles are fabricated by deep reactive ion etching and photolithography of silicon wafers, metals, and glass. Ceramics are fabricated using micromolding of ceramic slurries and subsequent casting and sintering. Lithography, wet, and dry etching are adapted from microelectromechanical systems technology. Coatings are applied by spray or dip coating techniques.

Dissolving microneedles are commercially the most important microneedle array. Implanted microneedles can be either fast dissolving, providing immediate release of an embedded drug or prolonged release based on the supporting substrate used to fabricate the microneedles. Typically, micromolds are filled by solvent casting where a liquid supporting material or polymeric monomer fills the mold and solidifies by solvent extraction or in situ polymerization. Appropriate extraction of residual monomers, initiators, and solvents and toxicology on the materials are needed for any of these materials. Drawing methods using polymer-sugar solutions and polymer-sugar melts have also been used [97]. Fast-dissolving substrates have included carboxymethyl cellulose, dextran, chondroitin sulfate, dextrin polyvinyl pyrrolidine, polyvinyl alcohol, poly(lactic-*co*-glycolic) acid, and sugars. Sugar melts have used maltose, and in situ polymerization by ultraviolet radiation has employed *N*-vinylpyrrolidone and methacrylic acid. Prolonged release microneedles are formulated with PLA, polyglycolic acid, and their copolymers as melts [100].

Parathyroid hormone (PTH) 1-34 has been delivered to postmenopausal women for treatment of osteoporosis via microneedles in Phase 1 and Phase 2 clinical studies [103–105]. Microneedles fabricated with dextran, chitosan, and beta-sodium glycerophosphate and incorporating levonorgestrel and levonorgestrel hydroxypropyl-β-cyclodextrin were evaluated in rats. The levonorgestrel hydroxypropyl-β-cyclodextrin formulation showed enhanced dissolution and bioavailability [106]. Etonogestrel microcrystal particles imbedded in hydroxymethylcellulose and polyvinylacetate to form microneedles were evaluated in rats. BA was about 64% [107].

More recently, 3D printing has been implemented in the laboratory for rapid prototyping, device fabrication, administration of self-healing polymers with improved mechanical strength, and developing scaffolds for tissue engineering. The 3D printers using fused deposition modeling (FDM) are preferred for medical applications since FDM is compatible with PLA polyesters and other biorenewable thermoplastic materials that are FDA approved including polyglycolic acid, polycaprolactone, and poly(lactic-*co*-glycolic) acid. FDM in combination with a new method of chemical etching showed improved feature size resolution of FDM

printed materials allowing for the fabrication of biocompatible microneedles capable of penetrating the outer layers of skin and delivering approximately 80% of a model therapeutic agent. Microneedles of varying shapes, lengths, and array densities without the need of a master template were produced. Using this reported method scalable fabrication of 3D printed microneedles is anticipated [108].

Considerable therapeutic interest has developed over the past decade in microneedles as prophylactic delivery devices for vaccines. The epidermis is rich in antigen-presenting cells with Langerhans cells covering 25% of skin area [109]. Dose-sparing strong immune responses, which are superior to intramuscular injections, have been elicited transdermally. Transdermal vaccinations against influenza, tetanus, diphtheria, and malaria have been shown to be comparable to parenteral administration [110–114]. . Rapidly dissolving microneedles containing ovalbumin elicited considerable Th1 $CD4^+$ and potent cytotoxic $CD8^+$ T cell responses [42]. Many types of vaccines and disease targets have been tested with microneedle patches [115].

7.10.2 Thermal or Radio Frequency Ablation

Another method designed to alter skin permeability is thermal or radio frequency ablation. Thermal ablation selectively removes the stratum corneum by local application of radio-frequency producing heat for a short period of time. Thermal ablation has been used to generate pores for delivery of hydrophilic drugs [116].

Short application of radio frequency to the skin can result in the development of microchannels approximately 2 orders of magnitude greater than the diameter of proteins and potentially allowing delivery through the stratum corneum and epidermis. The delivery of the permeant correlates with the area fraction of pores created, the aqueous solubility, the reciprocal molecular weight of the permeant, and the concentration in the patch. For greater peak delivery, printed patches have been developed and more traditional patches have been used for continuous delivery. Compared to passive skin permeation in guinea pigs, radio frequency ablation increased the skin permeation of the hydrophobic drug, testosterone, when the drug was encapsulated in sulfobutyl ethers of β-cyclodextrins to render the permeant water-soluble. After ablation, there was an immediate increase in permeation of several orders of magnitude [117]. The permeation returned to its baseline slowly with large increases over baseline still observed at 24 hour after ablation and by 36 hour the penetration was close to its baseline value.

In vivo delivery of human growth hormone transdermally was demonstrated in guinea pigs and rats [118]. While rats and guinea pigs are inappropriate models for passive diffusion through human skin, there is more relevance for channels which are artificially created. Topical immunization of adenovirus-based vaccines

after thermal ablation was also shown [119]. Delivery of nanoparticles and gene therapy vectors appeared promising through in vitro human skin [120].

PTH fragment 1-34 stimulates bone growth when delivered in a pulsatile manner, but may have the reverse effect when given continuously, and is currently administered as an injection (Forteo®). Delivery from a 1 cm^2 patch was examined over seven days in 48 postmenopausal women with pharmacokinetic profiles reflecting the dose-dependence. After these initial successes, there has been less research in this area.

7.10.3 Sonophoresis

Ultrasound is any sound of a frequency above 20 kHz, and for most applications has been based on the piezoelectric effect, where application of rapidly alternating electric potential on surfaces of a crystal results in oscillating dimensional changes that become high-frequency sound. Ultrasound has been used to facilitate enhanced skin permeability for a few decades. While diagnostic ultrasound is at high frequencies of 2–10 MHz, therapeutic ultrasound (0.7–3 MHz) was originally applied for sonophoresis, and more recently, power ultrasound or low frequency ultrasound (5–100 KHz) has found even greater applications to sonophoresis. Absorption of ultrasound energy leads to the desired biological effects and when longitudinal waves are applied perpendicular to tissue, the intensity diminishes exponentially with depth from the source depending on the absorption coefficient.

Clinical studies of ultrasound at the lower frequencies of the therapeutic range showed under-optimized conditions, some enhancement of the anesthetic effect of lignocaine and prilocaine [121], and vasodilation caused by methyl and ethyl nicotinate, but not the more lipophilic hexyl nicotinate [122–124]. The enhanced absorption from the ultrasound was attributed to disordering of skin lipid structure. Reductions in the lag time as well as enhanced permeation were reported in guinea pigs using high-frequency ultrasound [125, 126]. Kost et al. [127] observed that both lipophilic and hydrophilic routes of permeation were altered, and therefore, alteration of lipids was insufficient to explain this effect. In other studies on rats and guinea pigs, where temperature was carefully monitored, mixing and cavitation were consistent with the observed increased penetration [128].

In contrast to the work discussed above, Mitragori et al. [129] demonstrated that power ultrasound (20 kHz) increased the permeation of proteins through human skin by several orders of magnitude. Although different frequency ranges have been tested, low-frequency sonophoresis (LFS) in the range of 20–100 kHz has been shown to be most effective in the transdermal delivery of high-molecular weight drugs such as proteins and nucleotides. LFS has been reported to be effective for the transdermal delivery of peptides, proteins, vaccines, oligonucleotides,

nanoparticles, and liposomes [130]. LFS enhances skin permeability by acoustic cavitation, thermal effects, radiation forces, and physical agitation of a coupling fluid which reduces the boundary layer to diffusion [131, 132].

Cavitation occurs with a liquid being pulled apart when sonic wave forces exceeds the tensile strength of the liquid causing voids in the liquid. There are two types of cavitation, stable and inertial. Stable cavitation is characterized by oscillation of void bubbles, and inertial cavitation gives rise to violent growth and bubble collapse. Inertial cavitation is important in LFS since it leads to the production of shock waves in the coupling fluid, which results in a liquid microjet. This produces ultrastructural defects in regions of the stratum corneum. Using confocal microscopy, cavitation was observed in the keratinocytes and was hypothesized to induce lipid disorder in the stratum corneum [133]. Inertial cavitation in association with stable cavitation results in water migration into the disrupted lipid regions of the stratum corneum. The drug is carried by convection and penetrates the stratum corneum. Ultrasound is typically not applied continuously in order to control heat production. Prolonged continuous exposure to ultrasound can cause adverse effects in underlying tissue including burns, necrosis, and epidermal detachment [134].

Current research is focused on enhancing skin permeability by combining LFS and high-frequency ultrasound in order to maximize focal areas of skin penetration, and miniaturization and optimization of ultrasonic equipment. An FDA-approved sonophoresis device, SonoPrep7®, has been manufactured which can be used for drug delivery as well as extraction of interstitial fluid for bioassay. Clinical trials showed that it can reduce onset time of the topical anesthetic, lidocaine, to five minutes [135]. The primary interest in sonophoresis, however, has been in the delivery of macromolecules. With the need to control heat production to prevent epidermal damage, safety is a concern. At present, sonophoresis has not been commercialized on a large scale, requires trained personnel for use, and cannot be used for patient self-administration of drugs. Finally, ultrasound has been combined with microneedles to increase the fluxes further through skin [136].

7.10.4 Electrical

7.10.4.1 Electroporation

Electroporation is the application of high-voltage pulses of several hundred volts for durations of 10 μs–10 ms in order to disrupt the stratum corneum and produce transient or permanent hydrophilic pores. Drug delivery is primarily by passive diffusion through these pores. A broad range of molecules can be delivered by electroporation including small molecules, proteins, and oligonucleotides [137]. For example, transport of calcein was carefully studied with high pulses and

demonstrated creation of much larger pores for less-selective transport of higher molecular weight permeants [138, 139]. Clinical safety is a problem, however, since high-voltage pulses can rapidly change the resistance of the stratum corneum. This can result in electrical stimulation which is no longer confined to the stratum corneum. Stimulation of lower lying nerves and motor neurons in the dermis elicit pain and muscle contractions. These concerns have limited the interest in further development of electroporation as a transdermal enhancement technique.

7.10.4.2 Iontophoresis

In contrast to passive skin permeation with a driving force of only a chemical potential gradient, iontophoresis involves the application of electric current to drive charged molecules through the skin by means of an electric potential gradient across the stratum corneum. Except for early transient transport, passive skin permeation occurs largely through lipid regions. In contrast, iontophoresis involves polar and ionic permeants through a porous pathway, that is presumed based on visualization of permeants [140] corresponding to only a small area fraction of hair follicles and sweat glands.

The applied current, I, is given by Ohm's Law, the electrical analog of Fick's Law for diffusion,

$$I = \frac{\Delta V}{R} \tag{7.29}$$

where ΔV is the voltage gradient and R is the stratum corneum electrical resistance. To control the iontophoretic flux across skin, a constant total current is generally applied, and the flux is linear with current density. The pores in skin are negatively charged and exhibit slight selectivity for cations based on the charge and structure of the permeant. This results in selectivity of the stratum corneum for certain ions and is determined by measuring the transport number, t, and is an indication of the ionic mobility and fraction of the current carried by the permeating ion [141].

Current and current density have both been found to scale with pain thresholds [142]. While there is some debate, a pain threshold of 0.5 mA/cm^2 has been suggested [143]. For very short durations greater current densities are well tolerated [142]. Lower current densities for long duration are known to cause skin irritation. Skin irritation is a function of current density and duration, where for a pulsatile iontophoretic application, the duration is the sum of the durations all pulses. Provided the pH from the electrodes is controlled appropriately, skin irritation consists of transient erythema and is not clinically significant [144]. When greater current densities elicit moderate skin irritation, the irritation is often not uniform like observed with chemical irritation from passive transport. Instead, the

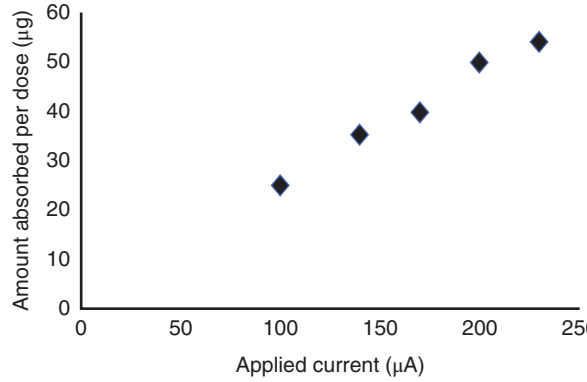

Figure 7.7 The linear relationship between applied current and amount of fentanyl hydrochloride absorbed per dose for an iontophoretic fentanyl device.

irritation may comprise a series of red spots centered on hair follicles or folliculitis. The skin irritation may show considerable intersubject variability.

The iontophoretic transport of fentanyl hydrochloride for patient-controlled analgesia [90] is marketed with on-demand pulsed delivery of 40 μg of fentanyl base equivalent for every 170 μA pulse when the patient pushes the button twice within three seconds. The system is designed to deliver no more than 6 doses per hour and 80 doses per day for a maximum of 3.2 mg per day. After either 80 doses per day or 24 hours, the system shuts off. The linear correlation between in vitro and in vivo delivery of fentanyl has been previously discussed in Figure 7.6. As previously mentioned in the discussion of Ohm's law, Eq. (7.29), the flux is linear with current density, and the total amount of drug delivered is proportional to the total applied current. This control of drug delivery through the skin by the total current results in the excellent in vitro/in vivo correlation, discussed previously in that section of this chapter. The linear dependence on applied current of the delivery of fentanyl hydrochloride [90] in pharmacokinetic studies in man is shown in Figure 7.7. The amount of fentanyl hydrochloride absorbed per dose in vivo was obtained using noncompartmental methods comparing the AUC for a particular pulsing period of the iontophoretic delivery to an intravenous infusion. For this set of data, the slope was 0.23 μg absorbed per dose/μA applied ($r^2 = 0.987$). The amount absorbed per dose-intercept is not significantly different from zero, and this agrees well with other pharmacokinetic data demonstrating that the passive delivery of fentanyl hydrochloride across skin (zero applied current) was negligible. The AUC (0–48 hour) for iontophoretic delivery of fentanyl hydrochloride through the chest (25.372 ng h/ml) and outer upper arm (25.835 ng h/ml) were approximately 20% greater than through the lower inner arm (23.93 ng h/ml). It is interesting to speculate that skin from the different regions may vary in ionic transport selectivity, as reflected by the transport number discussed previously.

Iontophoretic delivery that compared pulses of 25 and 40 μg of fentanyl hydrochloride were evaluated for plasma concentrations and pain scores by a visual analog scale (VAS). For both pulsed delivery rates, both the fentanyl concentrations and the VAS pain scores declined over the first few hours and reached nearly constant plasma concentrations after about six hours and throughout this period, the pain scores exhibited a slower steady decline [90]. Over this same time period, there was a linear correlation of fentanyl concentration with respiratory rate with respiratory depression being a major adverse event of opioid use.

Another application of iontophoresis is treatment of migraine headaches to the upper arm or thigh by iontophoretic delivery of sumatriptan succinate 6.5 mg (base) over four hours [80]. The bioavailability of iontophoretic delivery was compared to a 100 mg oral sumatriptan succinate tablet. The iontophoretic delivery achieved a near plateau in plasma concentrations within one hour that was maintained for the four-hour delivery period. In contrast, the oral tablet peaked within one hour at three times the level of the patch and then rapidly declined so that the plasma levels from the oral tablet did not substantially exceed the patch by the end of four hours. The rate and extent of delivery were much greater from the oral tablet with more than 15 times as much drug. The large reduction in C_{max} with iontophoretic delivery can, in principle, result in reduction in certain adverse events. A comparative study of the safety and efficacy with oral delivery was not conducted. The most common adverse events from iontophoretic delivery of sumatriptan were infrequent cases of allergic contact dermatitis (4%) and pain at the patch application site (4%) with 26% of the subjects on active patches reporting site pain.

While delivery from passive transdermal systems can be significantly affected by heat, the limitation of constant current limits the effect of heat on iontophoretic systems. Iontophoretic delivery of sumatriptan succinate was observed to be bioequivalent with and without an external therapeutic heat wrap around the system [80].

Iontophoretic systems offer an exciting alternative for delivery of ionizable drugs, particularly where variable delivery may have a therapeutic advantage and can justify the increased cost of a drug device combination. Further potential advantages are ability to limit the amount of drug in the system by relying on electric potential as the driving force and continuation of delivery of drug locally to the skin after the chemical gradient has been depleted. It has also been suggested and reviewed as a novel method of peptide delivery [145] and the role of electro-osmosis in iontophoretic transport has been extensively studied [146]. Electrosmosis of glucose has also been used as a means of iontophoretic extraction of glucose followed by detection and correlation with blood glucose levels [147]. Finally, iontophoresis for four to six hours of skin first treated with microneedles leads to short lag times and larger fluxes of drugs [148, 149].

7.11 Conclusion

Integrating transdermal mass transfer models with pharmacokinetic models is a powerful method providing predictable analytical drug disposition in vivo and the capability to evaluate transdermal delivery. In vivo assessment of transdermal drug delivery is the only truly viable way to evaluate delivery, tolerability, and adhesion of the patch. While mass transfer models provide insight, deconvolution is a necessary complement to prospective modeling in which the input function can be isolated and evaluated. Using these techniques, formulation factor effects can be investigated for strategic patch development and optimal therapeutic efficacy in the drug development process. If appropriate, IVIVCs can provide a regulatory bridge in the drug development process between manufacturing variables and in vivo transdermal drug delivery.

Over the past several decades, transdermal delivery has resulted in a series of a small number of successful drug products. Given the typical delay of over a decade to introduce new technologies to the market and the need to justify the added expense of the device, it is remarkable to see two recently approved iontophoretic products, a product with sonophoresis, and some highly promising vaccines in development. Although drug potency is a limiting factor for selection of drugs for transdermal delivery, the transdermal route of administration will remain an important mode of drug delivery for a select numbers of drug products.

References

1 Montagna, W. and Parakkal, P.F. (1974). *The Structure and Function of Skin*. New York: Academic Press.

2 Goldsmith, L.A. (1983). *Biochemistry and Physiology of the Skin*, vols. 1 and 2. New York: Oxford University Press.

3 Scheuplein, R.J. and Blank, I.H. (1971). Permeability of the skin. *Physiol. Rev.* 51: 702–747.

4 Keister, J.C. and Kasting, G.B. (1986). The use of transient diffusion to investigate transport pathways through skin. *J. Controlled Release* 4: 111–117.

5 Elias, P.M. (1981). Lipids and the epidermal permeability barrier. *Arch. Dermatol. Res.* 270: 95–117.

6 Yardley, H.J. and Summerly, R. (1981). Lipid composition and metabolism in normal and diseased epidermis. *Pharmacol. Ther.* 13: 357–383.

7 Guth, K., Schafer-Korting, M., Fabian, E. et al. (2015). Suitability of skin integrity tests for dermal absorption studies in vitro. *Toxicol. in Vitro* 29: 113–123.

8 Meidan, V.M. and Roper, C.S. (2008). Inter-and intra-individual variability in human skin barrier function: a large scale retrospective study. *Toxicol. in Vitro* 22: 1062–1069.

9 Godin, B. and Touitou, E. (2007). Transdermal skin delivery: predictions for humans from in vivo, ex vivo and animal models. *Adv. Drug Delivery Rev.* 59: 1152–1161.

10 Crank, J. and Park, G.S. (1968). *Diffusion in Polymers*, 1–39. New York: Academic Press.

11 Cooper, E.R. (1984). Increased permeability for lipophilic molecules. *J. Pharm. Sci.* 73: 1153–1156.

12 Katchalsky, A. and Curran, P.F. (1965). *Nonequilibrium Thermodynamics in Biophysics*, 113–132. Cambridge, MA: Harvard University Press.

13 Netzlaff, F., Schaefer, U.F., Lehr, C.M. et al. (2006). Comparison of bovine udder skin with human and porcine skin in percutaneous permeation experiments. *Altern. Lab. Anim.* 34: 499–513.

14 Jacobi, U., Kaiser, M., Tol, R. et al. (2007). Porcine ear skin: an in vitro model for human skin. *Skin Res. Technol.* 13: 19–24.

15 Gray, G.M. and Yardley, H.J. (1975). Lipid compositions of cells isolated from pig, human, and rat epidermis. *J. Lipid Res.* 16: 434–440.

16 Schmook, F.P., Meingassner, J.G., and Billick, A. (2001). Comparison of human skin or epidermis models with human and animal skin in in-vitro percutaneous absorption. *Int. J. Pharm.* 215: 51–56.

17 Lin, S.Y., Hou, S.J., Hsu, T.H.S., and Yeh, F.L. (1992). Comparisons of different animal skins with human skin in drug percutaneous penetration studies. *Methods Find. Exp. Clin. Pharmacol.* 14: 645–654.

18 Yalkowsky, S.H. (1981). *Techniques of Solubilization of Drugs*, 1–14. New York: Marcel Dekker.

19 Denbigh, K. (1981). *The Principles of Equilibrium*, 244. London: Cambridge University Press.

20 Kumins, C.A. and Kwei, T.K. (1968). Free volume and other theories. In: *Diffusion in Polymers* (eds. J.C. Crank and G.S. Park), 107–140. New York: Academic Press.

21 Potts, R.O. and Guy, R.H. (1992). Predicting skin permeability. *Pharm. Res.* 9: 663–669.

22 Kasting, G., Smith, R.L., and Cooper, E.R. (1987). Effect of lipid solubility and molecular size on percutaneous absorption. In: *Pharmacology of the Skin*, vol. 1 (eds. B. Shroot and H. Schaefer), 138–153. Basel: Karger Press.

23 Berner, B. and Coopeer, E.R. (1987). Models of skin permeability. In: *Transdermal Delivery of Drugs*, vol. 2 (eds. A.F. Kydonieus and B. Berner), 41–56. Boca Raton, FL: CRC Press.

24 Herman, A. and Herman, A.P. (2015). Essential oils and their constituents as skin penetration enhancer for transdermal delivery: a review. *J. Pharm. Pharmacol.* 67: 473–485.

25 Arora, A., Kisak, E., Karande, P. et al. (2010). Multicomponent chemical enhancer formulations for transdermal delivery: more is not always better. *J. Controlled Release* 144: 175–180.

26 Kunst, A. and Lee, G. (2016). Release and skin permeation of scopolamine from thin polymer films in relation to thermodynamic activity. *J. Pharm. Sci.* 105: 1496–1500.

27 Sachdeva, V., Bai, Y., Kydonieus, A., and Banga, A.K. (2013). Formulation and optimization of desogestrel transdermal contraceptive patch using crystallization studies. *Int. J. Pharm.* 44: 9–18.

28 Reismann, S. and Lee, G. (2012). Assessment of a five-layer laminate technique to measure the saturation solubility of drug in pressure-sensitive adhesive film. *J. Pharm. Sci.* 101: 2428–2438.

29 Jasti, B.R., Berner, B., Zhou, S.L., and Li, X. (2004). A novel method of determining drug solubility in polymeric matrices. *J. Pharm. Sci.* 93: 2135–2141.

30 Variankaval, N.E., Jacob, K.I., and Dinh, S.M. (2002). Polymorphism of 17-beta estradiol in a transdermal drug delivery system. *J. Mater. Sci. - Mater. Med.* 13: 271–280.

31 Rietveld, I.B. and Ceolin, R. (2015). Rotigotine: unexpected polymorphism with predictable overall monotropic behavior. *J. Pharm. Sci.* 104: 4117–4122.

32 Gupta, S.K., Gale, R., and Hwang, S.S. (1992). System functionality and, physicochemical model of fentanyl transdermal system. *J. Pain Symptom Manage.* 7: S17–S26.

33 Gale, R.M., Goetz, V., Lee, E.S. et al. (1986). Transdermal administration of fentanyl and device therefor. US Patent 4,588,580.

34 Berner, B., Otte, J.H., Mazzenga, G.C. et al. (1989). Ethanol-water mutually enhanced transdermal therapeutic system: I. Nitroglycerin solution properties and membrane transport. *J. Pharm. Sci.* 78: 314–318.

35 Berner, B., Mazzenga, G.C., Otte, J.H. et al. (1989). Ethanol-water mutually enhanced transdermal therapeutic system: II. Skin permeation of ethanol and nitroglycerin. *J. Pharm. Sci.* 78: 402–407.

36 Chandrasekaran, S.K. and Shaw, J.E. (1978). Factors influencing the percutaneous absorption of drugs. *Curr. Probl. Dermatol.* 7: 142–155.

37 Scheuplein, R.J. and Ross, L. (1970). Effects of surfactants and solvents on the permeability of epidermis. *J. Soc. Cosmet. Chem.* 21: 853–873.

38 Scheuplein, R.J. and Dugard, P.H. (1973). Effects of ionic surfactants on the permeability of human epidermis: an electrometric study. *J. Invest. Dermatol.* 60: 263–269.

39 Cooper, E.R. and Berner, B. (1985). Interactions of surfactants with epidermal tissues-physicochemical aspects. In: *Surfactants in Cosmetics* (ed. M.M. Rieger), 195–210. New York: Marcel Dekker.

40 Laughlin, R.G. (1978). Relative hydrophilicities among surfactant hydrophilic groups. In: *Advances in Liquid Crystals*, vol. 3 (ed. G.H. Brown), 99–148. New York: Academic Press.

41 Cooper, E.R. and Berner, B. (1987). Penetration enhancers. In: *Transdermal Delivery of Drugs*, vol. 2 (eds. A.F. Kydonieus and B. Berner), 57–62. Boca Raton, FL: CRC Press.

42 Berner, B., Wilson, D.R., Guy, R.H. et al. (1988). The relationship of pK_a and acute skin irritation in man. *Pharm. Res.* 5: 660–663.

43 Berner, B., Wilson, D.R., Steffens, R.J. et al. (1990). The relationship between pK_a and skin irritation for a series of basic penetrants in man. *Fundam. Appl. Toxicol.* 15: 760–766.

44 Berner, B., Mazzenga, G.C., Gargiulo, P.M., and Steffens, R. (1992). A transdermal nicotine system: feasibility studies. *J. Controlled Release* 20: 13–20.

45 Cooper, E.R. (1976). Pharmacokinetics of skin penetration. *J. Pharm. Sci.* 65: 1396–1397.

46 Berner, B. (1987). Pharmacokinetics of skin penetration. In: *Transdermal Delivery of Drugs*, vol. 2 (eds. A.F. Kydonieus and B. Berner), 134–148. Boca Raton, FL: CRC Press.

47 Nakashima, E., Noonan, P.K., and Benet, L.Z. (1987). Transdermal bioavailability and first-pass skin metabolism: a preliminary evaluation with nitroglycerin. *J. Pharmacokinet. Biopharm.* 15: 423–437.

48 Liu, P.F., Higuchi, W.I., Song, W. et al. (1991). Quantitative evaluation of ethanol effects on diffusion and metabolism of ß-estradiol in hairless mouse skin. *Pharm. Res.* 8: 865–872.

49 Zhang, Q., Grice, J.E., Wang, G., and Roberts, M.S. (2009). Cutaneous metabolism in transdermal drug delivery. *Curr. Drug Metab.* 10: 227–231.

50 Hikima, T., Tojo, K., and Maibach, H.I. (2005). Skin metabolism in transdermal therapeutic systems. *Skin Pharmacol. Physiol.* 18: 153–159.

51 Drugs@FDA. (2010) Butrans buprenorphine. Purdue Pharma LP. NDA: 021306 (approval date: 30 June 2010). https://www.accessdata.fda.gov/drugsatfda_docs/nda/2010/021306Orig1s000ClinPharmR.pdf.

52 Food and Drug Administration, Center for Drug Evaluation and Research (CDER) (2011). *Guidance for Industry: Residual Drug in Transdermal and Related Drug Delivery Systems*. Rockville, MD: Food and Drug Administration, Center for Drug Evaluation and Research (CDER).

53 Cooper, E.R. and Berner, B. (1985). Finite dose pharmacokinetics of skin penetration. *J. Pharm. Sci.* 74: 1100–1102.

54 Carslaw, H.S. and Jaeger, J.C. (1959). *Conduction of Heat in Solids*, 2nd ed., 100. London: Oxford University Press.

55 Noetzli, M. and Eap, C.B. (2013). Pharmacodynamic, pharmacokinetic, and pharmacogenetic aspects of drugs used in the treatment of Alzheimer's disease. *Clin. Pharmacokinet.* 52: 225–241.

56 Chandrasekaran, S.K., Bayne, W., and Shaw, J.E. (1978). Pharmacokinetics of drug permeation through human skin. *J. Pharm. Sci.* 67: 1370–1374.

57 Toon, S., Hopkins, K.J., Asrons, L., and Rowland, M. (1989). Rate and extent of absorption of clonidine from a transdermal therapeutic system. *J. Pharm. Pharmacol.* 41: 17–21.

58 MacGregor, T.R., Matzek, K.M., Keirns, J.J. et al. (1985). Pharmacokinetics of transdermally delivered clonidine. *Clin. Pharmacol. Ther.* 38: 278–284.

59 Berner, B. (1984). The pharmacokinetics of removal and re-application of transdermal patches. *J. Controlled Release* 1: 127–135.

60 Berner, B. and John, V.A. (1994). Pharmacokinetic characterization of transdermal delivery systems. *Clin. Pharmacokinet.* 26: 121–134.

61 Gibaldi, M. and Perrier, D. (1982). *Pharmacokinetics*, 2nd ed., 145–198. New York: Marcel Dekker, Inc.

62 Hildebrand, F.B. (1976). *Advanced Calculus for Applications*, 2e, 622–628. Englewood Cliffs, NJ: Prentice-Hall, Inc.

63 Li, J. and Cutler, D.J. (1998). Stability of finite difference deconvolution II: simulation studies. *Biopharm. Drug Dispos.* 19: 595–603.

64 Jansson, P.A. (1984). *Deconvolution with Applications in Spectroscopy*, 67–134. Orlando, FL: Academic Press, Inc.

65 Kiwada, H., Morita, K., Hayashi, M. et al. (1977). A new numerical calculation method for deconvolution in linear compartment analysis of pharmacokinetics. *Chem. Pharm. Bull.* 25: 1312–1318.

66 Altman, N.S. (1992). An introduction to kernel and nearest-neighbor nonparametric regression. *Am. Stat.* 46: 175–185.

67 Langenbucher, F. (2003). Handling of computational in vitro/in vivo correlation problems by Microsoft Excel: III. Convolution and deconvolution. *Eur. J. Pharm. Biopharm.* 56: 429–437.

68 Cutler, D.J. (1978). Numerical deconvolution by least squares: use of a prescribed input function. *J. Pharmacokinet. Biopharm.* 6: 227–241.

69 Veng-Pedersen, P. (1980). Novel approach to bioavailability testing: statistical method for comparing drug input calculated by a least-squares deconvolution technique. *J. Pharm. Sci.* 69: 318–324.

70 Gillespie, W.R. and Veng-Pedersen, P. (1985). A polyexponential deconvolution method. Evaluation of the "gastrointestinal bioavailability" and mean in vivo dissolution time of some ibuprofen dosage forms. *J. Pharmacokinet. Biopharm.* 13: 289–307.

71 Verotta, D. (1993). Estimation and model selection in constrained deconvolution. *Ann. Biomed. Eng.* 21: 605–620.

72 Verotta, D. (1996). Concepts, properties, and applications of linear systems to describe distribution, identify input, and control endogenous substances and drugs in biological systems. *Crit. Rev. Biomed. Eng.* 24: 73–139.

73 Debord, J., Risco, E., Harel, M. et al. (2001). Application of a gamma model of absorption to oral cyclosporine. *Clin. Pharmacokinet.* 40: 375–382.

74 Levitt, D.G. (2003). The use of a physiologically based pharmacokinetic model to evaluate deconvolution measurements of systemic absorption. *BMC Clin. Pharmacol.* 3: 1–29.

75 Food and Drug Administration (2014). *Draft Guidance on Buprenorphine*. Rockville, MD: Food and Drug Administration.

76 Drugs@FDA. (2007) Neupro® rotigotine. UCB Inc. NDA: 021829 (approval date: 5 September 2007). http://www.accessdata.fda.gov/drugsatfda_docs/nda/2007/021829s000_ClinPharmR_P1.pdf.

77 Drugs@FDA. (2006) Daytrana® methylphenidate. Noven Pharmaceuticals, Inc. NDA: 021514 (approval date: 6 April 2006). http://www.accessdata.fda.gov/drugsatfda_docs/nda/2006/021514s000_ClinPharmR_P1.pdf.

78 Cummings, J., Lefevre, G., Small, G., and Appel-Dingemanse, S. (2007). Pharmacokinetic rationale for the rivastigmine patch. *Neurology* 69: S10–S13.

79 Drugs@FDA. (2007) Exelon® rivastigmine. Novartis. NDA: 022083 (approval date: 6 July 2007). http://www.accessdata.fda.gov/drugsatfda_docs/nda/2007/022083s000_ClinPharmR_P1.pdf.

80 Drugs@FDA. (2013) Zecuity® iontophoretic sumatriptan succinate. Teva. NDA: 202278 (approval date: 17 January 2013). https://www.accessdata.fda.gov/drugsatfda_docs/nda/2013/202278Orig1s000ClinPharmR.pdf.

81 Food and Drug Administration, Center for Drug Evaluation and Research (CDER) (1997). *Guidance for Industry: Extended Release Oral Dosage Forms: Development, Evaluation and Application of In vitro/In vivo Correlations*. Rockville, MD: Food and Drug Administration, Center for Drug Evaluation and Research (CDER).

82 Lin, S., Kao, Y., and Chang, H. (1990). Preliminary evaluation of the correlation between in vitro release and in vivo bioavailability of two aminophylline slow-release tablets. *J. Pharm. Sci.* 79: 326–330.

83 Hussein, Z. and Friedman, M. (1990). Release and absorption characteristics of novel theophylline sustained-release formulations: in vitro-in vivo correlation. *Pharm. Res.* 7: 1167–1171.

84 Drewe, J. and Guitard, P. (1993). In vitro-in vivo correlation for modified-release formulations. *J. Pharm. Sci.* 82: 132–137.

85 Hayashi, T., Ogura, T., and Takagishi, Y. (1995). New evaluation method for in vitro/in vivo correlation of enteric-coated multiple unit dosage forms. *Pharm. Res.* 12: 1333–1337.

86 Jung, H., Milan, R.C., Girard, M.E. et al. (1997). Bioequivalence study of carbamazepine tablets: in vitro/in vivo correlation. *Int. J. Pharm.* 152: 37–44.

87 Abuzarur-aloul, R., Gjellan, K., Sjöund, M., and Graffner, C. (1998). Critical dissolution tests of oral systems based on statistically designed experiments III. In vitro/in vivo correlation for multiple-unit capsules of paracetamol based on PLS modeling. *Drug Dev. Ind. Pharm.* 24: 371–383.

88 Chan, K.K.H., Ross, H.D., Berner, B. et al. (1990). Pharmacokinetics of a single transdermal dose of nicotine in healthy smokers. *J. Controlled Release* 14: 145–151.

89 Kochak, G.M., Berner, B., Leal, M., and Sambol, N.C. (1992). Variational analysis of the transdermal delivery rate from two prototypical ethanol-water nitroglycerin TTS devices and Transderm Nitro™ 10 in the normal population. *J. Pharmacokinet. Biopharm.* 20: 443–459.

90 Drugs@FDA. (2006) Ionsys® iontophoretic fentanyl hydrochloride. The Medicines Co. NDA: 021338 (approval date: 22 May 2006). https://www.accessdata.fda.gov/drugsatfda_docs/nda/2006/021338s000_ClinPharmR.pdf.

91 Lefevre, G., Sedek, G., Huang, H.L. et al. (2007). Pharmacokinetics of a rivastigmine transdermal patch formulation in healthy volunteers: relative effects of body site application. *J. Clin. Pharmacol.* 47: 471–478.

92 Food and Drug Administration, Center for Drug Evaluation and Research (CDER) (1997). *Guidance for Industry: Skin Irritation and Sensitization Testing of Generic Transdermal Products*. Rockville, MD: Food and Drug Administration, Center for Drug Evaluation and Research (CDER).

93 Food and Drug Administration, Center for Drug Evaluation and Research (CDER) (2008). *Guidance for Industry and Review Staff: Nonclinical Safety Evaluation of Reformulated Drug Products and Products Intended for Administration by An Alternate Route*. Draft Guidance. Rockville, MD: Food and Drug Administration, Center for Drug Evaluation and Research (CDER).

94 Park, J.H., Choi, S.O., Seo, S. et al. (2010). A microneedle roller for transdermal drug delivery. *Eur. J. Pharm. Biopharm.* 76: 282–289.

95 Gupta, J., Felner, E.I., and Prausnitz, M.R. (2009). Minimally invasive insulin delivery in subjects with type I diabetes using hollow microneedles. *Diabetes Technol. Ther.* 11: 329–337.

96 Zhu, Q., Zarnitsyn, V.G., Ye, L. et al. (2009). Immunization by vaccine-coated microneedle arrays protects against lethal influenza virus challenge. *Proc. Natl. Acad. Sci. U.S.A.* 106: 7968–7973.

97 Lee, K., Lee, C.Y., and Jung, H. (2011). Dissolving microneedles for transdermal drug administration prepared by stepwise controlled drawing of maltose. *Biomaterials* 32: 3134–3140.

98 Moga, K.A., Bickford, L.R., Geil, R.D. et al. (2013). Rapidly-dissolvable microneedle patches via a highly scalable and reproducible soft lithography approach. *Adv. Mater.* 25: 5060–5066.

99 Indermum, S., Luttge, R., Choonara, Y. et al. (2014). Current advances in the fabrication of microneedles for transdermal delivery. *J. Controlled Release* 185: 130–138.

100 Park, K., Allen, M.G., and Prausnitz, M.R. (2005). Biodegradable polymer microneedles: fabrication, mechanics and transdermal drug delivery. *J. Controlled Release* 104: 51–66.

101 Bal, S., Kruithof, A.C., Liebl, H. et al. (2010). In vivo visualization of microneedle conduits in human skin using laser scanning microscopy. *Laser Phys. Lett.* 7: 242–246.

102 Kalluri, H. and Banga, A.J. (2010). Formation and closure of microchannels in skin following microporation. *Pharm. Res.* 28: 82–94.

103 Kim, Y.C., Park, J.H., and Prausnitz, M.R. (2012). Microneedles for drug and vaccine delivery. *Adv. Drug Delivery Rev.* 64: 1547–1568.

104 Cosman, F., Lane, N.E., Bolognese, M.A. et al. (2010). Effect of transdermal teriparatide administration on bone mineral density in postmenopausal women. *J. Clin. Endocrinol. Metab.* 95: 151–158.

105 Dadonna, P., Matriano, J., Mandema, J., and Maa, Y.-F. (2011). Parathyroid hormone (1-34)-coated microneedle patch system: clinical pharmacokinetics and pharmacodynamics for treatment of osteoporosis. *Pharm. Res.* 28: 159–165.

106 Yao, G., Quan, G., Lin, S. et al. (2017). Novel dissolving microneedles for enhanced transdermal delivery of levonorgestrel: in vitro and in vivo characterization. *Int. J. Pharm.* 534: 378–386.

107 He, M., Yang, G., Zhang, S. et al. (2017). Dissolving microneedles loaded with etonogestrel microcrystal particles for intradermal sustained delivery. *J. Pharm. Sci.* https://doi.org/10.1016/j.xphs.2017.11.013.

108 Luzuriaga, M.A., Berry, D.R., Reagan, J.C. et al. (2018). Biodegradable 3D printed polymer microneedles for transdermal drug delivery. https://chemrxiv.org/articles/Biodegradable_3D_Printed_Polymer_Microneedles_for_Transdermal_Drug_Delivery/5851950 (accessed 17 December 2020).

109 Glenn, G.M., Taylor, D.N., Li, X. et al. (2000). Transcutaneous immunization: a human vaccine delivery strategy using a patch. *Nat. Med.* 6: 1403–1406.

110 Kommareddy, S., Baudner, B.C., Oh, S. et al. (2012). Dissolvable microneedle patches for the delivery of cell-culture-derived influenza vaccine antigens. *J. Pharm. Sci.* 101: 1021–1027.

111 Raphael, A.P., Prow, T.W., Crichton, M.L. et al. (2010). Targeted, needle-free vaccinations in skin using multilayered, densely-packed dissolving microprojection arrays. *Small* 6: 1785–1793.

112 Sullivan, S.P., Koutsonanos, D.G., Del Pilar Martin, M. et al. (2010). Dissolving polymer microneedle patches for influenza vaccination. *Nat. Med.* 16: 915–920.

113 Zaric, M., Lyubomska, O., Touzeler, O. et al. (2013). Skin dendritic cell targeting via microneedle arrays laden with antigen-encapsulated poly-D, L-lactide-co-glycolide nanoparticles induces efficient antitumor and antiviral immune responses. *ACS Nano* 7: 2042–2055.

114 Matsuo, K., Hirobe, S., Yokota, Y. et al. (2012). Transcutaneous immunization using a dissolving microneedle array protects against tetanus, diphtheria, malaria, and influenza. *J. Controlled Release* 160: 495–501.

115 Suh, J., Shin, J., and Kim, Y.C. (2014). Microneedle patches for vaccine delivery. *Clin. Exp. Vaccine Res.* 3: 42–49.

116 Sintov, A.C., Krymberk, I., Daniel, D. et al. (2003). Radiofrequency-driven skin microchanneling as a new way of electrically assisted transdermal delivery of hydrophilic drugs. *J. Controlled Release* 39: 311–320.

117 Kam, Y., Sacks, H., Mevorat Kaplan, K. et al. (2012). Radio frequency-microchannels for transdermal delivery: characterization of skin recovery and delivery window. *Pharmacol. Pharm.* 3: 20–28.

118 Levin, G., Gershonowitz, A., Sacks, H. et al. (2005). Transdermal delivery of human growth hormone through RF-microchannels. *Pharm. Res.* 22: 550–555.

119 Bramson, J., Dayball, K., Evelegh, C. et al. (2003). Enabling topical immunization via microporation: a novel method for pain-free and needle-free delivery of adenovirus-based vaccines. *Gene Ther.* 10: 251–260.

120 Birchall, J., Coulman, S., Anstey, A. et al. (2006). Cutaneous gene expression of plasmid DNA in excised human skin following delivery via microchannels created by radiofrequency ablation. *Int. J. Pharm.* 312: 15–23.

121 Benson, H.A.E., McElnay, J.C., and Harland, R. (1988). Phonophoresis of lignocaine and prilocaine from Emla cream. *Int. J. Pharm.* 44: 65–69.

122 Benson, H.A.E., McElnay, J.C., McCallion, O. et al. (1989). Influence of ultrasound on the percutaneous absorption of a range of nicotinate esters. *J. Pharm. Pharmacol.* 40: 40.

123 Benson, H.A.E., McElnay, J.C., Harland, R., and Hadgraft, J. (1991). Influence of ultrasound on the percutaneous absorption of nicotinate esters. *Pharm. Res.* 8: 204–209.

124 McElnay, J.C., Benson, H.A.E., Harland, R., and Hadgraft, J. (1993). Phonophoresis of methyl nicotinate: a preliminary study to elucidate the mechanism. *Pharm. Res.* 4: 1726–1731.

125 Bommannan, D., Okuyama, H., Stauffer, P., and Guy, R.H. (1992). Sonophoresis I: the use of high-frequency ultrasound to enhance transdermal drug delivery. *Pharm. Res.* 9: 559–564.

126 Bommannan, D., Menon, G.K., Okuyama, H. et al. (1992). Sonophoresis II: examination of the mechanisms of ultrasound-enhanced transdermal drug delivery. *Pharm. Res.* 9: 1043–1047.

127 Kost, J., Macluf, M., and Langer, R. (1990). Experimental approaches to elucidate the mechanism of ultrasonically enhanced transdermal drug delivery. *Proc. Int. Symp. Controlled Release Bioact. Mater.* 17: 29–30.

128 Levy, D., Kost, J., Mashlulam, Y., and Landger, R. (1989). Effect of ultrasound on transdermal drug delivery in rats and Guinea pigs. *J. Clin. Invest.* 83: 2074–2078.

129 Mitragori, S., Blankschtein, D., and Langer, R. (1995). Ultrasound-mediated transdermal protein delivery. *Science* 269: 850–853.

130 Polat, B.E., Blankschtein, D., and Langer, R. (2010). Low-frequency sonophoresis: application to the transdermal delivery of macromolecules and hydrophilic drugs. *Exp. Opin. Drug Delivery* 7: 1415–1432.

131 Oberli, M.A., Schoellhammer, C.M., Langer, R., and Blankschtein, D. (2014). Ultrasound-enhanced transdermal delivery: recent advances and future challenges. *Ther. Delivery* 5: 843–857.

132 Wong, T.W. (2014). Electrical, magnetic, photomechanical and cavitational waves to overcome skin barrier for transdermal drug delivery. *J. Controlled Release* 193: 257–269.

133 Mitragori, S., Edwards, D., Blankschtein, D., and Langer, R. (1995). A mechanistic study of ultrasonically-enhanced transdermal drug delivery. *J. Pharm. Sci.* 94: 697–706.

134 Boucaud, A., Montharu, J., Machet, L. et al. (2001). Clinical, histologic, and electron microscopy study of skin exposed to low-frequency ultrasound. *Anat. Rec.* 264: 114–119.

135 Zempsky, W.T., Robins, B., and McKay, K. (2008). Reduction of topical anesthetic onset time using ultrasound: a randomized controlled trial prior to venipuncture in young children. *Pain Med.* 9: 795–802.

136 Han, T. and Das, D.B. (2015). Potential of combined ultrasound and microneedles for enhanced transdermal drug permeation: a review. *Eur. J. Pharm. Biopharm.* 89: 312–328.

137 Escobar-Chávez, J.J., Bonilla-Martínez, D., Villegas-González, M.A., and Revilla-Vázquez, A.L. (2009). Electroporation as an efficient physical enhancer for skin drug delivery. *J. Clin. Pharmacol.* 49: 1262–1283.

138 Prausnitz, M.R., Bose, V.G., Langer, R., and Weaver, J.C. (1993). Electroporation of mammalian skin: a mechanism to enhance transdermal drug delivery. *Proc. Natl. Acad. Sci. U.S.A.* 90: 10504–10508.

139 Prausnitz, M.R., Lee, C., Liu, C.H. et al. (1996). Transdermal transport efficiency during skin electroporation and iontophoresis. *J. Controlled Release* 38: 205–217.

140 Molitor, H. and Fernadez, L. (1939). Studies on iontophoresis. *Am. J. Med. Sci.* 198: 778–785.

141 DeNuzzio, J.D. and Berner, B. (1990). Electrochemical and iontophoretic studies of human skin. *J. Controlled Release* 11: 105–112.

142 Prausnitz, M.R. (1997). The effects of pulsed current on skin damage, sensation, and pain. *Proc. Int. Symp. Controlled Release Bioact. Mater.* 24: 25–26.

143 Schwarz, V., Sutcliffe, C.H., and Style, P.P. (1968). Some hazards of the sweat test. *Arch. Dis. Childh.* 43: 695–701.

144 Camel, E., O'Connell, M., Sage, B. et al. (1996). The effect of saline iontophoresis on skin integrity in human volunteers. *Fundam. Appl. Toxicol.* 32: 168–178.

145 Delgado-Charro, M.B. and Guy, R.H. (1998). Iontophoresis of peptides. In: *Electronically Controlled Drug Delivery* (eds. B. Berner and S.M. Dinh), 129–157. Boca Raton, FL: CRC Press.

146 Delgado-Charro, M. and Guy, R.H. (1994). Characterization of convective solvent flow during iontophoresis. *Pharm. Res.* 11: 929–935.

147 Tamada, J.A. and Potts, R.O. (1998). Glucose monitoring using electroosmotic transdermal extraction. In: *Electronically Controlled Drug Delivery* (eds. B. Berner and S.M. Dinh), 129–157. Boca Raton, FL: CRC Press.

148 Singh, N.D. and Banga, A.K. (2013). Controlled delivery of ropinirole hydrochloride using modulated iontophoresis and microneedles. *J. Drug Targeting* 21: 354–366.

149 Pawan, K.R., Smith, F., Kolli, C.S., and Babu, J. (2013). Effect of lipophilicity on microneedle mediated iontophoretic transdermal delivery across human skin in vitro. *J. Pharm. Sci.* 102: 3784–3791.

8

Formulation and Pharmacokinetic Challenges Associated with Targeted Pulmonary Drug Delivery

Tomoyuki Okuda[1] *and Hak-Kim Chan*[2]

[1] *Faculty of Pharmacy, Meijo University, Nagoya, Japan*
[2] *Advanced Drug Delivery Group, Faculty of Pharmacy, University of Sydney, Australia*

8.1 Progress on Formulations and Devices for Inhaled Drugs

Pharmacotherapy by pulmonary drug delivery has expanded well beyond the treatment of asthma and chronic obstructive pulmonary disease (COPD), as is evident in the types of marketed inhalation products which include indications for pulmonary arterial hypertension (PAH), cystic fibrosis, and neurological disorders (Table 8.1).

Pulmonary drug delivery is commonly achieved through pressurized metered-dose inhalers (pMDIs), nebulizers, and dry powder inhalers (DPIs). All three types of aerosol delivery systems have gone through rapid phases of development with innovation and improvement over the past 30 years. New excipients and metered-dose inhaler (MDI) valve materials developed to cater for the propellant transition from the chlorofluorocarbons (CFCs) to hydrofluoroalkanes (HFAs) in the formulation, along with a new mechanism to increase the lung dose by reducing the need to synchronize MDI actuation and aerosol inhalation and by slowing down the aerosol ballistic velocity [1, 2]. Nebulizers have progressed from the conventional design of continuous aerosol generation using either compressed gas or ultrasonic vibration, to newer technology with targeted delivery during a specific phase of the breathing cycle (adaptive aerosol, AKITA®, breath-enhanced), or technology which uses a vibrating mesh to push liquid through the orifices to generate aerosols with finer particle size and higher output rate [3, 4]. An innovative alternative to pMDI and nebulizers is the Respimat® Soft Mist™ Inhaler, which utilizes collision of opposing liquid jets to aerosolize a liquid formulation which can be ethanolic or aqueous solutions

Drug Delivery Approaches: Perspectives from Pharmacokinetics and Pharmacodynamics,
First Edition. Edited by Bret Berner, Toufigh Gordi, Heather A. E. Benson, and Michael S. Roberts.

Table 8.1 Current use of inhaled drugs for pharmacotherapy.

Drugs	Indications
Bronchodilators (e.g. β_2-agonists)	Asthma and COPD
Anti-inflammatory drugs (e.g. inhaled corticosteroids)	Asthma and COPD
Antibiotics (e.g. tobramycin)	Respiratory infections
Vasodilators (e.g. Iloprost)	Pulmonary arterial hypertension
Proteins (e.g. rhDNase, insulin)	Cystic fibrosis, diabetes
Osmolytes (e.g. mannitol)	Asthma diagnosis, mucus clearance
Analgesics (e.g. ergotamine)	Migraine pains
CNS drugs (e.g. loxapine)	Neurological disorders

[5]. Amid these advances, DPI has undergone the most changes in both the inhaler device and formulation designs, as shown by the number of patents [6, 7]. Lactose as a carrier is now understood to be playing a role more than just as a diluent for low-dose drugs or a bulking agent for improving the flow in device filling. Lactose is pivotal to the aerosol performance of the blend formulation, hence, the type of lactose, particle size distribution, fine particle fraction, particle morphology, surface roughness, moisture content, and electrostatic charge are factors to be considered in lactose formulation, and a special issue on the topic of lactose as a DPI carrier was published which was based discussions from a two-day symposium held in Parma in 2010 [8]. The discussions did not resolve all the problems related to lactose carrier, but highlighted the key issues and what needs to be done to address them. These include the confounding factors which can complicate the interpretation of the performance of DPI formulations and the lack of innovative methods which can analyze critical powder properties affecting powder dispersion. While lactose blend has been the mainstream for DPI formulations, lactose-free engineered particles have also been developed for marketed products, with spray-dried powders being the prime examples (e.g. Pulmosol™ in Exubera®, PulmoSphere™ in TOBI® Podhaler™, and mannitol in Aridol®) and, as discussed below, the trend will continue to rise in the future. Regarding the DPI devices, modeling and simulation using computational fluid dynamics (CFD) and discrete element method (DEM) have deepened the understanding on powder deagglomeration in the device, although these findings are yet to be utilized and applied to rational inhaler design. The general trend has been to move away from single-dose DPI toward multiple-dose DPI (Turbuhaler®, Twisthaler®), but interestingly single-dose products remain in recently marketed products (Spiriva® Handihaler®, TOBI Podhaler). While the first-generation DPI

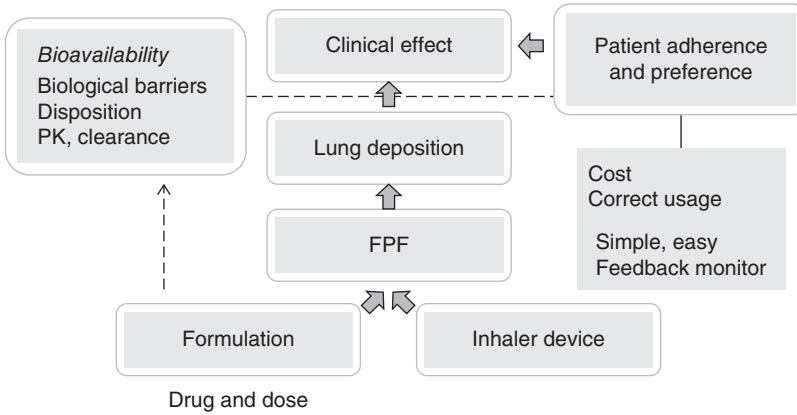

Figure 8.1 Design space considerations for development of inhalation products.

products (e.g. Rotahaler®, Spinhaler®) were known to perform rather poorly with a relatively low fine particle fraction (FPF) (<20%) [9, 10], newer products (e.g. Accuhaler®, Twisthaler) do not necessarily produce a much higher FPF (e.g. 30–35% for Twisthaler), but the emitted dose uniformity was shown to be more consistent [11]. From the formulation perspective, lactose blends still remain as the main stream. But due to the need to deliver a diversity of drugs (Figure 8.1) to the lungs, the situation is about to change, and with the change, it will bring along challenges and hurdles to overcome.

A starting point for the formulation and pharmacokinetic (PK) challenges associated with targeted pulmonary drug delivery is the design space for developing inhalation products (Figure 8.1). While the aspects on formulation and inhaler device are confined to DPI, the rest is applicable to any pulmonary delivery system such as pMDI and nebulizers. In this design space, the ultimate objective is to achieve desirable clinical outcome (therapeutic efficacy without unwanted side effects). Two important determinants for the clinical outcome are the patient usage and delivered lung dose. Regardless of how wonderful the performance of a pharmaceutical product may be, it is of no benefit to the treatment if a patient does not use it or uses it improperly. This, in turn, depends on other key factors such as pharmacoeconomics (cost to the patients, health-care providers, and/or government) and the product features (being simple and easy to use with feedback to patient to ensure correct usage). Once the patient usage is addressed, the next consideration is the dose delivered to the lungs. Although the lung dose impacts pharmacodynamic (PD) effects, the relationship between them is not necessarily linear. This is because the translation of a lung dose to a clinical outcome hinges on the bioavailability. Depending on whether the drug is intended for local action or for systemic effect and whether the drug is a small molecule or a macromolecule,

the drug deposited in the lungs needs to overcome various biological barriers (e.g. mucus, epithelium, and paracellular tight junctions) before reaching the target site. The drug will be also subject to absorption into the systemic circulation by passive diffusion or active transport, enzymatic degradation in the lungs, clearance by mucociliary mechanism, and macrophage uptake – with the dissolution rate and physicochemical properties of the aerosol particle properties controlling the fate of the drug.

FPF is determined by the inhaler device and formulation, but to a varying extent depending on the situation. FPF from nebulization is determined mainly by the nebulizer device efficiency and/or air flow, as the formulations are almost exclusively aqueous solution with little surface activity. FPF from pMDI is determined by both the metering valve features (i.e. metered volume, orifice diameter of the actuator) and the formulation (i.e. suspension vs. solution, particle size of the suspension, suspension stability, cosolvent amount, and propellant type) [1, 2]. For DPI, both the device and formulation interact closely to determine the FPF. For a given powder formulation with low dispersibility, a high-efficiency device will produce higher FPF than a low efficiency one such as the Rotahaler [9]. Conversely, for a highly dispersible powder formulation, even a low-efficiency inhaler can produce a reasonably high FPF [12, 13]. In other words, a readily dispersible powder formulation can reduce the dependence of FPF on the inhaler device.

8.2 Challenges for Inhaled Formulations

8.2.1 High-Dose Drugs and Amorphous Powders

Among the new inhalation products, inhaled antibiotics (e.g. tobramycin, colistin) require a large dose which usually is around 100 mg [14, 15]. This precludes the use of pMDI which generally delivers 1 mg or less and necessitates the administration by nebulizers and DPI. Nebulizers (e.g. TOBI solution) take more effort and a longer time for administration while DPI could cause unwanted coughing as a side effect [14, 15]. The challenge for DPI can be partly overcome by improving the aerosol performance so as to by-pass larynx-pharyngeal deposition to avoid cough triggers including mechanosensors and chemosensors in the extrapulmonary airways (larynx, trachea, and large bronchi). However, cough sensors are also present in the intrapulmonary airways and lung parenchyma [16]. For bacterial infection in the upper airways, a fine balance is necessary for the aerosol to minimize upper airway deposition, yet not to completely avoid it causing maximal deposition in alveoli which is not the site of action.

A formulation challenge for DPI is the high-dose requirement, which precludes the use of coarse lactose blends that would increase the bulk of the formulation,

resulting in extra effort and time required for inhalation. Hence, high-dose DPI contains mostly drug with very little excipient (e.g. tobramycin with distearoylphosphatidylcholine [DSPC], TOBI Podhaler) or pure drug only (e.g. inhaled mannitol, Aridol). These high-dose formulations were prepared by spray drying, not the conventional milling method. Milling is known to cause amorphization in solids and with the increased energy state, the powder becomes more adhesive and difficult to disperse. However, spray drying also tends to produce amorphous materials as the liquid spray is rapidly evaporated and turned into a dry powder. Because of the amorphous nature of the powder, another challenge for high-dose drug is the stability of the DPI formulation. It is necessary to mitigate any potential deleterious effect due to moisture contact. The amorphous powder is usually protected from humidity by packaging materials such as an aluminum blister (e.g. inhaled insulin in Exubera) or overwrap (TOBI Podhaler). Alternative methods which can produce crystalline powders would be highly desirable.

8.2.2 Generic DPI Formulations

A proven way to alleviate the respiratory health-care burden is the availability of generic medicines, as "on average, the cost of a generic drug is 80 to 85 percent lower than the brand name product" [17]. The US Food and Drug Administration (FDA) released the draft guidance on recommended in vitro and in vivo studies to establish bioequivalence of the test (i.e. generic) and reference DPIs containing fluticasone propionate and salmeterol xinafoate in September 2013. For the in vitro study, it requires supportive evidence for equivalent aerodynamic particle size distribution (APSD) data – including drug deposition on the individual stages of the cascade impactor along with the mass median aerodynamic diameter, geometric standard deviation, and fine particle mass at different air flow rates. To reproduce the same APSD data in the test DPI is not a trivial matter as the challenge lies in matching both the formulation and the generic inhaler device. For lactose-carrier formulations, although a carrier with the same specifications may be sourced from lactose suppliers, the drug particles will not be available from the innovator product company. This situation is becoming more complex for combination drug formulation where two (or more) different types of drugs will compete for occupancy on the same lactose surface. Understanding how drug particles interact with lactose carriers in the formulation is crucial. This requires knowledge on forces between the drug particles, between the drug and carrier particles, and between the powder formulation and inhaler device (turbulence and collision). Force information on particles obtained from atomic force microscopy and surface energy are useful for simplistic powder systems but have only limited translatability to the complex situation during formulation, powder mixing and aerosolization, where there are many confounding factors [18]. The major

problem is the lack of new and improved measuring techniques which can be used to predict the aerosol performance [8], and without any breakthrough technology on the horizon, it will remain a challenge in the foreseeable future.

8.2.3 Biologics and Macromolecules

The withdrawal of inhaled insulin Exubera from the market and the slow market sale of Afrezza® so far have tamed the enthusiasm of systemic delivery of proteins by inhalation. From another perspective, these two products are encouraging in (i) confirming small protein molecules (molecular weight [MW] of insulin ~6 kDa) that can be safely delivered to the blood from the lungs of patients, (ii) technology is available to achieve this outcome. The knowledge (preclinical and clinical) and experience gained from developing these products will likely benefit future development of other biologics and help shorten the bench-to-product timeline. In principle, biologics can be formulated in liquid or powder as long as they are stable. Large protein molecules (>40 kDa) have a significantly lower bioavailability, generally only <5% without any absorption enhancer [19]. Delivery of large proteins with increased bioavailability thus offers a challenge to inhalation formulators. Tackling the problem would require intimate knowledge of both the physicochemical aspects of formulation and the biological aspects of disposition of macromolecules in the lungs. The same challenge applies to respiratory delivery of other biologic cargos including nucleic acids, vaccines, cells, and bacteriophages – how to package the cargo to effectively avoid degradation, overcome biological barriers, enhance delivery, and unload the cargo to the target site safely without unwanted side effects [20–22]. In particular, cell therapy for lung injuries (e.g. burn injury, smoke injury from fires) and phage therapy (use of bacteriophages for combating multidrug resistance bacteria) for lung infections are still at their infancy and much is yet to be done – and the first challenge is how to prepare formulations in which the cells and phages are stable, not only during storage but also in the local environment encountered by the cells and phages in the lung where they can grow and multiply [23, 24].

8.2.4 Controlled Release Formulations

Currently, there is no inhaled controlled release product on the market. Controlled release to the lungs has been explored using liposomes and polymeric particles. The key questions are (i) is there a real need for controlled release? (ii) is it safe to inhale controlled release formulations? The safety concern stems from the potential chemical toxicity or local tolerability of the formulation and the possibility of its accumulation in the lungs over repeated uses. The problem of accumulation is not significant if the formulation is only to be administered for a short time at

low doses or only for a single use (e.g. inhaled vaccines). The chemical toxicity is potentially more difficult to handle. However, it is not conclusive whether the widely used FDA-approved polymer (poly(lactic-*co*-glycolic acid), PLGA) will induce inflammation in the lungs [25–27] or the degradation products such as lactic acid may cause myofibroblast differentiation and pulmonary fibrosis in humans [24]. In contrast, liposomes comprise lipids mostly naturally occurring in the lung tissues or surfactants, e.g. phosphatidylcholine (PC) and its derivatives such as dipalmitoylphosphatidylcholine (DPPC) and DSPC [28]. Although an elevated lipid level from inhaled liposomes may potentially upset the homeostasis in the lungs, so far clinical trials have shown adequate safety with no major adverse events reported [28]. For these reasons, liposomes by far are the most promising approach for controlled release. Ongoing clinical trials of liposomes have used only nebulization for aerosol generation. For ciprofloxacin liposomes, unilamellar vesicles formed by lipids with less fluidity were confirmed to be stable to nebulization [29, 30]. The main advantage is compliance by reducing administration to once daily, as compared with other inhaled antibiotics which require three to four times a day dosing. However, as discussed above, administration by nebulization is tedious. From the patient adherence perspective, it is preferred to have a DPI formulation which can be inhaled once daily. Converting a liposome liquid formulation into dry powder will disrupt the vesicle stability causing premature release of the drug content [31]. While it is possible to mitigate the deleterious effect using lyoprotectants which are mostly saccharides [32], the amount required is quite high (e.g. >50 wt%) which reduces the drug-loading capacity of the liposomes. The requirement to prepare stable dry powder formulations with high drug content will be an interesting challenge to formulators.

8.3 Factors Determining the Fate of Inhaled Drugs in the Body

There are various factors determining the fate of inhaled drugs in the body as described below, which is the essential information to understand and control the PK profiles of inhaled drugs, consequently leading to the optimized therapy with them. Device performance, handling skill of inhalers, and respiratory conditions of patients are also included in the factors, although they will not be discussed below.

8.3.1 Anatomical and Histological Characteristics of the Respiratory System

The respiratory tract has a highly branched structure, and the average number of airway generations (the number of levels of airway branches) in humans was estimated to be 23 by Weibel [33]. Larger-sized aerosol particles are deposited

on the upper respiratory tract by inertial impaction, while smaller-sized ones are deposited on the lower respiratory tract by sedimentation and diffusion. However, overly small-sized particles below 0.5 μm of the aerodynamic diameter are likely to escape deposition in the lungs by expiration. Thus, it has been widely known that aerosols comprised of 1–5 μm particles in aerodynamic diameter are suitable for clinical application as inhaled formulations [34].

Aerosols deposited on the bronchial epithelium can be moved by mucociliary clearance toward the larynx, and subsequently swallowed to the gastrointestinal tract. The clearance rate is fastest in the central airway and decreases as the airway generation increases [35]. In addition, mucus secreted by goblet cells covers the bronchial epithelium, which can restrict the dissolution and diffusion of deposited aerosols. On the other hand, aerosols deposited on the alveolar epithelium can be taken up by alveolar macrophages through phagocytosis, leading to lysosomal degradation or transfer toward the upper respiratory tract, followed by mucociliary clearance. The activity of phagocytosis greatly depends on the geometric particle size, being the greatest for 1–3 μm particles and least for particles less than 0.2 μm or more than 10 μm [36]. Moreover, lung surfactant, secreted by alveolar type II cells covering the alveolar epithelium, can affect deposited aerosols in the same way as mucus described above, as well as aiding in spreading and diffusing of deposited drug molecules [37].

In humans, the thickness of the alveolar epithelium (0.1–0.2 μm) is much thinner than that of the upper bronchial one (50–60 μm), which attributes to higher drug permeability in the deep lungs [38]. Furthermore, the alveolar region has attractive characteristics for drug absorption including a large surface area ($\sim$80 m^2), low enzymatic activity and extensive vasculature. Compared to other sites such as the small intestine, the lungs show higher bioavailability of a variety of drugs with wide-ranging molecular weights [39]. On the other hand, tight junctions in the intercellular space of the respiratory epithelium play a role in the barrier restricting paracellular permeation of hydrophilic and macromolecular drugs. In addition, various drug transporters including P-glycoprotein (P-gp), multidrug resistance proteins (MRPs), organic cation transporters (OCTs), organic anion transporters (OATs), and peptide transporters (PEPT1/PEPT2) have been found in the respiratory epithelium, although there is no clear evidence about their relation to the biodistribution of inhaled drugs [40].

8.3.2 Physicochemical Characteristics of Inhaled Drugs

In drug discovery, a widely accepted method for predicting oral bioavailabilities of drug candidates is the "Rule of Five" defined by Lipinski et al. [41], which is based on four physicochemical parameters: molecular weight (MW), number of hydrogen-bond donors (NHD), number of hydrogen-bond acceptors (NHA), and

octanol/water partition coefficient (log *P*). In the definition, drug candidates with MW > 500, NHD > 5, NHA > 10, or log *P* > 5 are predicted to exhibit poor absorption or permeation. Although this rule was led from the information of oral drug candidates, it is suggested to be not proper for the development of inhaled formulations [42].

In the same way as the other absorption sites, the drugs in the lungs are considered to permeate the respiratory epithelium by passive diffusion. Theoretically, therefore, hydrophobic drugs have higher bioavailability than hydrophilic ones in pulmonary absorption, although there was no parallel correlation between lipophilicity and permeability of various drugs with the log *P* ranged between −6 and 6 [43]. On the other hand, extremely hydrophobic drugs (e.g. amphotericin B and all-trans retinoic acid) cannot easily permeate the respiratory epithelium, consequently showing prolonged pulmonary retention [44, 45]. Positively charged drugs are expected to exhibit delayed mucus penetration or prolonged pulmonary retention through electrostatic interaction with the negatively charged mucus and epithelial membrane. Furthermore, both positively and negatively charged particles can promote phagocytosis of alveolar macrophages.

Molecular weight and size of drugs are also the important factors determining their membrane permeability in the lungs. Recently, the biodistribution of macromolecules and micro/nanoparticles after inhalation have been comprehensively studied from several perspectives including clinical application as drug delivery system (DDS) as well as health hazard caused by environmental particulate pollutants. For example, polyethylene glycol (PEG) is a clinically approved hydrophilic polymer. After pulmonary delivery into rats, smaller PEG with less than 2 kDa of the molecular weight was eliminated from the alveolar macrophages and the lung tissue within 48 hours, while larger PEG with more than 5 kDa of the molecular weight remained in these sites for up to seven days [46]. Besides, dendritic polymers (so-called "dendrimers") have attracted much attention because of some advantages such as precisely controlled nanostructure (∼2–20 nm in diameter), narrow molecular weight distribution, and easy surface multifunctionalization. The biodistribution of biodegradable PEGylated poly-L-lysine dendrimers after pulmonary delivery into rats was studied. About 20–30% of the dendrimers with molecular weight less than 22 kDa were partly degraded in the lungs to low molecular weight products and absorbed from the lungs into systemic circulation followed by renal elimination, while dendrimer with molecular weight 78 kDa showed more prolonged pulmonary retention with limited degradation, with only 2% of bioavailability [47]. Interestingly, the biodistribution study of various nanoparticles with different chemical composition, shape, size, and surface charge after pulmonary delivery into rats demonstrated that neutral and negatively charged nanoparticles with less than ∼34 nm of the hydrodynamic diameter rapidly translocated from the lungs to the mediastinal lymph nodes, irrespective

of chemical composition and shape, which could subsequently be transferred to the blood stream [48]. Furthermore, other reports about biodistribution of iridium (Ir) nanoparticles after pulmonary delivery into rats showed approximately 10% of Ir particles with 20 nm of the diameter being translocated to secondary target organs (liver, spleen, kidney, heart, and brain), skeleton, and soft tissue via pulmonary absorption, which was about one order of magnitude higher than that of Ir particles with 80 nm of the diameter [49]. Notably, it has been reported that both micro and nanoparticles have tendency to show more prolonged pulmonary retention in humans than other species including rodents [50].

8.4 Pharmacokinetic/Pharmacodynamic Correlation of Inhaled Drugs

So far, the relationship between biodistribution and subsequent therapeutic effects of inhaled drugs (i.e. PK/PD correlation) has been actively studied in preclinical and clinical trials, consequently leading to some successful clinical application [51]. In this section, the PK/PD correlation of clinically approved inhaled drugs is mainly discussed.

8.4.1 Desirable Pharmacokinetic Parameters of Inhaled Drugs for Local Action and Systemic Delivery

Biodistribution of inhaled drugs is schematically represented in Figure 8.2. All inhaled drugs are desired to achieve both high deposition efficiency in the lungs and avoidance of rapid elimination by mucociliary clearance and phagocytosis into alveolar macrophages. However, the desirable deposition site and subsequent behavior in the body depend on their objectives (i.e. local action or systemic delivery), consequently leading to the difference of suitable physicochemical properties and PK parameters among them.

In the inhaled drugs for local action, it is desirable for them to deposit near the action site. Therefore, inhaled drugs acting on the alveoli epithelium should have smaller aerodynamic diameter for effective delivery into the deep lungs than those acting on the bronchial epithelium. Longer-term pulmonary retention is suitable to extend therapeutic actions in the lungs. Furthermore, low pulmonary and oral bioavailability, rapid elimination in blood (i.e. short half-life ($t_{1/2}$) and high systemic clearance [CL_{sys}] as PK parameters), high plasma protein binding, and low volume of distribution (V_d) achieved by localized delivery to the lung are desirable to minimize systemic adverse effects.

Inhaled drugs for systemic delivery, on the other hand, are required to deposit in the alveolar region for effective absorption into systemic circulation. Extremely

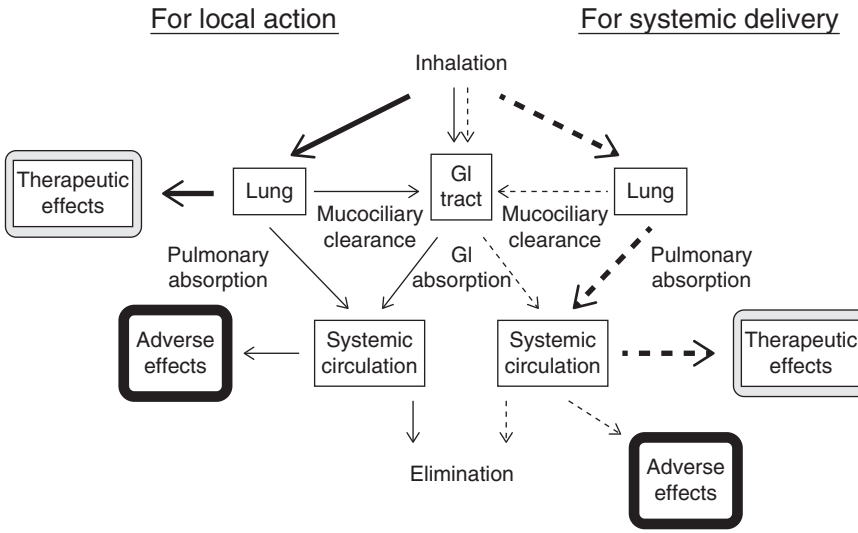

Figure 8.2 Biodistribution of inhaled drugs. Solid and dotted arrows mean translocations of inhaled drugs for local action and systemic delivery in the body, respectively. Thick arrows present desirable directions for each objective. GI, gastrointestinal.

lipophilic, hydrophilic, and high molecular weight drugs are not suitable because of their low membrane permeability. In systemic circulation after pulmonary absorption, proper PK parameters in blood (e.g. maximum blood concentration [C_{max}], time for maximum blood concentration [T_{max}], area under blood concentration-time curve [AUC], and $t_{1/2}$) are necessary to exhibit sufficient therapeutic effects and minimize adverse effects. For example, a short T_{max} is proper for rapid-acting drugs, while longer $t_{1/2}$ is proper for long-acting drugs. Prolonged pulmonary retention might achieve long systemic actions through sustained pulmonary absorption.

8.4.2 Pharmacokinetic/Pharmacodynamic Correlation of Clinically Approved Inhaled Drugs

8.4.2.1 Corticosteroids and Bronchodilators

Around the world, now, inhaled corticosteroids (ICSs) and bronchodilators (e.g. long-acting β_2-agonists [LABAs] and long-acting muscarinic antagonists [LAMAs]) are regarded as the golden standard for effective local therapies against asthma and COPD [52]. All corticosteroids target the same glucocorticoid receptors, while bronchodilators target β_2-adrenergic receptors as agonists or muscarinic receptors as antagonists. Their binding affinity with the relevant

receptors is one of the important factors directly related to their PD profiles. However, the higher binding affinity does not always guarantee more effective therapeutic index because of the possible adverse effects caused by binding to the same receptors present in other sites than the lungs. Therefore, PK parameters which minimize systemic delivery and actions are desirable in ICSs and inhaled bronchodilators. Such improvement can be clearly observed in the development history of ICSs; the newer ICSs (e.g. mometasone furoate and ciclesonide) have lower oral bioavailability and higher plasma protein binding than the older ones (e.g. beclomethasone dipropionate and budesonide) [52].

Ciclesonide, the newest ICS, was developed as a prodrug which is converted into desisobutyryl-ciclesonide (des-CIC), an active metabolite, by endogenous esterases in airway epithelial cells after inhalation [53]. In the solution formulation of ciclesonide (Alvesco®) with a HFA-MDI, the liquid aerosols with 1.1–2.1 μm of aerodynamic diameter are effectively delivered into the deep lungs (~50%) [53]. Less than 40% of ciclesonide was deposited on the oropharynx, and only 20% of this was converted into des-CIC [53]. Both ciclesonide and des-CIC show a low oral bioavailability (<1%) and high protein binding (~99%) [53]. Thus, ciclesonide can minimize oropharyngeal and systemic side effects.

Recently, the combination formulations such as ICS/LABA (e.g. budesonide/formoterol) and LAMA/LABA (e.g. tiotropium/olodaterol) have been clinically used for not only convenience but also possible synergistic effects [52], but it is necessary in new combination formulations to carefully confirm whether or not the combination can affect PK and PD parameters of each contained drug.

8.4.2.2 Antimicrobials

Some antimicrobials including antibacterials and antivirals have been introduced to clinical use as inhaled formulations for local action [54]. In many clinical trials of inhaled antimicrobials, sputum is collected from patients as a sample for measuring the drug concentration for PK analysis and evaluating the microbial colony-forming unit or plaque-forming unit (CFU or PFU) for PD analysis. The drug concentration in sputum is compared to the minimum inhibitory concentration (MIC) determined by in vitro susceptibility testing from sputum samples. However, such information obtained from the sputum might not sufficiently correspond to the true condition at the site of infection because of high variability in patients due to various factors (e.g. age, disease condition, and handling skill of inhalers), poor estimation about the contribution of drug binding to the epithelial membrane, and heterogeneous microbial population in different parts of the lungs, which consequently confuses the interpretation of PK/PD correlation of inhaled antimicrobials [55]. The use of alternative samples such as bronchoalveolar lavage (BAL) and epithelial lung fluid (ELF) to sputum may improve the accuracy of PK/PD correlation.

Tobramycin inhalation powder (TIP; TOBI Podhaler) was approved by the US FDA in 2013 for the treatment of chronic *Pseudomonas aeruginosa* infection in patients with cystic fibrosis. It comprises highly porous spherical particles with 1–2.7 μm of the geometric diameter produced by the PulmoSphere technology to achieve effective pulmonary delivery [56]. In the clinical trial with the comparison to nebulized tobramycin inhalation solution (TIS; TOBI), 112 mg in TIP was estimated to be equivalent to 300 mg in TIS regarding the dose of tobramycin [57]. Furthermore, TIP was demonstrated to be noninferior to TIS in therapeutic efficacy and have time-saving advantage in administration (~6 minutes in TIP vs. ~20 minutes in TIS), although TIP caused slightly more local irritation than TIS [58].

As a new anti-influenza drug, laninamivir octanoate formulated in an inhaled dry powder (Inavir®) has been clinically used in Japan from 2010, although it has not been approved in other countries so far. It was developed as a prodrug for long-lasting therapeutic action through conversion into laninamivir, an active metabolite, by hydrolysis in the lungs [59]. In the clinical trial with a single administration of Inavir, it was estimated that approximately 12% of the powder was deposited in the respiratory tract after inhalation, and approximately 3.4% of laninamivir octanoate was converted into laninamivir in systemic circulation [60]. Laninamivir octanoate itself was relatively rapidly eliminated from systemic circulation after pulmonary absorption (C_{max}; 0.162 μg/ml, T_{max}; 0.3 hours, $t_{1/2}$; 2.6 hours in plasma), while laninamivir retained in the lungs showed a much slower pulmonary absorption (C_{max}; 0.025 μg/ml, T_{max}; 3.5 hours, $t_{1/2}$; 45.7 hours in plasma) [61]. In addition, the $t_{1/2}$ in ELF for laninamivir was even longer (141 or 241 hours) than that in plasma, and the concentration in ELF was over the half maximal inhibitory concentration (IC_{50}) for viral neuraminidases for up to 240 hours [61]. Thus, the therapy with Inavir is achieved by only a single dose, as opposed to the Relenza® (zanamivir inhalation powder) which requires a total of 10 doses (twice daily for five days).

8.4.2.3 Prostacyclin Analogs

For therapeutic use against PAH, several prostacyclin analogs including Iloprost and treprostinil have been synthesized to overcome the low chemical stability and rapid elimination of the original endogenous prostacyclin (prostaglandin I_2; IP) in body ($t_{1/2}$ in blood; two to three minutes), which shows strong pulmonary vasodilation and inhibits proliferation of vascular smooth muscle cells [62, 63]. Furthermore, the clinical application as inhaled formulations is considered to be a superior strategy for successful therapy with prostacyclin analogs because of two possible advantages, i.e. effective delivery into pulmonary arteries and minimization of systemic adverse responses (e.g. hypotension, nausea, vomiting, jaw pain,

and headache) caused by their binding to IP receptors present in the sites other than pulmonary arteries.

Iloprost has been approved by the US FDA only as an inhaled formulation (Ventavis® in 2004), whereas treprostinil is available in different formulations for various administration routes (Remodulin® for subcutaneous and intravenous injections in 2002 and 2004, respectively; Tyvaso® for inhalation in 2009; Orenitram® for oral intake in 2013) [63]. Both Ventavis and Tyvaso use specific nebulizer systems for inhalation. In PK studies of Ventavis and Tyvaso, their blood concentrations immediately peaked after inhalation, with $t_{1/2}$ being 6.5–9.4 minutes and 44–52 minutes, respectively [64, 65]. In their PD studies, on the other hand, the physiological actions (the lowering effect on pulmonary vascular resistance, etc.) of Ventavis and Tyvaso peaked at ∼8 and ∼18 minutes, and continued for <60 and ∼180 minutes, respectively [66]. Consequently, Tyvaso was demonstrated to exhibit prolonged retention in body and sustained pulmonary vasodilation compared with Ventavis. The differences of PKs and PDs between Ventavis and Tyvaso reflect their recommended dosing schedules; six to nine times per day with at least two hours intervals in Ventavis and four times per day with at least four hours intervals in Tyvaso. New approaches for inhaled prostacyclin analogs such as the achievement of longer therapeutic action and the development as dry powder formulations will further improve the quality of life in patients with PAH through less dosing frequency and easier administration.

8.4.2.4 Loxapine

Inhaled loxapine (Adasuve®), an antipsychotic, was developed for rapid action through pulmonary absorption, and was approved by the US FDA in 2012 for the treatment of acute agitation associated with schizophrenia and bipolar disorder. A new single-use breath-actuated device (evaporation/condensation device; the Staccato® system) has been adopted to this product, in which a thin drug film is thermally evaporated to form condensed particles with 1–3 μm of the diameter in airstream for less than 0.5 seconds after inhalation [67]. The in vitro aerosol study estimated that irrespective of inspiratory flow rates (15–80 l/min), the emitted dose was large (≥91% of the dose contained in the device), while the deposited amount on the oropharyngeal region was relatively small (∼11% of the emitted dose) [67]. Clinical trials demonstrated that Adasuve showed extremely rapid pulmonary absorption (T_{max}; ∼2 minutes) and fast onset of action (10 minutes) [68–70].

8.4.2.5 Insulin

As inhaled formulations for systemic delivery of insulin to control the postprandial blood glucose level in patients with diabetes, only two dry powder products (Exubera in 2006 and Afrezza in 2014) were approved by the US FDA so far.

The comparison between Exubera and Afrezza was actively discussed in recent review articles including various key points related to PKs and PDs (known as "glucodynamics" in diabetes therapy) of insulin [71–73]. Both Exubera and Afrezza contain the same recombinant human insulin, but have different PK and PD parameters of insulin, which might be related to different delivered dose and solubility of insulin in the deep lungs obtained by their specialized particle designs; raisin-like particles with about 3 μm of mass median aerodynamic diameter produced by spray drying in Exubera [74] and highly porous particles with 2–2.5 μm of mass median aerodynamic diameters produced by Technosphere® technology in Afrezza [75]. These two formulations also differ in the solid form of insulin and the type of excipients used [76, 77].

As a PK parameter of insulin, the T_{max} for Exubera was 38–78 minutes, which was shorter than that of regular insulin and similar with that of insulin lispro (a rapid-acting insulin analog) for subcutaneous injection [73]. Their PD parameters were in good accordance with their different T_{max}; the peak and duration times of action (the lowering effect on blood glucose level) for Exubera were about 120 and 360 minutes, respectively, which were shorter than those of regular insulin and similar with those of insulin lispro for subcutaneous injection [73].

Regarding Afrezza, the T_{max} (12–15 minutes) was shorter than that for Exubera, clearly indicating the faster pulmonary absorption of insulin into systemic circulation [73]. It is noteworthy that the faster absorption allows patients to take Afrezza at the beginning of meals (or soon after starting to eat), while Exubera should be taken within 10 minutes before meals. Furthermore, the AUC for Afrezza in blood resembled that for endogenous insulin in healthy humans secreted after meals (i.e. the rapid increase of blood insulin concentration, followed by the rapid decrease), which is expected to minimize some undesirable side effects including hypoglycemia and weight gain. As for the PD parameters for Afrezza, the peak and duration times of action were about 53 minutes and 120–180 minutes, respectively, which were shorter than those for Exubera [73].

One concern for more general use of inhaled insulin is its low bioavailability (8–11% for Exubera and 21–30% for Afrezza relative to regular insulin for subcutaneous injection [73]), which can be explained by its limited pulmonary delivery accompanied with the loss in the capsule, device, oral cavity, and throat. Thus, a relatively high-loading dose is needed for effective therapy, consequently imposing a higher cost on patients. The cost of Afrezza (US$0.60 per unit) is twice as expensive as that of insulin lispro (US$0.30 per unit), and Sanofi ended the marketing partnership with MannKind Corp., the developer of Afrezza, in early 2016 [78]. Therefore, improved bioavailability by more effective pulmonary delivery is essential for successful clinical application of expensive biopharmaceutical drug candidates like insulin when used as inhaled formulations for systemic delivery.

8.5 Application of Drug Delivery System for Improving Pharmacokinetic/Pharmacodynamic Parameters of Inhaled Drugs

To closely control the PK parameters of drugs, consequently leading to desired PD outcomes, DDS has been actively studied in various formulations with different administration routes. Although the development of inhaled formulations is regarded as a practical DDS strategy for targeted lung delivery or effective systemic delivery, the introduction of further DDS functions as described below has been attempted to achieve the best PK and PD properties for each drug.

8.5.1 Chemical Modification

Chemical modification of drugs with functional molecules is one of the simplest techniques to achieve intended functions for DDS, although various modification conditions such as conjugated positions in the chemical structures of drugs, chemical binding modes between drugs and functional molecules (e.g. ester, amide, and imine), molecular ratios of functional molecules to drugs, and total molecular weight must be optimized in maintaining the original activity of the parent drugs. In clinically approved inhaled drugs, as described above, ciclesonide and laninamivir octanoate were synthesized by chemical modification as prodrugs to be converted into active metabolites in the lungs. Besides, chemical modification with water-soluble biocompatible polymers (e.g. PEG and dextran) has been used not only for prolonged lung retention but also for improved water solubility of hydrophobic drugs. In the absorption study of prednisolone (a corticosteroid) in the isolated and perfused rat lungs after nebulization, the di-substituted PEG conjugate by esterification was reported to prolong the residence and hydrolysis times of prednisolone in the lungs compared with free prednisolone and the mono-substituted conjugate [79]. The conjugate of cisplatin (cis-diamminedichloroplatinum (II) (CDDP); an anticancer drug) with hyaluronic acid (HA; a natural polysaccharide) as a metal complex (HA-Pt) could prolong higher concentration of platinum (Pt) in the lungs of rats after pulmonary delivery, keeping lower ratios of the concentrations of Pt in other organs to plasma, than intravenous injections of free CDDP and HA-Pt or pulmonary delivery of free CDDP [80]. Recently, a novel conjugate of doxorubicin (DOX; an anticancer drug) with a biodegradable PEGylated poly-L-lysine dendrimer was developed for effective therapy against lung cancers by prolonged pulmonary retention after pulmonary delivery into rat lung metastasis models [81]. The conjugate of superoxide dismutase (SOD; an antioxidant enzyme) with lecithin (a phospholipid mixture) which had a higher cell membrane affinity and longer $t_{1/2}$ in blood than free SOD [82] was reported to show higher therapeutic effects against

bleomycin-induced pulmonary fibrosis and lung dysfunction in mice than pirfenidone (an antifibrotic drug) after pulmonary delivery [83]. Interestingly, after systemic delivery of oligonucleic acids through pulmonary administration into mice, small interfering RNA (siRNA) and phosphodiester-linked locked nucleic acid (PO-LNA) were rapidly removed from the bodies by renal excretion, while phosphorothioate-linked locked nucleic acid (PS-LNA) was retained in systemic circulation, subsequently exhibiting the gene-silencing effect in the livers [84].

8.5.2 Functional Micro/Nanoparticle Formulations

Encapsulation into functional micro/nanoparticles is an alternative DDS strategy for prolonged pulmonary retention, sustained release, and targeted delivery of encapsulated drugs. Moreover, the surface modifications with PEG, cell penetrating peptides, and specific ligands (or antibodies) are expected to provide additional DDS functions for further prolonged pulmonary retention, cellular internalization, and active targeting, respectively. On the other hand, the interaction between these particles (or encapsulated drugs) and biocomponents (e.g. blood cells, proteins, and lipids) can cause a rapid release of encapsulated drugs in the body, consequently losing the functions as DDS. From this perspective, the application of functional micro/nanoparticles to inhaled formulations might be more practical than that to intravenous formulations due to fewer interacting biocomponents in the lungs.

In preclinical studies, lipid-based (e.g. liposomes and solid lipid nanoparticles) and polymer-based (e.g. polymeric micelles and micro/nanospheres) micro/nanoparticles have been mainly introduced for the encapsulation of drugs, followed by the PK and PD analyses after pulmonary delivery into small animals [85, 86]. Generally, the encapsulation of hydrophobic drugs can be achieved in all these particles, while that of hydrophilic drugs is limited to liposomes or polymeric micro/nanospheres prepared by water-in-oil-in-water (w/o/w) emulsion method. However, each drug must be encapsulated into the optimized micro/nanoparticles to achieve its desirable PK profile in the body. Some reports demonstrated that various drugs could be successfully encapsulated into these particles, resulting in the expected outcomes such as prolonged pulmonary retention, sustained release, and effective therapeutic effects after pulmonary delivery into small animals [87–92]. Among them, highly porous PLGA microspheres produced by the w/o/w emulsion method containing a gas-forming porogen (e.g. ammonium bicarbonate) in the inner aqueous phase or supercritical fluid pressure-quench technology are much promising as inhaled formulations since they have low densities and relatively large geometric particle sizes, which allow both high aerodynamic performance and escape of phagocytosis by alveolar macrophages [91, 92]. In case drug candidates are polyelectrolytes (e.g. hyaluronic acid and nucleic acids),

the electrostatic complex formation with the counter-charged carriers might be available as their micro/nanoparticle formulations. For successful pulmonary gene therapy with nucleic acid delivery, various cationic lipids and polymers have been developed to form the electrostatic complexes (so-called "lipoplex" and "polyplex") with cellular uptake and endosomal escaping functions [93, 94].

To date, there is still no clinically approved inhaled formulation based on these functional micro/nanoparticles. Currently, however, three nebulized liposomal formulations of antibiotics (amikacin [Arikace®] and ciprofloxacin [Lipoquin® and Pulmaquin®]) are in advanced stages of clinical testing. In Arikace, hydrophilic amikacin is efficiently encapsulated into the inner aqueous phase of liposomes composed of DPPC and cholesterol with approximately 250–300 nm of the diameter [95]. In Lipoquin, on the other hand, weakly basic ciprofloxacin is encapsulated by remote loading into the inner aqueous phase of liposomes composed of DSPC and cholesterol with approximately 50–100 nm of the diameter [96]. In Pulmaquin, rapid-acting free ciprofloxacin and slow-released liposomal ciprofloxacin (the same composition in Lipoquin) are mixed [97]. For prolonged retention and sustained release of encapsulated drugs in the human lungs, the once-daily treatments with these liposomal formulations have been carried out in clinical trials, consequently demonstrating their antimicrobial efficacy and tolerability in patients [98, 99].

8.5.3 Active Targeting

Several specific ligands, antibodies, and aptamers have been chemically conjugated with drugs or functional micro/nanoparticles encapsulating them for active targeting into relevant protein (e.g. receptors) overexpressing cells, consequently potentiating therapeutic actions of drugs. As the targets in the lungs, for example, vascular endothelial growth factor (VEGF), epidermal growth factor (EGF), transferrin, and folate receptors are overexpressed in some types of lung cancer cells [100], while a mannose receptor is present in alveolar macrophages [36]. However, systemic administration might not sufficiently achieve the active targeting of drugs into these cells since they are present not only in the lungs but also in other organs. Thus, active targeting in inhaled formulations is promising since it can directly deliver drugs near the targeted cells in the lungs and minimize the transfer of drugs to the targeted cells in the other organs, although the studies based on this strategy are few so far. Alveolar macrophages, which exist on the surface of alveolar epithelium, are especially attractive target sites due to easy accessing and wide clinical application including anti-inflammatory, antitubercular, and anticancer therapies [36]. So far the pulmonary delivery of mannose- and transferrin-modified liposomes, folate-modified polymeric micelles, and EGF-modified gelatin nanoparticles have been performed in the small animals for active targeting into alveolar

macrophages and lung cancer cells, demonstrating more effective delivery into the targeted cells and higher therapeutic effects of encapsulated drugs than the nonmodified ones, or good tolerability [101–104].

Inhaled antibodies are expected to achieve both prolonged pulmonary retention due to the large molecular weight (full-length monoclonal antibodies; ~150 kDa) and active delivery into targeted cells in the lungs. So far pulmonary delivery of anticancer full-length monoclonal antibodies (cetuximab and G6-31) demonstrated their anticancer therapeutic effects in mouse lung cancer models with low transfer into systemic circulation [105, 106]. Besides full-length antibodies, engineered antibody fragments such as antigen-binding fragments (Fabs), single-chain variable fragments (scFvs), and single-domain antibodies (sdAbs; Nanobodies®) are very attractive due to several advantages such as enhanced tissue and tumor penetration, binding to cryptic epitopes, and avoidance of crystallizable fragment (Fc) receptor-dependent adverse effects [107, 108]. Recently, a phase I clinical trial on treatment of respiratory syncytial virus infection was conducted using sdAb (ALX-0171) by nebulization at single and multiple doses. The results demonstrated that inhaled ALX-0171 had good tolerability at all doses evaluated with an apparent systemic $t_{1/2}$ of ~20 hours [109]. Furthermore, anti-interleukin Fabs was chemically conjugated with two-armed PEG (40 kDa) to show longer pulmonary retention and higher anti-inflammatory effects than the nonconjugated Fabs and the full-length antibodies following pulmonary delivery into mice [110]. Interestingly, it was demonstrated that mucoadhesion and escape of alveolar macrophages, rather than increased hydrodynamic size or improved enzymatic stability greatly contributed to the prolonged pulmonary retention by PEG modification.

8.6 Conclusion

Pulmonary drug delivery has experienced exponential growth in research and development over the past quarter of a century, leading to an expansion of inhaled drug products for treatment of diseases well beyond asthma and COPD. Facing the emerging challenges of delivering biologics and macromolecules, large dose drugs, molecules with poor aqueous solubility, controlled release formulations, and amorphous powders, the development of inhalation products will need innovative approaches in aerosol formulations and inhaler devices. Until now, PK and PD analyses of various inhaled drugs have successfully demonstrated their effectiveness for both local and systemic actions. Due to the increasing number of drug candidates delivered by the inhaled route, information about PK/PD correlation is expected to increase dramatically in the near future, although there are still issues to be overcome for more precise PK and PD analyses (e.g. novel

techniques for better sample collection from the lungs and correction methods for high variability in patients). This in vivo information is crucial for optimal development of the in vitro formulation in realizing the full benefits of targeted pulmonary drug delivery.

References

1 Myrdal, P.B., Sheth, P., and Stein, S.W. (2014). Advances in metered dose inhaler technology: formulation development. *AAPS PharmSciTech* 15: 434–455.

2 Stein, S.W., Sheth, P., Hodson, P.D., and Myrdal, P.B. (2014). Advances in metered dose inhaler technology: hardware development. *AAPS PharmSciTech* 15: 326–338.

3 Denyer, J. and Dyche, T. (2010). The adaptive aerosol delivery (AAD) technology: past, present, and future. *J. Aerosol Med. Pulm. Drug Delivery* 23 (Suppl. 1): S1–S10.

4 Fischer, A., Stegemann, J., Scheuch, G., and Siekmeier, R. (2009). Novel devices for individualized controlled inhalation can optimize aerosol therapy in efficacy, patient care and power of clinical trials. *Eur. J. Med. Res.* 14 (Suppl. 4): 71–77.

5 Dalby, R.N., Eicher, J., and Zierenberg, B. (2014). Development of Respimat® soft mist™ inhaler and its clinical utility in respiratory disorders. *Med. Devices (Auckl)* 4: 145–155.

6 Chan, H.K. (2013). Inhalation drug delivery devices and emerging technologies. *Expert Opin. Ther. Pat.* 13: 1333–1343.

7 Chougule, M.B., Padhi, B.K., Jinturkar, K.A., and Misra, A. (2007). Development of dry powder inhalers. *Recent Pat. Drug Delivery Formul.* 1: 11–21.

8 Marriott, C. and Frijlink, H.W. (2012). Lactose as a carrier for inhalation products: breathing new life into an old carrier. *Adv. Drug Delivery Rev.* 64: 217–219.

9 Chew, N.Y. and Chan, H.K. (1999). Influence of particle size, air flow, and inhaler device on the dispersion of mannitol powders as aerosols. *Pharm. Res.* 16: 1098–1103.

10 Adams, W.P., Lee, S.L., Plourde, R. et al. (2012). Effects of device and formulation on *in vitro* performance of dry powder inhalers. *AAPS J.* 14: 400–409.

11 Yang, T.T., Li, S., Wyka, B., and Kenyon, D. (2000). Assessment of dose uniformity and aerodynamic particle size distribution with the new Mometasone Furoate dry powder inhaler (Asmanex™ Twisthaler™). In: *Proceedings of Respiratory Drug Delivery VII*, vol. 2 (eds. R.N. Dalby, P.R. Byron, S.J. Farr and J. Peart), 499–502. Raleigh, NC: Serentec Press.

12 Chew, N.Y., Tang, P., Chan, H.K., and Raper, J.A. (2005). How much particle surface corrugation is sufficient to improve aerosol performance of powders? *Pharm. Res.* 22: 148–152.

13 Weers, J.G. and Miller, D.P. (2015). Formulation design of dry powders for inhalation. *J. Pharm. Sci.* 104: 3259–3288.

14 Velkov, T., Rahim, N.A., Zhou, Q.T. et al. (2015). Inhaled anti-infective chemotherapy for respiratory tract infections: successes, challenges and the road ahead. *Adv. Drug Delivery Rev.* 85: 65–82.

15 Zhou, Q.T., Leung, S.S., Tang, P. et al. (2015). Inhaled formulations and pulmonary drug delivery systems for respiratory infections. *Adv. Drug Delivery Rev.* 85: 83–99.

16 Mazzone, S.B. (2005). An overview of the sensory receptors regulating cough. *Cough* 1: 2.

17 U.S. Food and Drug Administration (2012). Facts about Generic Drugs. http://www.fda.gov/drugs/resourcesforyou/consumers/buyingusingmedicinesafely/understandinggenericdrugs/ucm167991.htm (accessed 24 February 2018).

18 de Boer, A.H., Chan, H.K., and Price, R. (2012). A critical view on lactose-based drug formulation and device studies for dry powder inhalation: which are relevant and what interactions to expect? *Adv. Drug Delivery Rev.* 64: 257–274.

19 Pfister, T., Dolan, D., Bercu, J. et al. (2014). Bioavailability of therapeutic proteins by inhalation – worker safety aspects. *Ann. Occup. Hyg.* 58: 899–911.

20 Mitragotri, S., Burke, P.A., and Langer, R. (2014). Overcoming the challenges in administering biopharmaceuticals: formulation and delivery strategies. *Nat. Rev. Drug Discovery* 13: 655–672.

21 Lam, J.K., Liang, W., and Chan, H.K. (2012). Pulmonary delivery of therapeutic siRNA. *Adv. Drug Delivery Rev.* 64: 1–15.

22 Tonnis, W.F., Lexmond, A.J., Frijlink, H.W. et al. (2013). Devices and formulations for pulmonary vaccination. *Expert Opin. Drug Delivery* 10: 1383–1397.

23 Garcia, O., Carraro, G., Navarro, S. et al. (2012). Cell-based therapies for lung disease. *Br. Med. Bull.* 101: 147–161.

24 Abedon, S.T. (2015). Phage therapy of pulmonary infections. *Bacteriophage* 5: e1020260.

25 Roberts, R.A., Shen, T., Allen, I.C. et al. (2013). Analysis of the murine immune response to pulmonary delivery of precisely fabricated nano- and microscale particles. *PLoS One* 8: e62115.

26 Nicolete, R., dos Santos, D.F., and Faccioli, L.H. (2011). The uptake of PLGA micro or nanoparticles by macrophages provokes distinct in vitro inflammatory response. *Int. Immunopharmacol.* 11: 1557–1563.

27 Dailey, L.A., Jekel, N., Fink, L. et al. (2006). Investigation of the proinflammatory potential of biodegradable nanoparticle drug delivery systems in the lung. *Toxicol. Appl. Pharmacol.* 215: 100–108.

28 Cipolla, D., Gonda, I., and Chan, H.K. (2013). Liposomal formulations for inhalation. *Ther. Delivery* 4: 1047–1072.

29 Cipolla, D., Wu, H., Gonda, I. et al. (2014). Modifying the release properties of liposomes toward personalized medicine. *J. Pharm. Sci.* 103: 1851–1862.

30 Cipolla, D., Wu, H., Gonda, I., and Chan, H.K. (2014). Aerosol performance and long-term stability of surfactant-associated liposomal ciprofloxacin formulations with modified encapsulation and release properties. *AAPS PharmSciTech* 15: 1218–1227.

31 Ingvarsson, P.T., Yang, M., Nielsen, H.M. et al. (2011). Stabilization of liposomes during drying. *Expert Opin. Drug Delivery* 8: 375–388.

32 Chen, C., Han, D., Cai, C., and Tang, X. (2010). An overview of liposome lyophilization and its future potential. *J. Controlled Release* 142: 299–311.

33 Weibel, E.R. (1963). *Morphometry of the Human Lung*. Heidelberg, New York: Springer Verlag and Academic Press.

34 Telko, M.J. and Hickey, A.J. (2005). Dry powder inhaler formulation. *Respir. Care* 50: 1209–1227.

35 Kreyling, W. and Scheuch, G. (2000). Clearance of particles deposited in the lungs. In: *Particle-Lung Interactions* (eds. P. Gehr and J. Heyder), 323–376. New York: Marcel Dekker.

36 Lee, W.H., Loo, C.Y., Traini, D., and Young, P.M. (2015). Nano- and micro-based inhaled drug delivery systems for targeting alveolar macrophages. *Expert Opin. Drug Delivery* 12: 1009–1026.

37 Hidalgo, A., Cruz, A., and Pérez-Gil, J. (2015). Barrier or carrier? Pulmonary surfactant and drug delivery. *Eur. J. Pharm. Biopharm.* 95: 117–127.

38 Patton, J.S. (1996). Mechanisms of macromolecule absorption by the lungs. *Adv. Drug Delivery Rev.* 19: 3–36.

39 Yamamoto, A., Iseki, T., Ochi-Sugiyama, M. et al. (2001). Absorption of water-soluble compounds with different molecular weights and [$Asu^{1,7}$]-eel calcitonin from various mucosal administration sites. *J. Controlled Release* 76: 363–374.

40 Gumbleton, M., Al-Jayyoussi, G., Crandon-Lewis, A. et al. (2011). Spatial expression and functionality of drug transporters in the intact lung: objectives for further research. *Adv. Drug Delivery Rev.* 63: 110–118.

41 Lipinski, C.A., Lombardo, F., Dominy, B.W., and Feeney, P.J. (1997). Experimental and computational approaches to estimate solubility and permeability in drug discovery and development settings. *Adv. Drug Delivery Rev.* 23: 3–25.

42 Choy, Y.B. and Prausnitz, M.R. (2011). The rule of five for non-oral routes of drug delivery: ophthalmic, inhalation and transdermal. *Pharm. Res.* 28: 943–948.

43 Patton, J.S., Fishburn, C.S., and Weers, J.G. (2004). The lungs as a portal of entry for systemic drug delivery. *Proc. Am. Thorac. Soc.* 1: 338–344.

44 Beyer, J., Schwartz, S., Barzen, G. et al. (1994). Use of amphotericin B aerosols for the prevention of pulmonary Aspergillosis. *Infection* 22: 143–148.

45 Brooks, A.D., Tong, W., Benedetti, F. et al. (2000). Inhaled aerosolization of all-trans-retinoic acid for targeted pulmonary delivery. *Cancer Chemother. Pharmacol.* 46: 313–318.

46 Gursahani, H., Riggs-Sauthier, J., Pfeiffer, J. et al. (2009). Absorption of polyethylene glycol (PEG) polymers: the effect of PEG size on permeability. *J. Pharm. Sci.* 98: 2847–2856.

47 Ryan, G.M., Kaminskas, L.M., Kelly, B.D. et al. (2013). Pulmonary administration of PEGylated polylysine dendrimers: absorption from the lung versus retention within the lung is highly size-dependent. *Mol. Pharmaceutics* 10: 2986–2995.

48 Choi, H.S., Ashitate, Y., Lee, J.H. et al. (2010). Rapid translocation of nanoparticles from the lung airspaces to the body. *Nat. Biotechnol.* 28: 1300–1303.

49 Kreyling, W.G., Semmler-Behnke, M., Seitz, J. et al. (2009). Size dependence of the translocation of inhaled iridium and carbon nanoparticle aggregates from the lung of rats to the blood and secondary target organs. *Inhalation Toxicol.* 21 (Suppl. 1): 55–60.

50 Geiser, M. and Kreyling, W.G. (2010). Deposition and biokinetics of inhaled nanoparticles. *Part. Fibre Toxicol.* 7: 2.

51 Forbes, B., Asgharian, B., Dailey, L.A. et al. (2011). Challenges in inhaled product development and opportunities for open innovation. *Adv. Drug Delivery Rev.* 63: 69–87.

52 Ricciardolo, F.L., Blasi, F., Centanni, S., and Rogliani, P. (2015). Therapeutic novelties of inhaled corticosteroids and bronchodilators in asthma. *Pulm. Pharmacol. Ther.* 33: 1–10.

53 Nave, R. (2009). Clinical pharmacokinetic and pharmacodynamic profile of inhaled ciclesonide. *Clin. Pharmacokinet.* 48: 243–252.

54 Stockmann, C., Roberts, J.K., Yellepeddi, V.K., and Sherwin, C.M. (2015). Clinical pharmacokinetics of inhaled antimicrobials. *Clin. Pharmacokinet.* 54: 473–492.

55 Mukker, J.K., Singh, R.S., and Derendorf, H. (2015). Pharmacokinetic and pharmacodynamic implications in inhalable antimicrobial therapy. *Adv. Drug Delivery Rev.* 85: 57–64.

56 Geller, D.E., Weers, J., and Heuerding, S. (2011). Development of an inhaled dry-powder formulation of tobramycin using PulmoSphere™ technology. *J. Aerosol Med. Pulm. Drug Delivery* 24: 175–182.

57 Geller, D.E., Konstan, M.W., Smith, J. et al. (2007). Novel tobramycin inhalation powder in cystic fibrosis subjects: pharmacokinetics and safety. *Pediatr. Pulmonol.* 42: 307–313.

58 Konstan, M.W., Flume, P.A., Kappler, M. et al. (2011). Safety, efficacy and convenience of tobramycin inhalation powder in cystic fibrosis patients: the EAGER trial. *J. Cyst. Fibros.* 10: 54–61.

59 Yamashita, M., Tomozawa, T., Kakuta, M. et al. (2009). CS-8958, a prodrug of the new neuraminidase inhibitor R-125489, shows long-acting anti-influenza virus activity. *Antimicrob. Agents Chemother.* 53: 186–192.

60 Yoshihara, K., Ishizuka, H., and Kubo, Y. (2013). Population pharmacokinetics of laninamivir and its prodrug laninamivir octanoate in healthy subjects and in adult and pediatric patients with influenza virus infection. *Drug Metab. Pharmacokinet.* 28: 416–426.

61 Ishizuka, H., Toyama, K., Yoshiba, S. et al. (2012). Intrapulmonary distribution and pharmacokinetics of laninamivir, a neuraminidase inhibitor, after a single inhaled administration of its prodrug, laninamivir octanoate, in healthy volunteers. *Antimicrob. Agents Chemother.* 56: 3873–3878.

62 Gessler, T., Seeger, W., and Schmehl, T. (2008). Inhaled prostanoids in the therapy of pulmonary hypertension. *J. Aerosol Med. Pulm. Drug Delivery* 21: 1–12.

63 LeVarge, B.L. (2015). Prostanoid therapies in the management of pulmonary arterial hypertension. *Ther. Clin. Risk Manag.* 11: 535–547.

64 Olschewski, H., Rohde, B., Behr, J. et al. (2003). Pharmacodynamics and pharmacokinetics of inhaled iloprost, aerosolized by three different devices, in severe pulmonary hypertension. *Chest* 124: 1294–1304.

65 Channick, R.N., Olschewski, H., Seeger, W. et al. (2006). Safety and efficacy of inhaled treprostinil as add-on therapy to bosentan in pulmonary arterial hypertension. *J. Am. Coll. Cardiol.* 48: 1433–1437.

66 Voswinckel, R., Enke, B., Reichenberger, F. et al. (2006). Favorable effects of inhaled treprostinil in severe pulmonary hypertension: results from randomized controlled pilot studies. *J. Am. Coll. Cardiol.* 48: 1672–1681.

67 Dinh, K.V., Myers, D.J., Noymer, P.D., and Cassella, J.V. (2010). In vitro aerosol deposition in the oropharyngeal region for Staccato® loxapine. *J. Aerosol Med. Pulm. Drug Delivery* 23: 253–260.

68 Spyker, D.A., Munzar, P., and Cassella, J.V. (2010). Pharmacokinetics of loxapine following inhalation of a thermally generated aerosol in healthy volunteers. *J. Clin. Pharmacol.* 50: 169–179.

69 Lesem, M.D., Tran-Johnson, T.K., Riesenberg, R.A. et al. (2011). Rapid acute treatment of agitation in individuals with schizophrenia: multicentre, randomised, placebo-controlled study of inhaled loxapine. *Br. J. Psychiatry* 198: 51–58.

70 Kwentus, J., Riesenberg, R.A., Marandi, M. et al. (2012). Rapid acute treatment of agitation in patients with bipolar I disorder: a multicenter, randomized, placebo-controlled clinical trial with inhaled loxapine. *Bipolar Disord.* 14: 31–40.

71 Santos Cavaiola, T. and Edelman, S. (2014). Inhaled insulin: a breath of fresh air? A review of inhaled insulin. *Clin. Ther.* 36: 1275–1289.

72 Rashid, J., Absar, S., Nahar, K. et al. (2015). Newer devices and improved formulations of inhaled insulin. *Expert Opin. Drug Delivery* 12: 917–928.

73 Al-Tabakha, M.M. (2015). Future prospect of insulin inhalation for diabetic patients: the case of Afrezza versus Exubera. *J. Controlled Release* 215: 25–38.

74 White, S., Bennett, D.B., Cheu, S. et al. (2005). EXUBERA®: pharmaceutical development of a novel product for pulmonary delivery of insulin. *Diabetes Technol. Ther.* 7: 896–906.

75 Angelo, R., Rousseau, K., Grant, M. et al. (2009). Technosphere® insulin: defining the role of Technosphere particles at the cellular level. *J. Diabetes Sci. Technol.* 3: 545–554.

76 Stevenson, C.L. and Bennett, D.B. (2014). Development of the Exubera® insulin pulmonary delivery system. In: *Mucosal Delivery of Biopharmaceuticals* (eds. J.D. Neves and B. Sarmento), 461–481. New York: Springer Science + Business Media.

77 Almeida, A.J. and Grenha, A. (2014). Technosphere®: an inhalation system for pulmonary delivery of biopharmaceuticals. In: *Mucosal Delivery of Biopharmaceuticals* (eds. J.D. Neves and B. Sarmento), 483–498. New York: Springer Science + Business Media.

78 Chan, J. and Cheng-Lai, A. (2017). Inhaled insulin: a clinical and historical review. *Cardiol. Rev.* 25: 140–146.

79 Bayard, F.J., Thielemans, W., Pritchard, D.I. et al. (2013). Polyethylene glycol-drug ester conjugates for prolonged retention of small inhaled drugs in the lung. *J. Controlled Release* 171: 234–240.

80 Xie, Y., Aillon, K.L., Cai, S. et al. (2010). Pulmonary delivery of cisplatin-hyaluronan conjugates via endotracheal instillation for the treatment of lung cancer. *Int. J. Pharm.* 392: 156–163.

81 Kaminskas, L.M., McLeod, V.M., Ryan, G.M. et al. (2014). Pulmonary administration of a doxorubicin-conjugated dendrimer enhances drug exposure to lung metastases and improves cancer therapy. *J. Controlled Release* 183: 18–26.

82 Igarashi, R., Hoshino, J., Ochiai, A. et al. (1994). Lecithinized superoxide dismutase enhances its pharmacologic potency by increasing its cell membrane affinity. *J. Pharmacol. Exp. Ther.* 271: 1672–1677.

83 Tanaka, K., Azuma, A., Miyazaki, Y. et al. (2012). Effects of lecithinized superoxide dismutase and/or pirfenidone against bleomycin-induced pulmonary fibrosis. *Chest* 142: 1011–1019.

84 Moschos, S.A., Frick, M., Taylor, B. et al. (2011). Uptake, efficacy, and systemic distribution of naked, inhaled short interfering RNA (siRNA) and locked nucleic acid (LNA) antisense. *Mol. Ther.* 19: 2163–2168.

85 Loira-Pastoriza, C., Todoroff, J., and Vanbever, R. (2014). Delivery strategies for sustained drug release in the lungs. *Adv. Drug Delivery Rev.* 75: 81–91.

86 El-Sherbiny, I.M., El-Baz, N.M., and Yacoub, M.H. (2015). Inhaled nano- and microparticles for drug delivery. *Glob. Cardiol. Sci. Pract.* 2015: 2.

87 Garbuzenko, O.B., Saad, M., Betigeri, S. et al. (2009). Intratracheal versus intravenous liposomal delivery of siRNA, antisense oligonucleotides and anticancer drug. *Pharm. Res.* 26: 382–394.

88 Li, Y.Z., Sun, X., Gong, T. et al. (2010). Inhalable microparticles as carriers for pulmonary delivery of thymopentin-loaded solid lipid nanoparticles. *Pharm. Res.* 27: 1977–1986.

89 Gill, K.K., Nazzal, S., and Kaddoumi, A. (2011). Paclitaxel loaded PEG(5000)-DSPE micelles as pulmonary delivery platform: formulation characterization, tissue distribution, plasma pharmacokinetics, and toxicological evaluation. *Eur. J. Pharm. Biopharm.* 79: 276–284.

90 Hu, X., Yang, F.F., Quan, L.H. et al. (2014). Pulmonary delivered polymeric micelles – pharmacokinetic evaluation and biodistribution studies. *Eur. J. Pharm. Biopharm.* 88: 1064–1075.

91 Oh, Y.J., Lee, J., Seo, J.Y. et al. (2011). Preparation of budesonide-loaded porous PLGA microparticles and their therapeutic efficacy in a murine asthma model. *J. Controlled Release* 150: 56–62.

92 Dhanda, D.S., Tyagi, P., Mirvish, S.S., and Kompella, U.B. (2013). Supercritical fluid technology based large porous celecoxib-PLGA microparticles do not induce pulmonary fibrosis and sustain drug delivery and efficacy for several weeks following a single dose. *J. Controlled Release* 168: 239–250.

93 Geiger, J., Aneja, M.K., and Rudolph, C. (2010). Vectors for pulmonary gene therapy. *Int. J. Pharm.* 390: 84–88.

94 Tros de Ilarduya, C., Sun, Y., and Düzgüneş, N. (2010). Gene delivery by lipoplexes and polyplexes. *Eur. J. Pharm. Sci.* 40: 159–170.

95 Li, Z., Zhang, Y., Wurtz, W. et al. (2008). Characterization of nebulized liposomal amikacin (Arikace™) as a function of droplet size. *J. Aerosol Med. Pulm. Drug Delivery* 21: 245–254.

96 Cipolla, D., Blanchard, J., and Gonda, I. (2016). Development of liposomal ciprofloxacin to treat lung infections. *Pharmaceutics* 8: 6.

97 Clancy, J.P., Dupont, L., Konstan, M.W. et al. (2013). Phase II studies of nebulised Arikace in CF patients with *Pseudomonas aeruginosa* infection. *Thorax* 68: 818–825.

98 Bruinenberg, P., Blanchard, J.D., Cipolla, D.C. et al. (2010). Inhaled liposomal ciprofloxacin: once a day management of respiratory infections. In: *Proceedings of Respiratory Drug Delivery 2010*, vol. 1 (eds. R.N. Dalby, P.R. Byron, J. Peart, et al.), 73–82. River Grove, IL: Davis Healthcare International Publishing.

99 Serisier, D.J., Bilton, D., De Soyza, A. et al. (2013). Inhaled, dual release liposomal ciprofloxacin in non-cystic fibrosis bronchiectasis (ORBIT-2): a randomised, double-blind, placebo-controlled trial. *Thorax* 68: 812–817.

100 Byrne, J.D., Betancourt, T., and Brannon-Peppas, L. (2008). Active targeting schemes for nanoparticle systems in cancer therapeutics. *Adv. Drug Delivery Rev.* 60: 1615–1626.

101 Wijagkanalan, W., Higuchi, Y., Kawakami, S. et al. (2008). Enhanced anti-inflammation of inhaled dexamethasone palmitate using mannosylated liposomes in an endotoxin-induced lung inflammation model. *Mol. Pharmacol.* 74: 1183–1192.

102 Gaspar, M.M., Radomska, A., Gobbo, O.L. et al. (2012). Targeted delivery of transferrin-conjugated liposomes to an orthotopic model of lung cancer in nude rats. *J. Aerosol Med. Pulm. Drug Delivery* 25: 310–318.

103 Rosière, R., Van Woensel, M., Mathieu, V. et al. (2016). Development and evaluation of well-tolerated and tumor-penetrating polymeric micelle-based dry powders for inhaled anti-cancer chemotherapy. *Int. J. Pharm.* 501: 148–159.

104 Tseng, C.L., Su, W.Y., Yen, K.C. et al. (2009). The use of biotinylated-EGF-modified gelatin nanoparticle carrier to enhance cisplatin accumulation in cancerous lungs via inhalation. *Biomaterials* 30: 3476–3485.

105 Maillet, A., Guilleminault, L., Lemarié, E. et al. (2011). The airways, a novel route for delivering monoclonal antibodies to treat lung tumors. *Pharm. Res.* 28: 2147–2156.

106 Hervé, V., Rabbe, N., Guilleminault, L. et al. (2014). VEGF neutralizing aerosol therapy in primary pulmonary adenocarcinoma with K-ras activating-mutations. *MAbs* 6: 1638–1648.

107 Nelson, A.L. and Reichert, J.M. (2009). Development trends for therapeutic antibody fragments. *Nat. Biotechnol.* 27: 331–337.

108 Muyldermans, S. (2013). Nanobodies: natural single-domain antibodies. *Annu. Rev. Biochem.* 82: 775–797.

109 Van Heeke, G., Allosery, K., De Brabandere, V. et al. (2017). Nanobodies® as inhaled biotherapeutics for lung diseases. *Pharmacol. Ther.* 169: 47–56.

110 Koussoroplis, S.J., Paulissen, G., Tyteca, D. et al. (2014). PEGylation of antibody fragments greatly increases their local residence time following delivery to the respiratory tract. *J. Controlled Release* 187: 91–100.

9

Oral Transmucosal Drug Delivery

Mohammed Sattar[1] *and Majella E. Lane*[2]

[1] *Department of Pharmaceutics, UCL School of Pharmacy, University College London, London, UK*
[2] *Department of Pharmaceutics, College of Pharmacy, University of Basrah, Basrah, Iraq*

9.1 Introduction

Oral transmucosal drug delivery (OTDD) may be defined as the administration of pharmaceutically active agents through the oral mucosa to achieve systemic effects. This route has several advantages over conventional drug delivery systems. Although oral delivery is the conventional method for drug administration in the form of tablets, capsules, or liquids, this route is not without its obstacles. Greater systemic absorption with OTDD is particularly attractive for molecules prone to gastric degradation or hepatic metabolism, because of the rich blood supply to the mucosal area, lower enzymatic content and reactivity, and avoidance of the first-pass effect [1, 2]. The bioavailability of peroral dosage forms is further influenced by factors such as pH, buffer species, gastric emptying rate, gastrointestinal (GIT) motility, and hydrodynamics which cause significant fluctuations in drug absorption from this route [3]. Holm et al. [4] suggested that OTDD should also be preferred for patients requiring rapid onset of action, with swallowing difficulties, gastric problems, and limited access to water at the time of drug administration.

The relative immobility of the buccal mucosa allows the flexible application of sustained release devices. Where necessary, such devices may easily be removed from the mouth and drug input halted; this cannot be achieved with an oral-sustained release dosage form [5]. Mucoadhesion of devices is possible in the oral cavity because the turnover time of approximately five to seven days [6] is comparatively longer than that of GIT. This means the adhesive device can be easily implanted from hours to days, and if mild irritation occurs upon removal of the device, a relatively fast recovery of the mucosa might be expected. The microenvironment of the oral cavity provides an additional advantage for

Drug Delivery Approaches: Perspectives from Pharmacokinetics and Pharmacodynamics,
First Edition. Edited by Bret Berner, Toufigh Gordi, Heather A. E. Benson, and Michael S. Roberts.

OTDD over oral delivery. The pH in the buccal mucosa may be manipulated to suit the applied dosage form more easily than the GIT [5]. A number of fentanyl buccal dosage forms are available that incorporate an effervescent reaction in the dissolution process; the reaction produces a large shift in salivary pH and enhanced fentanyl bioavailability [7].

In addition to these advantages, there are also a number of limitations associated with OTDD. The challenges facing OTDD are generally related to drug properties or to the physiology of the oral mucosa. If a drug has an unpleasant taste or smell, it will pose particular challenges for effective delivery via the oral transmucosal route. The oral mucosa has a smaller absorptive surface area than the small intestine, drug may be rapidly cleared by saliva, and there is a more limited volume of fluid for drug dissolution compared with the GIT. Devices may be dislodged from the mucosa by movement of the tongue, eating or drinking. Clearly, the possibility of swallowing devices is also a potential hazard for certain patient groups.

Only a limited number of drugs are administered as true oral transmucosal or sublingual dosage forms [8]. These include isosorbide dinitrate, ergot alkaloids, nicotine, testosterone, nitroglycerin, asenapine, buprenorphine, cannabis extracts, fentanyl, midazolam, naltrexone, prochlorperazine, selegiline, and zolpidem. The relatively low number of medicines on the market is surprising, given the suitability of OTDD for pediatric and geriatric patients. Sections 9.2–9.6 will explore in more detail the factors influencing effective OTDD, current OTDD technologies that are marketed and licensed, approaches to model and predict OTDD, and finally emerging strategies for enhanced delivery of molecules via this route.

9.2 Structure and Physiology of the Oral Mucosa

9.2.1 Buccal Mucosa

The buccal mucosa has an average surface area of 100 cm^2 and includes the area between the lips and gums and the inner lining of the cheeks. Functionally, the tissue protects underlying membranes from physical/chemical damage and prevents ingress of foreign substances [9]. The buccal mucosa includes the outer epithelium, the basement membrane, and connective tissue consisting of the lamina propria and submucosa (Figure 9.1). Mucus coats the surface of the epithelium which is stratified (40–50 layers) and nonkeratinized tissue; the thickness ranges from 500 to 600 μm [10]. Cells undergo mitosis in the deeper layers, of the epithelium and progress to become larger and flatter toward the outer areas. Four distinct layers are identified based on their morphological features, namely the basal, the prickle cell, intermediate layer, and superficial layers. As cells leave the basal layer, their lipid content increases and membrane coating granules (MCGs) that

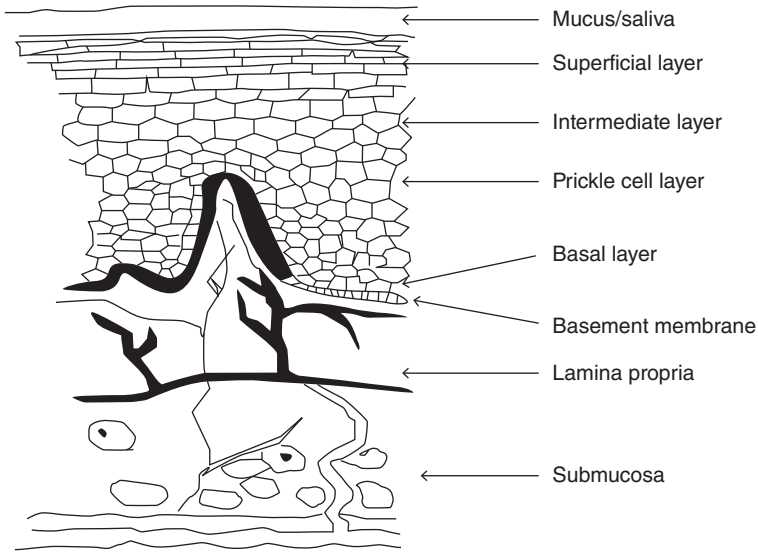

Figure 9.1 Schematic of the oral mucosa. Source: Reproduced from Sattar et al. [8] with permission.

accumulate lipid appear in the prickle cell layer. The lipid content is extruded into extracellular spaces following interaction of MCGs with cell membranes. These organelles expel their lipid content in the outer one-third of epithelium and are key to maintaining the barrier properties of the buccal mucosa [11]. Large amounts of phospholipids with comparatively smaller levels of ceramides are found in this outer area. The turnover time of buccal epithelial cells is five to seven days. The basement membrane is a layer of extracellular material forming the supporting structure for growth of epithelial cells and is approximately 1–2 μm in thickness [12]. From a drug permeation perspective, the lamina propria does not appear to be a significant barrier and is a loose, hydrated connective tissue composed of fibers of collagen smooth muscles and capillaries [13]. Where a submucosa is present, it consists of comparatively denser connective tissue than the lamina propria and may also contain salivary glands surrounded by myoepithelial cells [14]. The blood flow to the buccal mucosa is ~2.4 ml/min/cm^2 and the turnover time ranges from five to seven days [15].

9.2.2 Sublingual Mucosa

The sublingual mucosa is thinner (100–200 μm) than the buccal mucosa with a comparable multilayer structure. Not surprisingly, it is a more permeable tissue than the buccal mucosa [16, 17] and blood flow to the sublingual mucosal is slower (1.0 ml/min/cm^2) compared with the buccal mucosa.

9.2.3 Gingiva and Palate

The gingival and palatal epithelia are keratinized tissues with respective thickness of 250 and 200 μm [18]. Few studies have reported on the barrier characteristics of these membranes, but they are reported to be less permeable than the buccal and sublingual areas [17]. As for the buccal mucosa, they contain MCGs, and the lipids present are acylceramides or ceramides [17].

9.2.4 Saliva

Saliva is a viscous and colorless fluid that is secreted by parotid, submandibular, sublingual, and minor salivary glands in the submucosa [18]. The primary functions of this liquid are protection, lubrication, and moisturization of the oral cavity, as well as assisting with food mastication and prevention of teeth demineralization. Saliva also supports the growth of oral flora in the mouth and plays a role in carbohydrate metabolism [19]. Although largely composed of water saliva also contains mucus, enzymes, mineral salts, and protein. There may be variations in pH range (5.5–7) with changes in production rate and ionic composition, which in turn are influenced by various stimuli including taste and smell of food and time of day. The total daily volume of saliva produced ranges from 0.5 to 2 l, but because of continuous swallowing, the average amount in the mouth is approximately 1.1 ml [20]. For effective oral transmucosal delivery (OTMD), the candidate molecule must have adequate solubility in saliva and be rapidly absorbed. However, it will be impossible to prevent dilution and washing of some of the drug out of the mouth.

9.2.5 Mucus

Mucus is composed of water and glycoproteins or "mucins" with typical molecular weights ranging from 0.5 to 20 MDa. Mucins are negatively charged because of their high number of sialate and sulfur functional groups [20] which permits mucins to bind to epithelial cell surfaces and to form a "gel"-like coating [21]. This layer is the target for adhesion of mucoadhesive formulations, and if effective, prolonged residence time and subsequent enhanced drug delivery may be possible. Alternatively, the mucus layer may be a hindrance to OTMD as it is a physical barrier to drug diffusion, and there may be drug–mucus interactions which prevent the drug from accessing the epithelium.

9.2.6 Permeation Routes

The oral mucosa is considered to be more permeable than the skin, but less permeable than the small intestine [17] with the major barrier properties residing in the

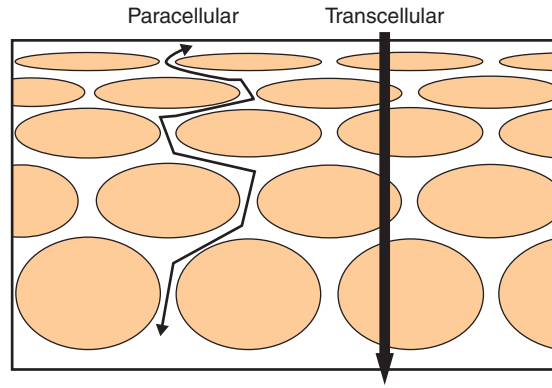

Figure 9.2 Schematic representation of pathways for oral transmucosal drug delivery.

outer epithelium [18, 22]. Active transport processes have been suggested for some drugs based on their stereochemistry but only limited evidence has been reported to date [23, 24]. Physically, the epithelium consists of cells embedded in an intercellular matrix. The greater permeability of the oral mucosa compared with the skin is suggested to reflect the presence of more polar lipids in this intercellular matrix as well as the more fluid nature of lipid organization [17, 22]. A molecule can penetrate the outer epithelium by diffusing between the cells through the matrix (intercellular pathway) or sequentially moving through the cells (Figure 9.2) in different layers (transcellular pathway). Some molecules appear to penetrate largely through one route, rather than another, but there is also the possibility of transport of drugs via both pathways.

9.3 Drug Properties Which Influence OTMD

Effective penetration of the oral mucosa tissue will be a function of drug physicochemical properties and specifically, molecular weight, lipophilicity, ionization, and partition/distribution coefficients. Considering the drugs that are currently known to deliver systemic effects when administered buccally or sublingually, it will be evident that some of them are also available as transdermal formulations. These include buprenorphine, fentanyl, nicotine, nitroglycerin, and testosterone. Buprenorphine and fentanyl are used as the salt forms in buccal preparations but as the corresponding free bases when delivered via the skin. In the saliva, both charged and uncharged fractions of these drugs will be present.

9.3.1 Molecular Weight

Passive diffusion through a biological membrane will be influenced by drug size or molecular weight as well as other factors. As the molecular weight

will determine drug diffusivity, small hydrophilic molecules (<75–100 Da) will traverse membrane pores faster than larger molecules. Evidence for oral mucosal penetration of dextrans with a molecular weight <20 000 Da has been found, but dextrans with larger molecular weights were not observed to permeate [25]. As such, the transport of large molecules (peptides and proteins) had previously been considered unlikely without the use of active transport mechanisms [12]. However, a buccal spray formulation for oral insulin delivery, Oral-lyn™, has recently been developed by Generex for the treatment of Type 1 and 2 diabetes [26, 27]. Goswami et al. [28] used polyethylene glycols (PEGs) as model hydrophilic permeants to establish theoretical pore sizes for permeation of hydrophilic molecules across various regions of the oral mucosa. Permeation studies were carried out in vitro with porcine buccal tissue for a period of 8–12 hours to obtain steady-state flux values for PEG oligomers with different molecular weights. PEG solutions with mean molecular weights varying from 300 to 1000 Da in isotonic phosphate buffer solution (pH 7.4). Theoretical diffusion and experimental permeability parameters for PEG molecules were used to calculate pore radii for aqueous pathways in sublingual and buccal tissues as 30–53 Å and 18–22 Å, respectively. The diameter of the insulin monomer is reported to be 27 Å [29]; therefore, an important factor in effective delivery of this molecule will be prevention of aggregation and the inclusion of penetration enhancers. The important role of penetration enhancers in the Oral-Lyn formulation has been emphasized in a recent review [30]. The paracellular route should be more accessible for peptides as most proteolytic enzymes in the buccal epithelium are located intercellularly [31]. Caon et al. [32] have recently reviewed approaches that have shown promise in enhancing the buccal mucosal transport of macromolecules, with major focus on proteins and peptides.

9.3.2 Lipid Solubility

The permeation of a drug through a biological membrane will also be influenced by its lipophilicity. The most commonly used measure of lipophilicity is the partition coefficient, usually expressed as the logarithm to base 10 of the partitioning of a drug between *n*-octanol and water, $\log P_C$, [33]. Beckett and Moffat [34] demonstrated a linear relationship between alkyl chain length and buccal absorption for a series of *p*-n-alkly phenyl acetic acids using a buccal absorption test in humans. In a separate study, the same authors determined the partition coefficients in *n*-heptane-0.1 N sodium hydroxide or 0.1 N hydrochloric acid for a series of amines and acids; linear relations between chain-lengths and the logs of their partition coefficients were reported [35]. A third study reported a positive correlation between the rate constants for buccal absorption of a series of carboxylic acids and their respective *n*-heptane: 0.1 N hydrochloric acid partition

coefficients [36]. Le Brun et al. [37] investigated the permeation of bupranolol, propranolol, oxprenolol, and acebutolol; a linear relationship was found between the permeability coefficient and the drug lipophilicity, which was expressed as the octanol–buffer distribution coefficient. A strong correlation for relative sublingual permeability and the $\log P$ in the range of 1.6–3.3 has been reported for uncharged molecules. Drugs with extremely high $\log P_{o/w}$, values will not be solubilized in aqueous salivary fluid, while it will be difficult for molecules with values $\ll 1$ to partition into the buccal membrane. The net result in both cases will be insignificant absorption [38].

9.3.3 Degree of Ionization

The vast majority of drugs have an ionizable group which means their lipophilicity will be pH-dependent. The distribution coefficient ($\log D$) describes the intrinsic lipophilicity of such a molecule in addition to the extent of drug ionization [39]. Kokate et al. [40] reported the in vitro flux values of three acidic (naproxen, warfarin, and nimesulide), seven basic (lidocaine, propranolol, verapamil, diltiazem, amitriptyline, metoprolol, and pindolol), and two uncharged (caffeine, antipyrine) molecules across porcine buccal mucosa. Saturated donor solutions of drugs with poor solubility (diltiazem, amitriptyline, nimesulide, naproxen, and warfarin) were used. The initial drug concentration for the remaining drugs was 1.0 mg/ml (verapamil), 5.0 mg/ml (lidocaine, propranolol, caffeine, antipyrine), 7.5 mg/ml (metoprolol), and 10 mg/ml (pindolol). When permeability coefficients were plotted against $\log P$, a poor correlation was obtained ($r^2 = 0.53$); however, the correlation improved significantly when $\log D_{6.8}$ ($r^2 = 0.73$) was plotted instead of $\log P$. The degree of ionization will be a function of the drug dissociation constant and the environmental pH. According to the pH partition hypothesis, the nonionized form of a molecule permeates a biological membrane via the transcellular route while charged molecules permeate through paracellular spaces [33]. Birudaraj et al. [41] reported that the dominant route for the buccal permeation of buspirone was the transcellular pathway at neutral pH, when the drug is unionized.

Kokate et al. [42] investigated the contribution of thermodynamic activities of ionized and unionized species on buccal drug permeation using nimesulide and bupivacaine as model drugs. In vitro studies were conducted with porcine tissue and horizontal side-by-side cells. Saturated or subsaturated buffered solutions of nimesulide were applied to the donor chamber at different pH values ranging from 5.0 to 8.0. Saturated and subsaturated buffered solutions of bupivacaine were investigated over the pH range 6.0–8.5. The receptor chamber contained McIlvaine buffer at the same pH as the respective donor solutions. The thermodynamic

activities of ionized and unionized drug species were expressed as the degree of saturation. The permeability of the ionized species was approximately fourfold lower than the unionized species, for both drugs. Theoretical estimations were made for the total drug flux values and percentage contribution of the ionized species to the total flux, with the assumption that both the ionized and unionized species contributed independently to total steady-state flux. When 90% of the drug was in the ionized state, the contribution of the ionized species to total flux was estimated to be equal to that of the unionized species.

9.3.4 Potency

It will be evident that all drugs currently delivered via the oral mucosal route for systemic effects are potent molecules with many of the dosage forms currently available containing only a few mg of drug (Table 9.1).

9.4 Buccal and Sublingual Formulations

9.4.1 Currently Used Technologies

Buccal tablets and lozenges are the most common oral transmucosal dosage forms currently available. Typically, the formulations available are similar to conventional tablets and may include suitable diluents, fillers, and coloring agents. Effervescent materials are employed in some fentanyl citrate formulations (e.g. Fentora) to maximize both drug solubility in the saliva as well as partitioning from the saliva into the tissues. Mucoadhesive polymers are also included in some tablet formulations to promote prolonged contact time with the buccal tissue – the modified release tablet formulation of testosterone includes both Carbomer® and polycarbophil for this purpose. Since the taste of the formulation is more critical for OTDD, than for conventional oral delivery, most dosage forms for the former route will also include flavoring agents. However, a simple buffered saline solution is used for delivery of midazolam hydrochloride in the management of epileptic fits.

Thin-film technology (TFT) is a delivery platform that is currently used for a number of buccal and sublingual medicines (Table 9.1). Typically, films are produced either by film casting or heat extrusion. Film-forming polymers are selected depending on the film thickness required and drug compatibility. Dixit and Puthli [43] have reviewed the materials used in TFT, as well as critical manufacturing aspects and applications.

Sprays have been used to deliver a number of molecules through oral mucosal tissue including delta-9-tetrahydrocannabinol, cannabidiol, nicotine, and nitroglycerine. Penetration enhancers are also included in some of these preparations.

Table 9.1 Examples of oral transmucosal formulations currently available.

Drug	Proprietary name	Dosage form and excipients
Buprenorphine HCl, naloxone HCl	Suboxone	*Film* Polyethylene oxide, hydroxypropyl methylcellulose, maltitol, acesulfame potassium, lime flavor, citric acid, sodium citrate, FD&C yellow #6, white ink
Cannabis extract	Sativex®	*Oromucosal spray* Ethanol anhydrous, propylene glycol, peppermint oil
Fentanyl citrate	Effentora®	*Tablets* Mannitol, sodium starch glycolate type A, sodium hydrogen carbonate, sodium carbonate anhydrous, citric acid anhydrous, magnesium stearate
	Actiq®	*Lozenge* Dextrates hydrated (containing glucose), citric acid, anhydrous, disodium phosphate, anhydrous, artificial berry flavor (maltodextrin, propylene glycol, artificial flavors, and triethylcitrate), magnesium stearate. Edible glue (modified maize-based food starch, sucrose and maize starch, water, purified). Imprinting ink (deionized water, dewaxed white shellac, propylene glycol, blue synthetic coal tar dye)
	Onsolis	*Film* Black ink, carboxymethylcellulose, citric acid, hydroxyethyl cellulose, hydroxypropyl cellulose, methylparaben, monobasic sodium phosphate, peppermint oil, polycarbophil, propylene glycol, propylparaben, sodium benzoate, sodium hydroxide, sodium saccharin, titanium dioxide, tribasic sodium phosphate, vitamin E acetate, and water
Nicotine	Nicorette®	*Chewing gum* (as resin) Polacrilin, chewing gum base, containing butylated hydroxy toluene, sorbitol, sodium carbonate anhydrous, sodium bicarbonate, flavor, glycerol, talcum *Lozenge* (as bitartrate); 2 mg Core: Mannitol, xanthan gum, winterfresh flavor, sodium carbonate anhydrous, sucralose, acesulfame potassium, magnesium stearate. Coating: Hypromellose, winterfresh flavor, titanium dioxide, sucralose, sepifilm gloss, acesulfame potassium, polysorbate 80, purified water
Testosterone	Striant	*Modified release tablet* Anhydrous lactose, carbomer 934P, hypromellose, magnesium stearate, lactose monohydrate, polycarbophil, colloidal silicon dioxide, starch, talc

For example, the Nitrolingual™ spray formulation contains ethanol as well as buffers, flavoring agents, and propylene glycol. As noted in Section 9.3.1, Generex have developed a spray formulation of recombinant human insulin (Oral-Lyn®) for buccal administration. A metered dose-type device is used to deliver the equivalent of one unit of insulin per spray to the oral cavity. The actual formulation is based on patented technology (RapidMist®), where the active is in solution with a combination of absorption enhancers and other excipients.

9.4.2 Investigation of Iontophoresis for Oral Transmucosal Drug Delivery

Iontophoresis has been investigated by a number of researchers with promising results reported recently for galantamine in pigs [44] and for naltrexone in pigs [45] and in man [46]. These short-term studies describe an "Intellidrug®" device which consists of intraoral and extraoral sections. The intraoral part consists of an outlet system embedded in a silicone-made mouth prop, whereas the extra-oral part contains a drug reservoir, a syringe pump, a flow sensor, and a power source for the flow sensor. No irritation or histological damage was reported for the studies in man (conducted over nine days) with further studies currently planned to test long-term use and tolerance of the device.

9.5 Models to Study OTDD

Several in vitro and in vivo methods have been used to assess the rate and extent of drug absorption, permeation mechanisms, and absorption kinetics in buccal tissue.

9.5.1 Studies in Man and Human Tissue Models

The "swirl and spit" test is an oral absorption measurement that was developed by Beckett and Triggs [47]. A known volume of a specific drug concentration is swirled around the mouth for a fixed period of time by human volunteers followed by expulsion of the solution. The volunteers then rinse their mouth with a known volume of buffer solution, and the rinses are combined and analyzed for drug content. The absorbed amount of drug is assumed to be the difference between the initial and final drug concentration in the solution. A series of research articles in the 1960s and 1970s described the application of this test to measure the buccal absorption of various drugs and the influence of pH on drug absorption [34–36, 48, 49]. Nonabsorbable markers have been included in the protocol to account for drug loss and dilution associated with swallowing and salivary secretion [50]. Limitations of this approach include (i) the absorption that takes place from all regions of the

oral cavity, with no control over the area across which absorption can take place; (ii) the disappearance from the oral cavity that is not necessarily an indication of complete transfer to the systemic circulation because of potential metabolism and/or tissue binding. Specialized perfusion cells for use in the oral cavity were subsequently developed to overcome some of these limitations. Using these cells, drug transfer takes place over an isolated area with avoidance of interference from salivary secretions; it is also possible to maintain control of the volume, pH, and temperature of the perfusant [51]. A modified version of the perfusion cells has been developed to compare the drug absorption from five sites in the mouth: dorsum, ventral side of the tongue, floor of mouth, labial, and buccal mucosa [52]. The modified perfusion cell has also been used to examine D-glucose transport through different oral sites [24].

A new in vivo Raman probe that allows depth profiling of the buccal epithelium has recently been developed [53]. A small external optical window is set at the end of a long pen-shaped device, which can be maneuvered against the buccal epithelium, with minimal discomfort to the subject. The probe is attached to an in vivo Raman spectrometer with three exit ports one of which directs the laser beam into the probe. Measurements of the oral mucosa were performed in a pilot study in two subjects by placing the probe inside the mouth on the cheek and depth scans were taken. The mouth was then rinsed with solutions (0.0183%, 0.183%, or 1.83% by weight) of epigallocatechin gallate (ECG). The ECG signal was observed clearly in the buccal epithelium and was still present after 15 minutes exposure for the 0.183% solution. The ability to probe the buccal epithelium at the molecular level with Confocal Raman Spectroscopy should facilitate a better understanding of the barrier properties of this tissue. Monitoring of actives may be possible where the molecule has a suitable Raman spectrum.

Although there are few in vitro studies with human biopsy or cadaver tissue reported in the literature, these models have been used by Nielsen and Rassing [54] to study buccal permeation of β blockers and testosterone, by Van Der Bijl et al. [55] to study sumatriptan, and by Meng-Lund et al. [56] to study metoprolol.

9.5.2 Porcine Tissue Models

Porcine oral mucosal tissue has similar histological characteristics to human oral mucosal tissue [57]. The water permeability of porcine buccal mucosa was reported to be similar to that observed for human buccal mucosa, but the floor of the mouth was more permeable in human tissue than in pig tissue [58]. No significant effect on permeability of tissue was observed following freezing. Porcine buccal mucosal absorption has been studied for a wide range of drug molecules both in vitro and in vivo.

Nicolazzo et al. [59] investigated the permeability of porcine buccal tissue using caffeine and estradiol as model permeants, in modified Ussing chambers. Permeation studies were conducted with full thickness epithelia and with fresh and frozen tissues. Tissue barrier properties were monitored with fluorescein isothiocyanate (FITC)-labeled dextran 20 kDa (FD20), and tissue viability was assessed using an MTT (3-[4,5-dimethylthiazol-2-yl]-2,5-diphenyltetrazolium bromide) biochemical assay as well as histological evaluation. Compared with full thickness buccal epithelium, permeability through the buccal epithelium was 1.8-fold greater for caffeine and 16.7-fold greater for oestradiol. Permeability for both compounds was comparable for fresh and frozen buccal epithelium, although histological evaluation demonstrated signs of cellular death in frozen tissue. The tissue appeared to remain viable for up to 12 hours postmortem using the MTT viability assay, which was also confirmed by histological evaluation.

Kulkarni et al. [60] conducted in vitro permeation studies with antipyrine, buspirone, bupivacaine, and caffeine as model permeants. The permeability of the model diffusants across buccal mucosae with thicknesses ranging from 250 to 700 μm was determined. A bilayer membrane model was developed to delineate the relative contribution to the barrier function of the epithelium and the connective tissue. The relative contribution of the connective tissue region as a permeability barrier significantly increased with increasing mucosal tissue thickness. Up to 500 μm, the epithelium acted as the major barrier to penetration of molecules; lipophilic molecules also diffused more easily through the epithelium compared with hydrophilic compounds. The authors concluded that for in vitro buccal penetration studies, porcine tissue should have a thickness of about 500 μm. In a further study with porcine tissue, the authors investigated the influence of mucosal region, tissue storage conditions, and processing on the permeability of the same group of model permeants [61]. Higher permeability was observed for a tissue behind the lip both compared with the thicker cheek region. The permeability of the buccal mucosae stored either in phosphate buffered saline at 4 °C for 6 hours or in Krebs-Ringer bicarbonate buffer (KBR) at 4 °C for 24 hours was similar to the permeability of fresh buccal mucosa. Heat treatment to separate the epithelium from underlying connective tissue did not affect tissue permeability and integrity characteristics compared with surgical separation. The experimental and biological variables highlighted in these two studies need careful consideration by researchers, given the widespread use of excised porcine tissue to model transbuccal delivery in man.

9.5.3 Dog, Monkey, and Rabbit Models

The buccal epithelium is nonkeratinized in dogs and monkeys, and a number of in vivo studies have been conducted in dogs [62–64] and monkeys [65]. Higher buccal permeability has been reported in both species compared with humans,

and the buccal epithelia in these animals have been reported to be thinner than that in humans [66–68]. The rabbit buccal mucosa is also nonkeratinized and has been used for both in vitro and in vivo studies [69–71]. The difficulties in isolating nonkeratinized tissue from keratinized tissue in rabbits were earlier highlighted by Squier and Wertz [68].

9.5.4 Chicken, Hamster, and Rat Models

Buccal drug delivery has been evaluated using in vitro studies with chicken pouch membranes by a number of researchers. There is no evidence to suggest that this is a suitable tissue for predicting buccal delivery in humans [72, 73]. This model has been used to study buccal delivery of tramadol from a hydrogel [73]. Chicken buccal tissue has also been used to evaluate mucoadhesion and residence time of metronidazole gel [74] and for measurement of glibenclamide from porous and nonporous films [75]. As the rat oral cavity and hamster cheek pouch are keratinized, they are not appropriate models to predict buccal delivery in humans. Nevertheless, many studies in the literature have employed these tissues. The hamster pouch has been used to determine bioadhesion of various oral gels [76] and for the in vitro evaluation of ergotamine permeation [77]. Tsutsumi et al. [77] prepared keratinized epithelium (KE) and keratinized free epithelium (KFE) from the full-thickness hamster pouch mucosa. The permeation of a range of hydrophilic and lipophilic compounds was subsequently examined in the KE and KEF membrane. The KEF-membrane was more permeable to hydrophilic molecules than the KE membrane; lipophilic compounds showed similar permeation in both membranes [78]. Keratinized hamster mucosa was used by Starokadomskyy and Dubey [79] as a screening tool to identify optimal enhancers for buccal delivery of proteins.

9.5.5 Cell Culture Models

A squamous cell carcinoma of the buccal mucosa, the TR 146 cell line, has been isolated [80] and developed as an in vitro model of the buccal mucosa by Rassing and coworkers [81, 82]. The barrier function of this model is lower than porcine or human buccal tissue [83]. Correlations between porcine buccal tissue and the TR 146, for in vitro studies, have been reported for nicotine [83]. Comparable permeability of metoprolol was demonstrated in both the TR 146 model and porcine buccal tissue; an in vitro–in vivo correlation was developed based on in vivo studies conducted in minipigs [4]. A limitation of the TR 146 cell line is the absence of the mucus layer. Teubl et al. [84] prepared an external mucus layer using film technology which was deposited on the TR 146 culture model. The permeability of 200 nm nanoparticles of different charges was evaluated in the modified cell culture model

and in excised porcine buccal mucosa. The absorption of negative nanoparticles was hindered by the negatively charged mucin with higher absorption of neutral and the positive nanoparticles. Similar results were obtained in porcine buccal tissue.

EpiOral™ is a three-dimensional tissue culture model derived from healthy human buccal keratinocytes. The permeation of three methylxanthines was investigated by Thakur et al. [85] in the EpiOral model and in porcine skin in vitro. The tissue culture model demonstrated greater permeability than skin to all tested compounds. Rai et al. [86] reported similar permeability parameters for naltrexone hydrochloride using this model and porcine buccal tissue. However, these investigators used a relatively thin porcine buccal membrane of 300–400 μm compared with the reported thickness of 500–600 μm [10]. In our own laboratory, we recently compared the permeability of domperidone in EpiOral and in porcine buccal mucosa; both tissues were mounted in conventional Franz cells [8]. Saturated solutions of domperidone in PEG 200, PEG 400, or Transcutol™ P were applied to the tissues and permeation was monitored over eight hours at 37 °C. For all formulations, flux values were always significantly higher in the EpiOral model compared with porcine tissue data.

9.6 Feasibility of Systemic Delivery Based on In Vitro Permeation Studies

From a pharmacokinetic point of view, the rate of drug absorption is equal to the rate of drug removal from the body at steady state. Steady-state flux (J_{ss}) may be used as an index of the rate of drug absorption after buccal administration. The mathematical expression for the rate of drug removal is dependent both on the drug steady-state concentration (C_{ss}) and its clearance (CL). Consequently, the potential plasma concentration of a molecule after buccal administration may be extrapolated from the in vitro steady-state flux and clearance. The steady-state plasma concentration that might be achieved in vivo is calculated from Eq. (9.1) [87]:

$$C_{ss} = \frac{J_{ss}}{CL} \tag{9.1}$$

where the drug is not a new chemical entity, the mean plasma concentration for a therapeutic effect (C_{ss}) is often known as will the volume of plasma from which the drug is removed over time, i.e. the clearance (CL). A limitation of this approach is that Eq. (9.1) does not take into consideration the salivary clearance, which may result in overestimation of the total drug absorption. The steady-state plasma concentration calculated from Eq. (9.1), for this purpose, represents the concentration after application of the dosage form to 1 cm^2 of the buccal mucosa. The ratio of the required drug mean plasma concentration to the calculated plasma concentration

may be used to estimate the total area of application for a buccal formulation in order to achieve the therapeutic level. The average surface area of the buccal mucosa is ~100 cm^2 [88]. An application area of 10 cm^2 or less has been suggested as a suitable area of application for buccal formulations [89]. Heemstra et al. [87] prepared a mucoadhesive gel containing risperidone and measured steady-state flux levels in porcine buccal mucosa. Using Eq. (9.1), these authors demonstrated that therapeutic drug levels would be attained following application of the formulation to an area of the buccal mucosa of 2–10 cm^2. More recently, we have used the same approach to confirm the suitability of naratriptan for delivery to the systemic circulation as a buccal formulation [90].

9.7 Conclusion

OTDD is often used to achieve faster therapeutic effects and lower drug metabolism when compared with conventional oral drug delivery. However, the number of drugs formulated for buccal or sublingual delivery remains low. This likely reflects (i) the critical need to ensure these dosage forms are palatable and acceptable to the patient, (ii) the dynamic environment in the oral cavity and the difficulty in ensuring prolonged residence times of these formulations, (iii) the loss of drug by swallowing which may also contribute to a fraction of drug absorption. New oral transmucosal carrier systems such as thin films and sprays have been launched in recent years, and there is clearly scope to investigate these technologies for delivery of other actives. Recent success with a buccal insulin formulation is encouraging and suggests that further opportunities may exist for effective oral transmucosal delivery of other peptides and proteins. The permeation of a wide range of molecules has been investigated using in vitro models; the most reliable of these appears to be that based on excised porcine buccal mucosa, rather than tissue from other species. Proof-of-principle data may be generated using this approach, allowing for prediction of likely plasma levels of a molecule in man and a determination of whether OTDD is a feasible option.

References

1 Nielsen, H.M. and Rassing, M.R. (2000). TR146 cells grown on filters as a model of human buccal epithelium: V. Enzyme activity of the TR146 cell culture model, human buccal epithelium and porcine buccal epithelium, and permeability of leu-enkephalin. *Int. J. Pharm.* 200: 261–270.

2 Pather, S.I., Rathbone, M.J., and Senel, S. (2008). Current status and the future of buccal drug delivery systems. *Expert Opin. Drug Delivery* 5: 531–542.

3 Mudie, D.M., Amidon, G.L., and Amidon, G.E. (2010). Physiological parameters for oral delivery and in vitro testing. *Mol. Pharmaceutics* 7: 1388–1405.

4 Holm, R., Meng-Lund, E., Andersen, M.B. et al. (2013). In vitro, ex vivo and in vivo examination of buccal absorption of metoprolol with varying pH in TR146 cell culture, porcine buccal mucosa and Gottingen minipigs. *Eur. J. Pharm. Sci.* 49: 117–124.

5 Pather, S.I., Rathbone, M.J., and Senel, S. (2008). *Modified-Release Drug Delivery Technology*, 53–74. New York: Informa Healthcare.

6 Sohi, H., Ahuja, A., Ahmad, F.J., and Khar, R.K. (2010). Critical evaluation of permeation enhancers for oral mucosal drug delivery. *Drug Dev. Ind. Pharm.* 36: 254–282.

7 Webster, L.R. (2006). Fentanyl buccal tablets. *Expert Opin. Invest. Drugs* 15: 1469–1473.

8 Sattar, M., Sayed, O.M., and Lane, M.E. (2014). Oral transmucosal drug delivery: current status and future prospects. *Int. J. Pharm.* 471 (1–2): 498–506.

9 Squier, C. and Brogden, K. (2011). *Human Oral Mucosa: Development, Structure and Function*, 77–97. Oxford, UK: Wiley-Blackwell.

10 Gandhi, R.B. and Robinson, J.R. (1994). Oral cavity as a site for bioadhesive drug delivery. *Adv. Drug Delivery Rev.* 13: 43–74.

11 Dawson, D.V., Drake, D.R., Hill, J.R. et al. (2013). Organization, barrier function and antimicrobial lipids of the oral mucosa. *Int. J. Cosmet. Sci.* 35: 220–223.

12 Harris, D. and Robinson, J.R. (1992). Drug delivery via the mucous membranes of the oral cavity. *J. Pharm. Sci.* 81: 1–10.

13 Veuillez, F., Kalia, Y.N., Jacques, Y. et al. (2001). Factors and strategies for improving buccal absorption of peptides. *Eur. J. Pharm. Biopharm.* 51: 93–109.

14 Young, B., Lowe, J.S., Stevens, A., and Heath, J.W. (2006). *Wheater's Functional Histology*, 82–101. London: Churchill Livingstone - Elsevier.

15 Rathbone, M., Drummond, B.K., and Tucker, I.G. (1994). The oral cavity as a site for systemic drug delivery. *Adv. Drug Delivery Rev.* 13: 1–22.

16 Pimlott, S.J. and Addy, M. (1985). A study into the mucosal absorption of isosorbide dinitrate at different intraoral sites. *Oral Surg. Oral Med. Oral Pathol.* 59: 145–148.

17 Squier, C.A. (1991). The permeability of oral mucosa. *Crit. Rev. Oral Biol. Med.* 2: 13–32.

18 Squier, C.A. and Rooney, L. (1976). The permeability of keratinized and nonkeratinized oral epithelium to lanthanum in vivo. *J. Ultrastruct. Res.* 54: 286–295.

19 Slomiany, B.L., Murty, V.L., Piotrowski, J., and Slomiany, A. (1996). Salivary mucins in oral mucosal defense. *Gen. Pharmacol.* 27: 761–771.

20 Gilles, P., Ghazali, F.A., and Rathbone, J. (1996). *Oral Mucosal Drug Delivery*, 241–285. New York: Marcel Dekker.

21 Bures, P., Huang, Y., Oral, E., and Peppas, N.A. (2001). Surface modifications and molecular imprinting of polymers in medical and pharmaceutical applications. *J. Controlled Release* 72: 25–33.

22 Squier, C.A. and Hall, B.K. (1985). In-vitro permeability of porcine oral mucosa after epithelial separation, stripping and hydration. *Arch. Oral Biol.* 30: 485–491.

23 Kurosaki, Y., Nishimura, H., Terao, K. et al. (1992). Existence of a specialized absorption mechanism for cefadroxil, an aminocephalosporin antibiotic, in the human oral cavity. *Int. J. Pharm.* 82: 165–169.

24 Kurosaki, Y., Yano, K., and Kimura, T. (1998). Perfusion cells for studying regional variation in oral mucosal permeability in humans. 2. A specialized transport mechanism in D-glucose absorption exists in dorsum of tongue. *J. Pharm. Sci.* 87: 613–615.

25 Hoogstraate, A.J., Cullander, C., Nagelkerke, J.F. et al. (1994). Diffusion rates and transport pathways of fluorescein isothiocyanate (FITC)-labeled model compounds through buccal epithelium. *Pharm. Res.* 11: 83–89.

26 Pozzilli, P., Manfrini, S., Costanza, F. et al. (2005). Biokinetics of buccal spray insulin in patients with type 1 diabetes. *Metab. Clin. Exp.* 54: 930–934.

27 Annabestani, Z., Sharghi, S., Shahbazi, S. et al. (2010). Insulin buccal spray (Oral-Lyn) efficacy in type 1 diabetes. *Iran. J. Diabetes Lipid Dis.* 29: 1–4.

28 Goswami, T., Jasti, B.R., and Li, X. (2009). Estimation of the theoretical pore sizes of the porcine oral mucosa for permeation of hydrophilic permeants. *Arch. Oral Biol.* 54: 577–582.

29 Shorten, P.R., McMahon, C.D., and Soboleva, T.K. (2007). Insultin transport within skeletal muscle transverse tubule networks. *Biophys. J.* 93: 3001–3007.

30 Shah, R.B., Patel, M., Maahs, D.M., and Shah, V.N. (2016). Insulin delivery methods: past, present, and future. *Int. J. Pharm. Invest.* 6: 1–9.

31 Wertz, P.W. and Squier, C.A. (1991). Cellular and molecular basis of barrier function in oral epithelium. *Crit. Rev. Ther. Drug Carrier Syst.* 8: 237–269.

32 Caon, T., Jin, L., Simões, C.M. et al. (2015). Enhancing the buccal mucosal delivery of peptide and protein therapeutics. *Pharm. Res.* 32: 1–21.

33 Malkia, A., Murtomaki, L., Urtti, A., and Kontturi, K. (2004). Drug permeation in biomembranes: in vitro and in silico prediction and influence of physicochemical properties. *Eur. J. Pharm. Sci.* 23: 13–47.

34 Beckett, A.H. and Moffat, A.C. (1969). Correlation of partition coefficients in *n*-heptane-aqueous systems with buccal absorption data for a series of amines and acids. *J. Pharm. Pharmacol.* 21 (Suppl. 1): 144S–150S.

35 Beckett, A.H. and Moffat, A.C. (1969). The influence of substitution in phenylacetic acids on their performance in the buccal absorption test. *J. Pharm. Pharmacol.* 21 (Suppl. 1): 139S–143S.

36 Beckett, A.H. and Moffat, A.C. (1970). Kinetics of buccal absorption of some carboxylic acids and the correlation of the rate constants and *n*-heptane: aqueous phase partition coefficients. *J. Pharm. Pharmacol.* 22: 15–19.

37 Le Brun, P.P.H., Fox, P.L.A., Vries De, M.E., and Boddé, H.E. (1989). In vitro penetration of some ß-adrenoreceptor blocking drugs through porcine buccal mucosa. *Int. J. Pharm.* 49: 141–145.

38 Florence, A.T. and Attwood, D. (2011). *Physicochemical Principles of Pharmacy*, 364–365. London: Pharmaceutical Press.

39 Bhal, S.K., Kassam, K., Peirson, I.G., and Pearl, G.M. (2007). The rule of five revisited: applying log D in place of log *P* in drug-likeness filters. *Mol. Pharmaceutics* 4: 556–560.

40 Kokate, A., Li, X., and Jasti, B. (2008). Effect of drug lipophilicity and ionization on permeability across the buccal mucosa: a technical note. *AAPS PharmSciTech* 9: 501–504.

41 Birudaraj, R., Berner, B., Shen, S., and Li, X. (2005). Buccal permeation of buspirone: mechanistic studies on transport pathways. *J. Pharm. Sci.* 94: 70–78.

42 Kokate, A., Li, X., Singh, P., and Jasti, B.R. (2008). Effect of thermodynamic activities of the unionized and ionized species on drug flux across buccal mucosa. *J. Pharm. Sci.* 97: 4294–4306.

43 Dixit, R.P. and Puthli, S.P. (2009). Oral strip technology: overview and future potential. *J. Controlled Release* 139: 94–107.

44 Giannola, L.I., De Caro, V., Giandalia, G. et al. (2005). Transbuccal tablets of carbamazepine: formulation, release and absorption pattern. *Int. J. Immunopathol. Pharmacol.* 18: 21–31.

45 Campisi, G., Giannola, L.I., Florena, A.M. et al. (2010). Bioavailability in vivo of naltrexone following transbuccal administration by an electronically-controlled intraoral device: a trial on pigs. *J. Controlled Release* 145: 214–220.

46 Paderni, C., Campisi, G., Schumacher, A. et al. (2013). Controlled delivery of naltrexone by an intraoral device: in vivo study on human subjects. *Int. J. Pharm.* 452: 128–134.

47 Beckett, A.H. and Triggs, E.J. (1967). Buccal absorption of basic drugs and its application as an in vivo model of passive drug transfer through lipid membranes. *J. Pharm. Pharmacol.* 19 (Suppl): 31S–41S.

48 Beckett, A.H. and Moffat, A.C. (1968). The influence of alkyl substitution in acids on their performance in the buccal absorption test. *J. Pharm. Pharmacol.* 20 (Suppl. 1): 239S–247S.

49 Beckett, A.H. and Pickup, M.E. (1975). A model for steroid transport across biological membranes. *J. Pharm. Pharmacol.* 27: 226–234.

50 Tucker, I.G. (1988). A method to study the kinetics of oral mucosal drug absorption from solutions. *J. Pharm. Pharmacol.* 40: 679–683.

51 Rathbone, M.J. (1991). Human buccal absorption. I. A method for estimating the transfer kinetics of drugs across the human buccal membrane. *Int. J. Pharm.* 69: 103–108.

52 Kurosaki, Y., Yano, K., and Kimura, T. (1997). Perfusion cells for studying regional variation in oral-mucosal permeability in humans. I: Kinetic aspects in oral-mucosal absorption of alkylparabens. *Pharm. Res.* 14: 1241–1245.

53 Pudney, P.D., Bonnist, E.Y., Caspers, P.J. et al. (2012). A new in vivo Raman probe for enhanced applicability to the body. *Appl. Spectrosc.* 66: 882–891.

54 Nielsen, H.M. and Rassing, M.R. (2000). TR146 cells grown on filters as a model of human buccal epithelium: IV. Permeability of water, mannitol, testosterone and beta-adrenoceptor antagonists. Comparison to human, monkey and porcine buccal mucosa. *Int. J. Pharm.* 194: 155–167.

55 Van Der Bijl, P., Penkler, L., and Van Eyk, A.D. (2000). Permeation of sumatriptan through human vaginal and buccal mucosa. *Headache: J. Head Face Pain* 40: 137–141.

56 Meng-Lund, E., Marxen, E., Pedersen, A.M.L. et al. (2014). Ex vivo correlation of the permeability of metoprolol across human and porcine buccal mucosa. *J. Pharm. Sci.* 103: 2053–2061.

57 Heaney, T.G. and Jones, R.S. (1978). Histological investigation of the influence of adult porcine alveolar mucosal connective tissues on epithelial differentiation. *Arch. Oral Biol.* 23: 713–717.

58 Lesch, C.A., Squier, C.A., Cruchley, A. et al. (1989). The permeability of human oral mucosa and skin to water. *J. Dent. Res.* 68: 1345–1349.

59 Nicolazzo, J.A., Reed, B.L., and Finnin, B.C. (2003). The effect of various in vitro conditions on the permeability characteristics of the buccal mucosa. *J. Pharm. Sci.* 92: 2399–2410.

60 Kulkarni, U., Mahalingam, R., Pather, S.I. et al. (2009). Porcine buccal mucosa as an in vitro model: relative contribution of epithelium and connective tissue as permeability barriers. *J. Pharm. Sci.* 98: 471–483.

61 Kulkarni, U., Mahalingam, R., Pather, I. et al. (2010). Porcine buccal mucosa as in vitro model: effect of biological and experimental variables. *J. Pharm. Sci.* 99: 1265–1277.

62 Voorspoels, J., Remon, J.P., Eechaute, W., and Desy, W. (1996). Buccal absorption of testosterone and its esters using a bioadhesive tablet in dogs. *Pharm. Res.* 13: 1228–1232.

63 Hosny, E.A., Elkheshen, S.A., and Saleh, S.I. (2002). Buccoadhesive tablets for insulin delivery: in-vitro and in-vivo studies. *Boll. Chim. Farm.* 141: 210–217.

64 Degim, T., Eglen, B., and Ocak, O. (2006). A sustained release dosage form of acyclovir for buccal application: an experimental study in dogs. *J. Drug Targeting* 14: 35–44.

65 Qiu, Y., Johnson, H.W., Reiland, T.L., and Lu, M.Y. (1999). Sublingual absorption of leuprolide: comparison between human and animal models. *Int. J. Pharm.* 179: 27–36.

66 Nagai, T. (1985). Adhesive topical drug delivery system. *J. Controlled Release* 2: 121–134.

67 Mehta, M., Kemppainen, B.W., and Stafford, R.G. (1991). In vitro penetration of tritium-labelled water (THO) and [^{3}H]PbTx-3 (a red tide toxin) through monkey buccal mucosa and skin. *Toxicol. Lett.* 55: 185–194.

68 Squier, C.A. and Wertz, P.W. *Oral Mucosal Drug Delivery*, 1–26. New York: Marcel Dekker.

69 Li, C., Bhatt, P.P., and Johnston, T.P. (1997). Transmucosal delivery of oxytocin to rabbits using a mucoadhesive buccal patch. *Pharm. Dev. Technol.* 2: 265–274.

70 Alur, H.H., Beal, J.D., Pather, S.I. et al. (1999). Evaluation of a novel, natural oligosaccharide gum as a sustained-release and mucoadhesive component of calcitonin buccal tablets. *J. Pharm. Sci.* 88: 1313–1319.

71 Rana, P. and Murthy, R.S. (2013). Formulation and evaluation of mucoadhesive buccal films impregnated with carvedilol nanosuspension: a potential approach for delivery of drugs having high first-pass metabolism. *Drug Delivery* 20: 224–235.

72 El-Samaligy, M.S., Yahia, S.A., and Basalious, E.B. (2004). Formulation and evaluation of diclofenac sodium buccoadhesive discs. *Int. J. Pharm.* 286: 27–39.

73 Kamel, R., Mahmoud, A., and El-Feky, G. (2012). Double-phase hydrogel for buccal delivery of tramadol. *Drug Dev. Ind. Pharm.* 38: 468–483.

74 Bhatia, M. and Ahuja, M. (2013). Thiol modification of psyllium husk mucilage and evaluation of its mucoadhesive applications. *Sci. World J.* 2013: 284182.

75 Kumar, A., Bali, V., Kumar, M., and Pathak, K. (2013). Comparative evaluation of porous versus nonporous mucoadhesive films as buccal delivery system of glibenclamide. *AAPS PharmSciTech* 14: 1321–1332.

76 Needleman, I.G. and Smales, F.C. (1995). In vitro assessment of bioadhesion for periodontal and buccal drug delivery. *Biomaterials* 16: 617–624.

77 Tsutsumi, K., Obata, Y., Takayama, K. et al. (1998). Effect of cod-liver oil extract on the buccal permeation of ergotamine tartrate. *Drug Dev. Ind. Pharm.* 24: 757–762.

78 Tsutsumi, K., Obata, Y., Takayama, K. et al. (1999). Permeation of several drugs through keratinized epithelial-free membrane of hamster cheek pouch. *Int. J. Pharm.* 177: 7–14.

79 Starokadomskyy, P.L. and Dubey, I.Y. (2006). New absorption promoter for the buccal delivery: preparation and characterization of lysalbinic acid. *Int. J. Pharm.* 308: 149–154.

80 Rupniak, H.T., Rowlatt, C., Lane, E.B. et al. (1985). Characteristics of four new human cell lines derived from squamous cell carcinomas of the head and neck. *J. Natl. Cancer Inst.* 75: 621–635.

81 Jacobsen, J., Nielsen, E.B., Brøndum-Nielsen, K. et al. (1999). Filter-grown TR146 cells as an in vitro model of human buccal epithelial permeability. *Eur. J. Oral Sci.* 107: 138–146.

82 Nielsen, H.M., Verhoef, J.C., Ponec, M., and Rassing, M.R. (1999). TR146 cells grown on filters as a model of human buccal epithelium: permeability of fluorescein isothiocyanate-labelled dextrans in the presence of sodium glycocholate. *J. Controlled Release* 60: 223–233.

83 Nielsen, H.M. and Rassing, M.R. (2002). Nicotine permeability across the buccal TR146 cell culture model and porcine buccal mucosa in vitro: effect of pH and concentration. *Eur. J. Pharm. Sci.* 16: 151–157.

84 Teubl, B.J., Absenger, M., Frohlich, E. et al. (2013). The oral cavity as a biological barrier system: design of an advanced buccal in vitro permeability model. *Eur. J. Pharm. Biopharm.* 84: 386–393.

85 Thakur, R.A., Michniak, B.B., and Meidan, V.M. (2007). Transdermal and buccal delivery of methylxanthines through human tissue in vitro. *Drug Dev. Ind. Pharm.* 33: 513–521.

86 Rai, V., Tan, H.S., and Michniak-Kohn, B. (2011). Effect of surfactants and pH on naltrexone (NTX) permeation across buccal mucosa. *Int. J. Pharm.* 411: 92–97.

87 Heemstra, L.B., Finnin, B.C., and Nicolazzo, J.A. (2010). The buccal mucosa as an alternative route for the systemic delivery of risperidone. *J. Pharm. Sci.* 99: 4584–4592.

88 Collins, L.M. and Dawes, C. (1987). The surface area of the adult human mouth and thickness of the salivary film covering the teeth and oral mucosa. *J. Dent. Res.* 66: 1300–1302.

89 Amores, S., Lauroba, J., Calpena, A. et al. (2014). A comparative ex vivo drug permeation study of beta-blockers through porcine buccal mucosa. *Int. J. Pharm.* 468: 50–54.

90 Sattar, M., Hadgraft, J., and Lane, M.E. (2015). Preparation, characterization and buccal permeation of naratriptan. *Int. J. Pharm.* 493 (1–2): 146–151.

10

PK/PD and the Drug Delivery Regimen for Infusion in the Critical Care Setting

Fekade B. Sime[1,2] *and Jason A. Roberts*[1,2,3,4]

[1] *Centre for Translational Anti-infective Pharmacodynamics, School of Pharmacy, The University of Queensland, Brisbane, QLD, Australia*
[2] *Faculty of Medicine, University of Queensland Centre for Clinical Research, The University of Queensland, Brisbane, QLD, Australia*
[3] *Department of Intensive Care Medicine, Royal Brisbane and Women's Hospital, Brisbane, QLD, Australia*
[4] *Pharmacy Department, Royal Brisbane and Women's Hospital, Brisbane, QLD, Australia*

10.1 Introduction

The first historical mention of intravenous infusions dates back to a fifteenth century unsuccessful blood transfusion for the ailing Pope Innocent VIII, 250th successor of the apostle Peter. The death of the Pope and three donors led to a ban of the use of intravenous infusions for any medical interventions for many years. Later in the second half of the seventeenth century, Sir Christopher Wren started experiments with parenteral injections in animals that paved ways for the introduction of this mode of drug delivery to humans. The first documented intravenous injection in humans was in 1662 CE by Johann D. Major. Unfortunately, he administered an unpurified compound resulting in a poor patient outcome that discouraged further attempts on infusions for centuries to follow. It was not until mid-nineteenth century when use of parenteral drug administration was first documented. By the mid-twentieth century, infusional drug delivery was well established due to increased understanding of associated risks, advances in microbiology, and infection control, as well as the advent of antibiotics [1–3]. To date, intravenous infusion is the mainstay of drug delivery in hospitalized and particularly critically ill patients because of the need for rapid drug action and patients' inability to take enteral drugs. Many antibiotics used in the treatment of serious infections are administered by intravenous infusion, some of which can only be given by infusion due to their physicochemical nature that makes other modes of delivery difficult [4]. This includes an inability to develop a formulation suitable for enteral use.

Drug Delivery Approaches: Perspectives from Pharmacokinetics and Pharmacodynamics,
First Edition. Edited by Bret Berner, Toufigh Gordi, Heather A. E. Benson, and Michael S. Roberts.

As far as antibiotic dosing is concerned, the ultimate goal of continuous intravenous infusions is to rapidly achieve and sustain effective antibiotic concentrations at the site of infection that ensure maximal bacterial killing and a quick resolution of infection. Given that sites of infection are often in deep tissue that are inaccessible for direct drug injection, intravenous infusion is the best option to rapidly achieve suitable blood concentrations that provide a concentration gradient that can enable sufficient distribution (usually diffusion) to enable adequate concentrations at the target site. Tissue (interstitial fluid) antibiotic concentration determines antibiotic efficacy for most types of infection. However, tissue concentrations are difficult to measure and as such plasma concentrations are used as surrogates to describe the concentration–effect relationship. This relationship between plasma concentrations and antibiotic activity is however not straightforward, with different classes of antibiotics having characteristic relationships [5]. These relationships have been described by the magnitude and time-course of antibiotic exposure (as described by pharmacokinetics, PK) in reference to the degree of the susceptibility of the target pathogen (described by pharmacodynamics, PD). Accordingly, the following PK/PD indices have been defined to be associated with maximal antibiotic effects for different antibiotic classes: ratio of peak concentration to the minimum inhibitory concentration, MIC (C_{max}/MIC), ratio of area under the concentration–time curve (AUC) to MIC, and duration of the dosing interval for which the free antibiotic concentration remains above MIC ($fT_{>MIC}$). This chapter aims to describe the influence of these PK/PD properties of antibiotic on the mode of infusional drug delivery regimen. It also describes PK/PD considerations on the design and optimization of antibiotic infusions in the critically ill. Further, it summarizes our current understanding on the clinical benefit of the different modes of antibiotic infusion advocated by PK/PD studies.

10.2 PK/PD Properties and the Mode of Infusional Drug Delivery for Antibiotics

For a given antibiotic, its unique PK property and the specific PK/PD dosing target define the optimal dosing regimen. Targeted C_{max}/MIC ratios can be effectively achieved with short intermittent infusions as compared to extended (infusion >2 hours) or continuous infusions. The C_{max} achieved with prolonged infusions is generally low, and particularly lowest with drugs that exhibit high clearance (CL) and high volume of distribution (V_d). On the other hand, the C_{max} achieved by short intermittent infusions is hardly affected by CL, but rather by the V_d; i.e. higher magnitude of the intermittent dose is required with an increased V_d. In some circumstances, a significant increase in V_d may even necessitate a loading dose to rapidly achieve C_{max}/MIC [6]. CL determines the

dosing frequency of short intermittent infusions although it does not significantly affect the magnitude of dose required to achieve the target C_{max}/MIC. However, if the dosing target is AUC/MIC or $fT_{>MIC}$, both CL and V_d influence the magnitude of an intermittent dosing regimen required to achieve the PK/PD target. Furthermore, alternative modes of infusion (extended infusion or continuous infusion) have a higher probability of achieving target $fT_{>MIC}$ as compared to intermittent infusions [7]. However for targeting specific AUC/MIC ratios, an increased V_d of antibiotics may necessitate a loading dose with prolonged infusion (i.e. extended or continuous infusion) regimens [8].

PD properties of antibiotics can also influence the drug delivery regimen. For example, in the presence of a long post-antibiotic effect (i.e. continual inhibition of bacterial growth after exposure to an antibiotic), the rate and extent of bacterial killing with intermittent exposure may be equivalent to continuous exposure [9]. Thus, less frequent intermittent dosing may be sufficient particularly for antibiotics with a C_{max}/MIC bacterial kill characteristic. With a prolonged post-antibiotic effect, a lesser dosing frequency of bolus infusion may be required, with carbapenems for examples, to achieve optimal $fT_{>MIC}$. However, the lack of post antibiotic effect for other β-lactams such as the cephalosporins, means that they required higher % $fT_{>MIC}$ for maximal activity [10]. Consequently, this requires the use of a relatively large dose of short intermittent infusions, as compared to prolonged infusions which can attain the same target with lower doses. The MIC of the antibiotic to the pathogen is another PD property that can dramatically influence the dosing regimen. A high MIC means that very high intermittent infusion doses are required to achieve target C_{max}/MIC, AUC/MIC, or $fT_{>MIC}$ ratios. In such cases, the antibiotic may be best given by prolonged infusion, which in particular, can maximize the $fT_{>MIC}$ without requiring a massive increase in the magnitude of the dose and hence potentially reducing the risk of toxicity.

10.3 Changes in PK/PD and Infusional Drug Delivery Regimens in Critically Ill Patients

Patients in the intensive care settings undergo complex physiological changes due to their underlying disease conditions as well as the aggressive therapeutic interventions associated with the resuscitation of patients and the management of major organ dysfunction. These changes can have a significant influence on antibiotic PK of thereby affecting the drug delivery regimen [11].

One of the most important pathophysiological phenomena associated with altered antibiotic PK is the progression of systemic inflammatory response syndrome (SIRS). This manifestation is triggered by multiple insults during critical

illness, including severe infections that can progress into severe sepsis or septic shock [12]. A complex set of inflammatory mediators released during SIRS affect the functions of major organs and systems that are primarily involved in drug disposition. The cardiovascular system is raised into a hyperdynamic state characterized by high cardiac output, increased regional blood flow, increased capillary permeability, and fluid extravasation [13]. A sharp increase in renal blood flow then results in a state of glomerular hyperfiltration [14]. These pathologic events are further augmented by therapeutic interventions. For example the large volume of fluid resuscitation during sepsis/septic shock or large volume hydration of patients with hematological malignancies [15] may accelerate fluid extravasation (edema) as well as glomerular hyperfiltration. These collective changes can alter the antibiotic concentrations in the critically ill. The antibiotics most affected are those that preferentially distribute into body water compartments and are dependent on renal function for elimination (hydrophilic antibiotics). The major changes to PK parameters that result from these pathophysiological processes include an increase in V_d and increase/decrease in CL (dependent on organ function).

Superimposed with the complex and hard-to-predict PK changes induced by this pathophysiology, the use of extracorporeal therapies in patients with renal and cardiac and/or respiratory dysfunction present an even more complex dosing challenge. In patients receiving extracorporeal renal replacement therapy (RRT), it is often challenging to quantify the extent of CL for such antibiotics, due to the interplay of multiple factors related to both the RRT and the patient. RRT-related factors include different modalities of RRT leading to different drug CL, operational settings (may affect drug CL), and filter materials used (may cause adsorption of antibiotic to filter membrane). Patient-related factors may also lead to an unpredictable total CL because of variable residual renal function and the presence/upregulation of nonrenal routes of elimination [16, 17]. Extracorporeal membrane oxygenation (ECMO) is another organ support intervention that can influence antibiotic PK. Accumulating data suggest, ECMO can significantly alter the V_d of some antibiotics and also can result in significant loss of the administered dose through sequestration in the circuit system [18, 19].

All in all, drug disposition in critically ill patients can be substantially different to disposition in general ward patients or healthy volunteers. Altered drug behavior translates into altered dosing needs. Since there are no objective clinical end points that can immediately signal dosing appropriateness, PK/PD analyses provide an invaluable means of gauging dosing adequacy. Further, with advances in PK study design, PK/PD analysis has emerged as robust tool for the design of optimal dosing regimens in challenging patient populations. In recent decades, such application of PK/PD has transformed the approaches to use of infusional dosing regimens in the critically ill, particularly, extended infusions, and continuous infusions.

10.4 Short Intermittent Infusions

In recent years, principles of PK/PD have been applied to antibiotics to adapt traditional intermittent dosing regimens so as to optimize antibiotic concentrations in line with PD properties, thereby leading to better patient outcome. A typical example is the introduction of single daily aminoglycoside intermittent infusions (typically 30-minute infusions) which have largely replaced the previous standard of care, thrice or twice daily intermittent infusions. This was based on some important PD considerations. Firstly, the antibacterial activity of aminoglycosides is maximized by increasing the C_{max}/MIC (i.e. concentration-dependent killing) [20]. Secondly, aminoglycosides have a prolonged post-antibiotic effect against most potential pathogens, which means that the antibacterial effect is sustained beyond the duration of exposure [9]. Thirdly, aminoglycoside toxicity correlates with trough concentrations [21] which are minimized with less frequent dosing, and that possibly saturable kinetics of renal tissue accumulation of aminoglycosides means high peak concentrations do not increase the risk of nephrotoxicity [22, 23]. Consequently, single daily dosing (also called extended interval dosing) is effective and offers an important advantage of ease of administration to reduce costs of treatment, and lower risks of nephrotoxicity [24]. Meta-analyses of clinical trials [25–30] have confirmed equivalence of once-daily vs. multiple-daily intermittent infusions in terms of clinical efficacy. Better patient outcomes in bacteriological/clinical cure rates and/or significantly reduced toxicity are also reported in some clinical trials and meta-analyses [26, 27, 29, 31]. In no report to our knowledge, have worse outcomes been described with once-daily dosing.

Another example of applications of advanced PK/PD analysis in the design of novel intermittent dosing schedules is the use of front-loaded dosing regimen. This involves high dose intermittent infusion in the early phase (hours to days) of treatment followed by a lower dose ongoing intermittent schedule. Front-loaded dosing regimens have been described, for instance, for fusidic acid [32], colistin [33], and linezolid [34]. Front-loading can maximize bacterial killing and suppress the emergence of pathogen resistance to antibiotics, and can optimize exposure in circumstances where the non-linear PK of a drug alters the disposition during the course of therapy [32]. In addition, considering intensive PK alteration during the early phase of infections and the associated high risk of initial sub-therapeutic concentration, front-loading provides a dosing approach that minimizes the risk of under-dosing [35]. Higher drug exposure is also beneficial to minimize the selection of resistant sub-populations that may initially exist when the bacterial load is highest (i.e. at the commencement of therapy). Further, it may offer a strategy for an appropriately aggressive early phase therapy in scenarios where highly resistant infections are encountered [34].

10.5 Extended Infusions

Although short intermittent infusions are the traditional mode of intravenous drug delivery for antibiotics in critically ill patients, this approach does not suit the PK/PD characteristics of time-dependent antibiotics ($fT_{>MIC}$, and some AUC/MIC drugs, e.g. vancomycin). This is because of PK alterations (increases in V_d and/or CL) which cause standard intermittent doses to result in potentially sub-optimal concentrations. This is typically true for β-lactam antibiotics, which exhibit a very short half-life (c. 1–2 hour), high CL, and are subject to augmented renal CL [36–38]. Since conventional intermittent doses of β-lactams are given up to three to four times per day, further increases in frequency are largely considered unreasonable from a nursing care perspective. Extended infusion of such time-dependent antibiotics over the first few hours of the dosing interval (i.e. 2–4 hour infusion) provides an attractive alternative to improve attainment of PK/PD targets with standard or less frequent dosing, and significantly lower total daily antibiotic dose than would be required with intermittent dosing [39–41]. Logistically, the use extended infusion can be easily implemented in routine practice with the wide availability of modern infusion pumps [42].

There is a clear evidence that extended infusion of β-lactams achieves better $fT_{>MIC}$ than short intermittent infusions [39, 43–45]. Especially when high PK/PD targets are aimed in severely ill patients (e.g. 100% $fT_{>4\times MIC}$), or when infections are caused by high MIC organisms, a higher proportion of patients achieve the desired target with extended infusion regimens relative to short intermittent infusions. However, in the critically ill, due to large PK variability between patients as well as within individual patients, a systematic extended infusion program is unlikely to attain desired target in all patients, unless guided by real time therapeutic drug monitoring (TDM) [38, 46, 47]. Nonetheless, extended infusion provides an effective strategy for TDM-guide dose adaptation [39]. For instance, we have previously demonstrated such an application for piperacillin–tazobactam in severely ill febrile neutropenic patients [48].

Beyond an increase in PK/PD target attainment, some clinical trials, and meta-analyses suggest that an extended infusion regimen can improve patient outcomes [49–51], although evidence on outcome benefit is generally limited. The relative advantage for patient outcome is likely to be greatest when less susceptible pathogens are encountered [7]. With highly susceptible infections (i.e. caused by pathogens with a low MIC), the efficacy of extended infusions is likely to be equivalent to that of short intermittent infusions. This was well shown by Felton et al. [52] in a hollow-fiber infection model investigation. Further, these authors reported that a higher trough concentration was required with extended infusion regimens (relative to bolus) to suppress emergence of resistance, which in essence seems to complicate the more basic $fT_{>MIC}$ data that preceded this study.

However, although clinical data is scarce on exposure response-relationships that suppress emergence of resistance, in vitro data suggest higher concentrations than those required for bacterial killing may be necessary [53–55]. Therefore, further characterization of the PD of β-lactams is warranted to describe the relative advantage of different infusion regimens on the suppression of antibiotic resistance.

Cost saving is another potential advantage of extended infusion regimens. In one institution which implemented a universal substitution of intermittent piperacillin/tazobactam dosing with a 4-hour extended infusion dose every 8–12 hours (based on renal function), the estimated total saving was greater than US$ 2 million over a period of two years [42] and was attributed to reduced drug expenditure and length of hospital stay (improved patient outcomes). Another study in a community medical center also reported significant cost savings from reduced pharmacy expenditure [50].

10.6 Continuous Infusion

Several PK/PD studies and clinical outcome trials have investigated the role of continuous infusion for optimization treatment by time-dependent antibiotics, mainly the β-lactams, and the glycopeptide vancomycin.

10.6.1 Continuous Infusion of β-Lactam Antibiotics

Following the strong evidence from preclinical in vitro and animal models of infection that the $fT_{>MIC}$ relates to antibacterial activity of β-lactams, a number of clinical studies have described the PK profile of continuous infusion. This subject has been extensively reviewed; for further detail, readers are referred to the examples of reviews by Mouton and Vinks [56, 57], Abdul-Aziz et al. [40], and Roberts et al. [7]. Overall, the available data strongly support superiority of continuous infusion regimens (combined with an initial loading dose, Figure 10.1) in maximizing exposure time above the MIC. However, the correlation of the improved PK/PD profile with a clinical outcome benefit is less well established; and has been a focus of ongoing investigations. This has been subjected to examination in both in vitro and in vivo pre-clinical studies as well as various clinical trials.

Few in vitro models that simulate changing drug concentrations have assessed the PD role of continuous infusion. A study by Tessier et al. [58] investigated the efficacy of cefepime continuous infusion against clinical isolates of *Pseudomonas aeruginosa*. More persistent bactericidal activity was noted for continuous infusion compared to intermittent dosing that was associated with a significant regrowth

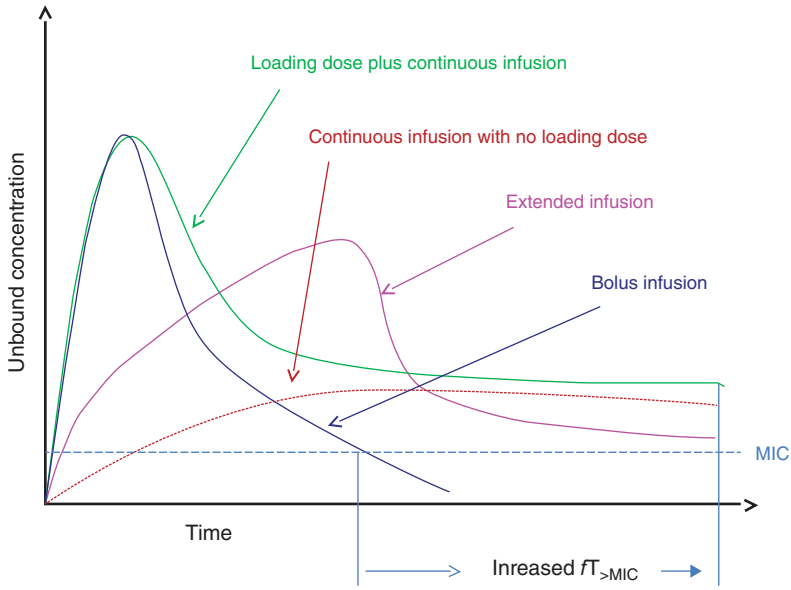

Figure 10.1 Schematic illustration of the concentration–time profile of different modes of infusion.

of bacteria. In another dynamic in vitro model investigation, Mouton and Den Hollander [54] found a higher kill rate by continuous compared with intermittent infusion of ceftazidime against *P. aeruginosa* strains. Findings of this study also suggested that regrowth of bacteria occurs when concentrations fall below a certain level despite the concentration being at or slightly above MIC. This observation, together with the fact that the PD activity of β-lactams does not increase at concentrations above four-times the MIC, suggests that maximal activity occurs at concentrations of about four to five times the MIC. Continuous infusion is not only efficient to maintain such steady concentrations, but also is more effective in maximizing bacterial kill and suppressing pathogen regrowth when concentrations are maintained at about four to five times the MIC [54]. The relative benefit of continuous infusion may be more evident with less susceptible organisms as demonstrated by Alou et al. [59] in a dynamic in vitro model simulating human-like PK of ceftazidime against strains of *P. aeruginosa* with varying susceptibility.

However, some in vivo data from animal models of infection suggest that even for susceptible strains, continuous infusion may be superior to intermittent administration. For example a study by Robaux et al. [60] found that ceftazidime continuous infusion was more effective against *P. aeruginosa* in a rabbit model of endocarditis. Further data from other animal models of infection, albeit limited

[57], suggest that very sick hosts (patients) such as those with febrile neutropenia or poor immunity may benefit from continuous infusion. For example, Roosendaal et al. [61, 62] showed in a rat model of pneumonia (*Klebsiella pneumoniae*) that continuous infusion of ceftazidime was more effective than intermittent dosing in neutropenic rats.

Several observational studies and randomized controlled trials have assessed the clinical benefit of β-lactam continuous infusion vs. short intermittent infusion and have been reviewed elsewhere [40, 57]. The collective outcome data from most of these studies have been subjected to meta-analyses [63–67] (Table 10.1). One such meta-analysis by Kasiakou et al. [63] included randomized control trials comparing outcomes of continuous infusion for antibiotics in general (including β-lactams, aminoglycosides, and vancomycin). The authors reported no significant reduction in clinical failures with continuous infusion regimens and no differences in mortality benefit or toxicity. However, the gross evaluation of multiple antibiotic classes with different PD activity in the same analysis would make the outcomes assessment difficult as antibiotics with different kill characteristics may benefit (or not) differently from continuous infusion. In particular, the inclusion of aminoglycosides might confound the analysis as their concentration-dependent activity is likely to favor intermittent daily dosing regimens particularly with regard to toxicity as discussed above. However, contrary to this, the authors observed clinical improvements with aminoglycoside continuous infusion. The heterogeneity of patients and dosing regimens in the analyzed studies could also be significant confounders of outcome of the analysis. This is actually reflected in the sub-group analysis of trials that used the same total daily dose, which showed reduced clinical failure with continuous infusion regimen. Given the studies available for this analysis were mostly underpowered and with low quality score [63], this study was limited to suggesting a potential benefit of continuous infusion for further confirmation in a well-designed randomized study. A later meta-analysis by Roberts et al. [64] included 14 randomized studies of only β-lactam antibiotics that compared relative outcomes of continuous (13 studies)/extended (1 study) infusion vs. intermittent bolus infusion. No significant improvement in clinical outcomes (clinical cure and mortality) was noted in this analysis. The authors further discussed the challenges of pooling data from existing studies in the context of the lack of benefit observed while abundant PK/PD data suggest the advantage of continuous infusion. Importantly, there was a considerable degree of heterogeneity of the available randomized studies in terms of patient's population, severity of participant's illness, distribution of organ dysfunction, and also in the magnitude of dose in the regimens including the use of loading dose with continuous infusion. Thus, the authors concluded that the results of the analysis were not sufficient to rule out the benefit of continuous infusion. However, the analysis provides important guidance that not

Table 10.1 Summary of meta-analyses assessing the outcome benefit of continuous infusion of β-lactam antibiotics.

Authors	Year	Antibiotics included	Number of RCTs	Inclusion of extended infusion	Outcome variable assessed	Number of participants (studies)	RR	95% CI	*p* value
Roberts et al. [68]	2016	β-Lactams	3	No	30-d hospital mortality	632 (3)	0.74	0.56 to 1.00	0.045
					Clinical cure		1.2	1.03 to 1.40	0.021
					ICU-free days at day 28		0	−3 to 3	0.9
					ICU mortality		0.82	0.58 to 1.16	0.26
Shiu et al. [65]	2013	Both time and concentration dependent	29	Yes (four studies)	All-cause mortality	1241 (19)	0.89	0.67 to 1.20	0.45
					Infection recurrence	398 (8)	1.22	0.35 to 4.19	0.76
					Clinical cure	975 (15)	1.04	0.95 to 1.13	0.98
					Super-infection	813 (12)	1.08	0.60 to 1.94	0.79
					Serious adverse events	871 (10)	1.36	0.8 to 2.3	0.26
					Withdrawal due to adverse events	871 (10)	2.03	0.52 to 7.95	0.31
					Adverse events	575 (5)	1.02	0.94 to 1.12	0.63
Falagas et al. [67]	2013	Carbapenems	14[a)]	Yes (six studies)	Mortality	1116 (12)	0.59	0.41 to 0.83	
		Piperacillin–tazobactam			Clinical cure	557 (8)	1.13	0.99 to 1.28	
Tamma et al. [66]	2011	β-Lactams	14	Yes (three studies)	In-hospital mortality	982 (8)	0.92	0.61 to 1.37	0.36
					Clinical cure	1380 (13)	1.00	0.94 to 1.06	0.58
Roberts et al. [64]	2009	β-Lactams	14	Yes (one study)	Clinical cure	755 (9)	1.04	0.74 to 1.46	0.83
					Mortality	541 (9)	1.00	0.48 to 2.06	1.00
Kasiakou et al. [63]	2005	β-Lactams, aminoglycosides, vancomycin	9	No	Clinical failure	730 (7)	0.73	0.53 to 1.01	0.78
					Mortality	(5)	0·89	0.48 to 1.64	0.71

RR, relative risk: CI, confidence interval.

a) 8 retrospective studies, 3 prospective studies, and 3 randomized controlled trials (RCTs).

all patients will gain a superior benefit from continuous infusion and that rational design of further studies should carefully address a more homogeneous study population. The meta-analysis by Tamma et al. [66] expanded upon the Roberts et al. meta-analysis and included two additional studies on prolonged β-lactam infusion but still concluded similarly. Another, relatively recent, meta-analysis by a Cochrane group [65] also failed to show any outcome benefit of continuous infusion over intermittent administration. However, the authors suggested that most of the available studies included in their analysis were not clear or were associated with high risk of bias in some methodological aspects. Further, this study pooled data from both concentration-dependent and time-dependent antibiotics and thus may be subject of further bias as discussed above. In addition, both continuous and extended infusion regimens were included in the analysis while a distinct PK/PD profile exists for these two modes of infusion which could potentially affect outcomes. Once again, the observation of no benefit of continuous infusion over intermittent dosing could not be considered to be definitive until further data from large randomized studies is available. The authors also underscored this fact given the wide confidence intervals they observed for effect estimates and the acknowledgment of lack of adequate data.

In an ongoing effort to address the lack of data, Dulhunty et al. [69] reported results from a large multicenter randomized trial assessing the efficacy of continuous vs. intermittent infusion in patients with severe sepsis. Similar to the meta-analyses, no benefit was reported based on the nonsignificant difference in median alive ICU-free days (18 and 20 days, $p = 0.83$), survival at day 90 (74.3% vs. 72.5%; hazard ratio (HR) 0.91, 95% confidence interval [CI] 0.63–1.31, $p = 0.61$), and clinical cure rate (54.2% vs. 49.5%; odds ratio (OR) 1.12, 95% CI 0.77–1.63, $p = 0.56$) for the continuous and intermittent group respectively. Although this study was well designed and targeted a specific patient population with severe sepsis, it recruited a large cohort of patients with considerable heterogeneity in organ dysfunction including those receiving RRT. This adds evidence that not all patient groups benefit equally from continuous infusion and very strict homogeneity in factors that affect PK and PD of antibiotics would be necessary in further trials to address the undescribed correlation between results of PK/PD studies and clinical outcome trials. Recently, a relatively homogenous cohort of critically ill patients, excluding those on RRT, were recruited by Abdul-Aziz et al. [70] in a two-center randomized study. Interestingly, the authors found significant advantage in clinical cure rate with continuous vs. intermittent infusion (56% vs. 34%, $p = 0.011$). This study also integrated PK/PD evaluation with outcome assessment; attainment of 100% $fT_{>MIC}$ at steady state was significantly high for the continuous infusion arm (97% vs. 68%, $p < 0.001$) which is in line with the outcome findings on clinical cure. Subsequent to this study, Roberts et al. [68] published the first report of mortality benefit from an individual patient-level

data meta-analysis. The authors combined data from three randomized trials and found not only that rate of clinical cure was significantly higher for continuous infusion (relative risk [RR] 1.20, 95% CI 1.03–1.40, $p = 0.021$) but also hospital mortality is significantly lower (RR 0.74, 95% CI 0.56–1.00, $p = 0.045$). This most recent analysis of outcome benefit explains, at least in part, the largely missing correlation between PK/PD studies illustrating increased exposure, and randomized studies assessing outcome benefit.

10.6.2 Continuous Infusion of Vancomycin

The antibacterial effect of vancomycin correlates with the ratio of AUC_{24}/MIC which relates to both the concentration and time of exposure (conventional target is $AUC_{24}/MIC \geq 400$) [71–73]. Data from in vitro time-kill studies comparing high vs. low concentration of vancomycin found no difference in bacterial kill rate, suggesting high peak concentrations may not have therapeutic advantage in patients [74]. Further, a trend in increased bacterial killing was observed with continuous infusion in another in vitro study although it did not yield the highest kill rate [75]. Such observations and the fact that vancomycin has considerable time-dependent activity, triggered interest in clinical studies to optimize vancomycin therapy with continuous infusion.

However, results from subsequent clinical studies show no superiority of continuous infusion. Because of the relatively longer half-life of about six to eight hours for vancomycin (normal renal function), intermittent infusion can successfully achieve required AUC/MIC target and consequently appear the preferred mode of administration given the lack of evidence of additional benefit for continuous infusion [72, 75]. In a prospective randomized cross-over study, James et al. [76] illustrated that continuous and intermittent infusion regimens achieve similar AUC/MIC ratios although the PK profile was more stable with continuous infusion. Similarly, another prospective randomized study [77] found no difference in microbiological outcomes, rates of treatment failure, and infection-related mortality. Data from non-randomized observational studies are not consistent with some suggesting possible underexposure when reduced susceptibility exist (e.g. MIC > 1 mg/l for *Staphylococcus aureus*) or otherwise continuous infusion may require a high dose of unknown safety to achieve the conventional target of $AUC_{24}/MIC \geq 400$ [8, 78, 79]. Other studies [80–82] found that a continuous infusion regimen was sufficient to achieve PK/PD targets provided that appropriate loading doses are given to avoid sub-therapeutic concentrations in the initial phase.

In general, data from randomized studies are limited, and no conclusive evidence exists at the moment on the benefit of continuous infusion with vancomycin. With the limited data available, the meta-analysis by Cataldo et al. [83]

showed that it is difficult to derive conclusion on relative exposure, treatment outcomes, and mortality benefit. However in their analysis of five studies [77, 84–87], the authors found that continuous infusion was associated with a reduced risk of nephrotoxicity, which they suggest may be related to the lower total daily dose required with continuous infusion regimen to achieve desired PK targets. An additional advantage may be that such reduced total dose, and hence expenditure on drug, could be associated with significant cost savings as demonstrated in one study [81].

10.7 Conclusions

Understanding of PK/PD properties of antibiotics is instrumental in the rational design of dosing regimens that maximize adequacy of exposure for improved outcome. Recent developments in the application of PK/PD using advanced modeling techniques are changing conventional dosing regimens for intravenous infusions to define new modes of delivery in the critical care settings. However, although significant advances in knowledge of dose–exposure relationships have been observed, there is only limited evidence on the relationship between the exposures obtained through novel infusional regimens, and improved clinical outcome. Particularly, a mortality benefit derived from a well-designed, large randomized controlled study is still outstanding. Such a study that assesses patient outcomes should integrate PK/PD evaluations within the same study so as to enhance the interpretation of findings.

References

1 Brazeau, G.A., Persky, A., and Napaporn, J. (2007). Dosage forms: parenterals. In: *Encyclopedia of Pharmaceutical Technology*, 3e, vol. 1 (ed. J. Swarbrick), 1001–1011. New York, NY, USA: Informa Healthcare USA, Inc.

2 Macht, D.I. (1916). The history of intravenous and subcutaneous administration of drugs. *J. Am. Med. Assoc.* 66: 856–860.

3 Barsoum, N. and Kleeman, C. (2002). Now and then, the history of parenteral fluid administration. *Am. J. Nephrol.* 22: 284–289.

4 Macielag, M.J. (2012). Chemical properties of antimicrobials and their uniqueness. In: *Antibiotic Discovery and Development* (eds. T.J. Dougherty and M.J. Pucci), 793–820. New York: Springer Science+Business Media.

5 Craig, W.A. (1998). Pharmacokinetic/pharmacodynamic parameters: rationale for antibacterial dosing of mice and men. *Clin. Infect. Dis.* 26: 1–10; quiz 11–12.

6 Goncalves-Pereira, J., Martins, A., and Povoa, P. (2010). Pharmacokinetics of gentamicin in critically ill patients: pilot study evaluating the first dose. *Clin. Microbiol. Infect.* 16: 1258–1263.

7 Roberts, J.A., Abdul-Aziz, M.H., Lipman, J. et al. (2014). Individualised antibiotic dosing for patients who are critically ill: challenges and potential solutions. *Lancet Infect. Dis.* 14: 498–509.

8 Roberts, J.A., Taccone, F.S., Udy, A.A. et al. (2011). Vancomycin dosing in critically ill patients: robust methods for improved continuous-infusion regimens. *Antimicrob. Agents Chemother.* 55: 2704–2709.

9 Gerber, A.U., Wiprachtiger, P., Stettler-Spichiger, U., and Lebek, G. (1982). Constant infusions vs. intermittent doses of gentamicin against *Pseudomonas aeruginosa* in vitro. *J. Infect. Dis.* 145: 554–560.

10 Turnidge, J.D. (1998). The pharmacodynamics of beta-lactams. *Clin. Infect. Dis.* 27: 10–22.

11 Roberts, J.A. and Lipman, J. (2009). Pharmacokinetic issues for antibiotics in the critically ill patient. *Crit. Care Med.* 37: 840–851; quiz 859.

12 Blot, S.I., Pea, F., and Lipman, J. (2014). The effect of pathophysiology on pharmacokinetics in the critically ill patient – concepts appraised by the example of antimicrobial agents. *Adv. Drug Delivery Rev.* 77: 3–11.

13 Young, J.D. (2004). The heart and circulation in severe sepsis. *Br. J. Anaesth.* 93: 114–120.

14 Udy, A.A., Roberts, J.A., Shorr, A.F. et al. (2013). Augmented renal clearance in septic and traumatized patients with normal plasma creatinine concentrations: identifying at-risk patients. *Crit. Care* 17: R35.

15 McBride, A. and Westervelt, P. (2012). Recognizing and managing the expanded risk of tumor lysis syndrome in hematologic and solid malignancies. *J. Hematol. Oncol.* 5: 75.

16 Jamal, J.A., Mueller, B.A., Choi, G.Y. et al. (2015). How can we ensure effective antibiotic dosing in critically ill patients receiving different types of renal replacement therapy? *Diagn. Microbiol. Infect. Dis.* 82: 92–103.

17 Jamal, J.A., Udy, A.A., Lipman, J., and Roberts, J.A. (2014). The impact of variation in renal replacement therapy settings on piperacillin, meropenem, and vancomycin drug clearance in the critically ill: an analysis of published literature and dosing regimens*. *Crit. Care Med.* 42: 1640–1650.

18 Shekar, K., Fraser, J.F., Smith, M.T., and Roberts, J.A. (2012). Pharmacokinetic changes in patients receiving extracorporeal membrane oxygenation. *J. Crit. Care* 27 (741): 741.e9–741.e18.

19 Shekar, K., Roberts, J.A., McDonald, C.I. et al. (2015). Protein-bound drugs are prone to sequestration in the extracorporeal membrane oxygenation circuit: results from an ex vivo study. *Crit. Care* 19: 164.

20 Turnidge, J. (2003). Pharmacodynamics and dosing of aminoglycosides. *Infect. Dis. Clin. N. Am.* 17: 503–528.

21 Selby, N.M., Shaw, S., Woodier, N. et al. (2009). Gentamicin-associated acute kidney injury. *QJM* 102: 873–880.

22 Conly, J.M. and Shafran, S.D. (1994). Intravenous-to-oral conversion therapy for antimicrobials. *Can. J. Infect. Dis.* 5: 15–16.

23 Giuliano, R.A., Verpooten, G.A., Verbist, L. et al. (1986). In vivo uptake kinetics of aminoglycosides in the kidney cortex of rats. *J. Pharmacol. Exp. Ther.* 236: 470–475.

24 Stankowicz, M.S., Ibrahim, J., and Brown, D.L. (2015). Once-daily aminoglycoside dosing: an update on current literature. *Am. J. Health Syst. Pharm.* 72: 1357–1364.

25 Hatala, R., Dinh, T., and Cook, D.J. (1996). Once-daily aminoglycoside dosing in immunocompetent adults: a meta-analysis. *Ann. Intern. Med.* 124: 717–725.

26 Barza, M., Ioannidis, J.P., Cappelleri, J.C., and Lau, J. (1996). Single or multiple daily doses of aminoglycosides: a meta-analysis. *BMJ* 312: 338–345.

27 Ferriols-Lisart, R. and Alos-Alminana, M. (1996). Effectiveness and safety of once-daily aminoglycosides: a meta-analysis. *Am. J. Health Syst. Pharm.* 53: 1141–1150.

28 Munckhof, W.J., Grayson, M.L., and Turnidge, J.D. (1996). A meta-analysis of studies on the safety and efficacy of aminoglycosides given either once daily or as divided doses. *J. Antimicrob. Chemother.* 37: 645–663.

29 Smyth, A.R. and Bhatt, J. (2012). Once-daily versus multiple-daily dosing with intravenous aminoglycosides for cystic fibrosis. *Cochrane Database Syst. Rev.* 2: CD002009.

30 Mavros, M.N., Polyzos, K.A., Rafailidis, P.I., and Falagas, M.E. (2011). Once versus multiple daily dosing of aminoglycosides for patients with febrile neutropenia: a systematic review and meta-analysis. *J. Antimicrob. Chemother.* 66: 251–259.

31 Marik, P.E., Lipman, J., Kobilski, S., and Scribante, J. (1991). A prospective randomized study comparing once- versus twice-daily amikacin dosing in critically ill adult and paediatric patients. *J. Antimicrob. Chemother.* 28: 753–764.

32 Tsuji, B.T., Okusanya, O.O., Bulitta, J.B. et al. (2011). Application of pharmacokinetic-pharmacodynamic modeling and the justification of a novel fusidic acid dosing regimen: raising Lazarus from the dead. *Clin. Infect. Dis.* 52 (Suppl. 7): S513–S519.

33 Rao, G.G., Ly, N.S., Haas, C.E. et al. (2014). New dosing strategies for an old antibiotic: pharmacodynamics of front-loaded regimens of colistin at simulated pharmacokinetics in patients with kidney or liver disease. *Antimicrob. Agents Chemother.* 58: 1381–1388.

34 Tsuji, B.T., Brown, T., Parasrampuria, R. et al. (2012). Front-loaded linezolid regimens result in increased killing and suppression of the accessory gene

regulator system of *Staphylococcus aureus*. *Antimicrob. Agents Chemother.* 56: 3712–3719.

35 Goncalves-Pereira, J. and Paiva, J.A. (2013). Dose modulation: a new concept of antibiotic therapy in the critically ill patient? *J. Crit. Care* 28: 341–346.

36 Udy, A.A., Roberts, J.A., De Waele, J.J. et al. (2012). What's behind the failure of emerging antibiotics in the critically ill? Understanding the impact of altered pharmacokinetics and augmented renal clearance. *Int. J. Antimicrob. Agents* 39: 455–457.

37 Udy, A.A., Lipman, J., Jarrett, P. et al. (2015). Are standard doses of piperacillin sufficient for critically ill patients with augmented creatinine clearance? *Crit. Care* 19: 28.

38 Roberts, J.A., Paul, S.K., Akova, M. et al. (2014). DALI: defining antibiotic levels in intensive care unit patients: are current beta-lactam antibiotic doses sufficient for critically ill patients? *Clin. Infect. Dis.* 58: 1072–1083.

39 Abbott, I.J. and Roberts, J.A. (2012). Infusional beta-lactam antibiotics in febrile neutropenia: has the time come? *Curr. Opin. Infect. Dis.* 25: 619–625.

40 Abdul-Aziz, M.H., Staatz, C.E., Kirkpatrick, C.M.J. et al. (2012). Continuous infusion vs. bolus dosing: implications for beta-lactam antibiotics. *Minerva Anestesiol.* 78: 94–104.

41 Chant, C., Leung, A., and Friedrich, J.O. (2013). Optimal dosing of antibiotics in critically ill patients by using continuous/extended infusions: a systematic review and meta-analysis. *Crit. Care* 17: R279.

42 Maddox, M.L., DeBoer, E.C., and Hammerquist, R.J. (2014). Administration of extended infusion piperacillin–tazobactam with the use of smart pump technology. *Hosp. Pharm.* 49: 444–448.

43 De, W.J., Carlier, M., Hoste, E. et al. (2014). Extended versus bolus infusion of meropenem and piperacillin: a pharmacokinetic analysis. *Minerva Anestesiol.* 80: 1302–1309.

44 Shea, K.M., Cheatham, S.C., Smith, D.W. et al. (2009). Comparative pharmacodynamics of intermittent and prolonged infusions of piperacillin/tazobactam using monte carlo simulations and steady-state pharmacokinetic data from hospitalized patients. *Ann. Pharmacother.* 43: 1747–1754.

45 Felton, T.W., Hope, W.W., Lomaestro, B.M. et al. (2012). Population pharmacokinetics of extended-infusion piperacillin–tazobactam in hospitalized patients with nosocomial infections. *Antimicrob. Agents Chemother.* 56: 4087–4094.

46 Carlier, M., Carrette, S., Roberts, J.A. et al. (2013). Meropenem and piperacillin/tazobactam prescribing in critically ill patients: does augmented renal clearance affect pharmacokinetic/pharmacodynamic target attainment when extended infusions are used? *Crit. Care* 17: R84.

47 Carlier, M., Carrette, S., Stove, V. et al. (2014). Does consistent piperacillin dosing result in consistent therapeutic concentrations in critically ill patients?

A longitudinal study over an entire antibiotic course. *Int. J. Antimicrob. Agents* 43: 470–473.

48 Sime, F.B., Roberts, M.S., Tiong, I.S. et al. (2015). Can therapeutic drug monitoring optimize exposure to piperacillin in febrile neutropenic patients with haematological malignancies? A randomized controlled trial. *J. Antimicrob. Chemother.* 70 (8): 2369–2375.

49 Bauer, K.A., West, J.E., O'Brien, J.M., and Goff, D.A. (2013). Extended-infusion cefepime reduces mortality in patients with *Pseudomonas aeruginosa* infections. *Antimicrob. Agents Chemother.* 57: 2907–2912.

50 Brunetti, L., Poustchi, S., Cunningham, D. et al. (2015). Clinical and economic impact of empirical extended-infusion piperacillin–tazobactam in a community medical center. *Ann. Pharmacother.* 49: 754–760.

51 Yang, H., Zhang, C., Zhou, Q. et al. (2015). Clinical outcomes with alternative dosing strategies for piperacillin/tazobactam: a systematic review and meta-analysis. *PLoS One* 10: e0116769.

52 Felton, T.W., Goodwin, J., O'Connor, L. et al. (2013). Impact of bolus dosing versus continuous infusion of piperacillin and tazobactam on the development of antimicrobial resistance in *Pseudomonas aeruginosa*. *Antimicrob. Agents Chemother.* 57: 5811–5819.

53 Tam, V.H., Schilling, A.N., Neshat, S. et al. (2005). Optimization of meropenem minimum concentration/MIC ratio to suppress in vitro resistance of *Pseudomonas aeruginosa*. *Antimicrob. Agents Chemother.* 49: 4920–4927.

54 Mouton, J.W. and Den Hollander, J.G. (1994). Killing of *Pseudomonas aeruginosa* during continuous and intermittent infusion of ceftazidime in an in vitro pharmacokinetic model. *Antimicrob. Agents Chemother.* 38: 931–936.

55 Feng, Y., Hodiamont, C.J., van Hest, R.M. et al. (2016). Development of antibiotic resistance during simulated treatment of *Pseudomonas aeruginosa* in chemostats. *PLoS One* 11: e0149310.

56 Mouton, J.W. and Vinks, A.A. (1996). Is continuous infusion of beta-lactam antibiotics worthwhile? – efficacy and pharmacokinetic considerations. *J. Antimicrob. Chemother.* 38: 5–15.

57 Mouton, J.W. and Vinks, A.A. (2007). Continuous infusion of beta-lactams. *Curr. Opin. Crit. Care* 13: 598–606.

58 Tessier, P.R., Nicolau, D.P., Onyeji, C.O., and Nightingale, C.H. (1999). Pharmacodynamics of intermittent- and continuous-infusion cefepime alone and in combination with once-daily tobramycin against *Pseudomonas aeruginosa* in an in vitro infection model. *Chemotherapy* 45: 284–295.

59 Alou, L., Aguilar, L., Sevillano, D. et al. (2005). Is there a pharmacodynamic need for the use of continuous versus intermittent infusion with ceftazidime against *Pseudomonas aeruginosa*? An in vitro pharmacodynamic model. *J. Antimicrob. Chemother.* 55: 209–213.

60 Robaux, M.A., Dube, L., Caillon, J. et al. (2001). In vivo efficacy of continuous infusion versus intermittent dosing of ceftazidime alone or in combination with amikacin relative to human kinetic profiles in a *Pseudomonas aeruginosa* rabbit endocarditis model. *J. Antimicrob. Chemother.* 47: 617–622.

61 Roosendaal, R., Bakker-Woudenberg, I.A., van den Berghe-van Raffe, M., and Michel, M.F. (1986). Continuous versus intermittent administration of ceftazidime in experimental *Klebsiella pneumoniae* pneumonia in normal and leukopenic rats. *Antimicrob. Agents Chemother.* 30: 403–408.

62 Roosendaal, R., Bakker-Woudenberg, I.A., van den Berg, J.C., and Michel, M.F. (1985). Therapeutic efficacy of continuous versus intermittent administration of ceftazidime in an experimental *Klebsiella pneumoniae* pneumonia in rats. *J. Infect. Dis.* 152: 373–378.

63 Kasiakou, S.K., Sermaides, G.J., Michalopoulos, A. et al. (2005). Continuous versus intermittent intravenous administration of antibiotics: a meta-analysis of randomised controlled trials. *Lancet Infect. Dis.* 5: 581–589.

64 Roberts, J.A., Webb, S., Paterson, D. et al. (2009). A systematic review on clinical benefits of continuous administration of beta-lactam antibiotics. *Crit. Care Med.* 37: 2071–2078.

65 Shiu, J., Wang, E., Tejani, A.M., and Wasdell, M. (2013). Continuous versus intermittent infusions of antibiotics for the treatment of severe acute infections. *Cochrane Database Syst. Rev.* 3: CD008481.

66 Tamma, P.D., Putcha, N., Suh, Y.D. et al. (2011). Does prolonged beta-lactam infusions improve clinical outcomes compared to intermittent infusions? A meta-analysis and systematic review of randomized, controlled trials. *BMC Infect. Dis.* 11: 181.

67 Falagas, M.E., Tansarli, G.S., Ikawa, K., and Vardakas, K.Z. (2013). Clinical outcomes with extended or continuous versus short-term intravenous infusion of carbapenems and piperacillin/tazobactam: a systematic review and meta-analysis. *Clin. Infect. Dis.* 56: 272–282.

68 Roberts, J.A., Abdul-Aziz, M.H., Davis, J.S. et al. (2016). Continuous versus intermittent beta-lactam infusion in severe sepsis: a meta-analysis of individual patient data from randomized trials. *Am. J. Respir. Crit. Care Med.*

69 Dulhunty, J.M., Roberts, J.A., Davis, J.S. et al. (2015). A multicenter randomized trial of continuous versus intermittent beta-lactam infusion in severe sepsis. *Am. J. Respir. Crit. Care Med.* 192: 1298–1305.

70 Abdul-Aziz, M.H., Sulaiman, H., Mat-Nor, M.B. et al. (2016). Beta-lactam infusion in severe sepsis (BLISS): a prospective, two-centre, open-labelled randomised controlled trial of continuous versus intermittent beta-lactam infusion in critically ill patients with severe sepsis. *Intensive Care Med.*

71 Moise-Broder, P.A., Forrest, A., Birmingham, M.C., and Schentag, J.J. (2004). Pharmacodynamics of vancomycin and other antimicrobials in patients with

Staphylococcus aureus lower respiratory tract infections. *Clin. Pharmacokinet.* 43: 925–942.

72 Rybak, M.J., Lomaestro, B.M., Rotschafer, J.C. et al. (2009). Vancomycin therapeutic guidelines: a summary of consensus recommendations from the infectious diseases Society of America, the American Society of Health-System Pharmacists, and the society of infectious diseases pharmacists. *Clin. Infect. Dis.* 49: 325–327.

73 Matsumoto, K., Takesue, Y., Ohmagari, N. et al. (2013). Practice guidelines for therapeutic drug monitoring of vancomycin: a consensus review of the Japanese Society of Chemotherapy and the Japanese Society of Therapeutic Drug Monitoring. *J. Infect. Chemother.* 19: 365–380.

74 Ackerman, B.H., Vannier, A.M., and Eudy, E.B. (1992). Analysis of vancomycin time-kill studies with *Staphylococcus* species by using a curve stripping program to describe the relationship between concentration and pharmacodynamic response. *Antimicrob. Agents Chemother.* 36: 1766–1769.

75 Houlihan, H.H., Mercier, R.C., and Rybak, M.J. (1997). Pharmacodynamics of vancomycin alone and in combination with gentamicin at various dosing intervals against methicillin-resistant *Staphylococcus aureus*-infected fibrin-platelet clots in an in vitro infection model. *Antimicrob. Agents Chemother.* 41: 2497–2501.

76 James, J.K., Palmer, S.M., Levine, D.P., and Rybak, M.J. (1996). Comparison of conventional dosing versus continuous-infusion vancomycin therapy for patients with suspected or documented gram-positive infections. *Antimicrob. Agents Chemother.* 40: 696–700.

77 Wysocki, M., Delatour, F., Faurisson, F. et al. (2001). Continuous versus intermittent infusion of vancomycin in severe *Staphylococcal infections*: prospective multicenter randomized study. *Antimicrob. Agents Chemother.* 45: 2460–2467.

78 Panday, P.N. and Sturkenboom, M. (2009). Continuous infusion of vancomycin less effective and safe than intermittent infusion, based on pharmacodynamic and pharmacokinetic principles. *Clin. Infect. Dis.* 49: 1964–1965; author reply 1965.

79 Jeurissen, A., Sluyts, I., and Rutsaert, R. (2011). A higher dose of vancomycin in continuous infusion is needed in critically ill patients. *Int. J. Antimicrob. Agents* 37: 75–77.

80 Saugel, B., Nowack, M.C., Hapfelmeier, A. et al. (2013). Continuous intravenous administration of vancomycin in medical intensive care unit patients. *J. Crit. Care* 28: 9–13.

81 De Waele, J.J., Danneels, I., Depuydt, P. et al. (2013). Factors associated with inadequate early vancomycin levels in critically ill patients treated with continuous infusion. *Int. J. Antimicrob. Agents* 41: 434–438.

82 Ampe, E., Delaere, B., Hecq, J.D. et al. (2013). Implementation of a protocol for administration of vancomycin by continuous infusion: pharmacokinetic, pharmacodynamic and toxicological aspects. *Int. J. Antimicrob. Agents* 41: 439–446.

83 Cataldo, M.A., Tacconelli, E., Grilli, E. et al. (2012). Continuous versus intermittent infusion of vancomycin for the treatment of Gram-positive infections: systematic review and meta-analysis. *J. Antimicrob. Chemother.* 67: 17–24.

84 Wysocki, M., Thomas, F., Wolff, M.A. et al. (1995). Comparison of continuous with discontinuous intravenous infusion of vancomycin in severe MRSA infections. *J. Antimicrob. Chemother.* 35: 352–354.

85 Vuagnat, A., Stern, R., Lotthe, A. et al. (2004). High dose vancomycin for osteomyelitis: continuous vs. intermittent infusion. *J. Clin. Pharm. Ther.* 29: 351–357.

86 Hutschala, D., Kinstner, C., Skhirdladze, K. et al. (2009). Influence of vancomycin on renal function in critically ill patients after cardiac surgery: continuous versus intermittent infusion. *Anesthesiology* 111: 356–365.

87 Ingram, P.R., Lye, D.C., Fisher, D.A. et al. (2009). Nephrotoxicity of continuous versus intermittent infusion of vancomycin in outpatient parenteral antimicrobial therapy. *Int. J. Antimicrob. Agents* 34: 570–574.

11

Virtual Experiment Methods for Integrating Pharmacokinetic, Pharmacodynamic, and Drug Delivery Mechanisms: Demonstrating Feasibility for Acetaminophen Hepatotoxicity

Andrew K. Smith[1], Ryan C. Kennedy[1], Brenden K. Petersen[2], Glen E.P. Ropella[3] and Carver Anthony Hunt[1]

[1] *Bioengineering and Therapeutic Sciences, The University of California,, San Francisco, CA, 04143*
[2] *Lawrence Livermore National Laboratory,, Livermore, CA, 94550*
[3] *Tempus Dictum, Inc., Olympia, WA, 98502*

11.1 Introduction

When a drug development effort fails or is abandoned, one or more contributing factors can often be traced to flawed explanatory mechanistic insight into often-entangled drug delivery (DD), pharmacokinetic (PK), and/or pharmacodynamic (PD) influences. New modeling and simulation (M&S) methods are needed to improve explanatory DD, PK, and PD mechanistic insight incrementally during drug development. To do so, we maintain that a single methodology is needed that is capable of addressing DD, PK, and pharmacological questions simultaneously as well as independently. The foremost challenges concern pharmacological phenomena. Pharmacology can be characterized as the pursuit of mechanism-oriented models that better explain those phenomena. It follows that advances in both pharmacology and drug development efficiency require models capable of better explaining such phenomena. In this chapter, we describe an advanced methodology that enables concurrent biomimetic simulation of DD, PK, and PD phenomena.

These two questions demonstrate the necessity of having a unified approach to DD, PK, and PD M&S. How can we engineer delivery of X in a particular set of patients to achieve a particular therapeutic effect, while also avoiding drug-induced liver injury? Within a cadre of patients following the same pharmaceutical treatment protocol, clinical endpoint effect exhibits considerable – potentially unacceptable – interindividual variability. Is DD system variability a major contributing factor? Answering both questions requires capabilities to conduct many exploratory virtual experiments in which the focus can

Drug Delivery Approaches: Perspectives from Pharmacokinetics and Pharmacodynamics,
First Edition. Edited by Bret Berner, Toufigh Gordi, Heather A. E. Benson, and Michael S. Roberts.

shift among DD, PK, and PD influences. Doing so is beyond the scope of currently used modeling methods [1, 2]. The purpose of this chapter is to review progress [3–6] made toward achieving those capabilities. We then draw on that material to present requirements for scientifically useful models capable of answering the above two questions.

The PD component of the demonstration focuses on mechanisms of acetaminophen (APAP) induced liver injury (AILI) in mice, which serves as model for xenobiotic induced liver injury in humans. We selected AILI because of the quantity and variety of published data characterizing PD phenomena spanning several biological levels [7–9]. The PK component of AILI is concerned primarily with the mechanisms governing the hepatic disposition and metabolism of APAP in rodents. For this chapter, the DD component is limited to demonstrating control over the absorption and disposition of APAP. A way for a virtual experiment to demonstrate its scientific usefulness is to improve explanatory insight via challenging mechanism-based hypotheses and, more importantly, falsifying mechanism-based hypotheses, i.e. demonstrating that a particular mechanism is inadequate to explain a particular, targeted phenomenon. Challenging and falsifying hypotheses is central to the scientific method, but it cannot be done using conventional PK, PD, or physiologically based (PB) PK or PD models.

We demonstrate how and why scientifically useful biological models need to mimic – be analogous to – their referent system in meaningful ways. When a goal is increasing explanatory, mechanism-based knowledge, explanatory models should have concrete mechanisms that mimic hypothesized referent mechanisms [10]. We show why simply reproducing referent measurements is inadequate.

11.1.1 Focus on Acetaminophen-Induced Liver Injury

A characteristic feature of APAP hepatotoxicity is necrosis occurring first adjacent to the lobule's central vein (CV) and progressing outward thereafter toward the periportal entrance (PP) [11, 12]. The weight of evidence supports this explanation: location dependent differences in consequences of reactive metabolite (*N*-acetyl-*p*-benzoquinone imine [NAPQI]) formation within hepatic lobules (NAPQI zonation) are necessary and sufficient to account for that early pattern of necrosis. Hereafter, we refer to that explanation as the NZ-Mechanism hypothesis. However, challenging that hypothesis directly in mice is currently infeasible in part because doing so would require sequential intra-lobular measurements within the same mouse along with the ability to control multiple zonation influencing features spanning several biological levels.

In Section 11.2, we describe results of virtual experiments that challenged and falsified NZ-Mechanism [6]. We call virtual mice Mouse Analogs because we claim that their virtual causal mechanisms and the actual mechanism

in mice are strongly analogous within and across multiple biological levels. Mouse Analogs contain a concretized Liver Analog comprising biomimetic lobules in which autonomous hepatocyte counterparts utilize a parsimonious version of NZ-Mechanism. As a prerequisite, we achieved multiple qualitative and quantitative validation targets (VTs), discussed below. Virtual hepatocytes can use a periportal entry-to-central vein (PP-to-CV) gradient to individualize responses to APAP and internal damage based on location (functional zonation). Searches of NZ-Mechanism's configuration space failed to identify particular configurations able to cause simulated necrosis to occur first adjacent to CV (an Analog's configuration space is analogous to the parameter space of conventional PK/PD models). We posited that at least one additional mechanism feature must exhibit zonation. We instantiated competing hypotheses. For Competing Mechanism A, the likelihood of glutathione (GSH) being depleted below a critical level (through early reaction with NAPQI) increases PP-to-CV. For Competing Mechanism B, each hepatocyte's ability to repair simulated NAPQI-induced mitochondrial damage (e.g. [13]) diminishes PP-to-CV. We hypothesized that inclusion of either feature would be sufficient to achieve the VT. But both mechanisms were falsified. Thus, an even more complicated yet still parsimonious mechanism-based explanation was required. We created Merged Mechanism by combining Competing Mechanisms A and B, and were able to identify configurations that achieved the VT. The Merged Mechanism during execution is a dynamic concrete hypothesis for how key features of APAP hepatotoxicity in mice may be generated.

We begin by reviewing results that lead to discovery of Merged Mechanism and enabled demonstrating a therapeutic intervention by separately administering a hypothetical inhibitor of hepatotoxicity. We follow with an abridged review of methods, which makes clear how desirable DD, PK, and PD capabilities can be achieved simultaneously within a single virtual system. We conclude with discussion of capabilities needed to improve the scientific usefulness of virtual experiments within pharmaceutical research and development.

11.2 Results

11.2.1 Engineering Parsimonious Fit for Purpose Virtual Mice

Figure 11.1 illustrates Mouse Analog components, features, and organization that proved to be essential to enable implementing a changeable NZ-Mechanism. A precondition for credible challenge experiments was to strengthen concrete analog-to-mouse micro- and mesoscale functional similarities by achieving a variety of stringent multi-attribute qualitative and quantitative VTs (see Section 11.3) while adhering to a strong parsimony guideline. Hereafter, virtual objects and features are capitalized to avoid confusion and reinforce that they are incomplete software representations of the biology.

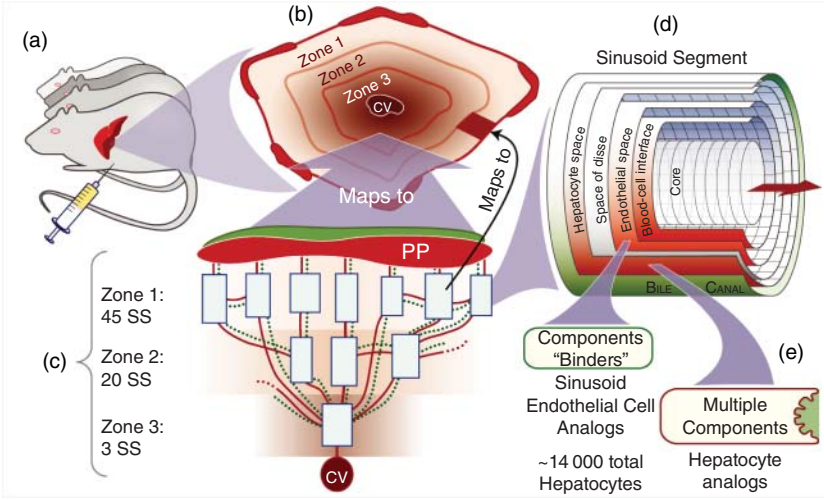

Figure 11.1 Mouse Analog components and their organization. (a) Mouse Analog comprises a Liver, Mouse Body, and a space (maps to peritoneal cavity) from which an APAP dose is absorbed. During execution, each discrete time step maps to ~1 second. (b) A Liver comprises Monte Carlo (MC)-determined Lobule variants. (c) A Lobule comprises a directed graph with a concrete Sinusoid Segment (SS) object (a software agent) at each graph node. Lobular configurations are the result of cycling many times through the Iterative Refinement Protocol and successfully achieving several quantitatively stringent Validation Targets [3, 14–16]. All flow paths follow the directed graph. Bile (dotted) flows separately from blood (solid) but is not a factor for the hypotheses tested herein. PP-to-CV gradients provide intra-Lobular location information to each Hepatocyte. (d) Each SS configures a parsimony-guided multiscale variety of components so that during execution it functions as an analog of sinusoid components and features averaged across many lobules; SS dimensions are MC-determined to mimic hepatic variability. Cell objects occupy most of Endothelial Cell (99%) and Hepatocyte (90%) spaces. APAP objects enter and exit an SS via Core and Interface, percolate stochastically through accessible spaces influenced by configuration-controlled local flow, and if not metabolized, exit to CV and return to Mouse Body. (e) Cells in Endothelial space control APAP entry and exit and contain a probability-specified number of Binders, which only bind and release APAP. Virtual Hepatocytes use three previously validated event management modules [17], which control (i) material entry and removal, (ii) binding and object transformations, and (iii) up- and down-regulation of events such as Metabolism (not used for this work). Source: (c) Based on Ropella et al. [3], Yan et al. [14], and Park et al. [16]. (e) Based on Petersen et al. [17].

Presented in Figure 11.2A is the minimum number of events needed to challenge NZ-Mechanism. All events are coarse grain analogs of actual processes. Each event is independent and does not necessarily occur each simulation cycle. The probability of occurrence is controlled by a value in the configuration file. All configuration values for the results that follow were arrived at using the Iterative Refinement (IR) Protocol.

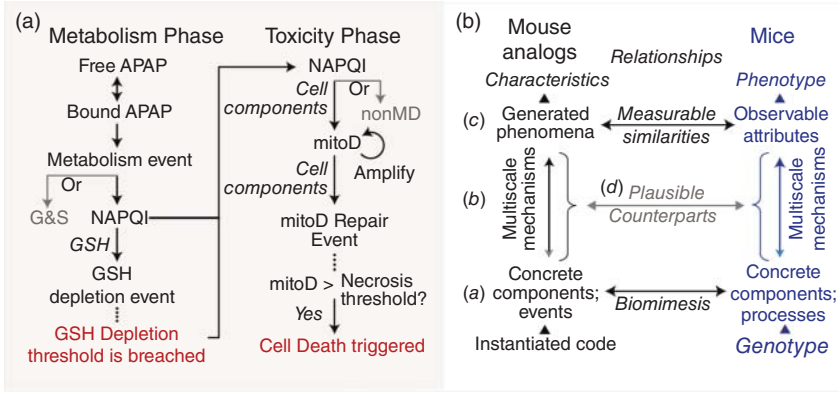

Figure 11.2 Events within vHPCs and Analog–mouse relationships. (A) Virtual experiments focus on Metabolism Phase events and key early events within the Toxicity Phase of injury [7]. Although illustrated as a sequential cascade, each event executes independently in pseudo-random order each time step. All events are stochastic. Some event probabilities are Lobule location-dependent. An APAP object maps to a small fraction of an actual APAP dose. G&S objects represent APAP-glucuronide and APAP-sulfate plus all other inactive metabolites. A GSH Depletion event maps to depletion of a portion of a hepatocyte's basal GSH. Mitochondrial Damage objects (mitoD) map to conflation of all influential damage products occurring within mitochondria [18]. Each mitoD may undergo one amplification event resulting in additional mitoD; doing so enables downstream events to be finer grain than Metabolism Phase events. A mitoD Repair event advances recovery processes; it maps to an incremental reduction in mitochondrial disruption and damage. (B) Experiments capable of challenging NAPQI zonation hypotheses must demonstrate four characteristics. (a) Components are concrete and biomimetic. (b) Virtual Mechanisms during execution are observable and independent of phenomena being generated. (c) Qualitative and quantitative similarity (or lack thereof) can be established between targeted and virtual phenomena. (d) The goal is to incrementally strengthen the claim that details of causal cascades in mice are strongly analogous [19] – quantitatively similar – to details of Mouse Analog's Causal Cascade within and across multiple levels. Source: (A) Based on Hinson [7] and Han et al. [18]. (B) Based on Bartha [19].

When the number of Mitochondrial Damage (mitoD) objects within a Hepatocyte exceeds the Death threshold value, a Cell Death trigger event occurs and the Hepatocyte stops metabolizing APAP. However, between a trigger event and actual Death, already generated NAPQI continues to react. Death maps to histologically identifiable necrosis. A trigger event and Death are separated by a Death Delay interval, which mimics the interval during which the necrotic process advances sufficiently to enable it to stain positive for necrosis. The duration of Death Delay is determined by a random draw from (6.8 to 10.6 hour); that range enabled achieving two VTs: (i) Some necrosis is evident at two hours and (ii) peak necrosis occurs at ~8 hours after dosing. The events in Figure 11.2A coupled with the features in Figure 11.1 enable achieving the four characteristics in Figure 11.2B.

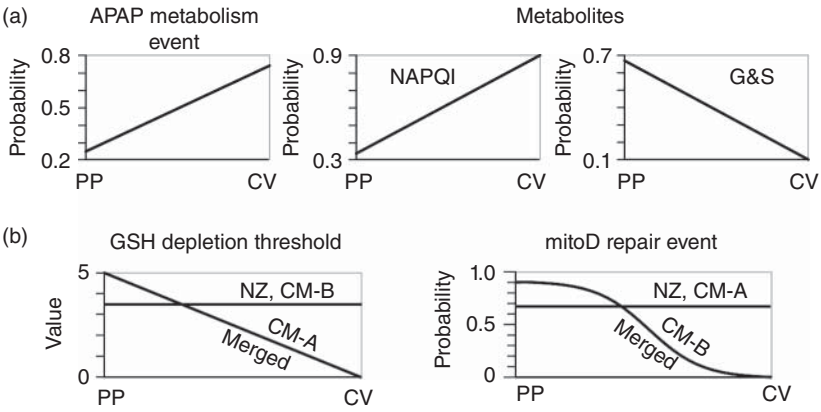

Figure 11.3 Three of four plausible Mechanisms falsified. (a) Only APAP metabolism and the type of Metabolite formed are location-dependent in NZ-Mechanism. Validation Target: necrosis first begins adjacent to CV and then moves (radially) outward toward PP entrance. (b) GSH Depletion Threshold and probability of mitoD Repair events are location-independent for NZ-Mechanism. However, one or both exhibit zonation (Section 11.3) for Competing Mechanisms A and B and Merged Mechanism.

11.2.2 Concrete Lobule Location-Dependent Mechanisms

NAPQI generation (Figure 11.3a) is Lobule location-dependent in all Mechanisms. Only the Figure 11.3a events are subject to zonation in NZ-Mechanism [20]. Each Hepatocyte uses the local value of a declining PP-to-CV gradient to specify its probability for a Metabolism event. The probability is 0.35 adjacent to PP. It increases progressively as distance from PP increases to a maximum of 0.95 adjacent to CV. The probability that Metabolite is NAPQI increases from 0.33 adjacent to PP to 0.9 adjacent to CV. Otherwise, with equal probability, the Metabolite is either G or S, which are represented together (Figure 11.2A). Those parameter values resulted in the largest amounts of NAPQI close to CV, while also enabling experimental results to achieve VTs.

For NZ-Mechanism and a given APAP dose, increasing (or decreasing) GSH Depletion and/or Death trigger threshold values, and/or probability of a mitoD repair event decreases (or increases) total Hepatocyte Death, but does not significantly alter Lobular locations of Hepatocyte Death. Zonation of GSH depletion and mitoD repair (Figure 11.3b) is what distinguishes the competing mechanistic hypothesis from the NZ-Mechanism.

Figure 11.4 shows the percent of Hepatocytes located in different regions relative to PP and CV. Note that Lobule does not have an actual mouse counterpart. Rather, it maps to a random sample of all PP-to-CV flow paths. Because of interconnections among periportal sinusoids, the number of hepatocytes encountered by sucrose moving PP-to-CV can be greater than the number of hepatocytes lining one side of the longest straight-through sinusoid.

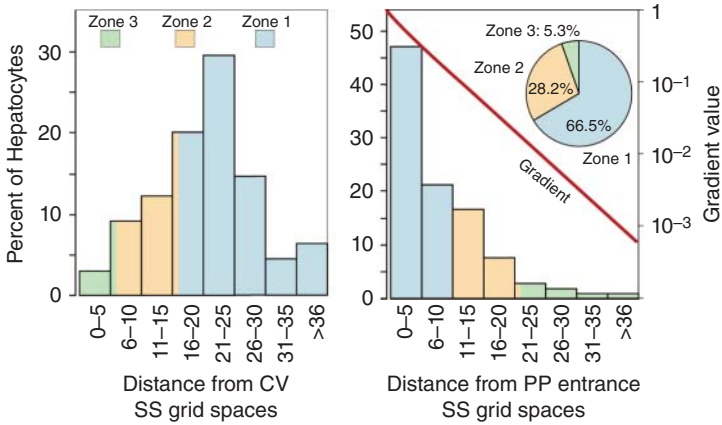

Figure 11.4 The relative locations of Hepatocytes are graphed in two different ways. Illustrated is the non-linear PP-to-CV gradient. It maps to measures of one or more common blood attributes, such as pO_2. The pie chart shows the percentage of Hepatocytes in each zone in Figure 11.1. Source: Based on Jungermann and Kietzmann [21].

11.2.3 Falsifying Virtual Mechanisms

For hypothesis testing, we focused on trigger events because, absent Inhibitor, each trigger event becomes a Death event. NZ-Mechanism is falsified because early measurements failed to fall within the Zone 3 validation range (Figure 11.5a). The average location of the earliest trigger events is in Zone 1. Later, the average location shifts toward CV, which is opposite to expectations: no such pattern has been reported. At about 10 minutes, the average location shifts again, this time in the expected direction toward PP. We see from Figure 11.3a that the maximum rate of NAPQI formation occurs adjacent to CV, so what is the explanation of that non-biomimetic pattern?

Due to the stochastic nature of events, some Hepatocytes at similar relative locations will be most "vulnerable" and will experience trigger events before their neighbors. For example, some Hepatocytes may have been randomly assigned a larger probability of metabolism and of producing NAPQI. Consider two Lobule regions at different distances from the CV. One region (R_{CV}) contains Hepatocytes closer to the CV, while the other region (R_{PP}) contains Hepatocytes closer to the PP. For NZ-Mechanism, the fraction of Hepatocytes experiencing an early trigger event will be larger in R_{CV}. However, the total number of Hepatocytes in R_{PP} will be larger (Figure 11.4). Consequently, the absolute number of early trigger events in R_{CV} and R_{PP} can be similar, or even larger in R_{PP}. Thus, relative to expectations, the average location of early trigger events (circled trend 1, Figure 11.5a) for the two regions will appear skewed toward R_{PP}. The remaining R_{PP} Hepatocytes will be less vulnerable, and so the average location of trigger events begins shifting

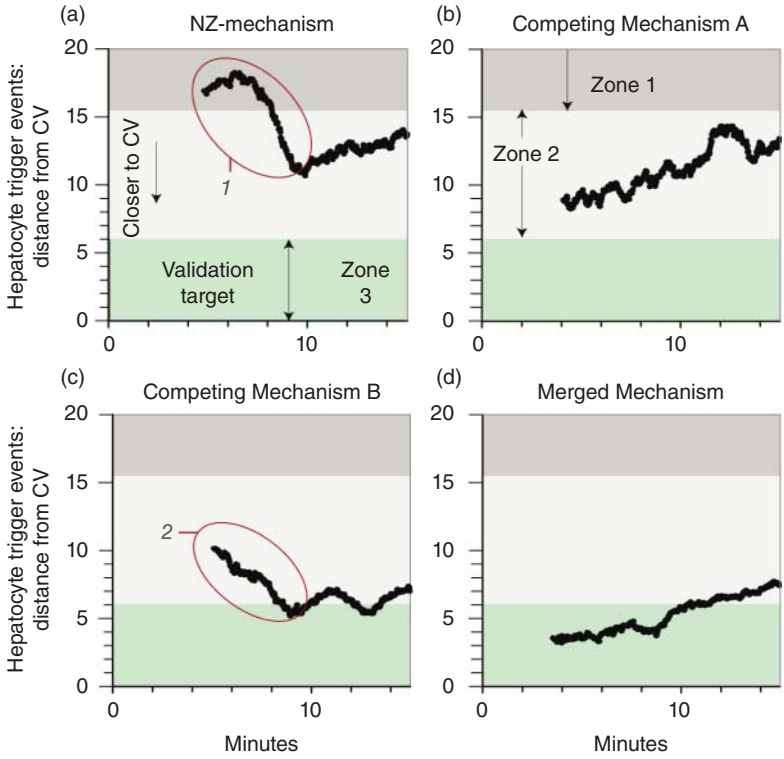

Figure 11.5 Shown are measurements from identical Mouse Analog experiments during which one of the four Mechanisms was implemented. Distances from CV (in SS grid spaces) of all Hepatocyte Death trigger events were recorded each time step. (a) NZ-Mechanism. (b) Results for Competing Mechanism A. (c) Results for Competing Mechanism B. (d) Results for Merged Mechanism. Values shown are 100-second moving averages to reduce the considerable variability within and between simulation steps. Only Merged Mechanism achieved the validation Target. Circled trends 1 and 2 help falsify Competing Mechanisms A and B.

toward R_{CV}. Concurrently, the fraction of Hepatocytes that are scheduled to Die is increasing significantly in R_{CV} but not R_{PP}, and that explains the direction change at around 10 minutes.

We posited that at least one additional feature must exhibit zonation, and conjectured that either one or both of the following might be sufficient. Competing Mechanism A specifies that GSH Depletion threshold values decrease PP-to-CV. Competing Mechanism B specifies that each Hepatocyte's ability to repair NAPQI-caused mitoD diminish sigmoidally PP-to-CV. We see from Figure 11.5b,c that both enhanced Mechanisms were falsified. Competing Mechanism A eliminated the early non-biomimetic NZ-Mechanism trend, but it is falsified

because the shift of early trigger events toward CV fell short of the validation range. Results for Competing Mechanism B are shifted considerably, but not sufficiently, toward the validation range and they exhibit a non-biomimetic trend, similar to NZ-Mechanism. Predecessors of Competing Mechanism B employed a parsimonious linear decrease in repair failed to shift trigger events sufficiently in the CV direction. We inferred that combining Competing Mechanisms A and B features into a Merged Mechanism might be sufficient to achieve the VT, and identified Merged Mechanism parameterizations that did so.

11.2.4 A Plausible Causal Cascade

To examine the multiplexed influences of zonation during Merged Mechanism execution, contents of each Hepatocyte were measured within three 5-grid-space-wide regions (Figure 11.6a). The value of a stochastic configuration determines the rate at which APAP and Extracellular Marker are transferred from the Dose input site to Mouse Body, (Figure 11.6b) mimicking IP or oral absorption. The function of Extracellular Marker is analogous to an internal standard. It is a verification marker: any unusual change following a software change alerts us to a possible unintended consequence of that change. It behaves the same as APAP except that it is excluded from Cells and it is not eliminated. The slow decline after about 80 minutes is a consequence of equilibrating within Lobular spaces. We used a quantitative Similarity Criterion to determine that the simulated APAP profile is sufficiently similar to a plasma level profile in mice to qualify as a "match."

To mimic hepatic blood flow, a parameter determines the fraction of APAP in Mouse Body that is transferred to PP each simulation cycle. G&S are transported out of Hepatocytes and, after exiting Lobule, are allowed to accumulate in Mouse Body. Having NAPQI in the CV region peak before doing so in the Midway region (Figure 11.6c) is a combined consequence of differences in APAP exposure, parameter zonation, and that Dead Hepatocytes stop Metabolizing APAP. APAP exiting Blood in the CV region partitions into fewer Hepatocytes than in the PP region, thus per Hepatocyte amounts are actually greater. Cell Death becomes measurable (Figure 11.6d) after being triggered. Regional patterns are similar to those in Figure 11.6c even though they are time-shifted. Mean amounts of G&S per Hepatocyte also reflect NAPQI patterns. Early mean GSH values adjacent to CV are much greater than adjacent to PP (Figure 11.6e), which may seem counterintuitive. Zonation of Metabolism is a factor, but more important is the relative number of Hepatocytes in different zones, with Zone 1 having more Hepatocytes than Zone 3 (Figure 11.4).

Cumulative GSH depletion events per Midway Hepatocyte continue accumulating after 20 minutes, whereas those adjacent to CV plateau (Figure 11.6f) because,

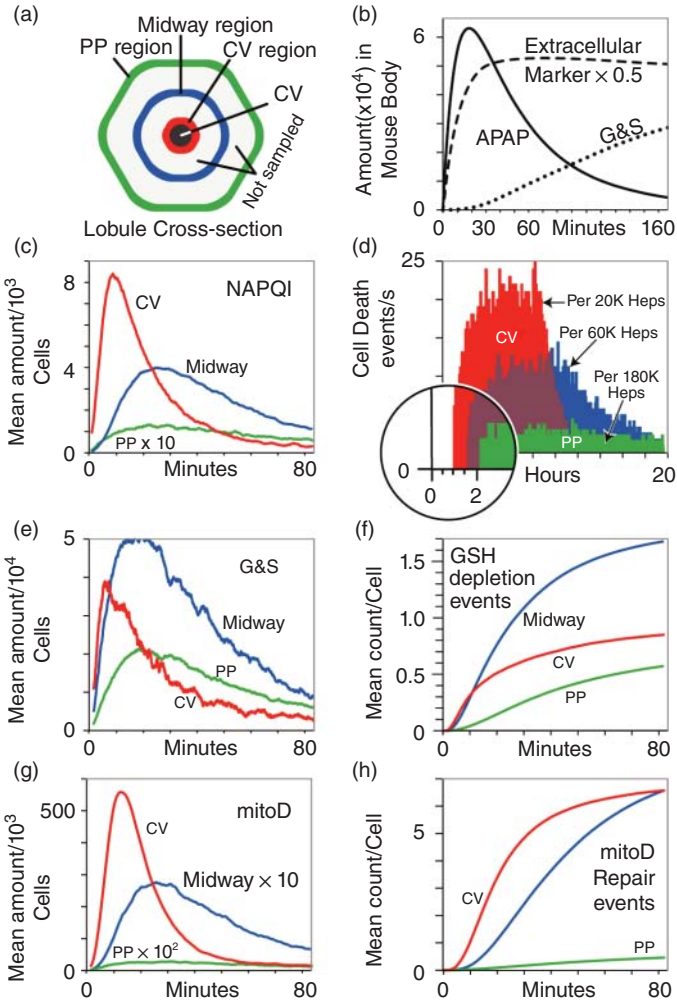

Figure 11.6 Cascading events within Lobules. (a) During an experiment that used Merged Mechanism, measurements were made within the three illustrated 5-grid-space-wide regions: PP region adjacent to PP entry; CV region adjacent to CV; and Midway region in between. The experiment used 332 Monte Carlo variants of the same Mouse Analog. (b) Amounts in Mouse Body. The APAP profile maps quantitatively to a blood level profile in a mouse. G&S are transported out of Hepatocytes and slowly accumulate. APAP Blood levels adjacent to PP are dramatically reduced as it distributes into the large number of accessible Hepatocytes. APAP in Blood close to CV partitions into far fewer Cells, so that per-Cell amounts adjacent to CV at early times is actually greater than that in Cells adjacent to PP. Data in (c) and (e–h) are 100-second moving averages from the experiment described in (a). (c) NAPQI profiles in each region. (d) Bar graphs of individual Cell Death events. Inset: earliest detectable Cell Deaths are seen one hour after APAP dosing; trigger events occur earlier. (e) Amounts of G&S in each region. (f) Cumulative mean GSH depletion events. (g) Mean amounts of mitoD; mitoD > 5 triggers Death. Significant mitoD accumulation begins only after GSH Depletion. (h) Cumulative mitoD Repair events.

by that time, Death has been triggered in most Hepatocytes adjacent to CV. Having peak mitoD values adjacent to CV occur early and be more than 10× those in Midway Hepatocytes (Figure 11.6g) proved necessary and essential to enable Hepatocyte Death to occur first near CV. The probability of a mitoD Repair event is smallest adjacent to CV, yet that is where the number of early Repair events is largest (Figure 11.6h). That is because mitoD amounts in those Hepatocytes at early times (Figure 11.6g) are more than 10× the amounts in Midway Hepatocytes. Although the probability of any one Repair Event is low, the cumulative number of such events can be larger than one might expect.

11.2.5 Drug Delivery and a Therapeutic Intervention

A goal is to expand Mouse Analog use cases to enable exploration of different DD scenarios. To demonstrate feasibility of doing so, we could demonstrate delivery of APAP using different techniques or demonstrate that a second compound can also be studied within the same virtual experiment. There is little practical interest in delivering APAP using novel strategies. So, we chose the latter: demonstrate that virtual experiments can be used to explore more effective pharmacological intervention scenarios.

The following is the targeted wet-lab observation. Dosing with c-JUN-N-terminal kinase (JNK) inhibitor SP600125 (which neither modulates GSH nor alters NAPQI production) one hour before a lethal dose of APAP, prevents death and dramatically reduces measured markers of liver injury thereafter [22]. Protection is significantly less when inhibitor is dosed two hours following APAP. By mimicking those observations, we demonstrate achieving Requirement 4. We prespecified two inhibition targeted attributes (TAs), but the similarity criterion (SC) was not prespecified. (i) The effectiveness of separately dosed Inhibitor objects (can map to SP600125) is significantly reduced (e.g. >25%) when dosed 2 hours as compared to 0.5 hours after the APAP dose. (ii) The reduction in Death Events caused by administering Inhibitor can be the same as that obtained a smaller APAP dose. There are three requisites to achieving those TAs. (i) Hepatocytes need an analog inhibition mechanism that operates at the same level of granularity as the events in Figure 11.2A. (ii) When the analog inhibition mechanism is deactivated, separately dosed Inhibitor objects do not interfere with Figure 11.2A processes. (iii) The disposition of Inhibitor is biomimetic. For this work, we simply specified that Inhibitor and APAP disposition be the same. We implemented the following coarse grain Inhibition Mechanism: if inhibition criterion INH is met, a scheduled Death event can be canceled. For each Hepatocyte, define INH = (Inhibitor count)/(mitoD count + 1). If a pseudo-random number draw from uniform [0.0, 1.0) ≤ INH, then delete the scheduled Death event. The trigger threshold is unchanged, so it can be triggered again. Results in Figure 11.7 demonstrate that the above two TAs were achieved.

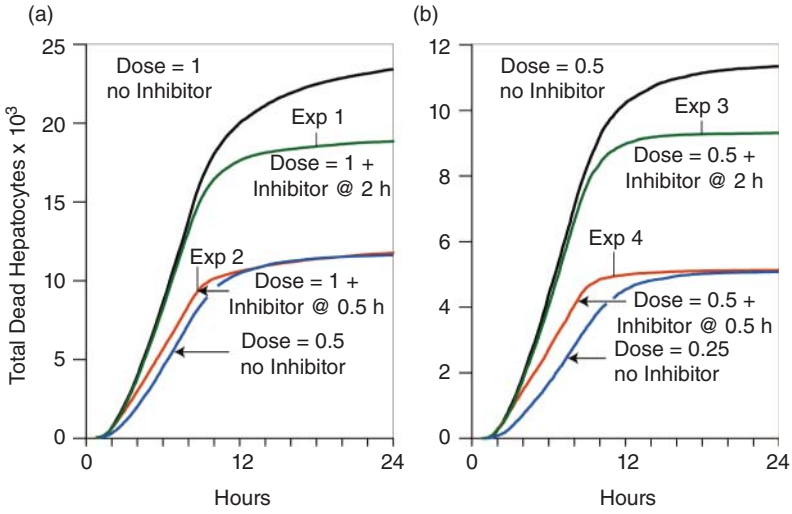

Figure 11.7 Inhibition of Hepatotoxicity. (a) Results are from four experiments in which an APAP dose is followed by a larger dose of Inhibitor. For simplicity, the disposition of APAP and Inhibitor in Mouse Body are the same. Experiment (Exp) 1: APAP dose is the same as in Figures 11.5 and 11.6 and the Inhibitor dose, administered two hours later, is twice as large. The same APAP dose without Inhibitor serves as reference. In Exp 2, both APAP and Inhibitor doses are the same as in Exp 1, except that the Inhibitor dose is administered after only 0.5 hours. A 50% smaller APAP dose without Inhibitor serves as control. (b) In Exps 3 and 4, all doses are reduced by 50%.

In separate work, unrelated to hepatotoxicity, Kim and coworkers [22, 23] demonstrated that DD features can even be individualized.

11.3 Methods

A use case is a statement, where a list of actions is implied, on how and why a Mouse Analog is used. The usage pattern for this chapter is performing virtual experiments to test PD, PK, and DD related hypotheses. We utilize virtual experiment concepts detailed recently [6, 24, 25]. Methods are driven by requirements, which are statements about concepts or tools needed to implement the usage patterns [2]. The sections that follow are organized starting with broad requirements and progressing to methods tailored to DD, PK, and PD use cases. Names of configuration features and parameters are italicized.

11.3.1 Broad Requirements

1. Components and spaces (Figure 11.1) are concrete and exist in a virtual space, which enables embodying knowledge within the Analog. Individual details

within the Analog are defined by experiment use cases to facilitate analogical reasoning [19, 26]. Components are modular, in schedule as well as state, to allow the following.

- Defining and annotating mappings between components and modules to their biological counterparts to make them explicit, intuitive, and easily understood.
- Making modules quasi-autonomous and thus more biomimetic [17, 27].
- Adapting components to represent different past and future experiment designs and protocols.
- Changing mechanism detail (granularity, resolution) to simulate additional attributes or experiment features.
- Scaling (translation) among differently configured systems [1, 17, 25] to represent transitions from in vitro to animal models, from one animal model to another, and from animal model to human cohorts.
- Reusing analogs and components to study new intervention scenarios under similar or different constraints or environmental influences.
- Versioning, where each component can evolve independent of other components.
- Building trust in validated Mouse Analogs

2. Coarse grain phenomena (from the perspective of biological organization) derive mostly from local component interactions at a finer grain, which enables distinguishing causes from effects. For this work, doing so is essential because it is likely that one or more hepatotoxicity phenomenon is a consequence rather than a direct contributor to causal events.
3. Modular components and spaces in Figure 11.1 can be assembled easily. Generating new knowledge requires generating many alternative, plausible, testable hypotheses, composed as a system of interacting components, for each function/structure, and then selecting against any that fail. By so doing:
   - It becomes increasingly easy to construct (plug together) and explore or test alternative mechanism-based hypotheses and intervention scenarios thereby generating new knowledge.
   - It facilitates comparing and contrasting predictions [17].
   - It enables improving mechanism-based explanations of hepatic injuries, and then extending those explanations to also account for injuries caused by other xenobiotics, co-morbidities, and individual variability [23, 28].
4. Different chemical entity objects, each mapping to a particular actual compound, exist (are concrete), and move within the Analog. Virtual experiments require that each quasi-autonomous component recognize those different objects and adjust the response appropriately.
5. Tools that enable completing three critical activities:
   - Explore and shrink spaces of competing mechanism-based hypotheses and alternative mechanism instantiations.

- Use quantitative cross-model validation methods to discover parsimonious options during an IR Protocol cycle.
- Discover testable hypotheses about how established wet-lab measurements at coarser biological levels (e.g. pathology necrosis score; serum markers of hepatic damage) might be linked mechanistically to changes in finer grain phenomena, such as molecular-level phenomena that contribute to APAP hepatotoxicity.

Meeting the above requirements is outside the scope [1, 25] of systems biology models currently in use to predict APAP hepatotoxicity [29]. To achieve these requirements, Mouse Analogs are written in Java, utilizing the MASON multi-agent simulation toolkit [30]. In silico experiments are run using virtual machines [31] on Google Compute Engine, running 64-bit Debian 2. For longer simulations, Monte Carlo (MC) trials are run in parallel.

11.3.2 Prediction

A prediction is a system behavior that is validated in the future. Each Mouse Analog execution generates predictions. However, Broad Requirements make clear that Mouse Analogs are primarily exploratory and explanatory devices. Thus, the focus of experiments is shifted away from precise prediction, for which continuous mathematics and/or statistical methods are unsurpassed. Instead the focus is shifted toward improving mechanistic explanations for how those features may be generated. Moreover, it is easy to add mechanism details that improve apparent realism (e.g. see Pogson et al. [32]). However, we strive to keep analog mechanisms parsimonious in order to retain scientific usefulness for mechanism falsification.

11.3.3 Iterative Refinement Protocol

The goal of stepping through the IR Protocol is to refine a formulated mechanism-based hypothesis by achieving VTs, which is accomplished when a *prespecified* SC is attained for a *prespecified* TA. A TA is typically a measured phenomenon, such as an actual PK profile. An SC can range from quantitative and stringent (e.g. mean predicted measurement is within 10% of wet-lab counterpart) to qualitative (e.g. necrosis occurs first in Zone 3).

A concrete mechanism can be falsified – proven inadequate for its VTs – in one of two ways. It cannot exhibit a TA, or we fail to discover configurations that enable achieving the latest VT, while still achieving earlier VTs. There are two IR Protocol requisites. First, have a set (larger sets strengthen all analogical arguments [19]) of prespecified TAs that characterizes the phenomena to be explained and rank-order them in terms of expected difficulty to achieve. Second, start with an analog that has already achieved at least one VT. IR Protocol stages are as follows.

1) Falsify the Mouse Analog that was just validated at step 6, and discover where, why, and when it was inadequate. To do so, select one of two strategies: (i) increase SC stringency for one TA (e.g. the SC at step 6 was that at least 50% of hepatocyte Deaths occur in Zone 3; increase SC to 75%). (ii) Add a new VT (e.g. no Hepatocyte Deaths within the first 60 minutes). Recovery from such a falsification improves credibility incrementally and shrinks the space of plausible, explanatory virtual mechanisms.
2) Specify a mechanism revision hypothesis; e.g. if we do *ABC*, then the altered Mouse Analog will achieve the new VT along with all previously achieved VTs. If necessary, specify changes to the mechanism's granularity, while adhering to a strong parsimony guideline. Making the updated mechanism too fine grained is analogous to over-parameterizing a mathematical model. Mechanism fine-graining can expand Mouse Analog behavior space and the space of configurations that enable achieving VTs beyond one's ability to efficiently manage. Adhering to a strong parsimony guideline helps avoid excessive fine-graining. It also helps separate causes from effects (Broad Requirement 2). A best practice is to take smaller steps that mostly fail. By doing so, we accumulate evidence for how and why the failure occurred, and that shrinks explanatory mechanism space.
3) Outline an Analog revision plan, which may include revising modules, components, use case(s), parameters, rules, and/or parameterization ranges. This step is the actual implementation of the virtual mechanism within the Analog.
4) Update SC and how Analog phenomena will be measured. Choice of SC is governed by the objective of the current IR Protocol cycle. When possible, SC are specified to reflect variability in wet-lab measurements, e.g. Mouse Analog values fall within ± 1 standard deviation of the corresponding wet-lab values. For time-course data, an additional SC specifies that a percentage (e.g. 80%) of in silico values that must fall within the prespecified range. When first applying a quantitative SC, we make it weak initially (e.g. measurements are within a factor of 2 of the target) and then at step 6, increase its stringency for the next IR Protocol cycle.
5) Conduct and evaluate many virtual experiments.
6) When the above revision fails, return to step 2. A failed mechanism revision provides new knowledge and shrinks plausible mechanism space for the next iteration of Mouse Analog. When successful, we have achieved a degree of validation and incrementally improved analogical credibility. It is not unusual for insights achieved or observations made during an IR Protocol cycle to alter opinions about TAs, SCs, and their priorities. Return to step 1.

11.3.4 Data Types, Reuse, and Sharing

Mouse Analogs are treated as a form of data, using both the implicit schema of Java, JavaScript, and R and the explicit schema of configuration settings. Mouse Analogs and configuration details are maintained, archived, and released using Subversion version control tool in two repositories, one private (Assembla) for rapid and prototyping development with project partners, another public (e.g. [33, 34]) for collaboration. Input–output (I/O) data is handled separately. Smaller data sets are stored in simple CSV. I/O data is tightly coupled to experiments and configuration versions, requiring a common versioning system, aggregating all three data types. Versioned I/O data is archived as downloadable packages.

The entire toolchain, including the operating system, used for Mouse Analogs, parameterization, and I/O handling are open-source, thereby ensuring repeatability. Similarly, all project-generated and released data is available to be licensed as open data. Mouse Analogs are built, maintained, and executed using a cloud environment (e.g. Google Compute Engine) to ensure platform and infrastructure repeatability across experiments, project team members, partners, and the wider community.

11.3.5 Quality Assurance and Control

Regression and unit tests are special cases of canonical use cases (e.g. a single pass Liver perfusion experiment). While use cases are instances of the class of experiments to which Mouse Analogs are being applied (e.g. hepatotoxicity research), they also provide the measures by which the software and methods are maintained. Each toolchain and Mouse Analog iteration can execute the canonical use cases so that current results can be compared to prior results for which credibility has been documented. Significant variations are documented, investigated, and explained. While the majority of variations are the result of model iterations, the process does catch artifacts introduced by code changes.

Unexpected variations in results first trigger a software verification process designed to test the toolchain from the bottom up: machine, OS, compiler, libraries, simulator, model, in order from generality, and widespread use. Absent unexpected variations, that same process is applied at least yearly. So doing is rigorous and avoids wasteful iterations that result from assuming that all variations are caused by the most specific layer. Anomalies at any layer below Mouse Analog are handled by methods specified by project team members. Should anomalies occur, they would trigger a source, data, parameter, and trace review in comparison with the design of experiments. Any unexpected variations that survive the verification process are then submitted to an IR Protocol based

falsification battery. Results satisfying canonical use cases, but yielding unexpected variation as a result of changes to Mouse Analog or toolchain, provide material that can be used to formulate a useful hypothesis.

11.3.6 Building Mouse Analog Credibility

11.3.6.1 Validation

Mouse Analogs are instantiated structural and behavioral hypotheses for mice (Figure 11.2B). As such, validation methods (success at step 6 of the IR Protocol) include both explanatory and predictive types, and are both qualitative and quantitative. Achieving VTs is the objective of each IR Protocol cycle, but IR is an ongoing process. To improve explanatory mechanism-based insight further, we must challenge Mouse Analog. If it fails the challenge, then some aspect of the instantiated hypothesis is false. We use a new IR Protocol cycle to overcome that failure. Thus, in advancing the science, validation is just one part of an ongoing two-part process. *Falsification* of a just-validated Mechanism (step 1) is the second essential part. At any iteration of the IR protocol, the Mouse Analog Mechanisms currently in use are those that have survived prior testing. The number and type of tests and/or falsification challenges a Mouse Analog has survived will establish its credibility. Making these validation–falsification cycles explicit, even when seemingly minor, improves credibility by providing a workflow record that insures that the work can be reproduced. It also provides a record of the engineering and biological reasoning used.

Quantitative tests consist of well-defined SC comparing Analog output with wet-lab data. Each Mouse Analog carries an inscribed variability from probabilistic configurations and MC sampling. Hence, surviving a quantitative test against wet-lab data requires two VTs for each pairing between an analog use case (e.g. mimic a wet-lab experiment) and the targeted wet-lab dataset (measurements of the particular target phenomenon):

VT1. The actual similarity being measured as a sample-space dependent, well-defined distance between measurements of wet-lab phenomenon and measurements of Mouse Analog's phenomenon; and

VT2. The extent to which Mouse Analog and wet-lab variations are comparable with the corresponding uncertainty.

Variation can be intra- and inter-individual, or within and across experiments. Where possible, components are alternately composed to achieve in vitro and in vivo VTs, thereby testing across two different use cases. Doing so provides an aspect-oriented validation method that, though behavior-based for each use case, facilitates multi-scale and structural validation (both qualitative and quantitative), and translation to application.

Qualitative tests consist of characteristic features of the wet-lab observations that can be generalized to a variety of wet-lab scenarios. Examples applied to all four Mechanisms include APAP metabolism and NAPQI production increases Portal Vein-to-Central Vein, and necrosis occurring first close to CV.

11.3.6.2 Verification

Because Mouse Analogs constitute concrete structural and mechanistic hypotheses, verification is limited mostly to mathematically well-defined sub-component requirements. Unit tests for those use cases are included side by side with the components in the repositories. Integrated verification is performed through the comparison of the expected against the measured systemic impact of a new or modified component.

11.3.7 Liver and Lobular Form and Function

Liver composition (Figure 11.1) is now stable and robust, having already achieved several VTs [3, 14–16, 34]. With each major improvement, we insure that those VTs continue to be achieved. Because rat and mouse lobule structures are similar, we designed Liver to be used in simulations of phenomena measured in rats as well as mice (Broad Requirement 1). We do so by changing analog-to-referent mapping functions [27] (e.g. the functional relationship between simulation cycles and real time is different for rats and mice). A Lobule maps to a very small random sample of all PP-to-CV flow paths, not to an idealized mouse or rat lobule. Actual lobules have interconnections between sinusoids. The number of these interconnections is greatest closer to PP; they have not been observed close to CV.

Earlier, we arrived at the Lobular composition in Figure 11.1 by incrementally achieving stringent quantitative SC for single pass rat liver perfusion profiles for eight compounds having very different physicochemical properties: APAP, atenolol, antipyrine, labetalol, diltiazem, propranolol, prazosin, and sucrose [14, 15]. A Cell-free analog of Space of Dissé was added, and earlier VTs reestablished. It was needed in part to accommodate larger doses and additional mobile objects, including G and S, which do not enter Cells. The following parsimonious Lobule configuration values enabled achieving multiple VTs for all compounds [3, 14–16, 34], and those specifications were fixed throughout this work. The three-zone interconnected graph network has 68 nodes, 45, 20, and 3 in Zones 1, 2, and 3, respectively. Nodes are connected using 94 edges: Zone 1-to-Zone 2 = 55; Zone 1-to-Zone 1 = 10; Zone 2-to-Zone 3 = 24; Zone 2-to-Zone 2 = 10; Zone 3-to-Zone 3 = 0. To represent both uncertainty and variability, edge connections between sinusoid segment (SS) are randomly assigned at the start of each MC Lobule execution.

One SS, which maps to aspects of tissue microarchitecture and function, is located at each node. SS sizes are MC determined. Each SS has a Core and concentric toroidal spaces. APAP and other mobile objects enter and exit an SS via Core and the Blood–Cell Interface, percolate through spaces influenced by analog flow (random walks biased toward CV), and, if not destroyed, eventually exit the CV. Having edges and SS sizes assigned pseudo-randomly at the start of each experiment simulates lobular variability within and between livers.

11.3.8 APAP Metabolism

Cell objects, absent the capabilities identified in Figure 11.2A, are identical to those described Petersen et al. [17, 24]. Within Endothelial Cell Space, the only event occurring within Cells mimics nonspecific binding of APAP. For this work, IR Protocol cycles focused on events occurring within Hepatocytes. This work uses four physiomimetic mechanism modules: *InductionHandler*, *EliminationHandler*, *MetabolismHandler*, and *BindingHandler*. The events and features illustrated in Figure 11.2A were added incrementally during IR stages.

The first refinement stage required arriving at an APAP metabolism configuration that would remain unchanged for all four Mechanisms. Within the literature, there is quantitative variability (within and between experiments) in zonal measurements of CYP2E1 (primarily responsible for formation of NAPQI) [35], the relative proportion of the three primary metabolites (glucuronide, sulfate, and NAPQI) [36], hepatic clearance, and hepatic extraction. However, there is qualitative agreement on key trends.

An APAP object maps to a tiny fraction of dose. For a particular experiment, there is a direct mapping between the single simulation cycle probability of an unbound APAP object being metabolized and amounts of metabolic enzymes [17, 24]. In mice, CYP2E1 levels per hepatocyte increase PP-to-CV. Reported fold changes range from 2 to >10. We specified this VT: probability of an APAP metabolic event generating NAPQI increase at least three-fold PP-to-CV. All other metabolites, which are nontoxic, are lumped together and called G&S (map mostly to APAP-glucuronide and APAP-sulfate). In most reports, the inactive metabolites (mostly the glucuronide and sulfate metabolites) are estimated to account for up to 85% of a dose, with NAPQI accounting for the balance. We specified that total NAPQI, as fraction of dose, be within 0.15–0.4. We specified that large range for convenience to insure that sufficient numbers of NAPQI are generated when dose is reduced. One of the above TAs is that toxicity be reduced by about 50% when the APAP dose is reduced by 50%.

This VT was the most demanding: APAP hepatic extraction ratio = 0.6, and for that we specified a stringent SC: 0.6 ± 0.06. To simplify achieving that VT, we used a virtual single pass Liver perfusion protocol with a constant rate of APAP input.

Once steady state was reached and APAP outflow values were within 34–46% of input values, the VT was reached. For convenience, we began the initial IR Protocol cycle by specifying that the hepatic clearance of APAP will be similar to that of prazosin, which is one of the compounds for which the Liver had already been validated [14, 15]. We then cycled through the IR Protocol seeking configuration changes that would enable achieving the three VTs. Those identified are illustrated in Figure 11.3a.

11.3.9 PP-to-CV Gradients

Lobules have a built-in PP-to-CV gradient [17], which maps to measures of one or more common blood attributes, such as pO_2 [21]. Each Hepatocyte can use its local gradient value to calculate values for its location-dependent configurations. We needed to explore multiple plausible gradients for several different events. Once these event-specific gradients have stabilized, they can be replaced by rules that use that built-in PP-to-CV gradient. Those rules, in turn, will be placeholders for yet to be discovered finer-grain mechanisms.

11.3.10 GSH Depletion

We started with the parsimonious operating guideline that, when specific damage products accumulate within a Liver above some threshold, then Hepatocyte Death would be irreversibly triggered. There is ample evidence that accumulation of APAP-induced damage products in mice occurs after available GSH has been sufficiently depleted. By analogy, we implemented a new event: each simulation cycle, with $p = 0.5$, each NAPQI object may be destroyed. We specified $p = 0.5$ arbitrarily because we had no wet-lab data to guide doing otherwise. NAPQI destruction maps to in vivo depletion of a fraction of hepatocyte's available GSH. Within Mouse Analog, a NAPQI destruction event is also a GSH depletion event. A small GSH Depletion threshold value maps to mice that are very sensitive to APAP hepatotoxicity; a larger GSH Depletion threshold maps to mice that are more resistant. The threshold value needed to be small enough to allow sufficient accumulation of Damage products (below), but large enough for toxicity to be reduced by about 50% when the APAP dose is reduced by 50%, which we imposed as a VT. Setting GSH Depletion threshold = 5 at PP decreasing to 0 at CV for Competing Mechanism A and Merged Mechanism proved adequate to enable elimination of circled trend 1 in Figure 11.5a.

In wet-lab studies, GSH is often measured in whole liver homogenates. To make Mechanisms 1 and 3 more directly comparable to Mechanisms 2 and 4 at the level of whole Lobule measurements, we specified that GSH Depletion threshold = 3.5 for NZ-Mechanism and Competing Mechanism B, which is the average value for all Hepatocytes using Competing Mechanism A and Merged Mechanism.

11.3.11 Damage Products

Each simulation cycle after the Depletion threshold is reached, with $p = 0.5$, each NAPQI object may be destroyed and replaced by a Damage product. The available evidence clearly implicates necrosis being triggered by mitochondrial damage. We parsimoniously specified that there be two classes of Damage product: a "mitochondrial damage product," called mitoD, and a "non-mitochondrial damage product," called nonMD. When a NAPQI object is destroyed, it is replaced with either nonMD or mitoD object selected randomly; we had no wet-lab data to guide specifying anything other than random.

11.3.12 Triggering Hepatocyte Death

We applied a simple, literature-derived working hypothesis. Upon accumulation of sufficient mitochondrial damage within hepatocyte mitochondria, a tipping point is reached and necrosis is triggered irreversibly.

In order for necrosis to be triggered, it is presumed to require reaction of possibly hundreds (or more) of NAPQI molecules. That number is a very tiny fraction, f, of the APAP dose. One analog NAPQI object maps to a very small fraction, f_A, of that same APAP dose. When Mouse Analog maps to a mouse that is very resistant to APAP hepatotoxicity (case 1), it is possible that $f > f_A$. When the referent mouse strain is more sensitive to APAP hepatotoxicity (case 2), it is likely that $f_A > f$. For case 2, one mitoD will be more than enough to trigger a Death event. For that case, one NAPQI => one mitoD is too coarse grain. We solved that problem by specifying that each mitoD be amplified to $(1 + n)$ mitoD. Explorations showed that specifying n be a random draw from either a uniform [1, 4] or Gaussian (mean = 4, standard deviation = 1) distribution proved sufficient to complete IR of the Mechanism and achieve the VTs. The mitoD amplification step is an example of making an analog mechanism locally more fine grain – increasing resolution [37] – without changing granularity elsewhere.

As with the GSH Depletion threshold, the Death Trigger threshold value needed to be small enough to allow sufficient accumulation of mitoD without a trigger event, but large enough for toxicity to be reduced by about 50% when the APAP dose is reduced by 50%. We imposed that feature as an additional VT. Setting Trigger threshold = 6 proved adequate.

11.3.13 Repair Events

Hepatocytes utilize multiple mechanisms to repair or reverse different types of damage, ranging from up-regulation of GSH to DNA repair to mitophagy. Consistent with our strong parsimony guideline, we started with a single analog

repair mechanism, which maps to a conflation of all actual repair/recovery mechanisms. Each simulation cycle, with $p = 0.5$, each nonMD and mitoD object may be destroyed. Again, lacking available wet-lab data, we specified $p = 0.5$ arbitrarily. For Competing Mechanism A, we made p(Repair event) independent of Lobule location because doing so is parsimonious.

Because hepatocytes closer to CV are known to experience increasing oxidative stress, it seemed reasonable to infer that repair mechanisms would be more robust closer to CV. However, when we increased p(mitoD Repair event) PP-to-CV, the NZ-Mechanism data in Figure 11.5a shifted further in the PP direction. To shift average location of Death trigger events in the CV direction, it was necessary to decrease p(mitoD Repair event) in the CV direction. Specifying a linear decrease from 0.9 at PP to 0 at CV, even when combined with a GSH Depletion threshold, failed to produce a sufficient shift. There were several options allowing sufficient shift improvement to achieve the VT. Each made the mechanism more complicated and finer grained. One option was to keep p Repair constant at (for example) 0.9 through Zone 2 and then have it decrease linearly to 0 at CV, but we conjectured that such a configuration risks being non-biomimetic. We opted for specifying that p(mitoD Repair event) for Competing Mechanism B and Merged Mechanism decreases PP-to-CV following a reverse sigmoid with the inflection centered approximately midway in Zone 2.

As with GSH Depletion threshold, to make NZ-Mechanisms and Competing Mechanism B more directly comparable to Competing Mechanism A and Merged Mechanism at the whole Lobule level, we determined that the average p value for all Hepatocytes using Competing Mechanism A and Merged Mechanism is 0.62. So, we specified that p(mitoD Repair event) for NZ-Mechanisms and Competing Mechanism B in Figure 11.3b increase from 0.5 to 0.62.

Once VTs were achieved, an essential next step (within an IR Protocol cycle) was to hypothesize about possible Analog-to-mouse mappings. Having p(mitoD Repair event) decreased sigmoidally PP-to-CV was essential for Merged Mechanism to validate. Can we suggest possible mouse counterparts? We could posit that normal mitochondrial repair processes exhibit little zonation. However, one or more of the processes that maintain necrosis-triggering pathways, is preferentially sensitive to NAPQI damage. As a consequence, the effectiveness of mitochondrial damage repair diminishes proportional to NAPQI, and that maps to p(mitoD Repair event) decreasing sigmoidally PP-to-CV in Mouse Analog.

11.3.14 Sensitivity Analyses and Uncertainty Quantification

Most Mouse Analog Mechanisms are inscribed with a probability distribution and executed according to MC sampling followed by aggregation of results. Simultaneous, small changes (e.g. 5–10%) in several configuration values can offset each

other and may produce no detectable change in measured events or an outcome. Thus, linear sensitivity studies are less informative and meaningful than complete location changes in Analog configuration space [4, 5]. A complication is that significant regions of Mouse Analog's configuration space are non-biomimetic. For example, having more SS in Zone 3 than in Zone 2, or having the probability of NAPQI formation in Zone 1 be greater than in Zone 3 are not biomimetic. Domain knowledge is used to select for analyses only in those regions that are known to be, or are plausibly, biomimetic. We used batch sampling of configuration values (as in [31]) to identify small subsets of configuration features (such as the values and their zonation in Figure 11.3b) that were most influential for particular AILI attributes.

No two Lobule simulations are the same because a combination of factors (e.g. MC variations in SS dimensions, graph composition, probabilistic events, networking of some events, and small numbers of objects) contributes to built-in uncertainty and causes measurements of some phenomena during a single execution to be very noisy. Consequently, experiments are comprised of 12 (Figure 11.5) to 332 (Figure 11.6) MC Lobule variants.

For each simulation, important event information, such as timing and location of Hepatocyte Death, are recorded along with a selection of other events influential in Hepatocyte Death patterns (e.g. zonation of GSH Depletion events). This record mimics possible experimental measurements and provides a sampling of the entire biomimetic mechanism space. The resulting information can be used to separate configuration space into some regions that have achieved validation and other regions that were falsified. Mappings between output variance, which is a consequence of inscribed stochasticity, and variance in wet-lab data provide a quantification of uncertainty.

11.3.15 Mouse Body

When we unplug Liver from Mouse Analog, we have Mouse Body. It contains a space (not to be confused with a PK compartment) that maps to all extra-hepatic tissues including blood along with a space to contain dose (can map to an IP injection site or the GI tract). For this work, no further Mouse Analog details were needed, but when needed, other objects can be added to Mouse Analog without influencing Liver. We prespecified two TAs. (i) APAP PK data in mice (from Fischer et al. [38]) for which we imposed a stringent SC: measurements of APAP in Mouse Body (maps to APAP concentrations in plasma) must be within one standard deviation of the wet-lab value. Results are presented in Figure 11.8a. (ii) Dose-dependent APAP PK data rats [39, 40]: plasma half-life (and the fraction of dose converted to NAPQI) increases with increasing APAP dose. Why rats? APAP PKs in mice and rats are somewhat similar, but rats are more resistant to APAP

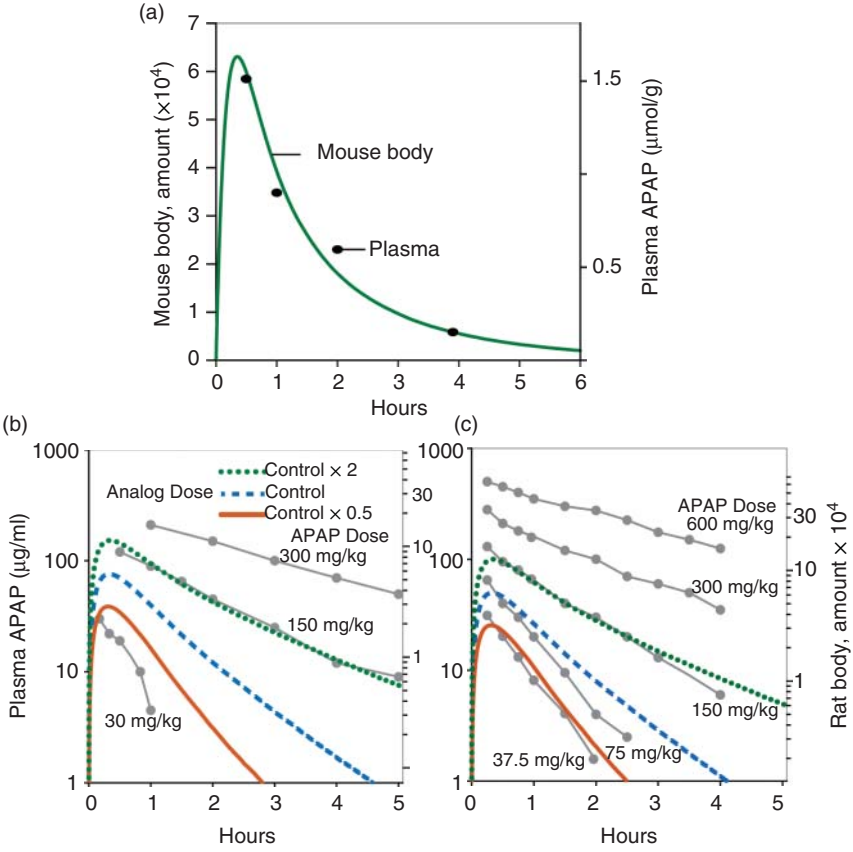

Figure 11.8 Targeted Attributes: pharmacokinetic similarities. (a) Shown are similarities between pharmacokinetic profiles in Mouse Body and in plasma from Swiss Webster mice administered 400 mg/kg APAP by oral intubation as reported by Fischer et al. [38]. The Analog to wet-lab data mapping [27] assumed a direct correlation between APAP in Mouse Body and APAP per gram in tissue samples, including plasma. We imposed a stringent Similarity Criterion (SC): measurements of APAP in Mouse Body (maps to APAP concentrations in plasma) must be within 1 standard deviation of the mouse data. The Mouse Analog and APAP dose were the same as in Figures 11.5 and 11.6. (b) We demonstrate reusing Mouse Analog as a Rat Analog. Unaltered Mouse Analog was used but the Targeted Attributes (TAs) were dose-dependent pharmacokinetic data from rats. We compared pharmacokinetic profiles in Mouse Body (right vertical axis in both (b) and (c)) to plasma profiles from Galinsky and Levy [39] (left vertical axis in both (b) and (c)). As in (a), the Analog to wet-lab data mapping assumes a direct correlation between APAP in Mouse Body and concentration of APAP in plasma. The qualitative SC was that dose-dependent changes in half-life in Mouse Analog be similar to those observed in rats. The Control dose (of APAP objects) was the same as in Figure 11.5. (c) The comparisons and SC were the same as in (b), except that the data are from Hjelle and Klaassen [40]. The Analog to wet-lab data mapping again assumed a direct correlation between APAP in Mouse Body and concentration of APAP in plasma. Source: (a) Based on Fischer et al. [38] and Hunt et al. [27]. (b) Based on Galinsky and Levy [39]. (c) Based on Hjelle and Klaassen [40].

hepatotoxicity. Our operating hypothesis was that if the same studies were done in mice, similar relative APAP PK profiles would be obtained. Results are presented in Figure 11.8b,c. The prespecified SC was that half-life in Mouse Analog increases with increasing APAP dose. Attaining VTs from different experiments in different species using the same Analog increases credibility.

Liver configurations from infusion experiments were carried forward and fixed while attaining the above two VTs. To achieve both, we adjusted values of two configuration settings. One controlled Absorption into Mouse Body and the other controlled metering of APAP from Mouse Body to Lobule PP. The latter maps to hepatic blood flow. We specified that Absorption into Mouse Body is first order and rapid. The resulting Mouse Body configurations were fixed for all experiments on all four Mechanisms.

11.3.16 Death Delay

Time course data for necrosis in mice is not available. Evidence from multiple sources indicates that necrosis is not detectable during the first hour following a toxic but non-lethal APAP dose, and further necrosis is not evident 12 hours after dosing. We used domain expert opinion as a TA placeholder for percent total necrosis following dosing in order to specify Death Delay. The prespecified SC was that mean Death events fall within the TA range.

11.4 Discussion

Most researchers seem to prefer descriptions of plausible explanatory mechanisms that are finer rather than coarser grain. Our simulations use relatively coarse grain model mechanisms because they are scientifically preferable and more informative. A validated coarse grain mechanism subsumes many different, yet equally plausible finer grain variants. When we falsify a coarse grain mechanism, we significantly shrink the space of equally plausible finer grain variants.

We expected Mouse Analog using NZ-Mechanism to show that simulated necrosis would occur first in first Zone 3. When we failed to find configurations that enable that outcome, we first suspected that the failure would be traced to some flaw in the software. We found none. A somewhat more complicated model mechanism would be needed. That failure generated new knowledge. Mouse Analog could not be made to do two things simultaneously: achieve the diverse set of quantitative and qualitative VTs, especially the PK TAs (Section 11.3) *and* cause Cell Death to occur first in Zone 3. A somewhat more complicated analog Mechanism was needed. We explored two Mechanism enhancements that we judged to be equally plausible and comparably parsimonious. We anticipate that others can be found. Making APAP metabolism a nonlinear function of distance from PP is one candidate. Experimenting on concrete biomimetic analogs, following

the IR Protocol (Section 11.3), provides the means to identify and challenge comparably parsimonious explanations of targeted phenomena. For questions posed, Mouse Analog's concreteness, coupled with the ability to observe and measure propagating causal events, make it easy for non-modeler domain experts to form opinions about credibility of similarities between virtual experiment results and real or envisioned wet-lab counterparts.

The immune system is known to influence the unfolding of APAP injury. However, adhering to our strong parsimony guideline, for the attributes targeted and the focus on early events, there is no need to represent immune system features. However, it is straightforward to add such features, when doing so is needed to achieve new TAs. Adding objects that map to Kupffer cells and circulating immune cells is straightforward.

The phenomenon that broke the NZ-Mechanism was that a few Hepatocytes in Zones 1 and 2 are vulnerable to an early Death trigger event (Figure 11.5). Closer to CV vulnerable Hepatocytes become the majority. Although that outcome falsified the tightly framed hypothesis (necrosis occurs first only adjacent to lobule's CV), can we rule out a mouse counterpart to NZ-Mechanism in which a small number of vulnerable hepatocytes actually exist in Zones 1 and 2? No. However, if deemed important, that phenomenon can be challenged directly using wet-lab experiments designed to identify hepatocytes distant from CV undergoing early necrosis. The results in Figure 11.5b,c also document the first use of virtual experiments to challenge the two competing mechanism-based hypotheses. The fact that both were falsified is another illustration of how virtual experiments shrink the space of plausible mechanism-based explanations for a targeted phenomenon.

Merged Mechanism during execution (Figure 11.6) is a dynamic hypothesis (in software) for how key features of APAP hepatotoxicity in mice are generated. It is clear from concurrent differences within the three regions (Figure 11.6c–h) that explanatory inferences drawn from molecular measurements made from whole liver homogenates or hepatic biopsies will at best be flawed and may be misleading. Fortunately, zonal differences in Analog measurements can guide design of wet-lab experiments intended to challenge particular Merged Mechanism features. The following are two examples of such features. (i) At 30 minutes post-dose, GSH depletion per mid-zonal hepatocyte is significantly greater than that in either pericentral or periportal hepatocytes. (ii) At 10 minutes post-dose, measures of mitochondrial damage in pericentral hepatocytes is an order of magnitude greater than that in mid-zonal hepatocytes. Experiments that challenge those predictions will be win–win: no matter the outcome, we will have useful new knowledge. Note that, absent the data in Figure 11.6, there would be no basis to undertake such narrowly focused experiments.

We argue that M&S methods capable of better explaining of DD, PK, and PD phenomena incrementally during all drug development stages should focus on

scientific usefulness [38], and that requires developing model types, such as Mouse Analog, which use model mechanisms to address DD, PK, and pharmacological questions simultaneously as well as independently. To that end, we propose six requirements that will enable model mechanisms to be scientifically useful [10]. They must be more than mere pedagogical or augmentative tools; *they must be an integral part of the scientific method*. During execution, following APAP Dosing, Mouse Analog is a biomimetic model mechanism. To be scientifically useful, such a model mechanism must be:

- *Falsifiable*. It is important to know when and how a model mechanism fails. When model mechanisms are falsified, we gain new knowledge by ruling out one or more competing explanations [41].
- *Suitable for experimentation*. One must be able to experiment on a model mechanism – to test hypotheses against it. So doing allows the scientific modeler to challenge existing hypotheses and/or generate new ones.
- *Use case specific*. Each model mechanism should be built for a particular use case. It need not be as broadly applicable as possible, and need not be meaningful outside of its particular use case.
- *Iteratively refined*. Explanatory model mechanisms should strive to be a perpetual work-in-progress. They are refined to overcome falsification efforts and/or to support new use cases. Just as refined wet-lab models increase phenotypic overlap between model and referent, refined biomimetic model mechanisms will expand their similarity to the referent system [1, 37, 42].
- *Concrete*. Model mechanisms need not be *physical* to be scientifically useful, but they must be concrete, in that they can be used to stand for particular referents for particular use cases. Concreteness is facilitated when mechanism components map to real-world biological counterparts. In contrast, a less concrete mechanistic model may simply relate model variable values to referent properties.
- *Biomimetic*. Scientifically useful biomimetic model mechanisms should *mimic* (be strongly analogous to) their referent system in meaningful ways, and they should strive to strengthen multi-attribute similarities. When a goal is increasing explanatory knowledge, computational models should have concrete mechanisms that mimic hypothesized referent mechanisms to the extent feasible. Simply generating output that matches referent measurements is inadequate.

Most of the requirements listed above are highly interconnected, if not redundant. For example, concreteness is a requisite to falsifiability; hypotheses are falsifiable by definition; experiments are always use case specific. Nevertheless, the requirements fit a central theme: scientifically useful model mechanisms must be flexible experimental devices that mimic particular aspects of the referent system.

References

1 Hunt, C.A., Ropella, G.E., Lam, T.N. et al. (2009). At the biological modeling and simulation frontier. *Pharm. Res.* 26: 2369–2400.

2 Hunt, C.A., Kennedy, R.C., Kim, S.H., and Ropella, G.E. (2013). Agent-based modeling: a systematic assessment of use cases and requirements for enhancing pharmaceutical research and development productivity. *Wiley Interdiscip. Rev. Syst. Biol. Med.* 5: 461–480.

3 Ropella, G.E., Kennedy, R.C., and Hunt, C.A. (2012). Falsifying an enzyme induction mechanism within a validated, multiscale liver model. *Int. J. Agent. Technol. Syst.* 4: 1–14.

4 Smith, A.K., Ropella, G.E., Kaplowitz, N. et al. (2014). Mechanistic agent-based damage and repair models as hypotheses for patterns of necrosis caused by drug induced liver injury. In: *Proceedings of the 2014 Summer Computer Simulation Multiconference*, Monterey, CA (7–11 July 2014), 112–120. San Diego, CA: Society for Computer Simulation International.

5 Smith, A.K., Ropella, G.E., Kaplowitz, N. et al. (2016). Virtual experiments help explain intra- and inter-strain variability of AILI-induced hepatic necrosis in mice. In: *Proceedings of the 2016 Spring Computer Simulation Multiconference*, Pasadena, CA (3–6 April 2016), 757–763. San Diego, CA: Society for Computer Simulation International.

6 Smith, A.K., Petersen, B.K., Ropella, G.E.P. et al. (2016). Competing mechanistic hypotheses of acetaminophen-induced hepatotoxicity challenged by virtual experiments. *PLoS Comput. Biol.* https://doi.org/10.1371/journal.pcbi.1005253.

7 Hinson, J.A. (2013). Mechanisms of acetaminophen-induced liver disease. In: *Drug-Induced Liver Disease* (eds. N. Kaplowitz and L.D. DeLeve), 305–329. San Diego, CA: Elsevier.

8 Jaeschke, H., Xie, Y., and McGill, M.R. (2014). Acetaminophen-induced liver injury: from animal models to humans. *J. Clin. Transl. Hepatol.* 2: 153–161.

9 Jaeschke, H., McGill, M.R., and Ramachandran, A. (2012). Oxidant stress, mitochondria, and cell death mechanisms in drug-induced liver injury: lessons learned from acetaminophen hepatotoxicity. *Drug Metab. Rev.* 44: 88–106.

10 Hunt, C.A., Erdemir, A., Lytton, W.W. et al. (2018). The spectrum of mechanism-oriented models and methods for explanations of biological phenomena. *Processes* 6: 56.

11 Mitchell, J.R., Jollow, D.J., Potter, W.Z. et al. (1973). Acetaminophen-induced hepatic necrosis. I. Role of drug metabolism. *J. Pharmacol. Exp. Therap.* 187: 185–194.

12 Roberts, D.W., Bucci, T.J., Benson, R.W. et al. (1991). Immunohistochemical localization and quantification of the 3-(cystein-*S*-yl)-acetaminophen protein adduct in acetaminophen hepatotoxicity. *Am. J. Pathol.* 138: 359–371.

13 Ni, H.M., William, J.A., Jaeschke, H., and Ding, W.X. (2013). Zonated induction of autophagy and mitochondrial spheroids limits acetaminophen-induced necrosis in the liver. *Redox Biol.* 1: 427–432.

14 Yan, L., Sheihk-Bahaei, S., Park, S. et al. (2008). Predictions of hepatic disposition properties using a mechanistically realistic, physiologically based model. *Drug Metab. Dispos.* 36: 759–768.

15 Yan, L., Ropella, G.E., Park, S. et al. (2008). Modeling and simulation of hepatic drug disposition using a physiologically based, multi-agent in silico liver. *Pharm. Res.* 25: 1023–1036.

16 Park, S., Ropella, G.E.P., Kim, S.H. et al. (2009). Computational strategies unravel and trace how liver disease changes hepatic drug disposition. *J. Pharmacol. Exp. Therap.* 328: 294–305.

17 Petersen, B.K., Ropella, G.E., and Hunt, C.A. (2014). Toward modular biological models: defining analog modules based on referent physiological mechanisms. *BMC Syst. Biol.* 8: 95–112.

18 Han, D., Dara, L., Win, S. et al. (2013). Regulation of drug-induced liver injury by signal transduction pathways: critical role of mitochondria. *Trends Pharmacol. Sci.* 34: 243–253.

19 Bartha, P. (2013). Analogy and analogical reasoning. In: *The Stanford Encyclopedia of Philosophy* (Fall 2013 Edition) (ed. E.N. Zalta). http://plato.stanford.edu/archives/fall2013/entries/reasoning-analogy/.

20 Gebhardt, R. and Matz-Soja, M. (2014). Liver zonation: novel aspects of its regulation and its impact on homeostasis. *World J. Gastroenterol.* 20: 8491–8504.

21 Jungermann, K. and Kietzmann, T. (2000). Oxygen: modulator of metabolic zonation and disease of the liver. *Hepatology* 31: 255–260.

22 Hanawa, N., Shinohara, M., Saberi, B. et al. (2008). Role of JNK translocation to mitochondria leading to inhibition of mitochondria bioenergetics in acetaminophen-induced liver injury. *J. Biol. Chem.* 283: 13565–13577.

23 Kim, S.H., Jackson, A.J., Hur, R., and Hunt, C.A. (2012). Individualized, discrete event, simulations provide insight into inter-and intra-subject variability of extended-release, drug products. *Theor. Biol. Med. Model.* 9 (1): 1.

24 Petersen, B.K., Ropella, G.E., and Hunt, C.A. (2016). Virtual experiments enable exploring and challenging explanatory mechanisms of immune-mediated P450 down-regulation. *PLoS One* 11: e0155855.

25 Petersen, B.K. and Hunt, C.A. (2016). Developing a vision for executing scientifically useful virtual biomedical experiments. In: *Proceedings of the 2016 Spring Simulation Multi-Conference*, Pasadena, CA (3–6 April 2016), 697–706. San Diego, CA: Society for Computer Simulation International.

26 Frigg, R. and Hartmann, S. (2012). Models in sciencec. In: *The Stanford Encyclopedia of Philosophy* (Fall 2012 Edition) (ed. E.N. Zalta). Available in: https://plato.stanford.edu/archives/spr2020/entries/models-science/.

27 Hunt, C.A., Ropella, G.E., Lam, T.N., and Gewitz, A.D. (2011). Relational grounding facilitates development of scientifically useful multiscale models. *Theor. Biol. Med. Model.* 8: 35–66.

28 Kim, S.H., Jackson, A.J., and Hunt, C.A. (2014). In silico, experimental, mechanistic model for extended-release felodipine disposition exhibiting complex absorption and a highly variable food interaction. *PLoS One* 9: e108392.

29 Bhattacharya, S., Shoda, L.K., Zhang, Q. et al. (2012). Modeling drug-and chemical-induced hepatotoxicity with systems biology approaches. *Front. Physiol.* 3: 462.

30 Luke, S., Cioffi-Revilla, C., Panait, L. et al. (2005). MASON: a multiagent simulation environment. *Simulation* 81 (7): 517–527.

31 Ropella, G.E.P. and Hunt, C.A. (2010). Cloud computing and validation of expandable In silico livers. *BMC Syst. Biol.* 4: 178.

32 Pogson, M., Smallwood, R., Qwarnstrom, E., and Holcombe, M. (2006). Formal agent-based modelling of intracellular chemical interactions. *Biosystems* 85: 37–45.

33 simTK.org Acetaminophen induced liver injury. https://simtk.org/projects/isl/ (accessed 17 December 2020).

34 Park, S., Kim, S.H.J., Ropella, G.E.P. et al. (2010). Tracing multiscale mechanisms of drug disposition in normal and diseased livers. *J. Pharmacol. Exp. Ther.* 334 (1): 124–136.

35 Anundi, I., Lähteenmäki, T., Rundgren, M. et al. (1993). Zonation of acetaminophen metabolism and cytochrome P450 2E1-mediated toxicity studied in isolated periportal and perivenous hepatocytes. *Biochem. Pharmacol.* 45: 1251–1259.

36 Godoy, P., Hewitt, N.J., Albrecht, U. et al. (2013). Recent advances in 2D and 3D in vitro systems using primary hepatocytes, alternative hepatocyte sources and non-parenchymal liver cells and their use in investigating mechanisms of hepatotoxicity, cell signaling and ADME. *Arch. Toxicol.* 87: 1315–1530.

37 Kirschner, D.E., Hunt, C.A., Marino, S. et al. (2014). Tuneable resolution as a systems biology approach for multi-scale, multi-compartment computational models. *Wiley Interdiscip. Rev. Syst. Biol. Med.* 6: 289–309.

38 Fischer, L.J., Green, M.D., and Harman, A.W. (1981). Levels of acetaminophen and its metabolites in mouse tissues after a toxic dose. *J. Pharmacol. Exp. Ther.* 219: 281–286.

39 Galinsky, R.E. and Levy, G.E. (1981). Dose-and time-dependent elimination of acetaminophen in rats: pharmacokinetic implications of cosubstrate depletion. *J. Pharmacol. Exp. Ther.* 219: 14–20.

40 Hjelle, J.J. and Klaassen, C.D. (1984). Glucuronidation and biliary excretion of acetaminophen in rats. *J. Pharmacol. Exp. Ther.* 228: 407–413.

41 Wimsat, W.C. (1987). False models as means to truer theories. In: *Neutral Models in Biology*, vol. 31 (eds. M.H. Nitecki and A. Hoffman), 23–55. Oxford University Press.

42 Weisberg, M. (2012). *Simulation and Similarity: Using Models to Understand the World*. Oxford University Press.

12

Personalized Medicine: Drug Delivery and Pharmacokinetics

Melanie A. Felmlee and Xiaoling Li

Department of Pharmaceutics & Medicinal Chemistry, Thomas J Long School of Pharmacy, University of the Pacific, Stockton, CA, USA

12.1 Personalized Medicine

Personalized medicine refers to all aspects of individualization of patient health care from disease prevention to diagnosis, intervention/therapy, and rehabilitation. Drug therapy is one of the important means in therapeutic treatments of diseases for patients. Individualized or personalized drug therapy can be divided into selecting or matching the medications and adjusting or tailoring the dose regimen for a specific patient based on physiology, pathological conditions, and molecular characteristics such as an individual's genetic profile, mRNA, or protein levels (Figure 12.1). With the advancement of science and technology, individualized drug therapy has become possible and is increasingly being implemented in patient care. Ideally, individualized drug therapy would result in improved therapeutic outcomes and circumvent adverse side effects. However, one of the major issues with current therapies is the drastic inefficiency of drugs with a large percentage of treated patients failing to respond to drug therapy [1]. This lack of response is seen across therapeutic areas [2, 3] and can be explained, at least in part, by patient variability in pharmacokinetics and pharmacodynamics. Pharmacokinetic variability results from individual differences in drug absorption, distribution, metabolism, and elimination (ADME) leading to variable drug exposure and effect. In contrast, pharmacodynamic variability results from differences in drug target interactions in the absence of individual differences in pharmacokinetics. The current "one size fits all" drug therapy approach to treat patients, where all patients receive the same drug and dose, does not account for the underlying differences between patients that contribute to drug response. Individual patients may have a beneficial response, or derive

Drug Delivery Approaches: Perspectives from Pharmacokinetics and Pharmacodynamics,
First Edition. Edited by Bret Berner, Toufigh Gordi, Heather A. E. Benson, and Michael S. Roberts.

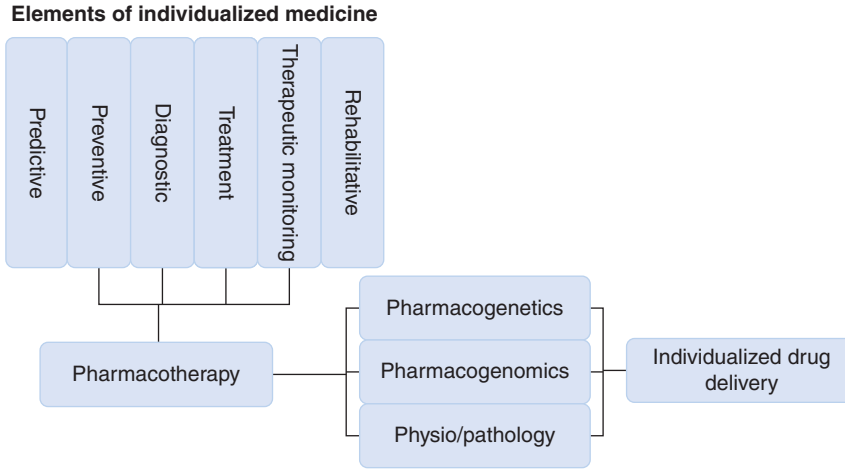

Figure 12.1 Pharmacotherapy and individualized drug therapy in the context of personalized medicine.

no benefit from drug therapy; individuals may also have a toxic response with or without the desired therapeutic benefits. Personalized medicine, also referred to as personalized molecular medicine, precision medicine, or stratified medicine, is an evolution of our therapeutic approach, where drug therapy elements and drug delivery are tailored to individual patients based on their diagnosis, individual biology, physiology, and disease pathology. Therefore, patient profiling should ideally occur prior to initiation of therapy. While personalized medicine in drug therapy has become synonymous with pharmacogenomics, i.e. the contribution of a patients' genetic make-up and global gene expression to drug response, a patients' environment and lifestyle should also be taken into account. The Food and Drug Administration (FDA), academia, and the US government have further expanded the concept of personalized medicine to include medical imaging, mobile phone health care applications, and direct to consumer genetic testing [1]. All of this information can provide clinicians with a greater understanding of the complex mechanisms governing a patient's drug exposure and response to aid in the development of an optimal individualized therapeutic regime.

The goal of personalized drug therapy is to identify which patients will most likely benefit from specific therapies, while eliminating therapies that would not be beneficial or modifying therapies that may result in toxicity prior to the initiation of drug therapy [4]. To accomplish this goal, there must be an established correlation between a molecular characteristic and a quantifiable physiological or pathophysiological process involved in drug disposition, drug effect, or disease progression [5]. These specific molecular phenotypes are referred to as clinical

biomarkers, and provide the underlying framework for personalized medicine and drug therapy. Patient-specific clinical biomarkers related to drug disposition or effect can then be utilized by physicians and pharmacists to design individualized therapeutic regimes through the selection of an appropriate targeted therapy or modification of dose, dosing interval, or drug release profile, thus personalizing drug therapy. Companion diagnostics are required to quantify specific clinical biomarkers and identify patient populations that would benefit from targeted therapy or require dose modifications [5]. Incorporation of these diagnostics into patient care can influence clinical decision-making and the delivery of personalized drug therapy, such as the measurement of Herceptin 2 (Her2) receptors to identify patients that would respond to anti-Her2 antibody therapy [5], or the use of CYP2D6 genotype to modify opioid dosage [6]. For personalized medicine to move forward, identification of relevant clinical biomarkers and quantitative diagnostic tests to identify patient subpopulations must be developed [7]. In 2015, the FDA approved 13 novel drugs that were classified as personalized medicine as their label contained information about a specific clinical biomarker and diagnostic tool to guide individualization of drug therapy [8]. Clinical biomarkers, diagnostics, and physiological information must be combined with the development of novel drug delivery approaches that allow for flexible dosage forms, release profiles, or targeted delivery to individualize drug therapy of novel drug molecules and previously existing therapies.

12.2 Drug Delivery in Personalized Medicine

Personalized drug delivery is not a new concept. The delivery principle has been evolving from selection of the optimal route of administration and adjustment of dose based on the patient disease state and physiological or pathological conditions to the contemporary individualized drug delivery based on a patient's molecular characteristics.

Early personalized drug delivery was carried out by pharmacists using the extemporaneous compounding approach or selecting a proper product for the disease state or patient characteristics (e.g. age or ability to voluntarily swallow). Pharmacists can alter the route of administration according to the patient's disease conditions or age. For example, a pharmacist may select or convert an existing product to a suppository to deliver drug to patients who have difficulty in swallowing or are unwilling to swallow. In addition to using different dosage forms to deliver medication based on the patient's disease conditions, the amount of drug delivered can also be individualized based on the patient's age, body weight, and metabolism phenotype. These early practices were limited to apparent disease state and patients' age or body weight. In contrast, modern

individualized drug delivery has a molecular basis. Targeted drug delivery can be achieved based on differential expression of molecular targets. Drug can be delivered to the intended target with a specific molecular marker in an individual patient, such as an over-expressed protein on the surface of cancer cells. The individualization of drug delivery can also be achieved by using pharmacokinetic and pharmacodynamic models that are built based on the patients' genetic profile, physiology, and pathophysiology to deliver a specific dose, and delivery mode tailored to the patients' disease condition.

Innovative drug delivery approaches are necessary for the implementation of personalized therapeutic strategies. Personalized drug therapy requires flexibility of dosing and release profiles, as well as targeted delivery to meet an individual patient's needs. Personalized drug delivery approaches do not involve chemical modification of the parent drug, but are comprised of solubilization, permeability enhancement, and modified release products [9]. Generation of a prodrug, a chemically modified form of the parent drug, does not fall under the umbrella of personalized drug therapy. Targeted delivery, may involve chemical modification, and functions to target the therapeutic agent to a specific location while minimizing exposure to off-target sites [9]. These approaches do not change the pharmacodynamic properties of the drug, but can alter the pharmacokinetic profile of a drug, which is the driving factor for drug effect.

Conventional oral dosage forms offer minimal flexibility and are not conducive to the range of dose levels that are required for personalized drug therapy to be successful. Intravenous dosing has more flexibility for individualization of doses, but there may be limitations based on the available dosing vials. The greatest potential for moving toward personalized medicine and drug therapy is for the development of dosage forms that allow for individualization of dose, release profile, or targeting to specific characteristics of the patients disease pathology. There are a number of reviews that discuss individualization of drug formulations and delivery approaches in detail, which will not be covered in this chapter [10–14]. This chapter will be focused on the novel approaches that are in development as well as the associated challenges.

12.2.1 Delivery Approaches to Alter Dose

The implementation of personalized medicine requires flexibility in drug doses that is not currently available in our "one size fits all" approach to drug therapy. Patient differences in drug ADME may require alterations in dose to achieve the same plasma concentrations or systemic drug exposure. For example, genetic variability in drug metabolizing enzymes affects their enzyme activity (extensive versus poor metabolizers), and therefore the clearance of substrates, leading to alterations in the concentration–time profile [15]. Dose adjustments can be utilized to account for the differences in enzyme activity, such as the lower dose

of 6-mercaptopurine in patients with reduced activity of thiopurine methyltransferase [16]. Dosage forms that are adaptable for individualized dosing are needed to ensure individual patients receive a safe and efficacious dose [11]. In addition, dosage forms should be suitable for the entire patient population, from children to the elderly [10, 17]. Very few examples of individual dosing have reached the market, with the best example being insulin dosage pens or pumps for the treatment of diabetes [11].

Wening and Breitkreutz proposed a general classification system for oral dosage forms and approaches that allowed for an individualized dosing regimen [11]. The authors separated the approaches into two categories that encompass both solid and liquid dosage forms: (i) dosing by accumulation, where several small carriers are combined to obtain the total dose and (ii) dosing by partition, where a larger drug carrier is subdivided to obtain the desired dose. Dosing by accumulation involves powder, pellets, granules, or mini-tablets that can be dispensed in individual dosages through the use of a dosing spoon or counting device. In contrast, dosing by partition involves scored tablets, oral films, or drug-loaded rods that can be cut using various approaches, or a liquid dosage forms with a dispensing device [11].

Multiparticulate dosage forms, such as powder, pellets, granules, or mini-tablets, can be utilized to individualize dosage by selecting a defined number or volume of the drug loaded particles [11, 12]. Volumetric dosing requires a device to dispense the correct amount of the formulation, such as a dosing spoon or pellet dispenser [11]. There are still constraints on the dosing flexibility with the volumetric approach, as it is dependent on a device. In addition, there is the potential for dosing errors, if the correct volume is not administered. Mini-tablets, defined as tablets with a diameter less than 3 mm, do not require volumetric dosing, but can be counted as subunits of the total dose. For individualize therapy with mini-tablets, dosing devices may be required to dispense the required number of tablets, ideally with the patients being able to dispense the correct number of mini-tablets with one actuation [12]. A number of mini-tablet dispensing devices have been described in the literature [11, 12, 18]. In addition to individualization of dosage, mini-tablets have the potential to be formulated as modified release dosage forms expanding their application in personalized medicine. These dosage forms are suitable for a wide age range allowing for personalized drug therapy, inclusive of pediatric, and geriatric populations that may have problems swallowing conventional oral dosage forms.

Dose flexibility could also be achieved by partitioning from a larger solid tablet. Traditional tablet formulations do not permit individualized dosing, as breaking the tablets may interfere with a functional coating or modified release. Scored tablets permit the tablet to be split in half or quarters which provides limited flexibility in dosage. However, there is often inaccuracy in splitting, leading to

variability in drug content between the segments [19]. Tablet-splitting devices reduce the risk of dose variability compared to breaking tablets by hand, but there can still be up to 10% variability in drug content [20]. Innovative tablet geometries or the use of drug-free compartments could be utilized to improve the accuracy of dosing [11, 19]. Solid dosage pens containing a drug-loaded rod have been proposed as a method to individualize dose. A cutting mechanism is contained within the device and cuts off predefined lengths of the drug-loaded rod [21]. These devices provide the dosing flexibility necessary for personalized drug therapy, and allow for tailoring of drug release [22]; however, the costs associated with the delivery device may be prohibitively high [11]. Oral film formulations utilizing printing technology are an emerging technology that has great potential for dose flexibility. Fixed dose oral film formulations of a number of drugs are currently on the market; individualized doses could be achieved by custom printing at the point of care enabling tailor-made drug therapies [13].

12.2.2 Delivery Approaches That Alter Pharmacokinetic Parameters

In drug development, pharmacokinetic parameters are optimized to maximize therapeutic efficacy and minimize side effects and toxicity. Typical pharmacokinetic parameters evaluated include maximum plasma concentration (C_{max}), time to reach C_{max} (T_{max}), half-life ($t_{1/2}$), and area under concentration–time curve (AUC). These parameters are dependent on the ADME properties of the drug, which is patient specific, and can be modified utilizing drug delivery approaches. In some cases, these approaches are not considered personalized medicine, as they are improving drug pharmacokinetics through formulations that will be administered to the whole population, and are not designed based on differences between individuals. One example of this would be liposomal drug formulations aimed at increasing drug half-life by decreasing clearance, such as vincristine sulfate liposomes [9]. However, as the need for individualized drug delivery rises in the evolution of personalized medicine, optimization of pharmacokinetic parameters for a specific patient could be an effective means for individualized drug delivery.

Individual variability in intestinal motility and gastric and intestinal pH leads to alterations in drug release profiles and subsequently pharmacokinetic parameters. Modification of drug release profiles is an approach that can be customized to personalize therapies based on differences in patient or disease state physiology. Several printing approaches have been proposed to formulate tablets or filaments with flexible release profiles using 3D printing technology [23, 24]. Drug-containing polymers can be printed into different shapes allowing for fully customizable tablets with any desired release profile; however, the cost of 3D printing needs to decrease for wide-spread utilization of this technology [23].

Further, for this technology to be implemented clinically, an understanding of the individual patient's intestinal physiology is required to personalize drug release profiles and optimize pharmacokinetic parameters. The Intellicap® device is a swallowable electronic oral delivery device that contains a wireless microprocessor which measures intestinal pH, temperature, and transit times, and can be utilized to quantify regional drug absorption [25]. This device represents a novel tool for the development of modified release formulations for personalized drug therapy.

12.2.3 Targeted Delivery Approaches

Targeted therapeutics are typically utilized in oncology to maximize drug concentration in tumor cells while minimizing the concentration in normal cells. When utilized in cancer therapy, targeted delivery approaches alter the in vivo disposition of the therapeutic agent, so that it is primarily taken up into tumor cells, through an interaction with a tumor cell specific molecule. Antibody-drug conjugates (ADCs) and nanoparticle-based formulations are targeted delivery approaches that combine a therapeutic agent with a targeted delivery platform.

Nanoparticle-based formulations currently on the market (Doxil®, DaunoXome, Marqibo, and Abraxane) that were designed to improve the pharmacokinetics or reduce toxicity of chemotherapeutic agents. Doxil, DaunoXome, and Marqibo are liposomal formulations containing chemotherapeutic agents that prolong the circulating half-life of the drug. Abraxane is an albumin-bound paclitaxel formulation that demonstrates reduced toxicity when compared to previous cremophor-based formulations. While these formulations alter in vivo drug disposition, they are not individualized based on a patients physiology and therefore do not fall under the umbrella of personalized medicine. Novel nanoparticle-based formulations that combine liposomes with targeted antibodies represent a move toward personalized nanoparticle-based delivery platforms [26]. Additionally, aptamer modifications (short single stranded DNA or RNA oligonucleotides) are an alternative to antibodies for targeting nanoparticles, and optimization of this technology may permit the development of aptamers unique to a patient's disease pathology [27].

ADCs involve the conjugation of an antibody to a therapeutic agent, where the antibody is targeted to a molecule that is overexpressed in the diseased cells [14]. The drug is covalently conjugated to the antibody via either a cleavable or non-cleavable linker [28]. ADCs are heterogeneous molecules with variations in the average number of drug molecules attached to the antibody, referred to as the drug:antibody ratio (DAR) [29]. Two ADCs are currently on the market, brentuximab vedotin (Adcetris), and ado-trastuzumab emtansine (Kadcyla), with more than 50 in the drug development pipeline primarily for oncology indications.

The challenge to developing ADCs is selecting targets and linking chemistry that result in selective delivery to diseased cells and efficient intracellular release of free drug [14, 30, 31]. There is also a requirement for the development of suitable diagnostic tests to determine whether a patient overexpresses the molecule to which the antibody is targeted to truly personalize therapy.

12.3 Pharmacokinetic Analysis for Personalized Drug Delivery

Clinical implementation of personalized drug delivery approaches has been limited, but a number of novel dosage forms, modified release formulations, and targeted therapeutics are in development to facilitate personalized drug therapy. In order to translate these approaches to the clinic, one needs to understand the physiological factors that contribute to the variability in pharmacokinetics and drug response, and how to leverage this information through the use of modeling and simulation tools to individualize therapeutic regimens. The modeling/simulation strategies will need to incorporate the drug delivery approach (targeted delivery versus modification of dose or dose release), and be dependent on the available pharmacokinetic data and whether there are diagnostic tests available to quantify clinical biomarkers prior to drug selection and administration.

12.3.1 Pharmacokinetic Analysis for Non-targeted Delivery Approaches

Compartmental models with covariate analysis or physiologically based pharmacokinetic (PBPK) models can be utilized to describe patient variability and determine dose, dosing interval, or modified release characteristics that result in the optimal drug exposure for efficacious therapy. The application of these modeling approaches is dependent on the type of pharmacokinetic data available; the use of compartmental models requires in vivo clinical concentration–time profiles (top-down approach to modeling), while PBPK models can be developed from in vitro and in silico data alone (bottom-up approach to modeling). The top-down approach to modeling involves the use of reduced models, compartmental, or physiological, where lumped tissues/compartments are used to estimate pharmacokinetic parameters from in vivo experimental data [32]. In this case, the structure and complexity of the models are determined by the available data. In contrast, the bottom-up approach utilizes a whole body PBPK modeling approach with in silico and in vitro data to simulate and predict pharmacokinetic profiles. The bottom-up approach is not dependent on clinical pharmacokinetic data.

A compartmental model approach is solely based on the drug-specific data set used to generate the model, and cannot be extrapolated to other drugs or physiological conditions [32]. While population modeling and covariate analysis can be utilized to describe the variability in pharmacokinetic parameters related to patient-specific physiological characteristics (e.g. weight, gender, creatinine clearance) or genotype/phenotype data (e.g. allelic variants of drug metabolizing enzymes), this approach does not quantify the differences in physiological processes, but utilizes an empirical equation to account for the differences between patients for specific pharmacokinetic parameters. Compartmental modeling approaches require in vivo clinical data to generate a structural model that adequately describes the observed concentration–time profile and estimate pharmacokinetic parameters; they cannot be constructed from in vitro data alone. Drug-specific compartmental models, and the associated pharmacokinetic parameters and covariates, can be used to tailor individualized therapeutic regimens, but they are limited based on the dose range and characteristics of the populations that were assessed during model development. This approach could be utilized to develop a dosing algorithm based on patient characteristics to determine an individualized dose, but is again limited based on the data used to develop the algorithm.

PBPK models have greater potential to account for pharmacokinetic variability in diverse patient populations, as they can quantitatively incorporate physiological, pathophysiological, and pharmacogenomic parameters [32]. Structural models based on physiological characteristics are critical for the implementation of personalized medicine and drug therapy, as they can be utilized to predict pharmacokinetics across the entire clinical population, from pediatrics through geriatrics, independent of in vivo clinical data in these populations [33]. One limitation to the wide-spread utilization of PBPK models is the need for a wide-range of physiological and pathophysiological data (system parameters that are independent of drug), as well as age-dependent changes in these processes, to develop PBPK models for healthy individuals and various disease states [32]. While the current commercial software platforms contain a wide-range of physiological data, there is limited information in certain areas, including tissue-specific expression of drug transporters, expression data in various disease states, and specific patient subpopulations, such as pediatrics. However, these platforms are constantly incorporating new physiological and pathophysiological data. PBPK models can be utilized from early drug development through clinical trials to prospectively predict and describe pharmacokinetic variability and optimize individualized therapeutic regimens. Personalized drug delivery approaches that focus on altering dose or drug release profile based on patient-specific physiology, pathophysiology, and genomics, as detailed in Section 12.2, can be readily explored using PBPK models, and they can be utilized to predict the

range of doses that may be needed clinically, thus informing the development of drug delivery approaches. This approach requires clinical biomarker data for individual patients to personalize drug therapy, and the data required will depend on the drug molecule.

PBPK (Simcyp Simulator or GastroPlus) or general modeling software (MATLAB, Berkeley Madonna, ADAPT-5, NONMEM, WinNonLin, STELLA) can be utilized to generate PBPK or compartmental models incorporating patient differences in physiological parameters related to drug metabolism and disposition to predict pharmacokinetics prior to drug administration. The commercial PBPK software packages incorporate complex intestinal absorption models that include parameters for intestinal physiological (intestinal pH, transit time, segmental differences in enzyme/transporter expression), and dissolution characteristics of the specific formulations being analyzed [32]. These models can then be utilized to simulate the impact of altering drug dose, dosing interval, or drug release characteristics, and design optimal therapeutic regimens based on patient-specific characteristics, which is the goal of personalized medicine and drug therapy. An understanding of the modifications required to deliver personalized therapy early in the drug development process can facilitate the design of drug delivery approaches that meet this need.

12.3.2 Pharmacokinetic Analysis for Targeted Delivery Approaches

Targeted therapeutics are novel modalities that leverage a molecule overexpressed in the target cells to deliver a pharmaceutical agent while minimizing delivery to off-target cells. For personalized therapy with targeted therapeutics, patients are subdivided into responder and non-responder groups based on analysis of the target molecule in the tumor cells; individuals without expression of the target molecule are non-responders and should not be treated with the therapy. The objective of personalized drug delivery using targeted therapeutics is to maximize the tumor payload of the conjugated drug to achieve an optimal pharmacodynamic effect. This can be accomplished by selecting tumor-specific targets, optimizing the DAR, and stability ADC in systemic circulation [34]. There is limited clinical experience with the pharmacokinetic analysis of these delivery platforms with only two agents (both ADCs) currently approved for oncology indications. As such the following paragraphs will focus on pharmacokinetic analysis of ADCs.

The pharmacokinetic analysis of these therapeutics is complex, as multiple components need to be evaluated. Analysis of the ADME of ADCs involves the analysis of the intact ADC, as well as the antibody alone and the small molecule, and the release of the small molecule from the delivery platform [34]. Researchers and pharmaceutical companies are evaluating diverse approaches for the characterization of ADC ADME, and these approaches have been discussed in a number

of recent reviews [29, 34, 35]. As with other personalized delivery approaches, compartmental, and PBPK models could be utilized; however, PBPK models for ADCs are not well established [29]. The PBPK models that have been developed for ADCs are hybrid PBPK models, which combine compartmental and physiological based approaches [36]. Compartmental models, which are more commonly used, contain structural components for the systemic disposition of the ADC and free drug, as well as tumor disposition of the antibody and drug release [29, 37]. Models for the individual components can be built separately and then merged together into the final ADC model [29]. These models take into account the variations in DAR, which can be measured in analytical assays to determine the amount of drug molecules for a give ADC dose [29, 35]. The DAR can alter the pharmacokinetic properties of the ADC, and its impact tumor accumulation of the ADC and drug molecule can be incorporated into a compartmental modeling approach [34]. Further personalization could be achieved by incorporating patient-specific clinical biomarker expression data into the structural models to predict and optimize drug delivery to the tumor.

12.4 Challenges and Opportunities in Personalized Drug Delivery

For clinical implementation of personalized drug therapy, therapies must be tailored to an individual's genetic makeup, physiological, and pathophysiological characteristics prior to their initiation. These patient-specific molecular characteristics can be leveraged to select beneficial therapies, while minimizing adverse side effects. Advances in drug delivery approaches facilitating personalized drug therapy must have a molecular basis, and clinical biomarkers must exist to identify patient subpopulations [7]. Personalized drug delivery can involve flexible dosage forms or modified release profiles to optimize systemic drug exposure, or targeted therapies that maximize drug concentrations in a specific cell type. Challenges associated with the implementation of personalized drug therapy include the cost associated with developing and manufacturing personalized dosage forms and targeted therapies, the requirement for diagnostic tests for relevant clinical biomarkers, and the lack of patient specific physiological and pathophysiological data to build PBPK models. In addition to the scientific and technological challenges, regulatory challenges are also present.

Personalized drug therapy and delivery approaches are a departure from the blockbuster "one size fits all" approach to drug therapy, as individualized therapy is tailored to smaller patient populations that will receive the greatest therapeutic benefit [38]. This change in therapeutic approach impacts the costs associated with drug development and manufacturing as well as pricing of the drug product [7].

Drug delivery devices proposed for individualization of oral dosage forms, such as mini-pellet dispensers or the solid dosage pen [11, 21], are more costly than conventional oral dosage forms, which may be a drawback to their wide-spread clinical implementation [10]. Further, the use of innovative tablet designs that are divisible, as well as a larger range of dose options necessitates a change in current manufacturing procedures. In contrast, clinical development costs may be lower due to identification of patient subpopulations that would have the highest drug response [7]. This may also reduce the size and number of the required clinical trials; however, it may take longer and require more clinical sites to obtain a suitable number of patients with the clinical biomarker. Personalized drug therapy can demonstrate a significant improvement compared to the standard of care. However, the smaller patient population can result in high costs for the course of therapy [7]. The high cost may reduce patient access due to an inability to pay for the therapy. For personalized drug therapy to be successfully implemented in the clinic, one needs to move away from the current blockbuster economic model.

Personalized medicine and drug therapy is dependent on development of high-throughput diagnostic assays for clinical biomarkers relevant to drug disposition and therapeutic efficacy. These diagnostic assays must quantitatively evaluate different biological levels (DNA, RNA, protein) to functionally characterize the patient and disease pathology [39]. Validation of clinical biomarkers to identify patient subpopulations should be done during drug development, and may increase development costs as the diagnostic assay requires regulatory approval [7]. As we move toward personalized drug therapy, these diagnostics must become low cost and widely available for this therapeutic approach to have wider implementation.

An additional limitation to the implementation of personalized drug therapy is the lack of quantitative physiological and pathophysiological data at the molecular level for the entire clinical population. Expanded knowledge of transporter expression in specific organs, physiological impact of specific diseases, and physiological changes in enzymes and transporters in pediatric and geriatric populations are needed to improve utility of PBPK models [10, 32]. This information is crucial for the development of PBPK models to predict drug disposition prior to clinical evaluation for new therapeutics and to inform the design and implementation of personalized drug delivery approaches.

12.5 Conclusions

As the initial wave of personalized medicine hits healthcare, the practice of individualized medicine is focused on the early steps of patient care, such as identification of an individual's unique molecular, biochemical, physiological, and pathological profile, and application of these clinical biomarker results as

the basis for subsequent treatments. Being an important element of personalized medicine, personalized pharmacotherapy plays an essential role in personalized patient care. Evaluation of pharmacogenetic, pharmacogenomic, and proteomic clinical biomarkers is becoming part of the standard of patient care. This is in part, due to the improvement in the affordability of genetic testing and protein quantification, through technological advances in genome sequencing and proteomic analysis. Patients are becoming more cognizant of the role of genetics in disease and drug therapy and are becoming active participants in the utilization of this information, as evidenced by the growing interest in direct-to-consumer genetic testing. Delivery of pharmacologically active agents according to the patients' molecular characteristics can be implemented by utilizing the drug delivery systems evolved in the past few decades to realize the precision and on demand nature of personalized drug delivery. Advancement in material sciences, nanotechnology, and microelectronics provides the foundation for delivery of drug to a specific target and/or for delivery of drug in a specific mode to meet the site, time, amount, and rate required by an individual patient. Personalized drug delivery is being achieved by targeted drug delivery for patients with specific molecular or biochemical markers. As more targets are identified using the genomic and proteomic data generated in the past decade, more personalized delivery plans can be drawn to increase therapeutic efficacy and reduce adverse events. Computer or microelectronic controlled infusion pumps have been a useful delivery system to administer drugs for flexible dosing and on demand mode. The application of this type of infusion pump will be an effective tool for tailoring the dose, delivery time, and rate in the individualized drug delivery of parenteral dosage forms. When this delivery system is coupled with biosensors, individualized dosing can reach another level of personalized medicine in pharmacotherapy. For oral dosage forms and implant devices, 3D printing technology can be a viable method to tailor the dose, delivery mode, and dosing kinetics for individualized drug delivery.

Individualized drug delivery is still in its infancy compared to other elements of individualized medicine. The integration and maturation of other elements of personalized medicine will be a propellant for individualized drug delivery. Incorporation of new technology such as the internet and artificial intelligent could also fuel the advancement of individualized drug delivery.

References

1 Guchet, X. (2015). What's in a word? The person of personalized (nano)medicine. *Nanomedicine (London)* 10: 3167–3179.

2 Carotenuto, P., Roma, C., Rachiglio, A.M. et al. (2011). Optimizing response to gefitinib in the treatment of non-small-cell lung cancer. *Pharm. Pers. Med.* 4: 1–9.

3 Ma, Q. and Lu, A.Y. (2011). Pharmacogenetics, pharmacogenomics, and individualized medicine. *Pharmacol. Rev.* 63: 437–459.

4 Cherny, N.I., de Vries, E.G., Emanuel, L. et al. (2014). Words matter: distinguishing "personalized medicine" and "biologically personalized therapeutics". *J. Natl. Cancer Inst.* 106: 1–5.

5 Waldman, S.A. and Terzic, A. (2015). Companion diagnostics at the intersection of personalized medicine and healthcare delivery. *Biomark. Med.* 9: 1–3.

6 Crews, K.R., Gaedigk, A., Dunnenberger, H.M. et al. (2014). Clinical pharmacogenetics implementation consortium guidelines for cytochrome P450 2D6 genotype and codeine therapy: 2014 update. *Clin. Pharmacol. Ther.* 95: 376–382.

7 Trusheim, M.R., Berndt, E.R., and Douglas, F.L. (2007). Stratified medicine: strategic and economic implications of combining drugs and clinical biomarkers. *Nat. Rev. Drug Discovery* 6: 287–293.

8 Pritchard, D. (2016). Personalized medicine at the FDA: 2015 progress report. *J. Precis. Med.* 5 (1): 40–41.

9 Wen, H., Jung, H., and Li, X. (2015). Drug delivery approaches in addressing clinical pharmacology-related issues: opportunities and challenges. *AAPS J.* 17: 1327–1340.

10 Breitkreutz, J. and Boos, J. (2007). Paediatric and geriatric drug delivery. *Expert Opin. Drug Delivery* 4: 37–45.

11 Wening, K. and Breitkreutz, J. (2011). Oral drug delivery in personalized medicine: unmet needs and novel approaches. *Int. J. Pharm.* 404: 1–9.

12 Aleksovski, A., Dreu, R., Gasperlin, M., and Planinsek, O. (2015). Mini-tablets: a contemporary system for oral drug delivery in targeted patient groups. *Expert Opin. Drug Delivery* 12: 65–84.

13 Preis, M., Breitkreutz, J., and Sandler, N. (2015). Perspective: concepts of printing technologies for oral film formulations. *Int. J. Pharm.* 494: 578–584.

14 Dawidczyk, C.M., Kim, C., Park, J.H. et al. (2014). State-of-the-art in design rules for drug delivery platforms: lessons learned from FDA-approved nanomedicines. *J. Controlled Release* 187: 133–144.

15 Ingelman-Sundberg, M., Sim, S.C., Gomez, A., and Rodriguez-Antona, C. (2007). Influence of cytochrome P450 polymorphisms on drug therapies: pharmacogenetic, pharmacoepigenetic and clinical aspects. *Pharmacol. Ther.* 116: 496–526.

16 Relling, M.V., Gardner, E.E., Sandborn, W.J. et al. (2011). Clinical pharmacogenetics implementation consortium guidelines for thiopurine methyltransferase genotype and thiopurine dosing. *Clin. Pharmacol. Ther.* 89: 387–391.

17 Stegemann, S., Ecker, F., Maio, M. et al. (2010). Geriatric drug therapy: neglecting the inevitable majority. *Ageing Res. Rev.* 9: 384–398.

18 Bredenberg, S., Nyholm, D., Aquilonius, S.M., and Nystrom, C. (2003). An automatic dose dispenser for microtablets – a new concept for individual dosage of drugs in tablet form. *Int. J. Pharm.* 261: 137–146.

19 van Santen, E., Barends, D.M., and Frijlink, H.W. (2002). Breaking of scored tablets: a review. *Eur. J. Pharm. Biopharm.* 53: 139–145.

20 McDevitt, J.T., Gurst, A.H., and Chen, Y. (1998). Accuracy of tablet splitting. *Pharmacotherapy* 18: 193–197.

21 Wening, K. and Breitkreutz, J. (2010). Novel delivery device for monolithical solid oral dosage forms for personalized medicine. *Int. J. Pharm.* 395: 174–181.

22 Laukamp, E.J., Vynckier, A.K., Voorspoels, J. et al. (2015). Development of sustained and dual drug release co-extrusion formulations for individual dosing. *Eur. J. Pharm. Biopharm.* 89: 357–364.

23 Basit, A. (2020). Recent innovations in 3D-printed personalized medicines: an interview with Abdul Basit. *Journal of 3D Printing in Medicine* 4 (1): 5–7.

24 Goyanes, A., Madla, C.M., Umerji, A. et al. (2019). Automated therapy preparation of isoleucine formulations using 3D printing for the treatment of MSUD: First single-centre, prospective, crossover study in patients. *Int. J. Pharm.* 567: 1–8.

25 Becker, D., Zhang, J., Heimbach, T. et al. (2014). Novel orally swallowable IntelliCap((R)) device to quantify regional drug absorption in human GI tract using diltiazem as model drug. *AAPS PharmSciTech* 15: 1490–1497.

26 Ramos-Cabrer, P. and Campos, F. (2013). Liposomes and nanotechnology in drug development: focus on neurological targets. *Int. J. Nanomed.* 8: 951–960.

27 Benedetto, G., Vestal, C.G., and Richardson, C. (2015). Aptamer-functionalized nanoparticles as "smart bombs": the unrealized potential for personalized medicine and targeted cancer treatment. *Target. Oncol.* 10: 467–485.

28 Nolting, B. (2013). Linker technologies for antibody-drug conjugates. *Methods Mol. Biol.* 1045: 71–100.

29 Singh, A.P., Shin, Y.G., and Shah, D.K. (2015). Application of pharmacokinetic-pharmacodynamic modeling and simulation for antibody-drug conjugate development. *Pharm. Res.* 32: 3508–3525.

30 Sassoon, I. and Blanc, V. (2013). Antibody-drug conjugate (ADC) clinical pipeline: a review. *Methods Mol. Biol.* 1045: 1–27.

31 Chari, R.V., Miller, M.L., and Widdison, W.C. (2014). Antibody-drug conjugates: an emerging concept in cancer therapy. *Angew. Chem. Int. Ed.* 53: 3796–3827.

32 Rowland, M., Peck, C., and Tucker, G. (2011). Physiologically-based pharmacokinetics in drug development and regulatory science. *Annu. Rev. Pharmacol. Toxicol.* 51: 45–73.

33 Leeder, J.S., Brown, J.T., and Soden, S.E. (2014). Individualizing the use of medications in children: making goldilocks happy. *Clin. Pharmacol. Ther.* 96: 304–306.

34 Kraynov, E., Kamath, A.V., Walles, M. et al. (2016). Current approaches for absorption, distribution, metabolism, and excretion characterization of antibody-drug conjugates: an industry white paper. *Drug Metab. Dispos.* 44: 617–623.

35 Kamath, A.V. and Iyer, S. (2015). Preclinical pharmacokinetic considerations for the development of antibody drug conjugates. *Pharm. Res.* 32: 3470–3479.

36 Chen, Y., Samineni, D., Mukadam, S. et al. (2015). Physiologically based pharmacokinetic modeling as a tool to predict drug interactions for antibody-drug conjugates. *Clin. Pharm.* 54: 81–93.

37 Wada, R., Erickson, H.K., Lewis Phillips, G.D. et al. (2014). Mechanistic pharmacokinetic/pharmacodynamic modeling of in vivo tumor uptake, catabolism, and tumor response of trastuzumab maytansinoid conjugates. *Cancer Chemother. Pharmacol.* 74: 969–980.

38 Panicucci, R. and Sanchez-Felix, M. (2015). Overview of challenges and opportunities in drug delivery and pharmaceutics. *Ther. Delivery* 6: 911–914.

39 Dietel, M. and Sers, C. (2006). Personalized medicine and development of targeted therapies: the upcoming challenge for diagnostic molecular pathology. A review. *Virchows Arch.* 448: 744–755.

Index

Drug Delivery Approaches: Perspectives from Pharmacokinetics and Pharmacodynamics,
First Edition. Edited by Bret Berner, Toufigh Gordi, Heather A. E. Benson, and Michael S. Roberts.

b

C

d

e

f

g

h

i

k

l

p

t